Muon to electron conversion, flavored leptogenesis and asymmetric dark matter in minimal extensions of the Standard Model

Mikaël Dhen

Service de Physique Théorique, Faculté des Sciences
Université Libre de Bruxelles

Doctoral Thesis in Theoretical Physics

September 2015

Thesis supervisor : Prof. Thomas Hambye

Fume, chante et bois,
On ne vit qu'une fois !

Oeuvre, ris et mange sainement,
Tu n'en vivras que plus longtemps !

Badine, danse et savoure,
Après tout, autant y mettre de l'amour !

Lis, comprends et analyse,
La vie n'est pas faite que de bêtises.

A TOUS LES SYBARITES, LES ULYSSES ET LES AMOUREUX QUI CROQUENT LA VIE À PLEINES DENTS.

Remerciements

Cette thèse de doctorat n'aurait jamais vu le jour sans un concours de circonstance somme toute particulier. En effet, bien qu'intéressé depuis tout petit par la science en général (mes parents n'étant pas étrangers à cela), je ne me suis pas dirigé vers la physique à l'ULB à la fin des secondaires, moment auquel j'ai préféré avec raison entamer des études afin de devenir ingénieur industriel électromécanicien. Après avoir terminé ces études avec succès, deux choix se sont alors présentés à moi : soit j'utilisais ce nouveau bagage directement en cherchant un emploi dans ce domaine, soit je profitais de ma relative jeunesse pour chercher des réponses aux divers questions fondamentales qui m'ont toujours interloqué. C'est vers ce dernier domaine que je me suis tourné, et que j'ai eu la chance de pouvoir emprunter... et non sans difficultés ! Recommencer quatre années d'études en Physique à l'ULB n'est clairement pas chose aisée, non seulement techniquement mais aussi moralement. Cependant, j'ai réussi à en venir à bout non sans plaisir, vu que ça m'a permis d'éclairer certaines zones d'ombres de ma pensée. Certaines, car alors que l'on croit mieux comprendre ce qui nous entoure, des problèmes insoupçonnés sont mis au jour car l'Univers n'a de cesse de donner du fil à retordre, à chaque fois que l'on croit pouvoir y mettre de l'ordre.

C'est pourquoi, j'ai voulu et j'ai eu la chance de pouvoir continuer sur ma lancée en effectuant un doctorat dans le service de Physique théorique. En même temps, je n'étais plus à quatre ans près ! Et me voici déjà au bout de cette épopée, non sans fierté. Ces années de doctorat furent extrêmement enrichissantes, tant du côté de la recherche et de l'enseignement que du côté humain et personnel.

En effet, j'ai eu la chance de travailler sur des projets intéressants, grâce à mon excellent promoteur Thomas. Il va de soit que je le remercie énormément pour tout ce qu'il m'a apporté. Sa passion de la science, sa patience, sa persévérance et sa sincérité m'ont notamment beaucoup touché. J'en profite aussi pour remercier, pour leur travail et disponibilité, mes collaborateurs Xiaoyong Chu, Rodrigo Alonso, Belen Gavela, Diego Aristizabal, Avelino Vicente et Chee Sheng Fong. Je remercie de même les membres du jury, Riccardo Argurio, Jean-Marie Frère, Belen Gavela, Thomas Hambye, Michel Tytgat et Francesco Vissani qui ont eu le courage et la patience de lire cet ouvrage.

En parallèle du travail de recherche, j'ai eu l'immense chance d'être témoin de plusieurs résultats expérimentaux, comme l'importante découverte du boson de Brout-Englert-Higgs au LHC ! Et ce n'est pas fini, vu que ce formidable outil nous réserve sûrement encore quelques surprises, et vu que de nombreuses autres expériences devraient encore tenir en haleine les physiciens affamés pendant encore quelques années...

Tout au long du doctorat, j'ai aussi eu le privilège de donner des séances d'exercices grâce notamment aux professeurs de notre service Michel et Peter, que je remercie aussi chaleureusement, tout comme Jean-Marie, Paul, Anastase et Etienne qui animent les laboratoires de physique générale. J'ai vraiment aimé enseigner parce que c'est gratifiant de transmettre et de partager. Après tout, étudiants nous l'avons tous été.

Le doctorat m'a aussi permis de rencontrer des gens formidables : vive les mariés Tiziana et Fabio, mais aussi Bryan, Camilo, Chaïmae, Federica, Federico, Isabelle, José-mi, Julian, Laura, Lorenzo, Maxim, Michael, Sabir, Simon et Yong. Doctorants ou post-docs, on a bien ri tous ensemble. Un tout grand merci à Isabelle pour son travail, son efficacité et sa gentillesse. Un clin d'oeil aussi à Thierry, Lucien, Alex, Simon, Champion, Gus, Edu, Nacho, Robson, Shyam, Lio, Yassin et toutes les personnes de l'ULB ou de la VUB avec qui j'ai eu la chance d'étudier, d'enseigner ou juste de jouer un match de foot.

Naturellement, tout au long de mon parcours original, j'ai reçu l'amour et le soutien de ma chérie, de ma famille et de mes amis. Sans ce carburant, il est clair que je n'aurais pas été si loin ! Et ce n'est que le début. . . vu mon réservoir, je pense pouvoir traverser la voie lactée. C'est donc naturellement à eux que cet ouvrage est dédié. Je souhaite finalement la bienvenue aux nouveaux arrivés, Eve et Matis, à qui j'espère communiquer mon intérêt et ma curiosité pour la science !

Abstract

It is well known that there must be a physics beyond the Standard Model of elementary particles. Among all the evidences, the mass of the neutrinos, the matter-antimatter asymmetry of our Universe and the dark matter constitute the three general contexts of this thesis.

The fact that neutrinos are massive is the first clearest evidence for a new physics beyond the Standard Model. Neutrino masses can find an explanation in the context of the famous and favorite "Seesaw models". These models also generate processes in which the flavor of the charged leptons changes, as in the decay of a muon into an electron and a photon, or the conversion of a muon into an electron in atomic nuclei without neutrino emission. These processes are very appealing because future experiments will reach impressive sensibilities on the measurement of their branching rate, and because their observation would confirm the existence of a new physics and could even potentially discriminate between different theoretical models. It is therefore important to have reliable expressions for their rate in each kind of Seesaw mechanism. In the first part of this thesis, we compute the rate of the conversion of a muon into an electron in the framework of type-1 Seesaw models, and we analyze the phenomenology it leads to.

The Seesaw models, on top of generating small neutrino masses and new interesting processes, also contain remarkably all the necessary ingredients to create enough matter-antimatter asymmetry in our Universe through the "leptogenesis" mechanism. This latter consists in generating a lepton asymmetry which is partially transferred in a baryon asymmetry. In the second part of this thesis, we study the leptogenesis in the context of type-2 Seesaw models, determining and analyzing for the first time the effect of the flavors and the spectator processes.

Finally, the third and last part of this thesis focuses on the possibility of generating not only the baryons in an asymmetric way but also the dark matter. To this end we consider the "inert doublet" model, as it contains an interaction which could generate dark matter in an asymmetric way. We therefore address the following question : is it possible to generate all the observed dark matter of our Universe in an asymmetric way in the inert doublet model ?

Résumé

Il est clair que le Modèle Standard des particules élémentaires n'est pas complet. Parmi tous les indices d'une physique au-delà du Modèle Standard, la masse des neutrinos, l'asymétrie matière-antimatière de notre Univers et la matière noire constituent les trois contextes généraux de cette thèse.

Le fait que les neutrinos soient massifs constitue la plus claire évidence d'une physique au-delà du Modèle Standard. La masse des neutrinos peut trouver une explication notamment dans le cadre des modèles favoris dits "modèles Seesaw". Ces modèles, en plus de générer une petite masse pour les neutrinos, génèrent aussi des processus dans lesquels la saveur d'un lepton chargé est changée, comme la désintégration d'un muon en un électron et un photon, ou la conversion d'un muon en un électron au sein d'un atome sans émission de neutrino. Ces processus sont importants car les expériences futures devraient atteindre des sensibilités impressionnantes sur leurs taux, mais aussi parce que leur observation confirmerait l'existence d'une physique nouvelle et pourrait peut-être discriminé parmi les différents modèles. Il est donc important d'avoir une expression analytique fiable du taux de ces processus dans le cadre de ces modèles Seesaw favoris. Dans la première partie de cette thèse, nous calculons l'expression du taux de conversion d'un muon en un électron au sein d'un atome dans le cadre des modèles Seesaw de type 1, et analysons la phénoménologie s'y rapportant.

Ces modèles Seesaw, en plus de générer une petite masse pour les neutrinos et des processus changeant la saveur leptonique, permettent aussi la création de l'asymétrie matière-antimatière dans l'Univers, à travers le mécanisme dit de "leptogenèse". Selon ce mécanisme, une asymétrie leptonique aurait d'abord été créée, avant d'être partiellement transférée en une asymétrie baryonique. Dans la seconde partie de cette thèse, nous calculons et analysons la leptogenèse dans le cadre des modèles Seesaw de type 2 avec, pour la première fois, la prise en compte des effets de saveurs.

Finalement, la troisième et dernière partie de cette thèse se concentre sur la possibilité de générer non seulement la matière baryonique à partir d'une asymétrie, mais aussi la matière noire. À cette fin, nous considérons le modèle dit "doublet inerte", car il contient une interaction qui pourrait à priori générer de la matière noire à partir d'une asymétrie. Nous adressons dès lors la question suivante et y répondons : est-il possible de générer toute la matière noire à partir d'une asymétrie de matière noire dans le contexte du modèle doublet inerte ?

Contents

Introduction

What else ? This is the question which is in everybody's mind since thousands of years, concerning any kind of field, scientific or not. This is particularly true in physics nowadays. After each improvement in our understanding of the physical phenomenon around us, it is each time more shadow zones that are discovered. This was and this will be surely like that forever. However, we are today very far in the elucidation of mysteries of Nature, thanks to the scientific input of thousands of people since thousand of years, thanks to wonderful mathematical tools and increasingly sophisticated experiments.

At the microscopic level, the building blocks of the Standard Model of elementary particles (SM) physics have been progressively assembled until to reach in the 1960-1970's his present form after the placement of the keystone, the Brout-Englert-Higgs boson which has been discovered experimentally in 2012 at the Large Hadron Collider (LHC). At the macroscopic level, the adjunction to the SM of the General Relativity (GR), the dark matter (DM) and dark energy (DE) has allowed to build the Standard Model of cosmology (ΛCDM), which amazingly describes very well the evolution of the Universe as confirmed by observations.

But we know that the monument is not yet achieved. As a first example, neutrinos are massless in the Standard Model while experiments have put forward the fact that neutrinos are actually massive particles. Second, our Universe is matter dominated so that an asymmetry between matter and antimatter should have been created in the early times, and unfortunately the Standard Model fails to generate it. Thirdly, on top of ordinary matter, there are clear evidences that the Universe is also composed by an invisible dark matter whose origin is still unknown. Finally, on top of these three examples, there are several other theoretical hints to believe that there exists a new physics beyond the Standard model (BSM) as : the hierarchy problem, the unification of forces, the inclusion of gravity, the strong CP problem, inflation, the origin of the dark energy, the smallness of the cosmological constant, the Big Bang singularity,...

Despite these facts and these hints, it is very difficult to put in evidence new physics beyond the Standard Model at the particle level, giving hard time to physicists. For now, all laboratory experiments are in impressive agreement with the Standard Model of elementary particles and don't show any evidence for new BSM particles. The neutrino masses have been put in evidence by both Universe observational means and laboratory experimental means, but its origin in terms of particles is still unknown. All the other hints, as for example dark matter, are purely observational.

So what's next ? At the experimental level, the present and future experiments should bring new discoveries soon. For example, the LHC second run could hopefully highlight the existence of new elementary or composite particles (if this is not already done), neutrino experiments should bring light on the nature of these particles, dark matter searches will also continue to bring hope on its discovery, and more and more experiments are planed so as to lighten the real new physics. At the theoretical level, lots of extensions to the Standard Model have been considered for years, which generally all predict new particles and phenomena to be discovered. Among all theses possibilities, Nature may be mild with us and could have chosen the ones that are within experimental reach.

This thesis lies in such an exciting context and focuses on three of the above puzzles which point towards new physics, namely neutrino masses, the matter-antimatter asymmetry of our Universe and dark matter. Even if each puzzle can be solved in many possible ways and may not be linked, clearly it is of special interest to see whether they could find an explanation from a common origin. This is the point of view and the guiding principle we will adopt all along this thesis. Actually, there are good reasons to believe that at least two or even the all three enigmas could be related. For instance, the small neutrino masses can be explained in the framework of the favorite Seesaw models, which are the most simple extensions of the Standard Model to account for it. As we will show in this thesis, these models not only generate interesting charged lepton flavor violation processes which we will study, but they also contain quite remarkably all the necessary ingredients to explain the matter-antimatter asymmetry of the Universe, as we will see too. The smallness of the mass of the neutrinos may therefore be related to the matter-antimatter asymmetry of the Universe. As another example, it is particularly intriguing that the quantity of visible matter and the quantity of dark matter in our Universe are very close to each other. It is thus important to study if such apparent coincidence could not be explained in various ways, as we will also discuss in this thesis. The thesis is structured as follows.

In chapter 1, we review the experimental evidence for neutrino oscillations. Since these necessarily imply that neutrinos are massive particles, we discuss how the Standard Model can be enlarged in order to account for their mass. In particular, we introduce the three types of Seesaw models, which are very attractive extensions of the Standard Model that can generate small neutrino masses and at the same time new processes that violate the charged lepton flavors. Furthermore, these models can generate enough matter-antimatter asymmetry in our Universe and they are very well motivated by Grand Unified Theories.

In chapter 2, we focus on the charged lepton flavor violation processes in the context of type-1 Seesaw models. First, we review the experimental and theoretical status of these promising processes, particularly the conversion of a muon into an electron in atomic nuclei since future experiments should reach impressive sensitivities on its rate. Second, we compute the analytical expression of the muon to electron conversion rate in the type-1 Seesaw models, on which there was actually no agreement in the literature. Finally, we show how the charged lepton flavor violation processes could lead to pretty nice predictions, how they could allow to determine the Seesaw scale and how they could allow to distinguish between the various kinds of Seesaw models. The computation of the conversion rate and the study of the phenomenology have lead to an original publication [1].

In chapter 3, we review the cosmological evidence for a matter-antimatter asymmetry in our Universe. Among all the possibilities, the Seesaw models possess quite remarkably all the ingredients to explain the matter-antimatter asymmetry, on top of generating small neutrino masses. The way the matter asymmetry is generated in the Seesaw models is via the so-called leptogenesis mechanism. We show how it works in the framework of the type-1 Seesaw models, and discuss the effect of the lepton flavors in the asymmetry production. Flavors are important because they could change dramatically the way leptogenesis occurs, but also because the structure of flavors is in fact directly related to another puzzle in the Standard Model, that is : why are there three families of fermions with such different masses and why are the flavor mixings in the lepton sector so different from the ones in the quark sector ?

In chapter 4, we focus on the leptogenesis mechanism in the framework of the type-2 Seesaw model. Because the way leptogenesis works in this case is in many ways different from the type-1 leptogenesis considered in the previous chapter, we first study the scalar triplet leptogenesis within the one-flavor approximation. Subsequently we show the importance of the lepton flavors and why they actually always matter in the scalar triplet leptogenesis mechanism. We then give all the necessary ingredients for computing the baryon asymmetry of the Universe, starting from the elementary interactions of the scalar triplet. In order to show how leptogenesis works within this framework, we finally analyze the effect of flavors in several new scenarios. The computation of the flavor effect in type-2 Seesaw leptogenesis and the study of the new scenarios have lead to an original publication in Ref. [2].

In the last chapter 5, we first review very briefly the evidence for dark matter in our Universe. Since here too the Standard Model doesn't posses any dark matter candidate, it also needs to be enlarged to account for it. In particular, in the so-called Inert Doublet Model (IDM), a second scalar doublet is introduced which can account for the dark matter relic density. In the last part of this thesis, we wonder if, alike to the baryonic matter in the previous chapters, dark matter can be generated in an asymmetric way within this model. The answer of this question has lead to an original publication in Ref. [3].

Part I

SEESAW MODELS AS THE ORIGIN OF NEUTRINO MASSES AND CHARGED LEPTON FLAVOR VIOLATION

1 Neutrino masses and BSM physics

Since the assumption of its existence by Wolfgang Pauli in 1930 [4], neutrinos are still fascinating the world. The "desperate" remedy to save energy conservation in the β-decay is a neutral particle of spin 1/2 and, at that time, supposed massless. Because of its very feeble interactions with the other particles of the Standard Model (SM), it is only years after that we had a proof of its existence. Chronologically, first was discovered the electron neutrino ν_e at Hanford [5] in 1956, then the muon neutrino ν_μ at Brookhaven [6] in 1962, and finally the tau neutrino ν_τ at Fermilab [7] in 2000. Three flavors of neutrinos were discovered, corresponding to the three charged lepton families. Experimentally, the number of neutrinos species lighter than $m_Z/2$ has been determined by measuring the cross-section of the e^+e^- annihilations near the Z mass. Adjusting the results from the experiments ALEPH, DELPHI, L3 and OPAL, the number of light neutrino families N_ν is in agreement with $N_\nu = 2.92 \pm 0.05$ [8].

In the SM of elementary particles, together with its associated left-handed charged lepton, each neutrino is a part a doublet $\ell_L \equiv (\nu_L \; e_L)^T$, which is charged under the gauge group $SU(2)_L \times U(1)_Y$. Since they are electrically neutral and colorless, they can only interact through the Z and the $W^\pm$ gauge bosons of the weak interaction. Because they are supposed massless, no right-handed neutrino has been introduced in the SM in order to give a mass to the neutrinos through the Brout-Englert-Higgs mechanism. At the same time, no right-handed neutrino has never been observed in nature so far.

As a consequence of the absence of right-handed neutrinos, the SM contains by construction three lepton flavor global symmetries $U(1)_{L_\alpha}$, with $\alpha = e, \mu, \tau$, in addition to the lepton and baryon global symmetries $U(1)_L$ and $U(1)_B$. From now on, greek letters $\alpha, \beta, \ldots$ will denote the different flavors (e, μ, τ). From Noether theorem, to each of these global symmetries corresponds a conserved quantity, which are respectively the electron L_e, the muon L_μ and the tau L_τ flavor numbers, and the lepton L and baryon B numbers. As a consequence, no lepton flavor changing interactions should exist, according to the SM.

In this section, we will fist review the physics of neutrino oscillations whose observation brought clear evidence that lepton flavor is violated in Nature and that neutrino are massive particles. We then present the present values of the mixing parameters and the best bounds on

the absolute neutrino mass from non-oscillation experiments. We will also discuss the prospects of future neutrino experiments. Finally, we will show how one can extend the SM in order to give a mass to the neutrinos. In particular, we will introduce the Seesaw mechanisms which constitute the framework of the main works of this thesis.

1.1 Neutrino oscillations

1.1.1 Puzzles from neutrino fluxes

Collisions between cosmic rays and nuclei produce lots of pions in the upper atmosphere. These pions decay mostly into muonic neutrinos and muons, which in turn decay into electrons, muonic neutrinos and electron neutrinos. As a result, an important flux of electron and muon neutrinos arrives at the surface of the earth. By measuring the muon neutrino flux coming from the top atmosphere, the Super-Kamiokande collaboration highlighted the existence of muonic neutrino oscillations in 1998 [9]. They detected a deficit of muon neutrinos compared to the predictions, which can find as an explanation the fact that some muon neutrinos oscillate to another neutrino flavor. Other explanations, as neutrino decay or decoherence, were ruled out. Few years after, several experiments confirmed that neutrinos coming from the sun [10], from nuclear reactor [11], and from accelerator beams [12] do oscillate as well.

Neutrino oscillations arise if the flavor eigenstates (the basis of the weak interactions) are not the mass eigenstates (the basis in which neutrino propagates). The discovery of neutrino oscillations has therefore drastic consequences : the global lepton flavor symmetries L_α are violated, and more important, at least two of the three left-handed neutrinos do actually have masses, as we will show in the next section. These both consequences are clearly not consistent with the SM, which therefore need to be extended in order to account for this phenomenon.

1.1.2 Theory of neutrino oscillations

The neutrinos which take part in weak interactions are the three flavor eigenstates ν_α (and the associated antiparticles $\bar{\nu}_\alpha$). By definition, these are the particles that interact with the corresponding charged leptons e_α (and $\bar{e}_\alpha$ respectively) through emission or absorption of W bosons. Their quantum states form an orthogonal basis $|\nu_\alpha\rangle$, such that $\langle\nu_\alpha|\nu_\beta\rangle = \delta_{\alpha\beta}$. However, the neutrino states that are relevant for propagation are the mass eigenstates ν_i, where $i = 1,2,3$, which coincide with the flavor eigenstate only if neutrinos are massless, or if the mass matrix is flavor diagonal in the flavor eigenstate basis. The mass eigenstates also form an orthogonal basis $|\nu_i\rangle$, such that $\langle\nu_i|\nu_j\rangle = \delta_{ij}$. If in the flavor basis the mass matrix is non-diagonal, one has in general

$$m_\nu = \begin{pmatrix} m_{\nu_{ee}} & m_{\nu_{e\mu}} & m_{\nu_{e\tau}} \\ m_{\nu_{\mu e}} & m_{\nu_{\mu\mu}} & m_{\nu_{\mu\tau}} \\ m_{\nu_{\tau e}} & m_{\nu_{\tau\mu}} & m_{\nu_{\tau\tau}} \end{pmatrix}, \tag{1.1}$$

and the flavor and mass eigenstates basis differ by a unitary transformation :

$$|\nu_\alpha\rangle = \sum_{i=1}^{3} \mathscr{U}_{\alpha i} |\nu_i\rangle \ , \quad \text{with} \quad \alpha = e, \mu, \tau \ , \tag{1.2}$$

such that

$$\mathscr{U}^\dagger m_\nu \mathscr{U} = \hat{m}_\nu = \text{diag}\left(m_{\nu_1}, m_{\nu_2}, m_{\nu_3}\right) \ . \tag{1.3}$$

The matrix $\mathscr{U}$ is called PMNS, for Pontecorvo-Maki-Nakagawa-Sakata. As what was done for the CKM matrix of the quark sector, one can parametrized $\mathscr{U}$ as

$$\mathscr{U} = \begin{pmatrix} 1 & 0 & 0 \\ 0 & c_{23} & s_{23} \\ 0 & -s_{23} & c_{23} \end{pmatrix} \begin{pmatrix} c_{13} & 0 & s_{13} e^{-i\delta} \\ 0 & 1 & 0 \\ -s_{13} e^{i\delta} & 0 & c_{13} \end{pmatrix} \begin{pmatrix} c_{12} & s_{12} & 0 \\ -s_{12} & c_{12} & 0 \\ 0 & 0 & 1 \end{pmatrix} \begin{pmatrix} e^{i\alpha_1} & 0 & 0 \\ 0 & e^{i\alpha_2} & 0 \\ 0 & 0 & 1 \end{pmatrix} , \tag{1.4}$$

where $s_{ij} = \sin\theta_{ij}$ and $c_{ij} = \cos\theta_{ij}$. The θ_{ij}'s are the mixing angles. The angles θ_{23} and θ_{12} are also called atmospheric and solar angles respectively, in relation with the experiments that have measured them. The phases δ and $\alpha_{1,2}$ are the Dirac and Majorana CP-violating phases, whose values are still unknown. The presence of the Majorana phases comes from the fact that neutrinos could be *a priori* of Dirac or Majorana type. In this latter case, neutrinos are there own antiparticles up to a phase. After redefinition of the fields, one ends up with the two phases $\alpha_{1,2}$. If neutrinos are of Dirac type, these latter are unphysical and can be put to zero in the above matrix.

Let's have a look to the production, propagation and detection of a neutrino in the plane wave approximation. Let's assume that a neutrino is produced at some space coordinate $x = 0, t = 0$. Just after being created through an EW interaction, it is in some flavor state $|\nu_\alpha\rangle$. This state is a superposition of mass eigenstates, and from Eq. (1.2), one has

$$|\nu_\alpha\rangle = \sum_i \mathscr{U}_{\alpha i} |\nu_i\rangle \ . \tag{1.5}$$

The produced neutrino will propagate in some direction x. After some distance L, the flavor state is given by

$$|\nu_\alpha(L)\rangle = \sum_i \mathscr{U}_{\alpha i} |\nu_i(L)\rangle = \sum_i \mathscr{U}_{\alpha i} e^{ip_i L} |\nu_i\rangle \ , \tag{1.6}$$

where $p_i = \sqrt{E_i^2 - m_{\nu_i}^2}$ is the momentum in the direction x of the neutrino of mass m_{ν_i} and energy E_i. The last equality has been obtained using the Schrödinger equation. We detect a neutrino through its weak interaction with matter. By measuring the state of the neutrino, one projects it into some flavor eigenstate $|\nu_\beta\rangle$. The corresponding transition amplitude is thus giving by

$$\mathscr{A}_{\alpha\beta} = \langle \nu_\beta | \nu_\alpha(L)\rangle = \sum_{i,j} \langle \nu_j | \mathscr{U}^*_{\beta j} \mathscr{U}_{\alpha i} e^{ip_i L} |\nu_i\rangle = \sum_i \mathscr{U}^*_{\beta i} \mathscr{U}_{\alpha i} e^{ip_i L} \ . \tag{1.7}$$

The probability to detect a flavor state ν_β after a distance L, given that the produced neutrino was

a flavor state $|\nu_\alpha\rangle$, reads therefore

$$\mathscr{P}\left(\nu_\alpha \to \nu_\beta, L\right) = |\mathscr{A}_{\alpha\beta}|^2 = \sum_{i,j} \mathscr{U}^*_{\beta i}\mathscr{U}_{\alpha i}\mathscr{U}^*_{\alpha j}\mathscr{U}_{\beta j} e^{i(p_i - p_j)L} \,. \tag{1.8}$$

If we assume that the neutrino has a well-defined energy $E \equiv E_i$, [1] and taking into account that the produced neutrinos are generally always ultra-relativistic $E \gg m_{\nu_i}$, one has $p_i \approx E - m^2_{\nu_i}/2E$, so that Eq. (1.8) can be expressed as

$$\mathscr{P}\left(\nu_\alpha \to \nu_\beta, L\right) = \sum_{i,j} \mathscr{U}^*_{\beta i}\mathscr{U}_{\alpha i}\mathscr{U}^*_{\alpha j}\mathscr{U}_{\beta j} e^{-i\frac{\Delta m^2_{ij}}{2E}L} \,, \tag{1.9}$$

where $\Delta m^2_{ij} \equiv m^2_{\nu_i} - m^2_{\nu_j}$. Using the unitarity of the PMNS matrix $\mathscr{U}$, Eq. (1.9) can also be expressed as

$$\begin{aligned}\mathscr{P}\left(\nu_\alpha \to \nu_\beta, t\right) = \delta_{\alpha\beta} &- 4\sum_{i>j} \Re e\left(\mathscr{U}^*_{\alpha i}\mathscr{U}_{\beta i}\mathscr{U}_{\alpha j}\mathscr{U}^*_{\beta j}\right)\sin^2\left(\pi\frac{L}{L_{ij}}\right) \\ &+ 2\sum_{i>j} \Im m\left(\mathscr{U}^*_{\alpha i}\mathscr{U}_{\beta i}\mathscr{U}_{\alpha j}\mathscr{U}^*_{\beta j}\right)\sin\left(2\pi\frac{L}{L_{ij}}\right) \,.\end{aligned} \tag{1.10}$$

where the oscillation length $L_{ij} \equiv 4\pi E/\Delta m^2_{ij}$ is the distance scale over which the oscillations effects can be appreciable. From this formula, we see that neutrino oscillations depend on the mass splitting between the neutrino mass eigenstates Δm^2_{ij}, on the travel distance L and on the mixing parameters through $\mathscr{U}_{\alpha i}$. This means that if neutrinos are massive, and if the mixing parameters are non-vanishing, one should be able to observe experimentally the oscillation of neutrinos. And this is actually the case.

Before going on, it should be stressed that in order to oscillate, the neutrino that has been produced must propagate coherently. A coherent propagation means that the wave packets of the mass eigenstates are superposed along the path, i.e. the group velocities v_{g_i} of the neutrino mass eigenstates are close to each other. Since $|v_{g_i} - v_{g_j}| \simeq \Delta m^2_{ij}/2E^2$, this is the case if $\Delta m^2_{ij} \ll E^2$, which is indeed satisfied by most of the neutrino experiments since the energy of the produced neutrinos is much bigger than their mass difference.

1.1.3 Experimental framework

There are mainly four sources that are used in neutrino oscillation experiments, depending on whether the detected neutrinos come from the sun, from the top atmosphere, from nuclear reactors or from accelerators. Each of these kind of experiment has specific travel distance L and neutrino energy spectrum E, which are more or less suitable for the measurement of mixing parameters. The experimental framework is generally conceived to measure the appearance or disappearance probability of some neutrino flavor.

Neutrinos are produced in the sun by the fusion reactions. In the late 1960s, the Homestake Experiment has observed a neutrino deficit from the sun compared to what was expected [14]. This

[1] This assumption leads to the correct result. However, this assumption is, strictly speaking, wrong. A more detailed analysis should be needed in order to account precisely for the wave packets propagation and coherence [13].

	Normal hierarchy ($\pm 1\sigma$)	Inverted hierarchy ($\pm 1\sigma$)
$\sin^2\theta_{12}$	$0.304^{+0.013}_{-0.012}$	$0.304^{+0.013}_{-0.012}$
$\theta_{12}(^\circ)$	$33.48^{+0.78}_{-0.75}$	$33.48^{+0.78}_{-0.75}$
$\sin^2\theta_{23}$	$0.452^{+0.052}_{-0.028}$	$0.579^{+0.025}_{-0.037}$
$\theta_{23}(^\circ)$	$42.3^{+3.0}_{-1.6}$	$49.5^{+1.5}_{-2.2}$
$\sin^2\theta_{13}$	$0.0218^{+0.0010}_{-0.0010}$	$0.0219^{+0.0011}_{-0.0010}$
$\theta_{13}(^\circ)$	$8.50^{+0.20}_{-0.21}$	$8.51^{+0.20}_{-0.21}$
$\delta_{CP}(^\circ)$	306^{+39}_{-70}	254^{+63}_{-62}
$\Delta m^2_{21}(\times 10^{-5}\ \mathrm{eV}^2)$	$7.50^{+0.19}_{-0.17}$	$7.50^{+0.19}_{-0.17}$
$\Delta m^2_{3k}(\times 10^{-3}\ \mathrm{eV}^2)$	$+2.457^{+0.047}_{-0.047}$	$-2.449^{+0.048}_{-0.0.47}$

Table 1.1 – Oscillation parameters from Ref. [19], in which they performed a fit to the global data, which come from 24 experiments. These are the solar experiments Gallex & GNO, SAGE, SK1-4, SNO and Borexino ; the combined data from the SK1-4 experiment for the atmospheric experiments ; KamLAND, CHOOZ, Palo Verde, Double Chooz, Daya Bay, RENO and SBL for the reactor experiments ; and MINOS and T2K for the accelerator experiments. In the last line, $\Delta m^2_{3k} = \Delta m^2_{31}$ in case of Normal Hierarchy, and $\Delta m^2_{3k} = \Delta m^2_{32}$ in case of Inverted Hierarchy.

deficit can be explained by the disappearance of ν_e through the $\nu_e \leftrightarrow \nu_\mu$ oscillations. Experiments, as for example SNO and KAMLAND, were in turn able to determined the solar mixing parameters θ_{12} and Δm^2_{21}. In the late 1980s, it is a deficit of ν_μ atmospheric neutrinos that is observed by several experiment as IMB, MACRO, and Kamiokande II, and it is well explained by the $\nu_\mu \leftrightarrow \nu_\tau$ oscillations. Experiments, as Super-Kamiokande, have determined the atmospheric mixing parameters θ_{23} and Δm^2_{31}. Finally, very recently, experiments as Daya Bay in 2012 [16, 15], followed by Double Chooz [17] and T2K experiment [18] have determined the last mixing angle θ_{13}, by measuring the electron neutrino disappearance from nuclear reactors. Until now, experiments have allowed the measurement of all three mixing angles θ_{12}, θ_{23} and θ_{13}, and two mass splittings Δm^2_{21} and $|\Delta m^2_{31}|$.

The present best fit values of the mixing parameters [19] are given in Table 1.1. It is remarkable that a so large variety of experiments can all be fitted so well in the picture of three light neutrinos. The fit is performed for normal and inverted hierarchy. Indeed, the knowledge of the parameters Δm^2_{21} and $|\Delta m^2_{31}|$ allows two possibilities for the mass hierarchy. Either the hierarchy is "normal" and one has $m_{\nu_1} < m_{\nu_2} < m_{\nu_3}$ with $\Delta m^2_{31} > 0$, either it is "inverted" and one has $m_{\nu_3} < m_{\nu_1} < m_{\nu_2}$ with $\Delta m^2_{31} < 0$. The mass hierarchy is still to be determined experimentally. From Eq. (1.10), we see that only the third term from the right-hand side of the equation could allow to determine it. Future experiments as Daya Bay 2, INO and Reno-50 should be sensitive on the mass hierarchy, and hopefully should allow to determine the mass spectrum in around 10 years [20, 21, 22].

The last mixing parameters that are still unknown are the CP-violating phases. Only the Dirac CP-violating phase δ_{CP} could be determined thanks to neutrino oscillations experiments. For example, we can show that the probability of $\nu_\mu \to \nu_e$ oscillation contains CP-violating terms

at next order [23]

$$\mathscr{P}\left(\nu_\mu \to \nu_e\right) \ni c_{13}^2 s_{13} s_{23} c_{23} s_{12} c_{12} \frac{\Delta m_{21}^2 L}{E} \left[c_\delta \sin\left(\frac{\Delta m_{31}^2 L}{2E}\right) - 2 s_\delta \sin\left(\frac{\Delta m_{31}^2 L}{4E}\right)\right], \tag{1.11}$$

where $c_\delta \equiv \cos\delta_{CP}$ and $s_\delta \equiv \sin\delta_{CP}$. For antineutrinos, the probability of $\bar{\nu}_\mu \to \bar{\nu}_e$ oscillations is obtained by replacing $\delta_{CP} \to -\delta_{CP}$. By comparing neutrino-induced and antineutrino-induced oscillations, one should therefore be able to determine the δ_{CP} phase. Note however that matter effect also introduces a neutrino-antineutrino asymmetry because of the presence of electrons and absence of positrons in the Earth. To disentangle the leptonic CP-violation effect from the matter effect, it is adequate to place the detector at $\sim$ 1000 km from the neutrino source. Future experiments, as LBNO, LBNE and Hyper-K [24, 25, 26] should be able to determine the mass hierarchy and to measure the CP-violating phase δ_{CP} by observing $\nu_\mu \to \nu_e$ oscillations coming from accelerators, through a precise measurement of the neutrino energy spectrum and by comparing neutrino-induced and antineutrino-induced oscillations. These long-baseline neutrino experiments could ideally determine the δ_{CP} phase at 5σ after 10 years of exposure (at least for ~half of the δ_{CP} possible values and more likely around $\pi/2$ and $3\pi/2$ where the CP-violating effect is maximized).

Let's mention that all the neutrino experiments have for now determined that at least two neutrinos are massive, so that there is the possibility that one of the three neutrinos is actually massless. Since they measure only squared mass differences, the oscillation experiments are not able to determine the absolute mass scale of the neutrino. However, one can already derive an obvious lower bound on the heaviest neutrino :

$$m_\nu^{\max} \gtrsim \sqrt{|\Delta m_{31}^2|} \simeq 0.05 \text{ eV}. \tag{1.12}$$

Several experiments, not based on neutrino oscillations, brought precious bounds on the neutrino masses, as we will now briefly discuss.

1.2 Non-oscillation experiments

1.2.1 β-decay

By measuring the highest possible energy in the tail of the energy spectrum of the electron emitted in a β-decay $n \to p\, e^- \bar{\nu}_e$, one should be able to determine the neutrino mass. Experiments of this kind are sensitive to neutrino masses that are typically large $\langle m_\nu \rangle \gg 0.05$ eV, in which case all the neutrino are quasi degenerate $\langle m_\nu \rangle \equiv m_{\nu_1} \simeq m_{\nu_2} \simeq m_{\nu_3}$. Experiments as MAINZ and TROITSK, based on Tritium β-decay, have provided an upper bound at 95% C.L. [27, 28] on the "effective electron neutrino mass" given by

$$m_\beta \equiv \sqrt{\sum_i m_{\nu_i}^2 |\mathscr{U}_{ei}|^2} \lesssim 2.2 \text{ eV}. \tag{1.13}$$

For quasi degenerate spectrum, one has $m_\beta \simeq \langle m_\nu \rangle$. In the next future, the KATRIN experiment should reach sensitivities of the order of 0.2 eV at 90% C.L. on $\langle m_\nu \rangle$ [29].

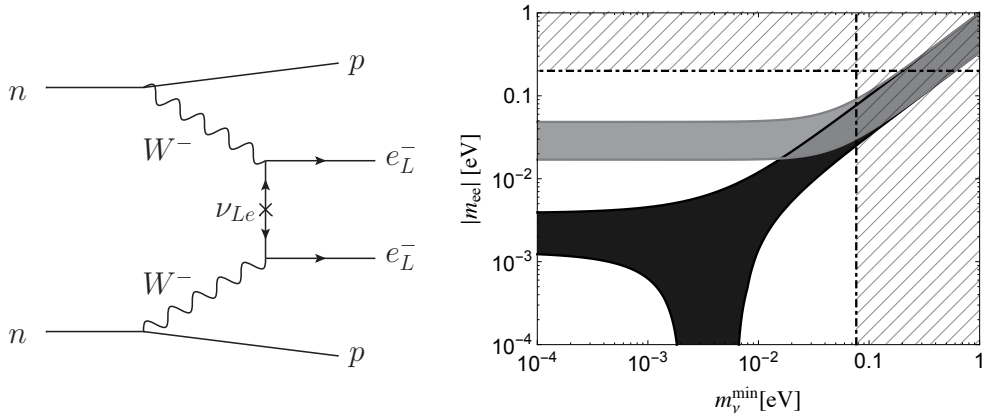

Figure 1.1 – Left : Feynman diagram of the $0\nu2\beta$ process. Right : $|m_{ee}|$ as a function of the lightest neutrino mass, in case of Normal (black) and Inverted (gray) hierarchy. The width of the bands reflects the uncertainties in phases, mixing angles and squared mass splittings at 1σ. The horizontal dot-dashed line correspond to the present best bound from $0\nu2\beta$ process, while the vertical dot-dashed line comes from cosmological bounds. We used the fact that we have $\sum_i m_{\nu_i} \simeq 3m_\nu^{\min}$ in the quasi-degenerate region.

1.2.2 Neutrinoless double β-decay ($0\nu2\beta$)

If neutrinos are Majorana particles, i.e. they are their own antiparticles, then a process such as the one depicted in Fig. 1.1 could be observed. This process consists in the decay of two neutrons into two protons and two electrons without emission of any neutrino. Its amplitude is proportional to neutrino mass matrix element

$$m_{ee} = \sum_i m_{\nu_i} \left(\mathscr{U}^2\right)_{ei} , \tag{1.14}$$

which according to Eq. (1.4) contains the Majorana CP-violating phases $\alpha_{1,2}$. The observation of such process would confirm the Majorana nature of neutrinos, and it could also determine the Majorana mass scale and potentially the hierarchy spectrum, as can be seen from the right panel of Fig. 1.1. The present best bounds come from the experiment GERDA, IGEX, EXO, NEMO, KamLAND-Zen and CUORICINO, which obtained that the half-time of the process should be grater than $\sim 2\cdot10^{25}$ years at 90% C.L. [30, 31, 32, 33, 34, 35]. The corresponding upper bound on $|m_{ee}|$ is given by

$$|m_{ee}| \lesssim 2\cdot10^{-1} \text{ eV} . \tag{1.15}$$

Future experiments, as SuperNEMO, Majorana, NEXT or SNO+ for exemple, should reach sensitivities as low as $|m_{ee}| \lesssim 2\cdot10^{-2}$ eV [36, 37, 38, 39].

1.2.3 Cosmology

Neutrinos have played several role in the evolution of our Universe. In particular, on the one hand their mass should have played a role in the structure formation of galaxies. Indeed, when becoming non-relativistic at a temperature around $T \sim m_\nu$, neutrinos do agglomerate and participate to the

structure formation of galaxies. The heavier they are, the earlier they participate. On the other hand, if they were non-relativistic at the decoupling epoch at a redshift of $z \sim 1100$, they should also have contributed to distort the Cosmic Microwave Background (CMB) spectrum.

The present best bound on the sum of the neutrino masses is provided by the Planck collaboration [40]. Using Planck, WMAP, baryon acoustic oscillation (BAO) and CMB data sets, they got the upper bound :

$$\sum_i m_{\nu_i} \lesssim 2.3 \cdot 10^{-1} \text{ eV} . \tag{1.16}$$

Planck also provided no evidence for additional neutrino-like relativistic particles beyond the three families of neutrinos in the SM. They find that the effective number of relativistic degrees of freedom is $N_{\text{eff}} = 3.30 \pm 0.27$, consistent with the SM prediction $N_{\text{eff}}^{SM} = 3.046$.

1.3 Neutrino mass, effective Lagrangian and Seesaw mechanisms

As illustrated by neutrino oscillations, it is now clear that at least two of the three neutrinos are massive particles. This constitutes an outstanding evidence for BSM physics. The SM needs therefore to be enlarged in order to account for the neutrino masses. A first question which arises is how to give mass to neutrinos ? The smallness of the neutrino masses is also quite disrupting, since these are of the order of $\sim 10^6$ lighter than the electron. So a second question is why are the neutrinos so light ?

There are many possibilities to generate neutrino masses, but let's first see if one cannot proceed as for the other fermions. In the SM, the mass of the quarks and the charged leptons are generated through the usual Brout-Englert-Higgs mechanism. To each left-handed doublet of particles, one has a right-handed particle that is a singlet under $SU(2)_L$, except for the neutrinos. Together with the Brout-Englert-Higgs scalar boson (quoted as SM scalar hereafter), they form Yukawa interactions that will generate Dirac mass for the quarks and charged leptons after Spontaneous Symmetry Breaking (SSB). So the way of generating a mass for the neutrinos which comes immediately to minds is to add right-handed neutrinos ν_R. By doing this, one can construct Yukawa interactions for the neutrinos :

$$\mathscr{L}_{\text{Yuk}} = -\overline{\nu_R}\,\tilde{\phi}^\dagger\, Y_\nu\, \ell_L + \text{H.c.} , \tag{1.17}$$

where $\ell_L = (\nu_L\, e_L)^T$ are the $SU(2)_L$ lepton doublets and $\phi = \left(\phi^+\, \phi^0\right)^T$ is the SM scalar doublet. One has defined $\tilde{\psi} = i\tau_2\psi^*$ where τ_2 is the second Pauli matrix. After SSB, the scalar field acquires a vacuum expectation value (vev), $\langle\phi^0\rangle = \text{v}/\sqrt{2}$ with $\text{v} = 246$ GeV, and the above operator therefore generates Dirac masses for the neutrinos given by $m_\nu^D = Y_\nu\, \text{v}/\sqrt{2}$.

This seems to be an easy and perfectly fine way of giving mass to the neutrinos. However, one is faced with some deeper questions. Indeed, the present bounds on the neutrino masses would require extremely small Yukawa couplings, typically of the order $Y_\nu \sim 10^{-12}$. This scale has to be compared to Yukawa coupling of the electron, muon and tau, whose value is approximately given by $Y_e \sim 10^{-6}$, $Y_\mu \sim 10^{-3}$ and $Y_\tau \sim 10^{-2}$ respectively. There are thus *six to ten orders* of magnitudes

that separate the mass of the two components of a same doublet. By comparison, the components of the quark doublets have Yukawa couplings that are about of the same order. The smallness of the neutrino Yukawa coupling seems therefore puzzling in this way.

Another question is the following. If one adds right-handed neutrinos to SM, these would be electrically neutral and singlets under all the gauge groups. So no fundamental symmetry would forbid them to have the following Majorana term :

$$\mathscr{L}_{\text{Maj}} = -\frac{1}{2}\overline{\nu_R}\, M\, \nu_R^c + \text{H.c.}\,, \tag{1.18}$$

where $\psi^c = C\bar{\psi}^T$ is the charged-conjugate of the field ψ. [2] Together with Eq. (1.17), this term violates lepton number by 2 units, but since lepton number is an accidental symmetry of the SM, this is not problematic. This small adjunction has a lot of interesting implications as we will see in the next sections. Let's just mention here that the mass M in Eq. (1.18) is a new energy scale that is not linked to the SM electroweak scale, i.e. it isn't linked to the vev of the SM scalar field. For this reason, it is not protected by the EW scale as the other SM fermion masses in the SM and it can be much more larger than the EW scale $\Lambda_{EW} \sim 100$ GeV. It constitutes therefore the energy scale of a new physics. Before going on, let's see how a new physics can manifest itself through the neutrino mass.

1.3.1 Effective Lagrangian and new physics

The neutrinos are Weyl spinors, and each neutrino is a left-handed particle with 2 degrees of freedom. Without adding any new particle to SM (as the right-handed neutrinos), one cannot construct any gauge invariant renormalizable interaction (as the Yukawa interactions) that will generate neutrino masses after $SU(2)_L \times U(1)_Y$ symmetry breaking. The only way is to add non-renormalizable higher dimension operators to the SM Lagrangian, i.e. operators whose field dimensions are bigger than $[E]^4$. Since they are not renormalizable, we expect these operators to be effective operators that come from beyond the SM physics. In this case, the low energy effective Lagrangian would read

$$\mathscr{L}_{\text{eff}} = \mathscr{L}_{SM} + \mathscr{L}^{d=5} + \mathscr{L}^{d=6} + \cdots = \mathscr{L}_{SM} + \frac{1}{\Lambda_{d=5}}\mathscr{O}^{d=5} + \frac{1}{\Lambda_{d=6}^2}\mathscr{O}^{d=6} + \dots\,, \tag{1.19}$$

where Λ_i are the scale suppression of the associated operator. These scales are not especially connected. If these are much larger than the EW scale, one expects the higher dimension operators to be more and more suppressed, i.e. Eq. (1.19) is a series expansion. If one or more of these operators actually generate neutrino masses, the scale suppression would naturally explains their smallness.

This is the same idea as in the Fermi V-A theory. Before the discovery of the W's and Z bosons, the muon decay was explained by a non-renormalizable dimension-6 operator, the four-fermion Fermi interaction. The theory of EW interactions, by Glashow, Weinberg and Salam, has shown

[2] The charge conjugation matrix C satisfied the following equalities $C^{-1}\gamma_\mu C = -\gamma_\mu^T$, $C^\dagger = C^{-1}$, and $C^T = -C$. One has also the following useful relations $(\psi^c)^c = \psi$, $\overline{\psi^c} = \psi^T C^{-1}$, and $\psi^c_{L,R} \equiv \left(\psi_{L,R}\right)^c = \left(\psi^c\right)_{R,L}$.

that this operator is in fact an effective operator that comes from the exchange of new heavy particles, the $W^{\pm}$ bosons which has been discovered experimentally in 1983. The smallness of the Fermi coupling was therefore partially explained by the scale suppression in $1/m_W^2$ in front of dimension-6 operator.

Interestingly, there is a single dimension-5 operators (allowed by gauge symmetries) that we can construct with the SM fields. This is the so-called Weinberg operator [41] :

$$\mathscr{L}^{d=5} = \frac{1}{2} c_{\alpha\beta}^{d=5} \left(\overline{\ell_{L\alpha}^{c}} \tilde{\phi}^{*}\right) \left(\tilde{\phi}^{\dagger} \ell_{L\beta}\right) + \text{H.c.} , \tag{1.20}$$

where $c_{\alpha\beta}^{d=5}$ are coefficients with dimension $[E]^{-1}$. This operator violates lepton number L by 2 units. After SSB, it leads to the following Majorana mass matrix for the neutrinos

$$m_{\nu} = -\frac{\mathrm{v}^2}{2} c^{d=5} . \tag{1.21}$$

This matrix can then be diagonalized by redefining the neutrino fields, according to Eq. (1.2). In order to generate neutrino masses of the order of 10^{-1} eV, which is the typical scale expected from experimental constraints, the dimension-5 coefficients should be of the order of $c_{\alpha\beta}^{d=5} \sim 10^{-14}$ GeV^{-1}. Together with its non-renormalisability, the dimension-5 operator should then be an effective operator coming from BSM physics whose scale could be has high as $\Lambda_{d=5} \sim 10^{14}$ GeV. But how could this dimension-5 operator be generated ?

A way to generate the Weinberg operator is by adding new fields to the SM. The easiest possibility is to connect the lepton and scalar doublets through the exchange of new heavy particles at tree-level. In this case, since one needs fields that couple to both scalar and left-handed lepton doublets, see Eq. (1.20), the only possibilities are to add either fermionic singlets, scalar triplets or fermionic triplets to the SM. [3] These are the three kinds of Seesaw mechanisms, respectively the type-1, type-2 and type-3 Seesaw mechanisms [43]. Each one generates a dimension-5 operator through the exchange of new heavy particles at tree-level. Since they constitute the framework of most of this thesis, we will further develop their main characteristics in the next sections. These Seesaw mechanisms also generate higher dimension operators, as the dimension-6 one. These latter are very interesting since they imply the existence of new observables, as the Charged Lepton Flavor Violation (CLFV) processes. These will be discussed in details in chapter 2.

Other possibilities do actually exist, where the dimension-5 operator is generated at loop-level. Let's mention for example the "scotogenic model" [44], where a new scalar doublet (the "inert" doublet) and new fermions singlets (right-handed neutrinos), both odd under a discrete Z_2 symmetry, are added to the SM. This model, where neutrinos masses are generated at one-loop, share common points with another part of this thesis, as we will see in chapter 5. Let's also mention the Zee model [46], where a charged scalar singlet is added to the SM which generates neutrino masses via one-loop diagrams, or the Zee-Babu model [47, 48, 49], in which two $SU(2)_L$ scalar singlets are introduced, one singly charged and one doubly charged, such that neutrino masses are generated at two-loop level.

[3] In principle, one could also add a single scalar singlet which couples to two lepton doublets. However, one can easily show that it cannot generate the dimension-5 Weinberg operator in Eq. (1.20) [42].

1.3.2 Type-1 Seesaw mechanism

The type-1 Seesaw mechanism consists in adding to the SM n_N right-handed fermions, singlets under $SU(2)_L$ and electrically neutral. They are called right-handed neutrinos and will be labelled by N_R instead of ν_R in what follows. As was anticipated before, we are in this case allowed to write new Yukawa and Majorana interaction terms for the neutrinos, so that the full Lagrangian reads

$$\mathscr{L}^{\text{type-1}} = \mathscr{L}_{SM} + i\overline{N_R}\partial\!\!\!/ N_R - \left[\overline{N_R}\,\tilde{\phi}^\dagger\, Y_N\,\ell_L + \frac{1}{2}\overline{N_R}\,M_N\,N_R^c + \text{H.c.}\right] , \tag{1.22}$$

where Y_N is a complex $n_N \times 3$ matrix, and M_N is a complex symmetric $n_N \times n_N$ matrix. After SSB, the Lagrangian in Eq. (1.22) contains the mass terms

$$\mathscr{L}^{\text{type-1}}_{\text{mass}} = -\overline{N_R}\,m_D\,\ell_L - \frac{1}{2}\overline{N_R}\,M_N\,N_R^c + \text{H.c.} , \tag{1.23}$$

where $m_D = Y_N\,\text{v}/\sqrt{2}$ is the Dirac mass matrix. Using the properties of the charge conjugation matrix (see footnote 2), this equation can also be expressed as

$$\mathscr{L}^{\text{type-1}}_{\text{mass}} = -\frac{1}{2}\begin{pmatrix}\overline{\nu_L^c} & \overline{N_R}\end{pmatrix}\begin{pmatrix}0_{3\times3} & m_D^T\\ m_D & M_N\end{pmatrix}\begin{pmatrix}\nu_L\\ N_R^c\end{pmatrix} + \text{H.c.} . \tag{1.24}$$

Since M_N is not protected by any scale, it is generally assumed that $M_N \gg m_D$. In this case, the diagonalization of the total neutrino mass matrix,

$$\mathscr{M}_\nu \equiv \begin{pmatrix}0_{3\times3} & m_D^T\\ m_D & M_N\end{pmatrix} , \tag{1.25}$$

leads to 3 light Majorana neutrinos whose mass matrix reads

$$m_\nu = -m_D^T\frac{1}{M_N}m_D + \mathscr{O}\left(m_D^4/M_N^3\right) \simeq -\frac{\text{v}^2}{2}Y_N^T\frac{1}{M_N}Y_N , \tag{1.26}$$

and to n_N heavy Majorana neutrinos whose matrix reads

$$m_N = M_N + \mathscr{O}\left(m_D^2/M_N\right) . \tag{1.27}$$

A more detailed analysis of the diagonalization will be done in chapter 2. It is straightforward to show that the matrix m_ν has rank equal or smaller than $\min[3, n_N]$ and possesses therefore the according number of eigenvalues. One needs in turn at least 2 right-handed neutrino singlets in order to account for neutrino experiments, i.e. $n_N \geq 2$.

A graphical way to see how neutrino masses are generated is from Fig. 1.2(a), which induces nothing but the dimension-5 operator in Eq. (1.20) with

$$c_{\alpha\beta}^{d=5} = \left(Y_N^T\frac{1}{M_N}Y_N\right)_{\alpha\beta} . \tag{1.28}$$

The suppression scale is therefore given by the right-handed mass scale $\Lambda_{d=5} \sim M_N$. Compared to the standard picture in Eq. (1.17), the presence of the Majorana mass in Eq. (1.22) allows m_ν to

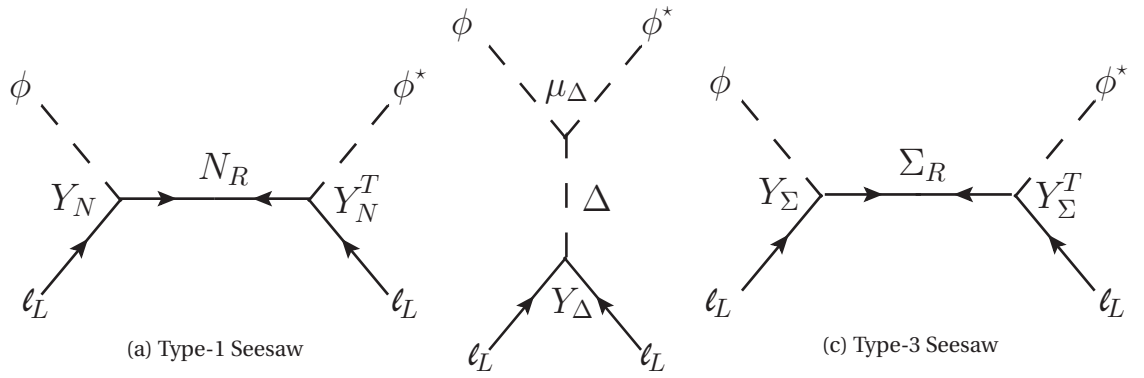

(a) Type-1 Seesaw

(b) Type-2 Seesaw

(c) Type-3 Seesaw

Figure 1.2 – Feynman diagrams responsible of the generation of the neutrino masses in the three Seesaw mechanisms. From left to right, these correspond to the exchange of fermionic singlets, scalar triplet(s) and fermionic triplets.

undergo an extra suppression from Y_N v/M_N. So the larger is the new scale, the lighter are the neutrinos. Within this framework, neutrinos are naturally very light, and their Yukawa couplings are not especially small compared to the other SM particles. These latter can even be large. For example, $m_\nu \approx 10^{-1}$ eV would need $M_N/Y_N^2 \sim 10^{14}$ GeV, which can be fulfilled for $Y_N \sim 1$ and $M_N \sim 10^{14}$ GeV, but also for $Y_N \sim 10^{-5}$ and $M_N \sim 10^4$ GeV.

Parameter counting. In the leptonic sector, one has the charged lepton Yukawa matrix Y_e, which is a 3×3 complex matrix, the neutrino Yukawa matrix Y_N, which is a $n_N \times 3$ complex matrix, and the Majorana matrix for the right-handed neutrinos M_N, which is a $n_N \times n_N$ complex symmetric matrix. All together, this makes a total of $9 + n_N(n_N+7)/2$ moduli and phases. However, we are free to redefine the fermion fields using unitary matrices. It is straightforward to show that this reduces considerably the number of physical parameters to [50] :

$$3+4n_N \quad \text{moduli, and} \quad 3(n_N-1) \quad \text{phases.} \tag{1.29}$$

Note that the moduli contain the 3 masses for the charged leptons, the n_N light neutrino masses, the n_N heavy neutrino masses and the different mixing angles in the light and heavy neutrino sectors. So in particular for $n_N = 2$, there are 14 parameters (3 charged lepton masses, 2 light neutrino masses, 2 heavy neutrinos masses, 3 low energy mixing parameters and 2 low energy CP-violating phases, one high energy mixing parameter and one high energy CP-violating phase), while for $n_N = 3$, there are 21 parameters.

Remark on lepton number violation. The presence of both Yukawa and Majorana interactions in Eq. (1.22) does violate lepton number by 2 units, as expected since the Weinberg operator is generated. The Majorana interaction is not forbidden by any fundamental principle here, but one could easily forbid it by imposing a $B-L$ symmetry to the Lagrangian. In this case, we recover the standard situation where the neutrino would be a Dirac particle with a mass $m_\nu = m_D$. However,

this situation requires an extra symmetry which has no reason to necessarily exists, and it is in this sense less minimal. Moreover, we have clear indications that the $B-L$ symmetry should be violated in Nature in order to generate a baryon asymmetry in the Universe – see chapter 3 – so that the presence of the Majorana term is actually well motivated by cosmology. The generation of the baryon asymmetry through the leptogenesis mechanism in the framework of type-1 Seesaw models will be discussed in section chapter 3.

Note that the $B-L$ symmetry is an anomaly-free global symmetry in the SM. Also, the global $B-L$ can be easily gauged just by adding 3 right-handed neutrinos. These must carry a lepton number $L(N)=1$ in order to cancel the $U(1)^3$ gauge anomaly. In this case, the $B-L$ symmetry could easily be spontaneously broken through the vev of a new complex scalar field ξ carrying $L(\xi)=-2$, which also generate a Majorana mass term for the right-handed neutrinos. More precisely, let's consider the following Lagrangian

$$\mathscr{L}_{\xi}^{\text{type-1}} = \mathscr{L}_{SM} + i\overline{N_R}\not{D}N_R - \left[\overline{N_R}\,\tilde{\phi}^{\dagger}\,Y_N\,\ell_L + \lambda_{\xi}\,\frac{1}{2}\overline{N_R}\,\xi^{*}\,N_R^{c} + \text{H.c.}\right], \tag{1.30}$$

where the covariant derivative reads

$$D_{\mu} = \partial_{\mu} - i g_{B-L}\,\frac{Q_{B-L}}{2}\,Z'_{\mu}\,, \tag{1.31}$$

with g_{B-L} the new gauge coupling, Q_{B-L} the $B-L$ charge associated to the particle, and Z'_{μ} the new gauge boson associated to the $B-L$ gauge symmetry. If the potential allows for a SSB of the $B-L$ symmetry through the Brout-Englert-Higgs mechanism, ξ acquires a vev $\langle\xi\rangle = \text{v}_{\xi}/\sqrt{2}$ and a mass $m_{Z'} = g_{B-L}\,\text{v}_{\xi}/2$ for the new gauge boson Z' is generated. In this case, the type-1 Seesaw Lagrangian in Eq. (1.22) appears with $M_N = \lambda_{\xi}\,\text{v}_{\xi}/\sqrt{2}$, and Majorana neutrino masses are generated via Eq. (1.26). This simple example is very interesting since (i) it generates the type-1 Seesaw and a small neutrino masses, (ii) it predicts the existence of a new massive gauge boson Z' which could be probed at colliders, (iii) new interactions with the SM particles are predicted too that could also be probed by experiments, (iv) a new complex scalar singlet is introduced which could be responsible for the inflation [51, 52], and (v) it is motivated by Grand Unified Theories (GUT) as SO(10) which contains $U(1)_{B-L}$ as a subgroup, as we will discuss below.

1.3.3 Type-2 Seesaw mechanism

Instead of adding fermion singlets, one can add one or more scalar triplets $\vec{\Delta}_k = \left(\Delta_k^1, \Delta_k^2, \Delta_k^3\right)$, where $k = 1, \ldots, n_{\Delta}$. Even if only one scalar triplet is in principle enough to generate three masses for the light neutrinos, we will consider here a general situation where we add n_{Δ} scalar triplets. In this case, the general Lagrangian reads

$$\begin{aligned}\mathscr{L}^{\text{type-2}} = &\left(D_{\mu}\vec{\Delta}_k\right)^{\dagger}\left(D^{\mu}\vec{\Delta}_k\right) - \vec{\Delta}_k^{\dagger} m_{\Delta_k}^2 \vec{\Delta}_k - V_{\text{pot}} \\ &+ Y_{\Delta_k}^{\alpha\beta}\,\ell_{L\alpha}^{T} C\, i\tau_2 \left(\frac{\vec{\tau}\cdot\vec{\Delta}_k}{\sqrt{2}}\right)\ell_{L\beta} + \mu_{\Delta_k}\tilde{\phi}^{\dagger}\left(\frac{\vec{\tau}\cdot\vec{\Delta}_k}{\sqrt{2}}\right)^{\dagger}\phi + \text{H.c.}\,,\end{aligned} \tag{1.32}$$

where $\vec{\tau} = (\tau_1, \tau_2, \tau_3)$ is a vector composed by the three Pauli matrices. Here, Y_{Δ} are n_{Δ} complex symmetric 3×3 matrices, and μ_{Δ_k} are n_{Δ} complex numbers. The hypercharge of the scalar triplet

is $Y(\Delta) = -2Y(\ell)$, so that the covariant derivative in (1.32) reads

$$D_\mu = \partial_\mu - ig\vec{T}\cdot\vec{W}_\mu - ig'B_\mu \,, \tag{1.33}$$

where $\vec{T}$ are the dimension-3 representations of the $SU(2)$ generators. The most general scalar triplet potential is given by

$$V_{\rm pot} = \lambda_2\left(\vec{\Delta}^\dagger\vec{\Delta}\right)^2 + \lambda_3\left(\vec{\Delta}^\dagger\vec{\Delta}\right)\left(\phi^\dagger\phi\right) + \lambda_4\left(\vec{\Delta}^\dagger T^i\vec{\Delta}\right)^2 + \lambda_5\left(\vec{\Delta}^\dagger T^i\vec{\Delta}\right)\left(\phi^\dagger\tau^i\phi\right) \,, \tag{1.34}$$

where the indices are left implicit. In this notation, the $SU(2)$ components of the fundamental scalar triplet representation have not all well defined electric charges. Electric charge eigenstates are instead given by

$$\boldsymbol{\Delta_k} \equiv \frac{\vec{\tau}\cdot\vec{\Delta}_k}{\sqrt{2}} = \begin{pmatrix} \frac{\Delta_k^+}{\sqrt{2}} & \Delta_k^{++} \\ \Delta_k^0 & -\frac{\Delta_k^+}{\sqrt{2}} \end{pmatrix} , \tag{1.35}$$

with the different components reading as

$$\Delta_k^0 = \frac{1}{\sqrt{2}}\left(\Delta_k^1 + i\Delta_k^2\right) \,, \qquad \Delta_k^+ = \Delta_k^3 \,, \qquad \Delta_k^{++} \equiv \frac{1}{\sqrt{2}}\left(\Delta_k^1 - i\Delta_k^2\right) \,. \tag{1.36}$$

After SSB, because of their interactions with the SM scalar doublet, the neutral component of each scalar triplet acquires a vev $\langle\Delta_k^0\rangle \equiv \mathrm{v}_{\Delta_k} \simeq \mu_{\Delta_k}\,\mathrm{v}^2/2m_{\Delta_k}^2$. The interactions of the triplets with the 2 lepton doublets then contains

$$\mathscr{L}^{\text{type-2}} \ni -\overline{\nu_{L_\alpha}^c}\; Y_{\Delta_k}^{\alpha\beta}\langle\Delta_k^0\rangle\,\nu_{L_\beta} + \text{H.c.} \,, \tag{1.37}$$

which give rise to a Majorana mass matrix for the neutrinos, given by

$$m_\nu = \sum_k m_\nu^{\Delta_k} = \sum_k 2\,\mathrm{v}_{\Delta_k}\; Y_{\Delta_k} = \sum_k \mu_{\Delta_k}\frac{\mathrm{v}^2}{m_{\Delta_k}^2}\; Y_{\Delta_k} \,. \tag{1.38}$$

For any general symmetric matrix Y_{Δ_k}, this mass matrix has three eigenvalues, which shows that a single triplet is enough to generate any neutrino mass matrix that could be measured. The smallness of the neutrino masses is here too quite natural. Indeed, because μ_Δ/m_Δ and Y_Δ are bounded by the perturbativity conditions, one has $\mathrm{v}_\Delta \ll \mathrm{v}$ provided that $m_\Delta \gg \mathrm{v}$.

A graphical way to see how m_ν is generated in Eq. (1.38) is from Fig. 1.2(b), which induces nothing but the dimension-5 operator in Eq. (1.20) with

$$c_{\alpha\beta}^{d=5} = \left(2\sum_k \mu_{\Delta_k}\frac{1}{m_{\Delta_k}^2}Y_{\Delta_k}\right)_{\alpha\beta} \,. \tag{1.39}$$

The suppression scale is therefore given by the combination $\Lambda_{d=5} \sim m_\Delta^2/\mu_\Delta$, and neutrino masses are naturally suppressed if this factor is large. Note that unlike the type-1 Seesaw, in the case where there is only one scalar triplet ($n_\Delta = 1$), the neutrino mass matrix is directly proportional to the Yukawa matrix Y_Δ. The measurement of m_ν gives therefore the fundamental Yukawa matrix up to a multiplicative constant, rather than a complicated combination of it as in Eq. (1.26).

Let's note that since the scalars are triplets under $SU(2)_L$, they interact directly via gauge interactions and are therefore very interesting to probe experimentally. Indeed, certainly one of the main differences between the type-1 and type-2 Seesaws resides on the feasibility of on-shell collider production of the Seesaw states. At LHC scalar triplet production proceeds mainly via Drell-Yan processes, with a cross-section which, depending on the triplet mass, can be as large as $\sim 1\,\text{pb}$ [53, 54]. Subsequent decay of the scalar triplet, in particular to the di-lepton channel, combined with possible displaced vertices may eventually allow the reconstruction of the Lagrangian parameters, as has been shown in [53]. Production, however, requires the scalar triplet to be below $\sim 1\,\text{TeV}$.

Parameter counting. Without the potential part of the Lagrangian, one has 9 moduli and phases in Y_e, 6 moduli and phases in each Y_{Δ_k}, and n_Δ moduli and phases in μ_{Δ_k}. This makes a total of $8n_\Delta$ moduli and $6n_\Delta - 3$ phases. Let's note that m_{Δ_k} has already been diagonalized, but there is still the freedom to redefine the individual phases of the triplets. So by redefining the lepton fields by unitary matrices and redefining the triplet phases, one are left with

$$3 + 8n_\Delta \quad \text{moduli, and} \quad 3(2n_\Delta - 1) \quad \text{phases.} \tag{1.40}$$

The moduli contains the 3 masses for the charged leptons, the 3 light neutrino masses, the n_Δ scalar triplet masses. The rest corresponds to the different low energy mixing angles and phases, and the high energy couplings μ_{Δ_k} and Y_{Δ_k}. For $n_\Delta = 1$, one has therefore 14 parameters (as in the type-1 Seesaw with $n_N = 2$, and so less than the case with $n_N = 3$).

Remark on lepton number violation. The presence of both lepton and scalar interactions in the second line of in Eq. (1.32) does violate lepton number by 2 units. As in the type-1 Seesaw case, one could forbid one of the two term by imposing a $B - L$ symmetry. However, there is an interesting situation where the dimension-full couplings μ_{Δ_k} would come from the vev of some new neutral scalar singlet fields ξ with lepton number $L_\xi = -2$. Indeed, in this case the $B - L$ conserving Lagrangian reads

$$\mathscr{L}_\xi^{\text{type-2}} \ni \ell_L^T C\, i\tau_2\, Y_\Delta \left(\frac{\vec{\tau}\cdot\vec{\Delta}_k}{\sqrt{2}}\right) \ell_L + \lambda_\xi\, \xi\, \tilde{\phi}^\dagger \left(\frac{\vec{\tau}\cdot\vec{\Delta}}{\sqrt{2}}\right)^\dagger \phi + \text{H.c.}\,. \tag{1.41}$$

By acquiring a vev $\langle\xi\rangle = \text{v}_\xi/\sqrt{2}$, the scalar singlet breaks spontaneously the $B - L$ symmetry and generates the type-2 Seesaw Lagrangian in Eq. (1.32) with $\mu_{\Delta_k} = \lambda_\xi\, \text{v}_\xi/\sqrt{2}$. Unlike in the expanded type-1 Seesaw model in Eq. (1.30), it is not possible to gauge the $B-L$ symmetry without introducing new fermion fields to cancel the anomalies (but this could be done easily by adding the right-handed neutrinos). As a result, the model in Eq. (1.41) with a broken global $B-L$ predicts the existence of a quasi massless Majoron [55]. In the case where $\text{v}_\xi \ll m_{\Delta_k}$, one has an interesting situation where neutrino masses undergo an extra $\text{v}_\xi/m_{\Delta_k}$ suppression compared to Eq. (1.38) since $\text{v}_\xi/m_{\Delta_k}$ is naturally suppressed compared to Y_{Δ_k}. This will motivate in particular the Purely Flavored Leptogenesis (PFL) scenario in section 4.5.

1.3.4 Type-3 Seesaw mechanism

The third possibility is to introduce n_Σ fermionic triplets $\vec{\Sigma}_k = \left(\Sigma_k^1, \Sigma_k^2, \Sigma_k^3\right)$ to the SM Lagrangian. This scenario is very similar to the type-1 Seesaw case. In this case, the general Lagrangian, omitting the indices, reads

$$\mathscr{L}^{\text{type-3}} = \mathscr{L}_{SM} + i\overline{\vec{\Sigma}_R}\not{D}\vec{\Sigma}_R - \left[\overline{\vec{\Sigma}_R}\, Y_\Sigma \left(\tilde{\phi}^\dagger\, \vec{\tau}\, \ell_L\right) + \frac{1}{2}\overline{\vec{\Sigma}_R}\, M_\Sigma\, \vec{\Sigma}_R^c + \text{H.c.}\right] , \tag{1.42}$$

where Y_Σ is a $n_\Sigma \times 3$ complex matrix, and M_Σ is a $n_\Sigma \times n_\Sigma$. Since the triplets carry zero hypercharge $Y(\Sigma) = 0$, the covariant derivative reads

$$D_\mu = \partial_\mu - i g \vec{T} \cdot \vec{W}_\mu \, . \tag{1.43}$$

The three components of each fermion triplet have the same Majorana mass term and have not well-defined electric charge. The eigenstates of the electric charge are instead given by

$$\Sigma_k^- = \frac{1}{\sqrt{2}}\left(\Sigma_k^1 + i\Sigma_k^2\right) , \qquad \Sigma_k^0 = \Sigma_k^3 , \qquad \Sigma_k^+ \equiv \frac{1}{\sqrt{2}}\left(\Sigma_k^1 - i\Sigma_k^2\right) . \tag{1.44}$$

As in the type-1 Seesaw mechanism, the light neutrino mass matrix after SSB is given by

$$m_\nu \simeq -\frac{\text{v}^2}{2}\, Y_\Sigma^T \frac{1}{M_\Sigma}\, Y_\Sigma \, , \tag{1.45}$$

and the heavy neutrino mass matrix reads

$$m_\Sigma \simeq M_\Sigma \, . \tag{1.46}$$

The neutrino mass matrix in Eq. (1.45) is not surprising since the neutral component Σ_k^0 has the same Yukawa interaction than a right-handed neutrino. A graphical way to see how m_ν is generated in Eq. (1.45) is from Fig. 1.2(c). Being charged under $SU(2)_L$, fermionic triplets have interesting phenomenology at colliders as LHC [53]. Since we won't consider this mechanism anymore in this thesis, we will stop here the analysis of the type-3 Seesaw model.

1.4 Dimension-6 operators and CLFV processes

The three types of Seesaw mechanisms do also generate dimension-6 operators, on top of the dimension-5 one. From the Lagrangian in Eq. (1.22),(1.32) and(1.42), one can show that these are given by [50, 56]

$$\mathscr{L}^{d=6}_{\text{type-1}} = c^{d=6}_{\alpha\beta}\left(\overline{\ell_{L\alpha}}\tilde{\phi}\right) i\not{\partial}\left(\tilde{\phi}^\dagger \ell_{L\beta}\right) \text{ , with } \quad c^{d=6}_{\alpha\beta} = \left(Y_N^\dagger \frac{1}{M_N^\dagger}\frac{1}{M_N} Y_N\right)_{\alpha\beta} , \tag{1.47}$$

for the type-1 Seesaw, and

$$\mathscr{L}^{d=6}_{\text{type-3}} = c^{d=6}_{\alpha\beta}\left(\overline{\ell_{L\alpha}}\vec{\tau}\tilde{\phi}\right) i\not{D}\left(\tilde{\phi}^\dagger \vec{\tau}\, \ell_{L\beta}\right) \text{ , with } \quad c^{d=6}_{\alpha\beta} = \left(Y_\Sigma^\dagger \frac{1}{M_\Sigma^\dagger}\frac{1}{M_\Sigma} Y_\Sigma\right)_{\alpha\beta} , \tag{1.48}$$

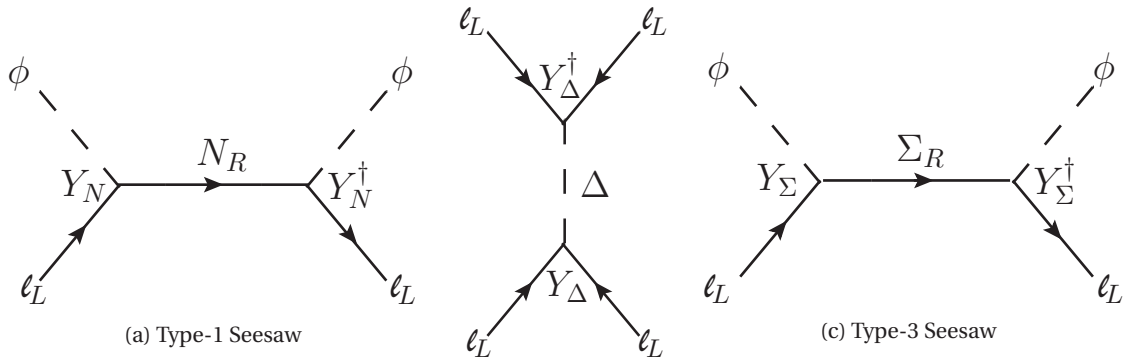

(a) Type-1 Seesaw

(b) Type-2 Seesaw

(c) Type-3 Seesaw

Figure 1.3 – Feynman diagrams responsible of the generation of dimension-6 operators in the three Seesaw mechanisms. From left to right, these correspond to the exchange of fermionic singlets, scalar triplet(s) and fermionic triplets.

for the type-3 Seesaw. These operators are generated by the diagrams (a) and (c) in Fig. 1.3, i.e. the same (a) and (c) diagrams as in Fig. 1.2 but with no lepton number flip from a Majorana mass insertion. The $\not{p}$ part of the propagator contributes rather than the M_N or M_Σ part, which explains the presence of the derivatives in these operators. As a consequence, these two operators do not break lepton number.

In the scalar triplet(s) case, there are several ones (as well as a dimension-4 one). Since we will need it in chapter 4, let's just mention the dimension-6 operator that involves 4 charged leptons, induced by the diagram (b) of Fig. 1.3, which can be written as

$$\mathscr{L}^{d=6}_{\text{type-2}} \ni c^{d=6}_{\alpha\beta\gamma\delta}\left(\overline{\ell_{L\alpha}}\gamma_\mu \ell_{L\gamma}\right)\left(\overline{\ell_{L\beta}}\gamma^\mu \ell_{L\delta}\right) \text{ , with } \quad c^{d=6}_{\alpha\beta\gamma\delta} = -\sum_k \frac{1}{m^2_{\Delta_k}}\left(Y^*_{\Delta_k}\right)_{\alpha\beta}\left(Y_{\Delta_k}\right)_{\gamma\delta} \,. \tag{1.49}$$

This operator too doesn't break lepton number L.

From Eqs. (1.47)-(1.49), or equivalently from Fig. 1.3, we see that to these different operators correspond new observable processes, such that $\mu \to e\gamma$ and $\mu \to e$ conversion, that violate the lepton flavor L_α but not the lepton number L. These are called Charged Lepton Flavor Violation processes (CLFV), and will be discussed at length in chapter 2.

Note that, in the type-1 Seesaw, it has been shown in Ref. [50] that the knowledge of all the low energy dimension-5 and dimension-6 coefficients is in principle enough to be able to reconstruct the high energy parameters in Y_N and M_N. [4] This is quite remarkable and not necessarily out of reach of future experiments. Unfortunately, from Eq. (1.19), the dimension-6 coefficients are in general expected to be small. Indeed, they involve the same number of couplings as the neutrino mass matrix but they scale as $\Lambda^2_{d=6}$ and, if $\Lambda_{d=6} \simeq \Lambda_{d=5}$, they undergo an extra high scale suppression compared to the neutrino mass suppression, see for example Eqs. (1.26) and (1.47) for the type-1 Seesaw. However, this is not always the case as we will show now.

[4] At least when the number of heavy neutrinos is less than or equal to the number of light lepton generations.

1.5 Inverse Seesaw models

An interesting class of Seesaw models are the so-called Inverse Seesaw models [57, 58], which are based on the approximate conservation of the lepton number L [59, 57, 60, 61, 62, 63, 64, 65, 56, 66, 67, 68]. In these models, the dimension-6 operators are not necessarily more suppressed than the dimension-5 ones. This is basically because Majorana neutrino mass requires lepton number violation, while CLFV processes do not.

In the type-1 Seesaw, lepton number is conserved by the Lagrangian in Eqs. (1.22) either if the Majorana mass matrix M_N is vanishing, or if the Yukawa and Majorana mass matrices Y_N and M_N have peculiar structures. In the first case, taking $M_N \ll m_D$ allows to have large dimension-6 coefficients, but then neutrinos are (quasi) Dirac particles and their small mass remains unexplained. In the second case, it has been shown that by assigning lepton number $L(N_1) = 1$, $L(N_2) = -1$, $L(N_3) = 0$ to the right-handed neutrinos, the Lagrangian is lepton number conserving if the neutrino mass matrix has the following structure [68, 69] :

$$\mathscr{M}_\nu = \begin{pmatrix} 0_{3\times3} & m_D^T \\ m_D & M_N \end{pmatrix}, \quad \text{with} \quad m_D = \frac{\mathrm{v}}{\sqrt{2}} \begin{pmatrix} Y \\ 0 \\ 0 \end{pmatrix}, \quad \text{and} \quad M_N = \begin{pmatrix} 0 & \Lambda & 0 \\ \Lambda & 0 & 0 \\ 0 & 0 & \Omega \end{pmatrix}. \tag{1.50}$$

This case shows that it is possible to conserve L while having both non zero m_N and non zero Yukawas Y_N. It is thus not surprising that the light neutrinos are massless but the dimension-6 coefficient in Eq. (1.47) is actually non vanishing. To generate masses for the light neutrinos, one needs to add small perturbations that break lepton number to the above matrix, which becomes

$$\mathscr{M}_\nu = \begin{pmatrix} 0_{3\times3} & m_D^T \\ m_D & M_N \end{pmatrix}, \quad \text{with} \quad m_D = \frac{\mathrm{v}}{\sqrt{2}} \begin{pmatrix} Y \\ \varepsilon Y' \\ \varepsilon Y'' \end{pmatrix}, \quad \text{and} \quad M_N = \begin{pmatrix} \mu' & \Lambda & \alpha \\ \Lambda & \mu & \beta \\ \alpha & \beta & \Omega \end{pmatrix}, \tag{1.51}$$

where $\epsilon \ll 1$ and $\mu, \mu', \alpha, \beta \ll \Lambda, \Omega$. In this case, keeping only dominant terms, the dimension-5 and dimension-6 coefficients in Eqs. (1.28) and (1.47) are given by

$$c^{d=5} \simeq \frac{1}{\mu'\mu - \Lambda^2} \left[Y^T \mu Y - \varepsilon \left(Y^T \Lambda Y' + Y'^T \Lambda Y \right) \right] \simeq \varepsilon \left(Y^T \frac{1}{\Lambda} Y' + Y'^T \frac{1}{\Lambda} Y \right), \tag{1.52}$$

$$c^{d=6} \simeq \frac{1}{\left(\mu'\mu - \Lambda^2\right)^2} \left[Y^\dagger \left(\Lambda^2 + \mu^2 \right) \right] \simeq Y^\dagger \frac{1}{\Lambda^2} Y \,. \tag{1.53}$$

We see that the dimension-5 coefficient is proportional to the small parameter ε. Therefore, one can have at the same time large dimension-6 coefficients and small dimension-5 ones, provided that $\varepsilon \ll 1$ and $Y \sim 1$. Note that in this scenario, two heavy neutrinos have quasi-degenerate masses :

$$m_{N_1} \simeq \Lambda - (\mu + \mu')/2 \,, \quad \text{and} \quad m_{N_2} \simeq \Lambda + (\mu + \mu')/2 \,. \tag{1.54}$$

The third heavy neutrino N_3 with $m_{N_3} \simeq \Omega$, already not mandatory to explain neutrino oscillation data, is nearly totally decouple from the rest since it only couples through small parameters.

In other words, we have seen that in the case of type-1 Seesaw, we have naively that the dimension-5 and dimension-6 coefficients go like $c^{d=5} \propto Y_N^2/M_N$ and $c^{d=6} \propto Y_N^2/M_N^2$ respectively. In order to generate neutrino masses of the order of $m_\nu \sim 0.1$ eV, one would need roughly $Y_N \sim 10^{-5}\dots 1$ for $M_N \sim 10^4 \dots 10^{14}$ GeV, what leads in general to an extremely suppressed dimension-6 coefficient, and therefore extremely small rate for the charged lepton flavor violation processes (CLFV). However, since the $c^{d=5}$ and $c^{d=6}$ don't involve the same combination of Y_N and M_N, we can take much larger values of Y_N while keeping m_N at the TeV scale which give larger $c^{d=6}$ without implying large $c^{d=5}$ and thus too large m_ν. Even if clearly less likely than the usual Seesaw, this offers a unique opportunity to probe the physics BSM through CLFV processes which is presumably the most likely to exist.

Comment on Extended Seesaw models. An important remark concern the μ' parameter in the type-1 Inverse Seesaw model. In order to generate a small mass for the light neutrinos and to have large dimension-6 coefficients, the difference between the right-handed neutrino masses can not be *a priori* too large. For example in the Inverse Seesaw introduced above, if the mass splitting is large, the parameters μ and/or μ' should be large, so that one expects from Eqs. (1.52)-(1.53) to have a small dimension-6 operator, since now $\mu, \mu' \gg \Lambda$. There is however an exception if one has $\mu \ll \mu'$, in which case one could a priori take larger values for μ' and still have small neutrino masses and large dimension-6 coefficients. This can be seen easily : if $\mu = \epsilon = 0$, the determinant of $\mathscr{M}_\nu$ in Eq. (1.51) remains equal to zero, leading to no masses for the light neutrinos even if μ' does break L. In this case, the conservation of the lepton number L is strongly violated and the heavy neutrino masses are no more degenerate. In fact, in the limit where $\mu' \gg \Lambda$, Eqs. (1.54) should be replaced by

$$m_{N_1} \simeq \mu - \Lambda^2/\mu' \,, \quad \text{and} \quad m_{N_2} \simeq \mu' + \Lambda^2/\mu' \,. \tag{1.55}$$

This kind of model, where $\mu' > \Lambda$, is called **"Extended Seesaw models"**, and presents additional attractive features that can help to achieve successful low-scale leptogenesis [70]. In this case, one has to be careful with possibly large one-loop corrections to the neutrino masses and $0\nu2\beta$ decay parameter m_{ee}, since there is no more symmetry protecting the neutrino masses [71, 72]. However, lepton number symmetry is actually restored at low energy for $\mu' \gg \Lambda$, so that one can actually have the Inverse Seesaw features with non-degenerate right-handed neutrino masses [72].

In the type-2 Seesaw, unlike the type-1 Seesaw, the $c^{d=6}$ coefficients have no reason to be small from the start. Indeed, L is violated by the existence of both μ_Δ and Y_Δ in the Lagrangian, see Eq. (1.32). As a result, the dimension-5 and dimension-6 coefficients go respectively like $c^{d=5} \propto (\mu_\Delta/m_\Delta)(Y_\Delta/m_\Delta)$ and $c^{d=6} \propto Y_\Delta^2/m_\Delta^2$. But μ_Δ/m_Δ and Y_Δ have no reasons to have the same value. So if $\mu_\Delta \to 0$, neutrinos are massless since these are proportional to μ_Δ, see Eq. (1.38), but the dimension-6 operator in Eq. (1.49) is non vanishing since it involves only the Yukawa matrix Y_Δ and the mass scale m_Δ. As a consequence, by taking $\mu_\Delta \ll m_\Delta$, lepton number is nearly conserved and one can have light neutrino masses together with large CLFV processes. No peculiar matrix structure is needed.

Finally, in the type-3 Seesaw, the situation is quasi-similar to the type-1 case.

1.6 $SO(10)$ GUT and L-R symmetry motivations for Seesaw models

1.6.1 $SO(10)$ GUT group

In the type-1 and type-2 Seesaw scenarios, we have discussed the possibility to enlarge the SM group with a new $B-L$ group. But the Seesaw mechanisms are in fact well motivated by a plethora of Grand Unified Theories (GUT), as for example the GUT group $SO(10)$ [73], that we now discuss briefly. An interesting aspect of $SO(10)$ is that each family of fermions is unified in a dimension-16 spinorial representation, which also contains generically the right-handed neutrinos. These are therefore naturally present in $SO(10)$. Furthermore, the $SO(10)$ group contains two maximal continuous subgroups which are

$$SO(10) \supset SU(5) \times U(1)_{B-L} \,, \tag{1.56}$$

$$SO(10) \supset SU(4)_c \times SU(2)_L \times SU(2)_R \,. \tag{1.57}$$

We recognize in Eq. (1.56) the $SU(5)$ GUT group [74], and the $B-L$ symmetry. The subgroup in Eq. (1.57) contains the left-right (L-R) symmetric model $SU(2)_L \times SU(2)_R \times U(1)_{B-L}$ [75, 76]. The breaking of $SO(10)$ to the SM group can be achieved in many ways through one of the two subgroups above. If we break $SO(10)$ according to Eq. (1.56), the following chain of symmetry breaking is possible

$$SO(10) \xrightarrow[\Lambda_{B-L}]{\{16\}} SU(5) \xrightarrow[\Lambda_5]{\{45\}} SU(3)_c \times SU(2)_L \times U(1)_Y \xrightarrow[\Lambda_{EW}]{\{10\}} SU(3)_c \times U(1)_{EM} \,. \tag{1.58}$$

The scalar boson representation of $SO(10)$ responsible of the SSB is displayed above the arrows, while the associated energy scale is displayed below the arrows. In the above chain, the breaking of the $B-L$ symmetry is expected to occur at $\Lambda_{B-L} \gg \Lambda_{EW} \simeq m_W$, scale at which a Majorana mass for the right-handed neutrino is generated. In this scenario, we have therefore naturally $M_N \gg m_D$ and the type-1 Seesaw is at work. This motivates for example the Lagrangian introduced in Eq. (1.30). Unfortunately, it has been shown that the $SU(5)$ group as a GUT group, embedding the SM group, doesn't provide the good running of the coupling constant, at least in usual realizations.

Another possible chain of spontaneous symmetry breaking is through the subgroups of Eq. (1.57), that is

$$\begin{aligned} SO(10) &\xrightarrow[\Lambda_{10}]{\{54\}} SU(4)_c \times SU(2)_L \times SU(2)_R \times Z_2 \xrightarrow[\Lambda_c]{\{45\}} SU(3)_c \times SU(2)_L \times SU(2)_R \times U(1)_{B-L} \\ &\xrightarrow[\Lambda_R]{\{126\}} SU(3)_c \times SU(2)_L \times U(1)_Y \xrightarrow[\Lambda_{EW}]{\{10\}} SU(3)_c \times U(1)_{EM} \,. \end{aligned} \tag{1.59}$$

Here too, the breaking of $B-L$ is expected to occur above the EW scale. An important remark to be done is that in order to generate a Majorana mass M_N for the right-handed neutrinos in a renormalizable way, one needs the vev of a $\overline{126}$ scalar representation. [5] This representation

[5] Given that $16 \times 16 = 10 + 120 + 126$, fermion bilinears can be formed via their couplings with the symmetric 10 and/or $\overline{126}$, and/or with the antisymmetric 120. To get correct masses for the quarks and charged leptons, it has been shown that one could in principle use any of the combination $(10, 120)$, $(10, \overline{126})$, $(120, \overline{126})$ or $(10, 120, \overline{126})$. To get the Seesaw mechanism at work, the $\overline{126}$ representation is however needed [77]. Under the gauge group $SU(4) \times SU(2)_L \times SU(2)_R$, the symmetric scalar representation $\overline{126}$ can be decomposed as $\overline{126} = (6,1,1) + (\overline{10},3,1) + (10,1,3) + (15,2,2)$, which contains scalar triplets under $SU(2)_L$ and $SU(2)_R$.

contains a scalar triplet under $SU(2)_L$ (Δ_L) and a scalar triplet under $SU(2)_R$ (Δ_R). On the one hand, if the neutral component of Δ_R acquires a vev, a heavy Majorana mass matrix M_N is generated. On the other hand, the scalar triplet Δ_L is nothing but a type-2 scalar triplet with $Y(\Delta_L) = 2$ which generates a Majorana mass for the left-handed neutrinos below SSB. Thus, unless one generates M_N from non-renormalizable interactions, the Seesaw framework is a type-1+2 one in $SO(10)$ [78, 79, 77]. Furthermore, this scenario is peculiarly interesting since it contains the L-R symmetric model, that we now discuss.

1.6.2 L-R symmetric model

The gauge group of this model is $SU(2)_L \times SU(2)_R \times U(1)_{B-L}$. As the left-handed sector of the SM, the right-handed particles are here embedded in doublets $\ell_R = (N_R\ e_R)$ and $Q_R = (u_R\ d_R)$, which transform under $SU(2)_R$. In this case, the electric charge formula has the attractive form

$$Q = I_L^3 + I_R^3 + \frac{B-L}{2}\,, \tag{1.60}$$

where $I_{L,R}^3$ are the left and right isospins respectively. After $SU(2)_R \times U(1)_{B-L} \to U(1)_Y$ symmetry breaking, the hypercharge Y is in this case simply given by $Y = 2I_R^3 + B - L$, which is interestingly in agreement with the SM if the leptons carry a charge $B-L=-1$ and the quarks carry a charge $B-L=1/3$.

The breaking of the L-R symmetric model to the SM gauge group can be done via different ways. A necessarily ingredient is the bi-doublet Φ which transforms under both $SU(2)_L$ and $SU(2)_R$, that is needed in order to give a mass to the fermions,

$$\Phi = \begin{pmatrix} \Phi^0 & \Phi'^+ \\ \Phi^- & \Phi'^0 \end{pmatrix}. \tag{1.61}$$

After SSB, the electrically neutral component of the bi-doublet acquire vev's $\langle \Phi^0 \rangle = \mathrm{v}_0$ and $\langle \Phi'^0 \rangle = \mathrm{v}_0'$, and fermions become massive. However, other scalars are needed to break the residual $U(1)_{L+R} \times U(1)_{B-L}$ to $U(1)_{EM}$, where the $U(1)_{L+R}$ symmetry is left because the neutral Φ^0 and Φ'^0 carry $I_L^3 + I_R^3 = 0$.

A possibility is to introduce two scalar ϕ_L and ϕ_R, doublets under $SU(2)_L$ and $SU(2)_R$ respectively and with charge $B-L=1$ [75, 76, 80, 81, 82, 83, 84]. By acquiring a vev, one of the doublet, let say ϕ_L, could therefore break $U(1)_{L+R} \times U(1)_{B-L} \to U(1)_{EM}$. This possibility is perfectly fine, but in this case it was shown that the neutrinos are Dirac particles whose small mass can not be explained easily.

Another interesting possibility is to introduce two scalar triplets Δ_L and Δ_R with $B-L=2$ on top of the scalar bi-doublet Φ [85], as in the case of $SO(10)$ breaking from Eq. (1.59) with renormalizable interactions to induce the right-handed Majorana mass M_N. Here, the breaking of $U(1)_{L+R} \times U(1)_{B-L}$ is done via the vev $\langle \Delta_R^0 \rangle = \mathrm{v}_{\Delta_R}$ of the electrically neutral component of Δ_R. In this case, a Majorana mass $M_N \propto \mathrm{v}_{\Delta_R}$ for the right-handed neutrinos is generated. One ends up therefore with the type-1 Seesaw scenario in Eq. (1.22), but also with the type-2 Seesaw scenario

in Eq. (1.32) [86]. [6]

The L-R symmetric model could therefore easily generate both the type-1 and the type-2 Seesaw model. In this case, the total Lagrangian is the sum of the Lagrangian in Eqs. (1.22) and (1.32), and the neutrino mass is the sum of Eqs. (1.26) and (1.38). Following the value of the different parameters, one or both types of Seesaw will be favored.

Final remark. Let's note that a more complicated possibility, based on the two previous ones, could lead to both Seesaw type-1 and type-2 Lagrangians in Eqs. (1.22) and (1.32). Indeed, let's take the scalar content of the L-R symmetric model to be constituted by 1 scalar bi-doublet $\Phi = (2,2,0)$, 2 scalar doublets $\phi_L = (2,1,1)$ and $\phi_R = (1,2,1)$, and 2 scalar triplets $\Delta_L = (3,1,2)$ and $\Delta_R = (1,3,2)$. In the brackets are given the corresponding $SU(2)_L \times SU(2)_R \times U(1)_{B-L}$ charges. [7] In this case, the general L-R symmetric Lagrangian contains

$$\begin{aligned} -\mathscr{L}_{LR} \ni & Y_\ell \, \overline{\ell_L} \, \Phi \, \ell_R + \tilde{Y}_\ell \, \overline{\ell_L} \, \tilde{\Phi} \, \ell_R \\ & + Y_{\Delta_L} \ell_L^T C \, i\tau_2 \, \Delta_L \ell_L + Y_{\Delta_R} \ell_R^T C \, i\tau_2 \, \Delta_R \ell_R + \mu_{\Delta_L} \tilde{\phi}_L \, \Delta_L^\dagger \phi_L + \mu_{\Delta_R} \tilde{\phi}_R \, \Delta_R^\dagger \phi_R + \text{H.c.} \,, \end{aligned} \tag{1.62}$$

where $\tilde{\Phi} = \tau_2 \Phi^* \tau_2$ transforms as Φ. The rest of the scalar potential is not explicitly written, but it is assumed to be such that at least Φ and ϕ_L acquire vev's. Let's note that it contains term proportional to $\phi_L^\dagger \, \Phi \, \phi_R$, which could be forbidden by imposing some discrete symmetry as Z_2. There are several possibilities of symmetry breaking, but let's assume that Φ, ϕ_R and ϕ_L acquire vev's

$$\langle \Delta_\Phi \rangle \equiv \begin{pmatrix} \kappa & 0 \\ 0 & \kappa' \end{pmatrix} , \quad \langle \phi_R^0 \rangle = \frac{\text{v}_{\phi_R}}{\sqrt{2}} , \quad \langle \phi_L^0 \rangle = \frac{\text{v}_{\phi_L}}{\sqrt{2}} . \tag{1.63}$$

In this case, scalar interactions also generate a vev for $\Delta_{L,R}$ given by

$$\langle \Delta_{L,R}^0 \rangle = \text{v}_{\Delta_{L,R}} = \frac{1}{2} \mu_{\Delta_{L,R}} \frac{\text{v}_{\phi_{L,R}}^2}{m_{\Delta_{L,R}}^2} . \tag{1.64}$$

As a consequence, a Majorana mass for the heavy right-handed neutrinos is generated with $M_N = 2 Y_\Delta \, \text{v}_{\Delta_R}$, as well as a type-2 Majorana mass term for the light left-handed neutrinos, given by Eq. (1.38). The neutrino mass matrix reads therefore

$$\mathscr{M}_\nu = \begin{pmatrix} 2 Y_{\Delta_L} \, \text{v}_{\Delta_L} & m_D^T \\ m_D & 2 Y_{\Delta_R} \, \text{v}_{\Delta_R} \end{pmatrix} , \tag{1.65}$$

where here $m_D = Y_\ell \kappa + \tilde{Y}_\ell \kappa'$. Then, if $\text{v}_{\Delta_R} \gg \text{v}_{\Delta_L}$, one also have that a type-1 Seesaw mechanism is at work, and the final light neutrino masses matrix is given by the sum of the two types of Seesaw

[6] The point is that the scalar potential of the Lagrangian contains a term $\gamma \text{Tr}[\Delta_L^\dagger \Phi \Delta_R \Phi^T]$ which give rise to a vev for Δ_L given by $\text{v}_{\Delta_L} \propto \gamma \, \text{v}_0^2 / \, \text{v}_{\Delta_R}$.

[7] This configuration has already been considered in [82]. We will here discuss briefly a scenario that is somehow slightly different.

$$m_\nu \simeq -m_D^T \frac{1}{2Y_{\Delta_R}\, v_{\Delta_R}} m_D + 2Y_{\Delta_L}\, v_{\Delta_L}\,. \tag{1.66}$$

Here too, both type-1 and type-2 Seesaw mechanisms are at work.

Another interesting possibility is that Φ, ϕ_L and Δ_R acquire a vev. In this case, if we also impose a Z_2 symmetry to ϕ_R in order to forbid the $\phi_L^\dagger\,\Phi\,\phi_R$ term such that ϕ_R doesn't acquire any vev, one ends up with a type-1+2 Seesaw with an inert scalar doublet ϕ_R as in the Inert Doublet Model, see section 5.2.

2 Muon to electron conversion in nuclei in type-1 Seesaw models

Muon conversion to electron in atomic nuclei – that in the following we will call $\mu \to e$ conversion – is a process that is not present in the SM (without neutrino oscillations). However, it is predicted to exist in some extension of the SM so that the observation of such a process would be a clear evidence for new physics. [1] Experimentally, this process is very appealing because future experiments should probe very high sensitivities on its rate, up to several orders of magnitude better than the present upper bound. It is therefore mandatory that minimal extensions of the SM own robust expressions for this rate.

The goal of this chapter is to compute the rate of this process in the type-1 Seesaw framework. We first write the type-1 Seesaw Lagrangian in the mass eigenstate basis, then introduce the Charged Lepton Flavor Violation processes, to which belong the $\mu \to e$ conversion. Subsequently we compute the analytical expression of the rate of this process, valid for any type-1 Seesaw model. In the next sections, we analyze the phenomenology one could derive from our result, and compare the predictions to the other kind of Seesaw mechanism.

2.1 Type-1 Lagrangian in the mass eigenstate basis

The type-1 Seesaw Lagrangian was introduced in section 1.3.2, Eq. (1.22). As anticipated, by redefining the different neutrino fields, the neutrino mass matrix in Eq. (1.25) can be diagonalized. This redefinition of the fields also leads to modifications in the neutrino interactions. To take care of that, one needs to write down the Lagrangian in the neutrino mass eigenstate basis. We perform in this first section the diagonalization step by step. We remind that the mass interactions of the type-1 Seesaw Lagrangian, as given in Eq. (1.23), can be expressed in terms of matrices as

$$\mathscr{L}_{\text{mass}}^{\text{type-1}} = -\frac{1}{2}\begin{pmatrix}\overline{\nu_L^c} & \overline{N_R}\end{pmatrix} \mathscr{M}_\nu \begin{pmatrix}\nu_L \\ N_R^c\end{pmatrix} + \text{H.c.}\,, \tag{2.1}$$

[1] Including neutrino oscillations, this process does actually exist. However, it is extremely rare – and experimentally unreachable – since its rate goes like the neutrino mass over the W mass to the 4th power.

where

$$\mathscr{M}_\nu \equiv \begin{pmatrix} 0_{3\times 3} & m_D^T \\ m_D & M_N \end{pmatrix} . \tag{2.2}$$

Here, $\nu_L = \left(\nu_{L_e}\ \nu_{L_\mu}\ \nu_{L_\tau}\right)^T$ and $N_R = \left(N_{R_1}\ \ldots\ N_{R_{n_N}}\right)^T$, with n_N the number of right-handed neutrinos. Without loss of generality, we will assume in what follows that the matrices M_N and Y_e have already been diagonalized after redefinition of respectively the right-handed neutrinos fields N_R and the charged lepton fields through unitary transformations. The matrix $\mathscr{M}_\nu$ is symmetric and, according to the Takagi's factorization, can be diagonalized by block thanks to a unitary matrix U_N :

$$\hat{\mathscr{M}}_\nu = U_N^T\, \mathscr{M}_\nu\, U_N . \tag{2.3}$$

Taking care of normalizing correctly the kinetic terms, this matrix U_N is in the limit where $M_N \gg m_D$ given by [88, 56]

$$U_N = \begin{pmatrix} \mathbb{1}_{3\times 3} - \frac{\epsilon_N}{2} & \left(M_N^{-1} m_D\right)^\dagger \\ -M_N^{-1} m_D & \mathbb{1}_{n_N\times n_N} - \frac{\epsilon'_N}{2} \end{pmatrix} + \mathscr{O}\left(m_D^3/M_N^3\right) , \tag{2.4}$$

where

$$\epsilon_N \equiv \left(M_N^{-1} m_D\right)^\dagger (M_N m_D) \quad \text{and} , \quad \epsilon'_N \equiv \left(M_N^{-1} m_D\right)\left(M_N^{-1} m_D\right)^\dagger . \tag{2.5}$$

The presence of the ϵ_N term in the diagonal can be understood as the following. Let's consider the low energy Lagrangian made of the dimension-5 Weinberg operator and the dimension-6 one in Eq. (1.47). The latter involves a derivative so that, after replacing the scalar field ϕ by its vev, it gives a correction to the kinetic term which takes the form $\bar{\nu_L}\, \partial\!\!\!/ (1+\epsilon_N)\nu_L$. In order to get back the canonical kinetic term, one must therefore perform a non-unitary transformation $\nu_L \to \nu_L(1+\epsilon_N/2)$, which leads to the form of the diagonal terms of the U_N matrix in Eq. (2.4) and explains at the same time why ϵ_N is nothing but proportional to the dimension-6 coefficient in Eq. (1.47). After having performed the unitary transformation of Eq. (2.4), the block-diagonal matrix is approximately given by [88, 56]

$$\hat{\mathscr{M}}_\nu = \begin{pmatrix} -m_D^T M_N^{-1} m_D + \mathscr{O}\left(m_D^4/M_N^3\right) & \mathscr{O}\left(m_D^3/M_N^2\right) \\ \mathscr{O}\left(m_D^3/M_N^2\right) & M_N + \mathscr{O}\left(m_D^2/M_N\right) \end{pmatrix} \simeq \begin{pmatrix} m_\nu & 0 \\ 0 & m_N \end{pmatrix} . \tag{2.6}$$

where $m_\nu \simeq -m_D^T M_N^{-1} m_D$ and $m_N \simeq M_N$. The light neutrino mass matrix m_ν can finally be diagonalized by a matrix $\mathscr{U}$, the PMNS matrix. All in all, the mass matrix $\mathscr{M}_\nu$ is fully diagonalized by a unitary matrix U given by

$$U = U_N\, \mathrm{diag}\left(\mathscr{U}, \mathbb{1}_{n_N\times n_N}\right) \simeq \begin{pmatrix} U_{\nu\nu} & U_{\nu N} \\ U_{N\nu} & U_{NN} \end{pmatrix} , \tag{2.7}$$

where

$$U_{\nu\nu} = \left(\mathbb{1}_{3\times3} - \frac{\epsilon_N}{2}\right)\mathscr{U}\,, \qquad U_{\nu N} = \left(M_N^{-1} m_D\right)^\dagger\,,$$
$$U_{N\nu} = -M_N^{-1} m_D\,\mathscr{U}\,, \qquad U_{NN} = \mathbb{1}_{n_N\times n_N} - \frac{\epsilon'_N}{2}\,. \tag{2.8}$$

The neutrino flavor eigenstates are related to the mass eigenstate n_i, with $i = 1$ to $3+n_N$, through

$$\nu_{L_\alpha} = \sum_{i=1}^{3+n_N} U_{\alpha i}\, P_L\, n_i \quad \text{and} \quad N_{R_k} = \sum_{i=1}^{3+n_N} U^*_{ki}\, P_R\, n_i\,, \tag{2.9}$$

where $k = 1$ to n_N. All the mass eigenstates are Majorana particles, i.e. $n_i^c = n_i$. Explicitly, we write $n_i = \left(\nu_1\ \nu_2\ \nu_3\ N_1 \ldots N_{n_N}\right)^T$, where the three first mass eigenstates ν_i are the light neutrinos, and the n_N last ones are the heavy neutrinos N_i. In this chapter, the indices $i, j, \ldots$ will denote the mass eigenstates, and the indices $\alpha, \beta, \ldots$ still denote the flavor eigenstates e, μ and τ.

The presence of the terms ϵ_N and ϵ'_N in Eq. (2.4) are crucial in order to have well defined kinetic terms. Because of these, the $U_{\nu\nu}$ entry of the matrix U is not a unitary matrix. In the mass eigenstate basis, the various gauge boson and scalar interactions read [67]

$$\mathscr{L}^{W^\pm} = \frac{g}{\sqrt{2}} W_\mu^-\, \overline{\ell}_\alpha \gamma^\mu U_{\alpha i} P_L n_i + \text{H.c.}\,, \tag{2.10}$$
$$\mathscr{L}^{Z} = \frac{g}{4c_w} Z_\mu\, \overline{n}_i \gamma^\mu \left[C_{ij} P_L - C^*_{ij} P_R\right] n_j\,, \tag{2.11}$$
$$\mathscr{L}^{\phi^\pm} = -\frac{g}{\sqrt{2} m_W} \phi^-\, \overline{\ell}_\alpha U_{\alpha i} \left(m_{l_\alpha} P_L - m_{n_i} P_R\right) n_i + \text{H.c.}\,, \tag{2.12}$$
$$\mathscr{L}^{\phi^3} = -\frac{ig}{4m_W} \phi^3\, \overline{n}_i \left[C_{ij}\left(m_{n_i} P_L - m_{n_j} P_R\right) - C^*_{ij}\left(m_{n_i} P_R - m_{n_j} P_L\right)\right] n_j\,, \tag{2.13}$$
$$\mathscr{L}^{h} = -\frac{g}{4m_W} h\, \overline{n}_i \left[C_{ij}\left(m_{n_i} P_L + m_{n_j} P_R\right) + C^*_{ij}\left(m_{n_i} P_R + m_{n_j} P_L\right)\right] n_j\,, \tag{2.14}$$

where the Majorana properties of the neutrino fields n_i have been used to obtain the above form of their coupling to bosons. In the above expressions, g is the weak isospin coupling constant, c_w is the cosine of the weak mixing angle, and C and m_n are $(3+k)\times(3+k)$ matrices defined as :

$$C_{ij} \equiv \sum_{\alpha=1}^{3} U^\dagger_{i\alpha} U_{\alpha j}\,, \qquad m_n = \text{Diag}\left(m_{n_i}\right) = \text{Diag}(m_{\nu_1}, m_{\nu_2}, m_{\nu_3}, m_{N_1}, ..., m_{N_{n_N}})\,, \tag{2.15}$$

where m_{n_i} are the mass eigenvalues of the mass eigenstates n_i. The electromagnetic and Z interactions of the charged leptons are not modified by the basis change, so there are no flavor changing neutral current at tree-level.

These modified interactions have interesting consequences. Indeed, from Eq. (2.10) we see that the W's couplings to lepton is no more diagonal. Worse, because the matrix $U_{\nu\nu}$ is not unitary, the Fermi constant G_F measured in experiments is no more the one defined as $G_F^{SM} = \sqrt{2} g^2/8 m_W^2$.

The Fermi constant extracted from the decay $\mu \to e\bar{\nu}_e\nu_\mu$ is actually given by [89]

$$G_F \simeq G_F^{SM}\left(1 - \frac{(\epsilon_N)_{ee} + (\epsilon_N)_{\mu\mu}}{2}\right). \tag{2.16}$$

Since $\epsilon_N \sim m_D^2/M_N^2$, see Eq. (2.5), one expects small deviation from the SM value. Another clear consequence of the modified interactions is the Charged Lepton Flavor Violation (CLFV) processes.

2.2 Charged Lepton Flavor Violation processes

Through the dimension-6 operator effects on the Lagrangian, from Eqs. (2.10)-(2.14) new interesting processes are predicted that violate lepton flavor but conserve lepton number. As we will illustrate below, the ones involving charged leptons as $\mu \to e\gamma$, $\mu \to eee$ or $\mu \to e$ conversion are experimentally very interesting. This new class of processes, in which lepton flavor is violated, are called Charged Lepton Flavor Violation processes (CLFV). For example in the type-1 Seesaw model introduced above, we see that the charged leptons don't have any flavor changing neutral interactions, but they still can change flavor through the emission and absorption of W's at loop-level, with a neutrino flavor transition in the loop.

The recent experimental evidences for neutrino masses has shown that lepton flavor is in fact violated in the neutrino sector. These implies that CFLV processes do already exist thanks to neutrino oscillations. However, proceeding through neutrino masses m_ν, they need two neutrino mass m_ν insertions in the diagram, which lead to a branching ratio proportional to $(m_\nu/m_W)^4$, which is extremely suppressed. For example, it has been shown in Ref. [90] that, assuming only neutrino oscillations, the branching ratio of the process $\mu \to e\gamma$ is of the order of $Br(\mu \to e\gamma) \sim 10^{-56}$, which is several tens of order of magnitude smaller than the present and future experimental bounds, see below.

The CLFV processes are not specific to type-1 Seesaw models. In fact, a lot of models do actually predict them, like the other two kinds of Seesaw models. This is because once a model generates a dimension-5 operator, it is generally expected to generate dimension-6 ones as well, see section 1.4. For example, as already mentioned above, the type-1 Seesaw generates a dimension-6 operator given by Eq. (1.47). We here write again the associated dimension-6 coefficient $c_{\alpha\beta}^{d=6}$ [50] :

$$c_{\alpha\beta}^{d=6} = \left(Y_N^\dagger \frac{1}{M_N^\dagger}\frac{1}{M_N} Y_N\right)_{\alpha\beta} = \sum_i^{n_N} Y_{N_i\alpha}^* \frac{1}{m_{N_i}^2} Y_{N_i\beta}\,, \tag{2.17}$$

where we used the fact that M_N can be taken without loss of generality as a diagonal matrix of real elements. Here and in what follows, we denote by $Y_{N_i\alpha}$ the matrix elements of Y_N. We have shown that this dimension-6 coefficient $c^{d=6}$ is remarkably nothing else than the ϵ_N in Eq. (2.5), up to a factor $v^2/2$. As we will see, it is in fact involved in all CLFV processes.

2.2.1 Experimental status

The CLFV processes are very promising because new experiments will reach very high sensitivities on the branching of some of them. One distinguishes the following processes.

- $\underline{\ell_\alpha \to \ell_\beta \gamma}$

The decay of a charged lepton ℓ_α in another charged lepton ℓ_β with emission of a photon. The rate of such process reads $\Gamma(\ell_\alpha \to \ell_\beta \gamma)$, and its branching ratio is normalized according to

$$Br\left(\ell_\alpha \to \ell_\beta \gamma\right) = \frac{\Gamma\left(\ell_\alpha \to \ell_\beta \gamma\right)}{\Gamma_{\ell_\alpha}}\,, \tag{2.18}$$

where Γ_{ℓ_α} is the total decay rate of the charged lepton ℓ_α. The present best bounds on the different branching ratios are provided by the experiments MEG for $\mu \to e\gamma$ [91] and BABAR for $\tau \to e\gamma$ and $\tau \to \mu\gamma$ [92]. In the near future, the upgrade of the MEG experiment, MEG-II, should increase the sensitivity by nearly one order of magnitude on the $\mu \to e\gamma$ process [93]. Concerning $\tau \to \ell_\beta \gamma$, SuperB and Belle II should also improve the sensitivity by approximately one order of magnitude in a near future (~2021) [94, 95, 96].

- $\underline{\ell_\alpha \to \ell_\beta \ell_\gamma \overline{\ell_\delta}}$

The decay of a charged lepton ℓ_α in 3 charged leptons ℓ_β, ℓ_γ and ℓ_δ. The rate of such a process is given by $\Gamma(\ell_\alpha \to \ell_\beta \ell_\gamma \overline{\ell_\delta})$ and the associated branching ratio by

$$Br\left(\ell_\alpha \to \ell_\beta \ell_\gamma \overline{\ell_\delta}\right) = \frac{\Gamma\left(\ell_\alpha \to \ell_\beta \ell_\gamma \overline{\ell_\delta}\right)}{\Gamma_{\ell_\alpha}}\,. \tag{2.19}$$

The present best bounds on this branching ratio are provided by SINDRUM I [97], BABAR [98] and BELLE experiments [99]. In the future, the experiment Mu3e is expected to improve the sensitivity by about ~4 orders of magnitude with respect to the present bound [100]. For $\tau \to \ell_\beta \ell_\gamma \overline{\ell_\delta}$, the SuperB experiment should improve the sensitivity by one to two orders of magnitude [95].

- $\underline{\mu\,(A,Z) \to e\,(A,Z) \text{ in an nucleus } {}^{A}_{Z}\mathcal{N}}$

The conversion of a muon into an electron in a nucleus $\mathcal{N}$ which has Z protons and $A-Z$ neutrons. This process will also be referred to "$\mu \to e$ conversion" in what follows. Explicitly, when a muon is stopped by some material, it is trapped by an atom and a muonic atom is formed. The muon falls from energy levels until it reaches the $1s$ ground state. From this moment, the muon has different possibilities : either it decays in orbit through $\mu \to e\nu_\mu\bar{\nu}_e$, or it is captured by the nucleus through $\mu\,(A,Z) \to \nu_\mu\,(A,Z-1)$, or it is converted into an electron without emitting any neutrino and this is the exotic $\mu \to e$ conversion process $\mu\,(A,Z) \to e\,(A,Z)$. In $\mu \to e$ conversion, the final state of the nucleus could be the ground state or an excited state. However, the transition to the ground state, called "coherent" capture, is in general enhanced with respect to the other transition ("incoherent" capture) by a factor equal to the number of nucleons in the nucleus [101].

Process	Upper bound (95% C.L.)	Experiment/Collaboration	Ref.
$\mu^+ \to e^+ \gamma$	5.7×10^{-13}	MEG	[91]
$\mu^+ \to e^+ e^+ e^-$	1.0×10^{-12}	SINDRUM I	[97]
$\tau^+ \to \mu^+ \gamma$	4.4×10^{-8}	BABAR	[92]
$\tau^+ \to e^+ \gamma$	3.3×10^{-8}	BABAR	[92]
$\tau^+ \to \mu^+ \mu^+ \mu^-$	3.2×10^{-8}	BELLE	[99]
$\tau^+ \to e^+ e^+ e^-$	3.6×10^{-8}	BELLE	[99]
$\tau^+ \to \mu^+ e^+ e^-$	2.7×10^{-8}	BELLE	[99]
$\tau^+ \to e^+ \mu^+ \mu^-$	3.7×10^{-8}	BABAR	[98]
$\tau^+ \to \mu^+ \mu^+ e^-$	2.3×10^{-8}	BELLE	[99]
$\tau^+ \to e^+ e^+ \mu^-$	2.0×10^{-8}	BELLE	[99]
$\mu^- Ti \to e^- Ti$	4.3×10^{-12}	SINDRUM II	[102]
$\mu^- Au \to e^- Au$	7×10^{-13}	SINDRUM II	[104]
$\mu^- Pb \to e^- Pb$	4.6×10^{-11}	SINDRUM II	[103]
Process	Future sensitivities	Experiment/Collaboration	Ref.
$\mu \to e \gamma$	4×10^{-14}	MEG	[93]
$\tau \to \mu \gamma$	2.4×10^{-9}	SuperB, Belle II	[102, 104, 103]
$\tau \to e \gamma$	3.0×10^{-9}	SuperB, Belle II	[102, 104, 103]
$\mu \to e e e$	$\sim 10^{-16}$	Mu3e	[100]
$\tau \to \ell\ell\ell$	$2.3 - 8.2 \times 10^{-10}$	SuperB, Belle II	[102, 104, 103]
$\mu Ti \to e Ti$	$\sim 10^{-18}$	PRISM	[105],[106]
$\mu Al \to e Al$	$\sim 10^{-17}$	Mu2e	[108]
$\mu Al \to e Al$	$\sim 10^{-17}$	COMET	[105],[106]

Table 2.1 – Present upper bound and expected sensitivities on different CLFV processes. The bounds are on the rate $R^{\mathcal{N}}_{\mu\to e}$, as defined in Eq. (2.20) for $\mu \to e$ conversion processes, and on the branching ratios, as defined in Eqs. (2.18) and (2.19), for the other processes.

The rate of such an event is $\Gamma(\mu\mathcal{N} \to e\mathcal{N})$, and it is generally normalized according to

$$R^{\mathcal{N}}_{\mu\to e} = \frac{\Gamma\left(\mu\mathcal{N} \to e\mathcal{N}\right)}{\Gamma^{\mathcal{N}}_{\text{capt.}}} , \tag{2.20}$$

where $\Gamma^{\mathcal{N}}_{\text{capt.}}$ is the capture rate of the muon by the nucleus $\mathcal{N}$. The present best bounds on the rate $R^{\mathcal{N}}_{\mu\to e}$ for different nuclei are provided by the SINDRUM II experiment [102, 103, 104]. In the next future, new experiments like COMET, PRISM and Mu2e should reach fantastic sensitivities on $\mu \to e$ conversion in Titanium and Aluminum [105, 106, 107, 108, 109]. They are planned to improve the sensitivities on such processes by up to ~6 orders of magnitude. This is very exciting since these processes are in general not expected to be more suppressed than the others. The reason why they will reach such sensitivities is multiple. First, there is only one particle produced, the electron. This one carries an energy

$$E_e = m_\mu - B_\mu - R_{\mathcal{N}} , \tag{2.21}$$

where $B_\mu \simeq Z^2\alpha^2 m_\mu/2$ is the binding energy of the $1s$ muonic atom and $R_{\mathcal{N}} \simeq m_\mu^2/2m_{\mathcal{N}}$ is the recoil energy of the nucleus [110]. For Titanium, one has typically $B_\mu \simeq 1.27$ MeV and $R_{\mathcal{N}} \simeq$

Process	Present upper bound (95% C.L.)	Experiment/ Collaboration	Ref.	Future sensitivities	Experiment/ Collaboration	Ref.
$Z \to \mu e$	7.5×10^{-7}	ATLAS	[114]	4.1×10^{-7}	LHC	[116]
$Z \to \tau e$	9.8×10^{-6}	OPAL	[112]	3.5×10^{-6}	LHC	[116]
$Z \to \tau \mu$	1.2×10^{-5}	DELPHI	[113]	3.5×10^{-6}	LHC	[116]
$h \to \tau \mu$	1.57×10^{-2}	CMS	[116]			
$\tau \to \mu \eta$	2.3×10^{-8}	Belle	[117]	10^{-10}	SuperB	[95]
$\tau \to \mu \eta'$	3.8×10^{-8}	Belle	[117]	10^{-10}	SuperB	[95]
$\tau \to \mu \pi^0$	2.2×10^{-8}	Belle	[117]	10^{-10}	SuperB	[95]
$B_d^0 \to \mu \tau$	2.2×10^{-5}	Babar	[118]			
$B_d^0 \to \mu e$	6.4×10^{-8}	CDF	[119]	1.5×10^{-8}	LHCb	[120]
$B_s^0 \to \mu e$	2.0×10^{-7}	CDF	[119]	6.5×10^{-8}	LHCb	[120]
$K_L^0 \to \mu e$	4.7×10^{-12}	BNL 871	[121]			

Table 2.2 – Present and expected sensitivities for some other CLFV observables.

0.12 MeV [111], so that the experimental signature of such a process is in good approximation a single mono-energetic electron with an energy $E_e \approx m_\mu \simeq 106$ MeV. This signature is very clear and far above the end-point energy of the muon decay spectrum, which is around ~52.8 MeV. The only relevant backgrounds come from muon decay in orbit (whose energy endpoint is around m_μ because of the presence of the nucleus [110]), from cosmic rays, and from beam particles. In this latter case for example, the muon may decays in flight and produce background events. In order to decrease it, future experiments will use different methods, like for example using a pulsed beam [106].

◦ **Summary**

The three kinds of processes above constitute promising way of searching for new physics. We summarize in Table 2.1 the present bounds at 95% C.L. and the expected sensitivities of the future experiments on these CLFV processes. Let's note there are also plethora of other CLFV processes that could be probed, for which we summarize in Table 2.2 the present bounds and future sensitivities and on which we will not focus on this thesis, for example :

- $Z \to \ell_\alpha \overline{\ell_\beta}$. The best bound on this process is provided by OPAL [112], DELPHI [113], and ATLAS experiments [114]. According to estimations [115], the LHC with a luminosity of 20 fb^{-1} could improve the sensitivity by a factor ~2.
- $h \to \ell_\alpha \overline{\ell_\beta}$. The best bound on this process is provided by the CMS experiment at LHC [116], which should also improve the sensitivity in the future.
- $\tau \to \mu\eta, \mu\eta', \mu\pi^0$. The best bounds on this processes are provided by the Belle experiment [117], and SuperB should improve the sensitivity by ~2 orders of magnitude [95].
- $B_{d,s}^0 \to \mu\tau, \mu e$. The best bounds on this process are provided by the Babar and the CDF experiments [118, 119]. LHCb at LHC should improve the sensitivity by a factor ~4 [120].

2.2.2 Theoretical status in the Seesaw models

It is clear that the CLFV processes represent great hope of new physics discovery. As we shown, this is on the one hand because future experiments should reach great sensitivities on their detection, and on the other hand because a multitude of theoretical models do predict them, as the Seesaw models. It is therefore very important to have the expressions of the branching ratios of these CLFV processes in each theoretical model. These have been extensively studied in the literature for all the Seesaw mechanisms. In particular, the rate of CLFV processes in type-2 Seesaw have been computed in Refs. [124, 125, 126, 127, 128], and the ones in the type-3 Seesaw in Refs. [56, 129]. Let's now focus on the rate of these processes in the type-1 Seesaw model.

- **$\ell_\alpha \to \ell_\beta \gamma$ in type-1 Seesaw**

The analytical expression of the rate $\ell_\alpha \to \ell_\beta \gamma$ in the type-1 Seesaw models, $\Gamma(\ell_\alpha \to \ell_\beta \gamma)$, is well-known [130, 131, 132, 133, 134]. Since we will need it in what follows, we show the analytical expression of the branching ratio of $\mu \to e\gamma$ (neglecting tiny corrections proportional to the electron mass) :

$$Br\left(\mu \to e\gamma\right) = \frac{\alpha_w s_w^2}{128\pi^4} \frac{G_F^2 m_\mu^5}{\Gamma_\mu} \left|G_\gamma^{\mu e}\right|^2 , \tag{2.22}$$

where $\Gamma_\mu \approx 2.996 \times 10^{-19}$ GeV is the total decay rate of the muon, and $G_\gamma^{\mu e}$ is a loop form factor whose analytical expression is given in Eq. (B.121) of Appendix B.4. The general expression for $Br(\ell_\alpha \to \ell_\beta \gamma)$ is easily obtained from the above formula by replacing $\{\mu, e\} \to \{\ell_\alpha, \ell_\beta\}$.

- **$\ell_\alpha \to \ell_\beta \ell_\gamma \overline{\ell_\delta}$ in type-1 Seesaw**

The analytical expression of the rate $\Gamma(\ell_\alpha \to \ell_\beta \ell_\gamma \overline{\ell_\delta})$ has been computed in Ref. [67]. Since we will need it below, one has for example that the branching ratio of the decay $\mu \to ee\bar{e}$ is given by :

$$\begin{aligned} Br\left(\mu \to ee\bar{e}\right) = \frac{\alpha_w^2}{12288\pi^5} \frac{G_F^2 m_\mu^5}{\Gamma_\mu} \Bigg\{ & 2\left|\frac{1}{2}F_{box}^{\mu eee} + F_Z^{\mu e} - 2s_w^2 (F_Z^{\mu e} - F_\gamma^{\mu e})\right|^2 + 4s_w^4 \left|F_Z^{\mu e} - F_\gamma^{\mu e}\right|^2 \\ & + 16 s_w^2 Re\left[(F_Z^{\mu e} + \frac{1}{2}F_{box}^{\mu eee}) G_\gamma^{\mu e *}\right] - 48 s_w^4 Re\left[(F_Z^{\mu e} - F_\gamma^{\mu e}) G_\gamma^{\mu e *}\right] \\ & + 32 s_w^4 |G_\gamma^{\mu e}|^2 \left[\ln \frac{m_\mu^2}{m_e^2} - \frac{11}{4}\right] \Bigg\} . \end{aligned} \tag{2.23}$$

The expression of the various loop form factors above are given in Eqs. (B.120)-(B.129) of Appendix B.4. The expression for $Br(\ell_\alpha \to \ell_\beta \ell_\beta \bar{\ell}_\beta)$ can be obtained by replacing $\{\mu, e\} \to \{\ell_\alpha, \ell_\beta\}$.

- **$\mu(A,Z) \to e(A,Z)$ in an nucleus ${}^A_Z\mathcal{N}$ in type-1 Seesaw**

While the expression of the branching ratio for $\ell_\alpha \to \ell_\beta \gamma$ and $\ell_\alpha \to \ell_\beta \ell_\gamma \overline{\ell_\delta}$ were well established in the type-1 Seesaw models, it was actually not the case of the $\mu \to e$ conversion rate $R_{\mu\to e}^{\mathcal{N}}$. It has been calculated in the literature for the various possible types of Seesaw : with right-

handed neutrinos in Refs. [136, 137, 138, 139, 140, 141, 142], scalar triplet(s) in Refs. [143, 144, 145] and fermion triplets in Ref. [129]. *However, for the type-1 Seesaw, a comparison of the various calculations showed that there were no agreement on what is actually the result.* This issue is also relevant for references using calculations in previous articles [145, 146]. Some of the discrepancies have a very significant impact on the predictions. Given both these experimental and theoretical situations, in this thesis, we first recalculate the $\mu \to e$ conversion rate for the type-1 Seesaw model. Subsequently we will check and compare our result with the previous calculations. The corresponding phenomenology it leads to is done in the next section 2.4.

Comments. Before going on, let's note that all the loop form factors involved in the expressions of these CLFV processes invoke the product of the mixing elements :

$$F_\gamma^{\mu e}, G_\gamma^{\mu e}, F_Z^{\mu e}, F_{box}^{\mu eee} \propto \sum_{N_i} U_{eN_i} U_{\mu N_i}^* \, f\left(m_{N_i}^2\right) \propto \sum_{N_i} \frac{Y_{N_i\mu}^*}{m_{N_i}} \frac{Y_{N_i e}}{m_{N_i}} \, f\left(m_{N_i}^2\right) , \tag{2.24}$$

where we recognize the $c_{\mu e}^{d=6}$ coefficient in Eq. (2.17), as anticipated. Note that in order to have observable rates for say $\mu \to e\gamma$, i.e. $Br(\mu \to e\gamma) \gtrsim 10^{-14}$, the combination Y_N / m_N should be roughly larger than $\sim 10^{-5}$ GeV^{-1}, or equivalently

$$Y_N \gtrsim 10^{-2} \cdot \frac{m_N}{1 \text{ TeV}} . \tag{2.25}$$

For TeV right-handed neutrino masses, this requires quite large Yukawa couplings ($Y_N \gtrsim 10^{-2}$). This could at first sight be in contradiction with the neutrino mass, which roughly requires $Y_N \sim 10^{-6} \cdot (m_N / 1 \text{ TeV})^{1/2}$ if one fixes the neutrino mass scale to $m_\nu \sim 0.1$ eV. However, we have shown in section 1.5 that the neutrino mass matrix can undergo an extra suppression in some peculiar models as the Inverse Seesaw, based on an approximate lepton symmetry, so that one can have observable rate for the CLFV processes together with small neutrino masses. Even if clearly less likely than the usual Seesaw, this offers a unique opportunity to probe the physics BSM which is presumably the most likely to exist.

2.3 $\mu \to e$ conversion rate for type-1 Seesaw models

We have derived in section 2.1 the type-1 Seesaw Lagrangian in the neutrino and charged lepton mass eigenstates, and this now allows us to compute the $\mu \to e$ conversion rate. This computation was made in collaboration with Rodrigo Alonso, Belen Gavela and Thomas Hambye [1]. Since the goal of the paper was to obtain a new formulae for the rate, one had to make sure that our result was totally correct. We therefore paid attention to take certain precautions, in particular:

1. all the steps of the computation have been cross-checked independently ;
2. several methods have been used to confirm the result, as the comparison with results obtained in the quark sector ;
3. the final result was carefully compared with the previous results, and the differences were highlighted.

Since this is a complex process that involves nuclear physics, we first present the general expression of the conversion rate, explaining briefly how to handle the nuclear part of the problem. We next present the methodology of the computation, i.e. the answer to the questions "How should we proceed ?". Finally, the different amplitudes are given, associated to the different contributions, and they are plugged in the formula that take care of nuclear physics and the final result is derived. The reader who would like to go to the original calculation of the type-1 Seesaw contribution can go directly to section 2.3.2.

2.3.1 General expression of the conversion rate and approximations

The muon interacts with a nucleus $\mathcal{N}$ by exchanging some particles with it. As Fig. 2.1 shows, the exchanged particle will probe different layers : the nucleus level, the nucleon level, and the quark level. But what is actually the typical momentum of the exchanged particle ? By making a fast analysis of the kinematics, the 4-momenta of the initial and final states are approximately given by

$$p \approx \left(m_\mu, \vec{0}\right) , \qquad p' \approx \left(m_\mu, m_\mu \vec{1}_n\right) , \tag{2.26}$$

$$p_{\mathcal{N}} \approx \left(m_{\mathcal{N}}, \vec{0}\right) , \qquad p'_{\mathcal{N}} \approx \left(m_{\mathcal{N}}, -m_\mu \vec{1}_n\right) , \tag{2.27}$$

where p and $p_{\mathcal{N}}$ are the momenta of the initial muon and nucleus state, while p' and $p'_{\mathcal{N}}$ are the momenta of the final electron and nucleus state. $\vec{1}_n$ is the direction of the outgoing electron. In Eq. (2.26)-(2.27), we assumed that the initial states are at rest, and we have neglected the mass of the electron compared to the nucleus mass $m_{\mathcal{N}}$ and muon mass m_μ. The transferred momentum is thus in good approximation given by

$$q = p - p' \approx \left(0, -m_\mu \vec{1}_n\right) . \tag{2.28}$$

Therefore, the exchanged particle probes the nucleus with an energy of the order of the muon mass, i.e. $|q|$ ~106 MeV. Since this momentum is smaller than 1 GeV, in a first approximation it doesn't probe the inner structure of the nucleons, and from this point of view the nucleons are made of 3 valence quarks, each one carrying one third of the nucleus momentum. However, as we will see, the strange quark contribution may bring significant correction. We now detail the main steps in calculating the conversion rate. We will mainly follow the approach of Ref. [153].

◦ General expression of the rate

The general expression of the rate of some nuclear transition $i \to f$ is given by Fermi's golden rule

$$\Gamma\left(i \to f\right) = 2\pi \, \rho\left(E_f\right) \left|\langle f|\mathscr{H}_{\text{eff}}|i\rangle\right|^2 . \tag{2.29}$$

where $\rho(E_f)$ is the density of final states of energy E_f and $\langle f|\mathscr{H}_{\text{eff}}|i\rangle$ is the matrix element of the effective Hamiltonian $\mathscr{H}_{\text{eff}}$ between the final and the initial states. In the present case of $\mu \to e$ conversion, this expression becomes [149]

$$\Gamma\left(\mu\mathcal{N} \to e\mathcal{N}\right) = \left(\frac{p_e E_e}{m_\mu^2}\right) \frac{1}{2} \sum_{\text{final states}} |\mathscr{M}|^2 \tag{2.30}$$

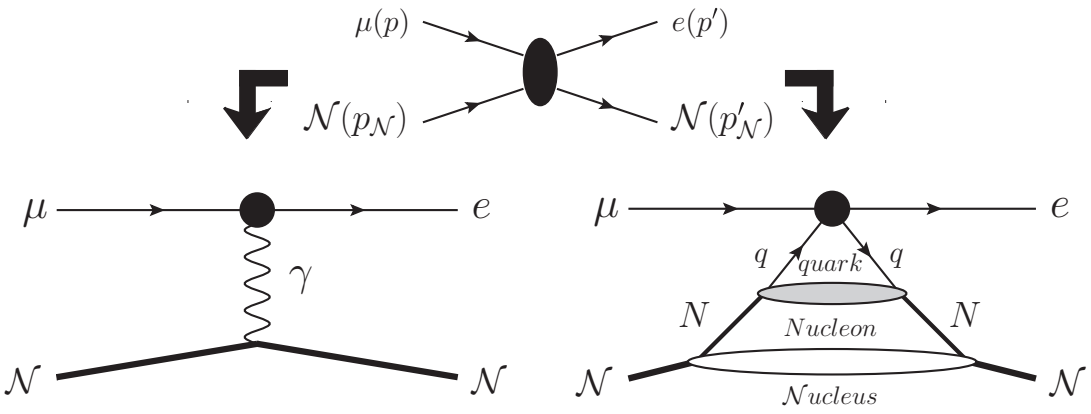

(a) Photonic contribution

(b) Non-photonic contribution

Figure 2.1 – Photonic and non-photonic contributions to the nuclear $\mu \to e$ conversion process. In the first case, the conversion occurs via an interaction with the electromagnetic field of the nucleus. In the second case, the muon interacts with one quark q of a nucleon N, which constitutes one part of the total nucleus $\mathcal{N}$.

where the factor $(p_e E_e / m_\mu^2)$ involves the density of the final states, such that the electron wave packet is well normalized (the factor 2π is absorbed in this normalization). From Eq. (2.26), one has that $(p_e E_e / m_\mu^2) \approx 1$. The muon bound state wave function is normalized to unity, and we also averaged on the initial spin and summed over the final states of the electron. The interacting Hamiltonian is related to the effective Lagrangian through

$$\mathcal{M} = \langle e, \mathcal{N} | \mathcal{H}_{\text{eff}} | \mu, \mathcal{N} \rangle = -\int d^3x \, \langle e, \mathcal{N} | \mathcal{L}_{\text{eff}} | \mu, \mathcal{N} \rangle \, . \tag{2.31}$$

In any general model, one can compute the effective Lagrangian at the quark level. Once this is done, one needs to compute the matrix element in Eq. (2.31) at the nucleus level. This pathway, of going to the quark to the nucleus level, involves nuclear physics and has been studied in details, see e.g. Refs. [147, 148, 149, 150, 151, 152, 153]. Here are the main steps.

At the quark level. The 4-fermions interaction of the $\mu \to e$ conversion is described by an effective Lagrangian $\mathcal{L}_{\text{eff}}$. For a rigorous calculation of the rate, it is necessary to separate the local contributions from the long-ranged ones. This stems from the fact that long-ranged contributions, unlike local ones, are sensitive to the atomic electric field effect. The Lagrangian contains therefore two distinct parts, respectively called usually "photonic" (long-ranged) contribution and "non-photonic" (local) contribution [147, 150, 151, 153]

$$\mathcal{L}_{\text{eff}} = \mathcal{L}_{\text{phot}} + \mathcal{L}_{\text{non-phot}} \, . \tag{2.32}$$

The general form of the photonic part is given by

$$\mathcal{L}_{\text{phot}} = -\frac{4G_F}{\sqrt{2}} \left(m_\mu A_R \bar{\mu} \sigma^{\alpha\beta} P_L e F_{\alpha\beta} + m_\mu A_L \bar{\mu} \sigma^{\alpha\beta} P_R e F_{\alpha\beta} + \text{H.c.} \right) , \tag{2.33}$$

where the coefficients $A_{R,L}$ are model-dependent. This part describes the interaction with the electromagnetic field of the nucleus. The non-photonic part is generically given by

$$\begin{aligned}\mathscr{L}_{\text{non-phot}} = -\frac{G_F}{\sqrt{2}} \sum_{q=u,d,s} \Big[& \left(g_{LS(q)}\, \bar{e} P_R \mu + g_{RS(q)}\, \bar{e} P_L \mu\right)\, \bar{q}\, q \\ & + \left(g_{LP(q)}\, \bar{e} P_R \mu + g_{RP(q)}\, \bar{e} P_L \mu\right)\, \bar{q}\, \gamma_5 q \\ & + \left(g_{LV(q)}\, \bar{e} \gamma^\alpha P_L \mu + g_{RV(q)}\, \bar{e} \gamma^\alpha P_R \mu\right)\, \bar{q}\, \gamma_\alpha q \\ & + \left(g_{LA(q)}\, \bar{e} \gamma^\alpha P_L \mu + g_{RA(q)}\, \bar{e} \gamma^\alpha P_R \mu\right)\, \bar{q}\, \gamma_\alpha \gamma_5 q \\ & + \frac{1}{2}\left(g_{LT(q)}\, \bar{e} \sigma^{\alpha\beta} P_R \mu + g_{RT(q)}\, \bar{e} \sigma^{\alpha\beta} P_L \mu\right)\, \bar{q}\, \sigma_{\alpha\beta} q + \text{H.c.}\Big] \,, \end{aligned} \tag{2.34}$$

and describes the interactions with the quarks of the nucleus. Following our conventions, $F_{\mu\nu} = \partial_\mu A_\nu - \partial_\nu A_\mu$ and $\sigma_{\mu\nu} = (i/2)[\gamma_\mu, \gamma_\nu]$. The various $g_{LX(q)}$ and $g_{RX(q)}$ are coefficients that need to be determined for each specific model. Here, X stand for S, P, V, A, T, respectively denoting scalar (S), pseudo-scalar (P), vector (V), axial-vector (A) and tensor (T) interactions.

At the nucleon level. Once the effective Lagrangian at the quark level has been computed in a given model, it must be sandwiched in nucleon matrix elements to rewrite the Lagrangian in terms of the nucleon fields (also called "hadronization"). It has been shown in Refs. [154, 148, 155] that this can be done by replacing the quark currents $\bar{q}\, \Gamma_X\, q$, where Γ_X stands for $\{1, \gamma_5, \gamma_\mu, \gamma_\mu\gamma_5, \sigma_{\mu\nu}\}$, by the corresponding nucleon currents :

$$\langle N | \bar{q}\, \Gamma_X\, q | N \rangle = G_X^{(q,N)}\, \bar{\Psi}_N\, \Gamma_X\, \Psi_N \,, \tag{2.35}$$

where Ψ_N stands for the wave functions of $N = p, n$ and $G_X^{(q,N)}$ are nuclear form factors, which have been determined for example in Refs. [148, 152, 156, 153]. Since the typical momentum transferred by the current is of the order of the muon mass which is small compared to typical nucleon structure scales ~ 1 GeV, see Eq. (2.28), the q^2 dependence of the nucleon form factors $G_X^{(q,N)}$ can be neglected. In the limit in which strong isospin is a good symmetry, that is up to terms proportional to the up and down mass difference, the neutron and proton form factors are related through

$$G_X^{(u,p)} = G_X^{(d,n)} \,, \quad G_X^{(u,n)} = G_X^{(d,p)} \text{ and } \quad G_X^{(s,p)} = G_X^{(s,n)} \,. \tag{2.36}$$

It can be shown that only the scalar and vector contributions do actually contribute to the coherent transition rate. This stems from the fact that the axial, pseudo-scalar and tensor nucleon currents couple to the nuclear spin and therefore to incoherent contributions. [2] As a consequence, we will neglect these latter in what follows. The scalar and vector form factors have been computed in Refs. [152, 156, 153] and are given by

$$G_S^{(u,p)} = G_S^{(d,n)} \approx 5.1\,(3.74) \,, \quad G_S^{(d,p)} = G_S^{(u,n)} \approx 4.3\,(2.69) \,, \quad G_S^{(s,p)} = G_S^{(s,n)} \approx 2.5\,(0.64) \,, \tag{2.37}$$

$$G_V^{(u,p)} = G_V^{(d,n)} = 2 \,, \quad G_V^{(d,p)} = G_V^{(u,n)} = 1 \,, \quad G_V^{(s,p)} = G_V^{(s,n)} = 0 \,. \tag{2.38}$$

[2] As previously mentioned, the coherent conversion process, in which the final state of the nucleus is the same as the initial one, gives generally a larger contribution than incoherent one approximately by a factor of the mass number of the target nuclei. We will consider only the coherent process in what follows.

The scalar form factors have been extracted from the baryon octet B mass spectrum, in combination with the data on the pion-nucleon scattering [152]. We show in bracket the smaller values obtained in Ref. [157], in which another method was used. Clearly, scalar nucleon form factors contain appreciable theoretical and experimental uncertainties. Conservation of vector current implies that the vector charge is equal to the number of valence quarks of the nucleon. From Eq. (2.37), one sees that the strange quarks of the nucleon sea can significantly contribute to the scalar nucleon form factor, so the first approximation of considering only valence quarks in the process is actually not so good, and one needs to take into account the strange quark contribution. However, as we will see below, only vector current receives a contribution in the type-1 Seesaw so that the strange quark will finally not contribute to the conversion rate.

At the nucleus level. The matrix element of the effective Hamiltonian with respect to the nucleus states is given by Eq. (2.31). From the above general Lagrangian in Eqs. (2.32)-(2.34) together with Eq. (2.35), we see that the matrix element can be divided in two contributions : a leptonic and a nucleonic part. So once the Lagrangian is known in a given model in terms of nucleon fields, it must still be sandwiched in the lepton and nucleus matrix elements. This will allow to rewrite the Lagrangian in terms of lepton fields and nucleon densities. The leptonic part contains matrix elements as $\langle e|\bar{e}\,\Gamma_X\,\mu|\mu\rangle$, which will give :

$$\langle e|\bar{e}\,\Gamma_X\,\mu|\mu\rangle = \bar{\Psi}_e(\vec{r})\,\Gamma_X\,\Psi_\mu(\vec{r})\,, \tag{2.39}$$

where $\Psi_e(\vec{r})$ and $\Psi_\mu(\vec{r})$ are the wave functions of the electron and the muon respectively. The initial muon state is the $1s$ state of the muonic atom, and the final electron state is a a plane wave with an energy $E_e \simeq m_\mu$, see Eq. (2.21). The wave function of the muon state can be determined by solving the Dirac equations in the electric field of the nucleus [153].

From Eq. (2.35), the nuclear part contains elements as $\langle\mathcal{N}|\bar{\Psi}_N\,\Psi_N|\mathcal{N}\rangle$ and $\langle\mathcal{N}|\bar{\Psi}_N\,\gamma_\mu\,\Psi_N|\mathcal{N}\rangle$. Since the nucleus $\mathcal{N} = (A,Z)$ contains Z protons and $A-Z$ neutrons, these nuclear matrix elements give [153, 158]

$$\langle\mathcal{N}|\bar{\Psi}_p\,\Psi_p|\mathcal{N}\rangle = Z\,\rho_p\,, \tag{2.40}$$
$$\langle\mathcal{N}|\bar{\Psi}_n\,\Psi_n|\mathcal{N}\rangle = (A-Z)\,\rho_n\,, \tag{2.41}$$
$$\langle\mathcal{N}|\bar{\Psi}_p\,\gamma^0\,\Psi_p|\mathcal{N}\rangle = Z\,\rho_p\,, \tag{2.42}$$
$$\langle\mathcal{N}|\bar{\Psi}_n\,\gamma^0\,\Psi_n|\mathcal{N}\rangle = (A-Z)\,\rho_n\,, \tag{2.43}$$
$$\langle\mathcal{N}|\bar{\Psi}_N\,\gamma^i\,\Psi_N|\mathcal{N}\rangle = 0\,, \tag{2.44}$$

where $\rho_p(\vec{r})$ and $\rho_n(\vec{r})$ are the proton and neutron densities of the nucleus. In good approximation the nucleus is spherically symmetric, and these densities are normalized as

$$\int_0^\infty 4\pi r^2 dr\;\rho_{p,n}(r) = 1\,. \tag{2.45}$$

The matrix element of spatial components of the vector current is proportional to the velocities of the constituents and is negligible in the present problem. The time component of the vector current counts the number of nucleons in the nucleus.

Summary. All in all, we can use the different results in Eq. (2.31)-(2.35),(2.39)-(2.44), to derive the final form of the matrix element, which reads

$$\mathcal{M} = \mathcal{M}_{\text{phot}} + \mathcal{M}_{\text{non-phot}} \tag{2.46}$$

where

$$\mathcal{M}_{\text{phot}} = \frac{4G_F}{\sqrt{2}} m_\mu \int d^3r \left(A_R^* \bar{\Psi}_e \sigma^{\alpha\beta} P_R \Psi_\mu + A_L^* \bar{\Psi}_e \sigma^{\alpha\beta} P_L \Psi_\mu \right) \langle \mathcal{N} | F_{\alpha\beta}(\vec{r}) | \mathcal{N} \rangle \,, \tag{2.47}$$

and

$$\begin{aligned} \mathcal{M}_{\text{non-phot}} = & \frac{G_F}{\sqrt{2}} \sum_{q=u,d,s} \int 4\pi r^2 dr \Bigg[\\ & \left(g_{LS(q)} \bar{\Psi}_e \quad P_R \Psi_\mu + g_{RS(q)} \bar{\Psi}_e \quad P_L \Psi_\mu \right) \left(Z G_S^{(q,p)} \rho_p + (A-Z)\, G_S^{(q,n)} \rho_n \right) \\ & + \left(g_{LV(q)} \bar{\Psi}_e \gamma^0 P_L \Psi_\mu + g_{RV(q)} \bar{\Psi}_e \gamma^0 P_R \Psi_\mu \right) \left(Z G_V^{(q,p)} \rho_p + (A-Z)\, G_V^{(q,n)} \rho_n \right) \Bigg] . \end{aligned} \tag{2.48}$$

The form factors $G_{S,V}^{(q,N)}$ are given in Eq. (2.37)-(2.38). The matrix element $\langle \mathcal{N} | F_{\alpha\beta}(\vec{r}) | \mathcal{N} \rangle$ in Eq. (2.47) has still to be determined. Assuming that the electric field of the nucleus is also spherically symmetric, and neglecting the contribution of the magnetic field compared to the electric one (since we assume a spherical symmetry), this element will give a contribution proportional to the total electric field of the nucleus $E(r)$.

The transition rate of the coherent conversion is given by Eq. (2.30). After squaring the amplitude, averaging on the initial muon spin and summing over the final states of the electron, the branching ratio $R_{\mu\to e}^{\mathcal{N}}$, defined in Eq. (2.20) as the final conversion rate over the capture rate $\Gamma_{\text{capt.}}^{\mathcal{N}}$, reads [153]

$$\begin{aligned} R_{\mu\to e}^{\mathcal{N}} = \frac{2G_F^2\, m_\mu^5}{\Gamma_{\text{capt.}}^{\mathcal{N}}} \Big[& \left| A_R^* D + \tilde{g}_{LS}^{(p)} S^{(p)} + \tilde{g}_{LS}^{(n)} S^{(n)} + \tilde{g}_{LV}^{(p)} V^{(p)} + \tilde{g}_{LV}^{(n)} V^{(n)} \right|^2 \\ & + \left| A_L^* D + \tilde{g}_{RS}^{(p)} S^{(p)} + \tilde{g}_{RS}^{(n)} S^{(n)} + \tilde{g}_{RV}^{(p)} V^{(p)} + \tilde{g}_{RV}^{(n)} V^{(n)} \right|^2 \Big] , \end{aligned} \tag{2.49}$$

where we defined

$$\tilde{g}_{LS,RS}^{(p)} = \sum_q G_S^{(q,p)} g_{LS,RS(q)} \,, \qquad \tilde{g}_{LS,RS}^{(n)} = \sum_q G_S^{(q,n)} g_{LS,RS(q)} \,, \tag{2.50}$$

$$\tilde{g}_{LV,RV}^{(p)} = \sum_q G_V^{(q,p)} g_{LV,RV(q)} \,, \qquad \tilde{g}_{LV,RV}^{(n)} = \sum_q G_V^{(q,n)} g_{LV,RV(q)} \,. \tag{2.51}$$

In Eq. (2.49), D, $S^{(p,n)}$ and $V^{(p,n)}$ are dimensionless overlap integrals. More precisely, D is a spatial integral involving the lepton fields and the electric field $E(r)$ of the nucleus, and $S^{(p,n)}$ and $V^{(p,n)}$ are spatial integrals involving the lepton fields and the nucleon densities $Z\rho_p$ and $(A-Z)\rho_n$. We won't write their analytical expressions here for shortness, but these can be found in Ref. [153]. Let's however discuss how one can evaluate them numerically.

Nucleus ${}^{A}_{Z}\mathcal{N}$	D	$S^{(p)}$	$V^{(p)}$	$S^{(n)}$	$V^{(n)}$	$\Gamma^{\mathcal{N}}_{\text{capt.}}$ $(10^6 s^{-1})$
${}^{27}_{13}$Al	0.0357	0.0153	0.0159	0.0163	0.0169	0.7054
${}^{48}_{22}$Ti	0.0870	0.0371	0.0399	0.0462	0.0495	2.59
${}^{197}_{79}$Au	0.167	0.0523	0.0859	0.0610	0.108	13.07
${}^{208}_{82}$Pb	0.162	0.0495	0.0838	0.0575	0.107	13.45

Table 2.3 – Nuclear form factors and capture rates for various nuclei. For Aluminum, Gold and Lead the overlap integrals have been obtained using neutron distributions from pionic atom experiments [161]. For Titanium the values have been obtained using neutron distributions from polarized proton scattering data [162, 163].

In order to evaluate these overlap integrals, the proton and the neutron densities are needed. While the proton density is precisely determined from electron scattering experiments [159, 160], the neutron distribution is less known. There are therefore two main sources of uncertainty in the calculation of the transition rate : (i) the scalar form factors in Eq. (2.37) and (ii) the neutron density. This latter uncertainty has been carefully discussed in Ref. [153], where several approaches have been reviewed to determine the neutron density, and to compute the overlap integrals. Whenever data from polarized proton scattering exists, the uncertainty on the overlap integrals $S^{(p,n)}$ and $V^{(p,n)}$ can be reduced to a few percent. Otherwise, it should be considered to be of the order of ~10%.

Numerical estimations of the overlap integrals can be found in Ref. [153]. We show in Table 2.3 their values for various relevant nuclei used in experiments. [3] For Aluminum, Gold, and Lead, the values have been obtained using pionic atom experiments [161], while for Titanium the values have been obtained from polarized proton scattering data [162, 163]. We also include in this table the associated muon capture rate found in Ref. [164]. Let's note that future experiments like AlCap aim to provide precision measurements of the products of nuclear capture on Aluminum, which is the target material for both COMET and Mu2e [165]. Also, improved knowledge of the neutron distribution in nuclei should improve the overlap integral values.

◦ Light nuclei approximation

Following Ref. [153], an approximation consists in taking the neutron density to be the same as the proton density $\rho_p = \rho_n$. For light nuclei, this is a good approximation because the number of neutrons and protons are approximately equal. We show in Fig. 2.2 from Ref. [153] the values of D, $S^{(p,n)}$ and $V^{(p,n)}$ obtained using this assumption. We see that for $Z \lesssim 30$, one has in good approximation that $S^{(n)} \simeq V^{(n)}$ and $S^{(p)} \simeq V^{(p)} \simeq D/8e$. If, in addition, we neglect the relativistic effect of the muon bound state and we replace the muon wave function by its average value in the nuclei, the conversion rate doesn't depend on the details of the neutron distribution, and the overlap integrals can be expressed as

$$V^{(p)} \approx S^{(p)} \approx \frac{1}{8\pi}\langle\phi_\mu\rangle\, F_p\, Z \;, \quad V^{(n)} \approx S^{(n)} \approx \frac{1}{8\pi}\langle\phi_\mu\rangle\, F_p\, (A-Z) \;, \quad D \approx 8eV^{(p)} \,, \tag{2.52}$$

[3] The normalization of the overlap integrals used here is not the same than the one in Ref. [153]. The two differ by a factor $m_\mu^{5/2}$.

Nucleus ${}^{A}_{Z}\mathcal{N}$	D	$S^{(p)}$	$V^{(p)}$	$S^{(n)}$	$V^{(n)}$	Z_{eff}	$\lvert F_p(-m_\mu^2)\rvert$
${}^{27}_{13}$Al	0.0362	0.0155	0.0161	0.0167	0.0173	11.5	0.64
${}^{48}_{22}$Ti	0.0864	0.0368	0.0396	0.0435	0.0468	17.6	0.54
${}^{197}_{79}$Au	0.189	0.0614	0.0974	0.0918	0.146	33.5	0.16
${}^{208}_{82}$Pb	0.161	0.0488	0.0834	0.0749	0.128	34.0	0.15

Table 2.4 – Nuclear form factors in the approximation of equal densities for proton and neutron, and taking the average value of the muon wave function in the nucleus. The values are taken from Ref. [153].

where F_p is some nucleus-dependent nuclear form factor, and $\langle\phi_\mu\rangle$ is the average value of the muon wave function in the nucleus divided by $m_\mu^{3/2}$,

$$\langle\phi_\mu\rangle = \sqrt{\frac{4\alpha^3 Z_{\text{eff}}^4}{Z}}\,, \tag{2.53}$$

with Z_{eff} the effective charge of the muon in the $1s$ state, and $\alpha = e^2/4\pi$ the fine structure constant. In the light nuclei approximation, the branching ratio $R^{\mathcal{N}}_{\mu\to e}$ reads

$$R^{\mathcal{N}}_{\mu\to e} \simeq \frac{\alpha^3 F_p^2}{8\pi^2}\frac{Z_{\text{eff}}^4}{Z}\frac{G_F^2 m_\mu^5}{\Gamma^{\mathcal{N}}_{\text{capt.}}}\left[\left|8eZA_R^* + Z\left(\tilde{g}^{(p)}_{LS}+\tilde{g}^{(p)}_{LV}\right)+(A-Z)\left(\tilde{g}^{(n)}_{LS}+\tilde{g}^{(n)}_{LV}\right)\right|^2 + \left|8eZA_L^* + Z\left(\tilde{g}^{(p)}_{RS}+\tilde{g}^{(p)}_{RV}\right)+(A-Z)\left(\tilde{g}^{(n)}_{RS}+\tilde{g}^{(n)}_{RV}\right)\right|^2\right]. \tag{2.54}$$

We show in Table 2.4 the evaluation of the form factors F_q and the effective charge of the muon Z_{eff} for relevant nuclei. The values are taken from Ref. [153]. We see that for light nuclei, as Aluminum or Titanium, the values of the overlap integrals are quite similar to the ones in Table 2.3, which have been obtained using experimental neutron densities. However, this is no more the case for heavier nuclei as Gold or Lead, where both results deviate by up to $\sim 30\%$, especially concerning the neutron form factors $S^{(n)}$ and $V^{(n)}$.

Validity of the approximation. It is important to stress that, firstly, the approximation $\rho_n = \rho_p$ is not necessarily a good approximation for $S^{(n)}$ and $V^{(n)}$, as can be seen by comparing their values in Table 2.4 with the one shown in Table 2.3 obtained from experiments. Secondly, from Fig. 2.2, taking $S^{(n)} \simeq V^{(n)}$ and $S^{(p)} \simeq V^{(p)}$ is clearly not consistent for heavy nuclei with $Z \gtrsim 30$. Finally, by taking the average value of the muon wave function in the nucleus in Eq. (2.53), we assume actually that the nucleus is point-like, which is equivalent to not separate the photonic and the non-photonic contributions. When does this last approximation ceases to be valid ? To answer this question, one needs to compare the different scales of the problem [150]. The wave function of the muon bounded in the lowest orbit is characterized by the Bohr radius $r_B = (\alpha Z m_\mu)^{-1}$. This radius has to be compared with the nucleus radius, $r_{\mathcal{N}}$. Using the Fermi model, one has approximately $r_{\mathcal{N}} \approx Z^{1/3}$ fm. The nucleus can be considered as point-like only if the Bohr radius is much larger than the radius of the nucleus. The requirement $r_B \gg r_{\mathcal{N}}$ implies $Z \ll 60$. As a consequence, all in all the above expression (2.54) is valid for relatively light nuclei, typically $Z \lesssim 30$.

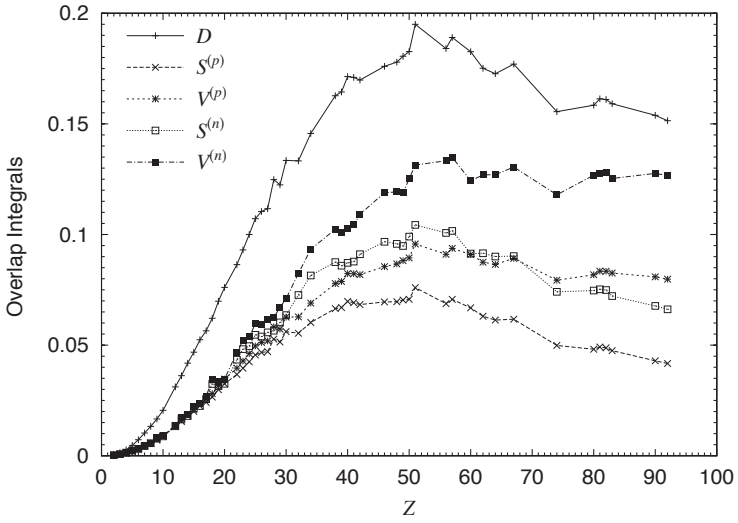

Figure 2.2 – Numerical values of the overlap integrals for various nuclei, using the approximation of equal densities for proton and neutron. The figure is taken from Ref. [153].

Comments. In Fig. 2.2 from Ref. [153] for example, we see that the values of the overlap integrals increase with Z until they reach a plateau around $Z \simeq 30$, and then decrease for $Z \gtrsim 60$. One expect therefore the conversion rate $R^{\mathcal{N}}_{\mu\to e}$ to be larger for nuclei with $Z \in [30,60]$. However, as seen previously in for example Table 2.1, future experiments plan to use Aluminum and Titanium nuclei, which have $Z = 13$ and $Z = 22$ respectively. Why ? The reason is the background reduction. First, the larger the Z, the smaller the Bohr radius r_B, and the larger is the capture rate. As a consequence, the muon in heavy nuclei has a shorter lifetime than in light nuclei, as can be seen in Table 2.3. This is not convenient experimentally because long lifetimes are required in order to eliminate the beam-related background. Secondly, the smaller the binding energy, the farther the electron energy is in the tail of the energy spectrum of the background. Since the binding energy increases with Z, light nuclei are again favored. This is why future experiments will use Aluminum and Titanium nuclei.

2.3.2 Methodology

How should we proceed ? From previous section, the methodology to follow is the following.

1. One needs to compute the effective Lagrangian at the quark-level in Eqs. (2.32)-(2.34), in order to derive the $g_{X(q)}$ coefficients and so the final result in Eq. (2.49). Starting from the general type-1 Seesaw Lagrangian in Eqs. (2.10)-(2.14), this is achieved by computing the amplitudes of the processes $\mu q \to e q$, to get the photonic and non-photonic parts.

2. The result must be verified. Several methods can be use to check the amplitudes and their relative factors. Also, several papers have provided other methods to get the conversion rate, which are generally approximations of the result presented in Eq. (2.49), as the one in Eq. (2.54). Finally, our result is compared with the various one obtained previously in the literature, and the origin of the inconsistencies are traced back.

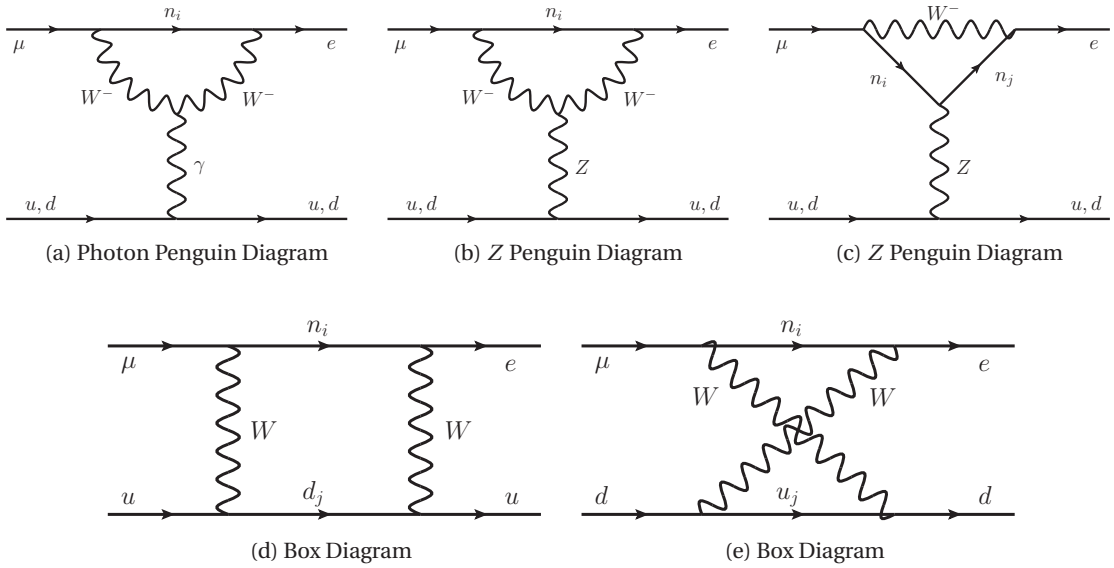

(a) Photon Penguin Diagram (b) Z Penguin Diagram (c) Z Penguin Diagram

(d) Box Diagram (e) Box Diagram

Figure 2.3 – The five classes of diagrams contributing to $\mu \to e$ conversion in the type-1 Seesaw model.

2.3.3 Computation of the rate in type-1 Seesaw models

◦ **Amplitudes**

In the type-1 Seesaw framework, violation of charged lepton number arises at the one loop level, as was anticipated in section 2.2. The $\mu \to e$ conversion is induced by a series of gauge boson mediated diagrams given in Fig. 2.3. The various contributions to the process can be divided in those in which the momentum is transferred by the photon, by the Z boson or via two W bosons. The first two proceed via penguin diagrams, whereas the latter proceeds via box diagrams. Alike to the quark case, the internal fermions in the loop must have non-degenerate masses and non trivial mixings, in order to avoid a GIM cancellation.

The detailed amplitudes associated to all the different parts of the process are given in Appendix B. In order to simplify the computation, we fixed the gauge $\xi = 1$, i.e. we went in the Feynman-t'Hooft gauge. [4] The only approximations used in our calculation are to neglect : i) the electron mass compared to the muon mass ; ii) higher orders in the external momentum over the W mass ; iii) the value of the three light neutrino masses compared to the heavier ones. [5] The first two approximations are accurate at a level better than $\mathcal{O}(10^{-4})$, that is to say better that what can be expected from higher loop contributions, and much better than the uncertainties on the nuclear form factors. The third approximation becomes excellent as soon as the right-handed neutrino masses are a few orders of magnitude above the light neutrino masses. We next show the contributions to the amplitude from the photon and then from the W and Z bosons.

[4] For specific diagrams, as the boxe ones, we made a computation of the amplitudes without fixing the gauge, in order to have supplementary check of the consistency of the result.

[5] This latter approximation is not made in the first equality of Eqs. (B.120)-(B.129), only in the second equality of these equations. One could therefore use those results for any value of the right-handed neutrino masses.

Note that, as we have seen in the previous section, for a rigorous calculation of the rate it is necessary to separate the local contributions (non-photonic) from the long-ranged (photonic) ones. This stems from the fact that long-ranged contributions, unlike the local ones, are sensitive to atomic electric field effects. The W and Z mediated diagrams are obviously all local. The γ-mediated diagrams contribute in fact to both classes of transitions, local and long-ranged. The word "photonic" must therefore be understood for long-ranged interactions, and not for all the QED contributions.

Photon contribution. The contribution from the photon exchange has a common basis with the $\mu \to e\gamma$ process. It is computed in Appendix B.3.2. The general matrix element of the $\mu \to e\gamma$ process can be written as

$$i\mathcal{M}_\gamma = \frac{ieg^2}{2(4\pi)^2 m_W^2}\epsilon_\lambda^\alpha(q)\overline{u}_e(p')\Big[F_\gamma^{\mu e}(q^2\gamma_\alpha - \not{q}q_\alpha)P_L - i\sigma_{\alpha\beta}q^\beta G_\gamma^{\mu e}(m_e P_L + m_\mu P_R)\Big]u_\mu(p)\,, \quad (2.55)$$

where q_α denotes the photon momentum, $q_\alpha = p_\alpha - p'_\alpha$. The analytical expressions for $G_\gamma^{\mu e}$ and $F_\gamma^{\mu e}$ can be found in Appendix B, Eqs. (B.120) and (B.121).

The second term in this equation (2.55) – mediated by the photon-lepton "dipole" $G_\gamma^{\mu e}$ coupling – is the only one contributing for an on-shell photon and is long-ranged, whereas the "monopole" term $F_\gamma^{\mu e}$ is local (i.e. it only accounts for off-shell photon exchange and it involves 2 powers of the photon momentum in the numerator which compensate the long range $1/q^2$ propagator of the photon between the lepton and nuclei lines [150]). Let's note that the $\mu \to e\gamma$ decay amplitude is obtained for on-shell photons, i.e. for $q^2 = 0$. In this case, obviously, only the dipole term survives. Therefore, the knowledge of the $\mu \to e\gamma$ amplitude, calculated long ago to determine the $\mu \to e\gamma$ branching ratio, is not sufficient. One needs to calculate the $F_\gamma^{\mu e}$ part.

In the case of $\mu \to e$ conversion, both dipole and monopole terms do contribute to the photonic and non-photonic effective Lagrangian respectively. The photonic contribution to the effective Lagrangian is given by the dipole term : [6]

$$\mathscr{L}^\gamma_{\text{phot}} = \frac{\alpha_w e m_\mu}{4(4\pi)m_W^2}\bar{e}\,G_\gamma^{\mu e}\sigma_{\alpha\beta}P_R\mu \quad F^{\alpha\beta}\,. \quad (2.56)$$

To get the non-photonic contribution from Eq. (2.55), one has to include the quark line and use the fact that the exchanged photon has momentum $q^2 = -m_\mu^2$, see Eq. (2.28). From the amplitude in Eq. (B.88) of the Appendix B.4, one gets : [7]

$$\mathscr{L}^\gamma_{\text{non-phot}} = \sum_{q=u,d,s}\frac{\alpha_w\alpha}{2m_W^2}\,\bar{e}\,F_\gamma^{\mu e}\gamma_\alpha P_L\mu \quad \bar{q}\,\gamma^\alpha Q_q\,q\,, \quad (2.57)$$

where Q_q is the electric charge of the quark $q = u, d$ ($Q_u = 2/3, Q_d = -1/3$), and $\alpha_w = g^2/4\pi$.

[6] To get the effective Lagrangian from Eq. (2.55), one just has (i) to multiply the amplitude by $-i$, (ii) to replace the $\epsilon_\lambda^\alpha(q)$ by A^α, $u_\mu(p)$ by μ , and $\bar{u}_e(p')$ by $\bar{e}$, and (iii) to use the fact that $\partial_\beta A_\alpha = iq_\beta A_\alpha$.

[7] The term proportional to q_α in Eq. (2.55) drops because of quark current conservation.

Z and W contributions. These are non-local diagrams, that therefore contribute only to the non-photonic effective Lagrangian. Their contributions are obtained from the amplitudes in Eqs. (B.89)-(B.90) in Appendix B.4, and are given by

$$\mathscr{L}^{Z}_{\text{non-phot}} = \sum_{q=u,d,s} \frac{\alpha_w^2}{2m_W^2} \bar{e} F_Z^{\mu e} \gamma_\alpha P_L \mu \quad \bar{q}\gamma^\alpha \left(I_q^3 P_L - Q_q s_w^2\right) q\,, \tag{2.58}$$

$$\mathscr{L}^{W}_{\text{non-phot}} = \sum_{q=u,d,s} \frac{\alpha_w^2}{4m_W^2} \bar{e} F_{box}^{\mu eqq} \gamma_\alpha P_L \mu \quad \bar{q}\gamma^\alpha P_L q\,. \tag{2.59}$$

where I_q^3 is the weak isospin ($I_u^3 = 1/2$, $I_d^3 = I_s^3 = -1/2$) and s_w is the sinus of the weak mixing angle. The analytical expressions of $F_Z^{\mu e}$ and $F_{box}^{\mu eqq}$ for the up and down quarks can be found in Appendix B, Eqs. (B.122), (B.124) and (B.127). Let's note that, as said above, whatever the loop form factors of the strange quark, since the associated scalar nuclear form factor vanishes, the strange quark doesn't contribute to the conversion rate, so that we omit its contribution in what follows.

Final photonic and non-photonic contributions to the effective Lagrangian. Putting all the contributions together, the total photonic part of the effective Lagrangian is therefore given by Eq. (2.56),

$$\mathscr{L}_{\text{phot}} = -\frac{4G_F}{\sqrt{2}} \left[m_\mu \left(\frac{-e}{2(4\pi)^2} G_\gamma^{\mu e} \right) \bar{e}\sigma^{\alpha\beta} P_R \mu \quad F_{\alpha\beta} + \text{H.c.} \right] , \tag{2.60}$$

and the total non-photonic part is obtained by summing Eqs. (2.57)-(2.59),

$$\mathscr{L}_{\text{non-phot}} = -\frac{G_F}{\sqrt{2}} \sum_{q=u,d} \left[\left(\frac{-\alpha_w}{\pi} \right) \bar{e}\,\gamma^\alpha P_L\, \mu \quad \bar{q}\gamma_\alpha \left(V_q^{\mu e} + A_q^{\mu e}\gamma_5 \right) q + \text{H.c.} \right] , \tag{2.61}$$

where $V_q^{\mu e}$ contains the contribution of the monopole $F_\gamma^{\mu e}$ term as well as that from the weak gauge-boson exchange diagrams. The term proportional to $A_q^{\mu e}$ is an axial-vector interaction, and therefore it doesn't contribute to the coherent conversion process. One has, from Eqs. (B.92) of Appendix B.4,

$$V_q^{\mu e} = Q_q s_w^2 F_\gamma^{\mu e} + \left(\frac{I_q^3}{2} - Q_q s_w^2 \right) F_Z^{\mu e} + \frac{1}{4} F_{box}^{\mu eqq}\,, \tag{2.62}$$

$$A_q^{\mu e} = -\frac{I_q^3}{2} F_Z^{\mu e} - \frac{1}{4} F_{box}^{\mu eqq}\,. \tag{2.63}$$

The coefficients $V_q^{\mu e}$, $A_q^{\mu e}$ and $G_\gamma^{\mu e}$ encode all the dependence on the internal fermion masses and mixing angles.

◦ Expression of the $\mu \to e$ conversion rate in type-1 Seesaw models

The effects of the nuclear form factors and of the average over the atomic electric field can be taken into account in the way described in section 2.3.1. A careful comparison with Eqs. (2.33)-(2.34)

allows to make the following replacements

$$A_R^* = -\frac{e}{2(4\pi)^2}\, G_\gamma^{\mu e}\,, \quad g_{LV(q)} = -\frac{\alpha_w}{\pi}\, V_q^{\mu e}\,, \quad g_{LA(d)} = -\frac{\alpha_w}{\pi}\, A_d^{\mu e}\,. \tag{2.64}$$

From these last two correspondences, we see that only the left-handed vector and axial-vector interactions do actually contribute to the non-photonic conversion rate, i.e. only the first terms of the third and fourth line of Eq.(2.34). However, as said above, only the vector interaction do actually contribute to the coherent conversion rate. The final expression for the ratio of the coherent $\mu \to e$ conversion over the capture rate $\Gamma^{\mathcal{N}}_{\text{capt.}}$ is given by Eq. (2.49) and reads

$$\boxed{R^{\mathcal{N}}_{\mu\to e} = \frac{2\alpha_w^2}{\pi^2}\frac{G_F^2 m_\mu^5}{\Gamma^{\mathcal{N}}_{\text{capt.}}}\left|\frac{s_w^2}{8e}G_\gamma^{\mu e}\, D + \left(2V_u^{\mu e} + V_d^{\mu e}\right)V^{(p)} + \left(V_u^{\mu e} + 2V_d^{\mu e}\right)V^{(n)}\right|^2}\,. \tag{2.65}$$

The nuclear information is encoded by the D, $V^{(p)}$ and $V^{(n)}$ overlap integrals whose values are given in Table 2.3, taken from Ref. [153]. The values of $\Gamma^{\mathcal{N}}_{\text{capt.}}$ are given in the same table and come from Ref. [164]. In the following, we will use Eq. (2.65) for all numerical results.

Let's note that the comparison of this equation with the analytical expression of the decays $\mu \to e\gamma$ and $\mu \to ee\bar{e}$ in Eqs. (2.19) and (2.18), illustrates the fact that $R^{\mathcal{N}}_{\mu\to e}$, $Br(\mu \to e\gamma)$ and $Br(\mu \to ee\bar{e})$ are sensitive to different combinations of the same form factors, which contain the dimension-6 coefficient as it should.

Light nuclei approximation. For low atomic number, $Z \lesssim 30$, and for comparison with other calculations, the result can be nevertheless simplified using the approximation in Eq. (2.54), in which case the branching ratio reads

$$R^{\mathcal{N}}_{\mu\to e} \simeq \frac{\alpha_w^2\alpha^3 F_p^2}{8\pi^4}\frac{Z_{\text{eff}}^4}{Z}\frac{G_F^2 m_\mu^5}{\Gamma^{\mathcal{N}}_{\text{capt.}}}\left|Z\left(2\tilde{V}_u^{\mu e} + \tilde{V}_d^{\mu e}\right) + (A-Z)\left(\tilde{V}_u^{\mu e} + 2\tilde{V}_d^{\mu e}\right)\right|^2\,, \tag{2.66}$$

where we defined, see Eq. (B.138)-(B.139) of the Appendix B.4,

$$\tilde{V}_q^{\mu e} \equiv V_q^{\mu e} + Q_q s_w^2 G_\gamma^{\mu e}\,. \tag{2.67}$$

The values of Z_{eff} and F_p are given in Table. 2.4, taken from Ref. [153]. Since in this light nuclei approximation we do not separate the photonic and non-photonic contributions, the result in Eq. (2.66) can also be obtained taking the long range contribution proportional to $G_\gamma^{\mu e}$ to be non-photonic, in which case the effective Lagrangian reads, using Eq. (B.96)

$$\mathscr{L}_{\text{non-phot}} \simeq -\frac{G_F}{\sqrt{2}}\sum_{q=u,d}\left[\left(\frac{-\alpha_w}{\pi}\right)\bar{e}\,\gamma^\alpha P_L\,\mu \quad \bar{q}\gamma_\alpha\left(\tilde{V}_q^{\mu e} + \tilde{A}_q^{\mu e}\gamma_5\right)q + \text{H.c.}\right]\,. \tag{2.68}$$

This effective Lagrangian leads indeed to Eq. (2.66), after the replacement

$$A_R^* = 0\,, \quad g_{LV(q)} = -\frac{\alpha_w}{\pi}\, \tilde{V}_q^{\mu e}\,, \quad g_{LA(d)} = -\frac{\alpha_w}{\pi}\, \tilde{A}_d^{\mu e}\,. \tag{2.69}$$

◦ **Cross-checks and comparison with the literature**

We gather here together the result of comparing our formula with those in previous literature. These latter are most often given in the approximation of low atomic number, although the first two items below hold for the exact formulae. A number of comments can be made :

- *Sign of the G_γ contribution.* Our results agree with the sign indicated in Refs. [137, 141, 142], and is opposite to that in Refs. [138, 139]. Note that G_γ contributes both to $\mu \to e$ conversion and to $\mu \to e\gamma$ decay – see Eq. (2.22) – and the loop integrals involved can be related with analogous amplitudes in the quark sector, once the internal quark charge is switched off : this allows to check that our results are consistent with those for K transitions [166] and for $b \to s\ell^+\ell^-$ decay [167].

- *Box diagrams.* Refs. [137, 138, 139] also exhibit differences in the relative size and/or sign of the crossed and not crossed box contributions, that is, in the amplitudes resulting from the last two diagrams in Fig. 2.3. As shown in the Appendix, we obtain a -4 factor between these contributions, in agreement with for instance the quark results for $\Delta S = 2$ or $\Delta B = 2$ processes in Ref. [168], and Refs. [141, 142]. Also, we obtain half the contribution considered in Ref. [146] for all box diagrams.

- *Constant terms in the F_γ and F_Z form factors.* In the case of right-handed neutrino masses heavier than the W mass, $m_N \geq m_W$, the different form factors can be expanded as in the right-handed Eqs. (B.130)-(B.135) of Appendix B.4. The associated expressions contain constant terms and terms proportional to $\ln(m_N^2/m_W^2)$. For right-handed masses sufficiently low to result in observable $\mu \to e$ conversion rates, the constant terms are numerically competitive with logarithmic ones and cannot be neglected. We get different results for them, though, than in Ref. [142], where some of them have been neglected. On the contrary, our results agree with the full expressions for those form factors given in Ref. [67] for the computation of the $\mu \to eee$ rate, to which they also contribute, see Eq. (2.23). Furthermore, the $\mu \to e$ conversion rate has been also calculated in the framework of the supersymmetric type-1 Seesaw model in Ref. [141] ; we checked that its non-supersymmetric limit results in logarithmic terms which agree with ours, but there too the constant terms have been neglected. [8]

- *Decoupling limit.* In the limit of infinite right-handed neutrino masses and fixed Yukawa couplings, the low-energy theory is renormalizable (e.g. the Standard Model with massless left-handed neutrinos) and, in consequence, the extra singlet degrees of freedom introduced must decouple, leaving no impact on low-energy observables, see for example [169]. We have checked explicitly that this condition is indeed fulfilled by our $\mu \to e$ conversion expression, but also by all the other rates mediated by right-handed neutrinos as for example $\mu \to e\gamma$ and $\mu \to eee$. This is in disagreement with the non-decoupling behavior obtained in Ref. [145] for the $\mu \to e$ conversion rate in the type-1 Seesaw models. [9]

[8] Numerically, to neglect the constant terms for these form factors can lead to rates which can differ by several orders of magnitude in the few TeV range.

[9] The analytic expressions used in Ref. [145] are the same ones that are valid for the case of a fourth generation of quarks and leptons [170] (that is, with an active extra neutrino instead of a singlet right-handed neutrino, which cannot decouple as the remaining low-energy theory would not be renormalizable).

- *Cross-checks using other methods.* The derivation of the rate from the expression of the amplitude can also be obtained from the effective Lagrangian following methods developed in other papers. For example we can use the result obtained in Ref. [151] or in Ref. [148], where they don't separate the photonic and the non-photonic part, so that their results are strictly correct in the light nuclei approximation. We have carefully checked that their methods also provide exactly the result in Eq. (2.66).

- Finally, let's note that with respect to the results in Ref. [140], we get different coefficients for several logarithmic and constant terms.

2.4 Predictions and constraints : degenerate case

The $\mu \to e$ transition rates expected in the type-1 Seesaw framework are clearly highly model dependent. For right-handed neutrino masses above the eV scale – as those considered in this work – for which the Seesaw approximation $U_{\nu N} \sim Y_N^\dagger \, \mathrm{v}/m_N$ in Eq. (2.8) holds – they scale in particular as the inverse of the right-handed neutrino masses at the fourth power, and contain four Yukawa couplings in the numerator, [10] bringing each one a flavor dependence. Nevertheless, it turns out that the models which can naturally give measurable rates are models which involve two or more quasi-degenerate right-handed neutrinos and for these models one can make remarkably clear predictions. The quasi-degenerate case is particularly natural, as it takes place for instance in scenarios in which lepton number (L) is approximately conserved [59, 57, 60, 61, 62, 63, 64, 65, 56, 66, 67, 68] : the degeneracy is protected by the symmetry. This assumption allows a natural decoupling between large Yukawa couplings (inducing L-preserving large rates) and small Yukawa couplings (guaranteeing small neutrino masses) and results in viable scenarios, even for low Seesaw scales. In other words, large Yukawa couplings to get large CLFV rates goes with quasi-degeneracy. This class of models is generically called Inverse Seesaw models [57, 58], which have been introduced in section 1.5.

For this quasi-degenerate case, we have found that the model lead to remarkable predictions. These predictions hold for the ratios of two rates where a same flavor transition occurs, for example $R^{\mathcal{N}}_{\mu\to e}/Br(\mu \to e\gamma)$ or $R_{\mu\to e}/Br(\mu \to eee)$. The point is simply that if at least two right-handed neutrinos are quasi degenerate, only one right-handed neutrino mass scale is relevant in the rates and the dependence on the elements of the mixing matrix (which contain the Yukawa dependence) factorizes from the mass dependence. For instance, for $m_{N_1} \simeq m_{N_2} \simeq ... \equiv m_N$, the rates in Eq. (2.65) for $\mu \to e$ conversion takes the factorized form

$$R^{\mathcal{N}}_{\mu\to e} \simeq \frac{2\alpha_w^2}{\pi^2} \frac{G_F^2 m_\mu^5}{\Gamma^{\mathcal{N}}_{\text{capt.}}} \left[\frac{s_w^2}{8e} G_\gamma \, D + (2V_u + V_d)\, V^{(p)} + (V_u + 2V_d)\, V^{(n)} \right]^2 \left| \sum_i^{n_N} U_{eN_i} U^*_{\mu N_i} \right|^2 , \quad (2.70)$$

[10] In this phenomenology section, higher orders in Yukawa couplings will be neglected, assuming a perturbative expansion holds, although this might not be the case for couplings larger than unity [141, 67]. This assumption is required for the factorization of the Yukawa (mixing) structure in the rates and the simple relations that follow as discussed below.

and Eq. (2.22) for $\mu \to e\gamma$ factorizes as

$$Br(\mu \to e\gamma) \simeq \frac{\alpha_w s_w^2}{128\pi^4} \frac{G_F^2 m_\mu^5}{\Gamma_\mu} G_\gamma^2 \left| \sum_i^{n_N} U_{eN_i} U_{\mu N_i}^* \right|^2 , \tag{2.71}$$

where $G_\gamma(x_N)$, $V_u(x_N)$ and $V_d(x_N)$ are functions of $x_N \equiv m_N^2/m_W^2$ given in Appendix B.4, Eqs. (B.99), (B.136) and (B.137). *In consequence, the flavor dependence in the mixing parameters drops in the ratio of both rates, leaving only a dependence on the mass m_N of the heavy neutrinos* [171] :

$$R_{\mu\to e\gamma}^{\mu-e(\mathcal{N})}(x_N) \equiv \frac{R_{\mu\to e}^{\mathcal{N}}}{Br(\mu\to e\gamma)} = \frac{256\pi^2\alpha_w}{s_w^2} \frac{\Gamma_\mu}{\Gamma_{\text{capt.}}^{\mathcal{N}}} \left[\frac{\frac{s_w^2}{8e} G_\gamma\, D + (2V_u + V_d)\, V^{(p)} + (V_u + 2V_d)\, V^{(n)}}{G_\gamma} \right]^2 . \tag{2.72}$$

Note that the cancellation of the mixing parameters dependence in the ratio is valid at the dominant order in the mixing angle expansion, that is to say that in Eqs. (2.71)-(2.72) we neglected terms which involve four insertions of light-heavy mixing in the amplitudes, see Eqs. (B.130)-(B.135) in Appendix B.4. This approximation is justified for the range of low right-handed neutrino masses we contemplate (i.e. m_N from 10^{-2} GeV to m_W) in view of the experimental constraints on the mixing, whereas for the large mass regime (i.e. m_N above m_W) it relies on the perturbativity of the Yukawa couplings.

In this first phenomenological section, we will show the predictions concerning the ratios of rates in the case where all the heavy neutrinos are degenerate. The result can in particular be applied to the Inverse Seesaw models, where two right-handed neutrino are quasi-degenerate and the third one provides tiny contribution to the CLFV rates, since it has very small mixings, see Eq. (1.51) in section 1.5. The non-degenerate case is analyzed in next section 2.5 below.

2.4.1 Ratios of rates involving one same flavour transition

If all the heavy neutrinos are degenerate, $m_{N_1} \simeq m_{N_2} = ... \equiv m_N$, the expressions in Eqs. (2.22), (2.23) and (2.65) allow to compare the relative strength of $\mu \to e$ conversion to the $\mu \to e\gamma$ branching ratio, $R_{\mu\to e\gamma}^{\mu-e(\mathcal{N})}$, and to the $\mu \to eee$ branching ratio, $R_{\mu\to eee}^{\mu-e(\mathcal{N})}$. As explained above, these ratios depend only on the right-handed neutrino mass scale m_N (at leading order in $Y_N\, v/M_N$). The results are illustrated in Fig. 2.4 as a function of m_N for various nuclei, in the large m_N regime. [11]

We see that the ratios to $\mu \to e\gamma$ and $\mu \to eee$ for Titanium, Gold and Lead fall on top of each other. Numerically the agreement holds at the % level. This is due to the conversion ratio $R_{\mu e}^{\mathcal{N}}$ in these nuclei being approximately equal, at the percent level (modulo possible nuclear physics uncertainties). The ratios entering this quantity vary from atom to atom solely through the square of the variables $V^{(p)}, V^{(n)}, D$ divided by $\Gamma_{\text{capt.}}^{\mathcal{N}}$, see Eq. (2.65), which differ by about 10% for Lead versus Titanium, and similarly for Gold for instance, see Table 2.3. But the combination in which these variables enter in Lead, Titanium and Gold, via the form factors $V_{u,d}^{\mu e}, G_\gamma^{\mu e}$ in Eq. 2.65,

[11] For $m_N \approx 100$ GeV, we get $R_{\mu\to e}^{Ti} \approx 6.9 \cdot Br(\mu \to e\gamma)$ and $Br(\mu \to eee) \approx 0.033 \cdot Br(\mu \to e\gamma)$. The first result differs numerically by two orders of magnitude with Eq. (3.21) of Ref. [142], by a factor 4 with the value we get from the analytic formulas of Refs. [142, 141], and by a factor 45 from the value we get from the analytic formula given in Ref. [139].

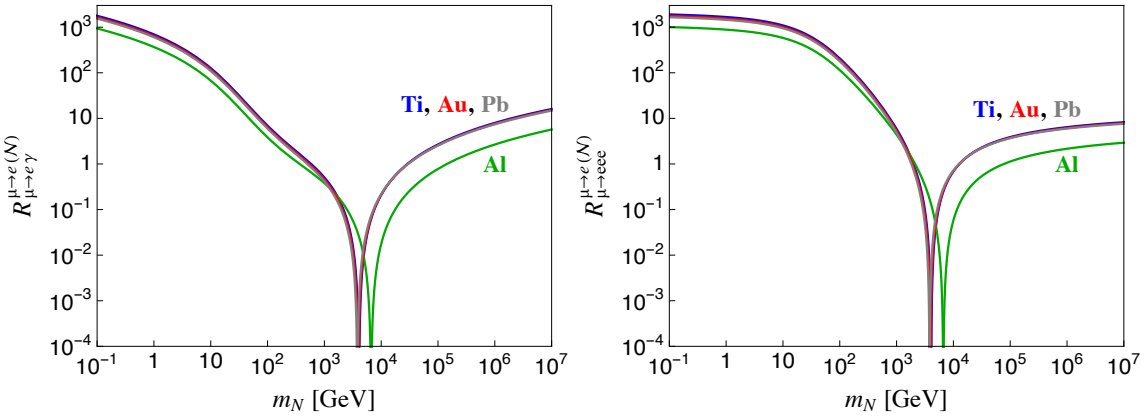

Figure 2.4 – $R^{\mu\to e(\mathcal{N})}_{\mu\to e\gamma} = R^{\mathcal{N}}_{\mu\to e}/Br(\mu\to e\gamma)$ (left panel) and $R^{\mu\to e(\mathcal{N})}_{\mu\to eee} = R^{\mathcal{N}}_{\mu\to e}/Br(\mu\to eee)$ (right panel) as a function of the right-handed neutrino mass scale m_N, for $\mu\to e$ conversion in various nuclei.

happens to be very close numerically. The coincidence at the % level of the $\mu\to e$ conversion ratios $R^{\mathcal{N}}_{\mu e}$ in Titanium, Gold and Lead in all the mass range is a prediction of the quasi-degenerate right-handed neutrino scenario. It is worth noting that the future experiment's choice of using Titanium and Aluminum is nicely not redundant, since the present scenario provides very different predictions .

One distinctive feature of these ratios is that they vanish for some value of m_N, when the $\mu\to e$ conversion rate in Eq. (2.65) vanishes. This peculiar feature is due to the up quark $V^{\mu e}_u$ and down quark $V^{\mu e}_d$ contributions in Eq. (2.65), having opposite signs as an outcome of their different charge and weak isospin, as can be seen from Eq. (2.62). The value where the $\mu\to e$ conversion rate vanishes is nuclei-dependent and, in the limit where $m_N \gg m_W$, it is given by

$$m_N^2\Big|_0 = m_W^2 \exp\left(\frac{\frac{9}{8}V^{(n)} + \left(\frac{9}{8}+\frac{37s_w^2}{12}\right)V^{(p)} - \frac{s_w^2}{16e}D}{\frac{3}{8}V^{(n)} + \left(\frac{4s_w^2}{3}-\frac{3}{8}\right)V^{(p)}}\right). \tag{2.73}$$

This shows that small variations on the nuclear form factor (i.e. the overlap integrals) may result in sizable variations on the value of $m_N^2|_0$, which is therefore sensitive to the nuclear physics uncertainties. The uncertainty in the ratio $V^{(p)}/V^{(n)}$ translates, for instance for 5-10% variations, into $\mathcal{O}$(TeV) shifts on the value of the right-handed neutrino mass at which the conversion rate vanishes. With the overlap integral values given in Table 2.3, the rate vanishes for mass values typically in the 2-7 TeV range, respectively 6.6, 4.1, 4.0 and 3.8 TeV for Al, Ti, Au and Pb respectively, as Fig. 2.5 shows. [12]

The left panel of Fig. 2.6 depicts the ratio $R^{Ti}_{\mu\to e}/R^{Al}_{\mu\to e}$. Sweeping over increasing m_N values, the ratio first vanishes when $R^{Ti}_{\mu\to e}$ does, and later goes to infinity when $R^{Al}_{\mu\to e}$ vanishes. On the right panel, we show the ratios $Br(\ell_\alpha\to\ell_\beta\gamma)/Br(\ell_\alpha\to\ell_\beta\ell_\beta\bar{\ell}_\beta)$ for the electron, muon and tau charged leptons. These ratios only differ by an overall factor, since the loop functions are the same. This ratio is continuous and don't display any m_N degeneracy for $m_N \gtrsim 100$ GeV.

[12] Note that a plot of the same ratio is displayed in Ref. [145], with quite different results, in particular vanishing rates for much lower m_N values, see footnote 8 above.

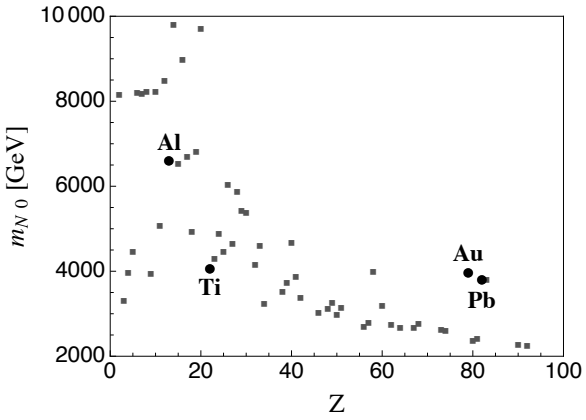

Figure 2.5 – Taking the nuclear form factor for each nuclei from Ref. [153], we show the mass values for which the $\mu \to e$ conversion rate vanishes for different nuclei. If possible, the values of the nuclear form factors D, $V^{(p)}$ and $V^{(n)}$ come from pionic atom experiment or proton scattering experiments. Otherwise, these are taken by using the approximation of taking equal proton and neutron densities, see Table. (2.4) and the associated discussion.

The fact that for the degenerate case the ratios depend only on the mass scale m_N, leading to very clear predictions, has been first pointed out in Ref. [171] precisely for the ratios $Br(\ell_\alpha \to \ell_\beta\gamma)/Br(\ell_\alpha \to \ell_\beta\ell_\beta\bar{\ell}_\beta)$. The $\mu \to e$ conversion rates provide other ratio predictions, which lead to a very interesting situation. Indeed, from the experimental determination of two $\mu - e$ transition processes, and up to discrete degeneracies, it is possible to determine the scale m_N of the generic framework considered. That pair of processes could be any two among the four processes which will be probed with improved sensitivity in near future : $\mu \to e\gamma$, $\mu \to eee$, $R^{Al}_{\mu\to e}$ and $R^{Ti}_{\mu\to e}$. To lift possible degeneracies, a third measurement may need to be considered. As an example, assume that from the MEG and COMET experiments, $R^{\mu-e(Al)}_{\mu\to e\gamma}$ is measured to be ~ 0.1 : the values $m_N \approx 2.5$ TeV or $m_N \approx 16.5$ TeV would then be singled out, see Fig. 2.4. To lift this degeneracy, the observation of a third $\mu \to e$ transition process would be necessary : for instance $R^{Ti}_{\mu\to e}$ at PRISM or $\mu \to eee$ at $\mu 3e - PSI$ [172]. If the ratio is as predicted by one of the two mass values, this would be a strong indication for this scenario. Alternatively, the measurement of two rates might be incompatible with the upper bound or the measurement of a third one, which would rule out the scenario. Similarly, the measurement of a single rate, together with the upper bound or measurement of another one, could exclude this scenario for ranges of m_N values (eventually excluding the whole mass range). Note also that, analogously, the measurement of $\tau \to \ell\gamma$ decay and of $\tau \to \ell\ell'\ell'$ decay would also allow to determine the m_N scale [171]. That determination could be compared with the $\mu \to e$ results above, to rule out or further confirm this scenario.

Although the full range of right-handed neutrino masses will be analyzed, we next discuss in detail the maximum and minimum right-handed neutrino mass scales that future sensitivities may reach, as well as the sensitivity reach for the charged-current mixing of steriles with the electrons and muon sector of the SM. We will denote by “large” mass regime the one in which the right-handed neutrino scale is larger than the electroweak scale, $m_N \geq m_W$, while the “low” mass regime will be the one in which the heavy right-handed neutrinos are lighter than m_W (although always much larger than the usual three light neutrinos). Let us consider first in detail the regime of singlet fermion masses larger than the electroweak scale.

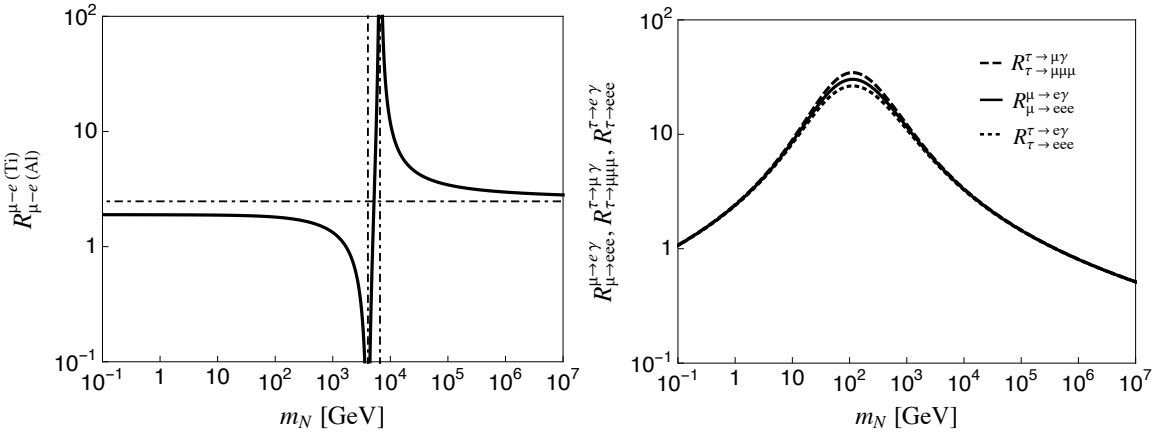

Figure 2.6 – Left : $R^{Ti}_{\mu\to e}/R^{Al}_{\mu\to e}$ as a function of m_N. The horizontal dot-dashed line show the large m_N asymptotic value of $R^{Ti}_{\mu\to e}/R^{Al}_{\mu\to e}$. The vertical dot-dashed lines correspond to the mass values for which $R^{Ti}_{\mu\to e}$ and $R^{Al}_{\mu\to e}$ vanish. Right : Ratios $R^{\mu\to e\gamma}_{\mu\to eee} = Br(\mu\to e\gamma)/Br(\mu\to eee)$ (solid), $R^{\tau\to e\gamma}_{\tau\to eee} = Br(\tau\to e\gamma)/Br(\mu\to eee)$ (dotted) and $R^{\tau\to\mu\gamma}_{\tau\to\mu\mu\mu} = Br(\tau\to\mu\gamma)/Br(\mu\to\mu\mu\mu)$ (dashed) as a function of the mass m_N.

2.4.2 Large mass regime ($m_N \geq m_W$) and constraints on the mixing parameters

◦ **Analytical results**

Expanding Eqs. (B.120-B.129) to lowest order in inverse powers of $x_{N_i} \equiv m^2_{N_i}/m^2_W$, the terms relevant for the ratio of the $\mu\to e$ conversion rate to the capture rate – see Eq. (2.65) – read

$$V^{\mu e}_u = \sum_{i=1}^{n_N} U_{eN_i} U^*_{\mu N_i} V_u(x_{N_i}), \qquad V_u(x) = \left(\frac{2}{3}s^2_w \frac{16\ln(x)-37}{12} - \frac{3+3\ln(x)}{8}\right), \tag{2.74}$$

$$V^{\mu e}_d = \sum_{i=1}^{n_N} U_{eN_i} U^*_{\mu N_i} V_d(x_{N_i}), \qquad V_d(x) = \left(-\frac{1}{3}s^2_w \frac{16\ln(x)-37}{12} - \frac{3-3\ln(x)}{8}\right), \tag{2.75}$$

$$G^{\mu e}_\gamma = \sum_{i=1}^{n_N} U_{eN_i} U^*_{\mu N_i} G_\gamma(x_{N_i}), \qquad G_\gamma(x) = \frac{1}{2}, \tag{2.76}$$

whereas for the particular case of light nuclei in Eq. (2.66), it results

$$\tilde{V}^{\mu e}_u = \sum_{i=1}^{n_N} U_{eN_i} U^*_{\mu N_i} \tilde{V}_u(x_{N_i}), \qquad \tilde{V}_u(x) = \left(\frac{2}{3}s^2_w \frac{16\ln(x)-31}{12} - \frac{3+3\ln(x)}{8}\right), \tag{2.77}$$

$$\tilde{V}^{\mu e}_d = \sum_{i=1}^{n_N} U_{eN_i} U^*_{\mu N_i} \tilde{V}_d(x_{N_i}), \qquad \tilde{V}_d(x) = \left(-\frac{1}{3}s^2_w \frac{16\ln(x)-31}{12} - \frac{3-3\ln(x)}{8}\right). \tag{2.78}$$

As an illustration of the well-behaved decoupling limit, consider the up quark contribution in Eq. (2.74). Although the loop integral exhibits a logarithmic m^2_N/m^2_W dependence, the $1/m_N$ dependence of the elements of the mixing matrix $U_{\nu N} \sim Y^\dagger_N \, \mathrm{v}/m_N$ – see Eq. (2.8) – ensures a total rate scaling as $\sim 1/m^4_N \ln^2(m^2_N/m^2_W)$ for $m_N \gg m_W$. In other words, a rate that vanishes in the decoupling limit as it should.

Using the analytical expression of the other processes in Eqs. (2.22) and (2.23), in the large mass regime $x_N = m^2_N/m^2_W \gg 1$, the leading term in the three types of rate under discussion scales

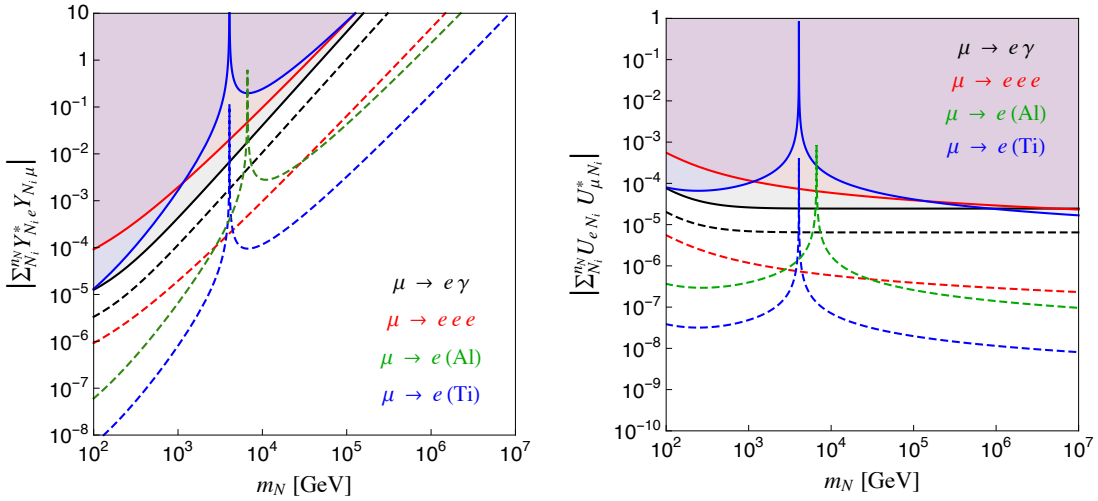

Figure 2.7 – Present bounds and future sensitivity on $|\sum_{N_i} Y_{N_{i\mu}} Y_{N^*_{ie}}|$ (left) and $|\sum_{N_i} U_{eN_i} U^*_{\mu N_i}|$ (right) as a function of the right-handed mass for scenarios characterized by one right-handed neutrino mass scale m_N. The solid lines are obtained from present experimental upper bounds in Table 2.1, that is $Br(\mu \to e\gamma) < 5.7 \cdot 10^{-13}$ [91], $Br(\mu \to eee) < 10^{-12}$ [97]. The dashed lines are obtained from the expected experimental sensitivities $Br(\mu \to e\gamma) < 4 \cdot 10^{-14}$ [93], $Br(\mu \to eee) < 10^{-16}$ [100].

therefore as

$$\Gamma \sim (\ln x_N)^2 / x_N^2, \qquad \text{for } \mu \to eee \quad \text{and} \quad \mu \to e \text{ conversion}, \tag{2.79}$$

$$\Gamma \sim 1/x_N^2, \qquad \text{for } \mu \to e\gamma. \tag{2.80}$$

◦ Maximum Seesaw scales that future experiments could probe

Fig. 2.7 shows the lower bounds resulting for the Yukawa couplings (left) and mixing parameters (right), if the various rates are required to be large enough to be observed in planned experiments. It also shows the upper bounds which hold today on these quantities from the non-observation of these processes. This figure illustrates well the impact of future $\mu \to e$ conversion measurements/bounds, as they will become increasingly dominant in exploring flavor physics in the $\mu - e$ charged lepton sector. Values of the Yukawa couplings as low as 10^{-1}, 10^{-3} and 10^{-4} could be probed, for $m_N = 100$ TeV, $m_N = 1$ TeV and $m_N = 100$ GeV, respectively, with Titanium experiments being the most sensitive. If the Yukawa couplings are required to lie in the perturbative regime, i.e. that each Yukawa coupling is smaller than $\sqrt{4\pi}$, the bounds of Fig. 2.7 can be rephrased as upper bounds on the m_N scale:

$$m_N \lesssim 3.4 \cdot 10^2 \text{ TeV} \cdot \left[\frac{4 \cdot 10^{-14}}{Br(\mu \to e\gamma)}\right]^{\frac{1}{4}}, \tag{2.81}$$

$$m_N \lesssim 1.7 \cdot 10^3 \text{ TeV} \cdot \left[\frac{10^{-16}}{Br(\mu \to eee)}\right]^{\frac{1}{4}}, \tag{2.82}$$

$$m_N \lesssim 9.7 \cdot 10^3 \,\text{TeV} \cdot \left[\frac{10^{-18}}{R^{Ti}_{\mu\to e}}\right]^{\frac{1}{4}}, \tag{2.83}$$

$$m_N \lesssim 3.9 \cdot 10^3 \,\text{TeV} \cdot \left[\frac{10^{-17}}{R^{Al}_{\mu\to e}}\right]^{\frac{1}{4}}. \tag{2.84}$$

Imposing instead that the Yukawa couplings should be smaller than 1 would lead to bounds smaller by about a factor of ∼ 3. Overall, this exercise shows that future experiments may in principle probe the type-1 Seesaw model beyond the ∼few 1000 TeV scale.

2.4.3 Low mass regime ($m_N \leq m_W$) and constraints on the mixing parameters

◦ **Analytical results**

In the low mass regime, expanding in powers of the small parameter $x_N = m_N^2/m_W^2 \ll 1$, the leading terms of the different form factors relevant for $\mu \to e$ conversion in an arbitrary nucleus – see Eq. (2.65) – are given by

$$V_u^{\mu e} = \sum_{i=1}^{n_N} U_{eN_i} U^*_{\mu N_i} V_u(x_{N_i}), \qquad V_u(x) = \left(\frac{2}{3} s_w^2 \frac{4\ln(x)+6}{4} + \frac{3+6\ln(x)}{8}\right) x, \tag{2.85}$$

$$V_d^{\mu e} = \sum_{i=1}^{n_N} U_{eN_i} U^*_{\mu N_i} V_d(x_{N_i}), \qquad V_d(x) = \left(-\frac{1}{3} s_w^2 \frac{4\ln(x)+6}{4} + \frac{3}{8}\right) x, \tag{2.86}$$

$$G_\gamma^{\mu e} = \sum_{i=1}^{n_N} U_{eN_i} U^*_{\mu N_i} G_\gamma(x_{N_i}), \qquad G_\gamma(x) = \frac{x}{4}, \tag{2.87}$$

whereas for conversion in light nuclei, Eq. (2.66), they take the form

$$\tilde{V}_u^{\mu e} = \sum_{i=1}^{n_N} U_{eN_i} U^*_{\mu N_i} \tilde{V}_u(x_{N_i}), \qquad \tilde{V}_u(x) = \left(\frac{2}{3} s_w^2 \frac{4\ln(x)+7}{4} + \frac{3+6\ln(x)}{8}\right) x, \tag{2.88}$$

$$\tilde{V}_d^{\mu e} = \sum_{i=1}^{n_N} U_{eN_i} U^*_{\mu N_i} \tilde{V}_d(x_{N_i}), \qquad \tilde{V}_d(x) = \left(-\frac{1}{3} s_w^2 \frac{4\ln(x)+7}{4} + \frac{3}{8}\right) x. \tag{2.89}$$

As a consequence, for $x_N = m_N^2/m_W^2 \ll 1$ the leading terms in the transition rates vanish as : [13]

$$\Gamma \sim x_N^2 (\ln x_N)^2, \qquad \text{for } \mu \to eee \quad \text{and} \quad \mu \to e \text{ conversion}, \tag{2.90}$$

$$\Gamma \sim x_N^2, \qquad \text{for } \mu \to e\gamma. \tag{2.91}$$

This is in contrast with the leading behaviour found for the large mass regime $x_N \gg 1$, Eq. (2.79), with the scaling law being inversely proportional to x_N^2, ensuring decoupling. Note that to get Eqs. (2.90)-(2.91) we assumed fixed $U_{\nu N}$ mixing parameters, as it is customary to express con-

[13] In the low mass regime, the amplitude for $\mu \to e\gamma$ is analogous to that for $b \to s\gamma$, while those for $\mu \to e$ conversion and $\mu \to 3e$ exhibit only a GIM cancelation quadratic in the light neutrino masses instead of the logarithmic one for quark transitions such as $b \to s e^+ e^-$, which are proportional to fermion electric charges inside the loop.

straints on sterile neutrino models in terms of these mixing parameters. [14]

◦ **Minimum Seesaw scales that future experiments could probe**

Taking $\mu \to e$ conversion experiments by themselves, the sensitivity to low singlet fermion masses is outstanding. This is illustrated in Fig. 2.8(a) (dashed lines), which shows a sensitivity down to 2 MeV for Titanium for large mixing. Nevertheless, a series of existing experimental bounds curtails the expected impact, to wit :

- *Unitarity bounds.* The mixing matrix elements $U_{\ell N}$ entering the rates are constrained by the bounds on the unitarity of the leptonic mixing matrix [89, 173]. The relevant bounds here are those holding for $m_N < m_W$, in which the strong constraint from $\mu \to e\gamma$ present for masses above m_W is lost due to the restoration of the GIM mechanism under the m_W scale. In the region ~ 100 MeV< $m_N < m_W$ the bounds are dominated by the constraints on β decay (lost under the GeV regime), kaon decays, universality constraints from τ and π decays, and tree-level μ decays. For very light N_i, under the pion and muon masses, the constraints from the decays of the latter are lost, since all eigenstates are then available in the decay, so that unitarity is recovered. Nevertheless, below 100 MeV the absence of zero distance effects in short baseline oscillation experiments (such as KARMEN [174] and NOMAD [175]) also sets constraints on the mixing elements [89]. Stronger constraints follow nevertheless in that region, mainly from “peak" and “decay" search experiments.

- *Peak experiments* explore the direct production of light ($< m_K, m_\pi$) extra singlet fermions in two-body ($\ell\, N_i$) particle decays of light mesons. From pion [176] and kaon decays [177, 178], the absence of a monochromatic line – or peak – in the charged lepton energy spectrum at $(m^2_{K,\pi} + m^2_\ell - m^2_{N_i})/2m_{K,\pi}$, [15] excludes at present the 30 MeV< m_N < 400 MeV region. Decay searches provide even stronger constraints.

- *Decay experiments* including more than 2 particles in the final state look for the effects of the production and decay of massive neutrinos. The relevant processes for constraining $\sum_i U_{eN_i} U^*_{\mu N_i}$ are $K, \pi, D \to \ell\, N_i \to \ell\, \ell' \nu_{\ell'} \ell''$ with $\ell, \ell', \ell'' = e, \mu$. Their non observation sets very strong constraints in the range 1 MeV< m_N < 2 GeV [179, 180, 181, 182]. Similarly searches for a $Z \to N_i \nu$ decay sets interesting constraints below the m_Z mass [183]. For a more detailed discussion of both decay and peak experimental bounds see Ref. [184], and also Refs. [185] and [186].

- *Supernovae and BBN limits.* Upper and lower bounds on the mixing can be obtained from supernova SN1987A data [187], since the known duration of the blast would be modified if the right-handed neutrinos are produced in the core and escape carrying energy away, and that depends on the mixing. BBN limits have also been explored for the very low mass region [186, 188, 189, 190].

[14] For small sterile masses above the eV, the Seesaw approximation $U_{\nu N} \propto Y_N^\dagger v/m_N$ ($\ll 1$) in Eq. (2.8) still holds, and an extra x_N^{-2} factor has to be added in Eqs. (2.90)-(2.91), so that the rates have a logarithmic or constant dependence on m_N. Below this range one enters the Dirac-dominated regime, where the mixing angles become free parameters, and the asymptotic behaviour is that in Eqs. (2.90)-(2.91).

[15] In the rest frame of the decaying meson.

- *LHC search for the decay of a 125 GeV scalar boson via the channel* $h \to \nu N \to \nu\nu\ell\ell$ provides new bounds on the Seesaw parameters [191, 192, 193, 194, 195], which can be translated into bounds on rare processes. The branching ratio of the SM scalar boson decaying into Majorana neutrinos enters the implementation of these bounds, which in the general Seesaw considered here reads

$$Br(h \to \nu N) = \frac{\alpha_w}{8}\frac{m_h}{\Gamma_h^{\rm tot}}\sum_i^{n_N}\left(\left|U_{eN_i}\right|^2+\left|U_{\mu N_i}\right|^2+\left|U_{\tau N_i}\right|^2\right)\frac{m_{N_i}^2}{m_W^2}\left(1-\frac{m_{N_i}^2}{m_h^2}\right)^2 , \tag{2.92}$$

  where the decay into all three light neutrinos ν_j and all heavy ones N_i is considered. $\Gamma_h^{\rm tot}$ denotes the total decay width of the scalar boson including the SM channels plus those producing the extra heavy neutrinos. The different decay widths of the heavy neutrinos also enter the analysis, mainly all $N \to \nu\ell^+\ell^-$ channels.

Following Ref. [184] (see also Refs. [185, 186, 190, 196]), Fig. 2.8(a) provides an approximate drawing of the regions excluded by these constraints (depicted as shaded areas). We included : non-unitarity bounds, kaon and pion peak searches, kaon decay searches by the PS191 experiment, D meson decay searches by the CHARM [181] and NuTeV [182] experiments, [16] Z decay searches by the Delphi experiment [183], and SM scalar decays data from LHC. The exclusion lines for the mixing parameter $|\sum_{N_i} U_{eN_i}U^*_{\mu N_i}|$ are valid at 90% C.L., for the present (continuous curves) and future (dashed curves) reach of the three types of measurements under discussion : $\mu \to e\gamma$, $\mu \to eee$ and $\mu \to e$ conversion. Note the impressive sensitivity expected from $\mu \to e$ conversion in Titanium taken by itself, reaching Seesaw masses down to 2 MeV. Nevertheless, the very stringent PS191, CHARM and NuTeV bounds on decay searches into N_i determine a lower bound on the mass at which conversion experiments would be competitive : 2 GeV. The SHiP experiment should further increase this lower bound to 5 GeV.

Fig. 2.8(b) shows the maximum rates allowed by the bounds on mixing depicted in Fig. 2.8(a) (shaded areas), as a function of the mass m_N, at the 90% C.L.. Horizontal lines in Fig. 2.8(b) indicate the present (continuous) and future (dashed) sensitivities of the different experiments : their intersection with the corresponding rate (depicted with the same color) determines the lowest mass for which the new experiments would improve present bounds.

About the SM scalar boson decay constraints, Fig. 2.8(a) depicts a model-independent bound, except for the assumption of degenerate heavy neutrinos. This bound is obtained [193] by translating the absence of an excess over the SM expectation for the channel $h \to \nu\bar{\nu}\ell^+\ell^-$ into an upper bound on ${\rm Br}(h \to \nu N) < 0.51$ (90% C.L.) [195] in Eq. (2.92), and employing then the general Cauchy-Schwarz inequality $|\sum_{N_i} U_{eN_i}U^*_{\mu N_i}| < \sum_{N_i,\alpha}|U_{\alpha N_i}|^2$. [17] Figs. 2.8(a) and 2.9 illustrate that

[16] The bounds from meson decay searches for masses below 2 GeV depicted in Fig. 2.8 are those provided by the experimental collaborations which assume decaying Dirac neutrinos ; for Majorana neutrinos they may differ by factors $\sim\sqrt{2}$ or less, depending on whether the decay channel is or is not self-conjugate [179]. The inclusion of those factors would require a reanalysis of the experimental data for masses lighter than 2 GeV, which we refrain from attempting here as that region turns out to be out of reach for the $\mu \to e$ conversion experiments under discussion.

[17] In Fig. 2.8(a) this bound is plotted down to 20 GeV, a point below which the typical cuts in the invariant mass of the lepton pair would remove the events coming from the scalar boson decay via the right-handed neutrino [193]. The equivalent bounds shown in [193, 194], which we used, do not extend further down than 50 GeV : in the region 20 – 50 GeV what Fig. 2.8(a) depicts is an extrapolation.

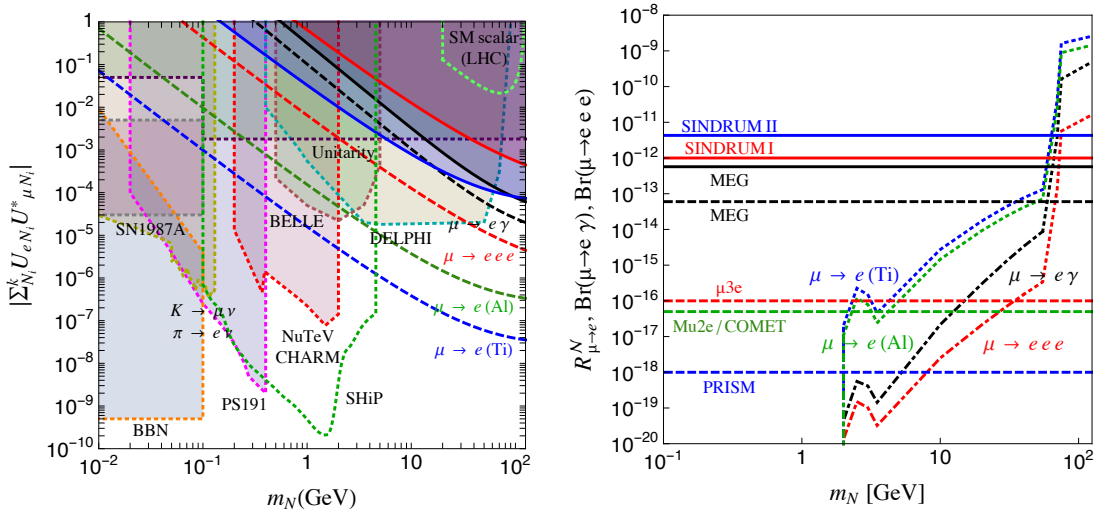

Figure 2.8 – The left panel shows the $|\sum_{N_i} U_{eN_i} U^*_{\mu N_i}|$ versus mass sensitivity regions for present (continuous curves) and future (dashed curves) $e-\mu$ flavor experiments. Black, red, green and blue curves result from $Br(\mu \to e\gamma)$, $Br(\mu \to eee)$, $R^{Al}_{\mu\to e}$ and $R^{Ti}_{\mu\to e}$, respectively. The regions already excluded by non-unitarity limits, π and K peak searches, π, K, D, Z decay searches, BBN, SN1987A and LHC collider searches (dotted lines) are also indicated. Shaded areas signal the regions already excluded experimentally. We also include the future SHiP experiment sensitivity [197]. The right panel shows the maximum allowed flavor changing rates compatible with the bounds of the first panel. The horizontal lines give the present (solid [102, 91, 97]) and future (dashed [198, 172, 106, 108, 105, 107]) sensitivities of the different experiments.

it turns out to be less stringent than for example the present MEG bound on $Br(\mu \to e\gamma)$. In the future, if LHC can reach a $\sim 1\%$ sensitivity on Br($h \to \nu N$), the constraint would be comparable to the present MEG one.

More stringent bounds follow in concrete realizations of the Seesaw. For instance, the Inverse Seesaw scenario with just two right-handed neutrinos added to the SM and approximate lepton number L conservation in section 1.5 [68, 69] (see also Refs. [62, 63, 64, 66]) is very predictive. The mixing-dependence of Br($h \to \nu N$) – the term between parenthesis in Eq. 2.92 – reduces in this case to an overall scale dependence, which can then be bounded from Fig. 2.8(a). Furthermore, in these scenarios the mixing elements $|U_{\alpha N_i}|$ are not arbitrary, but explicit functions of a few observable quantities such as the measured light neutrino mass differences and mixing angles, the overall scale and the Dirac (δ) and Majorana (α) phases. This allows to express bounds on $|U_{eN_i} U^*_{\mu N_i}|$ from SM scalar decay as a function of the values of those CP phases. This interesting fact is illustrated in Fig. 2.9, whose bands depict the maximum and minimum bounds obtained by varying those phases. The values of the neutrino parameters used in this figure are the ones given in Table 1.1, from Ref. [19]. For normal hierarchy (NH), the maximum and minimum boundary lines of the bands correspond approximately to $(\delta, \alpha = 0, \pi/2)$ and $(\delta, \alpha = 0, -\pi/2)$, respectively, while the equivalent values for the case of inverted hierarchy (IH) are $(\delta, \alpha = 3\pi/2, \pi)$ and $(\delta, \alpha = 0, -\pi/4)$. The allowed values never reach the absolute bound, also depicted. On the other side, note that the plot for IH allows some points in which the $\mu - e$ mixing tends to vanish : this is expected and well-known (first pointed out in Refs. [199, 200]), because in this class of

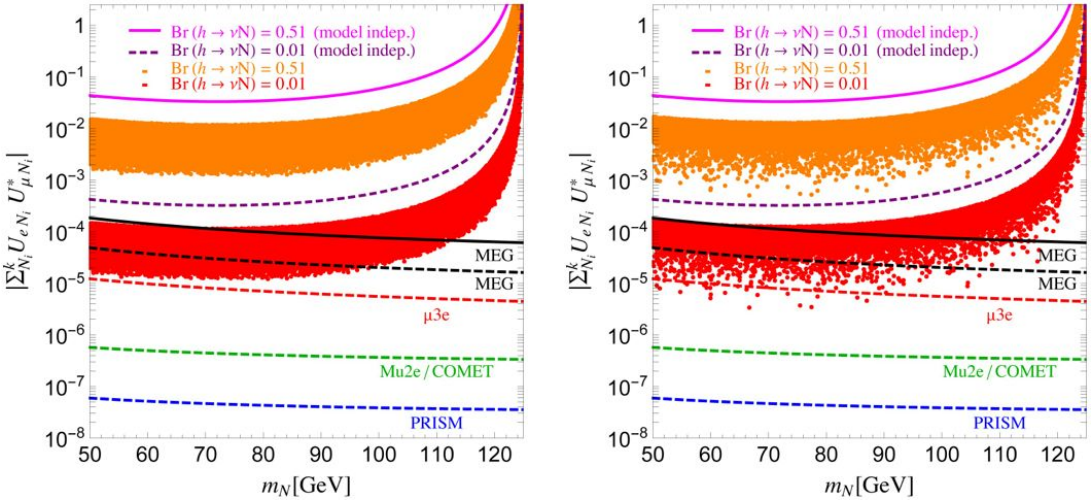

(a) Normal hierarchy

(b) Inverted hierarchy

Figure 2.9 – Bounds on $|\sum_{N_i} U_{eN_i} U^*_{\mu N_i}|$ from LHC scalar decay data and comparison with flavor violation searches. The constraints from LHC data are illustrated for a sensitivity of $Br(h \to \nu N) < 0.51$ (90% C.L.) [195], and a future one improved to the % level [194]. For these values, isolated purple curves are the absolute bounds for a generic Seesaw model. Bands in orange and red show instead the variation with the unknown values of the Dirac and Majorana CP phases, for the approximately L conserving scenario in Ref. [68], for normal (left panel) and inverted (right panel) hierarchy. The present (black) and future (dashed black) MEG sensitivities and the expected one for conversion in Titanium (blue), in Aluminum (green) and $\mu \to eee$ (red) are shown for comparison.

models some entries of the Yukawa couplings may vanish (and therefore the entry in the mixing $U_{\alpha N_i}$ would vanish too) for certain values of the CP phases and light neutrino mixing and mass differences within their 90% C.L. region [171]. As an example of the impact of the analysis for this type of models, with the present limit on $Br(h \to \nu N)$, if MEG observes a signal of order the present sensitivity, only particular ranges of the phases would be allowed in this model. In any case, for the μ-e channel it is not expected that LHC data will allow to approach, even from far, the sensitivities one expects in the new generation of $\mu \to e$ conversion experiments.

2.4.4 Comments

It is worth to remark that the sensitivities and exclusion plots obtained apply not only to the (quasi-degenerate) type-1 Seesaw scenario object of this section, but also to any BSM renormalizable theory containing Dirac or pseudo-Dirac singlet fermions, which mix with SM light leptons with strength $U_{\ell N}$.

Also, the predictions on the ratios of rates, such as that in Eq. (2.72) and the figures above, hold as well for the case where only one right-handed neutrino would dominate the rates, because in this case the Yukawa dependence also drops, leaving the same dependence on a unique mass. This situation is quite generic of scenarios where the right-handed neutrino mass spectrum is hierarchical, since in the large $m_N > m_W$ (low $m_N < m_W$) mass regime all but the lightest (heaviest) N_i contributions can be in general neglected, see Eqs. (2.79), (2.80), and Eqs. (2.90) and

(2.91) above. However, the price to obtain measurable flavor-changing rates with hierarchical spectra is to induce in general unacceptably large neutrino masses, disregarding eventual large fine-tuning between the various parameters.

Nevertheless, we have shown in section 1.5 that one could *a priori* take larger values of the μ' parameter in the Inverse Seesaw model, while still keeping the advantages of having small neutrino masses and large CLFV rates. In this case, one could have a large mass splitting between the two right-handed neutrinos, see Eq. (1.54). The price to pay is that this Extended Seesaw model is not anymore motivated by a nearly conserved lepton symmetry. Furthermore, one has to pay attention to possibly large one-loop corrections to neutrino masses and neutrinoless double beta decay parameter m_{ee}, see e.g. Refs. [191, 139, 71, 72]. This case is therefore less interesting *a priori* because there is no simple symmetry to explain it, but it is perfectly possible. This is why the next section is dedicated to the possibility that right-handed are not degenerate.

2.5 Ratios of rates involving one same flavor transition : non degenerate case

We now tackle the more general case where the right-handed neutrinos are no more degenerate. In this case, we will see that one can still factorize the mixing matrix element from the mass dependent terms. The reason is more subtle, and one needs first to parametrize correctly the Yukawa matrix elements. In this section, we will for simplicity restrict ourself to the two right-handed neutrinos case, $n_N = 2$, and our analytical study will focus on the situation where the right-handed neutrino masses are larger than the W mass, $m_{N_i} \gg m_W$, even if we will cover the whole mass range for the numerical results.

An important comment concerns the observability of the CLFV processes in the case where the right-handed neutrinos are not degenerate. Indeed, as shown above, it is easy to have large CLFV rates and small neutrino masses when at least two right-handed neutrinos are quasi-degenerate. Now, it is important to stress that such a situation can also be obtained with non-degenerate right-handed neutrinos, as in the Extended Seesaw mode, introduced in section 1.5. To show that, we will use the Casas-Ibarra parametrization that allows us to see that easily.

2.5.1 Casas-Ibarra parametrization

In order to analyze the non-degenerate case, we need to parametrize the various parameters that enter in the mixing elements U_{eN_i} and $U^*_{\mu N_i}$. Indeed, as shown in Eq. (2.24), it is the combination

$$\sum_i U_{eN_i} U^*_{\mu N_i} \, f\left(m^2_{N_i}\right) \propto \sum_i \frac{Y^*_{N_i\mu}}{m_{N_i}} \frac{Y_{N_i e}}{m_{N_i}} \, f\left(m^2_{N_i}\right) \equiv \sum_i c_{N_i} \, f\left(m^2_{N_i}\right) , \tag{2.93}$$

that enters in the various form factors of the concerned rates. To this end, it is useful to introduce the Casas-Ibarra matrix [201]

$$R \equiv \frac{\mathrm{v}}{\sqrt{2}} (M_N)^{-1/2} \; Y_N \, \mathscr{U} \; (\hat{m}_\nu)^{-1/2} , \tag{2.94}$$

where $\hat{m}_\nu$ is the diagonal matrix of the light neutrinos mass eigenstates, and $\mathscr{U}$ is the PMNS matrix. The matrix R is a complex $n_N \times 3$ matrix (where n_N is the number of right-handed neutrinos), which contains all the high energy parameters, i.e. the parameters that are not contained in the neutrino mass matrix $m_\nu = \mathrm{v}^2/2(Y_N^T M_N^{-1} Y_N) = \mathscr{U}^* \hat{m}_\nu \mathscr{U}^\dagger$. As a result, R is totally unknown except for the fact that it is complex orthogonal :

$$R R^T = \mathbb{1}_{n_N \times n_N} \quad , \quad R^T R = \mathbb{1}_{3\times 3} \, . \tag{2.95}$$

This matrix is very useful since, by inverting Eq. (2.94), it allows to factorize in the Yukawa matrix Y_N the low energy parameters, in m_ν and $\mathscr{U}$, from the high energy ones, in M_N and R :

$$Y_N = \frac{\sqrt{2}}{\mathrm{v}} (M_N)^{1/2} \; R \; (\hat{m}_\nu)^{1/2} \; \mathscr{U}^\dagger \, . \tag{2.96}$$

Or in component, using the fact that M_N can be taken diagonal $M_N = \mathrm{diag}(m_{N_i})$,

$$Y_{N_i \alpha} = \frac{\sqrt{2 m_{N_i}}}{\mathrm{v}} \left(\sum_j R_{N_i j} \sqrt{m_j} \mathscr{U}^*_{j\alpha} \right) , \tag{2.97}$$

where m_j is the mass of the neutrino eigenstate ν_j. That is to say this parametrization allows us to scan all the Y_N which could account for the data. To do so, one needs to enter the mixing data in $\mathscr{U}$, the neutrino mass difference in m_j, and vary the other parameters (the 3 CP-violating phases, $m_\nu^{\min}$ and the unknown high energy parameters in M_N and R) in their allowed range. It allows therefore to see easily how one can get large Y_N with still small neutrino masses. Clearly, large Y_N must come from large R entries, i.e. large imaginary part in R as we will see.

2.5.2 $\mathbf{n_N = 2}$ non-degenerate right-handed neutrinos

The two right-handed neutrinos case is particularly interesting as it is the one which contains the minimum number of independent parameters.

◦ Parametrization

In this case, the 2×3 matrix R contains only 1 complex angle $\hat{\theta} \equiv \alpha + i\beta$, and it can be parametrized as [202]

$$R = \begin{pmatrix} 0 & \cos\hat{\theta} & \sin\hat{\theta} \\ 0 & -\sin\hat{\theta} & \cos\hat{\theta} \end{pmatrix} \quad \text{(NH)} \quad , \quad R = \begin{pmatrix} \cos\hat{\theta} & \sin\hat{\theta} & 0 \\ -\sin\hat{\theta} & \cos\hat{\theta} & 0 \end{pmatrix} \quad \text{(IH)} \, , \tag{2.98}$$

in the case of normal and inverted hierarchies respectively. Since R is any complex orthogonal matrix, one has

$$\cos\hat{\theta} = \cos\alpha \cosh\beta - i \sin\alpha \sinh\beta \quad \text{and} \quad \sin\hat{\theta} = \sin\alpha \cosh\beta + i \cos\alpha \sinh\beta \, , \tag{2.99}$$

where $\alpha \in [0, 2\pi]$ is an angle, while β can take any value in $\Re$. The Yukawa matrix Y_N has therefore only 6 unknown parameters (see Eq. (1.29)) : the low energy CP-violating phases $\alpha \in [0, 2\pi]$ and $\delta \in [0, 2\pi]$, the 2 heavy neutrino masses m_{N_1} and m_{N_2}, and the complex high-energy angle

$\hat{\theta} \equiv \alpha + i\beta$ with $\alpha \in [0, 2\pi]$ and $\beta \in \Re$. On top of that, the neutrino mass hierarchy is also unknown. Since there are 2 right-handed neutrinos, only 2 light neutrinos receive masses so that the absolute neutrino mass scale is actually known, $m_\nu^{\rm min} = 0$ eV. Nevertheless, the number of unknown parameters is too large to make generic predictions on the various CLFV rates separately. However, as we will show now, one can still make remarkable prediction on the ratios of branching ratio, provided that the rates are not too suppressed.

◦ **Ratio of rates**

From Eq. (2.98) and (2.99), we see that the CLFV processes are proportional to some combination of $\cosh\beta$ and $\sinh\beta$. For large β, one has $\cosh\beta \simeq \sinh\beta$, so that all the Yukawas scale as $Y_N \propto \cosh\beta$. [18] The combination $\cosh\beta$ is therefore nothing else but the overall scale of the Yukawa couplings. In order to have observable rates, one needs quite large Yukawa couplings $Y_N \gtrsim 10^{-2} \cdot m_N/1$ TeV, see Eq. (2.25). From Eq. (2.96), this roughly requires $\beta \gtrsim 6 + \ln\sqrt{m_N/1\,\text{GeV}}$ so that, in order to have observable rates, one has indeed in a good approximation

$$Y_N \propto \cosh\beta \quad \text{with} \quad \beta \gg 1\,. \tag{2.100}$$

This parametrization therefore shows that indeed one can have large Y_N and small m_ν, provided that β is large. This shows also that this is possible even if m_{N_1} and m_{N_2} are not degenerate. More remarkable, one can see after development that in this case the different terms entering in the sum in Eq. (2.93) share a common factor. For example in the case of normal hierarchy, one has

$$\begin{aligned} c_{N_1} &\equiv \frac{Y^*_{N_1\mu}}{m_{N_1}}\frac{Y_{N_1 e}}{m_{N_1}} = \frac{2}{\text{v}^2 m_{N_1}}\left(\sum_j R^*_{N_1 j}\sqrt{m_{\nu_j}}\mathcal{U}_{j\mu}\right)\left(\sum_k R_{N_1 k}\sqrt{m_{\nu_k}}\mathcal{U}^*_{ke}\right) \\ &= \frac{2\cosh^2\beta}{\text{v}^2 m_{N_1}}\left[m_{\nu_2}\mathcal{U}_{2\mu}\mathcal{U}^*_{2e} + m_{\nu_3}\mathcal{U}_{3\mu}\mathcal{U}^*_{3e} + i\sqrt{m_{\nu_2}m_{\nu_3}}\left(\mathcal{U}_{2\mu}\mathcal{U}^*_{3e} - \mathcal{U}_{3\mu}\mathcal{U}^*_{2e}\right)\right]\,, \end{aligned} \tag{2.101}$$

and

$$\begin{aligned} c_{N_2} &\equiv \frac{Y^*_{N_2\mu}}{m_{N_2}}\frac{Y_{N_2 e}}{m_{N_2}} \propto \frac{2}{\text{v}^2 m_{N_2}}\left(\sum_j R^*_{N_2 j}\sqrt{m_{\nu_j}}\mathcal{U}_{j\mu}\right)\left(\sum_k R_{N_2 k}\sqrt{m_{\nu_k}}\mathcal{U}^*_{ke}\right) \\ &= \frac{2\cosh^2\beta}{\text{v}^2 m_{N_2}}\left[m_{\nu_2}\mathcal{U}_{2\mu}\mathcal{U}^*_{2e} + m_{\nu_3}\mathcal{U}_{3\mu}\mathcal{U}^*_{3e} + i\sqrt{m_{\nu_2}m_{\nu_3}}\left(\mathcal{U}_{2\mu}\mathcal{U}^*_{3e} - \mathcal{U}_{3\mu}\mathcal{U}^*_{2e}\right)\right]\,. \end{aligned} \tag{2.102}$$

That is, $c_2 = c_1 \cdot m_{N_1}/m_{N_2}$. One can easily show that the same relation stands for the inverted hierarchy. The combination in Eq. (2.93) can therefore be written as

$$\sum_i c_{N_i}\, f\left(m^2_{N_i}\right) \simeq c_{N_1}\,\left[f\left(m^2_{N_1}\right) + \frac{m_{N_1}}{m_{N_2}} f\left(m^2_{N_2}\right)\right]\,. \tag{2.103}$$

As a consequence, one can still factorize most of the unknown parameters contained in c_{N_1} from the branching ratios, so that the ratios of branching ratios will now only depend on both m_{N_1} and m_{N_2} (or equivalently on m_{N_1} and $r \equiv m_{N_2}/m_{N_1}$).

[18] More precisely, the approximation $\cosh\beta \simeq \sinh\beta$ holds at better than 1% for $\beta \gtrsim 3$.

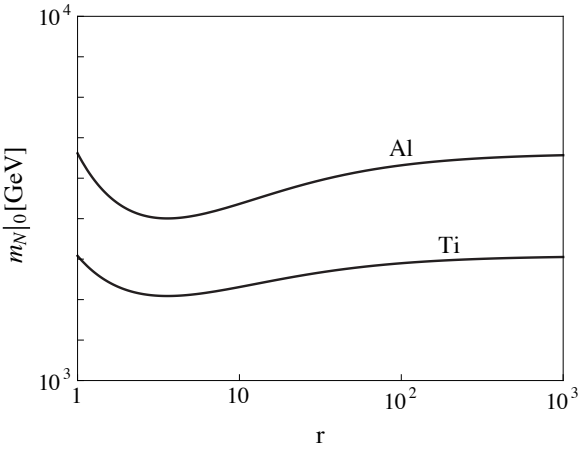

Figure 2.10 – Mass values of the lightest right-handed neutrino for which the $\mu \to e$ conversion rate vanishes for Aluminum and Titanum, as a function of $r \equiv m_{N_2}/m_{N_1}$. We required the conversion rates to be observable by future experiments.

Before commenting the results, it is instructive to compute the values $m_N|_0$ where the $\mu \to e$ conversion rate vanishes, which are shown in Fig. 2.10. For $m_{N_i} \gg m_W$, these are now given by

$$m_N^2\Big|_0 = m_W^2 \exp\left(\frac{\frac{9}{8}V^{(n)} + \left(\frac{9}{8} + \frac{37s_w^2}{12}\right)V^{(p)} - \frac{s_w^2}{16e}D}{\frac{3}{8}V^{(n)} + \left(\frac{4s_w^2}{3} - \frac{3}{8}\right)V^{(p)}} - 2\frac{\ln r}{1+r} \right), \tag{2.104}$$

where $r \equiv m_{N_2}/m_{N_1}$. The values of $m_N\big|_0$ vary by few TeV around the one obtained in the degenerate case, which is recovered for $r = 1$ as well as for large r, as expected from the decoupling theorem. The maximum deviation is obtained for $r_{\max} \approx 3.6$ whatever the nucleus, which is the value that maximizes the function $\ln r/(1+r)$. Quite remarkably, this value is also the value for which one has a maximum deviation for all the other rates, still for $m_{N_i} \gg m_W$. This can be understood because, for $m_{N_i} \gg m_W$, the different form factors only depend on the logarithm of $x_{N_i} = m_{N_i}^2/m_W^2$, see Eqs. (2.74)-(2.75). From Eq. (2.103), one has therefore

$$\sum_i c_{N_i}\, f\left(x_{N_i}\right) \simeq \sum_i c_{N_i}\, \left(A + B\ln x_{N_i}\right) = c_{N_1}\left[\left(A + B\ln x_{N_1}\right)\left(1 + \frac{1}{r}\right) + \frac{2B}{r}\ln r\right], \tag{2.105}$$

where A and B are some constants. We see that here too, the maximum deviation from the case $r = 1$ is obtained for $r_{\max}$ maximizing the function in the second term of the bracket, which gives also approximately $r_{\max} \approx 3.6$.

Let's note that for $m_{N_i} \leq m_W$, one expects things to be much less simple, since the different form factors depend now on x_{N_i} and $x_{N_i} \cdot \ln x_{N_i}$, see Eqs. (2.85)-(2.86), and one has

$$\sum_i c_{N_i}\, f\left(x_{N_i}\right) \simeq \sum_i c_{N_i}\, x_{N_i}\left(A + B\ln x_{N_i}\right) = c_{N_1}\, x_{N_i}\left[\left(A + B\ln x_{N_1}\right)(1+r) + 2Br\ln r\right]. \tag{2.106}$$

We see that in this case, the deviation increases with increasing r, and no simple prediction can be done.

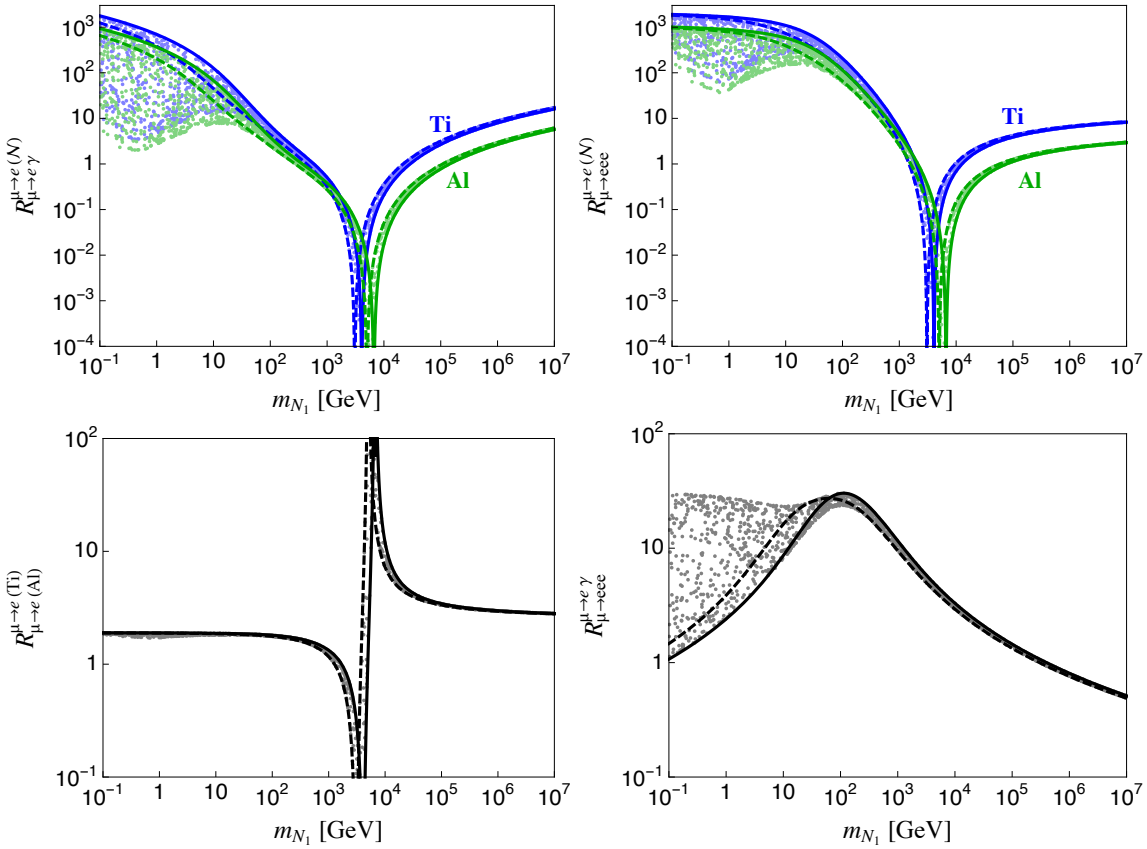

Figure 2.11 – Upper panels : $R^{\mu\to e(\mathcal{N})}_{\mu\to e\gamma} = R^{\mathcal{N}}_{\mu\to e}/Br(\mu\to e\gamma)$ (upper left panel) and $R^{\mu\to e(\mathcal{N})}_{\mu\to eee} = R^{\mathcal{N}}_{\mu\to e}/Br(\mu\to eee)$ (upper right panel) as a function of the lightest right-handed neutrino mass scale m_{N_1}, for $\mu\to e$ conversion in Aluminum (green) and Titanium (blue). Lower panels : $R^{Ti}_{\mu\to e}/R^{Al}_{\mu\to e}$ (lower left panel) and $R^{\mu\to e\gamma}_{\mu\to eee} = Br(\mu\to e\gamma)/Br(\mu\to eee)$ (lower right panel) as a function of m_{N_1}. In all the figures, the solid line corresponds to the degenerate case, while the dashed line corresponds to the maximum deviation for $m_{N_1}\gtrsim m_W$. The points has been obtained varying all the unknown parameters of the model, under the requirement of observable rates, and taking $r\equiv m_{N_2}/m_{N_1}$ in the range $r\in[1,10^3]$.

In the upper panels of Fig. 2.11, we show the ratios $R^{\mu\to e(\mathcal{N})}_{\mu\to e\gamma}$ (upper left panel) and $R^{\mu\to e(\mathcal{N})}_{\mu\to eee}$ (upper right panel) as a function of the lightest mass m_{N_1}, for Aluminum (green) and Titanium (blue) nuclei. The various points have been obtained by varying all the unknown parameters according to their domain, and r in the range $r\in[1,10^3]$. We also required the different branching ratios to be observable in the near future, that is we took $R^{Ti}_{\mu\to e}\geq 10^{-18}$, $R^{Al}_{\mu\to e}\geq 10^{-17}$, $Br(\mu\to e\gamma)\geq 4\cdot 10^{-14}$ and $Br(\mu\to eeee)\geq 10^{-16}$, see Table 2.1. The solid line corresponds to the degenerate case $r=1$, while the dashed line corresponds to the maximum deviation obtained analytically $r_{\max}\approx 3.6$, which fit well the points for $m_{N_1}\gtrsim m_W$.

The lower panels of Figure 2.11 show, as a function of m_{N_1}, the ratio $R^{Ti}_{\mu\to e}/R^{Al}_{\mu\to e}$ (lower left panel) and $Br(\mu\to e\gamma)/Br(\mu\to eee)$ (lower right panel), varying all the unknown parameters and requiring rates that could be observable by the future experiments. Here too, the solid and dashed lines correspond to $r=1$ and $r_{\max}\approx 3.6$ respectively.

As we can see from these figures, the ratios of rates is only mildly sensitive to the mass splitting of the right-handed neutrinos, at least for $m_{N_1} \gtrsim m_W$. As a consequence, the measurement of ratios would in this case provide a narrow range of possible values for m_{N_1}. The measurement of several ratios could even potentially lead to the determination of the two mass scales m_{N_1} and m_{N_2}. However, this should be very difficult in practice because : first, the measurement of the ratios goes always with uncertainties and, second, the nuclear overlap integrals have also associated uncertainties as we discussed before. Assuming for example $m_{N_1} \gtrsim m_W$, the measurement of ratios with their associated uncertainties could allow to determine a range of values for m_{N_1} and therefore also a (wide) range of possible values for m_{N_2} see Fig. 2.11. All together, this would lead in practice to uncertainties on the determination of the Seesaw scales m_{N_1}, but more hardly to the determination of the second scale m_{N_2}.

2.5.3 $n_N = 3$ non-degenerate right-handed neutrinos

In this case, the 3×3 matrix R contains 3 complex angles $\hat{\theta}_i \equiv \alpha_i + i\beta_i$ with $i = 1,2,3$, and it can be parametrize as [201]

$$R = \begin{pmatrix} \hat{c}_2\hat{c}_3 & -\hat{c}_1\hat{s}_3 - \hat{s}_1\hat{s}_2\hat{c}_3 & \hat{s}_1\hat{s}_3 - \hat{c}_1\hat{s}_2\hat{c}_3 \\ \hat{c}_2\hat{s}_3 & \hat{c}_1\hat{c}_3 - \hat{s}_1\hat{s}_2\hat{s}_3 & -\hat{s}_1\hat{c}_3 - \hat{c}_1\hat{s}_2\hat{s}_3 \\ \hat{s}_2 & \hat{s}_1\hat{c}_2 & \hat{c}_1\hat{c}_2 \end{pmatrix} . \tag{2.107}$$

Here, the number of unknown parameters is 13, see Eq. (1.29). The situation is more complicated than the previous case with only $n_N = 2$ right-handed neutrinos. However, one doesn't expect in general any simplification in ratios of rates, since now there are 3 complex angles in the R matrix. We won't go further into analytical details here. Let's just note that if one of the right-handed neutrinos is much heavier than the others, it will decouple from the rest so that one recovers the previous situation with $n_N = 2$. This is also the case if 2 of the 3 right-handed are degenerate.

2.6 Comparison between the different types of Seesaw

One question which naturally arises is the following : how could we determine which kind of Seesaw is at work ? The distinction between the different types of Seesaw can not be done only from the neutrino mass matrix, because the three types of Seesaw generate the same dimension-5 operator in Eq. (1.20), and any neutrino mass matrix that could be observed could be generated by any of the three Seesaw. One needs therefore informations coming from other experiments.

A way to distinguish between them is thus precisely through observations of CLFV processes they induce. This can be simply understood from the fact the dimension-6 operators of each kind of Seesaw are different, see Eqs. (1.47), (1.48) and (1.49). [19] This requires the CLFV processes to be not too suppressed, as in particular in the Inverse Seesaw models – see section 1.5. We will now show that the CLFV processes can indeed distinguish between the Seesaw types.

[19] Another way of distinction is to look at the direct production of the associated heavy particle at colliders. In the case of type-1 Seesaw, this is hardly feasible because they couple only to the fermions and the SM scalar through the Yukawas couplings. On the contrary, in the case of type-2 and type-3 Seesaw, since the heavy particle couple to gauge bosons, they are expected to be more easily detected.

2.6.1 Type-2 Seesaw ratios and maximum scales

In type-2 Seesaw with only one scalar triplet, the CLFV branching ratio are given by [203, 131, 124, 125, 127, 56, 145] : [20]

$$Br(\mu \to e\gamma) = \frac{\alpha}{192\pi G_F^2}\left(\frac{1}{m_{\Delta^+}^2}+\frac{8}{m_{\Delta^{++}}^2}\right)^2 \left|Y_\Delta^\dagger Y_\Delta\right|^2_{\mu e} \simeq \frac{27}{64\pi}\frac{\alpha}{G_F^2 m_\Delta^4}\left|Y_\Delta^\dagger Y_\Delta\right|^2_{\mu e}\,, \tag{2.108}$$

$$Br(\mu \to eee) = \frac{m_\mu^5}{192\pi^3\Gamma_\mu}\left|c^{d=6}_{\mu eee}\right|^2 = \frac{1}{G_F^2 m_\Delta^4}\left|Y_\Delta\right|^2_{\mu e}\left|Y_\Delta\right|^2_{ee}\,, \tag{2.109}$$

$$\begin{aligned} R^{\mathcal{N}}_{\mu\to e} &\simeq \frac{\alpha^5}{36\pi^4}\frac{m_\mu^5}{\Gamma^{\mathcal{N}}_{\text{capt.}}} Z_{\text{eff}}^4 Z\, F_p^2 \left[\frac{5}{24m_{\Delta^+}^2}+\frac{1}{m_{\Delta^{++}}^2}+\frac{1}{m_{\Delta^{++}}^2}\ln\left(\frac{m_\mu^2}{m_\Delta^2}\right)\right]^2 \left|Y_\Delta^\dagger Y_\Delta\right|^2_{\mu e} \\ &\simeq \frac{\alpha^5}{36\pi^4}\frac{m_\mu^5}{m_\Delta^4\Gamma^{\mathcal{N}}_{\text{capt.}}} Z_{\text{eff}}^4 Z\, F_p^2 \left[\frac{29}{24}+\ln\left(\frac{m_\mu^2}{m_{\Delta^{++}}^2}\right)\right]^2 \left|Y_\Delta^\dagger Y_\Delta\right|^2_{\mu e}\,, \end{aligned} \tag{2.110}$$

where the conversion rate is given in the light nuclei approximation. In the second equalities of the $\mu \to e\gamma$ and $\mu \to e$ expressions, we have neglected the mass splitting between the triplet components, i.e. we took $m_\Delta \equiv m_{\Delta^0} = m_{\Delta^+} = m_{\Delta^{++}}$. This approximation is generically justified only for high triplet mass, in which case the relative splittings $|\delta m|/m_\Delta$ is small because of the perturbativity of the quartic couplings. [21] Let's note that on the one hand, since the scalar triplet couples to two fermions, the process $\mu \to eee$ is generated at tree-level from the exchange of a scalar triplet, see Fig. 1.3(b). On the other hand, the processes $\mu \to e\gamma$ and $\mu \to e$ conversion come at loop-level. One expects therefore the $\mu \to eee$ rate (and the $\ell_\alpha \to \ell_\beta \ell\gamma\bar{\ell}_\delta$ in general) to be larger than the other rates.

We see from the above formula that the rates $R^{\mathcal{N}}_{\mu\to e}$ and $Br(\mu \to e\gamma)$ depend on the same combination of the Yukawa couplings $|Y_\Delta^\dagger Y_\Delta|_{\mu e} \propto \sum_\alpha c^{d=6}_{\mu\alpha\alpha e}$, contrarily to the $\mu \to eee$ rate which depends on $|Y_\Delta^\dagger|_{\mu e}|Y_\Delta|_{ee} \propto c^{d=6}_{\mu eee}$. As a result, the ratio $R^{\mu\to e(Ti)}_{\mu\to e(Al)}$ is fixed to

$$\frac{R^{Ti}_{\mu\to e}}{R^{Al}_{\mu\to e}} \simeq 1.8\,, \tag{2.111}$$

and in the same way as in the type-1 Seesaw case, the ratio $R^{\mu\to e(\mathcal{N})}_{\mu\to e\gamma} = R^{\mathcal{N}}_{\mu\to e}/Br(\mu \to e\gamma)$ depend only on the masses m_{Δ^+} and $m_{\Delta^{++}}$. In the approximation of degenerate triplet component masses, the various ratios depend only the unique mass scale m_Δ.

We show in Fig. 2.12 the ratio $R^{\mu\to e(\mathcal{N})}_{\mu\to e\gamma}$ as a function of the mass $m_\Delta \equiv m_{\Delta^+}$ for various nuclei.

[20] Note that these expressions can be expressed in terms of the dimension-6 coefficient, see section 1.4. One has indeed that $Br(\mu \to e\gamma) \propto |\sum_\alpha c^{d=6}_{\alpha\mu\alpha e}|^2$, $Br(\mu \to eee) \propto |c^{d=6}_{\mu eee}|^2$ and $R^{\mathcal{N}}_{\mu\to e} \propto |\sum_\alpha c^{d=6}_{\alpha\mu\alpha e}|^2$.

[21] The mass splitting goes like $|\delta m| \simeq \lambda m_W^2/g^2 m_\Delta$, where λ is some quartic coupling. Requiring $|\lambda| < \sqrt{4\pi}$ (4π), one has for example $|\delta m|/m_\Delta \lesssim 0.05$ (0.2) for $m_\Delta \gtrsim 1$ TeV. Below typically 1 TeV, the mass splitting may be larger so that the $\mu \to e\gamma$ and the $\mu \to e$ conversion rates depend in general on both m_{Δ^+} and $m_{\Delta^{++}}$, and the approximation is less consistent. However, experimentally the ATLAS and CMS collaborations have provided lower bounds on the doubly charged scalar through its dilepton signature $\Delta^{\pm\pm} \to \ell^\pm\ell^\pm$. At 7 TeV, with a luminosity of $L = 4.7\cdot\text{fb}^{-1}$ and assuming $Br(\Delta^{\pm\pm} \to \ell^\pm\ell^\pm) \sim 100\%$, ATLAS [204] excluded $m_{\Delta^{\pm\pm}}$ below 409, 398, 375 GeV at 95% C.L. in the ee, $\mu\mu$, $e\mu$ channel respectively. With the same assumption, CMS [205] set a lower bound ranging from 204 GeV to 459 GeV. Assuming for concreteness $m_{\Delta^{++}} \gtrsim 400$ GeV implies the upper bound $|\delta m|/m_\Delta \lesssim 0.3$ (1.2), requiring $\lambda < \sqrt{4\pi}$ (4π).

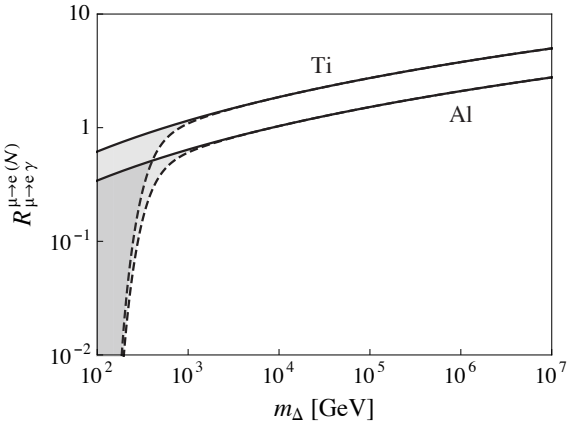

Figure 2.12 – $R^{\mu\to e(\mathcal{N})}_{\mu\to e\gamma} = R^{\mathcal{N}}_{\mu\to e}/Br(\mu\to e\gamma)$ as a function of the scalar triplet mass $m_\Delta \equiv m_{\Delta^+}$, for Aluminum and Titanium nuclei. The upper solid curve corresponds to the degenerate case $m_{\Delta^+} = m_{\Delta^{++}}$, while the lower dashed curve has been obtained varying the mass splitting in its allowed range.

The band has been obtained varying $m_{\Delta^{++}}$ in its allowed range for perturbative quartic couplings $|\lambda| < 4\pi$. We see that for $m_\Delta \gtrsim 900$ GeV the ratios are monotonous increasing functions. The determination of a ratio by experiments, typically above ~ 0.5 for Aluminum and ~ 1 for Titanium, leads to the determination of the mass scale m_Δ. As in the type-1 Seesaw, the determination of a second ratio could confirm or rule out the type-2 Seesaw scenario. For $m_\Delta \lesssim 900$ GeV, the allowed mass splitting doesn't allow the determination of the mass scale.

As in the type-1 Seesaw, one can compute the sensitivity on m_Δ we get from the various processes. Using the approximation $m_\Delta \equiv m_{\Delta^+} = m_{\Delta^{++}}$ and the perturbativity of the Yukawa couplings $Y_\Delta \leq \sqrt{4\pi}$, the maximum scalar triplet mass scales that future experiments could probe are given by

$$m_\Delta \lesssim 4.1\cdot 10^2 \text{ TeV}\cdot\left[\frac{4\cdot 10^{-14}}{Br(\mu\to e\gamma)}\right]^{1/4}, \tag{2.112}$$

$$m_\Delta \lesssim 1.0\cdot 10^4 \text{ TeV}\cdot\left[\frac{10^{-16}}{Br(\mu\to eee)}\right]^{1/4}, \tag{2.113}$$

$$m_\Delta \lesssim 8.3\cdot 10^3 \text{ TeV}\cdot\left[\frac{10^{-18}}{R^{Ti}_{\mu\to e}}\right]^{1/4}, \tag{2.114}$$

$$m_\Delta \lesssim 3.9\cdot 10^3 \text{ TeV}\cdot\left[\frac{10^{-17}}{R^{Al}_{\mu\to e}}\right]^{1/4}. \tag{2.115}$$

Imposing instead that the Yukawa couplings should be smaller than 1 would lead to bounds smaller by about a factor of ~ 3.

2.6.2 Type-3 Seesaw ratios and maximum scale

In type-3 Seesaw, the $\mu\to eee$ and $\mu\to e$ conversion CLFV processes arise all at tree-level. This is because the fermionic triplets Σ_k induce flavor mixings at the level of charged fermions, contrarily

to the type-1 Seesaw where flavor mixings arise only at the level of neutral fermions. Such a charged lepton flavor mixing simply comes from the fact that the Yukawa interaction of the Lagrangian contains $\mathscr{L} \ni \overline{\vec{\Sigma}_R} Y_\Sigma \tilde{\phi}^\dagger \vec{\tau} \ell_L \ni Y_\Sigma \, \mathrm{v} \Sigma_R^+ \ell_L^-$. Therefore, a muon can go to a Σ_R which can go to an electron without passing through neutral leptons. Nevertheless, $\mu \to e\gamma$ arises at loop-level because the electromagnetic couplings are still flavor diagonal in the charged lepton mass eigenstates basis. The expressions of the various rates, in the limit where $m_{\Sigma_k} \gg m_W$, are given by [129, 56]

$$Br(\mu \to e\gamma) = \frac{3\alpha}{32\pi} \left| \left(\frac{13}{3} - 6.56 \right) \frac{\mathrm{v}^2}{2} c_{e\mu}^{d=6} - \sum_i \frac{m_{\nu_i}^2}{m_W^2} (\mathscr{U})_{ei} (\mathscr{U})_{\mu i}^* \right|^2 \simeq \frac{15 \, \mathrm{v}^4 \alpha}{128\pi} \left| c_{\mu e}^{d=6} \right|^2 , \tag{2.116}$$

$$Br(\mu \to eee) = \mathrm{v}^4 \left(3 \sin\theta_w - 2 \sin^2\theta_w + \frac{1}{2} \right) \left| c_{\mu e}^{d=6} \right|^2 , \tag{2.117}$$

$$R_{\mu\to e}^{\mathscr{N}} \simeq \frac{\alpha^3}{2\pi^2} \frac{G_F^2 m_\mu^5}{\Gamma_{\text{capt.}}^{\mathscr{N}}} \frac{Z_{\text{eff}}^4}{Z} F_p^2 \left[(2Z+N) \left(1 - \frac{8}{3} s_w^2 \right) + (Z+2N) \left(-1 - \frac{4}{3} s_w^2 \right) \right]^2 \left| c_{\mu e}^{d=6} \right|^2 , \tag{2.118}$$

where we neglected the light neutrino mass contributions in the last equality of the first equation, and where the conversion rate is given in the light nuclei approximation. These three expressions depend on the same combination of the mixing parameters via the dimension-6 coefficient $c_{\mu e}^{d=6} = (Y_\Sigma^\dagger M_\Sigma^{\dagger -1} M_\Sigma^{-1} Y_\Sigma)_{\mu e}$, see Eq. (1.48). As a result, the ratio of two processes involving a same flavor transition doesn't depend on $c_{\mu e}^{d=6}$ anymore. Even better, in the limit where $m_{\Sigma_i} \gg m_W$, the ratios are fixed and are given by [129] : [22]

$$\frac{Br(\mu \to e\gamma)}{Br(\mu \to eee)} \approx \frac{Br(\tau \to \mu\gamma)}{Br(\tau \to \mu\mu\mu)} \approx \frac{Br(\tau \to e\gamma)}{Br(\tau \to eee)} \approx 1.4 \cdot 10^{-3} , \tag{2.119}$$

$$\frac{R_{\mu\to e}^{Ti}}{Br(\mu \to e\gamma)} \approx 1.5 \cdot 10^4 , \tag{2.120}$$

$$\frac{R_{\mu\to e}^{Al}}{Br(\mu \to e\gamma)} \approx 6.7 \cdot 10^3 . \tag{2.121}$$

Contrarily to the other kind of Seesaw models, one has $Br(\mu \to eee) > Br(\mu \to e\gamma)$ because $\mu \to eee$ arises at tree-level and $\mu \to e\gamma$ at loop-level. The predicted fixed ratios have drastic consequences, since the determination of a single ratio could rule out the type-3 Seesaw scenario as the one generating CLFV processes. Similarly, the measurement of one or better several ratios as predicted in Eqs. (2.119)-(2.121) would be a very strong indication for the type-3 Seesaw. Let's note that contrarily to the other kind of Seesaw, one cannot predict the mass scale from the determination of one ratio.

If all the triplets are degenerate in mass, one can finally compute the sensitivity of the future experiments on the mass scale $m_\Sigma \equiv m_{\Sigma_k}$. Using the perturbativity of the Yukawa couplings $Y_\Sigma \leq \sqrt{4\pi}$, the maximum fermionic triplet mass scales that future interesting experiments could

[22] Let's note that expression of $R_{\mu\to e}^{Ti}$ agrees with the one obtained in Eq. (40) of Ref. [129], but we get a ratio $R_{\mu\to e}^{Ti} / Br(\mu \to e\gamma)$ which is ~ 4 times larger compared to their Eq. (42).

probe are given by

$$m_\Sigma \lesssim 2.5\cdot 10^2 \text{ TeV}\cdot\left[\frac{4\cdot 10^{-14}}{Br(\mu\to e\gamma)}\right]^{1/4}, \tag{2.122}$$

$$m_\Sigma \lesssim 5.8\cdot 10^3 \text{ TeV}\cdot\left[\frac{10^{-16}}{Br(\mu\to eee)}\right]^{1/4}, \tag{2.123}$$

$$m_\Sigma \lesssim 3.9\cdot 10^4 \text{ TeV}\cdot\left[\frac{10^{-18}}{R^{Ti}_{\mu\to e}}\right]^{1/4}, \tag{2.124}$$

$$m_\Sigma \lesssim 1.8\cdot 10^4 \text{ TeV}\cdot\left[\frac{10^{-17}}{R^{Al}_{\mu\to e}}\right]^{1/4}. \tag{2.125}$$

2.6.3 Distinction between the Seesaw

From the above results in Fig. 2.11, Fig. 2.12, and Eqs.(2.111), (2.119)-(2.121), we can now compare the various ratios for the three kinds of Seesaw. The ratios $R^{\mu\to e(\mathcal{N})}_{\mu\to e\gamma}$ and $R^{\mu\to e(Ti)}_{\mu\to e(Al)}$ are the only ones that can be used to distinguish between the three types of Seesaw. Moreover, it is also possible to make the distinction between the type-1 and type-3 Seesaw via the ratios $R^{\mu\to e(\mathcal{N})}_{\mu\to eee} = R^{\mathcal{N}}_{\mu\to e}/Br(\mu\to eee)$ and $R^{\mu\to e\gamma}_{\mu\to eee} = Br(\mu\to e\gamma)/Br(\mu\to eee)$.

We show in Fig. 2.13, as a function of the mass scales of the heavy particles m_{N_1}, m_{Δ^+} and m_Σ, the various ratios for the type-1 Seesaw (black), type-2 Seesaw if possible (blue) and type-3 Seesaw (green). We focus on the region $m_X \gg m_W$, since it is the most predictive one. The solid lines correspond to the degenerate case in each Seesaw. The bands have been obtained varying all the unknown parameters in their allowed range. The regions that won't be probed by the future experiments are shown in red and are delimited by the dotted horizontal lines.

For Titanium, the present sensitivity on the ratio is $R^{\mu\to e(Ti)}_{\mu\to e\gamma} \approx 7.5$. MEG will improve the sensitivity on $\mu\to e\gamma$ to $Br(\mu\to e\gamma)\sim 4\cdot 10^{-14}$, so that the sensitivity on the ratio will increase to $R^{\mu\to e(Ti)}_{\mu\to e\gamma} \approx 107.5$. Then, thanks to the PRISM experiment, the sensitivity on the ratio should progressively decrease by ~ 6 orders of magnitudes to reach $R^{\mu\to e(Ti)}_{\mu\to e\gamma} \approx 2.5\cdot 10^{-5}$. For Aluminum, there is actually no bounds on the $\mu\to e$ conversion process. As the Mu2e and COMET will get in sensitivities, the sensitivity on the ratio will progressively decrease until reaching $R^{\mu\to e(Al)}_{\mu\to e\gamma} \approx 2.5\cdot 10^{-4}$. The PRISM experiment, using Titanium, should therefore not be able to probe the type-3 Seesaw through the ratio $R^{\mu\to e(Ti)}_{\mu\to e\gamma}$.

From Fig. 2.11, we see that it is in principle possible to distinguish between the various Seesaw mechanisms. Both measurements of $R^{\mu\to e(Ti)}_{\mu\to e\gamma}$ and $R^{\mu\to e(Al)}_{\mu\to e\gamma}$ could be necessary in order to remove the possible degeneracy. As an example, let's assume that experiments measure $R^{\mu\to e(Ti)}_{\mu\to e\gamma} \approx 1$. To this value corresponds two type-1 mass scales $m_{N_1} \approx 330$ GeV and $m_{N_1} \approx 120$ TeV, and a type-2 mass scale around 6 TeV, but the type-3 is ruled out as the one generating mainly the CLFV processes. To remove the degeneracy, the measurement of the $R^{\mu\to e(Ti)}_{\mu\to e\gamma}$ would be needed. This latter value could confirm either the type-1 or type-2 Seesaw, or rule out both possibilities.

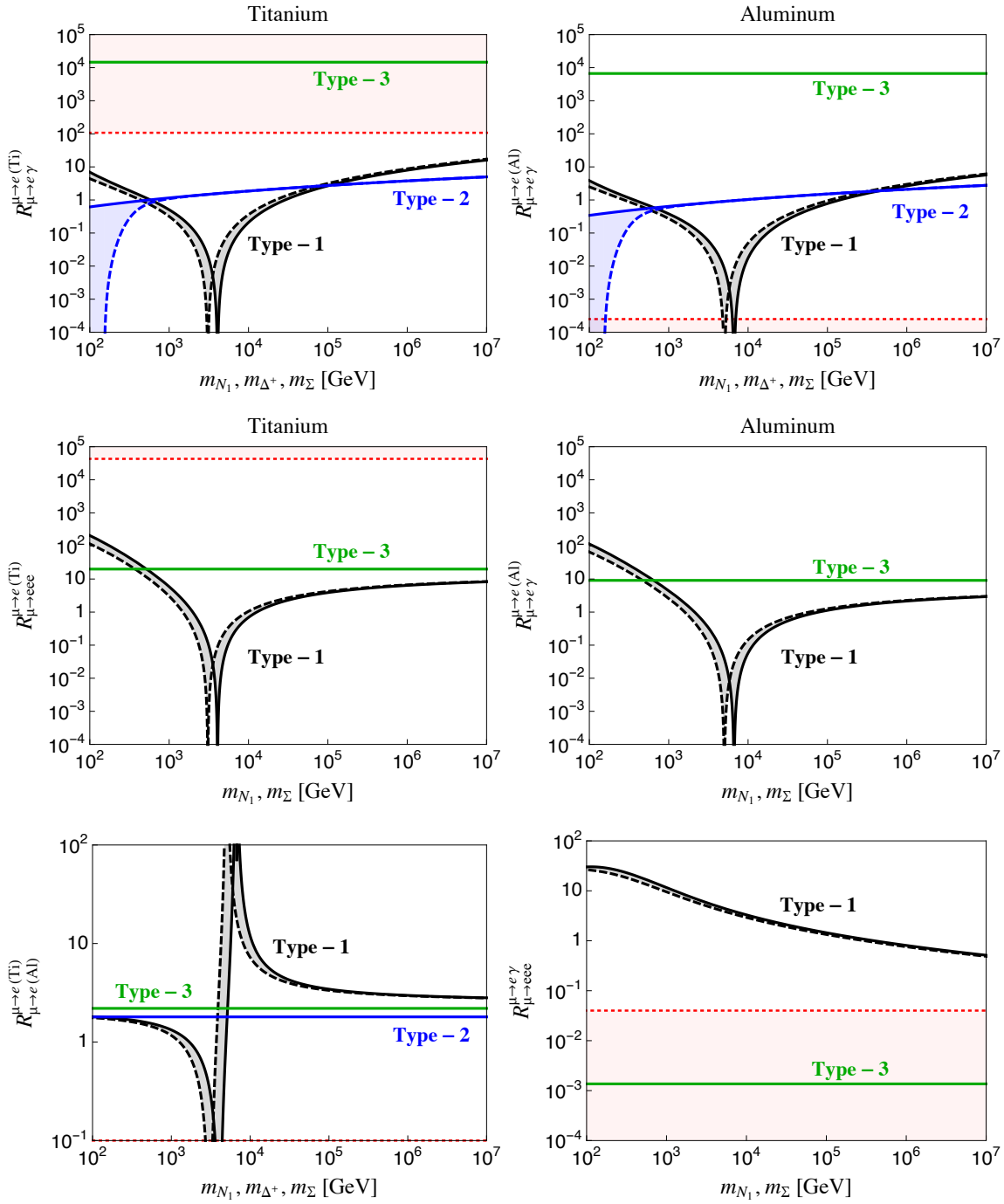

Figure 2.13 – Various ratios (i) for the type-1 Seesaw as a function of the lightest right-handed neutrino mass m_{N_1} (black), (ii) if possible for type-2 Seesaw as a function of the scalar triplet mass m_{Δ^+} (blue), and (iii) for type-3 Seesaw as a function of the scalar triplet mass m_Σ (green). The solid lines correspond to the degenerate case in each Seesaw model. The bands have been obtained varying the various parameters, allowing the non-degenerate case. The region above or below the dotted red lines could not be probed by future experiments.

2.7 Summary

In this chapter, we have analyzed the CLFV processes induced by the type-1 Seesaw models, as $\mu \to e\gamma$, $\mu \to eee$ and $\mu \to e$ conversion. Concerning this latter process, since there were no consensus on the expression of its rate, we have carefully computed it. We have found a new expression valid for any kind of nucleus. Our result is given in full generality by Eq. (2.65) with the form factors given in Eqs. (2.62) and (B.120)-(B.129). In the light nuclei approximation, it is given by Eq. (2.66) with the form factor given by Eq. (2.67). Although quite close to the one obtained in the literature, the new expression gives rise to a different phenomenology, that we have studied.

In particular, firstly we have analyzed the phenomenology in the case where all the right-handed neutrinos are degenerate. This case is well motivated by the Inverse Seesaw models, based on an approximate lepton conservation symmetry, in which one can have small masses for the light neutrinos, and at the same time observable CLFV rates. This is generally not the case because in the standard Seesaw mechanism, CLFV process rates are expected to be proportional to m_ν^2/m_N^2, thus very suppressed. In this context, where there is only one mass scale m_N, we have shown that the ratio of two CLFV rates involving a same flavor transition does depend on this unique mass scale m_N. This result has very interesting consequences since, on the one hand, it should allow us to get information on the energy scale of the Seesaw just from the knowledge of two (or three) CLFV rates (a third one may be needed to remove a potential degeneracy). On the other hand, the knowledge of only one rate and a bound on another one may be enough to rule the type-1 Seesaw as the main mechanism that generates CLFV processes. Taking into account that the processes $\mu \to e\gamma$ and $\mu \to eee$ will not reach sensitivities better than other low-energy experiments for $m_N \lesssim 40$ GeV and $m_N \lesssim 50$ GeV respectively (see Fig. 2.8), we show in Fig. 2.14 as a summary the ratios $R^{\mathcal{N}}_{\mu\to e}/Br(\mu \to e\gamma)$ (solid) and $R^{\mathcal{N}}_{\mu\to e}/Br(\mu \to eee)$ (dashed) as a function of the mass for various nuclei. Subsequently, we have analyzed the present and future constraints on the mixing parameters for the low and large mass regimes, and compared them to the sensitivities of other experiments. These will provide the best constraints for right-handed neutrino masses above ~2 GeV (before SHiP) and ~5 GeV (after SHiP). We have shown that future experiments could probe type-1 Seesaw masses as high as $m_N \sim 10^3$ TeV.

Secondly, we have analyzed the non-degenerate case with two right-handed neutrinos. We have shown analytically that, requiring observable rates, the ratio of two rates now depends on both neutrinos masses m_{N_1} and $m_{N_2} \geq m_{N_1}$. For $m_{N_1} \gtrsim m_W$, the results are very close to the ones obtained before, since they are just shifted by few TeV with respect to the degenerate case. The measurement of the ratios could in this case provide a narrow range of possible values of m_{N_1}, see Fig. 2.11. In the 3 right-handed neutrinos case, it seems not possible to make any compact analytical analysis. We didn't compute the various ratios numerically, but the situation is expected to be very similar to the two right-handed case.

Finally, we have compared the ratios obtained in the type-1 Seesaw with the ones in the other kind of Seesaw mechanisms, see Fig. 2.13. We have shown that the ratios have different expressions in all three types of Seesaw. In particular, for $m_\Delta \gg m_W$, the type-2 Seesaw predicts a ratio $R^{\mathcal{N}}_{\mu\to e}/Br(\mu \to e\gamma)$ that increases monotonically, and a fixed ratio $R^{Ti}_{\mu\to e}/R^{Ti}_{\mu\to e}$. It doesn't allow to make similar prediction on the other ratios because the expression of $\mu \to eee$ depends on another combination of the mixing parameters. Concerning the type-3 Seesaw, only fixed ratios

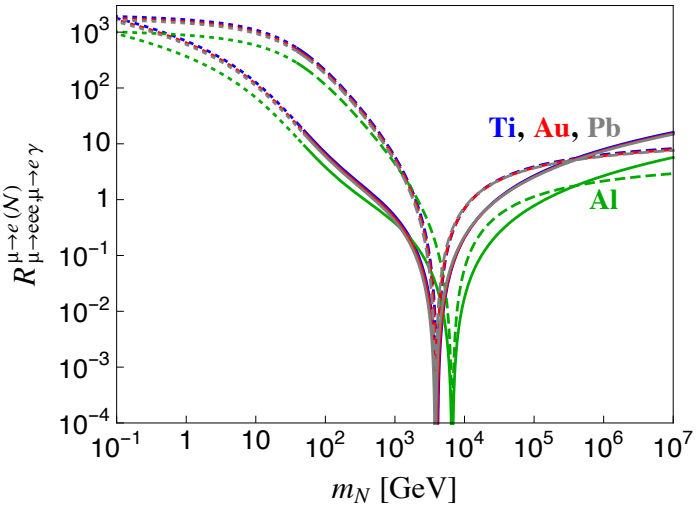

Figure 2.14 – Ratio of the $\mu \to e$ conversion rate over the $\mu \to e\gamma$ (solid) and over the $\mu \to eee$ (dashed) as a function of the degenerate mass m_N, for Aluminum (green), Titanium (blue), Gold (red) and Lead (gray) nuclei. Lines are dotted when they require, for $\mu \to e\gamma$ and $\mu \to eee$, a sensitivity better than the one expected at planned experiments.

are predicted. As a consequence, it is in principle possible to distinguish between the various types of Seesaw mechanism from the knowledge of two or, better, more rates. We have also shown that future experiments could probe mass sensitivities as high as 10^4 TeV for both type-2 and type-3 Seesaw.

Let's note, as a final remark, that in practice things may be more complicated, since the $\mu \to e$ conversion rates possess various uncertainties, in particular from nuclear physics which could shift the various curve by ~1 TeV order. In this case, the uncertainties should be treated correctly and would enlarge the bands in the various plots. Nevertheless, we don't expect any drastic impact the above conclusions, since the uncertainties could lead at most to order ~ 1 TeV shifts, as in the non-degenerate case.

Part II

Seesaw models as the origin of the Baryon asymmetry of the Universe

3 The Baryon Asymmetry of the Universe and standard leptogenesis

Since the discovery of the positron in1932 by Carl D. Anderson, it is clear that either a particle has an associated antiparticle as predicted by Paul Dirac few years before, or it is its own antiparticle. For example, a charged particle as the electron and its associated anti-particle (the positron) have exactly the same quantum numbers, except for their electric charge which are opposite. One could think naively that a perfect symmetry exists between particles and antiparticles in Nature. However, all what is made arounds us is made of matter, and not anti-matter. Protons, neutrons and electrons are the elementary blocks that constitute all the usual matter on earth. Antimatter can only be seen from creating it in accelerators or in the high atmosphere from cosmic rays interactions. Even beyond the earth, observations actually lead to the same verdict : there is no trace of any structure made of antimatter in the Universe. How is this possible ? Clearly, the matter-antimatter symmetry is broken. To understand this point, let's introduce very briefly the history of our Universe as it is actually understood.

The Standard Model of cosmology is the Lambda Cold Dark Matter (ΛCDM) model where Lambda denotes the dark energy. It is based on the theory of General Relativity using the Friedmann-Lemaître-Robertson-Walker metric. According to this model and using Planck observational data, our Universe seems to be constituted of approximately 4.9% of ordinary matter, 26.8% of Dark Matter (DM) and 68.3% of dark energy [40]. These two latter elements constitute the dark sector whose associated origin and nature has not yet been determined, which means that most of our Universe has still to be understood. The ΛCDM model is in excellent agreement with various properties of the cosmos, especially :

- the measurement of the Hubble-Lemaître expansion and the acceleration of the expansion of the Universe through the dark energy,
- the Cosmic Microwave Background (CMB) power spectrum, thanks in particular to the various density of ordinary matter and dark matter,
- the abundances of Hydrogen, Helium, and Lithium atoms, through the Big Bang Nucleosynthesis.

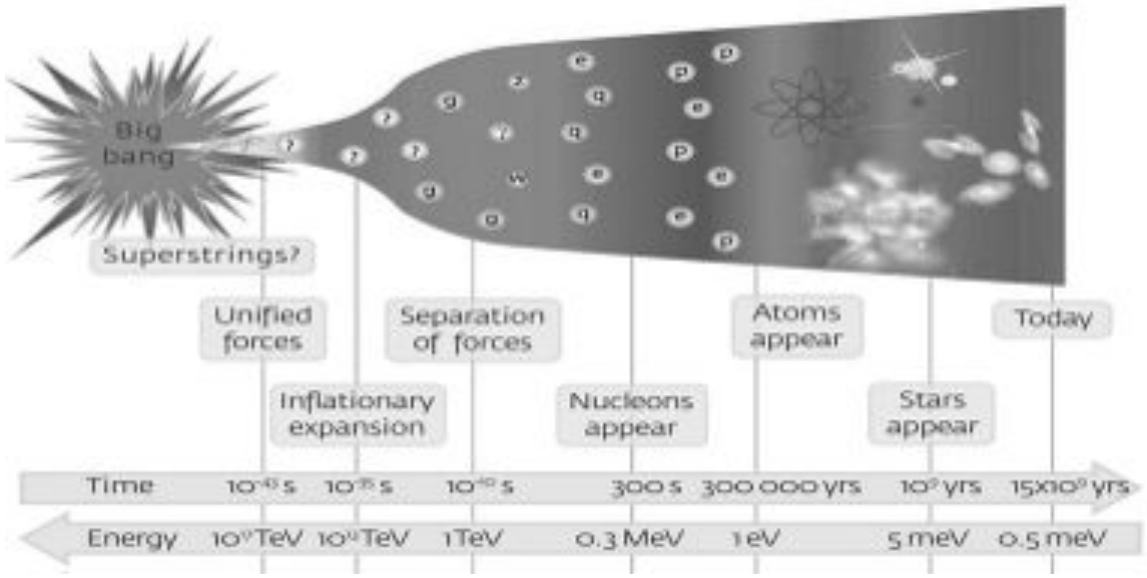

Figure 3.1 – Sketch of the evolution of our Universe since the Big Bang. ©Max Planck Institute for Physics

The existence of a CMB means that our Universe started in a hot, dense state and has been expanding over time. As we go back in time, our Universe was more and more hot and compact. Around 14 billion years ago, the Universe is expected to have been so hot and compact that the temperature could have reached a temperature close to the Planck temperature $T_{\text{Planck}} \sim 10^{32}$ K, or in terms of energy $E_{\text{Planck}} \sim 10^{19}$ GeV. This was the Big Bang era.

A sketch of the evolution of our Universe is presented in Fig. 3.1 . At early times, between the Big Bang era and the CMB decoupling which occurred about $\sim 3 \cdot 10^5$ seconds after, the Universe was constituted by a plasma of elementary particles. But what kind of elementary particles ? This depends on the temperature. Basically, for temperature values above the mass m_X of some particle X, the plasma will be populated by these particles X but also by the associated antiparticles $\bar{X}$. For example, for temperatures above ~500 keV, the kinetic energy of particles in the thermal bath is large enough for electron and positron species to be created in pairs and to populate the plasma. One could therefore naively expect that, at early times, our Universe was in good approximation symmetric regarding the particle and antiparticle abundances. However, following a totally symmetric cosmological evolution for both kind of particles, one can show that the present matter density would have been much less than the observed one, by approximatively ~ 9 orders of magnitudes. This means that at some point in our Universe, either the matter-antimatter symmetry must have been violated in order to account for the observed matter density, or the antimatter is living apart somewhere in the Universe. However, such a separation of population cannot be accounted by the ΛCDM model. Moreover, this would allow matter-antimatter annihilations to SM particles at the boundary between the matter and antimatter regions. In particular, high energy photons are expected to be created and since such annihilations have never been observed, the matter-antimatter symmetry violation is favored.

By matter asymmetry, one generally means baryon asymmetry because it dominates, since the baryons are much heavier than the leptons, and because it is known unlike the lepton asymme-

try (due to the neutrino asymmetry whose amount is not known). This is the Baryon Asymmetry of the Universe (BAU). The BAU is usually given as a ratio between the baryon number density n_B over the entropy density s, which doesn't vary due to the expansion and is constant in time. The analytical expression of these two quantities can be found in Appendix C.1. The present value of the baryon density, and therefore the baryon asymmetry, as measured by Planck is at 1 sigma level given by [206]

$$Y_B^{\text{today}} \equiv \left.\frac{n_B}{s}\right|_{\text{today}} \simeq \left.\frac{n_B - n_{\bar{B}}}{s}\right|_{\text{today}} = (9.2 \pm 0.1) \cdot 10^{-11} \,. \tag{3.1}$$

The BAU is sometimes instead defined as the ratio η_B between the baryon density and the photon number density n_γ, whose value is related to the previous one and is given by

$$\eta_B \equiv \left.\frac{n_B}{n_\gamma}\right|_{\text{today}} \simeq \left.\frac{n_B - n_{\bar{B}}}{n_\gamma}\right|_{\text{today}} = (6.5 \pm 0.1) \cdot 10^{-10} \,. \tag{3.2}$$

In this chapter, we will present the main experimental methods used to determine the baryon density of our Universe, and so the BAU. We discuss the ingredients needed in order to generate a baryon asymmetry, i.e. the Sakharov conditions. The generation of the baryon asymmetry is called baryogenesis. We discuss some of the various possible scenarios, in particular the leptogenesis one which consists in generating a baryon asymmetry through the production of a lepton asymmetry. This leptogenesis scenario is well motivated since it is naturally present in the different Seesaw models that we introduced previously. In order to understand more deeply the way leptogenesis proceeds, we focus on the type-1 Seesaw leptogenesis, firstly without distinguishing between the lepton flavors, and secondly taking into account the effect of the lepton flavors.

3.1 Experimental determination of the baryon density

The baryon density as defined in Eq. (3.1) or (3.2) can also be expressed in terms of the density parameters Ω_B. This quantity is generally the one furnished by experiments, and it is the one that enters in the Friedmann equations. It is defined as the ratio between the present baryon energy density ρ_B over the critical energy density ρ_c

$$\Omega_B \equiv \frac{\rho_B}{\rho_c} \,, \quad \text{where} \quad \rho_c \equiv \frac{3H_0^2}{8\pi G} \,, \tag{3.3}$$

with $H_0 = (67.74 \pm 0.46)$km/s/Mpc the present value of Hubble rate H [206], and G the gravitational constant. Let's note that H_0 is often given in terms of the reduced Hubble constant h according to $H_0 = 100 \cdot h \cdot$(km/s)/Mpc. The baryon density parameters Ω_B is related to Y_B and η_B through

$$Y_B = \frac{n_\gamma(T_0)}{s_0}\eta_B = \frac{3}{8\pi G m_p}\frac{H_0^2}{s_0}\Omega_B \,, \tag{3.4}$$

where $s_0 = s|_{\text{today}}$ is the present value of the entropy density and $n_\gamma(T_0) = n_\gamma|_{\text{today}}$ is the present value of the photon number density, whose analytical expression can be found in Appendix C.1. In Eq. (3.4), we have used the fact that the energy and the number density are related through $\rho_B = n_B m_B \simeq n_B m_p$, with m_p the mass of the proton.

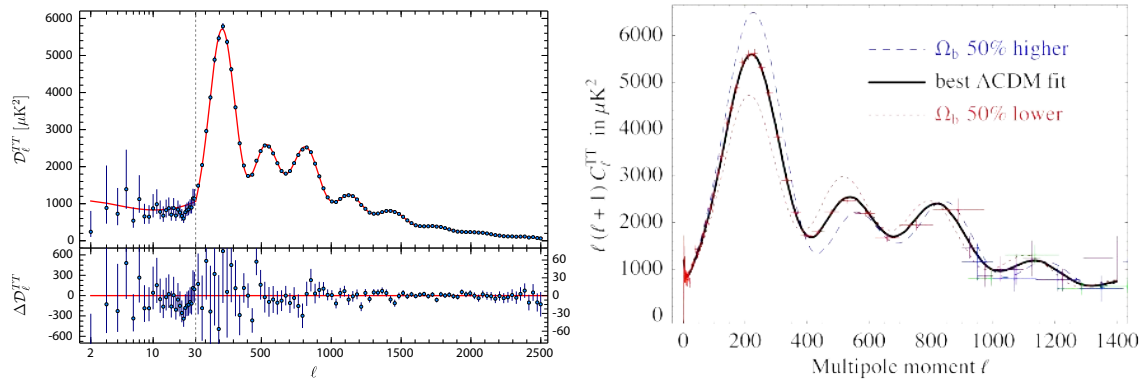

Figure 3.2 – Left : The most precise plots of the angular power spectrum of the CMB, as given by the Planck collaboration [206]. Right : effect of the variation of the baryon density on the CMB power spectrum. This figure is taken from [207].

The most precise determination of Ω_B has been performed by the Planck collaboration, which has provided, at 68% C.L., [206]

$$\Omega_B h^2 = 0.02230 \pm 0.00014 \,. \tag{3.5}$$

This is the value used to get Eqs. (3.1) and (3.2) through Eq. (3.4). To get this value, the Planck collaboration has combined data coming from the CMB spectrum and external sources as from Lensing and from Baryon Acoustic Oscillation (BAO). Let's now briefly discuss two of the several ways of determining the baryon asymmetry of our Universe.

3.1.1 From the Cosmic Microwave Background (CMB)

A possible way to determine Ω_B experimentally is from the angular CMB power spectrum, which basically gives us the amplitude of the temperature fluctuations of the CMB in function of the angular frequency ℓ. We show in left panel of Fig. 3.2 the power spectrum given by the Planck collaboration [206]. We will not provided here all details, just mention that the shape of the curve does in particular depend on Ω_B. In a sake of illustration, we show the effect of the baryon density variation on the CMB power spectrum in the right panel of Fig. 3.2, taken from Ref. [207].

3.1.2 From Big Bang Nucleosynthesis (BBN)

The Big Bang Nucleosynthesis describes how the various light element abundances have been generated as the Universe was cooling down. By light elements we mean the Deuterium D, the Helium ^3He and ^4He, and the Lithium ^7Li. Without going into details, let's mention the main steps of the scenario. For $T \gtrsim 1$ MeV, the weak interactions are in equilibrium, and processes as $n + \nu_e \leftrightarrow p + e^-$ maintain the p, n, e and ν_e particles in thermal equilibrium (the notion of thermal equilibrium is explained in Appendix C.1.5). If the protons and neutrons are non-relativistic, which is the case for $T < m_{p,n}$, this process implies that their abundances are directly related through $n_p/n_n \simeq e^{\delta m/T}$, where δm is the mass splitting $\delta m \equiv m_n - m_p \approx 1.3$ MeV. At $T \sim 0.7$ MeV, these weak interactions freeze out, so that the p and n abundance ratio is fixed to $n_p/n_n \approx 6$.

For 0.1 MeV $\lesssim T \lesssim$ 1 MeV, processes involving light nuclei are in thermal equilibrium. The Deuterium appears through $p+n \leftrightarrow D+\gamma$, the Tritium through $D+D \leftrightarrow T+n,p$, the Helium through $D+T \leftrightarrow {}^4He+n,p$ and $D+D \leftrightarrow {}^4He+\gamma$. The abundances of the various nuclei are thus directly related, but these are not definitively fixed since the inverse processes as $D+\gamma \rightarrow p+n$ still occur (because they are faster than the Hubble rate) and dissociate the nuclei. Below $T \sim 0.1$ MeV, these inverse processes are no more possible and the various light nuclei abundances are fixed, and related to each other. The sum of these light nuclei abundances is nothing but the total baryonic abundance n_B present in our Universe, and their relative abundances depend in fact on the ratio n_B/n_γ, since the rates of the above nuclear reactions depend on the density of baryons. Therefore, by measuring the light nuclei abundances fractions n_X/n_H with $X = D, {}^3He, {}^7Li$, one could determine the value of η_B.

A summary plot of the species abundances in function of the baryonic fraction $\eta_{10} \equiv 10^{10} \cdot \eta_B$ of the Universe is given in the left panel of Fig. 3.3 [8]. The bands show the 95% C.L. range. The yellow boxes represent the observed light abundance fractions at 95% C.L.. The largest vertical band indicates the BBN concordance range without the lithium constraint, $5.7 \lesssim \eta_{10} \lesssim 6.7$ (95% C.L.), and the narrow band represent the more precise CMB measurement of the cosmic baryon density, $6.4 \lesssim \eta_{10} \lesssim 6.6$ (95% C.L.).

The fraction of Deuterium D is the most precise one, because it could only have been produced during BBN. It has been measured from the observation of the absorption spectra of high redshift object as quasars, whose light has been partially absorbed by clouds of gas. The ${}^4He$ is not a so good indicator of the baryon density because it depends on the expansion rate. Indeed, since two neutrons are needed to produce one ${}^4He$ atom, the neutrons must not have decayed before they have been captured. Finally, the ${}^3He$ and ${}^7Li$ abundances are less precise since their determination is more complex and model dependent.

Finally, let's note that there are other ways to determine the baryon density of our Universe. Even if they are less precise than the CMB method, let's mention in particular methods based on : type-1 Supernovae (the velocity of these candles depends on the matter density), gravitational lensing (the matter density bends the light and acts as a lens), Baryon Acoustic Oscillation (BAO) (acoustic waves were generated as the plasma constituted by photons and baryons was attracted in dense regions, composed by ordinary and dark matter, and these sound waves have decoupled after the epoch of recombination, what can be seen from large scale structure of matter using astronomical surveys). The right panel of Fig. 3.3 shows a summary plot of the various experimental data, taken from Ref. [208]. It gives the preferred values of Ω_Λ and Ω_M densities from various kind of experiments, where the quantity Ω_Λ denotes the dark energy density and $\Omega_M = \Omega_B + \Omega_{DM}$ the total matter density. To get baryon density Ω_B, one can subtract Ω_{DM} as provided by the CMB.

3.2 Needed ingredients for baryogenesis

If we start with a B-symmetric Universe at early times, i.e. $n_B = \bar{n}_B$, then at $T \lesssim 1$ GeV a large amount of nucleons $N = (p,n)$ and anti-nucleons $\bar{N} = (\bar{p},\bar{n})$ are formed from quarks. From QCD interactions, one has therefore efficient $N + \bar{N} \rightarrow SM$ annihilations, which are in thermal equilibrium until $T \approx 20$ MeV. As a consequence, the final fraction density after the thermal

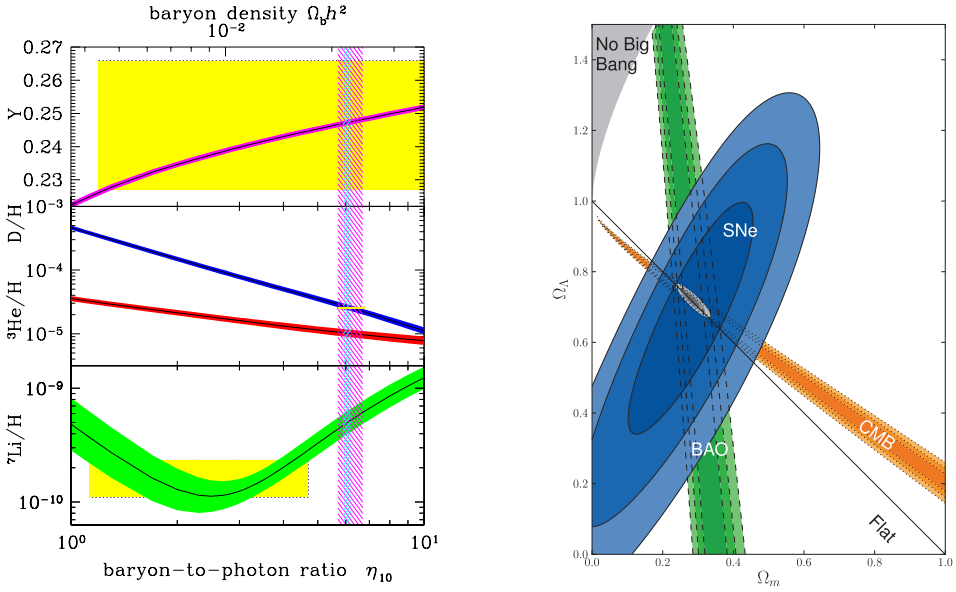

Figure 3.3 – Left : light nuclei abundance fractions as a function of the baryonic fraction $\eta_{10} \equiv 10^{10} \cdot \eta_B$, with $\eta_B = n_B/n_\gamma$. The plot has been taken from Ref. [8]. Right : summary plot of the various experimental measurement of Ω_Λ vs Ω_M, taken from Ref. [208].

decoupling of these annihilations at $T_{\rm fo} \approx 20$ MeV is given by

$$Y_B^{\rm today} = \frac{n_N^{\rm Eq}}{s}\bigg|_{\rm today} = \frac{n_N^{\rm Eq}(T_{\rm fo})}{s_0} = \frac{n_{\tilde{N}}^{\rm Eq}(T_{\rm fo})}{s_0} \approx 10^{-20} \ll 10^{-10} \,. \tag{3.6}$$

which is well below the observed value given in Eq. (3.1). One needs therefore an asymmetry before $T \approx 20$ MeV, given the fact that it would be difficult to create one after due to kinematical reasons.

A baryon asymmetry exists in our Universe, and it must have been generated at some epoch earlier than the BBN era. The generation of the baryon asymmetry is called "baryogenesis". Baryogenesis requires three basic elements to work. These are the Sakharov conditions [209] which say that, starting from a Universe composed by an equal amount of baryons and antibaryons ($\Delta B = 0$) and assuming CPT invariance, the processes that generated the baryon asymmetry must

1. *violate the baryon number B*. This is obvious since we start with $\Delta B = 0$ and finish with $\Delta B \neq 0$. There should thus exist a process $a \to b$ where a and b are initial and final states carrying different baryon number, $B_b - B_a \neq 0$.

2. *violate Charge (C) and the Charge·Parity (CP) symmetries.* If it is not the case, the B-violating processes $a \to b$ would occur at the same rate than $a^c \to b^c$ or $a^{cp} \to b^{cp}$, where the ^{c} (^{cp}) superscript denotes the C (CP) conjugate states, so that even if the baryon number B is violated in the process, it is in fact globally conserved.

3. *have departed from thermal equilibrium.* Otherwise, not only $a \to b$ processes do occur but also $b \to a$ do occur, and once a baryon asymmetry is generated it would be directly destroyed. The notion of thermal equilibrium is discussed in Appendix C.1.5.

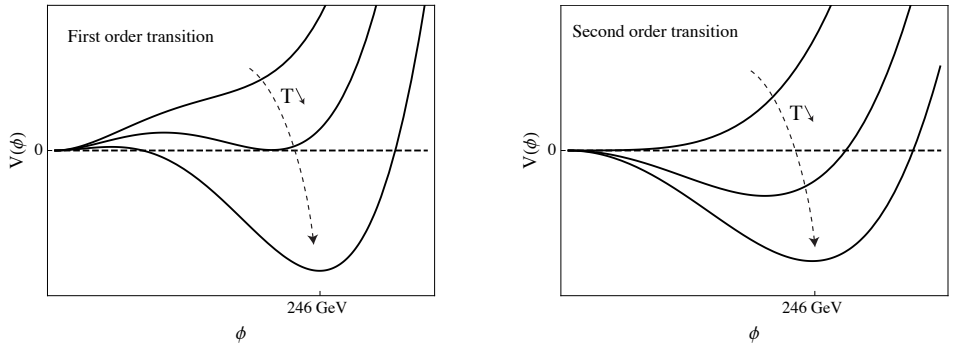

Figure 3.4 – Shape of the scalar potential as a function of the scalar field in case of a first order (left) and a second oder (right) phase transition. The curves go from bottom to top as the temperature increases.

These three ingredients must be fulfilled in order to generate the BAU. Interestingly, the SM satisfies the three conditions. Indeed, (i) the baryon number B, even if conserved globally, is violated at the quantum level by the sphalerons, which are non-perturbative processes (instantons) that violate the $B+L$ number. We will further discuss the sphalerons in section 3.3.3 below. (ii) C and CP are violated by weak interactions. (iii) The departure from thermal equilibrium may be assured by the ElectroWeak Phase Transition (EWPT) or by the expansion of the Universe.

However, as we will now see, the SM seems not to be able to produce enough BAU. This is on the one hand because CP-violation in the SM seems not to be sufficient to produce enough baryon asymmetry, and on the other hand because departure from thermal equilibrium requires a first order electroweak phase transition (see Fig. 3.4) while in the SM it is actually a crossover transition. These two failures are clear motivations for beyond the SM physics (BSM). We will next discuss briefly some of the well known baryogenesis scenario of BSM physics.

3.3 Baryogenesis possibilities

3.3.1 Electroweak baryogenesis

We know that the scalar potential of the SM is such that the scalar field has a vev, given by $\langle\phi\rangle = \mathrm{v}/\sqrt{2}$, with $\mathrm{v} = 246$ GeV. However, at high temperature, one must include the quantum loop corrections to the scalar potential. One can show that above some critical temperature T_{EW}, the minimum of the scalar potential is such that the scalar field ϕ has actually no vev, while below T_{EW} it gets a vacuum expectation value through the Brout-Englert-Higgs mechanism [210]. There is therefore an ElectroWeak Phase Transition (EWPT) at some temperature T_{EW}.

In the left panel of Fig. 3.5, we show the vev of the scalar field as a function of the temperature, computed in the SM framework. From this figure, one sees that the critical temperature is approximately given by $T_{EW} \simeq 165$ GeV, and one has therefore :

$$T \gtrsim 165 \text{ GeV} \quad \rightarrow \quad \langle\phi\rangle = 0 \,, \tag{3.7}$$

$$T \ll 165 \text{ GeV} \quad \rightarrow \quad \langle\phi\rangle = \frac{\mathrm{v}}{\sqrt{2}} \,. \tag{3.8}$$

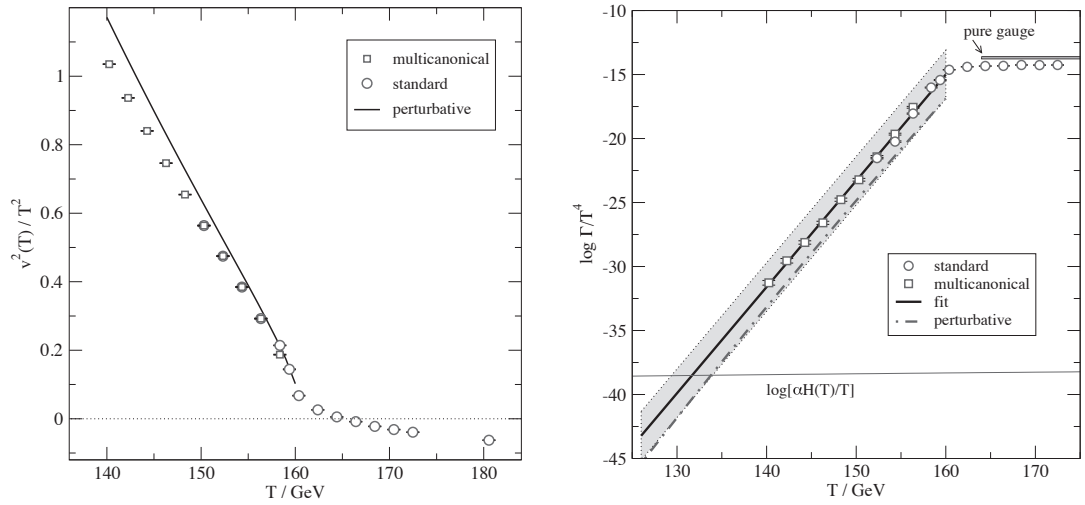

Figure 3.5 – Left : SM evolution of the vev of the scalar field, expressed as v^2/T^2, as a function of the temperature T using different methods. Right : SM evolution of the EW sphalerons rate $\Gamma_{EW} \equiv \Gamma/T^4$ as a function of the temperature, using different methods. Both plots are taken from Ref. [210].

One can show that if the phase transition is a first order transition, that is the vev of the scalar field jumps from $v = 0$ to $v \neq 0$ at some precise temperature (see the left panel of Fig. 3.4), it is in principle possible to generate a baryon asymmetry. [1] However, as already mentioned, the EW transition in the SM is not first order, in which case the vev changes smoothly from $v = 0$ to the $v = 246$ GeV as the temperature decreases (see the right panel of Fig. 3.4). In order to get a first order transition, one need to act on the EWPT, for example by adding new scalar particles as in the Two Scalar Doublet model (2HDM) or Supersymmetry.

3.3.2 GUT Baryogenesis

Grand Unified Theories, see section 1.6, on top of all the other advantages, also provide all the ingredients needed for baryogenesis. Indeed, they usually contain new heavy particles X, with new interactions that breaks B, C and CP, as in $SO(10)$ and L-R GUT theories. One expects generally (in particular from proton decay bounds) that the heavy particle masses should lie around the GUT scale, so that the out-of-equilibrium decays of these particle fulfill all the Sakharov conditions and can account for all the observed baryon asymmetry.

3.3.3 Sphalerons and baryogenesis through leptogenesis

The gauge symmetries and the particle content of the SM Lagrangian imply that the baryon number B and the three flavor numbers L_α are conserved at tree-level in the SM. From the

[1] Indeed, for a first order phase transition, most likely regions of non-zero vev nucleate bubbles at different space-time coordinates. When growing in the empty space with $v = 0$, bubbles with $v \neq 0$ filled progressively the whole Universe. During the conquest of the empty space, bubbles should have collided and it is these collisions that could be at the origin of the BAU. This is obviously not a thermal equilibrium process. For more details concerning this scenario, see for example Ref. [211, 212].

conservation of the three lepton flavor numbers L_α, the total lepton number L is (accidentally) conserved at tree-level as well. However, baryon and lepton numbers are anomalous : B and L numbers are in fact broken at the quantum level. Indeed, the SM contains non-perturbative processes called sphalerons [213] that break the $B+L$ number while conserving separately the $B/3-L_\alpha$ numbers and so the total $B-L$ one.

Sphalerons are complex processes, and our goal here is not to enter in the details of the way they are induced. For now, let's just say that they violate $B+L$ number but conserve $B/3-L_\alpha$ (and $B-L$), and that they are active for temperature within the range $T \in [132, 10^{12}]$ GeV. The lower value can be seen from the right panel of Fig. 3.5, taken from Ref. [210]. The higher value is obtained from Eq. D.44 in Appendix C.2 [214]. Therefore, since they break $B+L$ but conserve $B-L$, if some BSM physics has generated a lepton asymmetry ΔL above 132 GeV, a baryon asymmetry ΔB should have been generated too. As an example, let's suppose that a lepton asymmetry $\Delta L_{\rm ini} = L_{\rm ini}$ is generated above 132 GeV by some BSM physics. A naive computation allows us to determine the baryon asymmetry transferred by sphalerons :

$$(B+L)_{\rm fin} \simeq 0 \qquad \rightarrow \quad L_{\rm fin} \simeq -B_{\rm fin}\,, \tag{3.9}$$

$$(B-L)_{fin} - (B-L)_{\rm ini} = 0 \qquad \rightarrow \quad B_{\rm fin} = L_{\rm fin} - L_{\rm ini} \simeq -\frac{L_{\rm ini}}{2}\,. \tag{3.10}$$

In the first equation, we assumed that the EW sphalerons violates $B+L$ by typically bringing it to zero, and in the second equation we used the fact that sphalerons conserve $B-L$ so that $\Delta(B-L)=0$. The naive result $B_{\rm fin} \simeq -L_{\rm ini}/2$, even if not rigorous, does still provide the good order of magnitude, and we see that, starting from a zero initial baryon asymmetry $B_{\rm ini}=0$, we actually end up with $B_{\rm fin} \neq 0$. The correct relation between the $B-L$, L and B asymmetries is computed in Appendix C.5. Taking into account the various spectator processes, it is given by [215]

$$\Delta Y_B = \frac{28}{79}\Delta Y_{B-L} = -\frac{28}{51}\Delta Y_L \qquad \text{for} \quad T \gtrsim T_{EW}\,, \tag{3.11}$$

$$\Delta Y_B = \frac{12}{37}\Delta Y_{B-L} = -\frac{12}{25}\Delta Y_L \qquad \text{for} \quad T_{\rm sphal} \lesssim T \lesssim T_{EW}\,, \tag{3.12}$$

where $T_{\rm sphal} \simeq 132$ GeV is the temperature below which sphalerons are not active anymore. The above ratios are close to the naive result obtained in Eq. (3.10). For $T < T_{\rm sphal}$, sphalerons freeze out and if no baryon number violating process occurs the baryon asymmetry remains unchanged and given by Eq. (3.12). It is therefore the Eq. (3.12) that must be used in order to relate the present baryon asymmetry $\Delta Y_B^{\rm today}$ with the $B-L$ asymmetry produced above $T_{\rm sphal}$.

This scenario, of generating a baryon asymmetry starting from a lepton asymmetry, is called baryogenesis through leptogenesis, or just *leptogenesis*. Along this mechanism, the three Sakharov conditions become :

1. *the lepton number L must be violated,*

2. *C and CP must be violated,*

3. *the process must depart from thermal equilibrium.*

Leptogenesis is very appealing since all the above conditions are actually fulfilled in the now well-known Seesaw mechanisms, which contains new heavy particles whose out-of-equilibrium decays may violate L, C and CP. Thus, on top of generating small neutrino masses, Seesaw models could also provide an explanation for the baryon asymmetry of the Universe. This idea of leptogenesis has originally been carried in Ref. [216], where they considered leptogenesis in the framework of type-1 Seesaw models. We will now introduce in the next section the basics of leptogenesis in the type-1 Seesaw context. Leptogenesis in the framework of the type-2 Seesaw will be discussed in detail in chapter 4.

Definition of the total lepton and baryon asymmetries. In Eq. (3.11) and (3.12), the total lepton asymmetry is defined as $\Delta Y_L = Y_L - Y_{\bar{L}}$, where the total lepton abundance $Y_L \equiv n_L/s$ is equal to the sum of the lepton flavor densities $Y_{L_\alpha} = Y_{\ell_\alpha} + Y_{e_\alpha}$ (without Dirac right-handed neutrino) :

$$\Delta Y_L = \sum_\alpha^{N_f} \Delta Y_{L_\alpha} = \sum_\alpha^{N_f} \left(\Delta Y_{\ell_\alpha} + \Delta Y_{e_\alpha}\right) , \tag{3.13}$$

with $N_f = 3$ is the number of flavor families. In the same way, taking as usual $1/3$ for the baryon number of the quarks, the total baryonic asymmetry $\Delta Y_B = Y_B - Y_{\bar{B}}$ is defined by

$$\Delta Y_B = \frac{1}{3}\sum_\alpha^{N_f} \left(\Delta Y_{Q_\alpha} + \Delta Y_{u_\alpha} + \Delta Y_{d_\alpha}\right) , \tag{3.14}$$

The quantities conserved by sphalerons are the $B/3 - L_\alpha$ and so the $B - L$ ones, which are thus defined as

$$\Delta Y_{B/3-L_\alpha} = \frac{1}{9}\sum_\beta^{N_f} \Big(\Delta Y_{Q_\beta} + \Delta Y_{u_\beta} + \Delta Y_{d_\beta}\Big) - \left(\Delta Y_{\ell_\alpha} + \Delta Y_{e_\alpha}\right) , \tag{3.15}$$

$$\Delta Y_{B-L} = \sum_\alpha^{N_f} \left[\frac{1}{3}\left(\Delta Y_{Q_\alpha} + \Delta Y_{u_\alpha} + \Delta Y_{d_\alpha}\right) - \left(\Delta Y_{\ell_\alpha} + \Delta Y_{e_\alpha}\right)\right] . \tag{3.16}$$

3.4 Basics of Leptogenesis : the unflavored type-1 Seesaw case

We now introduce pedagogically the type-1 Seesaw leptogenesis mechanism because we will need it for the type-2 Seesaw leptogenesis in the next chapter. For a question of clarity, we first study the unflavored leptogenesis, i.e. we neglect the effects of the lepton flavors and the spectator processes. The flavor issue is addressed in the next section. The reader familiar with these concepts can directly go to chapter 4.

3.4.1 Lagrangian and interactions

The type-1 Seesaw mechanism contains right-handed neutrinos N_i that are expected to be heavy in order to generate small neutrino masses, see section 1.3. By heavy, here we mean typically

$m_{N_i} > 1$ TeV. The right-handed neutrino interactions read, see Eq. (1.22),

$$\mathscr{L}^{\text{type-1}} \ni -\overline{N_{R_i}}\,\tilde{\phi}^\dagger\, Y_{N_i\alpha}\,\ell_{L_\alpha} - \frac{1}{2}\overline{N_{R_i}}\,m_{N_i}\,N_{R_i}^c + \text{H.c.}\,. \tag{3.17}$$

As usual, we choose a right-handed neutrino basis such that the Majorana mass matrix is diagonal and real. We remind that lepton number is violated in the type-1 Seesaw Lagrangian because of the presence of both Yukawa and Majorana terms. From the above Lagrangian, we see that the right-handed neutrinos interact with the other SM particles through the Yukawa interactions. For a mass typically above the electroweak scale, they can decay in a lepton ℓ_α and a scalar boson ϕ through the Yukawa interactions $N_i \to \ell_\alpha \phi$. [2] As seen in section 1.3.2, because the Yukawa couplings $Y_{N_i\alpha}$ are complex matrices, these decays, on top of being L-violating, contain also in general a C and CP violating part. The first two Sakharov conditions are therefore satisfied from the start in the type-1 Seesaw Lagrangian. The third one is also satisfied as soon as the right-handed neutrino decays out-of-equilibrium. In particular, all along these next sections, we assume that the lepton asymmetry is generated by the out-of-equilibrium decay of the right-handed neutrino N_1, which is much lighter than the other right-handed neutrinos $T_{\text{sphal}} \ll m_{N_1} \ll m_{N_{k\neq 1}}$.

3.4.2 Unflavored statement and general scenario

In order to understand the main ideas behind leptogenesis, we will in this section consider the simple but representative scenario of the "unflavored leptogenesis". In this latter :

- the effects of the lepton flavors are neglected, i.e. *the right-handed neutrino N_1 is assumed to decay into only one lepton ℓ (carrying lepton number $L(\ell) = 1$) which encompasses all the lepton flavors,*
- the effects of the spectator processes are also neglected, i.e. *the SM reactions in the thermal bath as the quark Yukawa interactions don't play any role during the leptogenesis era.*

We will now illustrate the main steps in the generation of the $B-L$ asymmetry from the N_1 decays by considering a simple example where the N_1 are initially in thermal equilibrium with the thermal bath. Chronologically, one has typically the following steps as the temperature cools down.

1. At $T \gg m_{N_1}$, right-handed neutrinos N_1 are in thermal equilibrium. Their number is therefore known and given by the thermal distribution.
2. At $T \sim m_{N_1}$, the N_1's will progressively disappear from the thermal bath. If the decay/inverse decays are in thermal equilibrium $N_1 \leftrightarrow \ell\phi$ (i.e. they are faster than the Hubble rate), the N_1's disappear by following a Boltzmann suppressed thermal equilibrium distribution. If the inverse decay reaction is not in thermal equilibrium, they disappear simply by decaying $N_1 \to \ell\phi$. In both cases, since the decays violate L, C and CP, a total $B-L$ asymmetry ΔY_{B-L} is progressively generated. As long as processes like the inverse decays $\ell\phi \to N_1$ are

[2] From now on, ℓ_α and e_α designate the left-handed doublet ℓ_{L_α} and the right-handed singlet e_{R_α} respectively. In the quark sector, we also designate Q_α, u_α and d_α as the left-handed quark doublet, right-handed up-type quark singlet, and right-handed down-type quark singlet.

in thermal equilibrium, until some decoupling temperature $T_{\rm dec}$, the production of a final $B-L$ asymmetry may be slowed down.

3. At $T \sim T_{\rm dec}$, the inverse processes $\ell\phi \to N_1$ effectively stop. From this moment, all the N_1's left decay out-of-equilibrium and produce a net $B-L$ asymmetry.

4. At $T_{\rm sphal} \lesssim T \ll T_{\rm dec}$, all the right-handed neutrinos have decayed, and the present baryon asymmetry is related to the final $B-L$ asymmetry through

$$\Delta Y_B^{\rm today} = Y_B^{\rm today} = C_{\rm sphal} \cdot \left| \Delta Y_{B-L}^{\rm end} \right| , \tag{3.18}$$

where $C_{\rm sphal} = 12/37$ is the conversion factor due to sphalerons, given in Eq. (3.12) and determined explicitly in Appendix C.5.

This is the basic general picture, which gives an idea of how things work. From the above scenario, it is clear that the decays/inverse decays play a crucial role in leptogenesis. We now give the analytical expression of the tree-level decay rate and then the analytical expression of the CP-asymmetry in the unflavored leptogenesis.

3.4.3 Tree-level decay rate

From the Lagrangian in Eq. (1.22), it is straightforward to compute the tree-level partial decay rate in lepton (antilepton) :

$$\Gamma(N_1 \to \ell\phi) = \Gamma(N_1 \to \bar{\ell}\phi^*) = \frac{1}{16\pi} \left(Y_N Y_N^\dagger \right)_{11} m_{N_1} , \tag{3.19}$$

which is nothing but the sum over α of the flavored decay rates. The total tree-level decay rate is then given by the sum of the two partial decay rates :

$$\Gamma_{N_1} \equiv \Gamma(N_1 \to \ell\phi) + \Gamma(N_1 \to \bar{\ell}\phi^*) = \frac{1}{8\pi} \left(Y_N Y_N^\dagger \right)_{11} m_{N_1} . \tag{3.20}$$

To know how fast are these decays, this rate has to be compared to the Hubble rate H. It is convenient to express the ratio Γ_{N_1}/H at $T = m_{N_1}$ as

$$K_{N_1} = \frac{\Gamma_{N_1}}{H(z=1)} = \frac{\tilde{m}_1}{m^*} , \tag{3.21}$$

where $\tilde{m}_1$ is the effective neutrino mass

$$\tilde{m}_1 \equiv 4\pi \frac{\mathrm{v}^2}{m_{N_1}^2} \Gamma_{N_1} = \frac{\mathrm{v}^2}{2} \frac{1}{m_{N_1}} \left(Y_N Y_N^\dagger \right)_{11} , \tag{3.22}$$

which depends on the high energy parameters Y_N, and where m^* is the "equilibrium neutrino mass",

$$m^* \equiv 4\pi \frac{\mathrm{v}^2}{m_{N_1}^2} H(z=1) = \frac{20\pi}{3} \cdot \sqrt{g_*} \cdot \frac{\mathrm{v}^2}{m_{\rm Planck}} \simeq 1.08 \cdot 10^{-3} \text{ eV} , \tag{3.23}$$

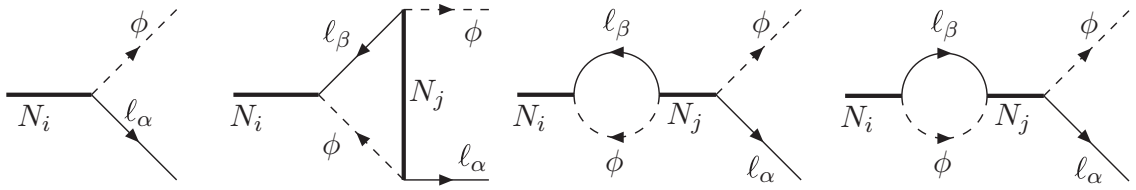

Figure 3.6 – Feynman diagrams needed in order to compute the CP-asymmetry $\epsilon_{N_1}^{\ell_\alpha}$.

which is a fixed quantity remarkably quite close to the expected neutrino mass value. It is worth to note that the quantity $\tilde{m}_1$ looks very similar to the neutrino mass expression in Eq. (1.26). From the Cauchy-Schwartz inequality $|Y_N^T Y_N| \leq |Y_N|^2$, one can actually have an idea on the lower bound on $\tilde{m}_1$:

$$\tilde{m}_1 \geq m_\nu^{\min} \,, \tag{3.24}$$

with $m_\nu^{\min}$ the smallest neutrino mass, whose value has still to be determined experimentally. This gives the lower bound $K_{N_1} \gtrsim m_\nu^{\min}/(10^{-3}\text{ eV})$. Since the second Sakharov condition is clearly not fulfilled by the tree-level expression in Eq. (3.19), we now compute the CP-asymmetry in N_1 decays.

3.4.4 Evaluation of the CP-asymmetry

In the unflavored regime, the CP-asymmetry of the decay $N_1 \to \ell\phi$ is simply given by the sum of the flavored CP-asymmetries :

$$\epsilon_{N_1} \equiv \frac{\Gamma\left(N_1 \to \ell\phi\right) - \Gamma\left(N_1 \to \bar{\ell}\phi^*\right)}{\Gamma_{N_1}} = \sum_\alpha \frac{\Gamma\left(N_1 \to \ell_\alpha\phi\right) - \Gamma\left(N_1 \to \bar{\ell}_\alpha\phi^*\right)}{\Gamma_{N_1}} \equiv \sum_\alpha \epsilon_{N_1}^{\ell_\alpha} \,. \tag{3.25}$$

Obviously, using the tree-level decay rate in Eq. (3.19) gives $\epsilon_{N_1} = 0$, and one needs to go at the loop level. In the type-1 Seesaw, the Feynman diagrams that are involved in the CP-asymmetry are given in Fig. 3.6. There are two kinds of loop diagrams : a "vertex" (second diagram) and a "self-energy" (third and fourth diagram). The self-energy part receives two contributions : a lepton number violating part (third diagram) and a lepton number conserving part (fourth diagram). Assuming $|m_{N_1} - m_{N_j}| \gg |\Gamma_{N_1} - \Gamma_{N_j}|$, a straightforward computation leads to the expression [217, 218]

$$\begin{aligned}\epsilon_{N_1}^{\ell_\alpha} = &\frac{1}{8\pi}\frac{1}{\left(Y_N Y_N^\dagger\right)_{11}} \sum_{j\neq 1} \Im m\left[Y_{N_1\alpha} Y_{N_j\alpha}^* \left(Y_N Y_N^\dagger\right)_{1j}\right] g(x_j) \\ &+ \frac{1}{8\pi}\frac{1}{\left(Y_N Y_N^\dagger\right)_{11}} \sum_{j\neq 1} \Im m\left[Y_{N_1\alpha} Y_{N_j\alpha}^* \left(Y_N Y_N^\dagger\right)_{j1}\right] \frac{1}{1-x_j} \,,\end{aligned} \tag{3.26}$$

where $x_j \equiv m_{N_j}^2/m_{N_1}^2$ and where the function $g(x)$ is given by

$$g(x) = \sqrt{x}\left[\frac{1}{1-x} + 1 - (1+x)\ln\left(\frac{1+x}{x}\right)\right] \xrightarrow[x\gg 1]{} -\frac{3}{2\sqrt{x}} \,, \tag{3.27}$$

and contains the contributions from the second and third diagrams of Fig. 3.6. The contribution from the lepton number conserving one is contained in the second line of Eq. (3.26). This latter vanishes when summing over the flavor indices, so that the unflavored CP-asymmetry is given by

$$\epsilon_{N_1} = \frac{1}{8\pi}\frac{1}{\left(Y_N Y_N^\dagger\right)_{11}}\sum_{j\neq 1}\Im m\left[\left(Y_N Y_N^\dagger\right)^2_{1j}\right] g(x_j)\,. \tag{3.28}$$

In the limit where $m_{N_j} \gg m_{N_1}$ and using the type-1 neutrino mass expression in Eq. (1.26), ϵ_{N_1} can also be recast in the form

$$\epsilon_{N_1} = -\frac{3}{32\pi}\frac{m^3_{N_1}}{\mathrm{v}^4\Gamma_N}\sum_{j\neq 1}\Im m\left\{\mathrm{Tr}\left[\left(m_\nu^{N_1}\right)\cdot\left(\sum_{j\neq 1} m_\nu^{N_j}\right)^\dagger\right]\right\}\,. \tag{3.29}$$

where $m_\nu^{N_i}$ is the contribution of the right-handed neutrino N_i to the light neutrino mass matrix $m_\nu = \sum_{N_i} m_\nu^{N_i}$.

∘ Upper bound on the CP-asymmetry and lower bound on the heavy neutrino mass

From the expression in Eq. (3.29), one can evaluate an upper bound on the CP-asymmetry, as Davidson and Ibarra shown [219] :

$$\left|\epsilon_{N_1}\right| \lesssim \frac{3}{8\pi}\frac{m_{N_1}}{\mathrm{v}^2}\frac{\Delta m^2_{\mathrm{atm}}}{m_{\nu_3}}\,, \tag{3.30}$$

where m_{ν_3} is the largest neutrino mass, and $m^2_{\mathrm{atm}} = |\Delta m^2_{31}|$ is the atmospheric mass splitting. This bound is very interesting because it allows us to determine a lower bound on the mass scale m_{N_1}. Indeed, using Eq. (3.18), we will show below that the present baryon asymmetry can be expressed as

$$\Delta Y_B^{\mathrm{today}} = C_{\mathrm{sphal}}\left|\Delta Y_{B-L}^{\mathrm{end}}\right| = \frac{12}{37}\,\epsilon_{N_1}\,\eta_{N_1}\,Y_{N_1}^{\mathrm{Eq}}\left(T \gg m_{N_1}\right)\,, \tag{3.31}$$

where $Y_{N_1}^{\mathrm{Eq}}(T)$ is the equilibrium abundance of N_1, and η_{N_1} is the so-called efficiency that reflects the out-of-equilibrium character of the N_1 decays. Basically, if all the right-handed neutrino decays $N_1 \to \ell\phi$ occur out-of-equilibrium, one has $\eta_{N_1} = 1$. Otherwise, and that is generally the case, $0 < \eta_{N_1} < 1$. The efficiency is the quantity that must be determined by solving to the Boltzmann equations, see below. Since the quantities $\Delta Y_B^{\mathrm{today}}$ and $Y_{N_1}^{\mathrm{Eq}}(T \gg m_{N_1})$ are fixed, one can express the CP-asymmetry in term of the efficiency :

$$\epsilon_{N_1} = \frac{Y_B^{\mathrm{today}}}{12/37\cdot\eta_{N_1}\,Y_{N_1}^{\mathrm{Eq}}\left(T \gg m_{N_1}\right)} \tag{3.32}$$

In the best situation, the efficiency is maximal $\eta_{N_1} = 1$, so that in order to get the observed value of the BAU in Eq. (3.1), the CP-asymmetry must be bigger than

$$\epsilon_{N_1} \geq \frac{Y_B^{\mathrm{today}}}{12/37\cdot Y_{N_1}^{\mathrm{Eq}}\left(T \gg m_{N_1}\right)} \simeq 5.7\cdot 10^{-8}\,. \tag{3.33}$$

This translates, using Eq. (3.30) and the atmospheric mass splitting value given in Table 1.1 of section 1.1, into a lower bound for the mass m_{N_1} given by : [3]

$$m_{N_1} \gtrsim 5.9 \cdot 10^8 \text{ GeV} . \tag{3.34}$$

This means that, in the unflavored limit, the right-handed neutrino scale should lie far beyond the EW scale if we want it to explain both leptogenesis and neutrino masses. Unfortunately, this scale is hardly testable by future experiments. However, this bounds can be lowered, for example by including the different lepton flavors or changing the right-handed neutrino mass spectrum, as in the resonant leptogenesis scenario. In this latter case, as can be seen from the self-energy diagram contribution in Eq. (3.26), the CP-asymmetry can be largely enhanced and the bound in Eq. (3.30) doesn't hold anymore [217, 220, 221, 222, 139].

◦ **Comment on the upper bound on the heavy neutrino mass**

Let's note that one generally assumes that, in order to be produced by the thermal bath, the right-handed neutrinos must be lighter than the reheating temperature $m_{N_1} \lesssim T_{\text{reheat}}$. Indeed, in order to explain the Universe homogeneity, it is generally assumed that there were a period of inflation at the early stage of our Universe, such that the Universe expanded by a factor bigger than $\sim e^{50}$. This inflation can be explained by the "slow-roll" slope of a scalar field in some particularly flat potential. At the end of inflation, when the field reaches the minimum of the potential, we expect that this field begins to oscillate and to decay in SM particles, which populate and reheat the Universe – this is what is called the reheating period. The reheating temperature is actually unknown, but following most inflationary models it may lie in the range 10 TeV $\lesssim T_{\text{reheat}} \lesssim 10^{16}$ GeV [223, 224]. As a consequence, one should have $m_{N_1} \lesssim 10^{16}$ GeV in order that the thermal bath (or the dilation field) could populate and maybe thermalize the right-handed neutrinos.

3.4.5 Boltzmann equations

Now that we have the analytical expression of the CP-asymmetry in Eq. (3.28) which differs in general from zero, we can write down the Boltzmann equations that will allow us to determine the value of the efficiency η_{N_1}. These equations describe the time evolution of the various densities by counting the number of particles which are destroyed/created. In fact, it is the solution of the Boltzmann equations that gives the final form of the $B-L$ asymmetry as introduced in Eq. (3.31).

The formalism of the Boltzmann equations is explained in Appendix C.4. We will closely follow the notation of Ref. [225]. Here, we will just write the final expressions. For the sake of illustration, we will only consider the contributions of the dominant interactions, as the decays $N_1 \to \ell\phi$, inverse decays $\ell\phi \to N_1$, and the on-shell contribution of the $\Delta L = 2$ scatterings $\ell\phi \leftrightarrow \ell\phi$ which must be included in order to have a correct thermodynamical behavior. A more complete approach consists in including also other processes as the off-shell contribution of the $\Delta L = 2$ scatterings or the $\Delta L = 1$ scatterings $\ell N_1 \leftrightarrow \bar{t}b$. These can be important in some cases as discussed in section 3.7 below, but this is not necessary in this introductory section.

[3] This lower bound stands in the case where the initial right-handed abundance is the equilibrium one. In case of a vanishing initial abundance, the lower bound becomes $m_{N_1} \gtrsim 10^9$ GeV, see below.

Neglecting the spectator processes, [4] the Boltzmann equations that describe the evolution of the N_1 comoving number density $Y_{N_1} \equiv n_{N_1}/s$ (also just called "density" or "abundance" in this thesis) and the evolution of the $B-L$ asymmetry ΔY_{B-L} as defined in Eq. (3.16), [5] read

$$\dot{Y}_{N_1} = -\left(\frac{Y_{N_1}}{Y_{N_1}^{\rm Eq}} - 1\right)\gamma_D \,, \tag{3.35}$$

$$\Delta\dot{Y}_{B-L} = -\left(\frac{Y_{N_1}}{Y_{N_1}^{\rm Eq}} - 1\right)\epsilon_{N_1}\gamma_D - \frac{1}{2}\frac{\Delta Y_{B-L}}{Y_\ell^{\rm Eq}}\gamma_D \,, \tag{3.36}$$

where $\dot{Y} \equiv sHz\,dY/dz$ can be interpreted as a time derivative, $s(z)$ is the entropy density, and $z \equiv m_{N_1}/T$. The decay/inverse decay reaction rate γ_D, which is nothing but the number of decays which occurs per unit time and unit volume, is given by

$$\gamma_D \equiv n_{N_1}^{\rm Eq}\frac{K_1(z)}{K_2(z)}\Gamma_{N_1} = n_{N_1}^{\rm Eq}\frac{K_1(z)}{K_2(z)}K_{N_1}H(z=1) \,. \tag{3.37}$$

The functions $K_1(z)$ and $K_2(z)$ are Bessel functions of the first and second kind – these must not be mixed up with the decay parameter K_{N_1} as defined in Eq. (3.21). In what follows, we take the Hubble rate and the entropy density to be

$$H(z) = \frac{2}{3}\sqrt{\frac{\pi^3 g_*}{5}}\frac{T^2}{m_{\rm Planck}} \quad , \quad s(z) = \frac{4}{\pi^2}g_*\,T^3 \,, \tag{3.38}$$

where $g_* = 106.75$ is the total number of relativistic degrees of freedom contributing to the energy density of the Universe, and $m_{\rm Planck} = 1.22\cdot 10^{19}$ GeV is the Planck mass. We also make the approximation of taking Maxwell-Boltzmann equilibrium distributions : [6]

$$n_{N_1}^{\rm Eq}(z) = g_{N_1}\frac{m_{N_1}^3}{2\pi^2}\frac{K_2(z)}{z} \quad , \quad n_\ell^{\rm Eq}(z) = g_\ell\frac{m_{N_1}^3}{2\pi^2}\frac{2}{z^3} \,, \tag{3.39}$$

where we used $K_2(z\ll 1)\simeq 2/z^2$ for the relativistic lepton species ℓ. In this thesis, the number of degrees of freedom of the species X is taken to be $g_X = 1,2,3$ for Dirac singlets, doublets (so $g_\ell = 2$) and triplets respectively, while $g_N = 2$ for the Majorana fermions singlets N_i, and $g_\gamma = 2$ for the two polarization states.

[4] As shown in Appendix C.5.2 the inclusion of spectator processes, even in the case of unflavored leptogenesis, can lead to a different numerical factor in front of the term proportional to ΔY_{B-L} in the r.h.s. of Eq. 3.36. For example, for $T \gtrsim 10^{15}$ GeV, the factor 1/2 should be replaced by 1, and for $T \in [10^{12}, 10^{15}]$ GeV, it should be replaced by 5/3. The inclusion of spectator processes thus in general increases the washout of the asymmetry. The effect of the spectator processes will be discussed in section 3.6.

[5] Since the sphalerons violate the lepton number L, it is rigorously not correct to write a Boltzmann equation for L without taking into account the effects of complex sphalerons reactions. Dealing with $B-L$ instead, which is conserved by sphalerons, allows us to not include these complex reactions in the Boltzmann equations. Let's note that we already took into account the effect of the chemical potential equilibrium conditions in Eq. (3.36), that relate the L and $B-L$ asymmetry – see the so-called C_ℓ matrix elements in Appendix C.5.

[6] Rigorously, one should take the Fermi-Dirac distribution for the fermions, and the Bose-Einstein distribution for the bosons. However, in this case, the Boltzmann equations would be more complexes and one would only gain few percent in precision. In contrast, the fact of using classical Boltzmann equations instead of quantum ones gives the same answer up to ~ 10 percent deviations.

Let's now analyze the physics behind the above Boltzmann equations. The r.h.s. of the equation for Y_{N_1} contains two parts, proportional to the reaction rate γ_D. The first term in the bracket represents the total decays of N_1, given by the sum of $N_1 \to \ell\phi$ and $N_1 \to \bar{\ell}\phi^*$, and is therefore negative while the second term represents the total inverse decays to N_1, i.e. $\ell\phi \to N_1$ and $\bar{\ell}\phi^* \to N_1$, and is then positive. As the N_1's decay/inverse decay, some lepton asymmetry (and then an opposite $B-L$ asymmetry) is produced/erased. This is represented by the first term of the r.h.s. of the equation for ΔY_{B-L}, which has therefore exactly the same form of as the r.h.s. of Eq. (3.35), but weighted by the CP-asymmetry ϵ_{N_1}. Finally, the equation for ΔY_{B-L} also contains a term proportional to ΔY_{B-L}, which reflects the fact that if there is more ℓ than $\bar{\ell}$ for example, there will be more inverse decay $\ell\phi \to N_1$ than $\bar{\ell}\phi^* \to N_1$, having consequently the effect of diminishing the asymmetry. [7] This is the "washout term".

The Boltzmann equation for the $B-L$ asymmetry contains therefore two distinct kind of terms : the **"source term"** that is responsible of an increase of the absolute $B-L$ asymmetry (the term proportional to ϵ_{N_1}), and the **"washout term"** that tends to prevent the enhancement of the lepton asymmetry. Starting with an equilibrium number density for N_1, the final $B-L$ asymmetry produced will be maximal if the washout terms are minimal. [8] Note that if the initial N_1 abundance is zero, the washout term is crucial for a $B-L$ asymmetry to develop. These washouts play therefore a crucial role in the leptogenesis scenario. But how fast are they ?

To answer this question, one needs to compare the reaction rates with the Hubble rate. Looking at the Boltzmann equations, the relative rapidity of the total decay of $N_1 \to \ell\phi$ can be evaluated by the quantity $\gamma_D/(Hn_{N_1}^{\rm Eq})$, with $\gamma_D/n_{N_1}^{\rm Eq}$ being the number of decays a single N_1 has per unit time, while the relative rapidity of the inverse decay $\ell\phi \to N_1$ can be evaluated by $\gamma_D/(Hn_{\ell}^{\rm Eq})$, with $\gamma_D/n_{\ell}^{\rm Eq}$ being the number of inverse decays a single ℓ (or a single ϕ) has per unit time. These reactions densities play a crucial role in the understanding of the evolution of the $B-L$ asymmetry, because they allow us to know if a reaction effectively occurs or not.

For example, we show in Fig. 3.7 the reaction densities as a function of $z = m_{N_1}/T$ for the decays (left) and inverse decays (right), fixing the decay parameter to $K_{N_1} = 50$ (solid), $K_{N_1} = 1$ (dashed), and $K_{N_1} = 1/50$ (dashed). From the left panel, we see that N_1 starts to decay typically around $T \sim m_{N_1}$. From the right panel, more interestingly we see that the $\ell\phi \to N_1$ inverse decay rate is always slower than the Hubble rate for $K_{N_1} \lesssim 1$ (in which case we say that the reaction never reaches thermal equilibrium). This means that for $K_{N_1} = 1/50$ for example, the inverse decays $\ell\phi \to N_1$ basically not occur, and one can safely neglect the corresponding washout term in the Boltzmann equation for $B-L$ (at least if one starts with a thermal N_1 density).

We show in Fig. 3.8 the evolution of the Y_{N_1} (left) and ΔY_{B-L} abundances (right), for the same choice of K_{N_1}. These curves have been obtained by solving numerically the Boltzmann equations, fixing $\epsilon_{N_1} = 1$ and taking at $z_0 \ll 1$ the initial conditions $Y_{N_1}(z_0) = Y_{N_1}^{\rm Eq}(z_0)$ and $\Delta Y_{B-L}(z_0) = 0$. Let's have a quick look at the evolution of the $B-L$ asymmetry.

[7] Let's note that the factor 1/2 in front of the third term of Eq. (3.36) comes from the fact that the decay rate $\Gamma(N_1 \to \ell\phi)$ is half of the total rate Γ_{N_1}.

[8] Note that by washout we here mean the term proportional to ΔY_{B-L} in Eq. (3.36). and not the total inverse decays to N_1.

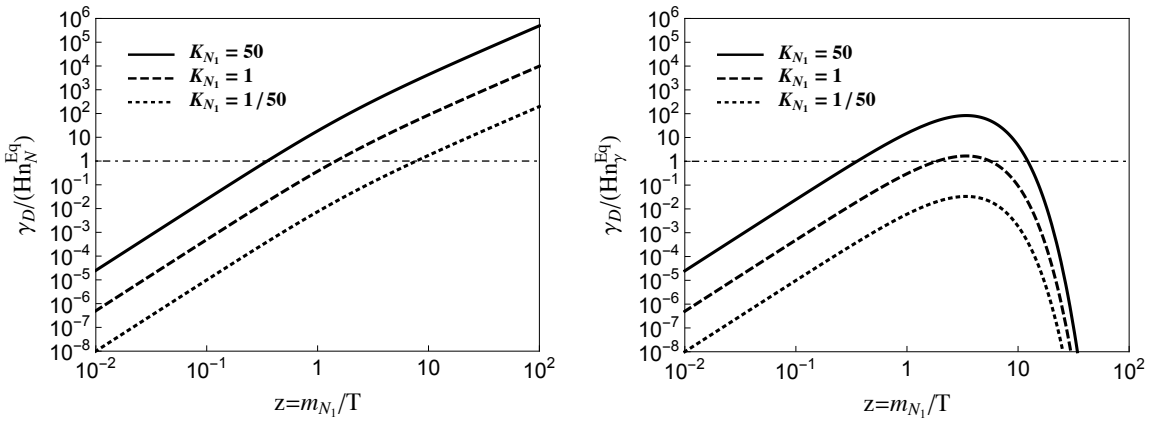

Figure 3.7 – Thermalization rates $\gamma_D/(Hn_{N_1}^{\mathrm{Eq}})$ (left) and $\gamma_D/(Hn_\ell^{\mathrm{Eq}})$ (right) for different values of K_{N_1}. These represent how fast are the decay and inverse decay rate with respect to the Hubble rate.

First, for $z \lesssim 1$, we see that the $B-L$ asymmetry increases progressively as the N_1's decay. For $K_{N_1} = 50$, it reaches a maximum around $z \sim 1$ before decreasing until $z \sim 10$. Looking at the right panel of Fig. 3.7, this value corresponds to the moment at which the inverse decay $\ell\phi \to N_1$ washout leaves thermal equilibrium. For $z \gtrsim 10$, the fraction $\gamma_D/(Hn_\ell^{\mathrm{Eq}})$ is always smaller than 1 and the $B-L$ asymmetry remains constant. For $K_{N_1} = 1/50$, we see on the contrary that the $B-L$ asymmetry never decreases. This is because the inverse decays never reaches thermal equilibrium as can be seen on the right panel of Fig. 3.7. The case where $K_{N_1} = 1$ lies at the boundary between the two above situations.

From the left panel of Fig. 3.8, we also see that the more the N_1's decay out-of-equilibrium (the more Y_{N_1} deviates from $Y_{N_1}^{\mathrm{Eq}}$), the more $B-L$ asymmetry will be produced. This clearly reflects the third Sakharov condition : the process that generates the lepton asymmetry must leave thermal equilibrium in order to have a non-zero lepton asymmetry at the end of leptogenesis.

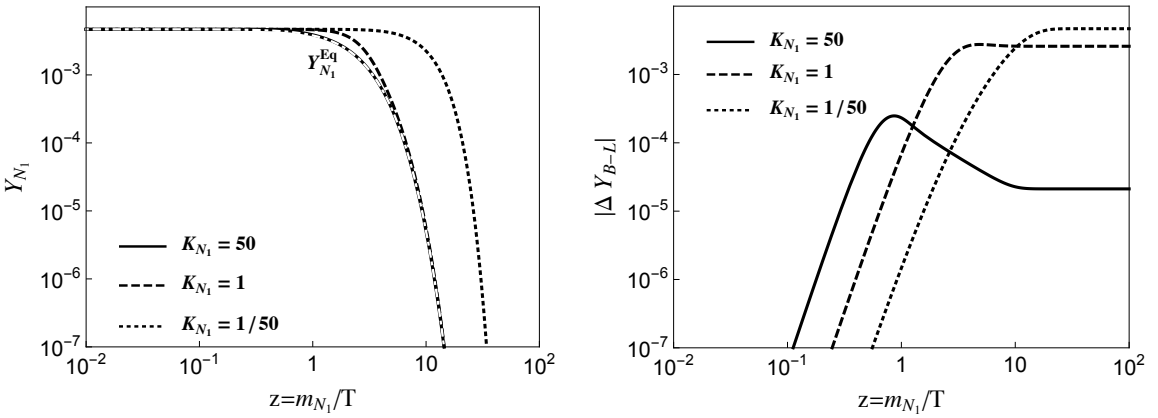

Figure 3.8 – Evolution of the N_1 density (left) and the $B-L$ asymmetry (right), for different values of the K_{N_1} parameter. The right panel also shows the equilibrium density $Y_{N_1}^{\mathrm{Eq}}$ in white dotted-dashed, which is in fact quasi superposed to the $K_{N_1} = 50$ curve.

3.4.6 Analytical solutions to the Boltzmann equations

It is in general difficult to get a simple expression for the final $B-L$ asymmetry by solving the system of Boltzmann equations analytically. Indeed, integrating Eq. (3.35) and (3.36) from z_0 to z using the integrating factor technique, the exact solution reads

$$\Delta Y_{B-L}(z) = \Delta Y_{B-L}(z_0)\; e^{-\int_{z_0}^{z} dz' W_1(z')} - \int_{z_0}^{z} dz' \epsilon_{N_1} \frac{dY_{N_1}}{dz'} e^{-\int_{z'}^{z} dz'' W_1(z'')} \,. \tag{3.40}$$

where $\Delta Y_{B-L}(z_0)$ is the initial asymmetry, and where we defined

$$W_1(z) \equiv \frac{1}{2Y_\ell^{\rm Eq}} \frac{\gamma_D(z)}{s(z)H(z)z} \,. \tag{3.41}$$

Starting with zero initial asymmetry $\Delta Y_{B-L}(z_0) = 0$ at $z_0 \ll 1$, the final asymmetry at the end of leptogenesis is given by

$$\left|\Delta Y_{B-L}^{\rm end}\right| \simeq \left|\Delta Y_{B-L}(z\to\infty)\right| = \epsilon_{N_1}\, \eta_{N_1}\, Y_{N_1}^{\rm Eq}(z_0) \,, \tag{3.42}$$

where we recover the efficiency η_{N_1} which is now defined as

$$\eta_{N_1} \equiv \frac{1}{Y_{N_1}^{\rm Eq}(z_0)} \int_{z_0}^{\infty} dz' \, \frac{dY_{N_1}(z_0)}{dz'} \, e^{-\int_{z'}^{\infty} dz'' W_1(z'')} \,. \tag{3.43}$$

This justifies the form introduced in Eq. (3.31). Note that in the case of thermal initial abundance $Y_{N_1}(z_0) = Y_{N_1}^{\rm Eq}(z_0)$, in the best case there is no washout, $W_1(z) \to 0$, and the efficiency is maximal $\eta_{N_1} = 1$, since $Y_{N_1}(\infty) \to 0$. The larger the washout, the closer to zero is the efficiency.

In some peculiar situations, the integral in Eq. (3.43) can be solved analytically at the cost of some approximations. For example, if one can neglect some terms compared to others in the Boltzmann equations, one can eventually derive a simple analytical expression for the final $B-L$ asymmetry that is physically understandable. As an illustration, we consider the analytical solutions in the weak and the strong washout regimes, corresponding to $K_{N_1} \ll 1$ and $K_{N_1} \gg 1$ respectively.

Weak washout regime ($K_{N_1} \ll 1$). Depending on the initial condition for Y_{N_1}, we can have different analytical results. *Firstly,* let's take the initial density to be the thermal one $Y_{N_1}(z \ll 1) = Y_{N_1}^{\rm Eq}(z \ll 1)$. In this case, as we illustrated in the example above for $K_{N_1} = 1/50$, the washouts from $\ell\phi \to N_1$ basically never occur since the inverse decay are much slower than the Hubble rate. The term proportional to ΔY_{B-L} in Eq. (3.36) can thus be neglected with respects to the source term. Injecting Eq. (3.35) in Eq. (3.36), one has simply

$$\Delta \dot{Y}_{B-L} \simeq \epsilon_{N_1} \dot{Y}_{N_1} \,, \tag{3.44}$$

and integrating from $z = z_0$ to z, the $B-L$ asymmetry at z is given by

$$\Delta Y_{B-L}(z) \simeq \Delta Y_{B-L}(z_0) + \epsilon_{N_1} \left[Y_{N_1}(z) - Y_{N_1}(z_0) \right] \,. \tag{3.45}$$

For $z \to \infty$, $Y_{N_1}(z)$ is Boltzmann suppressed $Y_{N_1}(z \to \infty) \ll 1$, so that taking $\Delta Y_{B-L}(z_0) = 0$ and $Y_{N_1}(z_0) = Y_{N_1}^{\rm Eq}(z_0)$ as initial conditions, we have finally

$$\left|\Delta Y_{B-L}^{\rm end}\right| \simeq \left|\Delta Y_{B-L}(z \to \infty)\right| \simeq \epsilon_{N_1}\, Y_{N_1}^{\rm Eq}(z_0)\ . \tag{3.46}$$

We see that this expression is nothing but Eq. (3.31) or (3.42) with a maximal efficiency $\eta_{N_1} = 1$, as it should be since there are no washout effects in this case. For $K_{N_1} = 1/50$, this analytical result is in very good agreement (at the ∼0.2% level) with the numerical solution, see Fig. 3.8.

Secondly, by taking $Y_{N_1}(z_0) = 0$ as an initial condition in Eq. (3.45), one would have obtained $\Delta Y_{B-L}(z \gg 1) = 0$, which is in fact not in agreement with the numerical solution. Starting with $Y_{N_1}(z_0) = 0$, one cannot neglect the washout effects because it is actually thanks to them that a non-zero $B-L$ asymmetry can develop. In this case, we can show that it is also possible to get an approximate analytical result given by [226]

$$\left|\Delta Y_{B-L}^{\rm end}\right| \simeq \frac{27}{16}\epsilon_{N_1}\, K_{N_1}^2\, Y_{N_1}^{\rm Eq}(z_0)\ . \tag{3.47}$$

This is again nothing but the form given in Eq. (3.31) or (3.42) with an efficiency $\eta_{N_1} = 27/16K_{N_1}^2$.

Strong washout regime ($K_{N_1} \gg 1$). Here, in good approximation the initial N_1 doesn't matter since even if one starts with $Y_{N_1}(z_0) = 0$ the inverse decays are so fast that the abundance Y_{N_1} has the time to reach the equilibrium density before the right-handed neutrinos start to decay at $z \sim 1$. In this case, as in the $K_{N_1} = 50$ example above, the washouts are very fast until some $z = z_{\rm dec}$ value at which the inverse decays become slower than the Hubble rate. For $z < z_{\rm dec}$, the $\gamma_D/n_\ell^{\rm Eq}$ inverse decay rate is in thermal equilibrium and occur so fast that one has a balance between the production and the destruction rate of $B-L$ asymmetry. This means that, for $z < z_{\rm dec}$ and in the limit where $\Gamma_D \gg H$, the washout term maintains the r.h.s. of Eq. (3.36) to zero and one has

$$\Delta Y_{B-L}(z) \simeq 2\cdot\epsilon_{N_1}\, Y_\ell^{\rm Eq}\frac{\dot{Y}_{N_1}}{\gamma_D}\ . \tag{3.48}$$

The above relation holds until the inverse decays decouple at $z = z_{\rm dec} \gg 1$, time at which the $B-L$ asymmetry freezes. Using $Y_{N_1}(z) \simeq Y_{N_1}^{\rm Eq}(z)$ and $dY_{N_1}^{\rm Eq}/dz \simeq -Y_{N_1}^{\rm Eq}(z)$ for $z \gg 1$, the asymmetry at $z = z_{\rm dec}$ can be expressed as

$$\Delta Y_{B-L}(z_{\rm dec}) \simeq -2\cdot\epsilon_{N_1}\, Y_\ell^{\rm Eq}\frac{Hzn_{N_1}^{\rm Eq}}{\gamma_D}\bigg|_{z_{\rm dec}\gg 1} \simeq -2\cdot\epsilon_{N_1}\frac{1}{z_{\rm dec}K_{N_1}}\, Y_\ell^{\rm Eq}(z_{\rm dec})\ , \tag{3.49}$$

and the final $B-L$ asymmetry is therefore given by

$$\left|\Delta Y_{B-L}^{\rm end}\right| \simeq \left|\Delta Y_{B-L}(z_{\rm dec})\right| \simeq \epsilon_{N_1}\frac{2}{z_{\rm dec}K_{N_1}}\, Y_{N_1}^{\rm Eq}(z_0)\ , \tag{3.50}$$

where we used the fact that $Y_\ell^{\rm Eq}$ is a constant whose values is equal to $Y_{N_1}^{\rm Eq}(z \ll 1)$. This expression corresponds to the form given in Eq. (3.31) or (3.42) with an efficiency $\eta_{N_1} = 2/(z_{\rm dec}K_{N_1})$. For $K_{N_1} = 50$, one has $z_{\rm dec} \approx 11$ and this analytical result gives the correct answer at the level of ∼ 20%.

3.4.7 Some results of successful leptogenesis

Efficiency. From Eqs. (3.22), (3.37), (3.41) and (3.43), we see that the efficiency depends in a first approximation on only one unknown parameter, that we choose to be $\tilde{m}_1$, and on the initial condition $Y_{N_1}^{\rm Eq}(z_0)$. We show in the left panel of Fig. 3.9 the efficiency η_{N_1} as a function of $\tilde{m}_1$ for initial conditions between $Y_{N_1}(z_0)=0$ (dashed) and $Y_{N_1}(z_0)=Y_{N_1}^{\rm Eq}(z_0)$ (solid). This plot is taken from Ref. [227] and also includes thermal corrections (RGE corrections), $\Delta L=1$ and $\Delta L=2$ scatterings (see section 3.7) and finite temperature effects (possibility of absorption and re-emission of the loop particles by the plasma). [9]

We see that in the strong washout regime, i.e. for $\tilde{m}_1 \gtrsim m^*$ with $m^* \simeq 1.08\cdot 10^{-3}$ eV (or equivalently $K_{N_1} \gtrsim 1$), the efficiency doesn't depend on the initial condition, and decreases linearly with $\tilde{m}_1 \propto K_{N_1}$, as expected from Eq. (3.50). On the contrary, in the weak washout regime, i.e. for $\tilde{m}_1 \lesssim m^*$ (or equivalently $K_{N_1} \lesssim 1$), the efficiency depends on the initial condition. For zero initial abundance $Y_{N_1}(z_0)=0$, the efficiency increases linearly with $\tilde{m}_1$, while for thermal initial abundance, the efficiency is quasi maximal $\eta_{N_1}\approx 1$, as expected from Eqs. (3.45) and (3.47) respectively. Any initial condition between the two last possibilities will give an efficiency lying in the gray region. Note that for $Y_{N_1}(z_0)=Y_{N_1}^{\rm Eq}(z_0)$ the efficiency decreases for $\tilde{m}_1 \ll m^*$ because in that case the N_1 decays out-of-equilibrium at a temperature so low that it actually reheats the thermal bath, which has the effect of decreasing the efficiency, see Ref. [227] for further details.

In section 3.4.3 we have shown that the parameter $\tilde{m}_1$ has nearly the same form as the expression of the neutrino mass matrix. In Eq. (3.24) we have shown that there is actually a lower bound on it : $\tilde{m}_1 \geq m_\nu^{\rm min}$. Accordingly, one could expects $\tilde{m}_1$ to be of the order of the atmospheric $(\Delta m^2_{\rm atm})^{1/2}\approx 0.05$ eV or solar mass splitting $(\Delta m^2_{\rm sol})^{1/2}\approx 0.01$ eV. Quite remarkably, in this both cases the efficiency doesn't depend on the initial conditions and the suppression is not too large, as can be seen from the left panel of Fig. 3.9.

Bounds on the right-handed neutrino mass m_{N_1} and on $\tilde{m}_1$. From Eq. (3.32), in order to generate the right amount of BAU, we see that the CP-asymmetry is now directly related to the parameter $\tilde{m}_1$ and the initial condition $Y_{N_1}(z_0)$ through the efficiency. Using Eq. (3.30), this can be translated on bounds on the $\tilde{m}_1$ and m_{N_1} parameters. This is what we show in the right panel of Fig. 3.9. This plot is also taken from Ref. [227] and includes thermal corrections, $\Delta L=1$ and $\Delta L=2$ scatterings, and finite temperature effects. As a result, one has a lower bound on m_{N_1} that now depends on $\tilde{m}_1$ as expected, and the absolute lower bound on the mass of the lightest right-handed neutrino N_1 is given by :

$$m_{N_1} \gtrsim \begin{cases} 2.9\cdot 10^9 & \text{GeV, in case } Y_{N_1}(z_0)=0\,, \\ 5.9\cdot 10^8 & \text{GeV, in case } Y_{N_1}(z_0)=Y_{N_1}^{\rm Eq}(z_0)\,. \end{cases} \tag{3.51}$$

Note that we recover the result of Eq. (3.34) in the case of thermal initial abundance. [10]

[9] A consequence of this is that the efficiency in fact also depends on the mass m_{N_1}, which has been fixed to $m_{N_1}=10^{10}$ GeV in the plot, but one can actually show that for $m_{N_1}\lesssim 10^{14}$ GeV the efficiency depends almost only on $\tilde{m}_1$ [227], see the discussion on the $\Delta L=2$ scatterings below.

[10] The values in Eq. (3.68) however differ by a factor ~ 1.3 with respect to the ones given in Ref. [227]. This is because, in the whole thesis, we use the Maxwell-Boltzmann distribution for the equilibrium number density of N_1, which

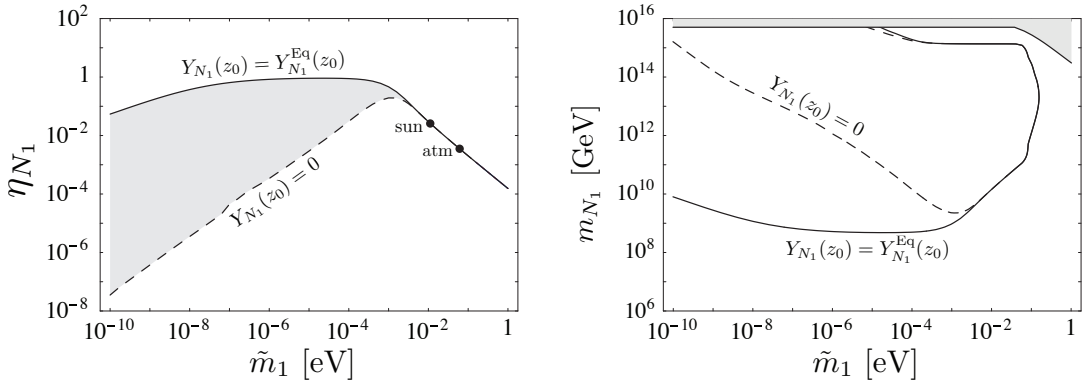

Figure 3.9 – In the case of thermal (solid) and zero initial abundance for $Y_{N_1}(z_0)$ (dashed), the left panel shows the efficiency η_{N_1} as a function of $\tilde{m}_1$ for $m_{N_1} = 10^{10}$ GeV, and in the right panel the lower and upper bound on m_{N_1} as a function of $\tilde{m}_1$. The two plots have been taken from Ref. [227]. The upper bound is obtained including the $\Delta L = 2$ scatterings – see section 3.7. In both plots, the lightest neutrino mass has been fixed to be $m_\nu^{\rm min} = 0$ eV.

Comment on $\Delta L = 2$ *scatterings.* Let's just mention why the $\Delta L = 2$ scatterings can be particularly dangerous in some cases for successful leptogenesis. One can show that these scatterings enter in thermal equilibrium for typically $m_{N_1} \gtrsim 10^{14}$ GeV and since their rate goes like $\gamma_{\Delta=2} \propto m_{N_1}(\sum_i m_i)$, they strongly suppress the efficiency η_{N_1}. This explains the upper bound on m_{N_1} in the right panel of Fig. 3.9. Furthermore, since the rate of the $\Delta L = 2$ scatterings is also proportional to the sum of the light neutrino masses m_i, the requirement of successful leptogenesis also leads to an upper bound on the maximum light neutrino mass [228]. As can be seen from the right panel of Fig. 3.9, it is given by :

$$m_\nu^{\rm max} \lesssim 0.12 \text{ eV} \,. \tag{3.52}$$

Above this value, washouts are too strong and one cannot generate enough baryon asymmetry. However, this bound is of relatively little interest. Indeed, remember that all these results apply when $m_{N_1} \ll m_{N_{2,3}}$, and if for example $m_\nu^{\rm max} \sim 0.12$ eV, this assumption is not much likely because it is difficult to explain the degenerate spectrum of the light neutrino from a hierarchical spectrum of heavy neutrinos, see Eq. (1.26). In the case where the heavy neutrinos are quasi-degenerate, all the bounds are not valid anymore due to a (resonant) enhancement of the CP-asymmetry – see self-energy diagram contribution in Eq. (3.26) – and they get considerably relaxed [217, 220, 221, 222, 139].

So far we have considered just one Boltzmann equation for the total number of lepton produced, and what has been done for now is valid within this approximation. However, as we will now see this is not always justified since lepton flavors should in some case be taken into account. But when do flavors matter in type-1 leptogenesis ?

differs by a factor ~ 3/4 with respect to the Fermi-Dirac distribution for $T \gg m_{N_1}$ – see Appendix C.1.

3.5 Flavor issue in type-1 leptogenesis

An important issue concerns the flavors. Indeed, until now we have considered the general case where the right-handed neutrino N_1 decays into only one lepton ℓ, which by definition contains all the lepton flavors. However, following the temperature at which leptogenesis takes place, two or three flavors *must* actually be considered. Indeed, the SM Lagrangian extended by the type-1 Seesaw Lagrangian contains the interaction of N_1 with the leptons ℓ_α in Eq. (3.17), but also the charged lepton Yukawa interactions :

$$\begin{aligned}\mathscr{L} \ni & -\sum_\alpha \overline{N_1}\,\tilde{\phi}^\dagger\, Y_{N_{1\alpha}}\,\ell_\alpha - \sum_\alpha \overline{e_\alpha}\,\phi^\dagger\, Y_{\ell_\alpha}\,\ell_\alpha + \text{H.c.} \\ & = -\overline{N_1}\,\tilde{\phi}^\dagger \left(\sum_\alpha Y_{N_{1\alpha}}\,\ell_\alpha\right) - \sum_\alpha \overline{e_\alpha}\,\phi^\dagger\, Y_{\ell_\alpha}\,\ell_\alpha + \text{H.c.}\,. \end{aligned} \tag{3.53}$$

Without loss of generality, we choose as usual a charged lepton basis such that the charged lepton Yukawa matrix is diagonal and real, see the parameter counting in Eq. (1.29).

If one considers only the first interaction term above, i.e. we forget about the charged Yukawa interaction, we see that the right-handed neutrino N_1 actually decays into a scalar ϕ and into a state ℓ_1 carrying $L(\ell_1) = 1$, which is a superposition of the three lepton flavors :

$$|\ell_1\rangle = \frac{1}{\sqrt{N}}\left(Y_{N_{1e}}\,|\ell_e\rangle + Y_{N_{1\mu}}\,|\ell_\mu\rangle + Y_{N_{1\tau}}\,|\ell_\tau\rangle\right)\,, \tag{3.54}$$

with $N \equiv \sum_\alpha |Y_{N_{1\alpha}}|^2$ a normalization factor such that $\langle\ell_1|\ell_1\rangle = 1$. This is equivalent of performing a rotation in the flavor basis. Indeed, one has the freedom to define a new basis $\ell' = R\,\ell = (\ell_1, \ell_2, \ell_3)$, with R a unitary matrix, such that the heavy right-handed neutrino does effectively decay in $|\ell_1\rangle = \sum_\alpha R_{1\alpha}|\ell_\alpha\rangle$ through an effective Yukawa coupling given by $\mathscr{Y}_{N_1 1} = \left(Y_N R^\dagger\right)_{11} = \sqrt{N}$, and such that it doesn't decay in either $|\ell_2\rangle$ or $|\ell_3\rangle$. From the above equation, we already know the first line of R which is $R_{1\alpha} = Y_{N_1\alpha}/\sqrt{N}$.

Therefore, by decaying, N_1 actually produces effectively a ΔY_{ℓ_1} asymmetry. This massless lepton state $|\ell_1\rangle$ is coherent, [11] in the sense that it is a superposition of undistinguishable massless flavor states. This is quite analogous to the coherent neutrino propagations, see section 1.1. Let's now consider the effect of the Yukawa interactions, i.e. the second term in Eq. (3.57). As propagating, one has two possibilities for the evolution of $|\ell_1\rangle$.

On the one hand, if the state $|\ell_1\rangle$ undergoes only interactions that doesn't make the distinction between the flavors $|\ell_\alpha\rangle$, this state propagates coherently until it eventually undergoes an inverse decay $\ell_1\phi \to N_1$. In this case, all the three flavors should obviously not play any role in the leptogenesis scenario, since all the interactions in the game are sensitive to only one flavor ℓ_1, which constitutes therefore the only relevant flavor. One needs in this case only one Boltzmann equation which simply counts the number of ℓ_1 created and annihilated. We recover therefore the unflavored leptogenesis situation studied in the previous section, with $\ell \equiv \ell_1$.

[11] Above $T_{EW} \simeq 165$ GeV, the scalar field has no vev, so that all the fermions are massless, except the right-handed neutrinos that are massive due to there Majorana mass term, see Fig. 3.5.

On the other hand, the state $|\ell_1\rangle$ may loose its coherence if it undergoes an interaction that is not flavor-blind, i.e. an interaction that makes the distinction between the flavors, as the charged Yukawa interactions (the second term in Eq. (3.57)) or the $N_{2,3}$ Yukawa interactions. These latter are in general much slower than the Hubble rate because Boltzmann suppressed since the $N_{2,3}$ are taken much heavier than N_1, so that they should not a priori be responsible of the decoherence of the state $|\ell_1\rangle$. This is not the case of the charged Yukawa interactions, which are not Boltzmann suppressed and are even much faster than the Hubble rate below some specific temperatures that can be easily determined. Quantitatively, the charged Yukawa interaction rate is given by

$$\Gamma_{\ell_\alpha}(T) \simeq 5 \cdot 10^{-3}\, Y^2_{\ell_\alpha}\, T\,. \tag{3.55}$$

To see if this interaction has the time to happen, this rate must be compared to the Hubble rate H, *but also* to the appropriate inverse decay (ID) rate $\Gamma^{ID}_\ell \equiv \Gamma(\ell\alpha\phi \to N_1)$, which for $\ell_1\phi \to N_1$ is simply given by Eq. (3.19). One has the following distinct possibilities :

1. **For $T \gtrsim 10^{12}$ GeV, one has always $\Gamma_{\ell_{e,\mu,\tau}} < H$**, and basically no charged lepton Yukawa interactions occur. In this case, the lepton state $|\ell_1\rangle$ propagates without loosing its coherence, and could possibly undergo an inverse decay $\ell_1\phi \to N_1$. In other terms, one can define a new orthonormal interaction basis $(|\ell_1\rangle, |\ell_2\rangle, |\ell_3\rangle)$, with $\langle\ell_{2,3}|\ell_1\rangle = \langle\ell_3|\ell_2\rangle = 0$ and $\langle\ell_i|\ell_i\rangle = 1$, such that a right-handed neutrino N_1 only decays and inverse decays in ℓ_1 and never in $\ell_{2,3}$. In this regime, called "**unflavored regime**", only one lepton "flavor" ℓ_1 participates to the leptogenesis mechanism and one needs one Boltzmann equation for ℓ_1. This is the regime we considered in details in the last section 3.4, with $\ell \equiv \ell_1$.

2. **For $10^9 \lesssim T \lesssim 10^{12}$ GeV, one has $\Gamma_{\ell_\tau} > H$ but still $\Gamma_{\ell_{e,\mu}} < H$**. Here, one has two cases :

   (a) **If $\Gamma_{\ell_\tau} < \Gamma^{ID}_{\ell_1}$**, the lepton state $|\ell_1\rangle$ will more likely inverse decay $\ell_1\phi \to N_1$ before interacting through the tau charged Yukawa interaction. This case reduces to the **unflavored regime** in item 1, i.e. there is a unique flavor ℓ_1 participating to the leptogenesis.

   (b) **If $\Gamma_{\ell_\tau} > \Gamma^{ID}_{\ell_1}$**, the lepton state $|\ell_1\rangle$ has the time to decohere thanks to the $\ell_\tau\phi \leftrightarrow e_\tau$ processes. In this case, the new interaction basis is $(|\ell_a\rangle, |\ell_b\rangle, |\ell_\tau\rangle)$, with $\langle\ell_{a,b}|\ell_\tau\rangle = \langle\ell_b|\ell_a\rangle = 0$ and $\langle\ell_i|\ell_i\rangle = 1$. The states $|\ell_a\rangle$ and $|\ell_b\rangle$ are coherent superpositions of e and μ flavors. One can choose a basis such that N_1 decays in either ℓ_a or ℓ_τ, but not in ℓ_b, i.e. the orthogonal combination ℓ_b doesn't enter into the game. In this case the state $|\ell_a\rangle$ is given by

   $$|\ell_a\rangle = \frac{1}{\sqrt{N'}}\left(Y_{N_{1e}}|\ell_e\rangle + Y_{N_{1\mu}}|\ell_\mu\rangle\right)\,, \tag{3.56}$$

   with $N' \equiv \sum_{\alpha=e,\mu}|Y_{N_{1\alpha}}|^2$ a normalization factor such that $\langle\ell_a|\ell_a\rangle = 1$. In this **"2-flavor regime"**, only the 2 flavors ℓ_a and ℓ_τ do actually participate to the leptogenesis scenario, and one needs two Boltzmann equations for ℓ_a and ℓ_τ.

3. **For $10^5 \lesssim T \lesssim 10^9$ GeV, one has $\Gamma_{\ell_\tau} > \Gamma_{\ell_\mu} > H$ but still $\Gamma_{\ell_e} < H$**. Here too, there are several possible cases :

(a) **If $\Gamma_{\ell_\tau} < \Gamma^{ID}_{\ell_1}$**, we recover the **unflavored regime**.

(b) **If $\Gamma_{\ell_\tau} > \Gamma^{ID}_{\ell_1}$ and $\Gamma_{\ell_\mu} < \Gamma^{ID}_{\ell_a}$**, we recover the **2-flavor regime** in item 2.(b), since the coherent lepton state $|\ell_a\rangle$ undergoes inverse decays $\ell_a\phi \to N_1$ before loosing its coherence.

(c) **If $\Gamma_{\ell_\tau} > \Gamma^{ID}_{\ell_1}$ and $\Gamma_{\ell_\mu} > \Gamma^{ID}_{\ell_a}$**, the lepton states $|\ell_1\rangle$ and also $|\ell_a\rangle$ loose their coherence through the $\ell_\tau\phi \leftrightarrow e_\tau$ and $\ell_\mu\phi \leftrightarrow e_\mu$ interactions respectively. The interaction basis is now given by $(|\ell_e\rangle, |\ell_\mu\rangle, |\ell_\tau\rangle)$ and it is such that the right-handed neutrino N_1 can decay to one of the three flavor states (through the usual Yukawa couplings $Y_{N_{1\alpha}}$). This regime is therefore called the **"3-flavor regime"** and one needs three Boltzmann equations for ℓ_e, ℓ_μ and ℓ_τ.

4. **For $T \lesssim 10^5$ GeV, one has $\Gamma_{\ell_\tau} > \Gamma_{\ell_\mu} > \Gamma_{\ell_e} > H$**, we recover exactly the same flavor regimes as the in the previous temperature range, plus a fourth case "4.(d)" where $\ell_e\phi \leftrightarrow e_e$ is faster than the inverse decays and the Hubble rate. This case corresponds also to a 3-flavor regime as in item 3.(c) but with different chemical equilibrium conditions, see Appendix C.5.

In practice, the analysis of a leptogenesis scenario must be done in one of the above flavor regimes if, during the creation of the major part of the $B-L$ asymmetry, the associated conditions are fulfilled. Since one has in good approximation that the major part of the asymmetry is created around $T \sim m_{N_1}$, we generally consider that the temperature $T_{\rm Lepto}$ at which the leptogenesis takes place is given by the mass of the heavy particle that generates the asymmetry, that is $T_{\rm Lepto} = m_{N_1}$. In this approximation, the above temperature regimes in items 1-4 can be associated to mass regimes, replacing T by $T_{\rm Lepto} = m_{N_1}$.

It is worth to remark that it is not sufficient to have a charged Yukawa interaction faster than the Hubble rate to guarantee a specific flavor regime : it must also be faster than the inverse decays $\ell_\alpha\phi \to N_1$. These considerations are very important since, following the flavor regime, the final lepton asymmetry can change by orders of magnitudes. In the previous section, we have analyzed the type-1 leptogenesis in the unflavored regime. Since the production of the $B-L$ essentially occurs at $T \sim m_{N_1}$, this approach is typically valid for a right-handed neutrino mass larger than $m_{N_1} \gtrsim 10^{9\ldots12}$ GeV. However, the unflavored regime may still be used in the whole temperature range $T \gtrsim T_{\rm sphal}$ in order to have a general idea on how things works and on the final $B-L$ asymmetry that can be reached.

Before going on, let's note too that, in this thesis, we will perform the analysis using classical Boltzmann equations to describe the evolution of the various quantities as the temperature cools down from $T \gg m_{N_1}$ to $T \ll m_{N_1}$. However, if the $B-L$ production covers different flavor regimes, one can wonder which is the flavor regime one needs to choose, and how one could account for the transition from one regime to another. In order to take care of this, a more rigorous but more complicated approach consists in using the density matrix formalism to describe the evolution of the $B/3-L_\alpha$ asymmetries, see for example Refs. [230, 231]. However, it has been shown that away from the transitions between the regimes, the two approaches (density matrix formalism and classical Boltzmann equations) essentially lead to the same results, in particular in the case where only the lightest right-handed neutrino species is assumed to be responsible for the generation of the asymmetry [232], as it is the case here.

3.6 Flavored type-1 leptogenesis

We now discuss what happens in the flavored leptogenesis scenario. We will proceed basically as in the unflavored case. The main difference, in the structure, is that now we also need to introduce the chemical equilibrium conditions, which relate in particular the flavor abundances Y_{ℓ_α} with the $B/3 - L_\alpha$ one, taking into account the effect of the spectator processes. We will in this end closely follow the approach of Ref. [233].

By definition of the flavored regime, the right-handed neutrino N_1 can now effectively decay in two or more flavors. We denote by n_f the number of "active" flavors, i.e. the number of flavors participating in leptogenesis. The effective right-handed interaction Lagrangian reads now

$$\mathscr{L}^{\text{type-1}}_{\text{flavored}} \ni -\sum_{\alpha}^{n_f} \overline{N_1}\,\tilde{\phi}^\dagger\,\mathscr{Y}_{N_1\alpha}\,\ell_\alpha - \sum_{i\neq 1}^{n_N}\sum_{\alpha}^{3} \overline{N_i}\,\tilde{\phi}^\dagger\,Y_{N_i\alpha}\,\ell_\alpha - \frac{1}{2}\sum_{i}^{n_N} \overline{N_i}\,m_{N_i}\,N_i^c + \text{H.c.}\,, \tag{3.57}$$

where we have defined the effective Yukawa coupling $\mathscr{Y}_N \equiv Y_N R^\dagger$ with R the unitary matrix of the corresponding flavor regime. In the case where only one flavor is active (the ℓ_1 flavor of the unflavored case), the effective Yukawa couplings is $\mathscr{Y}_{N_1 1} = (\sum_\alpha |Y_{N_1\alpha}|^2)^{1/2}$, see Eq. (3.54). When two flavors are active (the ℓ_τ and the "ℓ_a" flavors), the effective Yukawa couplings are $\mathscr{Y}_{N_1\tau} = Y_{N_1\tau}$ and $\mathscr{Y}_{N_1 a} \equiv (\sum_{\alpha=e,\mu} |Y_{N_1\alpha}|^2)^{1/2}$, see Eq. (3.56). Finally, in the 3-flavor case, these are the usual Yukawa couplings $\mathscr{Y}_{N_1\alpha} = Y_{N_1\alpha}$ with $\alpha = e,\mu,\tau$. In what follows, we don't specify the number of flavors labelled by the index α. We now give the analytical expression of the decay rates, CP-asymmetries and Boltzmann equations.

3.6.1 Tree-level decay rates

In analogy with section 3.4.3, we can compute the tree-level decay rate $\Gamma(N_1 \to \ell_\alpha \phi)$ of N_1 into one flavor ℓ_α, which is given by

$$\Gamma(N_1 \to \ell_\alpha \phi) = \Gamma(N_1 \to \bar{\ell}_\alpha \phi^*) = \frac{1}{16\pi}\left|\mathscr{Y}_{N_1\alpha}\right|^2 m_{N_1}\,. \tag{3.58}$$

The total tree-level decay rate into the flavor ℓ_α reads

$$\Gamma^\alpha_{N_1} \equiv \Gamma(N_1 \to \ell_\alpha \phi) + \Gamma(N_1 \to \bar{\ell}_\alpha \phi^*) = \frac{1}{8\pi}\left|\mathscr{Y}_{N_1\alpha}\right|^2 m_{N_1} = B_{\ell_\alpha}\Gamma_{N_1}\,, \tag{3.59}$$

where for practical reasons we introduced the branching fractions

$$B_{\ell_\alpha} \equiv \frac{\Gamma^\alpha_{N_1}}{\Gamma_{N_1}} = \frac{\left|\mathscr{Y}_{N_1\alpha}\right|^2}{\left(Y_N Y_N^\dagger\right)_{11}}\,, \quad \text{that satisfy} \quad \sum_\alpha B_{\ell_\alpha} = 1\,. \tag{3.60}$$

The total decay rate Γ_{N_1} is obtained by summing over the flavor in Eq. (3.59). Let's note that it doesn't depend on the flavor regime since $Y_N Y_N^\dagger = \mathscr{Y}_N \mathscr{Y}_N^\dagger$, as it should, so it is still given by Eq. (3.20).

3.6.2 Evaluation of the CP-asymmetry

The analytical expression of the CP-asymmetries in the decay $N_1 \to \ell_\alpha \phi$, as defined in Eq. (3.25), are already given in Eq. (3.26). Let's note that now the lepton number conserving diagram in Fig. 3.6 may contribute to each individual flavor CP-asymmetry $\epsilon^{\ell_\alpha}_{N_1}$. As a consequence, the Davidson-Ibarra bound in Eq. (3.30) on the separated flavored CP-asymmetries doesn't hold anymore. It however still applies on the sum of the flavored CP-asymmetries, obviously. As a consequence, flavored CP-asymmetries can be larger (but still smaller than 1), and smaller right-handed neutrino masses are allowed. In practice, it is nevertheless difficult to go sizably below $\sim 10^9$ GeV, see Eq. (3.68) below. Note that there exists still an upper bound on the individual CP-asymmetries, proportional to the absolute neutrino mass scale, given by [231]

$$\left|\epsilon^{\ell_\alpha}_{N_1}\right| \leq \frac{3}{8\pi}\frac{m_{N_1}}{\mathrm{v}^2}\,\langle m_\nu\rangle\,, \tag{3.61}$$

where we assumed for simplicity a quasi-degenerate light neutrino spectrum $\langle m_\nu\rangle = m_1 \simeq m_2 \simeq m_3$ (even if not likely for $m_{N_1} \ll m_{N_{2,3}}$). This allows to decrease a little bit the lower bound on m_{N_1}, as we will see below.

3.6.3 Boltzmann equations

The evolution of the total $B-L$ must now be determined through the evolution of the N_1 density Y_{N_1} and through the evolution of the separate $B/3-L_\alpha$ asymmetries $\Delta Y_{B/3-L_\alpha}$, which are the quantities that sphalerons preserve. Using the formalism given in Appendix C.4 and keeping only the dominant contributions for the sake of illustration, one can easily derive the set of flavored Boltzmann equations :

$$\dot{Y}_{N_1} = -\left(\frac{Y_{N_1}}{Y^{\mathrm{Eq}}_{N_1}} - 1\right)\gamma_D\,, \tag{3.62}$$

$$\Delta\dot{Y}_{B/3-L_\alpha} = -\left(\frac{Y_{N_1}}{Y^{\mathrm{Eq}}_{N_1}} - 1\right)\epsilon^{\ell_\alpha}_{N_1}\gamma_D + \frac{1}{2}\frac{\Delta Y_{\ell_\alpha} + \Delta Y_\phi}{Y^{\mathrm{Eq}}_\ell}\,B_{\ell_\alpha}\,\gamma_D\,, \tag{3.63}$$

where we use the equilibrium density $Y^{\mathrm{Eq}}_\ell = Y^{\mathrm{Eq}}_\phi$, since ℓ and ϕ have the same number of degrees of freedom and are relativistic. [12] This is not the final expression of the Boltzmann equations. Indeed, we see that to integrate Eq. (3.63) one needs to know what are the expressions of ΔY_{ℓ_α} and ΔY_ϕ. These asymmetries are in fact directly related to the $B/3-L_\alpha$ ones through the chemical equilibrium conditions. As explained in Appendix C.5, following the temperature regime (and in particular in the temperature range where the lepton flavors have to be taken into account $T \lesssim 10^{12}$ GeV), some SM interactions are in thermal equilibrium, i.e. they are much faster than the Hubble rate, and then enforce relations between the chemical potentials of the various species and thus between the asymmetries of the involved particles. These thermal processes are called "spectator processes". As a consequence, all the particle asymmetries can be expressed in terms of a single set of variables. Above T_{EW}, we choose this set to be $\{\Delta Y_{B/3-L_\alpha}\}$, since these are the quantities entering in the Boltzmann equations and are conserved by sphalerons. Therefore, the

[12] As in the unflavored case, we make the approximation of taking Maxwell-Boltzmann equilibrium distributions.

asymmetries ΔY_{ℓ_α} and ΔY_ϕ are in fact related to the $\Delta Y_{B/3-L_\alpha}$ through

$$\Delta Y_{\ell_\alpha} = -\sum_\beta C^\ell_{\alpha\beta}\, \Delta Y_{B/3-L_\beta} \qquad \text{and} \qquad \Delta Y_\phi = -\sum_\alpha C^\phi_\alpha\, \Delta Y_{B/3-L_\alpha}\,. \tag{3.64}$$

The matrices C^ℓ and C^ϕ have different expressions following the temperature regime at which leptogenesis takes place. The exact expressions can be found in for example in Ref. [233], and are given in Appendix C.5.2. [13] Inserting Eqs. (3.64) in the Boltzmann equations one gets

$$\dot{Y}_{N_1} = -\left(\frac{Y_{N_1}}{Y^{\rm Eq}_{N_1}} - 1\right)\gamma_D\,, \tag{3.65}$$

$$\Delta\dot{Y}_{B/3-L_\alpha} = -\left(\frac{Y_{N_1}}{Y^{\rm Eq}_{N_1}} - 1\right)\epsilon^{\ell_\alpha}_{N_1}\gamma_D - \frac{1}{2}\sum_\beta\left(C^\ell_{\alpha\beta} + C^\phi_\beta\right)\frac{\Delta Y_{B/3-L_\beta}}{Y^{\rm Eq}_\ell}\, B_{\ell_\alpha}\,\gamma_D\,. \tag{3.66}$$

These equations can be compared to the unflavored Boltzmann equations in Eqs. (3.35)-(3.36). We see that there are now n_f equations for the $B/3-L_\alpha$, which are inter-related. [14]

On top of the source terms, a major difference lies now in two flavor effects in the washout terms : (i) the branching fraction B_{ℓ_α}, and (ii) the chemical equilibrium matrices $C^\ell_{\alpha\beta}$ and C^ϕ_α. These have important consequences and can affect considerably the final $B-L$ asymmetry that could be reached.

3.6.4 Analytical solutions to the Boltzmann equations

Proceeding as in the unflavored case in section 3.4.6, it is straightforward to show that the final $B-L$ asymmetry produced at the end of leptogenesis has the form :

$$\left|\Delta Y^{\rm end}_{B-L}\right| = \left|\sum_\alpha \Delta Y^{\rm end}_{B/3-L_\alpha}\right| = \sum_\alpha^{n_f} \epsilon^{\ell_\alpha}_{N_1}\,\eta^{\ell_\alpha}_{N_1}\; Y^{\rm Eq}_{N_1}\left(T \gg m_{N_1}\right)\,, \tag{3.67}$$

with $\eta^{\ell_\alpha}_{N_1}$ the efficiencies for each flavor in the game. As in the unflavored case, it is possible to derive analytical expressions for these ones. However, we won't make an analytical study of the efficiency and the improvements with respect to the unflavored case, since this goes beyond our scope. This can be found in for example Ref. [234]. We will here just show some results, for specific parameter values.

[13] In a first approximation, the matrix C^ℓ is quite close to the identity matrix $\mathbb{1}_{n_f\times n_f}$, where n_f is the number of lepton flavors participating in leptogenesis. However, the vector C^ϕ is not close to zero even for $T > 10^{12}$ GeV, where lepton flavors are undistinguishable. This means that spectator processes induce modifications to the unflavored regime considered in the previous section, as already mentioned in footnote 4 in page 94.

[14] Let's note that in the 2-flavor regime $\{\ell_\tau, \ell_a\}$, one has actually a third Boltzmann equation which concerns the inactive flavor ℓ_b, which reads trivially $\Delta\dot{Y}_{B/3-\ell_b} = 0$. Any asymmetry in the b flavor that has been previously generated, by for example the N_2 and/or N_3 right-handed neutrino, will therefore remain unchanged. In this case its contribution must be added to the final $B-L$ asymmetry produced in the N_1 driven leptogenesis.

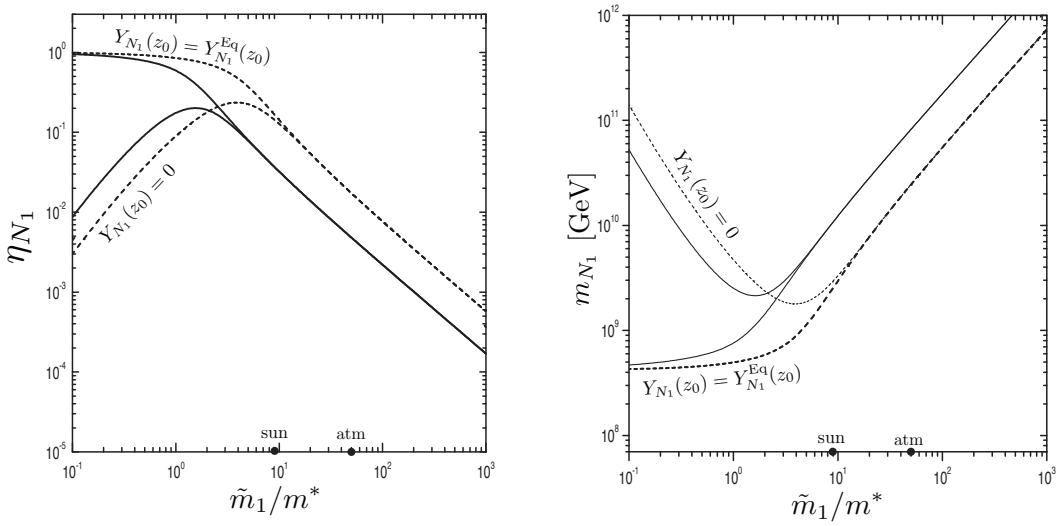

Figure 3.10 – In the case of thermal and zero initial abundance $Y_{N_1}(z_0)$, the left panel shows the efficiency η_{N_1} as a function of $K_1 \equiv \tilde{m}_1/m^*$, and in the right panel the lower bound on m_{N_1} as a function of $K_1 \equiv \tilde{m}_1/m^*$. In both plots, the one-flavor approximation is shown in solid black, while the dashed curve shows the flavor solution when taking equal CP-asymmetries and branching ratios. The two plots have been taken from Ref. [235].

3.6.5 Some results of successful leptogenesis

Efficiency. Since the parameter space is large, there are lots of specific cases leading to various values of the flavored efficiencies $\eta_{N_1}^{\ell_\alpha}$. Let's restrict ourselves here to a simple and limiting case where all the flavored CP-asymmetries and branching ratios are equal. In this case, from Eq. (3.67), one can define a total efficiency $\eta_{N_1} = \sum_\alpha \eta_{N_1}^{\ell_\alpha}$. Since now the $B-L$ asymmetry receive contributions from n_f flavors, one would expect roughly an enhancement of a factor $\sim n_f$ of the efficiency with respect to the unflavored case. But it doesn't work like that since the CP-asymmetries are also divided by n_f compared to the unflavored case. However, because of the presence of the branching ratios in Eq. (3.60), the washout is now reduced by a factor n_f. As a result, in this case the overall effect of the washout – controlled by the $\tilde{m}_1$ parameter – is shifted by a factor $\sim n_f$.

We show in the left panel of Fig. 3.10 the value of the efficiency as a function of the decay parameter $K_1 \equiv \tilde{m}_1/m^*$, in the case where three lepton flavors participate in leptogenesis. The plot has been taken from Ref. [235]. We see that the efficiency is shifted by a factor ∼3 to the right with respect to the unflavored case, as expect in this particular case.

Bounds on the mass m_{N_1} and on $\tilde{m}_1$. We show in the right panel of Fig. 3.10 the lower bound on the right-handed neutrino mass m_{N_1} as a function of $K_1 \equiv \tilde{m}_1/m^*$ in the case where all the flavored CP-asymmetries and branching ratios are equal. Here too, in this particular case the bounds are shifted by a factor ∼ 3 to the right with respect to the unflavored case. Furthermore, as in the unflavored scenario, one can derive in this case lower bounds on the right-handed neutrino

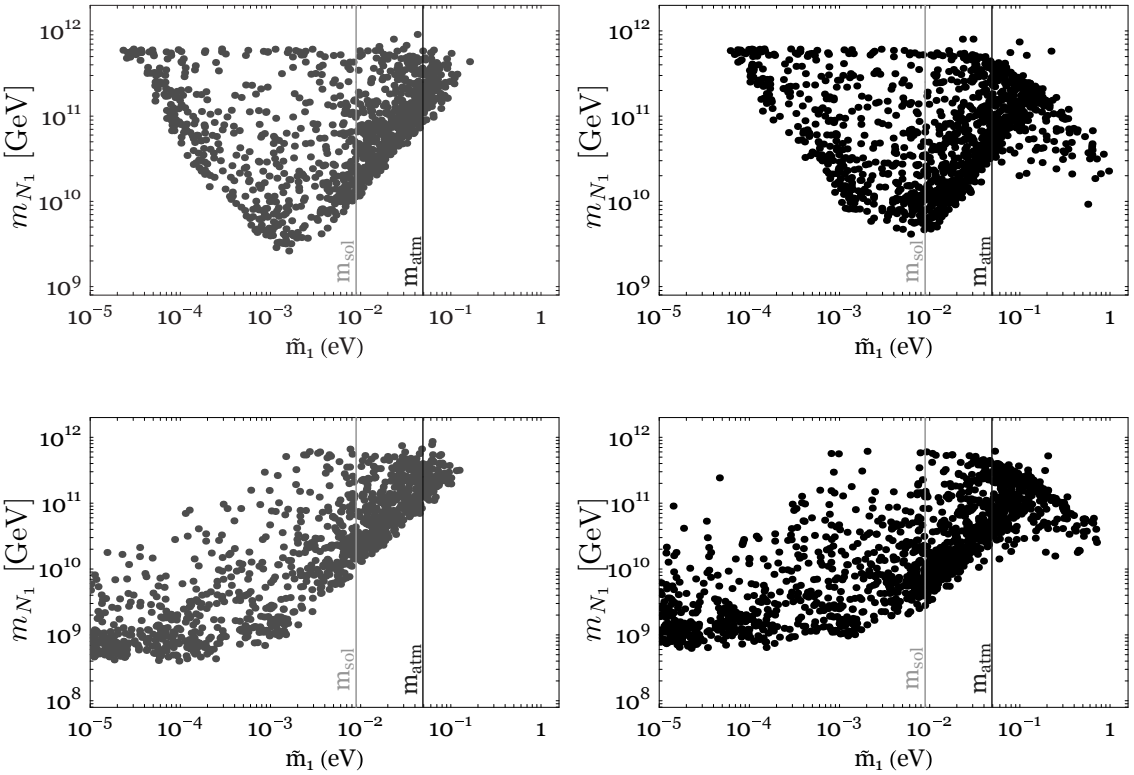

Figure 3.11 – The upper (lower) plots show the bounds on m_{N_1} in the case of zero (thermal) initial N_1 abundance. Left panels shows the unflavored approximation, while the right panels show the results when flavors are taken into account. These plots have been taken from Ref. [234].

masses, given by [235, 234] :

$$m_{N_1} \gtrsim \begin{cases} 2.5 \cdot 10^9 \text{ GeV} & \text{, in case } Y_{N_1}(z_0) = 0 \,, \\ 4.1 \cdot 10^8 \text{ GeV} & \text{, in case } Y_{N_1}(z_0) = Y_{N_1}^{\text{Eq}}(z_0) \,, \end{cases} \tag{3.68}$$

which are very close to the unflavored values in Eq. (3.68).

For more general flavor configurations, we show in Fig. 3.11 – taken from Ref. [234] – the parameter space values allowed by the requirement of successful leptogenesis, with (right-handed panels with black dots) or without (left-handed panels with gray dots) the inclusion of the flavor effects, and for thermal (upper plots) and zero (lower plots) initial N_1 abundance. We see that $\tilde{m}_1$ can take much larger values than in the unflavored case. This is because, in the flavored regime, the bound in Eq. (3.52) no longer holds because the upper-bounds on the separate CP-asymmetries are different. The bound has been estimated to be $m_\nu^{\max} \lesssim 2$ eV [236] (as confirmed by Fig. 3.11), to be compared with the unflavored result in Eq. (3.52), which is above the cosmological constraint given in Eq. (1.16). Note that all the points lie below $m_{N_1} \lesssim 10^{12}$ GeV in Fig. 3.11 because of the requirement to lie in a flavor regime.

3.7 Additional scattering processes

We previously considered only the dominant rates in the Boltzmann equations, i.e. only the decays and inverse decays on top of the CP-asymmetries. Since the latter are induced at the one-loop level, they involve 4 insertions of Yukawa couplings : $\epsilon_{N_1} \propto Y_N^4$. However, as already mentioned in section 3.4.7, other processes can have in some cases an important impact on the asymmetry production/washout in which case they must also be taken into account in the Boltzmann equations. For example, there are processes that are at the same order than the CP-asymmetries, as well as processes that are of the order $Y_N^2 Y_t^2$, where Y_t is the top Yukawa coupling. In particular, one has :

1. $\Delta L = 0$ scatterings mediated by a right-handed neutrino N_i, as the s, t, u-channel scatterings $\ell_\alpha \phi \leftrightarrow \ell_\beta \phi$ and $\phi\phi^* \leftrightarrow \ell_\alpha \bar{\ell}_\beta$;
2. $\Delta L = 1$ scatterings mediated by a SM scalar ϕ, as the s-channel scattering $\ell_\alpha N_i \leftrightarrow Q_3 \bar{t}$, the t-channel and u-channel scatterings $\ell_\alpha \bar{Q}_3 \leftrightarrow N_i \bar{t}$ and $\ell_\alpha t \leftrightarrow N_i Q_3$;
3. $\Delta L = 2$ scatterings mediated by a right-handed neutrino N_i, as the s, t, u-channel scatterings $\ell_\alpha \phi \leftrightarrow \bar{\ell}_\beta \phi^*$ and $\phi^*\phi^* \leftrightarrow \ell_\alpha \ell_\beta$. [15]

We show in Fig. 3.12 below the associated Feynman diagrams. These processes can bring significant corrections in the final $B-L$ asymmetry produced. Indeed, for example the $\Delta L = 0$ scatterings may have an impact on the relative washout of the $B/3 - L_\alpha$ asymmetries, the $\Delta L = 1$ scatterings can act as source term for heavy right-handed neutrino production and may have an impact on the washout, and finally the $\Delta L = 2$ scatterings may also contribute dramatically to the washout of the total $B-L$ asymmetry as we have discussed previously in section 3.4.7, page 100. Finally, let's note that there are also additional processes, as the $\Delta L = 1$ ones involving gauge bosons, or the $1 \leftrightarrow 3$ and $2 \leftrightarrow 3$ scatterings as $N_j \leftrightarrow \bar{Q} t \ell_i$ and $\ell_j \phi \leftrightarrow \bar{Q} t \ell_i$. These are in general even smaller contributions, either because of the couplings involved or because of a phase space factor suppression, and can safely be neglected.

It is not the goal of this thesis to go furthermore in the details of these scatterings in the type-1 Seesaw leptogenesis scenario. A proper derivation of the Boltzmann equations, as well as a consistent computation of the CP-asymmetry, has been carefully done in Ref. [225].

[15] Only the off-shell part of the s-channel scatterings $\ell_\alpha \phi \leftrightarrow \bar{\ell}_\beta \phi^*$ has to be considered since the on-shell one is already taken into account by the chain of processes $\ell_\alpha \phi \to N_1$ followed by $N_1 \to \bar{\ell}_\beta \phi^*$.

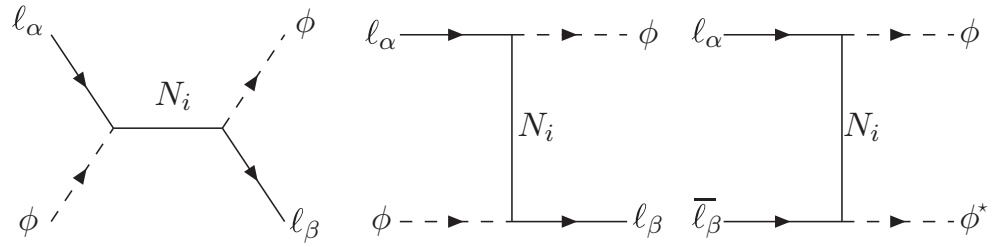

(a) $\Delta L = 0$ scatterings

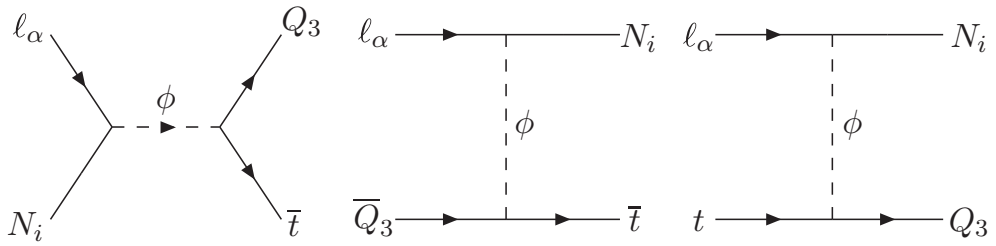

(b) $\Delta L = 1$ scatterings

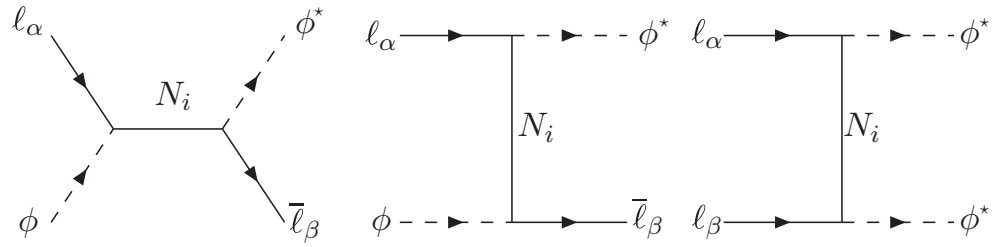

(c) $\Delta L = 2$ scatterings

Figure 3.12 – Feynman diagrams of the additional processes that need to be taken into account in the type-1 Seesaw leptogenesis. We don't show the u-channel diagrams associated to the t-channel ones.

4 Type-2 Seesaw leptogenesis

As already discussed in chapter 1, the type-2 Seesaw is a simple scenario in which Majorana neutrino masses are generated by the exchange of a heavy scalar electroweak triplet, see section 1.3.4. A single scalar triplet is enough in order to generate neutrino masses and mixings. At first sight, it also contains all the needed ingredients for leptogenesis, i.e. lepton number violation, CP-violating complex couplings and a heavy scalar triplet Δ that should have left thermal equilibrium at $T \sim m_\Delta$.

However, leptogenesis is not feasible in the standard type-2 Seesaw mechanism with only one scalar triplet added to the SM, because in this case the CP-asymmetry is expected to be generated only at higher loops than one-loop and is thus highly suppressed [237]. Indeed, the CP-asymmetries must be computed from the interference between the tree-level and the loop-level decay. In order to get non-zero CP-asymmetries at one-loop, we can show that this means that the one-loop diagrams must involve at least two heavy states with unequal couplings to leptons and/or scalar bosons, and both heavy states must have different masses, see for example Ref. [229]. If there is only one heavy state, or if for example there are several ones with exactly the same couplings to leptons and scalar bosons, the CP-asymmetry vanishes, since each coupling to leptons is automatically accompanied by its complex conjugate in the CP-asymmetry.

To activate leptogenesis in type-2 Seesaw framework, one needs to endow it with additional heavy fields, such as extra scalar triplets or right-handed neutrinos. In this case, the CP-asymmetries are no more vanishing and the type-2 leptogenesis can provide a compelling framework for baryogenesis via leptogenesis [229, 238, 239, 240, 241]. From now on, by type-2 leptogenesis we mean production of the BAU through the decays of the lightest scalar triplet, which are CP-violating thanks to heavier BSM fields. All along this chapter, we will mainly consider two representative possibilities :

(A) models featuring several scalar triplets, or in other words extended pure type-2 Seesaw models [238]. As we will see, the associated flavored CP-asymmetries contain in this case a lepton conserving part which will allow a Purely Flavored Leptogenesis (PFL) scenario, see section 4.5 below ;

(B) models involving a scalar triplet (minimal type-2 Seesaw) and heavier other Seesaw states, as for example right-handed neutrinos. In this general case, the CP-asymmetries generically break lepton number. This is particularly relevant for models where the generation of a $B-L$ asymmetry becomes possible due to the interplay between type-1 and type-2 Seesaws, scenarios arising in many well-motivated gauge extensions of the SM, see section 1.6.

For several reasons, the type-2 leptogenesis scenario is more intricate than the standard scenario based in the type-1 Seesaw introduced in sections 3.4-3.6. Let's already now specify the main differences with respect to the type-1 Seesaw leptogenesis scenario.

(1) **Gauge reactions.** First of all, while leptogenesis in type-1 Seesaw is driven by right-handed neutrinos which do not couple to gauge bosons, in type-2 Seesaw (as well as in type-3 Seesaw) the state which dynamically generates the $B-L$ asymmetry does have electroweak interactions. Because for temperatures below $T \sim 10^{14}$ GeV gauge reactions are much more faster than the Universe Hubble expansion, one may be tempted to believe that the third Sakharov condition is not fulfilled in scalar triplet leptogenesis so that leptogenesis is not viable, since gauge coupling seems to maintain the scalar triplet density in thermal equilibrium. As we will see in section 4.1, this is actually not the case [239, 237, 254, 241, 242, 243, 229]. Once the temperature of the heat bath decreases and reaches the mass of the decaying triplet, gauge reactions – being doubly Boltzmann suppressed – rapidly decouple and the dynamics becomes dominated by Yukawa reactions which then operate to a large extent as in the type-1 Seesaw case.

(2) **Triplet asymmetry.** Secondly, since the scalar triplet is not a self-conjugated particle as a right-handed neutrino is, a scalar triplet-antitriplet asymmetry develops [241, 229], thus calling for an additional Boltzmann equation accounting for the new asymmetry populating the heat bath. As a consequence, while the scalar doublet asymmetry in the type-1 case is fully determined by the evolution of the $B-L$ asymmetry, here it is determined in addition by the evolution of the triplet scalar asymmetry.

(3) **Decay channels.** Thirdly, while a right-handed neutrino decays via only one kind of channel $N \to \ell\phi$, a scalar triplet can decay via two channels : a "di-lepton" $\Delta \to \ell\ell$ and a "di-scalar" one $\Delta \to \phi\phi$, and this has important implications in particular concerning the flavor issue.

These three differences render leptogenesis much more difficult to understand. The chapter is organized as follow. In order to understand how the scalar triplet leptogenesis works, we first study in section 4.1 the scalar triplet leptogenesis within the "one-flavor approximation", which is a regime equivalent to the unflavored regime in the type-1 leptogenesis. The reason why we call it one-flavor approximation and not unflavored will appear in the next section 4.2, where we discuss the important flavor issue. Finally, in section 4.3 and after, we study the flavored type-2 leptogenesis scenario, which constitutes the original contribution of this chapter [2]. There were indeed no study of the effects of flavors in the type-2 leptogenesis when we started this project.

4.1 One-flavor approximation of the type-2 leptogenesis

We first remind the general expression of the type-1 and type-2 Lagrangian and the various interactions terms. Then, in order to understand the main features of the scalar triplet leptogenesis, we study in detail the one-flavor approximation, already well studied in the literature (see e.g. Ref. [241]). The reader familiar with this regime can directly go to the next section.

4.1.1 Lagrangians and interactions

The type-1 Seesaw Lagrangian with n_N right-handed neutrinos and the type-2 Seesaw Lagrangian with n_Δ scalar triplets are given by Eqs. (1.22) and (1.32) in sections 1.3.2 and 1.3.3. We remind here their expressions :

$$\mathscr{L}^{\text{type-1}} = i\overline{N_i}\partial\!\!\!/ N_i - \overline{N_i} Y_{N_i\alpha}\tilde{\phi}^\dagger \ell_\alpha - \frac{1}{2}\overline{N_i} M_{N_{ii}} C \bar{N}_i^T + \text{H.c.} \tag{4.1}$$

$$\mathscr{L}^{\text{type-2}} = \left(D_\mu \vec{\Delta}_k\right)^\dagger \left(D^\mu \vec{\Delta}_k\right) - \vec{\Delta}_k^\dagger m^2_{\Delta_k} \vec{\Delta}_k + \ell_\alpha^T C\, i\tau_2\, Y^{\alpha\beta}_{\Delta_k} \left(\frac{\vec{\tau}\cdot\vec{\Delta}_k}{\sqrt{2}}\right) \ell_\beta + \mu_{\Delta_k} \tilde{\phi}^\dagger \left(\frac{\vec{\tau}\cdot\vec{\Delta}_k}{\sqrt{2}}\right)^\dagger \phi + \text{H.c.}\,, \tag{4.2}$$

where $\ell^T = (\nu_L, e_L)$ and $\phi^T = (\phi^+, \phi^0)$ with $\phi^0 = (v + h^0 + i\phi_3^0)/\sqrt{2}$ are the lepton and scalar $SU(2)$ doublets. One has also $\tilde{\phi} = i\tau_2\phi^*$, $\vec{\tau}^T = (\tau_1, \tau_2, \tau_3)$ (with τ_i the 2×2 Pauli matrices) and the scalar Δ_k triplets given in the $SU(2)$ fundamental representation $\Delta_k = \left(\Delta_k^1, \Delta_k^2, \Delta_k^3\right)$. The n_Δ matrices Y_{Δ_k} are 3×3 symmetric matrices, while μ_{Δ_k} are n_Δ complex numbers. Since scalar triplets carry hypercharge $Y(\Delta) = -2$, the covariant derivative in Eq. (4.2) reads

$$D_\mu = \partial_\mu - i g \vec{T}\cdot\vec{W}_\mu - i g' B_\mu\,, \tag{4.3}$$

where $\vec{T}$ are the dimension three representations of the $SU(2)$ generators. The scalar triplet interactions with the leptons and scalars can be recast as

$$\mathscr{L}^{\text{type-2}} \ni \sum_k^{n_\Delta} \sum_{\alpha,\beta} Y^{\alpha\beta}_{\Delta_k} \ell_\alpha^T C i\tau_2 \mathbf{\Delta}_k \ell_\beta - \mu_{\Delta_k} \phi^T i\tau_2 \mathbf{\Delta}_k^\dagger \phi + \text{H.c.} \tag{4.4}$$

where $\mathbf{\Delta_k}$ is expressed in terms of electric charge eigenstates components

$$\mathbf{\Delta_k} \equiv \frac{\vec{\tau}\cdot\vec{\Delta}_k}{\sqrt{2}} = \begin{pmatrix} \frac{\Delta_k^+}{\sqrt{2}} & \Delta_k^{++} \\ \Delta_k^0 & -\frac{\Delta_k^+}{\sqrt{2}} \end{pmatrix}, \tag{4.5}$$

with the different components reading as

$$\Delta_k^0 = \frac{1}{\sqrt{2}}\left(\Delta_k^1 + i\Delta_k^2\right)\,, \qquad \Delta_k^+ = \Delta_k^3\,, \qquad \Delta_k^{++} \equiv \frac{1}{\sqrt{2}}\left(\Delta_k^1 - i\Delta_k^2\right)\,. \tag{4.6}$$

As said already in section 1.3.3, lepton number is broken in Eq. (4.2) because of the existence of both lepton and scalar interactions with the scalar triplet. The scalar interactions in Eq. (4.2) induce non-vanishing triplet vacuum expectation values which can be calculated from the minimization of the scalar potential : $\langle\Delta_k^0\rangle = \mathrm{v}_{\Delta_k} \simeq \mu_{\Delta_k}\, \mathrm{v}^2/2m^2_{\Delta_k}$.

Both Lagrangians in Eqs. (4.1) and (4.2), involving lepton number violating sources (from the coexistence of Y_N and M_N and of Y_Δ and μ_Δ), induce tree-level light neutrino Majorana masses through the standard type-1 (assuming $\mathrm{v}\, Y_N M_N^{-1} \ll 1$) and type-2 Seesaw mechanisms. The structure of the full neutrino mass matrix will of course depend on whether a single or both mechanisms is at work. Since here we will be dealing with scenarios determined by either the setup of Eq. (4.2) or an interplay between (4.1) and (4.2), in what follows we write the effective neutrino mass matrix in each case, namely

$$m_\nu^{\text{type-2}} = \sum_k m_\nu^{\Delta_k} = \sum_k \mu_{\Delta_k} \frac{\mathrm{v}^2}{m_{\Delta_k}^2} Y_{\Delta_k} \,, \tag{4.7}$$

$$m_\nu^{\text{type-1+2}} = \sum_k m_\nu^{\Delta_k} + m_\nu^N = \sum_k \mu_{\Delta_k} \frac{\mathrm{v}^2}{m_{\Delta_k}^2} Y_{\Delta_k} - \frac{\mathrm{v}^2}{2} Y_N^T M_N^{-1} Y_N \,. \tag{4.8}$$

The light neutrino mass spectrum is thus derived from these matrices by diagonalization through the leptonic mixing matrix $\mathscr{U} = U(\theta_{23})U(\theta_{13},\delta)U(\theta_{12})\hat{P}$, with θ_{ij} being the neutrino mixing angles, δ the Dirac CP phase and $\hat{P} = \mathrm{diag}(e^{i\alpha_1}, e^{i\alpha_2}, 1)$ containing the Majorana CP phases, see Eq. (1.4).

4.1.2 One-flavor approximation statement

In order to understand the main ideas behind the scalar triplet leptogenesis, we will in this section consider the simple but representative scenario of the "one-flavor approximation" of the scalar triplet leptogenesis. Similarly to the type-1 Seesaw leptogenesis, in this case :

- each component of the lightest scalar triplet $\Delta \equiv \Delta_1$ is assumed to decay in only one coherent lepton state ℓ, which encompasses all the lepton flavors,
- the effect of the spectator processes are neglected.

That is to say, this case doesn't distinguish the 3 flavors, and the associated Boltzmann equation for ℓ just counts the number of ℓ and $\bar{\ell}$ created or destroyed. An example of a general scenario of the production of a $B-L$ asymmetry will be given in section 4.1.5. The full one-flavor approximation analysis of the scalar triplet leptogenesis was first performed in detail in Ref. [241]. We will here follow closely the approach adopted in Ref. [229]. As in the type-1 Seesaw leptogenesis, decays/inverse decays play a crucial role during the leptogenesis era, so we first give the analytical expressions of the tree-level decay rate and of the CP-asymmetries.

4.1.3 Tree-level decay rates

Tree-level triplet decays involve leptonic and scalar final states. The Feynman diagrams are shown in Fig. 4.1 for the Δ^+ component, and the associated decay widths are computed in Appendix D.1. In the one-flavor approximation, the scalar triplet is assumed to decay into only one lepton state ℓ, which is constituted by the sum over the other flavors. The tree-level decay rates of each scalar triplet component to leptons and scalar are in this case given by, see Eqs. (D.9) and (D.11) in

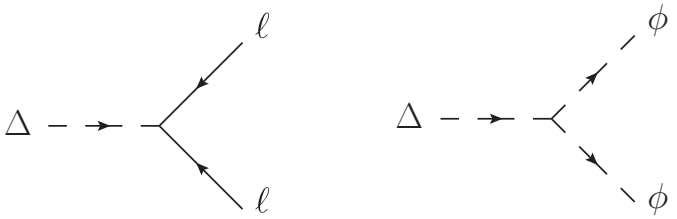

Figure 4.1 – Diagrams of the tree-level decay of the scalar triplet into leptons and into scalars.

Appendix D.1,

$$\Gamma\left(\Delta \to \bar{\ell}\bar{\ell}\right) \equiv \Gamma\left(\Delta^Q \to \bar{\ell}\bar{\ell}\right) = B_\ell \Gamma_\Delta = \frac{m_\Delta}{8\pi} \mathrm{Tr}\left[Y_\Delta Y_\Delta^\dagger\right] , \tag{4.9}$$

$$\Gamma\left(\Delta \to \phi\phi\right) \equiv \Gamma\left(\Delta^Q \to \phi\phi\right) = B_\phi \Gamma_\Delta = \frac{\left|\mu_\Delta\right|^2}{8\pi m_\Delta} , \tag{4.10}$$

where Q stands for the electric charges of the different $SU(2)$ triplet components, i.e. $\Delta_k^Q = (\Delta_k^0, \Delta_k^+, \Delta_k^{++})$. The parameters B_ℓ and B_ϕ are the branching fractions to two lepton doublets and two scalar doublets respectively ($B_\ell + B_\phi = 1$), and $\Gamma_\Delta \equiv \Gamma\left(\Delta \to \bar{\ell}\bar{\ell}\right) + \Gamma\left(\Delta \to \phi\phi\right)$ is the total decay width of one scalar triplet component Δ^Q. The total decay width can also be parametrized as :

$$\Gamma_\Delta = \frac{1}{8\pi} \frac{m_\Delta^2}{\mathrm{v}^2} \tilde{m}_\Delta^{\mathrm{eff}} , \tag{4.11}$$

where we defined the "effective neutrino mass-like" parameter $\tilde{m}_\Delta^{\mathrm{eff}}$ by

$$\tilde{m}_\Delta^{\mathrm{eff}} \equiv \tilde{m}_\Delta \frac{1}{\sqrt{B_\ell B_\phi}} , \tag{4.12}$$

in which the "neutrino mass-like" parameter $\tilde{m}_\Delta$ is given by

$$\tilde{m}_\Delta^2 \equiv \mathrm{Tr}[m_\nu^\Delta m_\nu^{\Delta\dagger}] = |\mu_\Delta|^2 \frac{\mathrm{v}^4}{m_\Delta^4} \mathrm{Tr}\left[Y_\Delta Y_\Delta^\dagger\right] . \tag{4.13}$$

As compared to the type-1 Seesaw leptogenesis, the decay rates depends on m_Δ and $\tilde{m}_\Delta$, but also on an extra parameter which is the branching ratio B_ϕ (or $B_\ell = 1 - B_\phi$). The total decay rate exhibits a minimum for $B_\ell = B_\phi = 1/2$ and the farther we are from this situation, the faster the scalar triplet decays, so that the decay rate obeys :

$$\Gamma_\Delta \geq \frac{1}{4\pi} \frac{m_\Delta^2}{\mathrm{v}^2} \tilde{m}_\Delta . \tag{4.14}$$

If the neutrino masses in Eqs. (4.7) or (4.8) are dominated by the light scalar triplet Δ, one has $m_\nu \simeq \mu_\Delta Y_\Delta \mathrm{v}^2 / m_\Delta^2$ and the neutrino mass like parameter is simply given by

$$\tilde{m}_\Delta^2 \simeq \mathrm{Tr}[m_\nu m_\nu^\dagger] = \sum_i m_i^2 \gtrsim |\Delta m_{\mathrm{atm}}^2| \approx (0.05 \text{ eV})^2 , \tag{4.15}$$

where m_i are the light neutrino masses and where $\Delta m_{\mathrm{atm}}^2$ is the atmospheric mass difference whose value is given in Table 1.1.

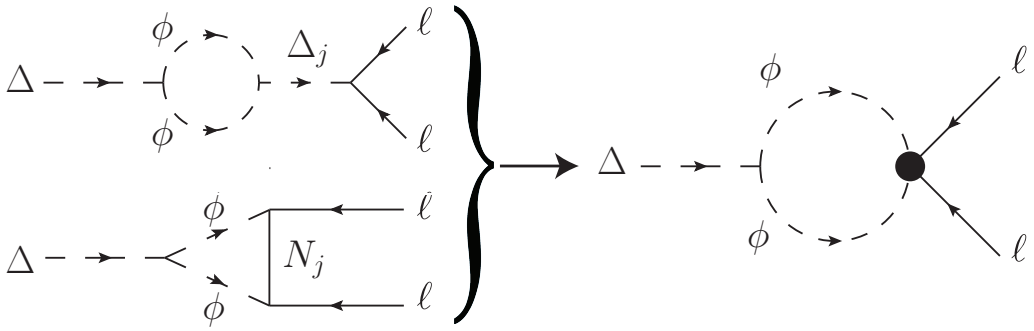

Figure 4.2 – One-loop diagrams contributing to the CP-asymmetry in scalar triplet decays (left). For heavy field value, they contain their contribution to the neutrino mass matrix.

4.1.4 Evaluation of the CP-asymmetry

Within this one-flavor approximation, the CP-asymmetry is simply given by the sum of the flavored CP-asymmetries, see Eq. (D.15)-(D.17) in Appendix D.2,

$$\epsilon_\Delta \equiv 2\frac{\Gamma\left(\bar{\Delta}\to\ell\ell\right)-\Gamma\left(\Delta\to\bar{\ell}\bar{\ell}\right)}{\Gamma_\Delta+\Gamma_{\Delta^*}}=\sum_\alpha \epsilon_\Delta^{\ell_\alpha}\,, \tag{4.16}$$

where the factor 2 comes from the fact that there are two leptons in the final state. This expression is nothing but the average lepton asymmetry ΔL produced per triplet decay. As already discussed at the beginning of this chapter, one needs one or more new heavy fields X in order to generate a non-vanishing CP-asymmetry. The Feynman diagrams where $X=\Delta_j, N_j$ are shown in Fig. 4.2. In the limit of hierarchical spectrum of heavy state $m_\Delta \ll m_X$, we can show – see also Eqs. (4.74), (4.75) and (4.78) below – that the CP-asymmetry is given by [241]

$$\epsilon_\Delta = -\frac{1}{2\pi}\frac{m_\Delta}{\mathrm{v}^2}\sqrt{B_\ell B_\phi}\frac{\Im m\left\{\mathrm{Tr}\left[m_\nu^\Delta m_\nu^{X\dagger}\right]\right\}}{\tilde{m}_\Delta}\,, \tag{4.17}$$

where the contribution of the heavy state comes only through its contribution to the neutrino mass matrix m_ν^X, as can be understood from Fig. 4.2. Therefore, for $m_\Delta \ll m_X$, leptogenesis in the one-flavor approximation can be studied in a fully general way independent of the exact heavy state which induces m_ν^X, i.e. whether it is a right-handed neutrino, a scalar triplet or a fermionic triplet. With this CP-asymmetry and from CPT invariance, the decay rates at one-loop read

$$\Gamma\left(\bar{\Delta}\to\ell\ell\right)=\Gamma_\Delta\left(B_\ell+\epsilon_\Delta/2\right)\,, \tag{4.18}$$
$$\Gamma\left(\Delta\to\bar{\ell}\bar{\ell}\right)=\Gamma_\Delta\left(B_\ell-\epsilon_\Delta/2\right)\,, \tag{4.19}$$
$$\Gamma\left(\bar{\Delta}\to\bar{\phi}\bar{\phi}\right)=\Gamma_\Delta\left(B_\phi-\epsilon_\Delta/2\right)\,, \tag{4.20}$$
$$\Gamma\left(\Delta\to\phi\phi\right)=\Gamma_\Delta\left(B_\phi+\epsilon_\Delta/2\right)\,. \tag{4.21}$$

As can be seen from the type-2 Seesaw Lagrangian in Eq. (4.2), in the situation where either $B_\ell=0$ or $B_\phi=0$, the lepton number is conserved and one cannot generate any lepton asymmetry. This is indeed confirmed by the above expression of the CP-asymmetry in Eq. (4.17), since $\epsilon_\Delta \propto (B_\phi B_\ell)^{1/2}$.

In a way similar to what has been done for type-1 Seesaw leptogenesis in section 3.4.4, it is possible to derive from Eq. (4.17) a Davidson-Ibarra-like bound given by [241] : [1]

$$\left|\epsilon_\Delta\right| \leq \frac{1}{2\pi}\frac{m_\Delta}{\mathrm{v}^2}\sqrt{B_\ell B_\phi \sum_i m_i^2}\,, \tag{4.22}$$

where as usual m_i stands for the light neutrino masses. Also, from perturbativity constraints, i.e. by requiring that the one-loop contribution to the various decay widths doesn't exceed the tree-level one, from Eqs. (4.18)-(4.21) one can derive another "model-independent" upper bound on the CP-asymmetry given by

$$\left|\epsilon_\Delta\right| \leq 2\cdot\min\left(B_\ell, B_\phi\right)\,. \tag{4.23}$$

This bound is an absolute bound from unitarity, while the one in Eq. (4.22) has been obtained assuming that the CP-asymmetry arises from heavier sources of neutrino masses. Now that we have computed the various CP-asymmetries, we are ready to write down the Boltzmann equations.

4.1.5 Boltzmann equations

In what follows we first present the main reactions involved in scalar triplet leptogenesis. Next, we derive the appropriate set of Boltzmann equations and we explain the origin of each term in these equations. Subsequently, in order to understand how scalar triplet leptogenesis works, a general leptogenesis scenario is analyzed, and the differences with respect to type-1 Seesaw leptogenesis are highlighted.

Reactions. In the hot plasma, triplets are subject to reactions that either tend to washout the $B-L$ asymmetry or to generate it. Depending on the interaction inducing the process, one can distinguish – at tree-level – four kind of reactions : pure Yukawa, pure scalar, pure gauge and Yukawa-scalar reactions. Explicitly, we have in general : [2]

- Yukawa and scalar-induced decay and inverse decays, $\Delta \leftrightarrow \bar{\ell}\bar{\ell}$ and $\Delta \leftrightarrow \phi\phi$, described by the reaction densities : $\gamma_D^\ell \equiv \sum_{\alpha,\beta}\gamma^\Delta_{\ell_\alpha\ell_\beta}$ and $\gamma_D^\phi \equiv \gamma^\Delta_{\phi\phi}$. The total decay reaction density is given by

$$\gamma_D = \gamma_D^\ell + \gamma_D^\phi = s\,\frac{K_1(z)}{K_2(z)}\,Y_\Sigma^{\mathrm{Eq}}\,\Gamma_\Delta\,, \tag{4.24}$$

  where we summed over the scalar triplet components (question of convention).

[1] This bound can be obtained by parametrizing the diagonal matrix of the light neutrino mass eigenstates as $\hat{m}_\nu^\Delta = \alpha\cdot\hat{m}_\nu$ and $\hat{m}_\nu^\Delta = \alpha\cdot\hat{m}_\nu$, where α is a real and diagonal matrix. From Eq. (4.17), looking just at the fraction, one get therefore that $|\epsilon_\Delta| \leq \ldots \sum_i (1-\alpha_i^*)\alpha_i m_{\nu_i}^2/(\sum_i |\alpha_i|^2 m_{\nu_i}^2)^{1/2}$. From Cauchy-Swartz inequality, one then obtains that $|\epsilon_\Delta| \leq \ldots (\sum_i |1-\alpha_i|^2 m_{\nu_i}^2)^{1/2}$, and the upper bound reads therefore $|\epsilon_\Delta| \leq \ldots \tilde{m}_X$ where $\tilde{m}_X^2 \equiv \mathrm{Tr}[m_\nu^X m_\nu^{X\dagger}]$. If one doesn't have any information about the structure of the light neutrino mass matrix (i.e. we don't know the α_i), this expression is bounded from above by $|\epsilon_\Delta| \leq \ldots (\sum_i m_{\nu_i}^2)^{1/2}$.

[2] Expressions for all the intervening reaction densities can be found in Appendix D.3.

- Gauge-induced $2 \leftrightarrow 2$ scatterings as follows : s-channel gauge-boson-mediated: $\Delta\Delta \leftrightarrow FF$ (F standing for SM fermions), $\Delta\Delta \leftrightarrow \phi\phi$ and $\Delta\Delta \leftrightarrow VV$ (V standing for SM gauge bosons) ; t and u channel triplet-mediated : $\Delta\Delta \leftrightarrow VV$ and four-point vertex $\Delta\Delta \leftrightarrow VV$ reactions. All together they are characterized by the reaction density γ_A.

- Lepton flavor and lepton number ($\Delta L = 2$) violating Yukawa-scalar-induced and triplet-mediated s and t channel $2 \leftrightarrow 2$ scatterings $\phi\phi \leftrightarrow \bar{\ell}_\alpha \bar{\ell}_\beta$ and $\phi\ell_\beta \leftrightarrow \bar{\phi}\bar{\ell}_\alpha$, which are accounted for by the reaction densities $\gamma^{\phi\phi}_{\ell_\alpha\ell_\beta}$ and $\gamma^{\phi\ell_\beta}_{\phi\ell_\alpha}$. In the one-flavor approximation, these become $\gamma^{\phi\phi}_{\ell\ell} = \sum_{\alpha,\beta}\gamma^{\phi\phi}_{\ell_\alpha\ell_\beta}$ and $\gamma^{\phi\ell}_{\phi\ell} = \sum_{\alpha,\beta}\gamma^{\phi\ell_\beta}_{\phi\ell_\alpha}$.

- Lepton-flavor-violating Yukawa-induced and triplet-mediated s and t channel $2 \leftrightarrow 2$ scatterings : $\ell_\gamma\ell_\delta \leftrightarrow \ell_\alpha\ell_\beta$ and $\ell_\beta\ell_\gamma \leftrightarrow \ell_\alpha\ell_\delta$, with reaction densities given by $\gamma^{\ell_\gamma\ell_\delta}_{\ell_\alpha\ell_\beta}$ and $\gamma^{\ell_\beta\ell_\gamma}_{\ell_\alpha\ell_\delta}$. In the one-flavor approximation, when summing over lepton flavors, theses interactions clearly don't affect the ℓ asymmetry and do not play any role. These reactions are therefore inherent to scalar flavored leptogenesis, see section 4.3.

Boltzmann equations. As said above in page 112, an important difference with the type-1 Seesaw leptogenesis is that the scalar triplet is not its own antiparticle. As a consequence, a triplet asymmetry ΔY_Δ can generate, leading to an additional Boltzmann equation. The network of Boltzmann equations for scalar triplet leptogenesis corresponds therefore to a system of coupled differential equations accounting for the temperature evolution of the triplet density $Y_\Sigma = Y_\Delta + Y_{\bar{\Delta}}$, the triplet asymmetry $\Delta Y_\Delta = Y_\Delta - Y_{\bar{\Delta}}$ and the ΔY_{B-L} charge asymmetry, where $L = \ell$ within this section. The resulting network will of course – and unavoidably – involve the scalar doublet asymmetry ΔY_ϕ. All together, the above reactions lead to the following network of classical Boltzmann equations [241] :

$$\dot{Y}_\Sigma = -\left(\frac{Y_\Sigma}{Y_\Sigma^{\rm Eq}} - 1\right)\gamma_D - 2\left[\left(\frac{Y_\Sigma}{Y_\Sigma^{\rm Eq}}\right)^2 - 1\right]\gamma_A\,, \tag{4.25}$$

$$\Delta\dot{Y}_\Delta = -\left[\left(B_\ell + B_\phi\right)\frac{\Delta Y_\Delta}{Y_\Sigma^{\rm Eq}} - B_\ell\frac{\Delta Y_{B-L}}{Y_\ell^{\rm Eq}} - B_\phi\frac{\Delta Y_\phi}{Y_\ell^{\rm Eq}}\right]\gamma_D\,, \tag{4.26}$$

$$\Delta\dot{Y}_{B-L} = -\left(\frac{Y_\Sigma}{Y_\Sigma^{\rm Eq}} - 1\right)\epsilon_\Delta\gamma_D + 2\left(\frac{\Delta Y_\Delta}{Y_\Sigma^{\rm Eq}} - \frac{\Delta Y_{B-L}}{Y_\ell^{\rm Eq}}\right)B_\ell\gamma_D + 2\left(\frac{\Delta Y_\phi}{Y_\ell^{\rm Eq}} - \frac{\Delta Y_{B-L}}{Y_\ell^{\rm Eq}}\right)\left(\gamma'^{\phi\phi}_{\ell\ell} + \gamma^{\phi\ell}_{\phi\ell}\right)\,, \tag{4.27}$$

where we have adopted the following conventions (details can be found in Appendix C.1). We use the particle number density-to-entropy ratio defined as $\Delta Y_X = \Delta n_X/s = (n_X - n_{\bar{X}})/s$, where n_X ($n_{\bar{X}}$) is the number density of species X ($\bar{X}$) and s is the entropy density. We have defined $Y_\Delta \equiv 3\cdot Y_{\Delta^Q}$, with Δ^Q denoting one of the three components of the scalar triplet, and $Y_\phi \equiv 2\cdot Y_{\phi^Q}$, with ϕ^Q denoting one of the two components of the scalar doublet. [3] The derivative is denoted according to $\dot{Y} \equiv sHzdY/dz$, with H the expansion rate of the Universe, and as usual $z = m_\Delta/T$. In order to avoid double counting, primed s-channel scattering reaction densities refer to the rates with resonant intermediate state subtracted : $\gamma' = \gamma - \gamma^{\text{on-shell}}$. Finally, we use the Maxwell-

[3] The triplet densities Y_Δ and $Y_{\bar{\Delta}}$ contain therefore all the three triplet components, i.e. $g_\Delta = g_{\bar{\Delta}} = 3$.

Boltzmann equilibrium distribution, and one has $Y_\ell^{\rm Eq} = Y_\phi^{\rm Eq}$ since both have the same number of degrees of freedom and are ultra-relativistic for the whole temperature range at which leptogenesis takes place.

In the above set of Boltzmann equations, one has still to determine the expression of the scalar doublet asymmetry ΔY_ϕ. One can derive a Boltzmann equation for it, but as we show in Appendix D.5, it is in fact directly related to the triplet and $B-L$ asymmetry through the hypercharge neutrality condition

$$2\Delta Y_\Delta + \Delta Y_\phi + \Delta Y_{B-L} = 0\,. \tag{4.28}$$

That is, the ϕ asymmetry is therefore fully determined by the triplet and the $B-L$ asymmetries through chemical equilibrium conditions, as it is done in the standard leptogenesis case [244, 245] (see Eq. (C.51) in the Appendix and the associated discussion). It is thus not necessary to consider it, but it is however very useful for our understanding to show the corresponding Boltzmann equation in the one-flavor approximation :

$$\Delta\dot{Y}_\phi = \left(\frac{Y_\Sigma}{Y_\Sigma^{\rm Eq}} - 1\right)\epsilon_\Delta \gamma_D + 2\left(\frac{\Delta Y_\phi}{Y_\ell^{\rm Eq}} - \frac{\Delta Y_\Delta}{Y_\Sigma^{\rm Eq}}\right)B_\phi \gamma_D + 2\left(\frac{\Delta Y_\phi}{Y_\ell^{\rm Eq}} - \frac{\Delta Y_{B-L}}{Y_\ell^{\rm Eq}}\right)\left(\gamma'^{\phi\phi}_{\ell\ell} + \gamma^{\phi\ell}_{\phi\ell}\right)\,. \tag{4.29}$$

Let's now try to understand the physical meaning of this set of Boltzmann equations (4.25)-(4.27) and (4.29). To this end, let's first describe the origin of each term.

1. **The first equation, describing the evolution of Y_Σ,** involves two terms : the first one, proportional to γ_D and also present in the type-1 leptogenesis, describes the decays/inverse decays of Δ. The second term, proportional to γ_A and not present in the type-1 leptogenesis, describes the gauge scatterings of the triplets $\Delta\Delta \leftrightarrow SM\,SM$ (with SM denoting a SM particle), and it involves therefore the square of the triplet density. Because of this, for $T \ll m_\Delta$ the gauge reaction rate is doubly Boltzmann suppressed $\gamma_A \propto e^{-2m_\Delta/T}$ and the thermalization rate goes like $\gamma_A/n_\Sigma^{\rm Eq}H \propto e^{-m_\Delta/T}/\sqrt{m_\Delta T}$. The rate is maximum for $T \approx m_\Delta$, where one has

   $$\frac{\gamma_A}{n_\Sigma^{\rm Eq}H} \approx \frac{10^{14}\ {\rm GeV}}{m_\Delta}\,. \tag{4.30}$$

   This means that for $m_\Delta \lesssim 10^{14}$ GeV, the gauge scatterings do enter in thermal equilibrium. The smaller the m_Δ, the larger the rate. As a consequence, for $m_\Delta \lesssim 10^{14}$ GeV, the gauge reactions thermalize the triplet density, even if the decay reaction γ_D is small.

2. **When decaying at one-loop,** the scalar triplet produces a $B-L$ (and a ϕ) asymmetry. The amount of asymmetry produced is proportional to the CP-asymmetry ϵ_Δ. This is represented by the usual source term in the first term in Eq. (4.27) (and Eq. (4.29)).

3. **The scalar triplet can decay/inverse decay at tree-level** in/from either leptons or scalars, with a rate proportional to B_ℓ and B_ϕ respectively. On the one hand, this means that once a $B-L$ (and so a ϕ) asymmetry is produced, the inverse decays $\ell\ell \to \bar{\Delta}$ (and $\bar{\phi}\bar{\phi} \to \Delta$) will create a triplet asymmetry. This is represented by the second term $\propto B_\ell$ (third term $\propto B_\phi$)

in the r.h.s. of Eq. (4.26) describing the evolution of the triplet asymmetry, and by the first term (second term) in the second bracket in the r.h.s. of Eq. (4.27) for the $B-L$ asymmetry (Eq. (4.29) for the ϕ asymmetry). On the other hand, it goes also the other way around, i.e. if there is a triplet asymmetry, the tree-level decays of the triplet will also generate $B-L$ and ϕ asymmetries. This is represented by the first term $\propto B_\ell + B_\phi$ in the r.h.s. of the Eq. (4.26) describing the evolution of the triplet asymmetry, and by the first (second) term in the second bracket in the r.h.s. of Eq. (4.27) describing the evolution of the $B-L$ asymmetry (Eq. (4.29) for the ϕ asymmetry).

4. **Finally, the last terms in Eqs.** (4.27) **and** (4.29) represent the $\Delta L = 2$ scattering processes $\phi\phi \leftrightarrow \bar{\ell}\bar{\ell}$ and $\phi\ell \leftrightarrow \bar{\phi}\bar{\ell}$. As in the type-1 Seesaw leptogenesis (see discussion at the bottom of page 99), the rates of theses scattering are proportional to the Seesaw mass scale m_Δ and to the light neutrino mass scale, since they involve the neutrino mass diagram. As a consequence, here too their effects are small for $m_\Delta \lesssim 10^{14}$ GeV, and we will neglect them in what follows. A quite accurate calculation of the resulting $B-L$ asymmetry can therefore be done by considering only decays, inverse decays and gauge induced reactions. As a justification example, fixing $m_\Delta = 10^{10}$ GeV, $\tilde{m}_\Delta = 0.05$ eV – parameter which drive the decay/inverse decay rate, see Eq. (4.13) – and $B_\phi = 10^{-2}$, we see in the left panel of Fig. 4.3 that these scatterings never reach thermal equilibrium. [4]

Gauge interactions. Before going on, an important remark concerns the gauge scatterings. Indeed, if the gauge reactions are active, in the sense that they are faster than the decay/inverse decay rate, the triplets will more likely gauge scatter than decay, and one doesn't expect an important production of $B-L$ asymmetry, as anticipated from page 112. *However, because the decay/inverse decay rate γ_D is only one time Boltzmann suppressed (because they involve one triplet) contrarily to γ_A which is two times Boltzmann suppressed for $T \ll m_\Delta$ (because they involve two triplets), the gauge reactions become slower than the inverse decays at some temperature* $z_A = m_\Delta/T_A$. This is also illustrated in the left panel of Fig. 4.3. From this moment z_A, the scalar triplet will more likely decay than gauge scatter, so that a more important $B-L$ can generate. This is why scalar triplet leptogenesis is feasible even in the presence of fast gauge reactions. We will come back to this point after.

General scenario. As an example, fixing $m_\Delta = 10^{10}$ GeV, $\tilde{m}_\Delta = 0.05$eV and $B_\phi = 10^{-2}$, we show in Fig. 4.3 as a function of $z = m_\Delta/T$ the reaction densities (left) and the evolution of the various densities (right). The latter figure has been obtained solving numerically the Boltzmann equations, taking a CP-asymmetry $\epsilon_\Delta = 1$ for illustration purpose, and $Y_\Sigma(z_0) = Y_\Sigma^{\rm Eq}(z \ll 1)$ as initial condition. The general scenario of the generation of the $B-L$ asymmetry is thus the following.

- For $z \ll 1$, whatever the initial triplet abundance, since $m_\Delta \lesssim 10^{14}$ GeV the gauge reactions thermalize the triplet density, so that $Y_\Sigma(T \gg m_\Delta) = Y_\Sigma^{\rm Eq}(T \gg m_\Delta)$. *There is therefore generally no dependence on the initial condition for the triplet abundance, unlike in type-1*

[4] More precisely, in the example of Fig. 4.3, the inclusion of these scattering processes leads to ~0.01% correction on the final $B-L$ asymmetry at the end of leptogenesis. That is to say, much less than the error we do by considering classical Boltzmann equations and Maxwell-Boltzmann equilibrium densities.

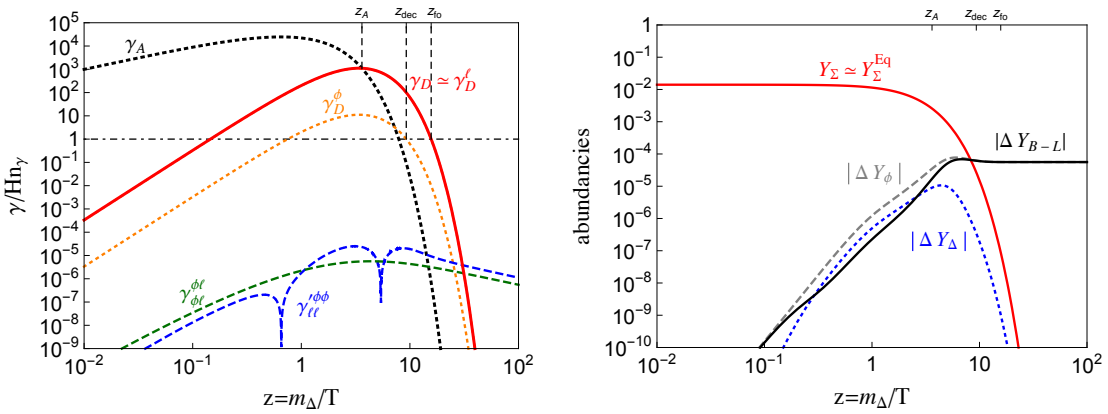

Figure 4.3 – Fixing the various parameters according to $m_\Delta = 10^{10}\,\mathrm{GeV}$, $\tilde{m}_\Delta = 0.05\,\mathrm{eV}$ and $B_\phi = 10^{-2}$ (which corresponds to $\tilde{m}_\Delta^{\mathrm{eff}} \approx 5\,\mathrm{eV}$), we show in the left panel the thermalization rates $\gamma/(Hn_\gamma)$ for the different processes involved in scalar triplet one-flavor leptogenesis, and in the right panel we show the evolution of the various densities as a function of $z = m_\Delta/T$. For this r.h.s. plot, we also fixed the CP-asymmetry to $\epsilon_\Delta = 1$ and the initial abundance to $Y_\Sigma(z_0) = Y_\Sigma^{\mathrm{Eq}}(z_0)$.

leptogenesis. This is why in what follows we will always assume a thermal initial abundance for the $\Sigma = \Delta + \bar{\Delta}$ abundance. Also, during all the leptogenesis scenario, the density follows closely the equilibrium density and one has approximately $Y_\Sigma(z) \approx Y_\Sigma^{\mathrm{Eq}}(z)$.

- For $1 \leq z < z_A$, the gauge reactions are faster than the decay/inverse decay rate (and faster than the Hubble rate). However, some triplets decay and produce slowly a $B-L$ asymmetry ΔY_{B-L} as well as a ϕ asymmetry ΔY_ϕ. At the same time, the creation of the $B-L$ and ϕ asymmetries automatically induces that a triplet asymmetry ΔY_Δ can develop.

- At $z = z_A$, the gauge reaction γ_A becomes slower than the decay/inverse decay γ_D. From this moment, all the triplets left decay and produce a $B-L$ asymmetry ΔY_{B-L}, as well as a ϕ asymmetry ΔY_ϕ.

- For $1 \ll z \leq z_{\mathrm{dec}}$, the triplet density is Boltzmann suppressed and, at some moment z_{dec}, the lepton number violating inverse decay reactions become slower than the Hubble rate. From this moment, all the triplets left decay without inverse decay and the triplet asymmetry decreases progressively to reach zero.

- At $z \gg z_{\mathrm{dec}}$, all the triplets have decayed, and the produced $B-L$ stays constant. The present baryon asymmetry of the Universe is as usual related to the $B-L$ asymmetry generated at the end of leptogenesis through

$$Y_B^{\mathrm{today}} = \Delta Y_B^{\mathrm{today}} = \frac{12}{37}\Delta Y_{B-L}^{\mathrm{end}}\,. \tag{4.31}$$

This is a basic example and one could have different situations as we will see. For example, with the chosen parameter values one had $z_A < z_{\mathrm{dec}}$, but one could also have $z_A > z_{\mathrm{dec}}$, in which case the final asymmetry is more suppressed since the decay/inverse decays are always overshadowed by the gauge reactions.

4.1.6 Analytical resolution of the Boltzmann equations and maximum $B-L$ asymmetry reachable

It is in general difficult to solve analytically the set of Boltzmann equations, because the point is that now the various equations are intricate. However, as in the type-1 Seesaw leptogenesis scenario, the final $B-L$ asymmetry can here too be expressed as

$$\left|\Delta Y_{B-L}^{\rm end}\right| = \epsilon_\Delta\, \eta_\Delta\, Y_\Sigma^{\rm Eq}(T \gg m_\Delta)\ , \tag{4.32}$$

where η_Δ is the efficiency, to be determined by solving the Boltzmann equation. In order to get an analytical expression of the efficiency, we now proceed by switching on the various interaction step by step, what will allow us to understand the main results.

Neglecting the washout terms. First, let's consider only the source term in the $B-L$ Boltzmann equation (4.27), i.e. we neglect the washout of the $B-L$ asymmetry from the inverse decay $\ell\ell \to \bar{\Delta}$. In this case, using Eq. (4.25), one gets

$$\Delta\dot{Y}_{B-L} = -\left(\frac{Y_\Sigma}{Y_\Sigma^{\rm Eq}} - 1\right)\epsilon_\Delta \gamma_D = \frac{\epsilon_\Delta\, \dot{Y}_\Sigma}{1+2\left(\frac{Y_\Sigma}{Y_\Sigma^{\rm Eq}}+1\right)\frac{\gamma_A}{\gamma_D}} \approx \frac{\epsilon_\Delta\, \dot{Y}_\Sigma}{1+4\frac{\gamma_A}{\gamma_D}}\ , \tag{4.33}$$

where we used $Y_\Sigma \approx Y_\Sigma^{\rm Eq}$. Let's consider two different situations :

1. If $\gamma_A/n_\Sigma^{\rm Eq} < H$ or $\gamma_A < \gamma_D/4$, the gauge scatterings are never active and the second term in the denominator can be neglected. One gets in this case $\Delta Y_{B-L}^{\rm end} \simeq Y_\Sigma\,(z \ll 1)$. Like in the type-1 leptogenesis, we recover the usual result that the efficiency is maximal $\eta_\Delta = 1$ if one starts with a thermal abundance $Y_\Sigma(z_0) = Y_\Sigma^{\rm Eq}(z_0)$.

2. If $\gamma_A > \gamma_D/4$, the triplet will more likely undergo gauge scatterings before decaying, and the first term in the denominator can be neglected, so that one has

$$\frac{d\Delta Y_{B-L}}{dz} \simeq \epsilon_\Delta\, \frac{dY_\Sigma}{dz}\, \frac{\gamma_D}{4\gamma_A}\ . \tag{4.34}$$

   This equation remains valid until the gauge scatterings decouple at some $z = z_A$. The value of z_A is determined by the moment at which $4\gamma_A$ becomes smaller than γ_D or, in the case where at the intersection $4\gamma_A/n_\Sigma^{\rm Eq}H = \gamma_D/n_\Sigma^{\rm Eq}H < 1$, by the moment at which the gauge reactions become slower than the Hubble rate. This means $4\gamma_A(z_A) = \gamma_D(z_A)$ or $4\gamma_A(z_A)/n_\Sigma^{\rm Eq}H|_{z=z_A} = 1$, see below. For $z > z_A$, the gauge reactions are no more active, and all the triplets left decay and produce a net $B-L$ asymmetry (negative following our convention). In this case, the final $B-L$ asymmetry is given by the sum of the two contributions :

$$Y_{B-L}^{\rm end} \simeq \epsilon_\Delta \int_{z_0}^{z_A} \frac{dY_\Sigma^{\rm Eq}}{dz}\frac{\gamma_D}{4\gamma_A}dz - \epsilon_\Delta Y_\Sigma^{\rm Eq}(z_A)\ . \tag{4.35}$$

   If we take take the limit $z \gg 1$ in the integrand, which is justified by the fact that the integrand differs significantly from zero only for $z \gtrsim 1$, we find that the integrand scales as z^3, and

Eq. (4.35) becomes : [5]

$$\left|Y_{B-L}^{\rm end}\right| \simeq \epsilon_\Delta \left(3 \frac{g_\Delta^2 \pi^2}{c_s g_*} \frac{\Gamma_\Delta}{m_\Delta} \frac{z_A^4}{4} + Y_\Sigma^{\rm Eq}(z_A) \right) . \tag{4.37}$$

Unless Γ_D is quite small, for example if $\tilde{m}_\Delta$ is small, one has always that $4\gamma_A / n_\Sigma^{\rm Eq} H|_{z=z_A} = \gamma_D / n_\Sigma^{\rm Eq} H|_{z=z_A} > 1$, so that z_A is in general given by the condition $4\gamma_A(z_A) = \gamma_D(z_A)$. This condition implies that the analytical value of z_A is approximately given by the solution of the equation :

$$z_A \simeq \ln \left[\frac{c_s}{6 \cdot g_\Delta \cdot (2\pi\, z_A)^{3/2}} \frac{m_\Delta}{\Gamma_\Delta} \right] , \tag{4.38}$$

which for $z_A \gg 1$ gives approximately

$$z_A \simeq \ln \left[\frac{c_s}{6 \cdot g_\Delta \cdot (2\pi)^{3/2}} \frac{m_\Delta}{\Gamma_\Delta} \right] - \frac{3}{2} \ln \left[\ln \left[\frac{c_s}{6 \cdot g_\Delta \cdot (2\pi)^{3/2}} \frac{m_\Delta}{\Gamma_\Delta} \right] \right] . \tag{4.39}$$

Using Eq. (4.38) in Eq. (4.37), one gets finally a simple expression for the final $B-L$ asymmetry,

$$\left|Y_{B-L}^{\rm end}\right| \simeq \epsilon_\Delta \left(\frac{z_A}{4} + 1 \right) Y_\Sigma^{\rm Eq}(z_A) , \tag{4.40}$$

to which corresponds an efficiency given by

$$\eta_\Delta \simeq \left(\frac{z_A}{4} + 1 \right) \sqrt{\frac{\pi}{8}}\, z_A^{3/2}\, e^{-z_A} . \tag{4.41}$$

The first term in this equation represents the $B-L$ asymmetry fraction produced before z_A, when the gauge scatterings are active, and the second term of this equation represent the $B-L$ asymmetry produced after. The faster the gauge reactions, the larger the z_A and the smaller the efficiency. Compared to $\eta_\Delta = 1$, this gives the gauge scattering suppression. This confirm the original intuition that the gauge scatterings slow down the production of the $B-L$ asymmetry, but we see that it is not so drastic (e.g. $\eta_\Delta = 0.2 \ldots 0.003$ for $z_A = 4 \ldots 10$).

We show in the left panel Fig. 4.4 the thermalization rates γ_D (solid) and γ_A (dotted) normalized to $n_\Sigma^{\rm Eq} H$ as a function of $z = m_\Delta / T$ for different values of m_Δ and $\tilde{m}_\Delta^{\rm eff}$, which is the effective neutrino mass parameter defined in Eq. (4.12) : $\tilde{m}_\Delta^{\rm eff} = \tilde{m}_\Delta / \sqrt{B_\ell B_\phi}$. In the right panel of Fig. 4.4, we show the value of z_A as function of $\tilde{m}_\Delta^{\rm eff}$ for different mass values. The dot-dashed line shows the limit between the value of z_A determined by $4\gamma_A(z_A) = \gamma_D(z_A)$ (the region on the r.h.s. of the curve) and by $4\gamma_A / n_\Sigma^{\rm Eq} H|_{z=z_A} = 1$ (the region on the l.h.s. of the curve). The dashed line represent the solution using Eq. (4.38), and we see that it is in very good agreement with the numerical solution in the region where z_A is determined through $4\gamma_A(z_A) = \gamma_D(z_A)$.

[5] Indeed, for $z \gg 1$ one has, with $c_s = 2 \cdot g_\Delta (15 C_1 - 3 C_2)/72\pi$ given in Appendix D.3 :

$$\frac{dY_\Sigma^{\rm Eq}}{dz} \to -\frac{g_\Delta \sqrt{\pi}}{4\sqrt{2} g_*}\, z^{3/2}\, e^{-z} , \quad \gamma_D \to 2 \cdot g_\Delta \left(\frac{m_\Delta^2}{2\pi} \right)^{3/2} \Gamma_\Delta\, z^{-3/2}\, e^{-z} , \quad \gamma_A \to \frac{m_\Delta^4}{96\pi^3}\, c_s\, z^{-3}\, e^{-2z} . \tag{4.36}$$

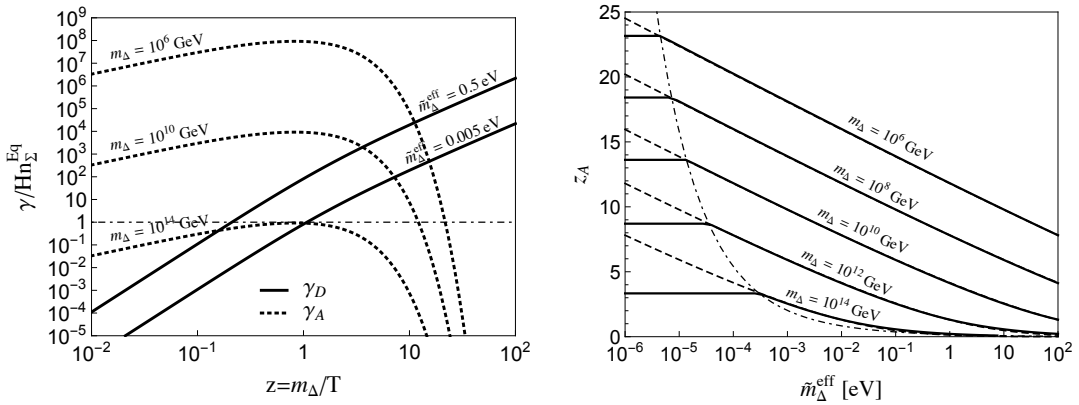

Figure 4.4 – Left : Decay (solid) and gauge (dotted) thermalization rates $\gamma/Hn_\Sigma^{\rm Eq}$ as a function of $z = m_\Delta/T$ for different values of m_Δ and $\tilde{m}_\Delta^{\rm eff}$. Right : z_A as a function of $\tilde{m}_\Delta^{\rm eff}$ for different mass values. The dot-dashed line represent the limit between z_A being determined by $4\gamma(z_A) = \gamma_D(z_A)$ and by $4\gamma_A/n_\Sigma^{\rm Eq}H|_{z=z_A} = 1$. The dashed lines represent the solution of Eq. (4.38).

Including the washout terms. The washouts will obviously have the effect of decreasing the efficiency. This means that Eq. (4.41) is actually an upper bound on the reachable efficiency :

$$\eta_\Delta \lesssim \eta_\Delta^{\max} = \left(\frac{z_A}{4}+1\right)\sqrt{\frac{\pi}{8}}\, z_A^{3/2}\, e^{-z_A}\,. \tag{4.42}$$

In the example above, associated to Fig. 4.3, we chose $m_\Delta = 10^{10}$ GeV, $\tilde{m}_\Delta = 0.05$ eV and $B_\phi = 10^{-2}$ which corresponds to $\tilde{m}_\Delta^{\rm eff} \approx 0.5$ eV. From Fig. 4.3 or Fig. 4.4 we see that for these values one has $z_A \approx 3.5$. This means from Eq. (4.42) that even when neglecting the washouts, the maximum efficiency reachable is $\eta_\Delta^{\max} \approx 0.23$. Taking into account the washouts, the efficiency we got in this example is in fact $\eta_\Delta \approx 0.005$, which is much smaller than $\eta_\Delta^{\max}$ reachable.

Quantitatively, the washout of the $B-L$ asymmetry occurs through the inverse decays $\phi\phi \to \Delta$ **and** $\ell\ell \to \bar{\Delta}$, which are active when $\gamma_D^\phi/n_\gamma^{\rm Eq} \geq H$ **and** $\gamma_D^\ell/n_\gamma^{\rm Eq} \geq H$. Indeed, it is the presence of both interactions that violates lepton number, so if one of these two interactions is not in thermal equilibrium, lepton number is effectively conserved by the inverse decays and there is no washout of the $B-L$ asymmetry. More precisely, the source terms in Eq. (4.27) and (4.29) generate a lepton asymmetry $\Delta\ell$ and a scalar doublet asymmetry $\Delta\phi$ respectively. If for example one has $B_\ell > B_\phi$, a negative triplet asymmetry can develop thanks to $\ell\ell \to \bar{\Delta}$ reactions. On the one hand, if the $\phi\phi \to \Delta$ reaction is in thermal equilibrium, the lepton asymmetry will be depleted through the chain $\phi\phi \leftrightarrow \Delta \leftrightarrow \bar{\ell}\bar{\ell}$. On the other hand, if the $\phi\phi \leftrightarrow \Delta$ is never in thermal equilibrium, which is the case when $B_\ell \gg B_\phi$, the scalar triplet Δ carries in this case an effective lepton number $L = -2$ and the total lepton asymmetry doesn't undergo any washout. In this case, at the end of leptogenesis when all the triplets have decayed, the whole triplet asymmetry is transferred back to a $\Delta\ell$ asymmetry – see also Eq. (4.28) – and the efficiency is large. A sketch of this scenario is depicted in Fig. 4.5. The same reasoning can be applied in the case where $B_\ell < B_\phi$. However, here when the reaction $\ell\ell \leftrightarrow \bar{\Delta}$ is never in thermal equilibrium, which is the case for $B_\ell \ll B_\phi$, one directly sees from Eq. (4.27) that the $B-L$ doesn't undergo any washout and the efficiency is large, see also Fig. 4.5.

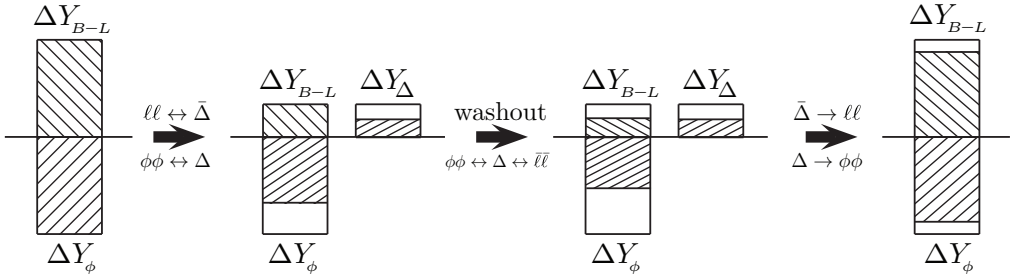

Figure 4.5 – Sketch of the washout in the situation $B_\ell > B_\phi$. The case where $B_\ell \gg B_\phi$, for which the $B-L$ asymmetry doesn't undergo any washout, is depicted by the white box. A sketch of the situation $B_\ell < B_\phi$ can be obtained by the exchange $\Delta Y_{B-L} \leftrightarrow \Delta Y_\phi$.

The inverse decays $\phi\phi \to \Delta$ and $\ell\ell \to \bar{\Delta}$ play therefore a crucial role in the washout of the $B-L$ asymmetry. In parallel with Fig. 4.4, we show in the left panel of Fig. 4.6 the inverse decay $\gamma_D/n_\gamma^{\rm Eq}H$ and the gauge $\gamma_A/n_\gamma^{\rm Eq}H$ thermalization rates as a function of z for various parameter values. The thermalization rate for γ_D^ϕ and γ_D^ℓ is obtained by multiplying $\gamma_D/n_\gamma^{\rm Eq}H$ by B_ϕ and B_ℓ respectively. Contrarily to decays, the inverse decays are Boltzmann suppressed for $z \gtrsim 3$. As we will discuss now, the washout effect of the $\phi\phi \to \Delta$ and $\ell\ell \to \bar{\Delta}$ inverse decays can in some case be overshadowed by gauge reactions. One distinguishes two distinct regimes, following that the inverse decays are active or not when the gauge reactions decouple :

1. **Gauge regime.** If $\gamma_D^\phi/n_\gamma^{\rm Eq} < H$ **or** $\gamma_D^\ell/n_\gamma^{\rm Eq} < H$ when the gauge reactions decouple at $z = z_A$, then for $z > z_A$ the inverse decays don't play any role in the evolution of the $B-L$ asymmetry and they can be neglected, so that the efficiency is still given in a good approximation by Eq. (4.41). This regime is called the "gauge regime", and from Eq. (4.42) if $z_A \gg 4$ one has in good approximation that

$$\eta_\Delta \simeq \frac{1}{4}\sqrt{\frac{\pi}{8}}\, z_A^{5/2}\, e^{-z_A} = \frac{g_\Delta^2\pi^2}{2c_s}\frac{\Gamma_\Delta}{m_\Delta}z_A^4\,, \tag{4.43}$$

   where in the second equality we expressed the efficiency in terms of the decay rate as in Eq. (4.37).

2. **Yukawa regime.** If now $\gamma_D^\phi/n_\gamma^{\rm Eq} > H$ **and** $\gamma_D^\ell/n_\gamma^{\rm Eq} > H$ at $z = z_A$, the inverse decays will substantially decrease the amount of $B-L$ produced, as discussed above. This regime is called the "Yukawa regime", for which the washout from inverse decays is important. In this regime, the efficiency can be determined in a way similar to the one used for the strong washout regime in the type-1 Seesaw leptogenesis, see page 98. Indeed, since $\gamma_D^{\phi,\ell}/n_\gamma^{\rm Eq} > H$, one can reasonably assume that there is a balance between the production and the destruction of the $B-L$ asymmetry until the inverse decays decouple at $z = z_{\rm dec}$, which is determined by the condition : $\min(B_\ell, B_\phi)\cdot\gamma_D/n_\gamma^{\rm Eq}H\big|_{z=z_{\rm dec}} = 1$. For $z_A < z < z_{\rm dec}$, one has therefore that the washouts maintain the r.h.s. of Eq. (4.27) to zero :

$$2\left(\frac{\Delta Y_\Delta}{Y_\Sigma^{\rm Eq}} - \frac{\Delta Y_{B-L}}{Y_\ell^{\rm Eq}}\right)B_\ell\gamma_D \simeq -\epsilon_\Delta\dot{Y}_\Sigma \simeq \epsilon_\Delta sHzY_\Sigma^{\rm Eq}\,. \tag{4.44}$$

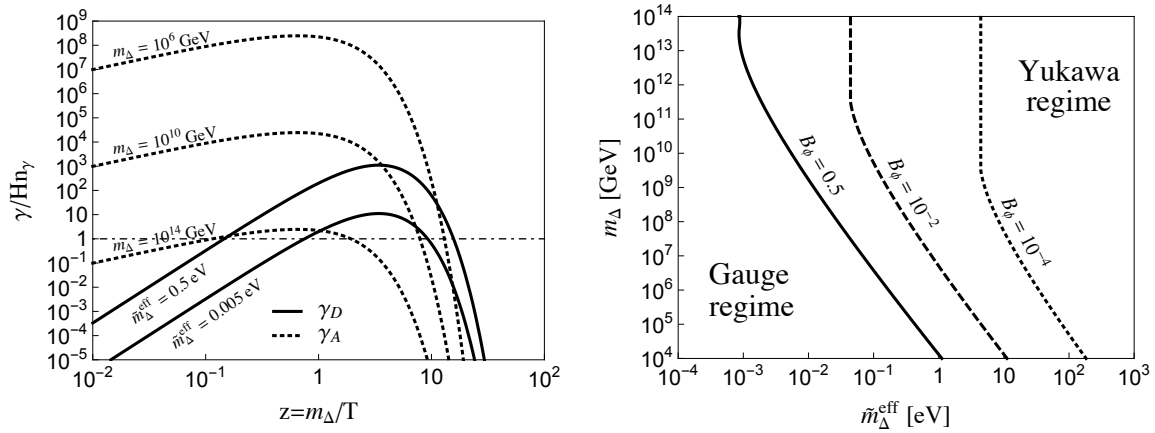

Figure 4.6 – Left : Same as the left panel of Fig. 4.6 but concerning the thermalization rates normalized to $Hn_\gamma^{\rm Eq}$. Right : Gauge versus Yukawa regimes as a function of $\tilde{m}_\Delta^{\rm eff}$ and m_Δ, for $B_\phi = (0.5, 10^{-2}, 10^{-4})$. The plot is symmetric in the exchange $B_\phi \leftrightarrow B_\ell$.

Note that we used Eq. (4.25) with the gauge term neglected, and $dY_\Sigma/dz \simeq dY_\Sigma^{\rm Eq}/dz \simeq -Y_\Sigma^{\rm Eq}$ for $z \gg 1$. Similarly, the washouts maintain the r.h.s. of Eq. (4.26) to zero too and one has

$$B_\ell \frac{\Delta Y_\Delta}{Y_\Sigma^{\rm Eq}} \simeq B_\ell \left(1 - B_\phi\right) \frac{\Delta Y_{B-L}}{Y_\ell^{\rm Eq}} + B_\ell B_\phi \frac{\Delta Y_\phi}{Y_\ell^{\rm Eq}} \,. \tag{4.45}$$

Putting these two equations together, one gets

$$2\left(\frac{\Delta Y_\phi}{Y_\ell^{\rm Eq}} - \frac{\Delta Y_{B-L}}{Y_\ell^{\rm Eq}}\right) B_\ell B_\phi \gamma_D \simeq \epsilon_\Delta s H z Y_\Sigma^{\rm Eq} \,. \tag{4.46}$$

This equation applies until the slower inverse decays decouple at $z = z_{\rm dec}$. At this moment, one has in good approximation that $\Delta Y_\Delta(z_{\rm dec}) \approx 0$ so that $\Delta Y_\phi(z_{\rm dec}) \simeq -\Delta Y_{B-L}(z_{\rm dec})$ from the hypercharge relation in Eq. (4.28), and one gets

$$\Delta Y_{B-L}(z_{\rm dec}) \simeq -\epsilon_\Delta \frac{Y_\ell^{\rm Eq}}{4B_\ell B_\phi} \frac{H z n_\Sigma^{\rm Eq}}{\gamma_D}\bigg|_{z_{\rm dec}\gg 1} \simeq -\epsilon_\Delta \frac{z_{\rm dec}}{4B_\ell B_\phi} \frac{H(z_{\rm dec})}{\Gamma_\Delta} Y_\ell^{\rm Eq}(z_{\rm dec}) \,, \tag{4.47}$$

and the final $B-L$ asymmetry is therefore given by

$$\left|\Delta Y_{B-L}^{\rm end}\right| \simeq \left|\Delta Y_{B-L}(z_{\rm dec})\right| \simeq \epsilon_\Delta \frac{1}{12 B_\ell B_\phi z_{\rm dec}^2 K_\Delta} Y_\Sigma^{\rm Eq}(z_0) \,, \tag{4.48}$$

where we used the fact that $Y_\ell^{\rm Eq}$ is a constant whose value is equal to $Y_\Sigma^{\rm Eq}(z \ll 1)/3$ (there are 3 triplet components). For convenience, we defined $K_\Delta \equiv \Gamma_\Delta/H(z=1) = z^2\Gamma_\Delta/H(z)$ so that this expression can be compared with the one obtained in Eq. (3.50) for the strong washout regime in type-1 leptogenesis. The factor 24 between the two expressions accounts for : (i) the 3 triplet components, (ii) the presence of B_ℓ and B_ϕ (one tends to the type-1 case in the limit where $B_\ell = B_\phi = 1/2$), (iii) the two ℓ in the final state of the process $\bar{\Delta} \to \ell\ell$.

The efficiency in this Yukawa regime can finally be expressed as

$$\eta_\Delta \simeq \frac{z_{\rm dec}}{12 B_\ell B_\phi} \frac{H(z_{\rm dec})}{\Gamma_\Delta} \,. \tag{4.49}$$

To each regime (gauge and Yukawa) corresponds a different efficiency behavior. Indeed, from Eqs. (4.43) and (4.49), we see that $\eta_\Delta \propto \tilde{m}_\Delta^{\rm eff}$ in the gauge regime while $\eta_\Delta \propto 1/\tilde{m}_\Delta^{\rm eff}$ in the Yukawa regime. From the above discussion, the delimitation between the gauge and the Yukawa regimes is given by the condition :

$$\min\left(B_\ell, B_\phi\right) \cdot \left.\frac{\gamma_D}{n_\ell^{\rm Eq} H}\right|_{z=z_A} = 1 \,. \tag{4.50}$$

We show in the right panel of Fig. 4.6 the delimitation between the two regimes as a function of $\tilde{m}_\Delta^{\rm eff}$ and m_Δ, for $B_\phi = (0.5, 10^{-2}, 10^{-4})$ (solid, dashed, dotted). The plot is symmetric with respect to $B_\ell \leftrightarrow B_\phi$. Note that below some values of $\tilde{m}_\Delta^{\rm eff}$, corresponding to $\tilde{m}_\Delta^{\rm eff} \lesssim (0.001, 0.04, 4)$ eV for $B_\phi = (0.5, 10^{-2}, 10^{-4})$, one of the two inverse decays $\ell\ell \to \bar{\Delta}$ or $\bar{\phi}\bar{\phi} \to \bar{\Delta}$ never reaches thermal equilibrium, and so it is the gauge regime that applies there (for all the mass values below $m_\Delta \sim 10^{14}$ GeV, since above gauge reactions never reach thermal equilibrium).

4.1.7 Some results of successful leptogenesis

Efficiency as a function of $\tilde{m}_\Delta^{\rm eff}$. Firstly, from Eqs. (4.11) and (4.12), the total decay rate γ_D depends on $\tilde{m}_\Delta^{\rm eff}$ and m_Δ. Secondly, the gauge scatterings γ_A depends on m_Δ. Finally, the quantities B_ϕ and $B_\ell = 1 - B_\phi$ enter in the Boltzmann equations in Eqs. (4.25)-(4.27). This means that, neglecting the $\Delta L = 2$ scatterings, one can obtain the efficiency as a function of $\tilde{m}_\Delta^{\rm eff}$, m_Δ and B_ϕ. This is illustrated in Fig. 4.7, which gives the efficiency as a function of $\tilde{m}_\Delta^{\rm eff}$ for different values of the mass m_Δ and the fraction B_ϕ. The plot is symmetric under the exchange $B_\phi \leftrightarrow B_\ell$. The curves have been obtained by solving numerically the set of Boltzmann equations.

The maximum of each curve corresponds approximately to the transition value between the gauge and the Yukawa regimes, as can be seen from the right panel of Fig. 4.6. On the one hand, on the l.h.s. of these maxima, the efficiency goes approximately like $\tilde{m}_\Delta^{\rm eff}$ and it doesn't depend on B_ϕ for a fixed $\tilde{m}_\Delta^{\rm eff}$, as expected from Eq. (4.43) in the gauge regime. On the other hand, on the r.h.s. of the maxima, we see that the efficiency goes approximately like $(\tilde{m}_\Delta^{\rm eff})^{-1}$ and doesn't depend on the mass m_Δ as also expected from Eq. (4.49) in the Yukawa regime. This confirms our analytical results as well as our physical interpretation of the scalar triplet leptogenesis mechanism.

Efficiency as a function of B_ϕ. From the left panel of Fig. 4.7, there is clear tendency that the efficiency increases as B_ϕ or B_ℓ departs from $B_\phi = B_\ell = 0.5$ in the Yukawa regime. We show in the right panel of Fig. 4.7 the efficiency as a function of B_ϕ for $m_\Delta = (10^6, 10^{10}, 10^{14})$ GeV, fixing $\tilde{m}_\Delta^{\rm eff} = 1$ eV. We see that the efficiency tends to a maximum when $B_\phi \lesssim (10^{-1}, 10^{-3}, 10^{-3})$ for $m_\Delta = (10^6, 10^{10}, 10^{14})$ GeV respectively. The plot is symmetric under the exchange $B_\phi \leftrightarrow B_\ell$, with a pivot point at $B_\phi = B_\ell = 1/2$. There are two questions one can address.

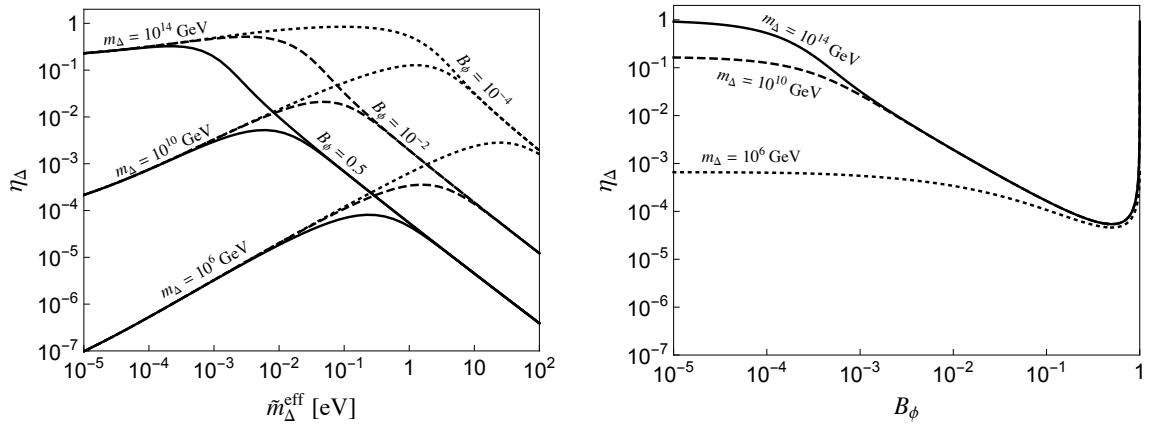

Figure 4.7 – Left : Efficiency as a function of $\tilde{m}_\Delta^{\rm eff}$, for $m_\Delta = (10^6, 10^{10}, 10^{14})$ GeV and $B_\phi = (0.5, 10^{-2}, 10^{-4})$ (solid, dashed, dotted). The maximum of each curve corresponds in good approximation to the transition value between the gauge and the Yukawa regime, see Fig. 4.6. Right : Efficiency as a function of B_ϕ for $m_\Delta = (10^6, 10^{10}, 10^{14})$ GeV and fixing $\tilde{m}_\Delta^{\rm eff} = 1$ eV. The minimum of each curve is obtained for $B_\ell = B_\phi = 0.5$.

First, why is the situation symmetric under $B_\phi \leftrightarrow B_\ell$? Analytically, this is because the decay rate in Eq. (4.11) and the set of Boltzmann equations in Eq. (4.25)-(4.27) are actually symmetric under $B_\phi \leftrightarrow B_\ell$, as can be seen from the sum rule in Eq. (4.28). However, at first sight one could think from Eq. (4.27) that for large B_ℓ, the washout would be more important than for small B_ℓ. As already mentioned above in page 125, the point is that lepton number violating washouts occur if both $\ell\ell \leftrightarrow \bar{\Delta}$ and $\phi\phi \leftrightarrow \Delta$ are in thermal equilibrium. If one of these two processes never reaches thermal equilibrium, i.e. if $B_\ell \gg B_\phi$ or $B_\phi \gg B_\ell$, the scalar triplet carries effectively lepton number -2 or 0 respectively and the efficiency tends to a maximum. This happens when $B_\phi \lesssim (10^{-1}, 10^{-3}, 10^{-3})$ for $m_\Delta = (10^6, 10^{10}, 10^{14})$ GeV respectively, see Fig. 4.6.

Second, in the limit where $B_\phi \to 0$ or $B_\ell \to 0$, lepton number is effectively conserved and the efficiency is maximal. But if lepton number is conserved, shouldn't we get a vanishing $B-L$ asymmetry ? The point here is that even if the efficiency is large, when $B_\phi \to 0$ or $B_\ell \to 0$ the CP-asymmetry is in this case suppressed since it goes like $\epsilon_\Delta \propto \sqrt{B_\ell B_\phi}$, as can be seen from Eq. (4.17), and so is the $B-L$ asymmetry. There is thus no contradiction and one has a correct behavior of the $B-L$ asymmetry produced, going to zero for $B_\phi \to 0$ or $B_\ell \to 0$, as we will see next.

Successful leptogenesis. The contours in Fig. 4.8 show the values of the CP-asymmetry parameter $\epsilon_\Delta / \sqrt{4 B_\ell B_\phi}$ needed in order to generate the baryon asymmetry of the Universe, as a function of the Yukawa coupling parameter $(Y_\Delta Y_\Delta^\dagger)^{1/2}$ and the triplet mass m_Δ, fixing $\tilde{m}_\Delta = 10^{-3}$ eV (left) and $\tilde{m}_\Delta = m_{\rm atm} \approx 0.05$ eV (right). The plots have been taken from Ref. [241]. The light green region is obtained assuming that the CP-asymmetry is bounded from above by unitarity consideration, see Eq. (4.23). The dark green region is obtained assuming that the CP-asymmetry arises from heavier sources of neutrino masses, see Eq. (4.22). Pertubativity of the coupling μ_Δ / m_Δ implies that the dark grey region is excluded. The diagonal black line corresponds to $B_\phi = B_\ell$. As expected, one cannot generate enough baryon asymmetry far from this line, even if the efficiency is larger, because in this case the CP-asymmetry is too suppressed. The further we are from this line, the

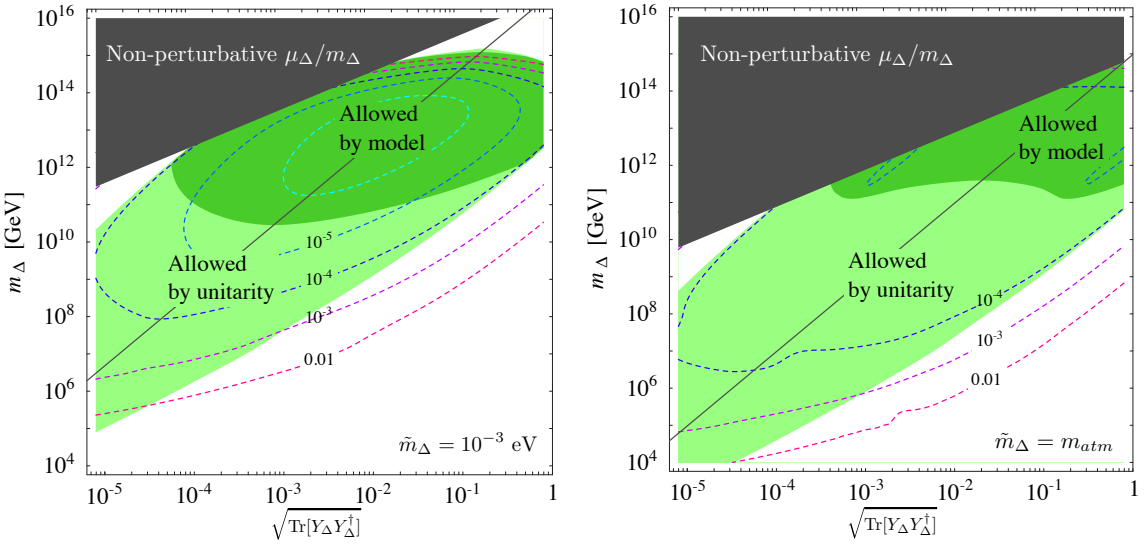

Figure 4.8 – Iso-curves of $\epsilon_\Delta/\sqrt{4B_\ell B_\phi}$ needed in order to have successful leptogenesis in the $\sqrt{Y_\Delta Y_\Delta^\dagger}$ plane, for $\tilde{m}_\Delta = 10^{-3}$ eV (left) and $\tilde{m}_\Delta = 0.05$ eV (right). The light green region is obtained assuming that the CP-asymmetry is bounded only by unitarity, i.e. fulfilling Eq. (4.23). The dark green region is the allowed region assuming that the CP-asymmetry arises from heavier sources of neutrino masses, i.e. fulfilling Eq. (4.22). The grey region is not allowed by pertubativity of the scalar coupling $\mu_\Delta/m_\Delta \leq 1$. The plots have been taken from Ref. [241].

bigger the efficiency but the smaller the CP-asymmetry. As a consequence, the maximum baryon asymmetry producible lies in fact around the line $B_\ell = B_\phi = 0.5$, but not necessarily on it as shown by the right panel of Fig. 4.8.

From these figures, one can see that there is a minimal value of the triplet mass below which there is not enough baryon asymmetry generated. In the case where the CP-asymmetry is bounded from above by Eq. (4.22), i.e. in the case where the CP-asymmetry arises from heavier sources of neutrino masses, since $\epsilon_\Delta \propto m_\Delta$ one has

$$m_\Delta \gtrsim 2.8 \cdot 10^{10}\ \text{GeV} \quad \text{for} \quad \tilde{m}_\Delta = 10^{-3}\ \text{eV}\,, \tag{4.51}$$

$$m_\Delta \gtrsim 1.3 \cdot 10^{11}\ \text{GeV} \quad \text{for} \quad \tilde{m}_\Delta = 0.05\ \text{eV}\,. \tag{4.52}$$

In the case where the CP-asymmetry is bounded from above by unitarity in Eq. (4.23), i.e. not for $m_\Delta \ll m_X$ but for example for two degenerate triplets, the lower bound get relaxed. If we also consider the Sommerfeld corrections, which account for the effect of a potential on the interaction cross section in case where particles are non-relativistic, the lower bound reads [246]

$$m_\Delta \gtrsim 1.6\ \text{TeV}\,. \tag{4.53}$$

This result can be visualized in Fig. 4.9, taken from Ref. [246], which shows the needed CP-asymmetry as a function of the triplet mass for $B_\ell = B_\phi = 0.5$ and for different values of the parameter $\tilde{m}_\Delta$. The gray region is the region excluded by unitarity, i.e. $|\epsilon_\Delta| \geq 2 \cdot \min(B_\ell, B_\phi)$.

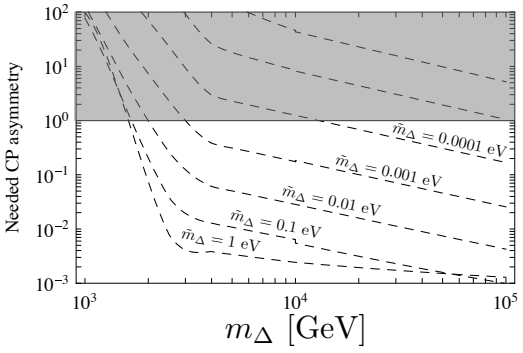

Figure 4.9 – Needed CP-asymmetry as a function of the triplet mass, for different values of $\tilde{m}_\Delta$ and for $B_\ell = B_\phi = 0.5$. The gray region is the region excluded by unitarity, i.e. one necessarily needs $|\epsilon_\Delta| \leq 2 \cdot \min(B_\ell, B_\phi)$. The plot has been taken from Ref. [246].

Now that we have analyzed how things work in the one-flavor approximation, we can tackle the more general analysis of the flavored scalar triplet leptogenesis, including the effect of spectator processes. But when do we need to consider the lepton flavors in scalar triplet leptogenesis ?

4.2 Flavor issue in type-2 leptogenesis

In the previous section, we have described the mechanisms and the properties of the type-2 leptogenesis in the one-flavor approximation. We can now go a step further and study the effect of the lepton flavors and spectator processes. But when do flavors matter in type-2 leptogenesis ? As in section 3.5 for the type-1 Seesaw leptogenesis scenario, this question needs to be addressed in order to determine the various flavor and temperature regimes. As we will show next, the situation differs drastically from the type-1 Seesaw leptogenesis scenario.

Indeed, let's already mention that the three flavors actually always matter in the scalar triplet leptogenesis, whatever the temperature at which leptogenesis takes place. This issue was first pointed out in Ref. [247], where they show, by solving the Boltzmann equations using the density matrix formalism, that there are flavor effects even above $T \sim 10^{12}$ GeV, i.e. even when no charged Yukawa interaction is active. Strictly speaking, this issue could have only been clarified using this density matrix formalism, that describes rigorously the (de)coherence of the lepton states. We will here follow the semi-classical approach, equivalent to the one in section 3.5, which is based on simple arguments and which leads to the same conclusion.

Let's denote as usual by $\Delta \equiv \Delta_1$ the lightest scalar triplet responsible for the leptogenesis. The SM Lagrangian, extended with the type-2 Seesaw Lagrangian, contains the interaction of the lightest triplet Δ with the leptons ℓ_α in Eq. (4.4), but also the charged lepton Yukawa interactions :

$$\mathscr{L} \ni \sum_{\alpha,\beta} \ell_\alpha^T C i\tau_2 \, \mathbf{\Delta} \, Y_\Delta^{\alpha\beta} \, \ell_\beta - \sum_\alpha \overline{e_\alpha} \phi^\dagger \, Y_{\ell_\alpha} \, \ell_\alpha + \text{H.c.} \,. \tag{4.54}$$

As usual, we choose a charged lepton basis such that the charged lepton Yukawa matrix is diagonal and real, see the parameter counting in Eq. (1.29). We remind that Y_Δ is a general 3×3 symmetric matrix.

The main difference with the type-1 Seesaw case is that now the scalar triplet doesn't decay into one, but into two coherent lepton states. As a consequence, *if leptons don't undergo any other flavor interaction*, all what we can do is to perform a rotation in the flavor space such that the matrix Y_Δ becomes diagonal. Indeed, in that case one can define a new flavor basis $|\ell'\rangle = R\,|\ell\rangle$, with R a unitary matrix, such that the scalar triplet interaction becomes

$$\mathscr{L} \ni \ell'^T C i\tau_2\, \mathbf{\Delta}\, \mathscr{Y}_\Delta\, \ell' \,, \tag{4.55}$$

where the new coupling matrix $\mathscr{Y}_\Delta$ is diagonal and is given by $\mathscr{Y}_\Delta = R^*\ Y_\Delta\ R^\dagger$ with R a unitary matrix. In the new basis $|\ell'\rangle \equiv (|\ell_1\rangle, |\ell_2\rangle, |\ell_3\rangle)$, since in general all the diagonal elements of $\mathscr{Y}_\Delta$ are non-vanishing, the scalar triplet Δ effectively decays via the di-lepton channels : $\bar{\Delta} \to \ell_1\ell_1$, $\bar{\Delta} \to \ell_2\ell_2$ and $\bar{\Delta} \to \ell_3\ell_3$, where all the three states $|\ell_{1,2,3}\rangle$ are a superposition of the three lepton flavors e, μ and τ.

Accordingly, if leptons don't undergo any other flavor interaction, the scalar triplet decays effectively via only 3 di-lepton channels instead of the 6 from the original symmetric matrix Y_Δ. *Even if the states $|\ell_{1,2,3}\rangle$ stay coherent, one has therefore in general always three flavors in the scalar triplet leptogenesis, whatever the temperature regime. It seems thus not possible to define an unflavored regime as in the type-1 Seesaw leptogenesis.*

4.2.1 Flavor regimes

Even if there are always three flavors in the game, one still has different flavor regimes as in the type-1 leptogenesis. Indeed, the states $|\ell_{1,2,3}\rangle$ can loose their coherence if they undergo an interaction that is not flavor-blinded. Among them, one has the charged Yukawa interactions (the second term in Eq. (4.54)), the $\Delta_{2,3,...}$ di-lepton interactions (in the case of pure scalar triplet scheme) or $N_{1,2,...}$ Yukawa interactions (in the case of mixed type-1+2 scheme). These two latter interactions are in general much slower than the Hubble rate because Boltzmann suppressed, since the extra heavy states are taken much heavier than Δ, so that they should not a priori be responsible of the decoherence of the states $|\ell_{1,2,3}\rangle$.

On the contrary, the charged Yukawa interactions are not Boltzmann suppressed and are even much faster than the Hubble rate below some specific temperatures, as already discussed for type-1 leptogenesis in section 3.5. If they are fast, they could in principle decohere the states $|\ell_{1,2,3}\rangle$ and another lepton flavor base must be used. As in the type-1 Seesaw case, to see if this interaction has the time to happen, the charged Yukawa interaction rate $\Gamma_{\ell_\alpha}(T)$ must be compared to the Hubble rate H, *but also* to the appropriate inverse decay (ID) rate $\Gamma_\ell^{ID} \equiv \Gamma(\ell\ell \to \bar{\Delta}_1)$. One has the following possibilities :

1. **For $T \gtrsim 10^{12}$ GeV, one has always $\Gamma_{\ell_{e,\mu,\tau}} < H$**, and basically no charged lepton Yukawa interactions occur. In this case, the three lepton states $|\ell_{1,2,3}\rangle$ propagate without loosing their coherence, and could possibly undergo an inverse decay $\ell_\alpha\ell_\alpha \to \bar{\Delta}$. In this regime, by performing a rotation R of the flavor basis, the scalar triplet interactions with the letpons

are effectively flavor diagonal in the flavor basis given by $(|\ell_1\rangle, |\ell_2\rangle, |\ell_3\rangle)$:

$$\mathscr{Y}_\Delta = R^*\ Y_\Delta\ R^\dagger = \begin{pmatrix} Y_\Delta^{11} & 0 & 0 \\ 0 & Y_\Delta^{22} & 0 \\ 0 & 0 & Y_\Delta^{33} \end{pmatrix}. \tag{4.56}$$

This regime will be denoted as "**full-diagonal regime**" in what follows.

2. **For $10^9 \lesssim T \lesssim 10^{12}$ GeV, one has $\Gamma_{\ell_\tau} > H$ but still $\Gamma_{\ell_{e,\mu}} < H$.** Here, one has two possible cases :

   (a) **If $\Gamma_{\ell_\tau} < \Gamma^{ID}_{\ell_\alpha}$**, with $\alpha = 1,2,3$, the lepton states $|\ell_\alpha\rangle$ will more likely inverse decay $\ell_\alpha \ell_\alpha \to \bar{\Delta}$ before interacting through the tau charged Yukawa interaction. This case reduces to the **full-diagonal regime** in item 1.

   (b) **If $\Gamma_{\ell_\tau} > \Gamma^{ID}_{\ell_1} > H$**, where $\Gamma^{ID}_{\ell_1}$ stands for the smallest of the three inverse decay rates $\Gamma^{ID}_{\ell_{1,2,3}}$, whatever the value of $\Gamma^{ID}_{\ell_{2,3}}$ the lepton state $|\ell_1\rangle$ has the time to decohere thanks to the $\ell_\tau \phi \leftrightarrow e_\tau$ processes. In this case, the new interaction basis is $(|\ell_a\rangle, |\ell_b\rangle, |\ell_\tau\rangle)$, with $\langle \ell_{a,b}|\ell_\tau\rangle = \langle \ell_b|\ell_a\rangle = 0$ and $\langle \ell_i|\ell_i\rangle = 1$. The states $|\ell_a\rangle$ and $|\ell_b\rangle$ are coherent superpositions of e and μ flavors. Even if the other states $\ell_{2,3}$ didn't loose their coherence through the charged Yukawa interaction, i.e. even if $\Gamma_{\ell_\tau} < \Gamma^{ID}_{\ell_{2,3}}$, the thermal bath contains now pure τ leptons which can interact with $\ell_{2,3}$ through $\ell_\tau \ell_{2,3} \to \bar{\Delta}$ and these interactions break the coherence of the states $\ell_{2,3}$. In this case, one can define the new interaction basis such that the scalar triplet doesn't decay via $\bar{\Delta} \to \ell_a \ell_b$, i.e. one can still define a flavor basis such that the scalar triplet interactions has the following structure

   $$\mathscr{Y}_\Delta = R^*\ Y_\Delta\ R^\dagger = \begin{pmatrix} Y_\Delta^{aa} & 0 & Y_\Delta^{a\tau} \\ 0 & Y_\Delta^{bb} & Y_\Delta^{b\tau} \\ Y_\Delta^{a\tau} & Y_\Delta^{b\tau} & Y_\Delta^{\tau\tau} \end{pmatrix}. \tag{4.57}$$

   This regime will be denoted as "**semi-diagonal regime**" in what follows. In this regime, the scalar triplet has 5 di-lepton channels.

3. **For $10^5 \lesssim T \lesssim 10^9$ GeV, one has $\Gamma_{\ell_\tau} > \Gamma_{\ell_\mu} > H$ but still $\Gamma_{\ell_e} < H$.** Here too, there are several possible cases :

   (a) **If $\Gamma_{\ell_\tau} < \Gamma^{ID}_{\ell_\alpha}$**, with $\alpha = 1,2,3$, we recover the **full-diagonal regime**.

   (b) **If $\Gamma_{\ell_\tau} > \Gamma^{ID}_{\ell_1}$ and $\Gamma_{\ell_\mu} < \Gamma^{ID}_{\ell_{a,b}}$**, we recover the **semi-diagonal regime** in item 2.(b), since the coherent lepton states $|\ell_{a,b}\rangle$ undergo inverse decays $\ell_a \ell_a \to \bar{\Delta}$ or $\ell_b \ell_b \to \bar{\Delta}$ before loosing their coherence.

   (c) **If $\Gamma_{\ell_\tau} > \Gamma^{ID}_{\ell_1}$ and $\Gamma_{\ell_\mu} > \Gamma^{ID}_{\ell_a} > H$**, where $\Gamma^{ID}_{\ell_a}$ stands for the smallest of the two inverse decay rates $\Gamma^{ID}_{\ell_a} < \Gamma^{ID}_{\ell_b}$, the lepton state $|\ell_a\rangle$ looses its coherence through the $\ell_\mu \phi \leftrightarrow e_\mu$ interactions. The interaction basis is now given by $(|\ell_e\rangle, |\ell_\mu\rangle, |\ell_\tau\rangle)$ and their interactions with the scalar triplet are given by the original matrix Y_Δ. This regime will therefore be denoted as **"general regime"**.

4. **For $T \lesssim 10^5$ GeV, one has $\Gamma_{\ell_\tau} > \Gamma_{\ell_\mu} > \Gamma_{\ell_e} > H$**, and one recover exactly the same flavor regimes as the in the previous temperature range, plus a fourth case where $\ell_e \phi \leftrightarrow e_e$ is faster than the inverse decays and the Hubble rate. This last case corresponds also to a **general regime**. Only the chemical equilibrium conditions do actually change, see below.

The fact that one cannot define a general unflavored regime explains why we called the previous section "one-flavor approximation". This one-flavor approximation is the analog of the unflavored regime of the type-1 Seesaw leptogenesis, and its study has allowed us to understand the main feature of the scalar triplet leptogenesis. Strictly speaking, this situation only applies when spectator processes are neglected and when the flavored CP-asymmetries and the various branching ratios to leptons are aligned, i.e. $\epsilon_\Delta^{\ell_\alpha} \equiv \epsilon_\Delta/3$ and $B_{\ell_{\alpha\beta}} \equiv \delta_{\alpha\beta} B_\ell/3$, see below. We now determine more precisely the parameter space where each flavor regime applies.

4.2.2 Parameter space of the flavor regimes

Now that we have defined the different flavor regimes, we can determine explicitly to which parameter values they correspond. We remind that lepton flavor decoherence is a delicate issue which requires a pure quantum treatment, which in full generality does not even exist for the more widely considered *standard* leptogenesis picture. Here in this section, rather than providing an exhaustive treatment of this issue, we will consider a simplified treatment by considering the two most relevant processes : SM lepton Yukawa reactions (given approximately by Eq. (3.55)) and the *total* lepton-related triplet inverse decays, basically along the lines of Ref. [248]. [6] We will proceed starting from the "full-diagonal" regime, which is the analog of the unflavored regime in type-1 leptogenesis, and then consider the domain of validity of the "semi-diagonal" and "general" regimes.

Full-diagonal regime and tau-decoherence temperature $T^\tau_{\mathbf{decoh}}$. In the full-diagonal regime, the lepton basis reads $|\ell'\rangle = (|\ell_1\rangle, |\ell_2\rangle, |\ell_3\rangle)$. In this case, the flavors that need to be treated in the Boltzmann equations are the $B - L_\alpha$, with $L_\alpha = \ell_\alpha$ where $\alpha = 1,2,3$. The interactions between the scalar triplet and these coherent states are diagonal and described by the diagonal matrix $\mathscr{Y}_\Delta = R^*\, Y_\Delta\, R^\dagger$ as in (4.56), where R is a unitary matrix. [7] Let's now determine more precisely for which parameter value this regime holds.

The charged tau Yukawa interactions $\ell_\tau \leftrightarrow e_\tau \phi$ are faster than the Hubble rate for $T_\tau \approx 10^{12}$ GeV. This temperature is determined by the condition $\Gamma_{\ell_\tau}(T_\tau) = H(T_\tau)$, where the charged lepton Yukawa interaction rate $\Gamma_{\ell_\tau}(T)$ is approximately given by Eq. (3.55). However, as explained above, if at the time when a lepton Yukawa interaction rate becomes faster than the Hubble rate, *all* the triplet inverse decay processes $\ell_\alpha \ell_\alpha \to \bar{\Delta}$ are much faster than this reaction, the coherent

[6] As highlighted previously, one should in fact compare the Yukawa interaction rate with the *slowest* inverse decay rate. However, in this case one cannot make any general statement since the slowest inverse decay rate depends on the matrix element values $\mathscr{Y}_\Delta$. Therefore, in what follows, for illustrative purpose and in order to compare with the other flavor regimes, we make the approximation of considering instead the total inverse decay $\ell\ell \to \bar{\Delta}$ to determine the flavor regimes.

[7] It is worth to mention that one can choose the unitary transformation so that the matrix elements of Y_Δ are real numbers.

superposition of leptons produced from the decay of a scalar triplet will inverse decay before it has the time to undergo any charged lepton Yukawa interaction. In this case, it is expected that decoherence is fully achieved only later, when the inverse decay rate (which is Boltzmann suppressed at low temperatures) gets smaller than the SM lepton Yukawa rate, at a temperature $T \equiv T^{\tau}_{\rm decoh}$.

Since the rate of the process $\ell\ell \to \bar{\Delta}$ is proportional to $B_\ell \Gamma_\Delta$, the parameters which determine $T^{\tau}_{\rm decoh}$ are m_Δ and the inverse leptonic decay effective parameter $B_\ell \tilde{m}^{\rm eff}_\Delta$, where $\tilde{m}^{\rm eff}_\Delta = \tilde{m}_\Delta / \sqrt{B_\ell B_\phi}$ is the effective neutrino mass-like parameter defined in Eq. (4.12). Imposing that charged tau Yukawa reaction never get faster than the lepton-related triplet inverse decays at a given temperature :

$$\Gamma_{\ell_\tau} \lesssim B_\ell \, \frac{\gamma_D}{n^{\rm Eq}_\ell} \, , \tag{4.58}$$

in the same way it has been done in the type-1 seesaw case [248], one can derive a lower bound on the triplet mass m_Δ as a function of $B_\ell \tilde{m}^{\rm eff}_\Delta$ which fixes the values that these parameters should have in order to assure that triplet dynamics takes place in the "full-diagonal" flavor regime, namely : [8]

$$m_\Delta \gtrsim \min\left[1 \, , \, \frac{10^{-3}{\rm eV}}{B_\ell \tilde{m}^{\rm eff}_\Delta}\right] \cdot 10^{12} \ {\rm GeV} \, . \tag{4.59}$$

Semi-diagonal regime and muon-decoherence temperature $T^{\mu}_{\rm decoh}$. In this flavor regime, the basis reads $|\ell''\rangle = (|\ell_a\rangle, |\ell_b\rangle, |\ell_\tau\rangle)$, where $|\ell_a\rangle$ and $|\ell_b\rangle$ are coherent superpositions of $|\ell_e\rangle$ and $|\ell_\mu\rangle$ states. In this case, the flavors that need to be treated in the Boltzmann equations are the $B-L_{a,b,\tau}$, with $L_{a,b} = \ell_{a,b}$ and $L_\tau = \ell_\tau + e_\tau$. The interactions between the scalar triplet and these coherent states are now "semi-diagonal" and described by the matrix $\mathscr{Y}_\Delta = R^* \ Y_\Delta \ R^\dagger$ as in (4.57), where $R = {\rm diag}[S, 1]$ is a unitary matrix such that S diagonalizes the (e,μ) bloc of the matrix Y_Δ.

As in the full-diagonal regime, the lepton states $|\ell_a\rangle$ and $|\ell_b\rangle$ can loose their coherence at a temperature $T^{\mu}_{\rm decoh}$ if they undergo a charged muon Yukawa interaction $\ell_\mu \leftrightarrow e_\mu \phi$. This interaction is faster than the Hubble rate for $T_\mu \approx 10^9$ GeV, which is obtained by the condition $\Gamma_{\ell_\mu}(T_\mu) = H(T_\mu)$. But this interaction must also be compared with the inverse decays $\ell\ell \to \bar{\Delta}$. The analytical condition to lie in the semi-diagonal regime reads thus

$$\Gamma_{\ell_\mu} \lesssim B_\ell \, \frac{\gamma_D}{n^{\rm Eq}_\ell} \lesssim \Gamma_{\ell_\tau} \, , \tag{4.60}$$

which translates in a condition on the mass of the scalar triplet :

$$\min\left[1 \, , \, \frac{10^{-3}{\rm eV}}{B_\ell \tilde{m}^{\rm eff}_\Delta}\right] \cdot 10^9 \ {\rm GeV} \quad \lesssim m_\Delta \lesssim \quad \min\left[1 \, , \, \frac{10^{-3}{\rm eV}}{B_\ell \tilde{m}^{\rm eff}_\Delta}\right] \cdot 10^{12} \ {\rm GeV} \, . \tag{4.61}$$

[8] In relation with footnote 6, rigorously, B_ℓ should be replaced by $B_{\ell_{11}}$ in this expression. However, since $B_{\ell_{11}} \leq B_\ell$, this bounds constitutes in fact an absolute condition for lying in the full-diagonal regime.

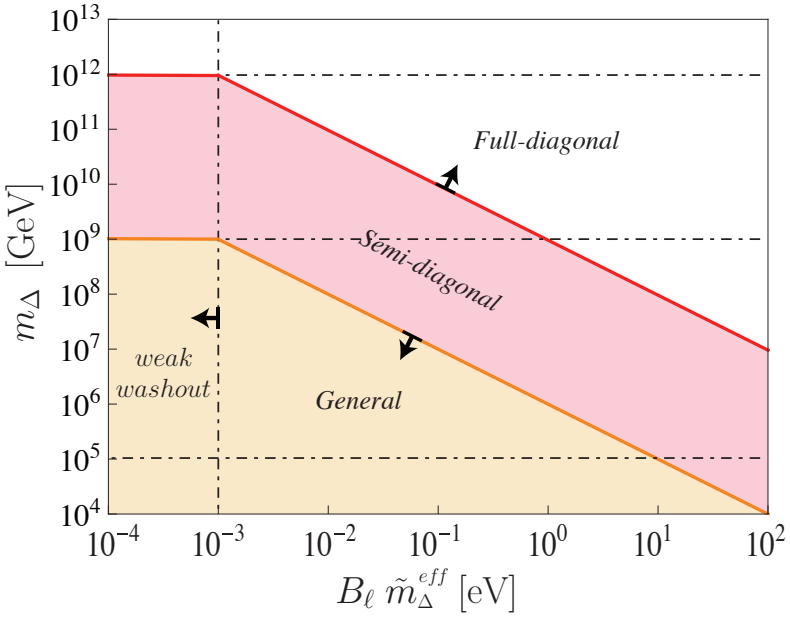

Figure 4.10 – Regions determining the different flavor regimes as a function of $B_\ell \tilde{m}_\Delta^{\rm eff}$ and m_Δ. The region above the solid red line is obtained by the requirement that the τ Yukawa rate is never faster than the $\ell\ell \to \bar{\Delta}$ inverse decay rate, determining the full-diagonal regime. The region between the red and orange solid lines is obtained by the requirement that the $\tau(\mu)$ Yukawa rate is faster (slower) than H and the $\ell\ell \to \bar{\Delta}$ inverse decay rate, and corresponds therefore to the semi-diagonal regime. Finally, the region below the dashed line corresponds to the general regime. The horizontal dot-dashed lines correspond to the value of m_Δ above which the τ, μ and e Yukawa never reach thermal equilibrium. The vertical dot-dashed line corresponds to the value of $B_\ell \tilde{m}_\Delta^{\rm eff}$ below which inverse decays never reach thermal equilibrium.

General regime. In this regime, the flavor basis is $|\ell\rangle = (|\ell_e\rangle, |\ell_\mu\rangle, |\ell_\tau\rangle)$, and the Boltzmann equations must be written in terms of $B - L_\alpha$ asymmetries, with $L_e = \ell_e (+e_e)$, $L_\mu = \ell_\mu + e_\mu$ and $L_\mu = \ell_\tau + e_\tau$. [9] The absolute condition to lie in the general regime reads simply

$$m_\Delta \lesssim \min\left[1\,,\, \frac{10^{-3}\text{eV}}{B_\ell \tilde{m}_\Delta^{\rm eff}}\right] \cdot 10^9\ \text{GeV}\,. \tag{4.62}$$

Summary. We show in Fig. 4.10 a summary of the regions corresponding to each specific flavor regime, in function of m_Δ and $B_\ell \tilde{m}_\Delta^{\rm eff}$. The white, red and orange region correspond to the full-diagonal, semi-diagonal and general regimes. The horizontal lines show the temperature (and thus m_Δ) value for which the tau ($T \sim 10^{12}$ GeV), muon ($T \sim 10^9$ GeV) and electron ($T \sim 10^5$ GeV) charged Yukawa interactions are faster than the Hubble rate. To the left of the vertical line one has $B_\ell \tilde{m}_\Delta^{\rm eff} \approx 10^{-3}$ eV, and one lies therefore in the "weak washout" regime (in analogy with the type-1 Seesaw leptogenesis), where the inverse decays $\ell\ell \to \bar{\Delta}$ never reach thermal equilibrium.

[9] Let's note that here one has two possibilities since the charged electron Yukawa interaction may or not be in thermal equilibrium.

4.3 Flavored type-2 leptogenesis

In this section, we aim to study the generation of the $B-L$ asymmetry arising from the CP-violating and out-of-equilibrium decays of a scalar triplet, taking into account in a systematic way any relevant effect that a SM interaction could have at a given temperature. This includes the flavor effects of the charged lepton Yukawa couplings and the "spectator" effects of the quark Yukawa couplings and the sphalerons processes. To this end, we first write the expressions of the decay rates and the CP-asymmetries valid in every regime, then consider the redistribution of the $B/3-L_\alpha$ asymmetries in the heat bath, which in turn requires considering the conservation laws and chemical equilibrium conditions implied by slow and fast reactions, as has been done in type-1 Seesaw leptogenesis. Finally, we derive the full network of flavored classical Boltzmann equations that included all the above effects.

This study was made in collaboration with Diego Aristizabal Sierra and Thomas Hambye [2]. At the time of writing our paper, the role played by lepton flavor effects in production as well as the evolution of the flavored $B/3-L_\alpha$ asymmetries have been partially considered in Ref. [250]. In particular, the author of Ref. [250] first published a paper in which they just computed the CP-asymmetries, and then updated later their paper including Boltzmann equations and short discussions. While we agree with their result concerning the CP-asymmetries, a careful analysis of their paper shows many clear discrepancies for example in their analytical expressions of the Boltzmann equations.

Few months ago, i.e. in March 2015, another paper has been published in which they analyze the type-2 flavored leptogenesis using the density matrix formalism [247]. In this paper, they highlighted the fact that the lepton flavors actually always play a role in leptogenesis. This interesting result was not found in our original paper [2], since we analyzed flavored leptogenesis in the semi-classical approach. Indeed, a rigorous treatment of the flavor (de)coherence can only be done through density matrix formalism, which was beyond our scope. However, the consequences of Ref. [247] can be straightforwardly applied to all what has been done in Ref. [2]. They basically just mean that all the results and scenarios in Ref. [2] still apply but with extended temperature windows.

Taking into account the considerations of Ref. [247], the precise determination of the flavor regimes as a function of the various parameters is a delicate task which has been addressed in section 4.2. We have seen that to each flavor regime corresponds a specific flavor basis, and therefore a specific effective Yukawa coupling matrix $\mathscr{Y}_\Delta$. Accordingly, one has to consider specific decay rates, CP-asymmetries and $B/3-L_\alpha$ asymmetries for each flavor regime. Here, we will derive general expressions that hold whatever the flavor regime, whatever the triplet Δ_k.

The reader who would like to compute the baryon asymmetry in a scalar triplet leptogenesis can find in the next section 4.4 a summary of the procedure to follow. We now detail the main steps in the determination of the flavor effects.

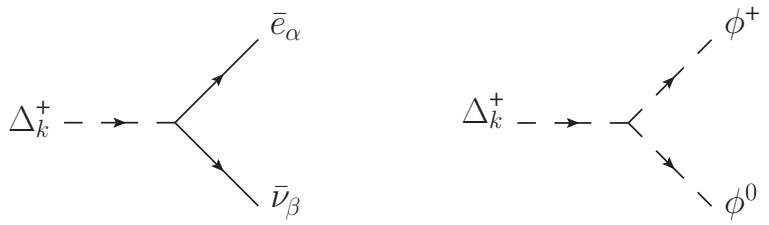

Figure 4.11 – Feynman diagrams of tree-level decay of the scalar triplet component Δ_k^+ to leptons and scalars respectively.

4.3.1 Tree-level decay rates

Tree-level triplet decays involve leptonic and scalar final states. The Feynman diagrams are shown in Fig. 4.11 for the Δ_k^+ component, and the associated decay widths are computed in Appendix D.1. The leptonic partial decay widths, depending on the lepton flavor composition of the final states, involve extra factors of $1/2$ which avoid double-counting : [10]

$$\Gamma\left(\Delta_k^Q \to \bar{\ell}_\alpha \bar{\ell}_\beta\right) = \frac{m_{\Delta_k}}{8\pi}\left|\mathscr{Y}_{\Delta_k}^{\alpha\beta}\right|^2 \left[1 + |Q-1|\left(1-\delta_{\alpha\beta}\right)\right] , \tag{4.63}$$

where Q stands for the electric charges of the different $SU(2)$ triplet components, $\Delta_k^Q = (\Delta_k^0, \Delta_k^+, \Delta_k^{++})$. The matrix $\mathscr{Y}_{\Delta_k}$ is related to the matrix Y_{Δ_k} through the transformation $\mathscr{Y}_{\Delta_k} = R^*\ Y_{\Delta_k}\ R^\dagger$, where R is a unitary matrix that diagonalize totally or partially the Yukawa matrix Y_{Δ_1} of the triplet responsible for leptogenesis $\Delta \equiv \Delta_1$, following that the full-diagonal or the semi-diagonal regime applies. On the other hand, scalar triplet decay modes can be written according to :

$$\Gamma\left(\Delta_k^Q \to \phi\phi\right) = \frac{\left|\mu_{\Delta_k}\right|^2}{8\pi m_{\Delta_k}} , \tag{4.64}$$

Since $\mathrm{Tr}[\mathscr{Y}_\Delta \mathscr{Y}_\Delta^\dagger] = \mathrm{Tr}[Y_\Delta Y_\Delta^\dagger]$, the total decay rate to leptons doesn't depend on the flavor regime, as it should. It is given as in Eq. (4.11) by

$$\Gamma_{\Delta_k} \equiv \Gamma_{\Delta_k^0} = \Gamma_{\Delta_k^+} = \Gamma_{\Delta_k^{++}} = \frac{1}{8\pi}\frac{m_{\Delta_k}^2}{\mathrm{v}^2}\tilde{m}_{\Delta_k}^{\mathrm{eff}} , \tag{4.65}$$

where the effective neutrino mass-like parameter $\tilde{m}_{\Delta_k}^{\mathrm{eff}}$ is defined as in Eq. (4.12) :

$$\tilde{m}_{\Delta_k}^{\mathrm{eff}} \equiv \tilde{m}_{\Delta_k}\frac{1}{\sqrt{B_\ell^k B_\phi^k}} , \tag{4.66}$$

with

$$\tilde{m}_{\Delta_k}^2 \equiv \mathrm{Tr}[m_\nu^{\Delta_k} m_\nu^{\Delta_k\dagger}] = |\mu_{\Delta_k}|^2 \frac{\mathrm{v}^4}{m_{\Delta_k}^4}\,\mathrm{Tr}\left[Y_{\Delta_k} Y_{\Delta_k}^\dagger\right] . \tag{4.67}$$

[10] One could think in a first sight that the total decay rate of the three triplet components are not the same, which would not be gauge invariant. This is actually not the case, because a peculiar attention has to be taken when summing over the lepton channels, see Appendix D.1.

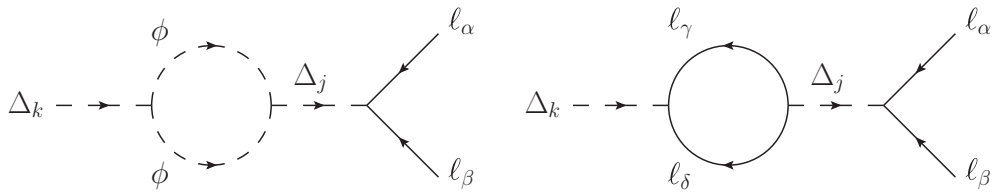

Figure 4.12 – One-loop Feynman diagrams responsible for the flavored CP asymmetry $\epsilon^{\ell_\alpha}_{\Delta_k}$ in the pure type-2 Seesaw scenario.

The B^k_ℓ and B^k_ϕ stand for the Δ_k triplet decay branching ratios to lepton and scalar final states :

$$B^k_\ell = \sum_{\alpha=e,\mu,\tau} B^k_{\ell_\alpha} = \sum_{\alpha,\beta=e,\mu,\tau} B^k_{\ell_{\alpha\beta}} = \sum_{\alpha,\beta=e,\mu,\tau} \frac{m_{\Delta_k}}{8\pi\Gamma_{\Delta_k}} \left|\mathscr{Y}^{\alpha\beta}_{\Delta_k}\right|^2 ,$$
$$B^k_\phi = \frac{\left|\mu_{\Delta_k}\right|^2}{8\pi m_{\Delta_k}\Gamma_{\Delta_k}} , \tag{4.68}$$

where of course the relation $B^k_\ell + B^k_\phi = 1$ holds. As in the one-favor approximation in Eq. (4.14), one sees directly from Eqs. (4.65) and (4.66) that Γ_{Δ_k} exhibits a minimum at $B^k_\ell = B^k_\phi = 1/2$, for fixed $\tilde{m}_{\Delta_k}$ and m_{Δ_k}. Thus, the farther we are from $B^k_\ell = B^k_\phi = 1/2$, the faster the scalar triplet decays.

4.3.2 Computation of the CP-asymmetries

The one-loop corrections to the tree-level decay depend on the details of the corresponding model. As mentioned at the beginning of the chapter in page 111, we focus here on (A) models featuring several scalar triplets ("pure type-2 Seesaw states"), and (B) models involving a scalar triplet and heavier right-handed neutrinos ("type-1+2 Seesaw states").

◦ Pure type-2 Seesaw states

In purely triplet models, that is to say models entirely determined by the Lagrangian in Eq. (4.2), the corrections to the leptonic tree-level decay mode involve only wave-function type corrections [238]. The CP-asymmetry follows from the interference between the tree-level and wave-function corrections shown in Fig. 4.12. The computation of the CP-asymmetries is done explicitly in Appendix D.2. The final CP-asymmetry therefore consists of two pieces : a lepton number *and* flavor violating one (first diagram with scalars in the loop) and a purely flavor violating part (second diagram with leptons in the loop). The total flavored CP-asymmetry in Δ_k decays can then be written as

$$\epsilon^{\ell_\alpha}_{\Delta_k} = \epsilon^{\ell_\alpha(\not{L},\not{F})}_{\Delta_k} + \epsilon^{\ell_\alpha(\not{F})}_{\Delta_k} , \tag{4.69}$$

where the two pieces read

$$\epsilon^{\ell_\alpha(\not{L},\not{F})}_{\Delta_k} = \frac{1}{2\pi} \sum_{j\neq k} \frac{\Im m\left[\left(\mathscr{Y}^\dagger_{\Delta_k}\mathscr{Y}_{\Delta_j}\right)_{\alpha\alpha}\mu^*_{\Delta_k}\mu_{\Delta_j}\right]}{m^2_{\Delta_k}\,\mathrm{Tr}\left[\mathscr{Y}_{\Delta_k}\mathscr{Y}^\dagger_{\Delta_k}\right] + |\mu_{\Delta_k}|^2} g\left(m^2_{\Delta_k}/m^2_{\Delta_j}\right) , \tag{4.70}$$

and

$$\epsilon_{\Delta_k}^{\ell_\alpha(\not{F})} = \frac{1}{2\pi}\sum_{j\neq k} m_{\Delta_k}^2 \frac{\Im m\left[\left(\mathscr{Y}_{\Delta_k}^\dagger \mathscr{Y}_{\Delta_j}\right)_{\alpha\alpha} \mathrm{Tr}\left[\mathscr{Y}_{\Delta_k}\mathscr{Y}_{\Delta_j}^\dagger\right]\right]}{m_{\Delta_k}^2 \mathrm{Tr}\left[\mathscr{Y}_{\Delta_k}\mathscr{Y}_{\Delta_k}^\dagger\right] + |\mu_{\Delta_k}|^2} g\left(m_{\Delta_k}^2/m_{\Delta_j}^2\right), \tag{4.71}$$

with

$$g(x) = \frac{x(1-x)}{(1-x)^2 + xy} \tag{4.72}$$

and $y = (\Gamma_{\Delta_j}/m_{\Delta_j})^2$. Note that the CP-asymmetry in Eq. (4.70) is in-line with what has been found in Ref. [251], and that the one in Eq. (4.71) is in-line with what has been found in Ref. [250]. This piece, which we refer to as *purely flavored CP-violating asymmetry*, satisfies the total lepton number conservation constraint

$$\sum_\alpha \epsilon_{\Delta_k}^{\ell_\alpha(\not{F})} = 0\,, \tag{4.73}$$

and so the total CP-asymmetry can consequently be written as

$$\epsilon_{\Delta_k} = \sum_{\alpha=e,\mu,\tau} \epsilon_{\Delta_k}^{\ell_\alpha} = \sum_{\alpha=e,\mu,\tau} \epsilon_{\Delta_k}^{\ell_\alpha(\not{L},\not{F})}\,. \tag{4.74}$$

For $m_{\Delta_j}^2 \gg m_{\Delta_k}^2$, the total flavored asymmetries can be recast in terms of triplet decay observables

$$\epsilon_{\Delta_k}^{\ell_\alpha} = -\frac{1}{2\pi\,\mathrm{v}^2}\sum_{j\neq k}\frac{m_{\Delta_j}^2}{m_{\Delta_k}}\frac{\sqrt{B_\ell^k B_\phi^k}}{\tilde{m}_{\Delta_k}}\Im m\left[\left(m_\nu^{\Delta_k\dagger} m_\nu^{\Delta_j}\right)_{\alpha\alpha}\left(1 + \frac{m_{\Delta_k}}{m_{\Delta_j}}\frac{\mathrm{Tr}[m_\nu^{\Delta_k} m_\nu^{\Delta_j\dagger}]}{\tilde{m}_{\Delta_k}\tilde{m}_{\Delta_j}}\sqrt{\frac{B_\ell^k B_\ell^j}{B_\phi^k B_\phi^j}}\right)\right] \times g(m_{\Delta_k}^2/m_{\Delta_j}^2)\,, \tag{4.75}$$

with $m_\nu^{\Delta_k}$ given in Eqs. (4.7).

Important comment on a purely flavored scenario. If flavor effects are operative, the purely flavored CP-asymmetry in (4.71) will play a role in the generation of the $B-L$ asymmetry. These asymmetries, conserving total lepton number, involve only the Yukawa couplings Y_Δ and not the lepton number violating parameter μ_Δ. Hence, as also noted in Ref. [250], they are not necessarily suppressed by the smallness of the neutrino masses. As can be seen by comparing (4.70) and (4.71), when the condition

$$\mu_{\Delta_k}^* \mu_{\Delta_j} \ll m_{\Delta_k}^2 \mathrm{Tr}[Y_{\Delta_k} Y_{\Delta_j}^\dagger] \tag{4.76}$$

is satisfied, the purely flavored CP-asymmetry overshadows the lepton number violating piece. This opens the path to a special regime where leptogenesis could be entirely driven by flavor dynamics. In terms of scalar triplet interactions, this means that a purely flavored scalar triplet leptogenesis scenario naturally emerges whenever the triplets couple substantially less to SM scalars than to leptons, $B_\phi^k \ll B_\ell^k$ for at least one value of k. This can for example be motivated from symmetry arguments, see the discussion associated to Eq. (1.41) in page 21.

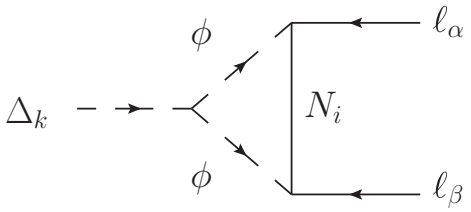

Figure 4.13 – One-loop Feynman diagrams accounting for the flavored CP asymmetry $\epsilon^{\ell_i}_{\Delta_\alpha}$ in scenarios featuring type-1 and type-2 interplay.

Note that although Purely Flavored Leptogenesis (PFL) scenarios in type-1 Seesaw can be defined as well, they differ significantly from the purely flavored scalar triplet leptogenesis scenario in that the latter just requires suppressed lepton number violation in a single triplet generation, i.e. suppression of lepton number breaking interactions in the full Lagrangian is not mandatory, as can be seen by noting that condition (4.76) can be satisfied even if $\mu_{\Delta_k}/m_{\Delta_k} \ll Y_{\Delta_k}$ for a single value of k. PFL scenario in type-2 leptogenesis is thus much more "natural" and straightforward than in type-1 leptogenesis. This possible scenario will be considered in section 4.5.

◦ Type-1+2 Seesaw states

We now turn to the case where the new states beyond the scalar triplet are right-handed neutrinos, which is a scenario well-motivated by GUT, see section 1.6. In these scenarios the tree-level triplet decay involves only a vertex one-loop correction as shown in Fig. 4.13. The interference between the tree and one-loop level diagrams leads to the following CP-asymmetry [240, 241] :

$$\epsilon^{\ell_\alpha}_{\Delta} = -\frac{1}{4\pi}\sum_{i,\beta} m_{N_i}\frac{\Im m\left[\mu_\Delta \mathscr{Y}^{\alpha\beta}_{\Delta} Y^*_{N_i\alpha} Y^*_{N_i\beta}\right]}{m^2_\Delta \mathrm{Tr}\left[\mathscr{Y}_\Delta \mathscr{Y}^\dagger_\Delta\right] + |\mu_\Delta|^2}\ln\left(1+\frac{m^2_\Delta}{m^2_{N_i}}\right) . \tag{4.77}$$

Here the triplet generation index, being superfluous, has been dropped. In contrast to what has been found in the previous case, the resulting flavored CP-asymmetry violates lepton flavor as well as lepton number. So, unless a specific (and somehow arbitrary) flavor alignment is assumed, so that $\sum_\alpha \epsilon^{\ell_\alpha}_{\Delta} = 0$, in these "hybrid" schemes PFL scenarios are not definable.

In the hierarchical case, $m_\Delta \ll m_{N_i}$, the flavored CP-asymmetry can be recast in terms of triplet decay observables, namely

$$\epsilon^{\ell_\alpha}_{\Delta} = -\frac{1}{2\pi}\frac{m_\Delta}{\mathrm{v}^2}\sqrt{B_\ell B_\phi}\frac{\Im m\left[\left(m^\Delta_\nu m^{N\dagger}_\nu\right)_{\alpha\alpha}\right]}{\tilde{m}_\Delta} , \tag{4.78}$$

with m^Δ_ν and m^N_ν given by Eqs. (4.7) and (4.8). Note that in type-1+type-2 scenarios, opposite to the scenario we consider here, it is also possible to generate the $B-L$ asymmetry from the decay of right-handed neutrinos via a vertex diagram involving a virtual scalar triplet, see in particular Refs. [240, 252, 253].

◦ **Upper bound on the CP-asymmetries**

The upper bounds in Eqs. (4.22) and (4.23) on the sum of the flavored CP-asymmetries still hold. As was done in the one-flavor approximation in Eq. (4.23), from perturbativity constraints, i.e. by requiring that the one-loop contribution to the various decay widths doesn't exceed the tree-level one, one can derive an upper bound on the CP-asymmetry given by

$$\left|\epsilon^{\ell_\alpha}_{\Delta_k}\right| \leq 2 \cdot \min\left(B^k_{\ell_\alpha}, B^k_\phi\right) . \tag{4.79}$$

However, it seems in general not possible to derive any model-independent upper bound on the separated flavor CP-asymmetries from light neutrino mass values. For example, *in the pure type-2 Seesaw with 2 scalar triplets,* we find that the CP-asymmetry in Eq. (4.69) is bounded from above by

$$\left|\epsilon^{\ell_\alpha}_{\Delta_1}\right| \leq \frac{1}{2\pi}\frac{m_{\Delta_1}}{\mathrm{v}^2}\sqrt{B_\ell B_\phi \sum_i m^2_{\nu_i}} + 2\,\frac{m^2_{\Delta_1}}{m^2_{\Delta_2}}\left[\sum_\beta \sum_{\gamma,\delta\neq\alpha}\sqrt{B_{\ell_{\alpha\beta}}}\sqrt{B_{\ell_{\gamma\delta}}} + \sum_{\beta\neq\alpha}\sqrt{B_{\ell_{\alpha\alpha}}}\sqrt{B_{\ell_{\alpha\beta}}}\right] , \tag{4.80}$$

where we assumed perturbative Yukawa couplings for the second triplet generation, i.e. $|Y_{\Delta_2}| \leq \sqrt{4\pi}$. [11] Note that the second term comes from the L-conserving CP-asymmetry in Eq. (4.71).

In the mixed type-1+2 scheme, we find that the upper bound on the separated flavor CP-asymmetries is given by the first term of the above equation, which is nothing but the general upper bound on the sum of the flavored CP-asymmetries in Eq. (4.22), to wit

$$\left|\epsilon^{\ell_\alpha}_{\Delta}\right| \leq \frac{1}{2\pi}\frac{m_{\Delta}}{\mathrm{v}^2}\sqrt{B_\ell B_\phi \sum_i m^2_i} . \tag{4.81}$$

We see therefore that the upper bound on each flavored CP-asymmetry depends on which kind of heavy particles activates leptogenesis.

Now that we have computed the various CP-asymmetries, we can compute the chemical equilibrium conditions that are needed to write down the set of flavored Boltzmann equations.

4.3.3 $B/3 - L_\alpha$ asymmetries and chemical equilibrium conditions

In order to set the Boltzmann equations, one needs to derive the chemical equilibrium conditions, as what has been done in section 3.6.3 for type-1 leptogenesis. As also already discussed in section 4.2.2, in each flavor regime the associated flavor asymmetries that need to be treated in the Boltzmann equations are the ΔY_{B-L_α}, with $L_\alpha = \ell_\alpha (+ e_\alpha)$ where e_α are the right-handed charged leptons. The ΔY_{B-L_α} are directly related to ΔY_{ℓ_α} through chemical equilibrium conditions. Indeed, following the temperature some SM processes can be in thermal equilibrium. These spectator processes induce relations between the chemical potentials and so between the asymmetries of various species.

[11] The upper bound on the CP-asymmetry depends crucially on the perturbativity condition. Taking instead $|Y_\beta| \leq 1$ would lead to the same expression divided by 4π.

As explained in Appendix C.5, there is in principle a chemical potential (an asymmetry) for each particle in the thermal bath, which implies that *a priori* there are as many chemical potentials as particles in the plasma : 61. This number is however largely reduced due to the constraints imposed by the set of chemical equilibrium conditions. These constraints depend on the temperature regime where the $B-L$ asymmetry is generated. For $T > T_{EW}$ (which is required in order to generate a $B-L$ asymmetry before the sphalerons decouple), one has that the possible constraints on the chemical potentials are, in this type-2 Seesaw case : [12]

1. Chemical potentials for gauge bosons vanish $\mu_{W^i} = \mu_{\mathscr{B}} = \mu_g = 0$, and so the components of the electroweak and color multiplets have the same chemical potentials [215].

2. Regardless of the temperature regime, cosmological hypercharge neutrality must be obeyed, namely

$$\mathscr{Y} = \sum_\alpha \left(\mu_{Q_\alpha} + 2\mu_{u_\alpha} - \mu_{d_\alpha} - \mu_{\ell_\alpha} - \mu_{e_\alpha}\right) + 2\mu_\phi + 6\mu_\Delta = 0 \,. \tag{4.82}$$

   Compared to the type-1 Seesaw expression in Eq. (C.55) in Appendix, since the scalar triplet carries a hypercharge, this equation involves now the chemical potential of the scalar triplet μ_Δ. These two first items already reduce to 16 the number of independent asymmetries.

3. Non-perturbative QCD instanton and electroweak sphaleron reactions – if in thermal equilibrium – enforce the following constraints :

$$\sum_\alpha \left(2\mu_{Q_\alpha} - \mu_{u_\alpha} - \mu_{d_\alpha}\right) = 0 \quad \text{(QCD)} \,, \qquad \sum_\alpha \left(3\mu_{Q_\alpha} + \mu_{\ell_\alpha}\right) = 0 \quad \text{(EW)} \,. \tag{4.83}$$

   The temperature range at which the QCD instanton reactions attain equilibrium has been estimated to be $T^{QCD}_{\text{sphal}} \in [132, 10^{13}]$ GeV [255, 214] while for electroweak sphaleron processes, being controlled by α_{EW} rather than α_S, it has been found to be about a factor 20 smaller for the upper value [214] so that $T^{EW}_{\text{sphal}} \in [132, 10^{12}]$ GeV. For a question of simplicity, we will here assume that they both are in thermal equilibrium for $T_{\text{sphal}} \in [132, 10^{12}]$ GeV.

4. Finally, when the SM charged Yukawa reactions are in thermal equilibrium, i.e. they are faster than the Hubble rate and faster than any other rate involving the charged fermion, one has the following chemical equilibrium constraints :

$$\text{Up-type quarks:} \qquad \mu_{u_\alpha} - \mu_{Q_\alpha} - \mu_\phi = 0 \,, \tag{4.84}$$

$$\text{Down-type quarks:} \qquad \mu_{d_\alpha} - \mu_{Q_\alpha} + \mu_\phi = 0 \,, \tag{4.85}$$

$$\text{Charged leptons:} \qquad \mu_{e_\alpha} - \mu_{\ell_\alpha} + \mu_\phi = 0 \,. \tag{4.86}$$

   Top Yukawa-induced reactions are faster than the Hubble rate for $T \lesssim 10^{15}$ GeV. Bottom, charm and tau Yukawa-induced processes are faster than the Hubble rate for $T \lesssim 10^{12}$ GeV, strange and muon for $T \lesssim 10^9$ GeV, and the first generation Yukawa-induced processes for $T \lesssim 10^5$ GeV [230, 233, 231].

[12] Theses ranges are based on the assumption that all SM interactions that approximately enter in thermal equilibrium at a similar temperature do it effectively at the same temperature. We stress that some of these temperature "windows" differ from those used in Ref. [233], in particular in what regards the charged lepton Yukawa reaction equilibrium temperatures. They however match with those pointed out in Ref. [230].

Following the temperature regime, the effective Lagrangian possesses global symmetries and the associated charges, the asymmetries, are conserved. This means that if at early stage there were zero initial asymmetry for all the species present in the thermal bath (which is a reasonable assumption) some of the chemical potentials can be set to zero, see discussion in Appendix C.5.2. As a consequence, the exact number of non-vanishing chemical potentials as well as the number of chemical equilibrium conditions are thus fixed only when a specific temperature window is settled. Once this is done, the resulting system of equations is solved in terms of a single set of variables, which we take to be $\mu_{B/3-L_\alpha}$ and μ_Δ, since it is the evolution of these quantities on which we are interested in. The solution thus provides the relations between the asymmetries of all the particles in the heat bath with the independent asymmetries ΔY_Δ and $\Delta Y_{B/3-L_\alpha}$.

In particular, the scalar asymmetry ΔY_ϕ and the lepton flavor asymmetries ΔY_{ℓ_α} are determined by the triplet asymmetry ΔY_Δ and the ΔY_{B-L_α} asymmetries through

$$\Delta Y_\phi = -\sum_k C_k^\phi \Delta Y_k \qquad \text{and} \qquad \Delta Y_{\ell_\alpha} = -\sum_k C_{\alpha k}^\ell \Delta Y_k \,, \tag{4.87}$$

where the asymmetries ΔY_k are given by the components of the asymmetry vector

$$\Delta \vec{Y} = \begin{pmatrix} \Delta Y_\Delta & \Delta Y_{B/3-L_\alpha} \end{pmatrix}^T \,. \tag{4.88}$$

The matrices C^ℓ and C^ϕ depend on the flavor regime *and* on the temperature at which leptogenesis takes place (i.e. the mass of the scalar triplet m_Δ), and their value are given in Table 4.1 for all the flavor and temperature regimes, see next page. [13] Indeed, in each flavor regime, the structure of the C^ℓ and C^ϕ matrices are determined by the constraints coming from the global symmetries of the effective Lagrangian and the chemical equilibrium conditions enforced by those SM reactions which in the relevant temperature regime (the regime at which the $B-L$ asymmetry is generated) are faster than the Universe Hubble expansion rate. All in all, one has a set of 5 pairs of matrices for the full-diagonal regime, 3 for the semi-diagonal and 3 for the general regime. This makes a total of 11 different matrices for C^ℓ and C^ϕ.

We are now in a position to compute the set of classical Boltzmann equations that describes how the scalar triplet leptogenesis works taking into account the lepton flavors and the spectator processes, whatever the flavor or temperature regime.

m_Δ (GeV)	Regime	C^ℓ	C^ϕ
$\gtrsim 10^{15}$	Full-diag.	$\begin{pmatrix} 0 & 1 & 0 & 0 \\ 0 & 0 & 1 & 0 \\ 0 & 0 & 0 & 1 \end{pmatrix}$	$\begin{pmatrix} 2 & 1 & 1 & 1 \end{pmatrix}$

…see next page for the other regimes…

[13] Note that some of these matrices reduce to those found in the type-1 Seesaw case when removing their first column.

m_Δ (GeV)	Regime	C^ℓ	C^ϕ
$[10^{12}, 10^{15}]$	Full-diag.	$\begin{pmatrix} 0 & 1 & 0 & 0 \\ 0 & 0 & 1 & 0 \\ 0 & 0 & 0 & 1 \end{pmatrix}$	$\begin{pmatrix} \frac{4}{3} & \frac{2}{3} & \frac{2}{3} & \frac{2}{3} \end{pmatrix}$
$[10^9, 10^{12}]$:			
$[T^\tau_{\rm decoh}, 10^{12}]$	Full-diag.	$\begin{pmatrix} 0 & \frac{13}{15} & -\frac{2}{15} & -\frac{2}{15} \\ 0 & -\frac{2}{15} & \frac{13}{15} & -\frac{2}{15} \\ 0 & -\frac{2}{15} & -\frac{2}{15} & \frac{13}{15} \end{pmatrix}$	$\begin{pmatrix} \frac{1}{2} & \frac{1}{4} & \frac{1}{4} & \frac{1}{4} \end{pmatrix}$
$[10^9, T^\tau_{\rm decoh}]$	Semi-diag.	$\begin{pmatrix} -\frac{4}{359} & \frac{307}{359} & -\frac{52}{359} & -\frac{36}{359} \\ -\frac{4}{359} & \frac{-52}{359} & \frac{307}{359} & -\frac{36}{359} \\ \frac{26}{359} & -\frac{21}{359} & \frac{-21}{359} & \frac{234}{359} \end{pmatrix}$	$\begin{pmatrix} \frac{172}{359} & \frac{82}{359} & \frac{82}{359} & \frac{112}{359} \end{pmatrix}$
$[10^5, 10^9]$:			
$[T^\tau_{\rm decoh}, 10^9]$	Full-diag.	$\begin{pmatrix} 0 & \frac{13}{15} & -\frac{2}{15} & -\frac{2}{15} \\ 0 & -\frac{2}{15} & \frac{13}{15} & -\frac{2}{15} \\ 0 & -\frac{2}{15} & -\frac{2}{15} & \frac{13}{15} \end{pmatrix}$	$\begin{pmatrix} \frac{1}{2} & \frac{1}{4} & \frac{1}{4} & \frac{1}{4} \end{pmatrix}$
$[T^\mu_{\rm decoh}, T^\tau_{\rm decoh}]$	Semi-diag.	$\begin{pmatrix} -\frac{4}{359} & \frac{307}{359} & -\frac{52}{359} & -\frac{36}{359} \\ -\frac{4}{359} & \frac{-52}{359} & \frac{307}{359} & -\frac{36}{359} \\ \frac{26}{359} & -\frac{21}{359} & \frac{-21}{359} & \frac{234}{359} \end{pmatrix}$	$\begin{pmatrix} \frac{172}{359} & \frac{82}{359} & \frac{82}{359} & \frac{112}{359} \end{pmatrix}$
$[10^5, T^\mu_{\rm decoh}]$	General	$\begin{pmatrix} -\frac{4}{179} & \frac{151}{179} & -\frac{20}{179} & -\frac{20}{179} \\ \frac{11}{179} & -\frac{25}{358} & \frac{344}{537} & -\frac{14}{537} \\ \frac{11}{358} & -\frac{25}{358} & -\frac{14}{537} & \frac{344}{537} \end{pmatrix}$	$\begin{pmatrix} \frac{82}{179} & \frac{37}{179} & \frac{52}{179} & \frac{52}{179} \end{pmatrix}$
$\lesssim 10^5$:			
$[T^\tau_{\rm decoh}, 10^5]$	Full-diag.	$\begin{pmatrix} 0 & \frac{13}{15} & -\frac{2}{15} & -\frac{2}{15} \\ 0 & -\frac{2}{15} & \frac{13}{15} & -\frac{2}{15} \\ 0 & -\frac{2}{15} & -\frac{2}{15} & \frac{13}{15} \end{pmatrix}$	$\begin{pmatrix} \frac{4}{11} & \frac{2}{11} & \frac{2}{11} & \frac{2}{11} \end{pmatrix}$
$[T^\mu_{\rm decoh}, T^\tau_{\rm decoh}]$	Semi-diag.	$\begin{pmatrix} -\frac{2}{244} & \frac{209}{244} & -\frac{35}{244} & -\frac{24}{244} \\ -\frac{2}{244} & -\frac{35}{244} & -\frac{209}{244} & -\frac{24}{244} \\ \frac{13}{244} & -\frac{33}{488} & -\frac{33}{488} & \frac{156}{244} \end{pmatrix}$	$\begin{pmatrix} \frac{86}{244} & \frac{41}{244} & \frac{41}{244} & \frac{56}{244} \end{pmatrix}$
$[T^e_{\rm decoh}, T^\mu_{\rm decoh}]$	$B/3 - L_{e,\mu,\tau}$	$\begin{pmatrix} -\frac{8}{481} & \frac{407}{481} & -\frac{52}{481} & -\frac{52}{481} \\ \frac{22}{481} & -\frac{1}{13} & \frac{70}{111} & -\frac{4}{111} \\ \frac{22}{481} & -\frac{1}{13} & -\frac{4}{111} & \frac{70}{111} \end{pmatrix}$	$\begin{pmatrix} \frac{164}{481} & \frac{2}{13} & \frac{8}{37} & \frac{8}{37} \end{pmatrix}$
$\lesssim T^e_{\rm decoh}$	General	$\begin{pmatrix} \frac{3}{79} & \frac{442}{711} & -\frac{32}{711} & -\frac{32}{711} \\ \frac{3}{79} & -\frac{32}{711} & \frac{442}{711} & -\frac{32}{711} \\ \frac{3}{79} & -\frac{32}{711} & -\frac{32}{711} & \frac{442}{711} \end{pmatrix}$	$\begin{pmatrix} \frac{26}{79} & \frac{16}{79} & \frac{16}{79} & \frac{16}{79} \end{pmatrix}$

Table 4.1 – C^ℓ and C^ϕ matrices for all the flavor regimes and temperature ranges.

4.3.4 Flavored Boltzmann equations

The network of Boltzmann equations for scalar triplet leptogenesis, no matter whether lepton flavor effects are active or not, corresponds to a system of coupled differential equations accounting for the temperature evolution of the triplet density $Y_\Sigma = Y_\Delta + Y_{\bar{\Delta}}$, the triplet asymmetry $\Delta Y_\Delta = Y_\Delta - Y_{\bar{\Delta}}$ and the $\Delta Y_{B/3-L_\alpha}$ charge asymmetries. We give in Appendix D.4 the details of the derivation of the set of Boltzmann equations, which ultimately reads

$$\dot{Y}_\Sigma = -\left(\frac{Y_\Sigma}{Y_\Sigma^{\rm Eq}} - 1\right)\gamma_D - 2\left[\left(\frac{Y_\Sigma}{Y_\Sigma^{\rm Eq}}\right)^2 - 1\right]\gamma_A\,, \tag{4.89}$$

$$\Delta\dot{Y}_\Delta = -\left[\frac{\Delta Y_\Delta}{Y_\Sigma^{\rm Eq}} - \sum_k\left(\sum_\alpha B_{\ell_\alpha}C^\ell_{\alpha k} - B_\phi C^\phi_k\right)\frac{\Delta Y_k}{Y_\ell^{\rm Eq}}\right]\gamma_D\,, \tag{4.90}$$

$$\begin{aligned}\Delta\dot{Y}_{B/3-L_\alpha} = &-\left(\frac{Y_\Sigma}{Y_\Sigma^{\rm Eq}} - 1\right)\epsilon^{\ell_\alpha}_\Delta\gamma_D + 2\sum_\beta\left(\frac{\Delta Y_\Delta}{Y_\Sigma^{\rm Eq}} - \frac{1}{2}\sum_k C^\ell_{\alpha\beta k}\frac{\Delta Y_k}{Y_\ell^{\rm Eq}}\right)B_{\ell_{\alpha\beta}}\gamma_D \\ &- 2\sum_{\beta,k}\left(C^\phi_k + \frac{1}{2}C^\ell_{\alpha\beta k}\right)\frac{\Delta Y_k}{Y_\ell^{\rm Eq}}\left(\gamma'^{\phi\phi}_{\ell_\alpha\ell_\beta} + \gamma^{\phi\ell_\beta}_{\phi\ell_\alpha}\right) - \sum_{\beta,\gamma,\delta,k}C^\ell_{\alpha\beta\gamma\delta k}\frac{\Delta Y_k}{Y_\ell^{\rm Eq}}\left(\gamma'^{\ell_\gamma\ell_\delta}_{\ell_\alpha\ell_\beta} + \gamma^{\ell_\beta\ell_\gamma}_{\ell_\alpha\ell_\delta}\right)\,.\end{aligned} \tag{4.91}$$

The matrices $C^\ell_{\alpha\beta k}$ and $C^\ell_{\alpha\beta\gamma\delta k}$ are defined according to

$$C^\ell_{\alpha\beta k} = C^\ell_{\alpha k} + C^\ell_{\beta k} \qquad \text{and} \qquad C^\ell_{\alpha\beta\gamma\delta k} = C^\ell_{\alpha k} + C^\ell_{\beta k} - C^\ell_{\gamma k} - C^\ell_{\delta k}\,, \tag{4.92}$$

where the C^ℓ and C^ϕ matrices relate the asymmetry in lepton and scalar doublets with the $B/3-L_\alpha$ and triplet asymmetries according to Eqs. (4.87). The asymmetries ΔY_k are given by the components of the asymmetry vector in Eq. (4.88) : $\Delta\vec{Y} = (\Delta Y_\Delta\,,\,\Delta Y_{B/3-L_\alpha})$. The final baryon asymmetry is as usual given by

$$\Delta Y_B^{\rm today} = \frac{12}{37}\sum_\alpha \Delta Y^{\rm end}_{B/3-L_\alpha}\,, \tag{4.93}$$

where $\Delta Y^{\rm end}_{B/3-L_\alpha}$ are the flavor asymmetries at the end of leptogenesis. The various rates have already been introduced in section 4.1.5, page 117. In particular, in the second line of the Boltzmann equation (4.91), we took into account : (i) the lepton flavor and lepton number ($\Delta L = 2$) violating Yukawa-scalar-induced and triplet-mediated s and t channel $2 \leftrightarrow 2$ scatterings $\phi\phi \leftrightarrow \bar{\ell}_\alpha\bar{\ell}_\beta$ and $\phi\ell_\beta \leftrightarrow \bar{\phi}\bar{\ell}_\alpha$, which are accounted for by the reaction densities $\gamma^{\phi\phi}_{\ell_\alpha\ell_\beta}$ and $\gamma^{\phi\ell_\beta}_{\phi\ell_\alpha}$; (ii) the lepton-flavor-violating Yukawa-induced and triplet-mediated s and t channel $2 \leftrightarrow 2$ scatterings $\ell_\gamma\ell_\delta \leftrightarrow \ell_\alpha\ell_\beta$ and $\ell_\beta\ell_\gamma \leftrightarrow \ell_\alpha\ell_\delta$, with reaction densities given by $\gamma^{\ell_\gamma\ell_\delta}_{\ell_\alpha\ell_\beta}$ and $\gamma^{\ell_\beta\ell_\gamma}_{\ell_\alpha\ell_\delta}$. The analytical expression of the rate of these scattering processes are given in Appendix D.3.

We show in Fig. 4.14 the different reaction densities as a function of $z \equiv m_\Delta/T$ by fixing the relevant parameters according to $m_\Delta = 10^9$ GeV, $\tilde{m}_\Delta = 10^{-2}$ eV and $B_\phi = 10^{-4}$ ($B_\phi = 0.5$) for the plot on the left (right). For the scattering rates, for convenience we summed over all the initial and final flavor configurations. We see that the various $2 \leftrightarrow 2$ scattering rates are always smaller than the Hubble rate for these parameter choices. This is actually the case for most of the parameter space. Accordingly, as in the one-flavor approximation, from now on and throughout

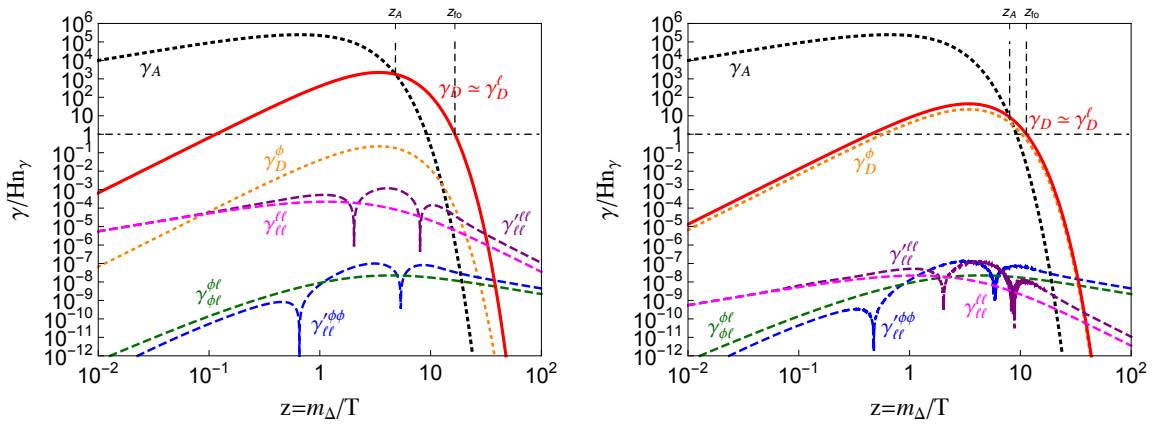

Figure 4.14 – Reaction densities for the different processes involved in scalar triplet flavored leptogenesis. In the left-hand side plot $B_\phi = 10^{-4}$ while in the right-hand side plot $B_\phi = B_\ell = 0.5$ ($B_\ell = 1 - B_\phi$). The remaining parameters have been fixed according to $m_\Delta = 10^9\,\text{GeV}$ and $\tilde{m}_\Delta = 10^{-2}\,\text{eV}$.

the numerical calculation we will drop the third and fourth term in the r.h.s. of Eq. (4.91) (i.e. the second line). For the numerical example we will consider below, this approximation is valid up to better than ~1%.

4.3.5 Formal integration of Boltzmann equations

Now that we know the Boltzmann equations for each flavor regime, it must be explained how to deal with them to get the final asymmetry produced. We here try to solve analytically the set of Boltzmann equations. Keeping only leading order terms in Eq. (4.91), i.e. dropping third and fourth terms, an analytic formal integration of the equations responsible for the $B-L$ asymmetry can be accomplished, basically along the same lines of the type-1 Seesaw case [256]. In all the flavor regimes, one has to consider 3 flavors, that we will label a, b and c. [14] The asymmetry vector introduced in Sec. 4.3.3 (see Eq. (4.88)) is given by

$$\Delta\vec{Y} = \left(\Delta Y_\Delta \quad \Delta Y_{B/3-L_a} \quad \Delta Y_{B/3-L_b} \quad \Delta Y_{B/3-L_c}\right)^T . \tag{4.94}$$

In terms of this vector, Eqs. (4.89) and (4.91) can be casted in matricial form, namely

$$\frac{d}{dz}\Delta\vec{Y}(z) = -\left(\frac{Y_\Sigma}{Y_\Sigma^{\text{Eq}}} - 1\right) D(z)\,\vec{\varepsilon} - D(z)\,\mathscr{M}(z)\,\Delta\vec{Y}(z)\,, \tag{4.95}$$

with

$$D(z) = \frac{\gamma_D(z)}{s(z)\,H(z)\,z}\,, \tag{4.96}$$

[14] The flavors (ℓ_a, ℓ_b, ℓ_c) correspond to (ℓ_1, ℓ_2, ℓ_3) In the full-diagonal regime, $(\ell_a, \ell_b, \ell_\tau)$ in the semi-diagonal regime, and $(\ell_e, \ell_\mu, \ell_\tau)$ in the general regime.

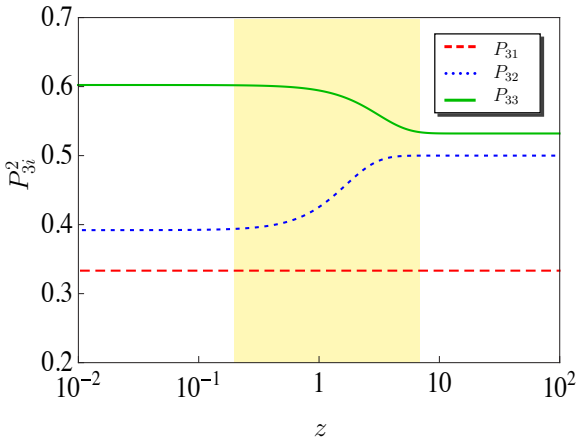

Figure 4.15 – $\mathscr{P}$ eigenvectors-third-component $\mathscr{P}_{3i}$ as a function of z. The eigenvectors have been evaluated for the flavor configuration $B_{\ell_{\alpha\alpha}} = 0$ and $B_{\ell_{ab}} = B_{\ell_{ba}} = (1 - B_\phi)/2$, with $B_\phi = 10^{-4}$, in the two-flavor approximation for simplicity. We have checked that this result is quite insensitive to changes in the flavor configuration. The vertical yellow stripe indicates the range where the matrix $\mathscr{P}$ slightly depends upon z.

and where the CP-asymmetry vector $\vec{\varepsilon}$ is defined as

$$\vec{\varepsilon} = \begin{pmatrix} 0 & \epsilon^{\ell_a}_{\Delta} & \epsilon^{\ell_b}_{\Delta} & \epsilon^{\ell_c}_{\Delta} \end{pmatrix}^T , \tag{4.97}$$

while the matrix $\mathscr{M}$ according to

$$\mathscr{M}(z) = \begin{pmatrix} \frac{1}{Y^{\rm Eq}_\Sigma} - \frac{\sum_\beta B_{\ell_\beta} C^\ell_{\beta\Delta} - B_\phi C^\phi_\Delta}{Y^{\rm Eq}_\ell} & -\frac{\sum_\beta B_{\ell_\beta} C^\ell_{\beta a} - B_\phi C^\phi_a}{Y^{\rm Eq}_\ell} & -\frac{\sum_\beta B_{\ell_\beta} C^\ell_{\beta b} - B_\phi C^\phi_b}{Y^{\rm Eq}_\ell} & -\frac{\sum_\beta B_{\ell_\beta} C^\ell_{\beta c} - B_\phi C^\phi_c}{Y^{\rm Eq}_\ell} \\ -2\sum_\beta B_{\ell_{a\beta}} \left(\frac{1}{Y^{\rm Eq}_\Sigma} - \frac{C^\ell_{a\beta\Delta}}{2Y^{\rm Eq}_\ell} \right) & \sum_\beta B_{\ell_{a\beta}} \frac{C^\ell_{a\beta a}}{Y^{\rm Eq}_\ell} & \sum_\beta B_{\ell_{a\beta}} \frac{C^\ell_{a\beta b}}{Y^{\rm Eq}_\ell} & \sum_\beta B_{\ell_{a\beta}} \frac{C^\ell_{a\beta c}}{Y^{\rm Eq}_\ell} \\ -2\sum_\beta B_{\ell_{b\beta}} \left(\frac{1}{Y^{\rm Eq}_\Sigma} - \frac{C^\ell_{b\beta\Delta}}{2Y^{\rm Eq}_\ell} \right) & \sum_\beta B_{\ell_{b\beta}} \frac{C^\ell_{b\beta a}}{Y^{\rm Eq}_\ell} & \sum_\beta B_{\ell_{b\beta}} \frac{C^\ell_{b\beta b}}{Y^{\rm Eq}_\ell} & \sum_\beta B_{\ell_{b\beta}} \frac{C^\ell_{b\beta c}}{Y^{\rm Eq}_\ell} \\ -2\sum_\beta B_{\ell_{c\beta}} \left(\frac{1}{Y^{\rm Eq}_\Sigma} - \frac{C^\ell_{c\beta\Delta}}{2Y^{\rm Eq}_\ell} \right) & \sum_\beta B_{\ell_{c\beta}} \frac{C^\ell_{c\beta a}}{Y^{\rm Eq}_\ell} & \sum_\beta B_{\ell_{c\beta}} \frac{C^\ell_{c\beta b}}{Y^{\rm Eq}_\ell} & \sum_\beta B_{\ell_{c\beta}} \frac{C^\ell_{c\beta c}}{Y^{\rm Eq}_\ell} \end{pmatrix} . \tag{4.98}$$

In the case $\mathscr{M}(z) = \mathscr{M}$, the system of equations in (4.95) can be decoupled via a rotation of the asymmetry vector $\Delta\vec{Y}$, the matrix accounting for the rotation being determined by the similarity transformation

$$\mathscr{P}^{-1}\,\mathscr{M}\,\mathscr{P} = \hat{\mathscr{M}} , \tag{4.99}$$

which brings $\mathscr{M}$ to diagonal form. Strictly speaking, $\mathscr{M}$ does depend on z, but it turns out that the z dependence of the rotation matrix $\mathscr{P}$ is quite moderate (only the first colon of $\mathscr{M}$ do actually depend on z). As can be seen in Fig. 4.15, in the high as well as in the low temperature regime $\mathscr{P}(z) = \mathscr{P}$ whereas within the window $z \subset [0.2, 7]$ there is a rather soft dependence.

Thus, we will make the approximation to take a z independent change-of-basis-matrix $\mathscr{P}$ and rotating the asymmetry vector, as

$$\Delta\vec{Y}'(z) = \mathscr{P}^{-1}\,\Delta\vec{Y}(z) . \tag{4.100}$$

In this way, we finally get a decoupled system of differential equations :

$$\frac{d}{dz}\Delta\vec{Y}'(z) = -\left(\frac{Y_\Sigma}{Y_\Sigma^{\rm Eq}} - 1\right) D(z)\,\vec{\varepsilon}' - D(z)\hat{\mathscr{M}}(z)\Delta\vec{Y}'(z)\,, \tag{4.101}$$

where the rotated CP-asymmetry vector $\vec{\varepsilon}'$ has been introduced:

$$\vec{\varepsilon}' = \mathscr{P}^{-1}\vec{\varepsilon}\,. \tag{4.102}$$

The decoupled system of equations in (4.101) can then be formally integrated through their integrating factor. By doing so, and assuming vanishing primordial asymmetries, $\Delta\vec{Y}(z_0) = 0$ with $z_0 \ll 1$, the solution reads

$$\Delta\vec{Y}'(z) = -\int_{z_0}^{z} dz' \,\frac{\gamma_D(z')}{\gamma_D(z') + 4\gamma_A(z')}\frac{dY_\Sigma(z')}{dz'}\, e^{-\int_{z'}^{z} dz'' D(z'')\hat{\mathscr{M}}(z'')}\,\vec{\varepsilon}'\,. \tag{4.103}$$

We used Eq. (4.90) and the fact that $Y_\Sigma(z)$ follows quite closely the equilibrium distribution function. In terms of the "new" asymmetries, and due to the diagonal structure of the matricial damping factor $\hat{\mathscr{M}}$, one can define efficiency functions $\eta'_i(z)$, which account for the evolution of the primed asymmetries and their corresponding values at freeze-out ($z \to \infty$), namely

$$\left[\Delta\vec{Y}'(z)\right]_i = -\eta'_i(z)\,\varepsilon'_i\, Y_\Sigma^{\rm Eq}(z_0)\,, \tag{4.104}$$

where the efficiency functions can be directly read from (4.103) by taking into account that, as usual, they have been normalized to the scalar triplet equilibrium distribution evaluated at z_0.

The evolution of these asymmetries, however, does not describe the evolution of the actual $B/3 - L_\alpha$ asymmetries but instead, as can be seen in (4.100), of a superposition which involves the triplet asymmetry as well. A meaningful description requires switching back to the non-primed variables, which yields

$$\Delta\vec{Y}(z) = -\int_{z_0}^{z} dz' \,\frac{\gamma_D(z')}{\gamma_D(z') + 4\gamma_A(z')}\frac{dY_\Sigma(z')}{dz'}\, e^{-\int_{z'}^{z} dz'' D(z'')\mathscr{M}(z'')}\,\vec{\varepsilon}\,, \tag{4.105}$$

where we used $\mathscr{P}e^{\hat{\mathscr{M}}}\mathscr{P}^{-1} = e^{\mathscr{M}}$. In the non-primed basis the matricial damping factor is no longer diagonal and therefore defining efficiency functions, as it was done in the primed basis, is no longer possible : $B/3 - L_{a,b,c}$ are a superposition of three terms weighted by the corresponding CP-asymmetries $\epsilon_\Delta^{\ell_{a,b,c}}$. Let us discuss this in more detail. The i-th component of the asymmetry vector in (4.105) can be written as

$$\left[\vec{Y}_\Delta(z)\right]_i = -\int_{z_0}^{z} dz' \,\frac{\gamma_D(z')}{\gamma_D(z') + 4\gamma_A(z')}\frac{dY_\Sigma(z')}{dz'}\sum_{k=1,2,3}\left[e^{-\int_{z'}^{z} dz'' D(z'')\mathscr{M}(z'')}\right]_{ik}\varepsilon_k\,, \tag{4.106}$$

thus implying that the flavored asymmetries become

$$\begin{aligned}
\Delta Y_{B/3-L_a}(z) &= -\left[\eta_{aa}(z)\epsilon_\Delta^{\ell_a} + \eta_{ab}(z)\epsilon_\Delta^{\ell_b} + \eta_{ac}(z)\epsilon_\Delta^{\ell_c}\right] Y_\Sigma^{\rm Eq}(z_0)\,, \\
\Delta Y_{B/3-L_b}(z) &= -\left[\eta_{ba}(z)\epsilon_\Delta^{\ell_a} + \eta_{bb}(z)\epsilon_\Delta^{\ell_b} + \eta_{bc}(z)\epsilon_\Delta^{\ell_c}\right] Y_\Sigma^{\rm Eq}(z_0)\,, \\
\Delta Y_{B/3-L_c}(z) &= -\left[\eta_{ca}(z)\epsilon_\Delta^{\ell_a} + \eta_{cb}(z)\epsilon_\Delta^{\ell_b} + \eta_{cc}(z)\epsilon_\Delta^{\ell_c}\right] Y_\Sigma^{\rm Eq}(z_0)\,,
\end{aligned} \tag{4.107}$$

with the flavored efficiency functions defined as :

$$\eta_{\alpha\beta}(z) = \frac{1}{Y_\Sigma^{\rm Eq}(z_0)} \int_{z_0}^{z} dz' \, \frac{\gamma_D(z')}{\gamma_D(z') + 4\gamma_A(z')} \frac{dY_\Sigma(z')}{dz'} \left[e^{-\int_{z'}^{z} dz'' D(z'') \mathscr{M}(z'')} \right]_{\alpha\beta} . \tag{4.108}$$

It is interesting to note that even if one (or even two) CP-asymmetry vanishes, e.g. $\epsilon_\Delta^{\ell_c} \to 0$, an asymmetry will develop in this flavor anyway, provided that the efficiency is not zero. So, once lepton flavors are taken into account the efficiencies are in general no longer flavor diagonal. The presence of the flavor off-diagonal efficiencies is a manifestation of flavor coupling which persists even when $C^\ell = \mathbb{1}$ due to the intricate structure of the matrix $\mathscr{M}$.

More precisely, as already said above, this occurs because, in contrast to the type-1 Seesaw leptogenesis case, an asymmetry in the state generating the $B-L$ asymmetry develops (ΔY_Δ), and so an additional Boltzmann equation accounting for this asymmetry turns out to be mandatory. Due to the presence of this equation the asymmetries in flavor a, b, c are indirectly coupled, and such coupling becomes manifest in the exponential function in Eq. (4.108). In other words, this is the precise reason why, unlike standard leptogenesis, flavor coupling effects are unavoidable in scalar triplet leptogenesis ! [15]

[15] A specific case where flavored efficiency functions, in the same sense of (4.104), can be properly defined corresponds to a purely flavored leptogenesis (PFL) scenario, see section 4.5.

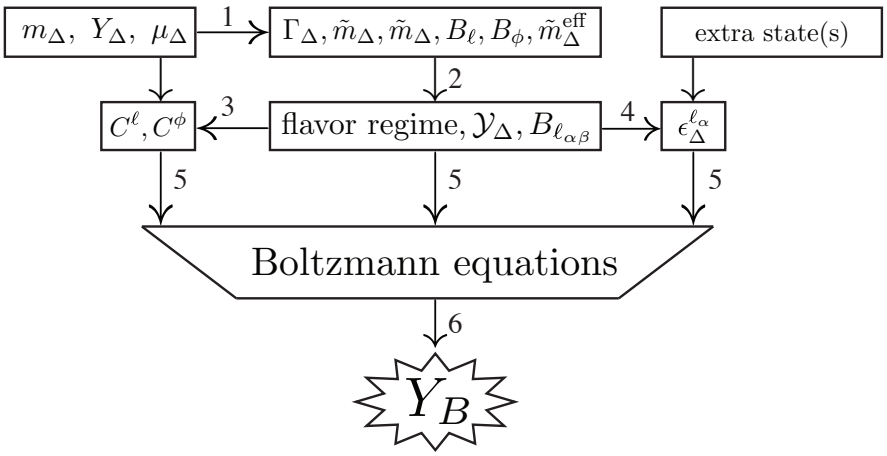

Figure 4.16 – Sketch of the procedure to follow to take into account flavor effects in any given type-2 Seesaw model, where the lightest triplet Δ is responsible for the generation of the baryon asymmetry.

4.4 Summary : leptogenesis procedure to follow in any given type-2 Seesaw model

As we have seen, the type-2 leptogenesis is clearly more complex that the standard type-1 leptogenesis. On top of the fact that scalar triplet undergoes gauge reactions, carries in general an asymmetry and decays through two different channels (di-lepton and do-scalar ones), we have shown in section 4.2 that flavor effects are always present during all the leptogenesis era. It is therefore necessary to provide a clear procedure to follow for a reader who would need to compute the baryon asymmetry produced from some given parameter inputs.

The procedure is summarized in Fig. 4.16 below. From the knowledge of the fundamental parameters of the Lagrangian m_Δ, Y_Δ and μ_Δ, where Δ is the scalar triplet responsible for leptogenesis, one must follow the following steps :

1. From Eqs. (4.9) and (4.10) in page 115, one can determine the partial decay rates to leptons and scalars respectively. As a consequence, one can determine the B_ℓ and B_ϕ, as well as $\tilde{m}_\Delta$ and $\tilde{m}_\Delta^{\rm eff}$ from Eqs. (4.12) and (4.13), page 115.

2. From Fig. 4.10 in page 135, one can determine what is the flavor regime to be considered.

   - In the case where the full-diagonal regime applies, one must compute the new Yukawa matrix $\mathscr{Y}_\Delta = R^* Y_\Delta R^\dagger$, where R is a unitary matrix that diagonalizes Y_Δ, i.e. $\mathscr{Y}_\Delta$ must be brought into the form as in Eq. (4.56).
   - In the case where the semi-diagonal regime applies, one must compute the new Yukawa matrix $\mathscr{Y}_\Delta = R^* Y_\Delta R^\dagger$, where $R = {\rm diag}[S,1]$ is a unitary matrix such that S diagonalizes the (e,μ) bloc of the matrix Y_Δ, i.e. $\mathscr{Y}_\Delta$ must have the form as in Eq. (4.57).
   - In the case where the general regime applies, one has simply $\mathscr{Y}_\Delta = Y_\Delta$.

   Now that the matrix elements of $\mathscr{Y}_\Delta$ are known, one can determine the $B_{\ell_{\alpha\beta}}$ matrix elements from Eq. (4.68), page 138.

3. Together with the mass value m_Δ, one has also access to the value of the C^ℓ and C^ϕ matrices for the associated temperature regime from Table 4.1, page 144.

4. One must then compute the values of the flavored CP-asymmetries, using the triplet's Yukawa matrix $\mathscr{Y}_\Delta$. These depend on the extra heavy states (scalar triplet or right-handed neutrinos) which allow to have non-vanishing CP-asymmetries.

   - In the case these are extra scalar triplets, flavored CP-asymmetries are given by Eqs. (4.69)-(4.71), page 138.
   - In the case these are extra right-handed neutrinos, flavored CP-asymmetries are given by Eq. (4.77), page 140.

5. One has now all the ingredients to compute numerically the $B/3-L_\alpha$ asymmetries produced at the end of leptogenesis from the Boltzmann equations in Eqs. (4.89)-(4.91), page 145.

6. The final baryon asymmetry as observed today is finally related to the $B/3-L_\alpha$ asymmetries through Eq. (4.93), page 145.

We will now study the phenomenology of the flavored scalar triplet leptogenesis. In order to illustrate how scalar triplet flavored leptogenesis works, we will analyze two scenarios in the next sections. [16]

(i) A scenario where the extra degrees of freedom correspond to additional scalar triplets, with the lepton number conserving flavored CP-asymmetries naturally dominating the generation of the $B-L$ asymmetry : this is the *Purely Flavored Leptogenesis (PFL) scenario* we will analyze in section 4.5 [257, 258, 259, 260].

(ii) *General triplet leptogenesis models* involving lepton number violating CP-asymmetries stemming from the presence of any Seesaw state heavier than the decaying scalar triplet (right-handed neutrinos or extra scalar electroweak triplets). This will be analyzed in section 4.6.

4.5 Purely Flavored Leptogenesis

As previously argued (see Eq. (4.76) and the corresponding discussion in section 4.3.2), when the scalar triplet CP-asymmetries arise from the presence of another scalar triplet, there exists an overall regime in which the purely flavored CP-asymmetries are larger than the lepton number violating CP-asymmetries, thus leading to a natural realization of a PFL successful scenario (to a very good approximation). Strictly speaking, PFL scenarios are defined by the condition $\sum_\alpha \epsilon_\Delta^{\ell_\alpha} = 0$ [257]. However, in a more general fashion, whenever the condition $|\sum_\alpha \epsilon_\Delta^{\ell_\alpha}| < |\epsilon_\Delta^{\ell_\beta}|$ (for any given value of β) is satisfied a PFL scenario can be defined as well. This is actually the condition which is generically satisfied, as soon as Eq. (4.76) holds, i.e. if one or both scalar triplets couple substantially less to scalars than they do to leptons, $\mu_{\Delta_k}/m_{\Delta_k} \ll Y_{\Delta_k}$ or equivalently $B_\phi^k \ll B_\ell^k$. This condition is interesting since it is also the one needed to provide large rate for the Charged Lepton Violation processes, as we will discuss in section 4.7 below.

Since there are a lot of parameters in the game, it is in general difficult to make a general analysis. This is why, for concreteness and in order to analyze as well as to demonstrate the viability of this scenario, we will fix the triplet mass spectrum to be hierarchical ($m_{\Delta_1} \ll m_{\Delta_\beta}$ with $1 < \beta$) and assume that the $B-L$ asymmetry is entirely due to the dynamics of the lightest state $\Delta \equiv \Delta_1$ (henceforth we drop the triplet generation index). For simplicity, we will also consider the example of a two-flavored regime situation where the $B-L$ asymmetry is distributed along the τ and a lepton flavor directions (a being an admixture of μ and e flavors). That is, we suppose that the semi-diagonal regime applies, in which the third lepton flavor "b" doesn't play any role during leptogenesis. [17] This could be the case if the couplings involving the flavor b are much smaller than the one involving a and τ flavors. This hypothesis is not mandatory, but it will allow us to understand the main features of this PFL scenario.

[16] A scheme of item (ii) has been already studied in the context of $SO(10)$-inspired left-right symmetric models in Ref. [253]. However, our analysis differs from the one presented in [253] in that the $B-L$ asymmetry in their case is entirely dictated by the lightest and next-to-lightest right-handed neutrinos, whereas in the analysis we will carry out the $B-L$ yield is driven only by the scalar triplet.

[17] This is also equivalent of taking a two-flavor approximation, in which we sum over the a and b flavors, in parallel to the one-flavor approximation studied in section 4.1.

In order to lie in the semi-diagonal regime, this scenario requires leptogenesis to occur at $T^{\mu}_{\rm decoh} \leq T \leq T^{\tau}_{\rm decoh}$ (see section 4.2.1), [18] and furthermore it requires more than a dominance of the purely flavored CP-asymmetries. Since the sum of the purely flavored CP-asymmetries vanishes (total lepton number is conserved), if there were only source terms, a net non-vanishing $B-L$ asymmetry would not develop due to an exact cancellation among the different $B/3-L_\alpha$ asymmetries. This cancellation has to be mandatorily avoided in order that a net non-vanishing total $B-L$ asymmetry develops.

In the type-1 Seesaw leptogenesis, this is possible due to the lepton flavor dependence of the washout effect, which allows the $B/3-L_\alpha$ asymmetries to be washed out in different amounts. In other words, the production of a net $B-L$ asymmetry in the PFL type-1 Seesaw case, which involves L-conserving CP-asymmetries as well, is closely related to the action of L-violating inverse decay rates larger than the Hubble Universe expansion rate (fast L-violating inverse decays), so that they reprocess the $B/3-L_\alpha$ asymmetries in different amounts, in such a way that these asymmetries do not compensate each other anymore.

In the type-2 Seesaw scenario, a similar effect is also possible provided decay/inverse decay to leptons and to scalars reach thermal equilibrium at some stage during the production of the $B-L$ asymmetry, so that L-violating processes do induce a washout. Additionally, and this is a new effect which does not exist in the PFL type-1 scenario, this is also possible even if the L-breaking inverse decay processes present in the heat bath never reach thermal equilibrium !

4.5.1 Mechanism

Let us explain already at this point how does this new effect work. To this end, we display in Fig. 4.17 the evolution of the different abundances as a function of $z = m_\Delta/T$ for the following parameter choice : [19]

$$\begin{aligned} &m_\Delta = 10^9\,\text{GeV}\,, && \tilde{m}_\Delta = 10^{-2}\,\text{eV}\,, && B_\phi = 10^{-4}\,, \\ &\epsilon^{\ell}_{\Delta} \equiv \epsilon^{\ell_\tau}_{\Delta} = -\epsilon^{\ell_a}_{\Delta} = 1\,, && B_{\ell_{aa}} = B_{\ell_{a\tau}} = 0\,, && B_{\ell_{\tau\tau}} = 1 - B_\phi\,. \end{aligned} \tag{4.109}$$

As we will discuss further on in this section, this $B_{\ell_{\alpha\beta}}$ flavor configuration actually maximizes the final efficiency.

Fig. 4.14 (left-hand side plot) clearly shows that for $B_\phi = 10^{-4}$ the inverse decays $\phi\phi \to \Delta$ have always a rate slower than the Hubble expansion rate. The fact that for the type-2 PFL case, we do get nevertheless a net non-vanishing $B-L$ asymmetry can then at first sight appear counterintuitive. If for instance only the channel to leptons does get in thermal equilibrium, as it turns out to be the case for $B_\phi = 10^{-4}$, the scalar triplets have effectively lepton number $L=-2$ and the only active (fast) inverse decays in the thermal bath, $\Delta \to \bar{\ell}\bar{\ell}$ and $\bar{\Delta} \to \ell\ell$, do not break total lepton number.

[18] Note that in the regime where all the charged lepton SM Yukawa interactions are in thermodynamic equilibrium ($T \ll 10^5$ GeV) lepton flavor equilibrating processes from generation-mixing interactions would render this PFL scenario unviable [259].

[19] Using Eq. (4.66), this choice corresponds to $B_\ell \tilde{m}^{\rm eff}_\Delta = 1$ eV. From Fig. 4.10, this parameter choice ensures the $B-L$ asymmetry generation process to take place in the semi-diagonal regime, where Eqs. (D.73) and (D.74) hold.

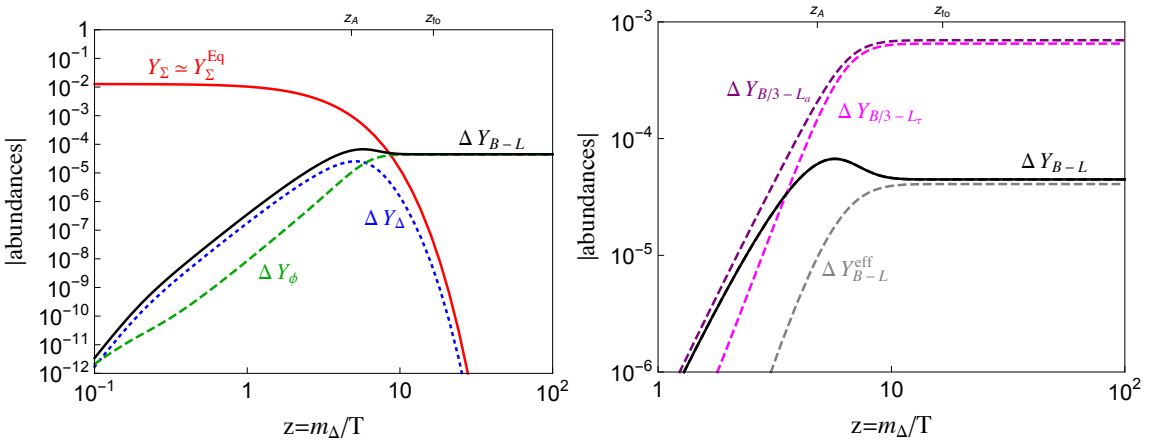

Figure 4.17 – Evolution of the different quantities Y_Σ, ΔY_Δ, ΔY_{B-L}, ΔY_ϕ and $\Delta Y_{B-L}^{\rm eff}$ as given by Eq. (4.110), as a function of $z = m_\Delta/T$ for the flavor configuration : $B_{\ell_{aa}} = B_{\ell_{a\tau}} = 0$, $B_{\ell_{\tau\tau}} = (1 - B_\phi)$. The remaining parameters have been fixed according to: $m_\Delta = 10^9$ GeV, $\tilde{m}_\Delta = 10^{-2}$ eV and $B_\phi = 10^{-4}$.

However, although the scalar doublet channel never reaches thermal equilibrium, still a portion of the scalar triplets in the heat bath undergoes decays to scalar doublets ($\Delta \to \phi\phi$), and these processes do break L. If the processes $\Delta \to \phi\phi$ and $\bar{\Delta} \to \bar{\phi}\bar{\phi}$ take place at different rates, the thermal bath gets a fraction of total lepton number each time these reactions occur. Quantitatively, since $\Delta \to \phi\phi$ and $\Delta \to \bar{\ell}\bar{\ell}$ are the only processes to violate this effective $B-L$ number, this means that we can define an effective $B-L$ yield, $\Delta Y_{B-L}^{\rm eff}$, determined by the counting of how many scalar triplets decay times their branching ratio into scalar doublets, namely

$$\Delta Y_{B-L}^{\rm eff}(z) \simeq -2 \int_{z_0}^{z} \frac{dz'}{sHz'} \frac{\Delta Y_\Delta}{Y_\Sigma^{\rm Eq}} B_\phi \gamma_D \,, \tag{4.110}$$

where the factor 2 comes from the fact that the decay to scalar doublets violates lepton number by 2 units. This effective quantity holds for the total $B-L$ asymmetry available if one assigns to Δ ($\bar{\Delta}$) a lepton number equal to -2 (2), as we have previously pointed out. It is related to the usual $B-L$ yield (where triplets have vanishing lepton number) according to

$$\Delta Y_{B-L}(z) = -2\Delta Y_\Delta(z) + \Delta Y_{B-L}^{\rm eff}(z) \,. \tag{4.111}$$

Since ultimately all triplets decay (their density vanishes), the final $B-L$ asymmetry simply reads

$$\Delta Y_{B-L}^{\rm end} = \Delta Y_{B-L}^{\rm eff}(z \to \infty) \simeq -2 \int_{z_0}^{\infty} \frac{dz'}{sHz'} \frac{\Delta Y_\Delta}{Y_\Sigma^{\rm Eq}} B_\phi \gamma_D \,. \tag{4.112}$$

In order to prove that this formula reproduces the correct $B-L$ asymmetry yield at freeze-out, we have inserted in Eq. (4.110) the ΔY_Δ asymmetry obtained by solving numerically the set of Boltzmann equations. The result is shown in Fig. 4.17 (right panel) by the dashed gray curve. It clearly shows that Eq. (4.112) reproduces very well the numerical result (solid black curve) for the $B-L$ asymmetry yield at freeze-out, up to a small deviation of order 10%. This deviation can be fully traced back to the effect of the inverse decay processes, $\phi\phi \to \Delta$ and $\bar{\phi}\bar{\phi} \to \bar{\Delta}$, i.e. of the term

proportional to B_ϕ in Eq. (4.89). These scalar inverse decays are not as numerous as scalar decays, because they are Boltzmann suppressed, but they are not negligible either.

As Eq. (4.112) shows, the generation of a baryon asymmetry, through decays rather than through inverse decay washout effects, is thus closely related to the possibility of creating a scalar triplet asymmetry (something obviously not possible for a right-handed neutrino due to its Majorana nature). The role of flavor effects is in fact to generate such a triplet asymmetry. To see that, it is useful to write down the relevant terms in Eq. (4.90),

$$\Delta\dot{Y}_\Delta \supset \sum_k \sum_\alpha B_{\ell_\alpha} C^\ell_{\alpha k} \frac{\Delta Y_k}{Y^{\rm Eq}_\ell} \gamma_D \,. \tag{4.113}$$

This expression clearly shows that a triplet asymmetry can be generated by two kinds of flavor effects :

A. The first possibility arises if the $C^\ell_{\alpha k}$ have a flavor structure. For instance, if the τ Yukawa is in equilibrium, once a lepton doublet ℓ_τ is produced, it has the time to interact through the Yukawa coupling and a fraction of the τ flavor is transferred from ℓ_τ lepton doublets to e_τ lepton singlets, while this is not the case for flavor a. These transferred fractions are just given by the C^ℓ matrices which are dictated by the chemical potential equilibrium equations, see Eq. (4.87). This means that there are less ℓ_τ than ℓ_a lepton doublets available for inverse decays to scalar triplets. So, even if there is no flavor structure in the branching ratios (i.e. $B_{\ell_a} = B_{\ell_\tau}$) and even if, at the onset, $\Delta Y_{L_\tau} = -\Delta Y_{L_a}$, the number of Δ produced is different from the number of $\bar{\Delta}$ produced because their production rate is proportional to $Y_{\bar{\ell}_\tau} + Y_{\bar{\ell}_a}$ and $Y_{\ell_\tau} + Y_{\ell_a}$ respectively, which are unequal. [20]

B. The second possibility arises from the flavor structure of scalar triplet decays, i.e. the B_{ℓ_α}. If $B_{\ell_a} \neq B_{\ell_\tau}$, a triplet asymmetry can be produced even if the C^ℓ coefficients do not distinguish the a and τ flavors. In this case, even if at the onset, $\Delta Y_{L_\tau} = -\Delta Y_{L_a}$, with for example $B_\tau \gg B_a$ and $Y_{L_\tau} > 0$, inverse decays involving the τ flavor are much more frequent than those involving the a flavor and inverse decays $\ell_\tau \ell_{a,\tau} \to \bar{\Delta}$ occur more frequently than $\ell_a \ell_{a,\tau} \to \bar{\Delta}$ inverse decays, resulting in the generation of a ΔY_Δ asymmetry (of negative sign in this case).

In other words, even if in the PFL case there is no L-violating CP- asymmetry, a final $B-L$ asymmetry can be generated in this case, even without L-violating processes attaining thermal equilibrium, i.e. even if $B_\phi \ll B_\ell$. The mechanism can be understood as a three step process, summarized in Fig. 4.18. **Firstly**, an asymmetry $\Delta Y_{L_\tau} = |\Delta Y_{L_a}| \neq 0$ is created from the source term in Eq. (4.91). **Secondly**, thanks to flavor effects, this asymmetry induces a triplet asymmetry via Eq. (4.113), due to the flavor structure encoded in $C^\ell_{\alpha k}$ and/or due to the flavor structure encoded in the B_{ℓ_α}. And **finally**, once a scalar triplet asymmetry is created, a $B-L$ asymmetry develops in turn because each time a triplet (anti-triplet) decays to scalars, a pair less of anti-leptons (leptons)

[20] It is worth noting that we have the same reprocessing concerning the ϕ asymmetry created from the slow Δ decays. This latter asymmetry is partly reprocessed through L-conserving SM Yukawa interactions into chiral asymmetries for charged leptons, which modifies back the Δ asymmetry, hence the number of Δ decaying into SM scalars, hence the $B-L$ asymmetry. This effect is nevertheless mild, since $B_\phi \ll B_\ell$ in this PFL case.

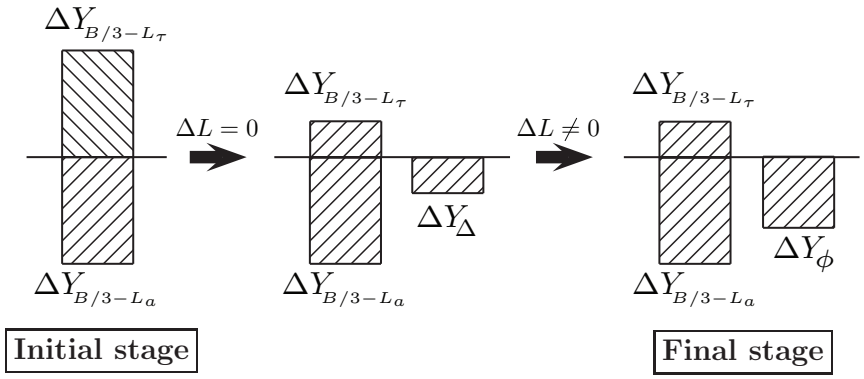

Figure 4.18 – Sketch of the type-2 PFL mechanism. See text for further details.

is produced back from the decay of a triplet (anti-triplet). The more ΔY_Δ asymmetry is produced, the bigger the efficiency. This PFL production mechanism, based on the chain of processes $\ell_\alpha \ell_\beta \leftrightarrow \bar{\Delta} \rightarrow \bar{\phi}\bar{\phi}$ and $\bar{\ell}_\alpha \bar{\ell}_\beta \leftrightarrow \Delta \rightarrow \phi\phi$, is therefore very different from the PFL type-1 scenario. It stems from the fact that in the type-2 scenario, a Seesaw state asymmetry develops, and in its last step this asymmetry generates a final $B-L$ asymmetry from a production mechanism which is due to out-of-thermal equilibrium decays ($B_\phi \ll B_\ell$), i.e. from the L-violating processes $\Delta \rightarrow \phi\phi$ and $\bar{\Delta} \rightarrow \bar{\phi}\bar{\phi}$. [21]

Let us emphasize once again that this $B_\phi \ll 1$ case is the situation which leads naturally to PFL, since this condition leads to a natural dominance of the purely flavored CP-asymmetries. It must be noted that PFL could nevertheless work for larger values of B_ϕ too, in a way more similar to the more involved PFL scenarios in the type-1 context, see section 4.5.2 below.

In the following subsection we will analyze, along these lines, the efficiency dependence upon the relevant parameters. We will discuss in particular the flavor configurations which minimize, or maximize, the production of ΔY_Δ. We will then discuss the flavored CP-asymmetry parameter dependence and show how the configurations that maximize the efficiency minimize the flavored CP-asymmetry. The production of the $B-L$ asymmetry, which is given by the product of the flavored CP-asymmetry and the efficiency, results therefore from the balance of both effects.

4.5.2 PFL scenario efficiency

Interestingly, in this PFL scenario within a two-flavor approximation, it is possible to define flavor efficiencies. What actually happens in this case is that due to the PFL condition $\sum_\alpha \epsilon_\Delta^{\ell_\alpha} = 0$, which implies $\epsilon_\Delta^\ell \equiv -\epsilon_\Delta^{\ell_a} \approx \epsilon_\Delta^{\ell_\tau}$, the off-diagonal efficiency functions can be hidden by suitable

[21] This production mechanism driven by a tiny coupling is in many ways similar to the dark matter freeze-in production mechanism, as Eq. (4.112) shows. However there are important differences. Firstly, this equation involves as a source term an asymmetry, ΔY_Δ, and not the symmetric component of a particle species as in the freeze-in scenario. Secondly, since we are dealing with decay rates much larger that the one of the dark matter freeze-in, still a small amount of inverse decays occurs, as we have pointed out.

redefinitions, see Eq. (4.107) :

$$\Delta Y_{B/3-L_a}(z) = \left[\eta_{aa}(z) - \eta_{a\tau}(z)\right]\epsilon_\Delta^\ell\, Y_\Sigma^{\rm Eq}(z_0) \to \eta_a(z)\,\epsilon_\Delta^\ell\, Y_\Sigma^{\rm Eq}(z_0)\,,$$
$$\Delta Y_{B/3-L_\tau}(z) = \left[\eta_{\tau a}(z) - \eta_{\tau\tau}(z)\right]\epsilon_\Delta^\ell\, Y_\Sigma^{\rm Eq}(z_0) \to \eta_\tau(z)\,\epsilon_\Delta^\ell\, Y_\Sigma^{\rm Eq}(z_0)\,, \tag{4.114}$$

and so the total $B-L$ asymmetry can be written as

$$\Delta Y_{B-L}(z) = \eta(z)\,\epsilon_\Delta^\ell\, Y_\Sigma^{\rm Eq}(z_0) = \left[\eta_a(z) + \eta_\tau(z)\right]\epsilon_\Delta^\ell\, Y_\Sigma^{\rm Eq}(z_0)\,, \tag{4.115}$$

with the final value (the value at freeze-out) given by $\Delta Y_{B-L}^{\rm end} = \Delta Y_{B-L}(z\to\infty)$. The problem of quantifying the final efficiency $\eta \equiv \eta_a + \eta_\tau$ – defined in Eq. (4.115) and taking $z\to\infty$ to get the final value – is in principle an eight parameters problem : $\epsilon_\Delta^{\ell_{\tau,a}}$, m_Δ, $\tilde{m}_\Delta$, B_ϕ, $B_{\ell_{aa}}$, $B_{\ell_{\tau\tau}}$ and $B_{\ell_{a\tau}}$, which reduces to six parameters due to the constraints $B_\ell + B_\phi = 1$ and $\epsilon_\Delta^\ell \equiv \epsilon_\Delta^{\ell_\tau} = -\epsilon_\Delta^{\ell_a}$. Since the efficiency does not depend on ϵ_Δ^ℓ – see Eq. (4.115) – we will analyze the dependence of the efficiency upon the 5 remaining parameters: m_Δ, $\tilde{m}_\Delta$, B_ϕ, $B_{\ell_{aa}}$ and $B_{\ell_{\tau\tau}}$.

We start by analyzing the dependence upon $B_{\ell_{\alpha\beta}}$ for fixed B_ϕ, m_Δ and $\tilde{m}_\Delta$. Different flavor configurations $B_{\ell_{\alpha\beta}}$ will produce a minimal or maximal efficiency. However, as we will show latter, the configurations that maximize the efficiency do not necessarily maximize the final $B-L$ asymmetry. We then proceed by analyzing the dependence of the efficiency with $\tilde{m}_\Delta$ for fixed B_ϕ, m_Δ and $B_{\ell_{\alpha\beta}}$, and finally the dependence of the efficiency with B_ϕ for fixed $\tilde{m}_\Delta$, m_Δ and $B_{\ell_{\alpha\beta}}$. This will allow us to understand and distinguish the main features of the type-2 Seesaw PFL scenario.

∘ $B_{\ell_{\beta\gamma}}$ dependence of the efficiency.

In order to proceed, we first solve numerically the system of kinetic equations in (4.89)-(4.91) for different flavor configurations. We then provide some physical arguments supporting the special flavor configurations that maximize/minimize the efficiency. For concreteness, we fix three out of the five relevant parameters as follows :

$$m_\Delta = 10^9\,{\rm GeV}\,, \quad \tilde{m}_\Delta = 10^{-2}\,{\rm eV}\,, \quad B_\phi = 10^{-4}\,. \tag{4.116}$$

Once these parameters are fixed, the efficiency is entirely dictated by the flavor configurations determined by the values of the $B_{\ell_{\alpha\beta}}$ parameters. It turns out that the flavor dependence is well described by the quantity :

$$R \equiv \frac{B_{\ell_a}}{B_{\ell_\tau}} = \frac{B_{\ell_{aa}} + B_{\ell_{a\tau}}}{B_{\ell_{\tau a}} + B_{\ell_{\tau\tau}}}\,, \tag{4.117}$$

which represents the ratio of triplet decay branching ratios to different lepton-flavor final states. The importance of this quantity can be understood from Eq. (4.113), where we see that it is precisely through the B_{ℓ_a} that a triplet asymmetry is generated. We plot in Fig. 4.19 the efficiency as a function of this parameter R for the parameters fixed according to Eq. (4.116). It clearly shows that the efficiency exhibits four special configurations, namely $(i,\, ii)$ two global maxima at $R \ll 1$ and $R \gg 1$, (iii) one local maximum and (iv) one global minimum near $R \sim 1$. We now aim to understand the physical reasons behind these special configurations.

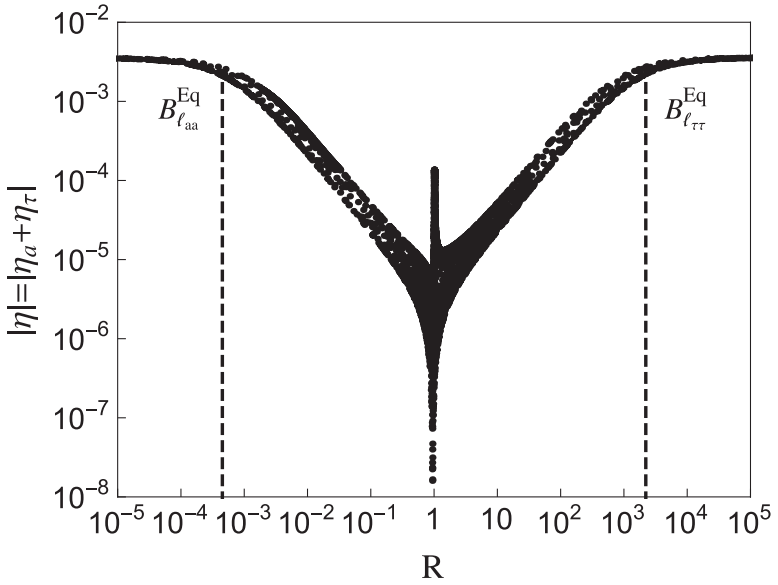

Figure 4.19 – Efficiency as a function of the R parameter for $m_\Delta = 10^9$ GeV, $\tilde{m}_\Delta = 10^{-2}$ eV and $B_\phi = 10^{-4}$. The vertical dashed line at the left (right) shows the value below (above) which the $\ell_a\ell_a \to \bar{\Delta}$ ($\ell_\tau\ell_\tau \to \bar{\Delta}$) inverse decays never reach thermal equilibrium.

• **Configurations (i) and (ii) :** following Eq. (4.117), these global maxima correspond to the flavor alignments $B_{\ell_a} \ll B_{\ell_\tau}$ and $B_{\ell_a} \gg B_{\ell_\tau}$. The effect seems entirely driven by the B_{ℓ_α}, so we will not consider the possible effects of the $C^\ell_{\alpha k}$ and C^ϕ_k elements in the analysis. More precisely, these maxima are reached whenever the inverse decays involving the a or τ flavor never enter in thermal equilibrium, i.e. for $B_{\ell_{\alpha\alpha}} < B^{\rm Eq}_{\ell_{\alpha\alpha}}$ where $B^{\rm Eq}_{\ell_{\alpha\alpha}}$ is determined by :

$$B^{\rm Eq}_{\ell_{\alpha\alpha}} \left.\frac{\gamma_D}{H n^{\rm Eq}_\ell}\right|_{\rm max} = 1 \quad \text{which gives} \quad B^{\rm Eq}_{\ell_{\alpha\alpha}} \approx 5\cdot 10^{-4}\,, \tag{4.118}$$

where we used in this last expression the parameter values given in Eq. (4.116). This value is in good agreement with the numerical results shown in Fig. 4.19, where the two maxima are reached for $R \lesssim 5\cdot 10^{-4}$ and $R \gtrsim 2\cdot 10^3$. For these configurations, only the asymmetry produced in one flavor is transferred through inverse decays $\ell_\alpha\ell_\alpha \to \bar{\Delta}$ to a triplet asymmetry, which is therefore maximal since the two flavor asymmetries have opposite signs. As a consequence, one asymmetry is depleted through the chain $\ell_\alpha\ell_\alpha \leftrightarrow \bar{\Delta} \to \bar{\phi}\bar{\phi}$, while the other flavor asymmetry remains unaffected, clearly leading to a maximal efficiency.

• **Configuration (iii) :** this local maximum is in fact reached for $R \approx 1$ when $B_{\ell_{aa}}, B_{\ell_{\tau\tau}} \ll B_{\ell_{a\tau}}$. In this configuration, only the inverse decays $\ell_a\ell_\tau \to \bar{\Delta}$ reach thermal equilibrium, and one expects no production of a triplet asymmetry, and therefore no production of a final $B-L$ asymmetry, since the flavor asymmetries are depleted by the same amount. However, this is not the case because the $C^\ell_{\alpha k}$ elements have a flavor structure, which here plays a crucial role. The point is that when inverse decays are in thermal equilibrium, the combination of processes $\ell_a\ell_\tau \leftrightarrow \bar{\Delta} \to \bar{\phi}\bar{\phi}$ and $\bar{\ell}_a\bar{\ell}_\tau \leftrightarrow \Delta \to \phi\phi$ tends to equilibrate the flavor asymmetries in lepton doublets $\Delta Y_{\ell_\tau} \approx -\Delta Y_{\ell_a}$,

while in the meantime decreasing the separated asymmetries by a small amount. [22] But due to the chemical equilibrium conditions, the total lepton flavors asymmetries $\Delta Y_{B/3-L_\alpha}$ are in general different. Indeed, using Eq. (4.87), the total $B-L$ asymmetry at freeze-out is related to the lepton flavor doublet asymmetries through :

$$\Delta Y_{B-L} = \Delta Y_{B/3-L_a} + \Delta Y_{B/3-L_\tau} = -\frac{\Delta Y_{\ell_a}\left(C^\ell_{\tau\tau} - C^\ell_{\tau a}\right) + \Delta Y_{\ell_\tau}\left(C^\ell_{aa} - C^\ell_{a\tau}\right)}{C^\ell_{\tau\tau}C^\ell_{aa} - C^\ell_{a\tau}C^\ell_{\tau a}} \,. \tag{4.119}$$

In the PFL regime, in the case where the final lepton doublet asymmetries are equal and opposite, $\Delta Y_{\ell_\tau} \approx -\Delta Y_{\ell_a}$ (as for the case $B_{\ell_{\alpha\alpha}} = 0$), a final $B-L$ asymmetry can be produced only if the $C^\ell_{\alpha k}$ elements have a flavor structure. This $B-L$ asymmetry can be quite large because the flavor asymmetries in lepton doublets ΔY_{ℓ_α} decrease only slightly for this special configuration.

Any significant deviation from this special configuration, e.g. $B_{\ell_{\alpha\alpha}} > B^{\rm Eq}_{\ell_{\alpha\alpha}}$, would not only tend to equilibrate the flavor asymmetries in the lepton doublets, but also tend to decrease the ΔY_{ℓ_α} separately through the chain $\bar{\ell}_\alpha \bar{\ell}_\alpha \leftrightarrow \Delta \to \phi\phi$. All in all, the efficiency has in consequence a local maximum for $B_{\ell_{a\tau}} \approx (1 - B_\phi)/2$.

• **Configuration (iv) :** shifted to the left of the maximum defining configuration (iii), a minimal efficiency (apparently vanishing efficiency) can be seen, it lies at about $R \approx 3/4$. In order to understand the reason for this configuration to show up, we can look in a first step if analytically the efficiency may vanish for some value of the flavor parameters $B_{\ell_{\alpha\beta}}$. Using Eq. (4.115), we see that a vanishing efficiency is obtained whenever $\eta_\tau(z) = -\eta_a(z)$ for all z, which means through Eq. (4.108) :

$$\sum_{\alpha,\beta=2,4} \left(e^{-\int_{z_0}^z dz' D(z')\mathcal{M}(z')}\right)_{\alpha\beta} (-1)^{1+\beta/2} = 0 \quad \forall z \,, \tag{4.120}$$

which is satisfied as long as all the coefficients of the exponential power series expansion vanish, i.e.

$$\sum_{\alpha,\beta=2,4} \int_{z_0}^z dz' D(z') (-1)^{1+\beta/2} \left[\mathcal{M}_{\alpha\beta}(z') - \frac{1}{2}\int_{z_0}^z dz'' D(z'') \sum_{\gamma=1}^4 \mathcal{M}_{\alpha\gamma}(z')\mathcal{M}_{\gamma\beta}(z'') + \ldots\right] = 0 \,. \tag{4.121}$$

We have found this turns out to be the case if the entries of the matrix $\mathcal{M}$ satisfy the following two conditions

$$\mathcal{M}_{12} = \mathcal{M}_{14} \quad \text{and} \quad \sum_{\alpha,\beta=2,4} (-1)^{1+\beta/2} \mathcal{M}_{\alpha\beta} = 0 \quad (\text{i.e. } \mathcal{M}_{22} - \mathcal{M}_{24} + \mathcal{M}_{42} - \mathcal{M}_{44} = 0) \,, \tag{4.122}$$

where the corresponding elements must not depend on z which is indeed our case, see Eq. (4.98). This result in turn can be understood using Eqs. (4.89) and (4.91). In the two-flavor PFL scenario, since the source terms for both flavors are equal and opposite, a vanishing efficiency will be

[22] Indeed, if $Y_{\ell_a} \cdot Y_{\ell_\tau} > Y_{\bar{\ell}_a} \cdot Y_{\bar{\ell}_\tau}$, that is if $\Delta Y_{\ell_\tau} + \Delta Y_{\ell_a} > 0$, there will be more $\ell_a \ell_\tau \leftrightarrow \bar{\Delta} \to \bar{\phi}\bar{\phi}$ processes than $\bar{\ell}_a \bar{\ell}_\tau \leftrightarrow \Delta \to \phi\phi$ processes, so that statistically $\Delta Y_{\ell_\tau} + \Delta Y_{\ell_a}$ will decrease, as well as the separated asymmetries ΔY_{ℓ_τ} and $|\Delta Y_{\ell_a}|$. This lasts until $\Delta Y_{\ell_\tau} \approx -\Delta Y_{\ell_a}$, and from that moment no more triplet asymmetry can be generated and the asymmetries ΔY_{ℓ_τ} and $|\Delta Y_{\ell_a}|$ are left invariant.

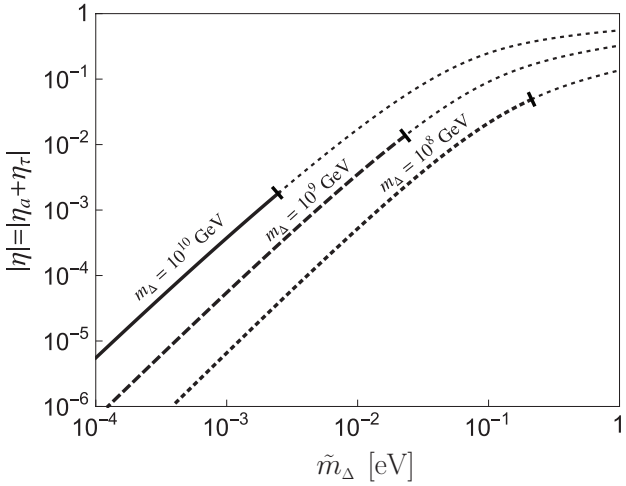

Figure 4.20 – Efficiency as a function of $\tilde{m}_\Delta$ for several values of the scalar triplet mass. The parameters have been fixed according to $B_\phi = 10^{-4}$ and $B_{\ell_{aa}} = B_{\ell_{a\tau}} = 0$. The lines are cut whenever the semi-diagonal regime condition ceases to be fulfilled (see section 4.2.1) – we don't expect however a very different behavior since only the C^ℓ and C^ϕ matrices would change.

generated if the washouts of the two flavors are also equal and opposite, which is nothing but the conditions in Eq. (4.122).

More precisely, for this to be achieved, we need that $\Delta Y_{B/3-L_\tau} = -\Delta Y_{B/3-L_a}$ remains valid at any time. As Eq. (4.91) shows, this requires: (a) $\Delta Y_\Delta = 0$ and (b) $\sum_{\alpha,\beta,k} C^\ell_{\alpha\beta k} B_{\ell_{\alpha\beta}} \Delta Y_k = 0$ at any time. These two relations hold simultaneously if both conditions in Eq. (4.122) are fulfilled. Indeed, if relation (a) holds, (b) can be rewritten as the second condition in Eq. (4.122). On the other hand, if relation (b) holds, (a) can be rewritten using Eq. (4.90) as $\sum_{\alpha,k}(C^\ell_{\alpha k} B_{\ell_\alpha} - B_\phi C^\phi_k)\Delta Y_k = 0$, which is nothing but the first condition in Eq. (4.122).

Using Eq. (4.98), these conditions can be simultaneously fulfilled only in the limit $B_\phi \to 0$, in which case the triplet flavor configuration must satisfy the simple relation :

$$R = \frac{B_{\ell_{aa}} + B_{\ell_{a\tau}}}{B_{\ell_{\tau a}} + B_{\ell_{\tau\tau}}} = \frac{C^\ell_{\tau\tau} - C^\ell_{\tau a}}{C^\ell_{aa} - C^\ell_{a\tau}} \approx 0.74\,. \tag{4.123}$$

Strictly speaking, since $B_\phi \neq 0$, the efficiency is not vanishing for any value of $B_{\ell_{\alpha\beta}}$. However, for small B_ϕ, the efficiency does not vanish exactly anymore but shows now a minimum for $R \approx 3/4$, which is in good agreement with the numerical results shown in Fig. 4.19.

∘ $\tilde{m}_\Delta$ dependence of the efficiency.

By fixing $B_\phi = 10^{-4}$ as in the previous section, and taking as an example $B_{\ell_{aa}} = B_{\ell_{a\tau}} = 0$, and $B_{\ell_{\tau\tau}} = 1 - B_\phi$, we display in Fig. 4.20 the dependence of the efficiency with $\tilde{m}_\Delta$, for the three benchmark triplet masses $m_\Delta = 10^8, 10^9, 10^{10}$ GeV. It can be seen that irrespective of the triplet mass, the smaller $\tilde{m}_\Delta$ the smaller the resulting efficiency. The reason for this behavior follows directly from the relative strength of gauge and Yukawa induced reactions : the larger $\tilde{m}_\Delta$ the most likely triplets will decay rather than scatter, thus implying a larger efficiency.

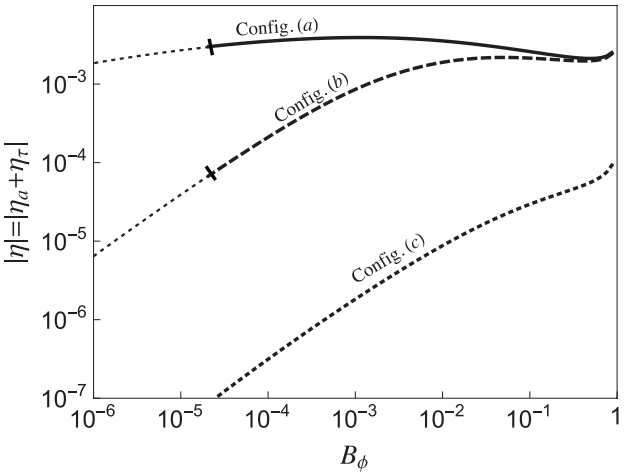

Figure 4.21 – Efficiency as a function of B_ϕ for $m_\Delta = 10^9$ GeV and $\tilde{m}_\Delta = 10^{-2}$ eV. Configuration (a), in solid, corresponds to $B_{\ell_{aa}} = B_{\ell_{a\tau}} = 0$ (i.e. $R = 0$). Configuration (b), in dashed, corresponds to $B_{\ell_{aa}} = B_{\ell_{\tau\tau}}/99 = (1 - B_\phi)/100$ (i.e. $R \simeq 10^{-2}$). Configuration (b), in dotted, corresponds to $B_{\ell_{aa}} = B_{\ell_{\tau\tau}} = (1 - B_\phi)/2$ (i.e. $R = 1$). The lines are cut when the semi-diagonal regime condition ceases to be fulfilled (see section 4.2.1) – we don't expect however a very different behavior since only the C^ℓ and C^ϕ matrices would change.

On the other hand, we see that the efficiency decreases with m_Δ. This is also due to gauge reactions : the smaller m_Δ the most likely the triplet will scatter rather than decay, thus implying a smaller efficiency. More precisely, as for the one-flavor case, when gauge scatterings are faster than decays they suppress $Y_\Sigma - Y_\Sigma^{\rm Eq}$ in Eq. (4.90) by a factor γ_D/γ_A, which implies an equal suppression of the source term in Eq. (4.91).

In the one-flavor approximation one have distinguished two regimes, see section 4.1.6 in page. 122 : the gauge and Yukawa regimes, depending on the values of m_Δ, $\tilde{m}_\Delta$ and B_ϕ. While in the one-flavor approximation a maximum efficiency is obtained at the transition between both regimes, this is in general not anymore the case in the flavored leptogenesis scenario. Depending on the flavor configuration, a maximum efficiency can be obtained far in the Yukawa regime because of flavor effects, see section 4.6 below for a more detailed explanation.

◦ **B_ϕ dependence of the efficiency.**

We present in Fig. 4.21 the dependence of the efficiency upon B_ϕ in the range $[10^{-6}, 1]$ for fixed values of m_Δ and $\tilde{m}_\Delta$. We considered two particular flavor configurations for $B_{\ell_{\alpha\beta}}$. The solid curve – configurations (a) – corresponds to one of the two flavor configurations that maximize the efficiency (see section 4.5.2). The dashed curve – configurations (b) – corresponds instead to the particular configuration $B_{\ell_{aa}} = B_{\ell_{\tau\tau}}/99 = (1 - B_\phi)/100$ and $B_{\ell_{a\tau}} = 0$. The dotted curve (configurations (c)) corresponds to the flavor alignment configuration $B_{\ell_{aa}} = B_{\ell_{\tau\tau}} = (1 - B_\phi)/2$ and $B_{\ell_{a\tau}} = 0$, i.e. without any flavor structure. These three configurations show two different behaviors, that are in fact representative of any other flavor configuration. We now describe briefly their behavior.

For $B_\phi \leq 10^{-1}$, which is the interesting region for this PFL scenario, we can distinguish two distinct regimes. They are separated by $B_\phi^{\rm Eq}$, the value at which the inverse decays $\phi\phi \to \Delta$ become active, determined by the condition

$$B_\phi^{\rm Eq} \left.\frac{\gamma_D}{H n_\ell^{\rm Eq}}\right|_{\rm max} = 1 \quad \text{which gives} \quad B_\phi^{\rm Eq} \approx 5\cdot 10^{-4}\,, \tag{4.124}$$

where we used in the last equality the parameter value domain-of-validity $\tilde{m}_\Delta = 10^{-2}$ eV. The way the efficiency scales with B_ϕ depends on the flavor configurations. For $B_\phi \lesssim B_\phi^{\rm Eq}$ the efficiency always increases with B_ϕ as a result of the fact that the larger B_ϕ the faster the decay to SM scalars, as can be seen in Eq. (4.112), but the exact scaling actually also depends on the interplay of the ΔY_Δ and $\Delta Y_{B/3-L_\alpha}$ asymmetries.

Now, as soon as $B_\phi \gtrsim B_\phi^{\rm Eq}$, inverse decays $\phi\phi \to \Delta$ become efficient, implying that lepton number is broken by processes in thermal equilibrium (fast processes). This brings a new $\sqrt{B_\phi}$ suppression in the efficiency, resulting in an efficiency increasing less with B_ϕ or even decreasing, depending on the flavor configuration, see Fig. 4.21.

To conclude, we see that for the flavor configuration that maximizes the efficiency, the value of B_ϕ which gives the maximal efficiency is obtained for $B_\phi \sim B_\phi^{\rm Eq}$, that is to say for the value of B_ϕ at which the $\phi\phi \to \Delta$ inverse decays are about to be active. In this case, the efficiency can be as large as unity for values of $m_\Delta \gtrsim 10^{12}$ GeV, or less for smaller values of m_Δ (due to the gauge scattering thermalization effect). For other configurations that lead to smaller efficiencies, the maximum efficiency is obtained for much larger values near $B_\phi \sim 1$.

4.5.3 Minimal and maximal $B-L$ asymmetry

As stressed above, a PFL scenario is naturally favored as soon as $\epsilon_{\Delta_1}^{\ell_\alpha(\not{F})}$ dominates the CP-asymmetry, which naturally holds if Yukawa couplings are larger than scalar couplings, i.e. when Eq. (4.76) holds. If leptogenesis is activated by a second scalar triplet Δ_2, this equation can also be recast in terms of the triplet branching ratios to scalar and lepton final states

$$\sqrt{\frac{B_\phi^1 B_\phi^2}{B_\ell^1 B_\ell^2}} \ll \frac{m_{\Delta_1}}{m_{\Delta_2}} \frac{{\rm Tr}[m_\nu^{\Delta_1} m_\nu^{\Delta_2\dagger}]}{\tilde{m}_{\Delta_1}\tilde{m}_{\Delta_2}} \leq \frac{m_{\Delta_1}}{m_{\Delta_2}}\,, \tag{4.125}$$

where the last inequality comes from the Cauchy-Schwarz inequality :

$$|{\rm Tr}\,[AB]| \leq \sqrt{{\rm Tr}\left[AA^\dagger\right]}\sqrt{{\rm Tr}\left[BB^\dagger\right]}\,. \tag{4.126}$$

As an example, taking a smooth triplet mass hierarchy $m_{\Delta_1}/m_{\Delta_2} \sim 10^{-1}$ (10^{-2}) and assuming the upper bound ${\rm Tr}[m_\nu^{\Delta_1} m_\nu^{\Delta_2\dagger}] \approx \tilde{m}_{\Delta_1}\tilde{m}_{\Delta_2}$, a PFL scenario will be naturally dominant as soon as $B_\phi^{1,2} \ll 10^{-1}$ (10^{-2}).

We have seen in the previous sections that the efficiency strongly depends on the flavor parameters $B_{\ell_{\alpha\beta}}$. Explicitly, we have shown that the efficiency has a minimum at $R \approx 3/4$, global maxima at $B_{\ell_{aa}} = B_{\ell_{a\tau}} \approx 0$ and $B_{\ell_{\tau\tau}} = B_{\ell_{a\tau}} \approx 0$, and a local maximum at $B_{\ell_{aa}} = B_{\ell_{\tau\tau}} \approx 0$. However,

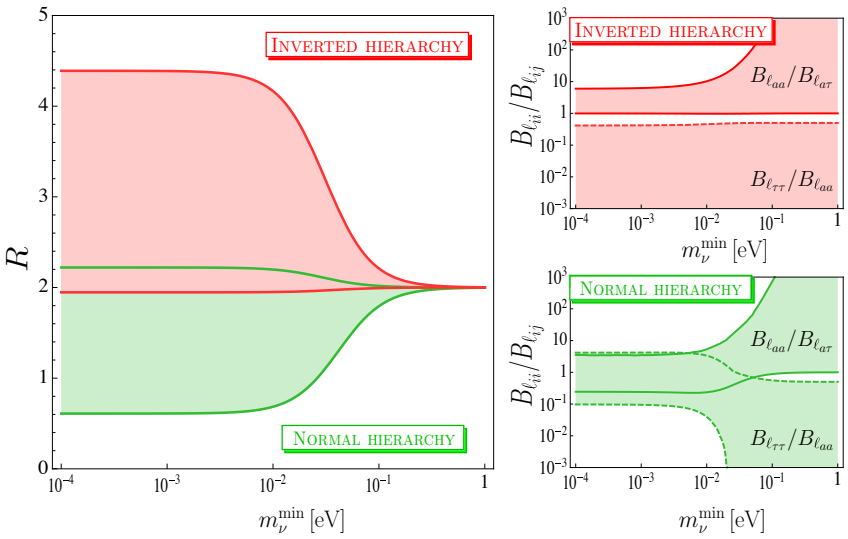

Figure 4.22 – Allowed ranges for R (left plot) and the ratios of branching ratios $B_{\ell_{\beta\beta}}/B_{\ell_{\beta\gamma}}$ (right plots) as a function of the lightest neutrino mass for both normal (green) and inverted mass spectrum (red). The results have been derived by varying the neutrino oscillation parameters in the 3σ range according to Ref. [19].

a maximal efficiency does not imply a maximal $B-L$ asymmetry. Indeed, using Eq. (4.71), we can actually compute a general upper bound for the purely two-flavored CP-asymmetry from Eq. (4.80) :

$$\left|\epsilon_\Delta^\ell\right| \leq 2\, g(m_{\Delta_1}^2/m_{\Delta_2}^2)\left[\sqrt{B_{\ell_{aa}}B_{\ell_{\tau\tau}}}+\sqrt{B_{\ell_{a\tau}}\left(B_{\ell_{aa}}+B_{\ell_{\tau\tau}}\right)}\right], \tag{4.127}$$

where we assumed perturbative Yukawa couplings for the second triplet generation, i.e. $|Y_{\Delta_2}| \leq \sqrt{4\pi}$. [23] This expression shows clearly that the three configurations that maximize the efficiency give vanishing CP-asymmetries ! This can be understood easily from the fact these configurations involve a Yukawa coupling only for one flavor. We see also that the upper bound on the CP-asymmetry is directly related to the hierarchy between the different triplet masses, which is compatible with the requirement in Eq. (4.125), i.e. a smooth triplet mass hierarchy favors PFL scenario and allows for a large CP-asymmetry.

A viable scalar triplet leptogenesis setup requires of course consistency with neutrino data [262, 345, 264, 19]. If the most relevant contribution to the neutrino mass matrix in Eq. (4.7) is given by the lightest triplet, which can be regarded as a quite reasonable possibility (assumption), the determination of the available flavor configurations can be done directly via neutrino oscillation data. We present in Fig. 4.22 the constraints on R (left panel) and on the ratios of branching

[23] The upper bound on the CP-asymmetry depends crucially on the perturbativity condition. Taking instead $|Y_{\Delta_2}| \leq 1$ would lead to the same expression divided by 4π. The upper bound one can take on Y_Δ depends on the scale at which new physics is expected to arise. Indeed, following the perturbativity condition, the Yukawa coupling Y_Δ could eventually become infinite at some scale, which is the case taking $Y_\Delta = \sqrt{4\pi}$. This is the so-called Landau pole, which can be computed using the renormalization group equations given for example in Ref. [261]. Running the RGE's from starting from $Y_\Delta = \sqrt{4\pi}$ at $\Lambda = m_\Delta = 10^9$ GeV (10^6 GeV), the Landau pole is reached at $\Lambda_L \simeq 5\cdot 10^{10}$ GeV (10^8 GeV). Since the scalar triplet extension of the SM is well motivated by BSM physics, we here assume that new physics arises at a scale below the Landau pole, see section 1.6.

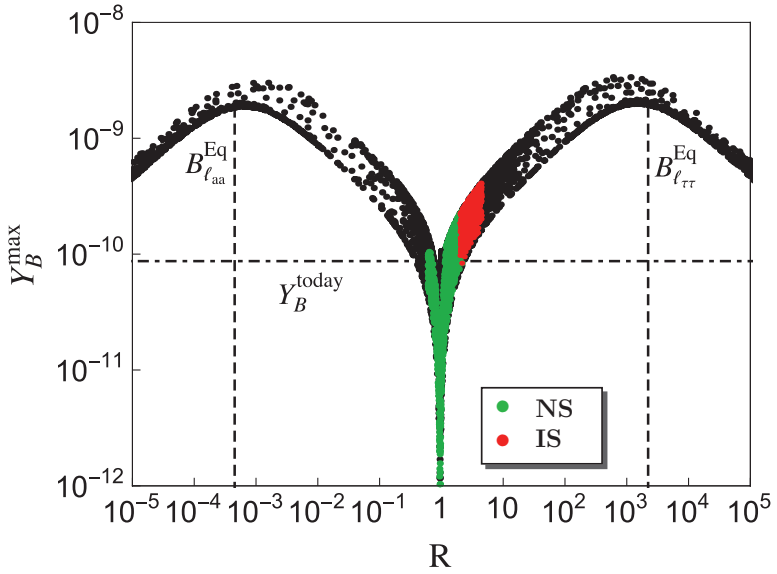

Figure 4.23 – Maximum reachable final $B-L$ asymmetry as a function of the R parameter, for $m_{\Delta_1} = 10^9$ GeV, $m_{\Delta_2} = 10^{10}$ GeV, $\tilde{m}_\Delta = 10^{-2}$ eV and $B_\phi = 10^{-4}$. The green (red) dots indicate the allowed range for the efficiency, as required by neutrino data (3σ level [262]) for the inverted (normal) hierarchical light neutrino mass spectrum. In addition to the constraints on R, we also took into account the constraints imposed by data on the different $B_{\ell_{ij}}$ elements (see Fig. 4.22). We stress that these constraints apply only if the neutrino mass matrix is entirely dominated by the lightest scalar triplet contribution.

ratios $B_{\ell_{\alpha\alpha}}/B_{\ell_{\alpha\beta}}$ (right panel) as a function of the lightest neutrino mass, for the normal (green) and inverted (red) light neutrino mass spectrum. We fixed the neutrino oscillation parameters according to their upper and lower 3σ limits [19]. It can be seen that the R configuration leading to a vanishing $B-L$ asymmetry, although showing up at the 3σ level in the normal spectrum case, can be readily evaded, thus showing the viability of the PFL scenario even in its most constrained form.

We plot in Fig. 4.23 the resulting maximal $B-L$ final asymmetry that can be achieved, as a function of the flavor parameter R, for $m_{\Delta_1}/m_{\Delta_2} = 10^{-1}$. To this end we have considered the same parameter configuration used in Fig. 4.19. It can be seen that the maximal $B-L$ asymmetry that can be achieved can account for the observed baryon asymmetry of the Universe for a large range of R values, except at $R \approx 3/4$. We also point out that, if the neutrino mass matrix is dominated by the light scalar triplet, the constraints coming from neutrino data are compatible with successful PFL scenario. One realizes as well that two of the $B-L$ asymmetry global maxima are shifted with respect to the efficiency maxima, and are now located around the points at which $\ell_\alpha \ell_\alpha \to \bar{\Delta}$ inverse decay rates are of the order of the Universe Hubble expansion rate, where $B_{\ell_{\alpha\alpha}} = B^{\rm Eq}_{\ell_{\alpha\alpha}}$, see Eq. (4.118). As a final remark, it is worth noting that the local maximum at $R \approx 1$ has gone away.

This result has to be compared with the one-flavor approximation case, where the CP-asymmetry is very suppressed for $B_\phi \ll B_\ell$ or $B_\phi \gg B_\ell$, since it is proportional to $\sqrt{B_\phi B_\ell}$ – see Eq. (4.17). This is no more the case in PFL leptogenesis, since the lepton number conserving and flavor violating CP-asymmetries depend only on Yukawa couplings.

4.6 General triplet flavored leptogenesis

Having discussed the viability of the PFL scenario in pure type-2 Seesaw models, we are now in a position to analyze the impact that flavor effects may have in general triplet flavored leptogenesis models. Here, as already defined previously in page 111 and 151, by "general models" we refer to models where the lepton number violating CP-asymmetries are relevant or even dominate over the lepton number conserving CP-asymmetries which drive PFL. Accordingly, if the extra degrees of freedom enabling a non-vanishing CP-asymmetry are additional triplets, a general model will be defined by Eq. (4.69), while if the extra degrees of freedom are right-handed neutrinos – as will be the case in models featuring interplay between type-1 and type-2 Seesaw – the CP-asymmetry in Eq. (4.77), being lepton number violating, will always define a "general model".

As in the PFL section, in what follows we will assume that the asymmetry is entirely generated via the decays of the lightest triplet, something that can be achieved by taking a heavy mass spectrum obeying the following hierarchy : $m_\Delta \ll m_{\Delta_{2,3,\ldots},N_k}$, and we focus on a two-flavor approximation of the semi-diagonal regime. In "general" scenarios, since the CP-asymmetries are lepton number breaking, successful leptogenesis is possible in the absence of lepton flavor effects, in contrast to PFL where flavor effects are mandatory. We will now quantify the enhancement that the inclusion of flavor effects may have in the final $B-L$ asymmetry.

4.6.1 Efficiency-like parameter

We recall that in the one-flavor approximation, an efficiency function accounting for the z (temperature) evolution of the unflavored $B-L$ asymmetry can be defined, see section 4.1.6 :

$$\left|\Delta Y^{\rm end}_{B-L}\right| = \epsilon_\Delta\, \eta_\Delta\, Y^{\rm Eq}_\Sigma(z_0)\,. \tag{4.128}$$

As in fermion triplet leptogenesis, in this case one can also define a gauge and a Yukawa regime, which boundaries in the $\tilde{m}^{\rm eff}_\Delta - m_\Delta$ parameter space plane are determined by the values of B_ϕ, as displayed in the right-hand side plot of Fig. 4.6, page 126. [24] While in the gauge regime, triplet dynamics is dominated by gauge-mediated triplet annihilation, in the Yukawa regime the dynamics is driven by Yukawa-induced reactions, and so it is in the latter where flavor effects can have striking implications. For a fixed triplet mass, the transition between both regimes becomes determined by a "critical" $\tilde{m}^{\rm eff}_\Delta$, given in the right panel of Fig. 4.6. [25]

The behavior of the efficiency (i.e. of the $B-L$ asymmetry) is to a large extent determined by the regime where leptogenesis takes place (gauge or Yukawa), or in other words by the location of the boundary in the $\tilde{m}^{\rm eff}_\Delta - m_\Delta$ plane, determined in turn by the value of B_ϕ. As we have shown in section 4.1.6, in the gauge (Yukawa) regime the efficiency increases (decreases) with $\tilde{m}^{\rm eff}_\Delta$. In the gauge regime this is due to the fact that there is no substantial production of the asymmetry until z approaches the value $z = z_A$ where γ_A/γ_D goes below unity. In the Yukawa regime instead,

[24] Let's recall that the effective neutrino mass-like parameter is defined in Eq. (4.12) to be $\tilde{m}^{\rm eff}_\Delta \equiv \tilde{m}_\Delta/(B_\ell B_\phi)^{1/2}$. It is such that the decay rate of the triplet $\Gamma_\Delta \propto m^2_\Delta \tilde{m}^{\rm eff}_\Delta$.

[25] In practice, for a given value of m_Δ, the transition between the gauge and Yukawa regimes is defined as the value of $\tilde{m}^{\rm eff}_\Delta$ above (below) which the inverse decays are (not) in thermal equilibrium once the gauge scatterings cease to dominate the whole process (i.e. it leads to $\gamma_D/n^{\rm Eq}_\ell H = 1$ when γ_A goes below γ_D at a temperature $z = z_A$).

the efficiency decreases with $\tilde{m}_\Delta^{\rm eff}$ because in this case still there is no substantial asymmetry produced until z approaches z_A, and because the asymmetry produced afterwards is further washed-out by the inverse decay whose magnitude increases with $\tilde{m}_\Delta^{\rm eff}$. Note that, even if large efficiencies can be obtained for $B_\phi \ll 1/2$, since lepton number is unbroken in the $B_\phi \to 0$ limit, these efficiency enhancements are accompanied by a suppression of the CP-asymmetry, so that still the maximum $B-L$ asymmetry is obtained for values of B_ϕ not far from its maximum value $B_\phi = 1/2$.

The picture described in the items above is expected to change as soon as one hits the (two-)flavor regime, in particular if the parameters are such that triplet dynamics takes place in the Yukawa regime. In order to discuss the impact that flavor effects may have, *it is convenient to introduce an efficiency-like parameter* $\tilde{\eta}_\Delta$. Indeed, as noticed in section 4.3.5, flavor coupling does not allow a conventional definition of an efficiency. However, in the two-flavor approximation as we assume here, a parameter resembling the efficiency of the unflavored case can be defined : [26]

$$\left|\Delta Y_{B-L}^{\rm end}\right| = \epsilon_\Delta\, \tilde{\eta}_\Delta\, Y_\Sigma^{\rm Eq}(z_0)\ , \tag{4.129}$$

with $\tilde{\eta}_\Delta$ given by

$$\tilde{\eta}_\Delta \equiv \frac{1}{2}\left[\eta_{aa} + \eta_{a\tau} + \eta_{\tau a} + \eta_{\tau\tau} + \bar{\epsilon}_\Delta\left(\eta_{aa} - \eta_{a\tau} + \eta_{b\tau} - \eta_{\tau\tau}\right)\right]\ , \tag{4.130}$$

where the flavored efficiency functions have been defined in Eq. (4.108) and with

$$\epsilon_\Delta = \epsilon_\Delta^{\ell_a} + \epsilon_\Delta^{\ell_\tau} \qquad \text{and} \qquad \bar{\epsilon}_\Delta = \frac{\epsilon_\Delta^{\ell_a} - \epsilon_\Delta^{\ell_\tau}}{\epsilon_\Delta}\ . \tag{4.131}$$

Note that the definition of $\tilde{\eta}_\Delta$ is such that in the limit $\epsilon_\Delta^{\ell_a} \to \epsilon_\Delta^{\ell_\tau}$ one recovers the usual definition of the efficiency as in the one-flavor approximation, while in the limit $\epsilon_\Delta^{\ell_a} \to -\epsilon_\Delta^{\ell_\tau}$ one recovers the efficiency as defined in the PFL section. This parameter proves to be useful in particular when comparing the results obtained in the flavored regime with those arising from the one-flavor limit. Instead, the parameter $\bar{\epsilon}_\Delta$, introduced in the definition of $\tilde{\eta}_\Delta$, has a two-fold utility : first of all it "measures" the deviation from the PFL ($\bar{\epsilon}_\Delta \gg 1$) and the general scenarios ($\bar{\epsilon}_\Delta \ll 1$) ; secondly, it "measures" the flavor misalignment of the source terms in the evolution equations of the $B/3 - L_\alpha$ charges.

◦ Efficiency as a function of $\tilde{m}_\Delta^{\rm eff}$

In order to quantify the impact that flavor effects have on the $B-L$ asymmetry, it is useful to consider first a case where both CP-flavored asymmetries are equal, i.e. $\bar{\epsilon}_\Delta = 0$, that is to say in a way the extreme opposite to the PFL case. This will allow to discuss flavor effects that are different from the ones we discussed in the previous section for the PFL case. For this case, we show in Fig. 4.24 the efficiency-like parameter $\tilde{\eta}_\Delta$ as a function of $\tilde{m}_\Delta^{\rm eff}$ for different values of $(m_\Delta,\, B_\phi)$, overlapped with the results we got for the unflavored case, see Fig. 4.7 in page 128.

[26] In the general three-flavor situation, it seems not possible to define such a simple quantity that can be compared to the one-flavor approximation efficiency.

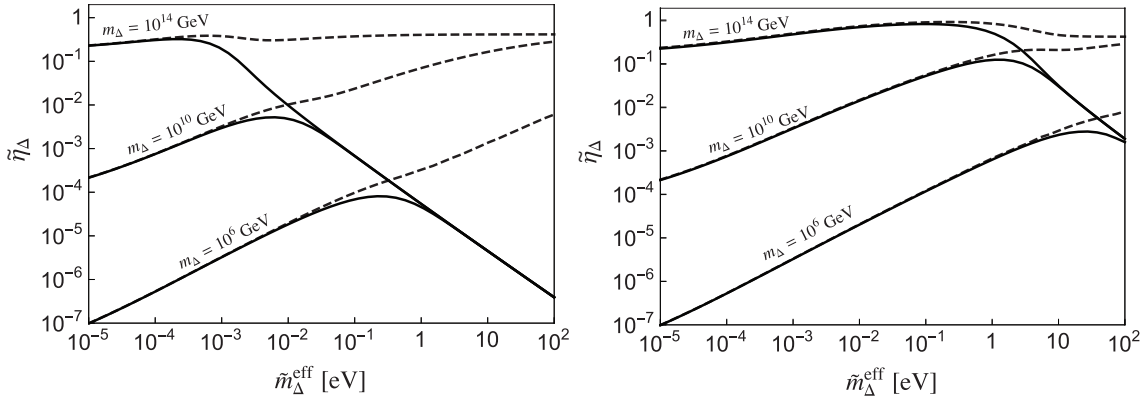

Figure 4.24 – Dependence of the efficiency with the effective mass parameter $\tilde{m}_\Delta^{\rm eff}$, for $B_\phi = 0.5$ (left) and $B_\phi = 10^{-4}$ (right). The effect of the flavor is shown in dashed, which shows the efficiency-like parameter $\tilde{\eta}_\Delta$, fixing $\bar{\epsilon}_\Delta = 0$ and the flavor configuration according to $B_{\ell_{aa}} = B_{\ell_{a\tau}} = 0$ and $B_{\ell_{\tau\tau}} = 1 - B_\phi$. For the unflavored case in solid, $\tilde{\eta}_\Delta$ refers to the usual efficiency, see Fig. 4.7.

Some comments are in order regarding these results. Gauge scatterings, being flavor "blind", are insensitive to lepton flavor effects and so the suppressions they induce cannot be overcome. This means that, as long as we consider values of parameters which in the one-flavor case gives Eq. (4.42), i.e. the maximum efficiency allowed by gauge scattering, flavor effects cannot further enhance the efficiency. However, in the Yukawa regime, for large values of $\tilde{m}_\Delta^{\rm eff}$, since inverse decay washouts are flavor sensitive, flavor effects allow to largely avoid this effect, so that the efficiency goes on to increase also there, as Fig. 4.24 shows. As a result in this case too, one is left only with the unavoidable gauge scattering suppression. This suppression is nevertheless very mild for large values of $\tilde{m}_\Delta^{\rm eff}$ (i.e. small values of z_A).

Hence, large enhancement of the efficiency can be obtained from flavor effects, especially for large values of B_ϕ (since this means small B_ℓ and therefore large $\tilde{m}_\Delta^{\rm eff}$). *We see from Fig.* (4.24) *that the efficiency can even be increased by several orders of magnitude.* In other words, deep inside the Yukawa region where gauge scattering suppression is faint, flavor effects start showing up and become even striking as $\tilde{m}_\Delta^{\rm eff}$ increases and B_ϕ approaches 1/2. Summarizing, in this equal flavored CP-asymmetries case we consider here ($\bar{\epsilon}_\Delta = 0$), Eq. (4.42) can still be used as an approximate upper bound of the $B - L$ asymmetry one can reach in all regimes, even deep in the Yukawa regime. We have checked that this bound can be saturated in all regimes up to a factor ~ 2.

∘ Efficiency as a function of B_ϕ

To further emphasize the effects of flavors in the $\bar{\epsilon}_\Delta = 0$ case, we have calculated the efficiency-like parameter $\tilde{\eta}_\Delta$ as a function of B_ϕ. The calculation has been done for fixed parameters m_Δ and $\tilde{m}_\Delta$, and for three flavor configurations (a), (b) and (c) – the one already used in Fig. 4.21. The results are displayed in Fig. 4.25 (left-hand side plot), where the flavored and unflavored outputs are compared. It can be seen that considering only the effects of the SM interactions (i.e. configuration (c)), one can get an enhancement of order 2 with respect to the unflavored case, whereas for the flavor configuration (a) one can get further orders of magnitude enhancement, as can be seen in particular for $B_\phi = B_\ell = 1/2$.

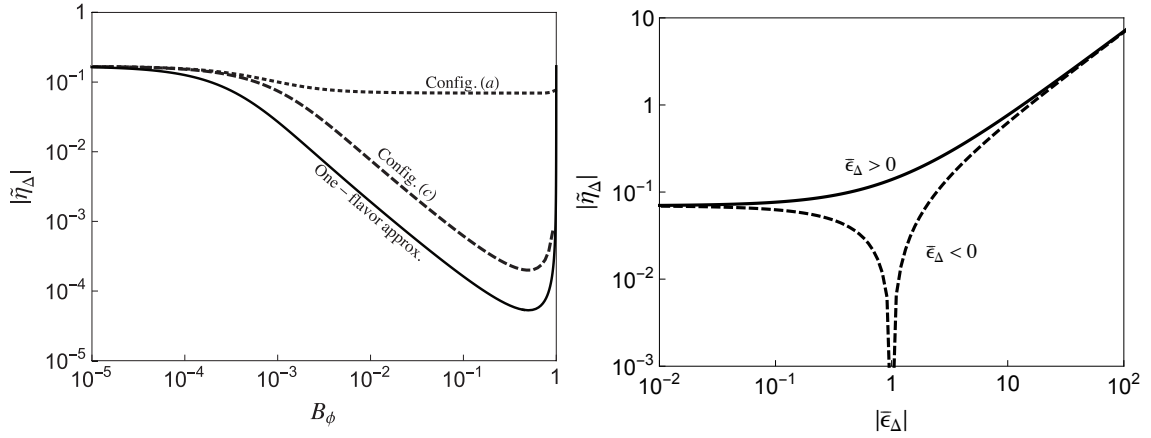

Figure 4.25 – Left-hand plot : Efficiency-like parameter $\tilde{\eta}_\Delta$ as a function of B_ϕ, for $\epsilon_\Delta^{\ell_a} = \epsilon_\Delta^{\ell_\tau}$. The flavor configurations (a), (b) and (c) correspond to the ones used in Fig. 4.21 (for the unflavored case $\tilde{\eta}_\Delta$ refers to the usual efficiency). Right-hand plot : Efficiency-like parameter $\tilde{\eta}_\Delta$ as a function of $|\bar{\epsilon}_\Delta|$ for $B_\phi = 1/2$ and the flavor configuration (a). In both plots we fixed $m_\Delta = 10^{10}$ GeV and $\tilde{m}_\Delta^{\rm eff} = 1$ eV.

◦ Efficiency as a function of $\bar{\epsilon}_\Delta$

Finally, let us discuss what happens very qualitatively in cases other than the pure PFL case, $\epsilon_\Delta^{\ell_\tau} = -\epsilon_\Delta^{\ell_a}$ and the "opposite" case, $\epsilon_\Delta^{\ell_\tau} = \epsilon_\Delta^{\ell_a}$. In these "intermediate" cases, the "efficiency-like" parameter as defined in Eq. (4.129) cannot be considered as an efficiency anymore, because it can be larger than one. For instance in the pure PFL case it is infinity since $\epsilon_\Delta = 0$. As a result it is difficult to span the range of possibilities in simple terms for these cases. To get a reliable idea of the behavior of the efficiency-like parameter, and thus of the $B-L$ asymmetry, in a specific case, the most efficient procedure is probably to integrate first the full set of Boltzmann equations in a "blind" way and see what the result looks like before trying to understand it by simple means.

But the basic picture qualitatively remains clear. As long as $z < z_A$ any flavor asymmetry production is suppressed by a factor of γ_D/γ_A, and afterwards the $B-L$ asymmetry that can be produced can anyway not be larger than the number of triplets remaining at $z \sim z_A$ times the sum of the absolute values of the flavor asymmetries. The important flavor effects stressed above, from the L-violating inverse decays as well as from the L-violating decays, will be operative in a way which may depend non trivially on basically all parameters, the flavored CP-asymmetries, the $C^{\ell,\phi}$ constants, the total decay rate and the various branching ratios.

As an illustration of the efficiency dependence on the mismatch between the flavored CP-asymmetries, parameterized by $\bar{\epsilon}_\Delta$, on the right-hand side plot in Fig. 4.25 we show the dependence of $\tilde{\eta}_\Delta$ with $\bar{\epsilon}_\Delta$ for $B_\phi = 1/2$ for the flavor configuration (a). In the region where $\bar{\epsilon}_\Delta \ll 1$ is small ($\epsilon_\Delta^{\ell_a} \sim \epsilon_\Delta^{\ell_\tau}$), as previously stressed, any possible mismatch between the asymmetries in flavor a and τ can only be due to the flavor dependence of the washout terms. As $\bar{\epsilon}_\Delta$ increases, the source terms start having a flavor dependence as well, and so an imbalance between production in flavor a and τ appears. The flavor dependence of both production and washout at large $\bar{\epsilon}_\Delta$, yields larger values for $\tilde{\eta}_\Delta$. In other words, flavor effects are diminished in those regions of parameter space where $\bar{\epsilon}_\Delta \ll 1$ and become more remarkable in regions where $\bar{\epsilon}_\Delta \gg 1$.

Accordingly, in the various flavor regimes, enhancements of the efficiency-like parameter $\tilde{\eta}_\Delta$ with respect to the unflavored case are a consequence of combined effects: the mismatch between the different flavored CP-asymmetries $\epsilon_\Delta^{\ell_\alpha}$, the SM interactions through the C^ℓ and C^ϕ matrices, and the flavor configurations encoded in $B_{\ell_{\alpha\beta}}$.

4.6.2 Successful leptogenesis

Using the general upper bound on the flavored CP-asymmetries given in Eq. (4.81), it is possible to see for which value of the parameters one can have successful leptogenesis. We didn't make this exercise, as it involves too many parameters. However, since larger efficiencies can be obtained for example in the case where $\epsilon_\Delta^{\ell_a} = \epsilon_\Delta^{\ell_\tau}$, the most striking feature is clearly that flavored leptogenesis allows for smaller values of the CP-asymmetry compared to the results obtained in the one-flavor approximation in Figs. 4.8. In the situation where $B_\ell = B_\phi = 1/2$, one can even enhance the efficiency up to 3 orders of magnitudes – see Fig. 4.25 – and so allow for an accordingly smaller CP-asymmetry. As a result and for comparison purpose, the green zones in Figs. 4.8 can be enlarged consequently in the case where $\epsilon_\Delta^{\ell_a} = \epsilon_\Delta^{\ell_\tau}$.

4.7 Compatibility with CLFV processes

For completeness, we now discuss briefly if whether it is possible to have both successful leptogenesis and observable CLFV processes in the type-2 Seesaw scenario, together with the correct light neutrino mass scale. This will also allow to emphasize the clear possible links which exists between this chapter and chapter 2 about $\mu \to e$ conversion. We will here consider only orders of magnitude, to have an idea of wether or not this is possible, and consider the case where the lightest scalar triplet dominates over the other heavier degrees of freedom.

- **Constraints from CLFV and neutrino masses**

CLFV. We already gave in section 2.6.1 the various analytical expressions of the CLFV processes when the SM is endowed with only one scalar triplet, or when one the lightest scalar triplet gives the most dominant contribution to the CLFV processes. Assuming this is indeed the case, their rate are roughly proportional to the square of the dimension-6 coefficient. Saturating the perturbativity condition $Y_\Delta \simeq \sqrt{4\pi}$, the lightest scalar triplet mass must obey the inequalities in Eqs. (2.112)-(2.115) in order to give a rate which is reachable by future experiment sensitivities. Keeping only the most stringent sensitivity coming from the μ3e experiment, i.e. $Br(\mu \to eee) \lesssim 10^{-16}$, and using Eq. (2.109), the dimension-6 coefficient must be roughly larger than :

$$c^{d=6} \sim \frac{Y_\Delta^2}{m_\Delta^2} \gtrsim 10^{-13}\,\text{GeV}^{-2}\,, \quad \text{i.e.} \quad \frac{Y_\Delta}{m_\Delta} \gtrsim 10^{-6}\,\text{GeV}^{-1}\,. \tag{4.132}$$

Neutrino masses. From Eq. (1.38) or (4.7) with a dominant contribution from the lightest scalar triplet, to get roughly $m_\nu \sim 0.1$ eV, one needs the Yukawa coupling to obey

$$\frac{Y_\Delta}{m_\Delta} \approx 10^{-15} \frac{m_\Delta}{\mu_\Delta} \text{GeV}^{-1} \,. \tag{4.133}$$

◦ **Compatibility with the scenarios considered previously**

In order to provide both large CLFV and small neutrino masses, Eq. (4.133) together with condition (4.132) imply that the scalar coupling must obey

$$\frac{\mu_\Delta}{m_\Delta} \lesssim 10^{-9} \,, \tag{4.134}$$

which is not in conflict with the perturbativity condition on μ_Δ/m_Δ. Let's now analyze if one can have successful leptogenesis and both large CLFV and small neutrino masses in the scenarios (i) PFL and (ii) general leptogenesis considered in sections 4.5 and 4.6 respectively.

PFL scenario In the case of the PFL scenario, we have seen that one needs firstly $B_\phi^k \ll B_\ell^k$ in order to lie in the PFL regime, and secondly large Yukawa couplings $Y_{\Delta_k} \sim 1$ as well as a mild hierarchy between the lighter and the heavier scalar triplet in order to generate enough baryon asymmetry (large enough CP-asymmetry). These conditions are therefore compatible with the CLFV and neutrino mass requirements in Eqs. (4.132)-(4.134). For example, one can have $Y_\Delta \sim 1 \cdots \sqrt{4\pi}$, in which case one has $m_\Delta \lesssim 10^6 \ldots 10^7$ GeV and $\mu_\Delta \lesssim 10^{-3} \ldots 10^{-2}$ GeV.

General scenario In the general scenario where leptogenesis is activated by other heavier states, as right-handed neutrinos, the CP-asymmetry involves both μ_Δ and Y_Δ couplings, see Eq. (4.77). In this case, maximal CP-asymmetry is obtained for $B_\ell \sim B_\phi$, i.e. $\mu_\Delta/m_\Delta \sim Y_\Delta$. This condition is not compatible with the CLFV and light neutrino mass conditions, since from Eq. (4.133) one would need $Y_\Delta \sim \mu_\Delta/m_\Delta \lesssim 10^{-9}$, that leads using Eq. (4.132) to a triplet mass $m_\Delta \lesssim 10^{-3}$ GeV way too small to get a large enough CP-asymmetry, and surely already excluded by accelerators.

4.8 Summary

In this long chapter, we have analyzed the scalar triplet leptogenesis with the inclusion of the flavor effects as well as the spectator effects. We have shown that, as highlighted in Ref. [247], flavors always matter in type-2 Seesaw leptogenesis. Indeed, contrarily to the type-1 Seesaw case, one can at best find a lepton flavor basis such that the scalar triplet decays following three pairs of coherent states. This is because the scalar triplet decays into three pairs of lepton, and not only one. As a consequence, the "unflavored" scalar triplet leptogenesis already studied in the literature appears to be an approximation of the general flavor leptogenesis, whatever the temperature regime. This "one-flavor approximation" is good as soon as the flavored CP-asymmetries and the various branching ratios into leptons are aligned. We have first studied this case that allowed us to understand the main features of the scalar triplet leptogenesis.

We then analyzed the general flavored case, in particular we have derived for the first time the complete set of flavored classical Boltzmann equations governing the evolution of the different relevant asymmetries, including the effects of those SM reactions which in the leptogenesis era may be fast : charged lepton and quark Yukawa reactions as well as QCD and electroweak sphaleron processes. The resulting network of kinetic equations with the chemical equilibrium conditions provide the tools for studying triplet scalar leptogenesis in full generality. Furthermore, by requiring that the decoherence rate is faster than the leptonic inverse decay rate during the leptogenesis era, we determined the domain of validity of the various flavor regimes. The reader who would like to determine the effects of flavors in any given type-2 Seesaw model can find in section 4.4 the procedure to follow, with all the references to the equations that are needed.

In scenarios involving an additional triplet (purely type-2 Seesaw scenarios), we have identified a novel class of models where the flavored CP-asymmetries, consisting of a lepton number violating and a lepton number conserving contributions, become dominated by the lepton number conserving piece. Such a dominance naturally shows up as soon as the couplings of at least one triplet (i.e. not necessarily of all Seesaw states as for PFL type-1 Seesaw scenarios) approximately conserve lepton number L, which in practice simply means that it couples more to leptons than to scalars. The purely flavored CP-asymmetries have no reasons to be suppressed by the smallness of the light neutrino masses since, in contrast to the lepton number violating CP-asymmetries, they only involve L-conserving couplings.

With the aid of the derived flavored Boltzmann equations and chemical equilibrium conditions, we have carried out a thorough study of the PFL scenario in the two-flavor approximation, for definiteness. The way this PFL scenario works is totally novel (for small values of B_ϕ which gives natural dominance of the purely flavored CP-asymmetries) : in this case there is no L-violating process in thermal equilibrium at any epoch but yet flavor effects do allow the creation of a $B-L$ asymmetry from the L-violating slow decay of the triplet to SM scalars. We have proved its viability by calculating the $B-L$ yield, finding that, for reasonable and wide ranges of parameter values, a baryon asymmetry consistent with observation can always be achieved. By exploring the $B-L$ asymmetry parameter space dependence, we have determined the lepton flavor configuration that maximizes the efficiency, finding that the same structure renders the flavored CP asymmetry minimal. Our findings show that maximal $B-L$ yield is achieved for intermediate lepton flavor configurations.

Finally, we discussed general scenarios, which we have defined by the condition of the CP-asymmetry involving lepton number violation. These scenarios can arise either in models with extra triplets or with right-handed neutrinos (models exhibiting interplay between type-1 and type-2 Seesaw). We discussed the impact that lepton flavor effects may have in the final $B-L$ asymmetry, showing that relevant flavor effects can only be achieved in the Yukawa regime, being more striking as deeper one moves into that regime, and depending on the parameter flavor configuration. Our results show that for certain flavor structures the asymmetry may be enhanced by several orders of magnitude.

Part III

The inert doublet model as the origin of dark matter

5 Asymmetric dark matter in the Inert Doublet Model

Beside the fact that one needs to enlarge the SM with new physics in order to generate neutrino masses and enough baryon asymmetry in the Universe, there is the dark matter paradigm. But what is dark matter ? In 1933, Zwicky has made the amazing observation that the gravitational mass of the Coma galaxy cluster is ~ 400 hundred times larger than the mass expected from the measured luminous matter from stars. This means that most of the gravitational mass of this cluster is actually dark, i.e. it doesn't emit any light. Few years after, this observation was confirmed by Vera Rubin who observed that the rotation curve of various galaxies doesn't follow the expected behavior from Newton's law using the luminous matter. More recently, the observations of "bullet clusters" showed that of the distribution of gravitational mass, obtained from lensing, doesn't correspond to the distribution of luminous matter in these clusters. Also recently, the measurement of the shape of the temperature power spectrum of the Cosmic Microwave Background (CMB) showed that it is not in agreement with a Universe made only with the observed luminous matter density. Finally, clusters are parts of a largest structure in the Universe, and the overall structure is made of filaments and bubbles. The observed amount and distribution of these clumps is actually not in agreement with the galaxy distribution obtained from numerical simulations using only the observed luminous matter.

In order to explain these discrepancies with the expected behavior, one has imagined mainly two possibilities : either the theory of gravity must be modified, either there is a huge amount of non-luminous, feebly interacting and yet unknown matter inside the galaxies. The first possibility lead to new theories known as MOdified Newton Dynamics theories (MOND), which we won't introduce in this thesis. The second possibility, the favorite one, is what we called the Dark Matter (DM).

In this chapter, we made the choice to review very briefly the main properties of the dark matter particle, detection techniques and the ways to account for its relic density. From that we will directly go to the last main part of this thesis, which is the analysis of how one could generate enough dark matter in the Inert Doublet Model (IDM) in an asymmetric way. The asymmetric way to produce dark matter is in many ways similar to the way the baryon asymmetry is produced. This chapter is therefore directly linked to the previous two chapters.

5.1 Generalities

5.1.1 Evidences for dark matter

We will not review the very well known evidences for DM. Just mention that beside galaxy rotation curves and bullet clusters, gravitational well effect due to DM is absolutely necessary to reproduce the CMB spectrum (already introduced in chapter 3, see Fig. 3.2 in page 82). This gives the most precise determination of the ratio of the DM density over the critical density $\Omega_{DM} = \rho_{DM}/\rho_c$. The CMB analysis by the Planck collaboration has provided at 68% C.L. [206] :

$$\Omega_{DM} h^2 = 0.1188 \pm 0.0010 \,, \tag{5.1}$$

after combining data coming from the CMB spectrum and external sources as Lensing and BAO. This means, comparing with Eq. (3.5), approximately 5 times the present baryonic matter density :

$$\frac{\Omega_{DM}}{\Omega_B} = 5.4 \pm 0.1 \,. \tag{5.2}$$

Note that it is peculiarly intriguing that the DM and baryon densities are so close to each other.

5.1.2 DM properties

From all the (non-)observation we have done so far, we already know several properties of the dark matter. It should be for example :

- massive, obviously ;
- electrically neutral, otherwise it could interact with atoms and photons in the Universe and we should have observe that since long. More generally, it should be at most weakly interacting with SM particles and thus non-colored ;
- long-lived, or even stable for now. Indeed, DM is expected to have been produced during the early stage of our Universe, as the other SM particles (~ some fraction of second after the Big Bang). Since it is still present in our galaxies today, its lifetime should at least be larger than the age of the Universe, i.e. $\tau_{DM} \gtrsim 4 \cdot 10^{17}$ s. This constraint can be improved considerably if one includes the fact that we don't have observed any decay of DM in our Universe. Indeed, if DM can decay in SM particles as photons or neutrinos, one should observe the residuals of these decays coming for example from the center of the galaxies. Experiments like HESS, Fermi-LAT and IceCube have provided stringent bounds on the DM lifetime if it has a decay channel with photons or neutrinos in its final state. As an illustration, we show in Fig. 5.1, taken from Ref. [267], the present best bounds on the DM lifetime as a function of its mass, if the DM candidate can decay through $DM \to \gamma + \nu$.
- most probably "cold", i.e. basically non-relativistic at the time of freeze-out. This is indeed necessary for DM to have formed such structures in our Universe.

But what is dark matter made off, i.e. how can we account for the DM in the SM ?

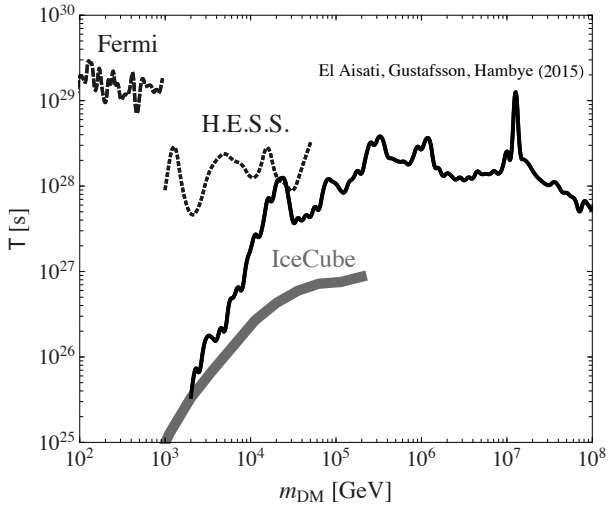

Figure 5.1 – Left : best lower bounds on the DM lifetime as a function of the DM mass m_{DM}, if this latter can decay into monochromatic lines $\nu + \gamma$. The plot has been taken from Ref. [267].

5.2 Models for dark matter

In this section, we present some models from the literature that were proposed in order to account for the DM properties. The list we give is non exhaustive, given the large amount of possibilities. Since there are no DM candidates in the SM, [1] one needs to go beyond the SM. We will just mention few candidates which are relevant for the subsequent model we will consider. [2]

5.2.1 Scalar singlet.

Real scalar singlet. Probably the simplest possibility, which doesn't rely on neutrinos, is to add a real scalar singlet to the SM [268, 269] (see for example Ref. [270] for an updated analysis of the associated phenomenology). In this case, the scalar potential of the SM contains the following interactions :

$$V \ni V_\phi + \frac{1}{2}\mu_S^2 S^2 + \frac{1}{2}\lambda_{S\phi} S^2|\phi|^2 + \frac{\lambda_S}{4} S^4 \,, \tag{5.3}$$

and thus, after diagonalizing the scalar mass matrix, the mass of the scalar singlet reads $m_S = (\mu_S^2 + \lambda_{S\phi}\, \mathrm{v}^2/2)^{1/2}$. The new scalar singlet is obviously neutral and massive, but since the scalar potential should also contain a term $\propto |\phi|^2 S$, the S particle could in principle decay at tree-level (if $m_S > 2m_h$) or at one-loop (if $m_S < 2m_h$) into SM particles. In order to be consistent with the

[1] Light neutrinos are too hot relics and have too small masses to account for DM. Indeed, as already mentioned in section 3.1.2, weak interactions freeze out at around $T \sim 1$ MeV, which is also the temperature at which neutrinos freeze out. This temperature is much greater than the neutrino mass so the neutrinos were highly relativistic at that time and until the structure formation. But if the light neutrinos account for the total DM relic density, structure formation should have occurred much later (typically for $z \lesssim 1$) than what we actually observe (structure are observed for $z \gtrsim 3$).

[2] Note that, even if massive and totally neutral, right-handed neutrinos cannot in general account for DM simply because these are not stable : from the Yukawa coupling it should rapidly decay into a light neutrino and a scalar. However, it is possible to render one of the right-handed neutrinos very long-lived, by making it light and by giving it very small mixing with the SM neutrinos. In this case, the right-handed neutrino could decay via the channel $N \to \nu\gamma$, in which case constraints from Fig. 5.1 do apply.

lifetime constraint, one should therefore either make these decay extremely slow, by putting artificially the associated coupling very close to zero, either one could forbid the linear and cubic terms in S by imposing a discrete Z_2 symmetry to the Lagrangian, such that all the SM are even under this Z_2 while S is odd. In this case, the stability of the S particle is ensured by the Z_2 symmetry. Let's note that since we don't want this symmetry to be broken, one has to make sure that the parameters of the scalar potential are such that $\langle S \rangle = 0$ (i.e. $\mu_S^2 > 0$).

Complex scalar singlet. A slightly more complicated possibility is to introduce a complex scalar singlet $S = S_1 + iS_2$, see for example [271, 272]. Interactions with the SM scalar doublet ϕ generate a mass splitting between S_1 and S_2, so that the DM candidate is the lightest particle between S_1 and S_2, which depends on the parameter value. As in the previous case, one needs to stabilize the dark matter candidate. To this end, one can further impose a Z_2 or $U(1)$ symmetry to the Lagrangian, and the parameters of the scalar potential must be such that $\langle S \rangle = 0$. However, this is not mandatory and it is still possible to have viable DM candidate while breaking the $U(1)$.

In fact, even if this possibility looks very similar to real scalar singlet case (with one more degree of freedom and extra couplings to the SM scalar doublet), the phenomenology is much richer. In particular, as we will see in the next section, since S is complex there is in fact the possibility to generate DM through an S asymmetry.

Note on the discrete symmetry. The discrete symmetry Z_2 that is imposed in order to stabilize the DM candidate could appear artificial. However, one can easily generate such kind of symmetry from local/global special unitary group as $U(1)$ or $SU(3)$. Indeed, consider the global group example of a simple model of two self-interacting scalar fields ($\sigma_{1,2}$) subject to the following global $U(1)$ transformations [273, 274] :

$$\sigma_1 \to e^{iN\alpha}\sigma_1 \quad \text{and} \quad \sigma_2 \to e^{-i\alpha}\sigma_2 \,. \tag{5.4}$$

The $U(1)$-invariant renormalizable as well as non-renormalizable Lagrangian describing such system is given by :

$$\mathscr{L} = \mu_i^2 \sigma_i^* \sigma_i + \lambda_{ij}(\sigma_i^* \sigma_i)(\sigma_j^* \sigma_j) + \frac{\lambda_{\sigma_M}}{\Lambda^{M(N+1)-4}} \sigma_1^M (\sigma_2^N)^M \,, \tag{5.5}$$

with μ_i dimension one and $\lambda_{ij}, \lambda_{\sigma_M}$ dimensionless couplings. M and N some positive integers, and Λ some high energy scale. If σ_1 acquires a vev the resulting Lagrangian will involve a collection of terms $(\sigma_2^N)^M$, thus being Z_N invariant, namely

$$\sigma_2 \to \eta_N^n \sigma_2 \quad \text{with} \quad \eta_N = e^{2\pi i/N} \quad (n = 0, 1, \ldots, N-1) \,. \tag{5.6}$$

The origin of the $SU(N)$ symmetries can come from exotic physics or can also come from the global abelian $U(1)$ or non-abelian $SU(3)$ flavor symmetries of the kinetic terms of the SM [275, 276, 277, 278, 279, 280, 281, 282, 283, 284, 285, 286, 287, 288, 289]. For example, in Ref. [289] made in collaboration with Diego Aristizabal, Chee Sheng Fong and Avelino Vicente, we have shown that the Z_2 discrete symmetry of the scotogenic model can be obtained as a residual

symmetry resulting from the SSB of a global $U(1)_{\nu_R}$, where $U(1)_{\nu_R}$ is a global symmetry of the kinetic Lagrangian of the right-handed neutrinos. Other ways of stabilizing the DM from the existence of gauge symmetries also exist.

5.2.2 The Inert Doublet Model (IDM)

The Inert Doublet Model (IDM) [44, 290, 291, 292] simply consists in adding to the Standard Model (SM) a single scalar doublet H_2 which is odd under a Z_2 symmetry, while all the SM fields are even. The most general scalar potential is in this case

$$\begin{aligned} V =& m_1^2|H_1|^2 + m_2^2|H_2|^2 + \lambda_1|H_1|^4 + \lambda_2|H_2|^4 \\ &+ \lambda_3|H_1|^2|H_2|^2 + \lambda_4|H_1^\dagger H_2|^2 + \frac{\lambda_5}{2}\left[\left(H_1^\dagger H_2\right)^2 + \text{H.c.}\right], \end{aligned} \tag{5.7}$$

where the SM and the inert scalar doublets can be written as

$$H_1 = \begin{pmatrix} \phi^+ \\ \text{v}/\sqrt{2} + \phi^0 \end{pmatrix} \quad \text{and} \quad H_2 = \begin{pmatrix} \eta^+ \\ \eta^0 \end{pmatrix}, \tag{5.8}$$

with $\phi^0 \equiv (h + i\phi^3)/\sqrt{2}$ and $\eta^0 \equiv (H^0 + iA^0)/\sqrt{2}$. In the scalar potential, m_2^2 is assumed to be positive to insure that H_2 doesn't acquire a vev, so that it's lightest neutral component (A^0 or H^0) is stable. Prior to electroweak symmetry breaking (EWSB), all H_2 components have mass $m_{H_2} = m_2$, whereas after EWSB they get split in mass (see section 3.3.1 in page 85)

$$m_{H^0}^2 = m_2^2 + \lambda_{H^0}\,\text{v}^2\,,\; m_{A^0}^2 = m_2^2 + \lambda_{A^0}\,\text{v}^2\,,\; m_{\eta^+}^2 = m_2^2 + \lambda_{H^c}\,\text{v}^2\,, \tag{5.9}$$

with $\lambda_{H^c} = \lambda_3/2$ and $\lambda_{H^0,A^0} = (\lambda_3 + \lambda_4 \pm \lambda_5)/2$. The λ_5 interaction in Eq. (5.7) is therefore responsible of the generation of a mass splitting between H^0 and A^0, so that the DM candidate can be either H^0 or A^0 following the sign of λ_5. This inert doublet model is very interesting since very predictive. It is subject to the following general constraints :

- For the vacuum to be stable and bounded from below, one necessary needs $\lambda_{1,2} > 0$, as well as $\lambda_{H^0,A^0,H^c} > -\sqrt{\lambda_1\lambda_2}$.
- Scalar couplings have to be perturbative, so that $\lambda_i \leq 4\pi$. A more conservative bound is $\lambda_i \leq \sqrt{4\pi}$. If the coupling do saturate the upper bound, radiative corrections are such that the coupling can become infinite for some high energy value – this is the Landau pole – so that a new physics is expected before the divergence of the couplings. The determination of the Landau pole can be performed using the renormalization group equations in the IDM framework given in Appendix E.3, from Ref. [290].
- Because of the gauge coupling of the inert scalar, Z decay width constraint at LEP requires $m_{A^0} + m_{H^0} > m_Z$ and $m_{\eta^+} > m_Z/2$, otherwise one could have already produced the inert doublet components at LEP or LHC.
- EW precision tests require $\Delta T \simeq \left(m_{\eta^+} - m_{A^0}\right)\left(m_{\eta^+} - m_{H^0}\right)/12\pi^2\alpha\,\text{v}^2 \lesssim 10^{-1}$. The EW precision tests consist in searching for new physics by analyzing small deviations between

SM predictions and associated quantities that are very well measured, as branching ratios, forward-backward asymmetries, left-right asymmetries, etc. These deviations can be partly parametrized by the useful "oblique" parameters S, T and U, which differ from zero if the new physics generates corrections in the gauge boson self-energy propagators, as it is the case for the IDM. The present best fit on the oblique parameters are [8]

$$S = -0.03 \pm 0.10\,, \quad T = 0.01 \pm 0.12\,, \quad U = 0.05 \pm 0.10\,. \tag{5.10}$$

Accordingly, one can allow deviations of these parameters only in the range given by the uncertainties, i.e. typically $|\Delta S|, |\Delta T|, |\Delta U| \lesssim 0.1$. In the IDM, only the T parameter receive important corrections [290], which lead to the upper bound given above.

- The gauge interactions imply the existence of Z-mediated inelastic scattering $H^0\mathcal{N} \to A^0\mathcal{N}$, whose cross section is much larger than the present direct detection upper bounds (see below). In order to kinematically forbid this interaction, one must have $m_{A^0} - m_{H^0} \gtrsim \mu_r \beta_{DM}^2/2$, where $\beta_{DM} c$ is the DM halo velocity with respect to the earth, and $\mu_r = m_{H^0} m_{\mathcal{N}}/(m_{H^0} + m_{\mathcal{N}})$ is the reduced mass of the system for the nucleus $\mathcal{N}$ used by the experiment. For $m_{H^0} \gg m_{\mathcal{N}}$ and Xenon nucleus, using an average velocity of ~ 270 km/s, this constraint can be rephrased as $m_{A^0} - m_{H^0} \gtrsim \delta m_{\rm min} \sim 50$ keV. Taking into account the velocity distribution around this central value, and the recoil energy sensitivity of the experiments, the minimum splitting becomes $\delta m_{\rm min} \sim 180$ keV, although a more robust constraint is $\delta m_{\rm min} \sim 100$ keV [293], which translates as

$$|\lambda_5| \gtrsim 3.3 \cdot 10^{-6} \cdot \left(\frac{m_{H^0}}{\rm TeV}\right) \cdot \left(\frac{\delta m_{\rm min}}{100\,{\rm keV}}\right). \tag{5.11}$$

5.2.3 Other possibilities

Note that there are several other possibilities of DM candidates that have been proposed in the literature, just mention a few :

- scalar or fermion multiplets with ad hoc Z_2, which generalize the inert doublet model. Note that a high multiplet fermion (quintuplet or more) is automatically stable, as it cannot have renormalizable interactions with the SM fields (neither dimension-5 ones) [312].
- the axion, which has been introduced by Peccei-Quinn in 1977 in order to solve the strong CP problem in QCD.
- the supersymmetric candidates, as the sneutrinos, which are the supersymmetric partner of the neutrino, or the lightest neutralino, the neutralinos being the supersymmetric partners of the neutral gauge and scalar bosons.
- Kaluza-Klein particles, which appear in models with extra dimensions trying to unify gravity with the other forces.

But how could we distinguish between all these possibilities ? Clearly, one first need to detect dark matter.

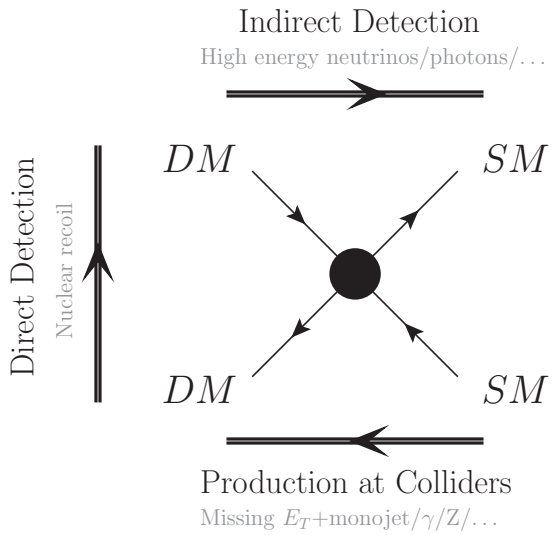

Figure 5.2 – DM detection principles.

5.3 Dark matter detection and constraints

Assuming that the DM candidate can interact through $DM\,DM \leftrightarrow SM\,SM$, there are basically three ways one can detect a DM particle, which are summarized in Fig. 5.2. This picture is quite representative of all DM detection experiment's principles. These are :

- $DM\,DM \rightarrow SM\,SM$: this is the process which is also responsible for the depletion of the DM density during the freeze-out. Even if it is out-of-equilibrium, still two DM candidates can meet and annihilate into SM particles. These annihilations are more likely to happen where the DM density is important, as in the center of galaxies or stars. If such annihilations occur, some of the decay products could reach the Earth where one could detect them. This detection principle is called "Indirect Detection".

- $DM\,SM \rightarrow DM\,SM$: the scattering of one DM particle with a SM particle. In particular, if the DM interacts with quarks, one could have for example that the DM can scatter with one of the nucleons of the Earth. In this case, one could be able to observe a nuclear recoil without detecting any colliding particle. This detection principle is called "Direct Detection".

- $SM\,SM \rightarrow DM\,DM$: the direct production of two DM particles from the collision of two SM particles. This is for example possible in accelerators as the LHC. Since the two particles in the final states cannot be detected, the signature of such an event would be... nothing. So what we are actually hunting for is this process but with the emission of a gauge boson $SM\,SM \rightarrow DM\,DM + g/Z/\gamma$, whose signature is a monojet/EM-shower/Z-remanant+missing energy ($\not{E}_T$).

In what follows we remind briefly all the present experimental constraints for each kind of detection principle.

5.3.1 Direct Detection

Direct Detection experiments have provide stringent bounds on the scattering cross section of the DM with nucleus as function of the DM mass. The detection rate R of a DM particle X of mass m_X that scatters on a nucleus $\mathcal{N}$ of mass $m_\mathcal{N}$ is generally expressed as : [3]

$$R = \int_{E^T_{\rm min}}^{E^T_{\rm max}} dE_R \frac{\rho_\odot}{m_X m_\mathcal{N}} \int_{v_{\rm min}}^{v_{\rm esc}} d^3v\, v\, f(v)\, \frac{d\sigma_{X\mathcal{N}}(v,E_R)}{dE_R}\,, \tag{5.12}$$

where E_R is the recoil energy of the nucleus, $\rho_\odot$ is the local DM density, v is the relative velocity of the DM with respect to the nucleus, $f(v)$ is the local velocity distribution of the DM at Earth, and $\sigma_{X\mathcal{N}}$ is the scattering cross section.

The lower integration boundaries of the recoil energy integral are the minimum and maximum threshold energy of the detector, $E^T_{\rm min}$ and $E^T_{\rm max}$. This depends clearly on the experiment sensibility. One has for example $E^T_{\rm min} \sim 1$ keV and $E^T_{\rm max} \sim 100$ keV for the famous LUX experiment.

The velocity distribution and local density of the DM are actually unknown. However, we know from Large Scale Structure formation that the DM halo in a galaxy is almost non-rotating. As a consequence, the relative velocity distribution between the DM and a nucleus should be centered on the velocity of the Sun around the galactic center, which is $v_\odot \approx 220$ km/s. In standard halo, the velocity distribution of the DM wind is assumed to be Maxwellian. Also from astrophysical considerations, one can estimate the DM local density which is centered around $\rho_\odot \approx 0.3$ GeV/cm^3.

For the velocity integral, one integrates between the minimal relative velocity $v_{\rm min}$ and the maximal velocity which is typically the escape velocity of the DM particle in our galaxy $v_{\rm esc} \approx 650$ km/s. The minimal velocity reads

$$v^{\rm El}_{\rm min} = \sqrt{\frac{m_\mathcal{N} E_R}{2\mu^2}}\,, \qquad \text{for an elastic scattering, and} \tag{5.13}$$

$$v^{\rm Inel}_{\rm min} = \frac{1}{\sqrt{2 m_\mathcal{N} E_R}}\left(\frac{m_\mathcal{N} E_R}{\mu} + \delta m_X\right)\,, \qquad \text{for an inelastic scattering [294],} \tag{5.14}$$

where $\mu = m_X m_\mathcal{N}/(m_X + m_\mathcal{N})$ is the reduced mass and δm_X stands for the mass splitting between the incoming and outgoing DM particles.

Finally, the cross section $\sigma_{X\mathcal{N}}$ involves nuclear physics, as well as the DM-nucleon cross section σ_0, which is the interesting quantity that we want to probe. For example, in the case where the DM-nucleon scattering doesn't depend on the spin of the nucleon ("Spin-Independent (SI) scattering"), one has

$$\frac{d\sigma^{SI}_{X\mathcal{N}}(v,E_R)}{dE_R} \simeq \frac{m_\mathcal{N} \sigma^{SI}_0 F^2_\mathcal{N}}{2\mu^2 v^2}\,, \tag{5.15}$$

where $F^2_\mathcal{N}$ is some nuclear for factor. Taking care of the nuclear part and the astrophysical

[3] The rate R as introduced here is the number of detections by day and by kg of the detector mass. It is therefore a dimensionless quantity.

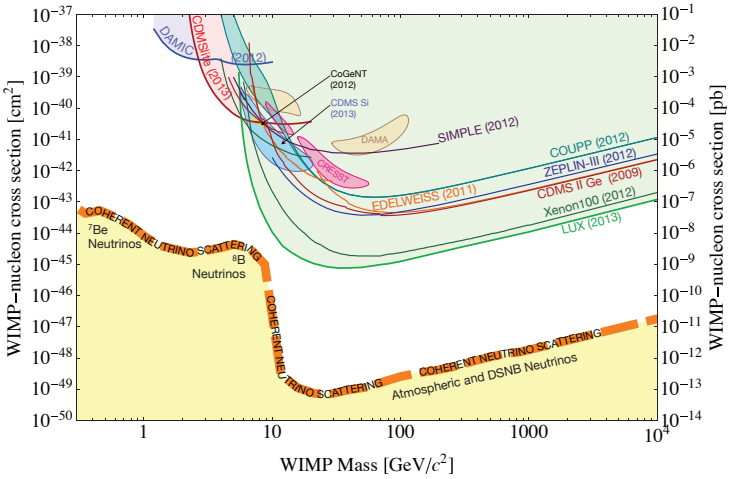

Figure 5.3 – Present upper bound on the spin-independent DM-nucleon cross section as a function of the mass of the DM particle. The region below the thick orange dashed curve shows the limitation of future experiments with respect to the neutrino background. The plot has been taken from Ref. [295].

consideration, the observation (or non-observation) of a DM-nucleon scattering could therefore give some information (or some bound) on the DM-nucleon cross section as well as on the mass of the DM particle.

All in all, we show in Fig. 5.3 the current upper bounds on the spin-independent cross section σ_0^{SI} as a function of the DM mass. The plot has been taken from Refs. [296, 295]. The current bounds and future sensitivities on the spin-dependent cross section can also be found in Ref. [296]. The best present upper bound is provided by the LUX experiment for $m_{DM} \gtrsim 6$ GeV. For $m_{DM} \gtrsim 100$ GeV, this bound is in good approximation given by

$$\sigma_0^{SI} \lesssim 1.2 \cdot 10^{-11} \left(\frac{m_{DM}}{1\,\text{GeV}}\right) \text{pb} \qquad \text{(LUX)} \,. \tag{5.16}$$

Let's note that some experiments as DAMA, which search an annual modulation of DM scatterings due the Earth movement, have claimed the observation of DM signals. However, this is highly controversial – since in conflict with other experiments – and it has been suggested that the observed modulation could be due to unexpected background, see for example Ref. [297].

5.3.2 Indirect Detection

Indirect Detection is a much more complicated issue. There are several reasons. Firstly, suppose the DM can annihilate in SM stable particles. If the decay products are charged, as proton or electrons, they won't obviously propagate straight towards the Earth, since they will undergo deviations from collisions with other particles or from the galactic magnetic field. Because of that, one expects to measure on Earth only a diffuse flux of charged particles. For neutral decay products, as photons or neutrinos, there are practically no deviations so that one could measure a flux coming from specific regions where the DM is dense, as in the center of galaxies. This is especially the case for neutrinos, but these are unfortunately very difficult to detect.

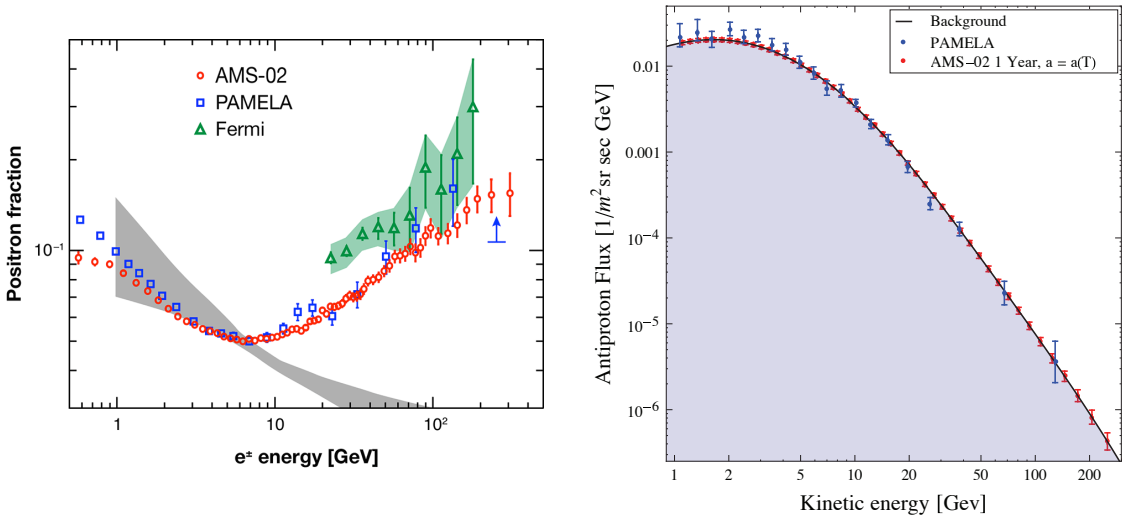

Figure 5.4 – Left : Positron fraction (positron flux normalized to the sum of electron and positron fluxes) as a function of the energy, as measured by several experiments. The gray band shows the expected positron fraction from astrophysical sources. The figure has been taken from Ref. [298]. Right : antiproton flux as a function of the energy. The gray region shows the expected flux from astrophysical background, which fit very well the data, contrarily to the positron flux. The plot has been taken from Ref. [299].

Secondly, suppose we detect some residual flux on Earth. In this case one still needs to be sure that it doesn't come from some unexpected background. Indeed, the Universe is very rich, and even if one can identify lots of astrophysical objects thanks to telescopes, there are surely still some exotic ones that escaped our present listing.

Nevertheless, it is still possible to search for DM annihilations signals. For example, most of the astrophysical processes produce mainly particles, and much less antiparticles. This is generally not the case of DM annihilations, which are expected to produce an equal amount of matter and antimatter in most of the theoretical models. As a consequence, any excess in antiparticle flux can be a hint of DM annihilation.

For illustration purpose, we show in Fig. 5.4 the positron fraction $\Phi_{e^+}/(\Phi_{e^+}+\Phi_{e^-})$ (left) and the antiproton flux $\Phi_{\bar{p}}$ (right) as a function of the energy. The data points have been obtained by several experiments. The gray band represent the expected fraction from astrophysical sources. While for the antiproton fluxes these fit very well the data, it is not the case for the positron flux. The excess could be explained by DM annihilations, but it is for now more likely due to an unexpected background or due to the astrophysical model. From antiproton flux measurement, it is possible to derive upper bounds on the annihilation cross section. These can for example be found in Ref. [299]. We won't comment furthermore on the Indirect Detection results.

In practice, the DM annihilation cross section is the same than the one that is responsible for the DM depletion in the usual freeze-out mechanism, see below. Therefore, it is generally fixed for a given DM mass, since the relic DM abundance is known. As a consequence, the DM annihilation rate can be computed and the decay products are known. The associated flux can finally be estimated and confronted to the observed flux.

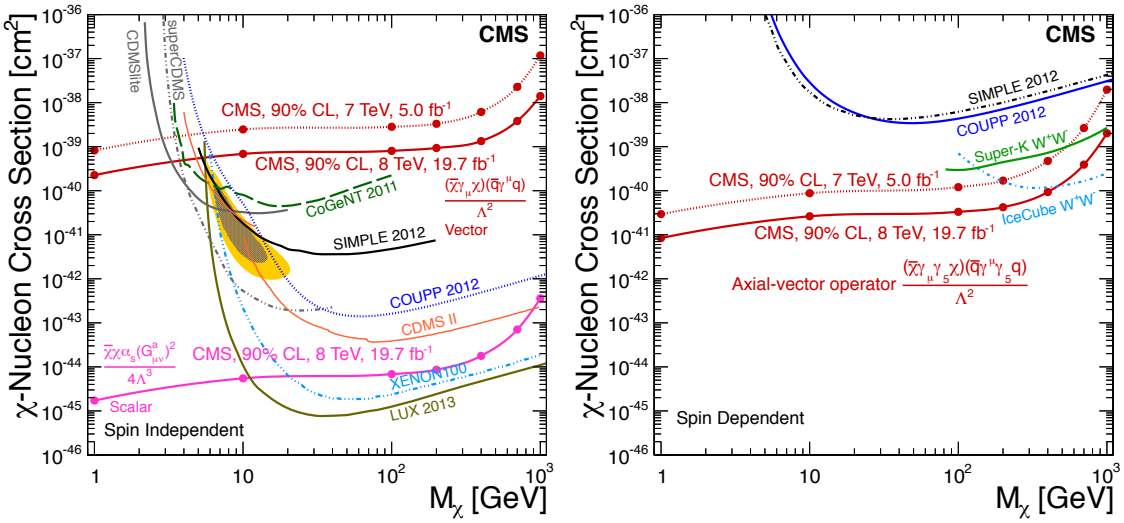

Figure 5.5 – Present best upper bounds on the Spin Independent – scalar and vector interactions – (left) and Spin Dependent – axial-vector interaction – (right) cross sections as a function of the DM mass, provided by the CMS collaboration [300]. Results from CMS are confronted to the other present bounds provided by detection experiments.

5.3.3 Collider constraints

Since pure DM production (only DM particles in the final state) is obviously not observable, colliders such as LHC look for specific signatures as a single monojet or monophoton in the final state with missing transverse momentum E_T. For example, a quark of an initial proton can radiate a gluon or a photon before annihilating into two DM particles. By searching for such signatures, the LHC already provided bounds on the Spin Dependent and Spin Independent DM-nucleon cross section. We show in Fig. 5.5 the present upper bound on the DM-nucleon cross section as provided by the CMS collaboration, for scalar and vector interactions (left) and axial-vector interactions (right).

Concerning the Inert Doublet Model, in the left panel of Fig. 5.6, the gray-shaded region indicates the region of the (m_{H^0}, m_{A^0}) plane excluded by LEP data. The plot has been taken from Ref. [301]. The lower left triangle, where $m_{H^0} + m_{A^0} < m_Z$, is excluded by LEP I data on the Z boson width. The remaining part of the shaded region is excluded by the LEP II analysis performed in Ref. [301]. Note that the upper left region is not accessible by the requirement that $m_{H^0} < m_{A^0}$. The right panel of Fig. 5.6 below, taken from Ref. [302], shows the allowed parameter region (at 95% C.L.) in the $(m_{\eta^\pm}, \lambda_3)$ parameter space from the requirement that the $h \to \gamma\gamma$ scalar decay width doesn't exceed the allowed range, and assuming that there are no invisible decays of the SM scalar. These two plots illustrate that, beside the constraints from Direct Detection, there is still few constraints on the Inert Doublet Model for $m_{H_2} \gg 100$ GeV which is the case we will consider here after.

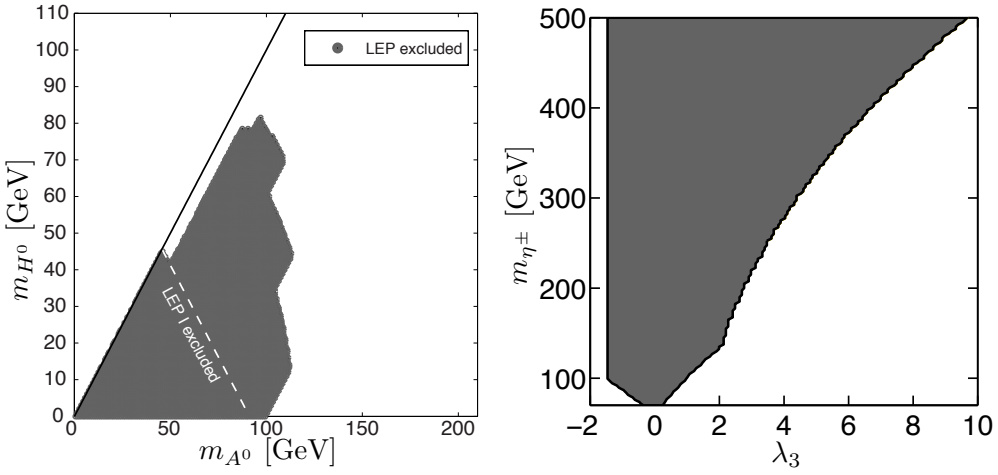

Figure 5.6 – In gray are shown the excluded regions for the parameter space (m_{H^0}, m_{A^0}) (left plot taken from Ref. [301]) and for $(m_{\eta^\pm}, \lambda_3)$ (right plot taken from Ref. [302]) in the framework of the Inert Doublet Model.

5.4 Dark matter production mechanisms

5.4.1 Symmetric production and WIMP miracle

The usual way one can explain the DM relic density is through the usual freeze-out mechanism. This latter can be described as follows. At $T \gg m_{DM}$, the DM is in thermal equilibrium because of fast interactions with SM particles. The DM follows the thermal density until $T = T_{\rm fo} \ll m_{DM}$, where the interactions freeze out, and from when the DM density remains constant. The mechanism, even if similar to the leptogenesis one, differs by the fact that we just focus on the total DM density, and not on an asymmetry generated through CP-violating decays. In order to quantify the amount of DM particles left after freeze-out, one needs to solve the corresponding Boltzmann equation(s).

◦ Boltzmann equation

To illustrate more precisely the freeze-out mechanism, let's consider a simple case where the DM is its own antiparticle, is stable, and annihilates in SM particles through the symmetric scattering channel $SS \leftrightarrow XX$, where S denotes the DM candidate and X some lighter SM particle, i.e. $m_X \ll m_S$. This example corresponds for example to the real scalar singlet DM introduced in section 5.2.1, with the replacement $X \to H$. In this case, it is straightforward to derive the Boltzmann equation for the DM number density $Y_S \equiv n_S/s$, which reads

$$\dot{Y}_S = -\left[\left(\frac{Y_S}{Y_S^{\rm Eq}}\right)^2 - 1\right]\gamma_S\,, \tag{5.17}$$

where $\dot{Y}_S = sHz\,dY_S/dz$ with $z \equiv m_S/T$, $Y_S^{\rm Eq} = n_S^{\rm Eq}/s$ with the equilibrium density given by $n_S^{\rm Eq} \simeq m_S^3/(2\pi^2 z)K_2(z)$ with $K_2(z)$ the Bessel function, and where γ_S the thermal scattering rate of the process $SS \leftrightarrow XX$, which is a model-dependent quantity that must be computed. In the case

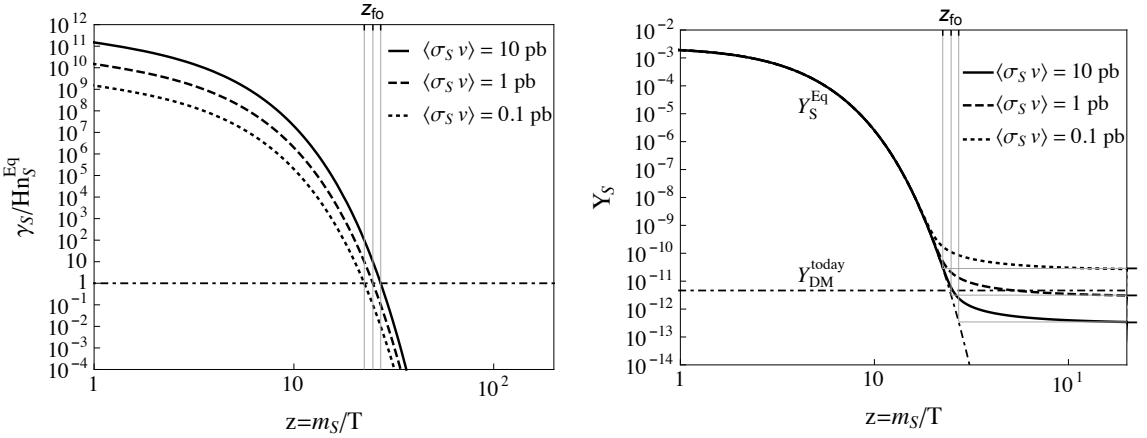

Figure 5.7 – Left : reaction density $\gamma_S/(Hn_S^{\rm Eq})$ as a function of $z = m_S/T$ for different values of the cross-section. Below the horizontal line, the reaction is no more in equilibrium and the associated process basically never occurs. Right : density Y_S as a function of z for different values of the cross-section. The dotted-dashed curve shows the equilibrium density, and the horizontal dotted-dashed curve is the DM density as measured by Planck. The ticks on the right-handed y-axis gives the density Y_S as given by Eq. (5.19). In both plot we fixed $m_S = 100$ GeV.

where this interaction freezes out at $z_{\rm fo} \gg 1$ (cold relics), the thermal rate in Eq. (5.17) can be approximated by

$$\gamma_S = n_S^{\rm Eq}\Gamma_S \approx n_S^{\rm Eq} n_S^{\rm Eq}\langle\sigma_S v\rangle \,, \tag{5.18}$$

where $\langle\sigma_S v\rangle$ is the thermal average of the non-relativistic annihilation cross-section times the relative velocity of the initial interacting particles.

∘ Analytical solution of the Boltzmann equation

We now study the analytical solution of the above Boltzmann equation. We introduce two different methods. Each method provides an analytical solution which is in good approximation with the value of the final relic density obtained by integrating numerically the Boltzmann equation. The result of the second method will actually be very useful in the section 5.5 below.

Method 1. Within this method, the resolution of the Boltzmann equation is straightforward. We proceed in the same way as in the leptogenesis chapters. As long as $\Gamma_S > H$, the annihilations $SS \leftrightarrow XX$ are in thermal equilibrium so that Y_S follows $Y_S^{\rm Eq}$. This can be easily verified analytically because this amounts to putting the l.h.s. of the Boltzmann equation to zero. At $z = z_{\rm fo}$, one has $\Gamma_S(z_{\rm fo}) = H(z_{\rm fo})$ and the annihilations freeze out : the Hubble expansion rate is larger than the annihilation rate so basically no annihilation can occur anymore. Around this moment, the DM density has left the thermal equilibrium distribution and remains more or less constant until now. The DM relic density is in this case given by

$$Y_S^{\rm end} \approx Y_S(z_{\rm fo}) \,, \tag{5.19}$$

which has to be compared to the observed value of the DM abundance

$$\frac{\Omega_{DM}}{\Omega_B} = \frac{m_{DM}}{m_p}\frac{Y_{DM}}{Y_B}\bigg|_{\text{today}} \quad \Rightarrow \quad Y_{DM}^{\text{today}} \approx 4.6\cdot 10^{-10}\cdot\left(\frac{1\,\text{GeV}}{m_S}\right). \tag{5.20}$$

Let's note that the result in Eq. (5.19) can also be written as

$$\Omega_{DM}h^2 \approx \frac{4.3\cdot 10^7}{g_*}\cdot\frac{m_S}{\text{GeV}}\cdot\frac{z_{\text{fo}}^{3/2}}{e^{z_{\text{fo}}}}. \tag{5.21}$$

The result in Eq. (5.19) is illustrated in Fig. 5.7, where in the left panel we show the ratio $\gamma_S/(Hn_S^{\text{Eq}})$ as a function of $z = m_S/T$ for different values of the cross-section $\langle\sigma_S v\rangle$. In the right-panel, we show the numerical solution of the Boltzmann equation (5.17) as a function of z for these same cross-section. In both plots, we fixed $m_S = 100$ GeV. We see that the larger the cross-section, the larger the z_{fo} and the smaller the relic density, as expected from Eq. (5.19).

It is worth to note that for a DM particle of the order of the EW scale, $m_S = 100$ GeV, the right relic abundance is obtained for a cross-section $\langle\sigma_S v\rangle \approx 1$ pb, which is the typical value of the weak interactions ! This is the so-called "WIMP miracle", where WIMP stands for Weakly Interacting Massive Particle. This miracle, or coincidence, clearly points towards a new physics scale which could be not so larger than the EW scale.

From Eqs. (5.19) and (5.21), one still needs to determine the analytical expression of the freeze-out temperature, which seems clearly related to the mass and the cross-section. The freeze-out temperature is determined by the solution of the equation

$$\frac{\gamma_S}{Hn_S^{\text{Eq}}}\bigg|_{z_{\text{fo}}} = 1\,, \qquad \text{or equivalently if } z_{\text{fo}} \gg 1, \qquad \frac{n_S^{\text{Eq}}\langle\sigma_S v\rangle}{H}\bigg|_{z_{\text{fo}}} = 1\,. \tag{5.22}$$

This translates as

$$\frac{e^{z_{\text{fo}}}}{\sqrt{z_{\text{fo}}}} \approx 0.038\cdot\frac{m_{\text{Planck}}m_S\langle\sigma_S v\rangle}{\sqrt{g_*}}\,, \tag{5.23}$$

whose resolution gives approximately

$$z_{\text{fo}} \approx \ln\left[0.038\cdot\frac{m_{\text{Planck}}m_S\langle\sigma_S v\rangle}{\sqrt{g^*}}\right] + \frac{1}{2}\ln\left\{\ln\left[0.038\cdot\frac{m_{\text{Planck}}m_S\langle\sigma_S v\rangle}{\sqrt{g^*}}\right]\right\}. \tag{5.24}$$

It is important to stress that this value of z_{fo} doesn't represent exactly the value at which the density starts to leave the equilibrium density. This freeze-out value is the one that needs to be injected in the approximated solution in Eq. (5.19), which is valid up to ~ 20 % compared to the numerical solution of the Boltzmann equation (5.17). Injecting Eq. (5.23) in Eq. (5.21), one gets

$$\Omega_{DM}h^2 \approx \frac{0.94\cdot 10^9\cdot z_{\text{fo}}\,\text{GeV}^{-1}}{\langle\sigma_S v\rangle\sqrt{g_*}m_{\text{Planck}}}\,. \tag{5.25}$$

In order to generate the correct DM relic abundance, one has generally that the freeze-out value $z_{\text{fo}} \equiv m_S/T_{\text{fo}}$ lies around $z_{\text{fo}} \simeq 25$.

Method 2. There exists another method, which we develop briefly here since we will need it in the next section. It gives in general a more accurate result, see Ref. [303]. Instead of defining the freeze-out temperature as the temperature at which $\Gamma_S = H$ as in Eq. (5.22), the freeze-out temperature $T'_{\rm fo}$ is instead determined as the temperature at which the density Y_S ceases to follow the equilibrium density. Taking as a criterion $|1 - Y_S/Y_S^{\rm Eq}|_{z'_{\rm fo}} \sim 1$, we can show that this freeze-out value $z'_{\rm fo} \equiv m_S/T'_{\rm fo}$ is in very good approximation determined by [303]

$$\left.\frac{\gamma_S}{zHn_S^{\rm Eq}}\right|_{z'_{\rm fo}} = 1\,, \qquad \text{or equivalently if } z'_{\rm fo} \gg 1, \qquad \left.\frac{n_S^{\rm Eq}\langle\sigma_S v\rangle}{zH}\right|_{z'_{\rm fo}} = 1\,. \tag{5.26}$$

This translates as

$$e^{z'_{\rm fo}}\sqrt{z'_{\rm fo}} \approx 0.038 \cdot \frac{m_{\rm Planck} m_S \langle\sigma_S v\rangle}{\sqrt{g_*}}\,, \tag{5.27}$$

whose resolution gives approximately [4]

$$z'_{\rm fo} \approx \ln\left[0.038 \cdot \frac{m_{\rm Planck} m_S \langle\sigma_S v\rangle}{\sqrt{g^*}}\right] - \frac{1}{2}\ln\left\{\ln\left[0.038 \cdot \frac{m_{\rm Planck} m_S \langle\sigma_S v\rangle}{\sqrt{g^*}}\right]\right\}\,. \tag{5.28}$$

The evolution of the density is then given as follows. For $z < z'_{\rm fo}$, the S density follows closely the equilibrium density, while for $z > z'_{\rm fo}$, the density evolution is given by the solution of the Boltzmann equation (5.17) with the inverse process $SM\,SM \to SS$ neglected, i.e. by the equation

$$\dot{Y}_S = -\left(\frac{Y_S}{Y_S^{\rm Eq}}\right)^2 \gamma_S \simeq -Y_S^2 s^2 \langle\sigma_S v\rangle\,. \tag{5.29}$$

This means that each time two S annihilate, it is definitively two S less in the thermal bath. The resolution of the above equation is straightforward. Using as initial condition $Y_S^{\rm Eq}(z'_{\rm fo})$, it is given by

$$Y_S(z) \approx \frac{Y_S^{\rm Eq}(z'_{\rm fo})}{1 + \frac{s(z)z}{H(z)} Y_S^{\rm Eq}(z'_{\rm fo}) J(z'_{\rm fo})}\,, \tag{5.30}$$

where $J(z'_{\rm fo})$ is an integral given by

$$J(z'_{\rm fo}) = \int_{z'_{\rm fo}}^{z} dz' \frac{\langle\sigma_S v\rangle}{z'^2}\,. \tag{5.31}$$

If the cross section doesn't depend on z, it becomes

$$Y_S(z) \approx \frac{Y_S^{\rm Eq}(z'_{\rm fo})}{1 + \frac{\langle\sigma_S v\rangle s(z)}{H(z)}\left(\frac{z}{z'_{\rm fo}} - 1\right) Y_S^{\rm Eq}(z'_{\rm fo})}\,. \tag{5.32}$$

[4] Let's note the minus sign in front of the second term in the r.h.s. with respect to Eq. (5.24).

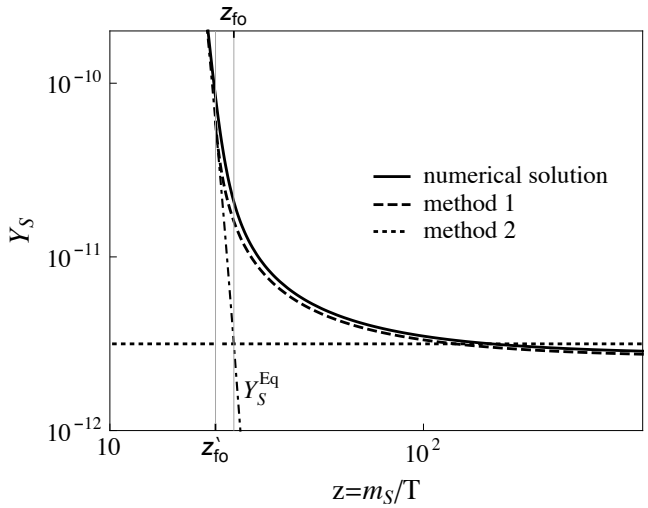

Figure 5.8 – Density Y_S as a function of z for $m_S = 100$ GeV and a fixed cross section $\langle\sigma v\rangle = 1$ pb. The solid curve shows the numerical solution of the Boltzmann equation (5.17). The dotted horizontal line shows the solution using the first method, i.e. $Y_S^{\rm end} = Y_S^{\rm Eq}(z_{\rm fo})$ where $z_{\rm fo}$ is given by the condition $\Gamma_S = H$. The dotted curve shows the solution using the second method, Eq. (5.30), which is based on a semi-analytical approach. Method 1 gives the correct result up to ∼20 % deviation while method 2 up to ∼5 %.

For $z \to \infty$, the asymptotic value of the DM density is finally given by

$$Y_S^{\rm end} \approx \frac{Y_S^{\rm Eq}(z'_{\rm fo})}{1 + \frac{\langle\sigma_S v\rangle s(z)}{H(z)} \frac{z}{z'_{\rm fo}} Y_S^{\rm Eq}(z'_{\rm fo})} \,. \tag{5.33}$$

If the second term of the denominator is much greater than 1, which is generally the case in order to generate the right relic abundance, this latter result leads to nothing else than the usual freeze-out solution

$$\Omega_{DM} h^2 \approx \frac{1.07 \cdot 10^9 \cdot z'_{\rm fo} {\rm GeV}^{-1}}{\langle\sigma_S v\rangle \sqrt{g_*} m_{\rm Planck}} \,. \tag{5.34}$$

This result gives the right relic abundance up to deviation of the order of ∼ 5 %. In order to generate the correct DM relic abundance, one has generally that the freeze-out value lies around $z'_{\rm fo} \simeq 21$. We show in Fig. 5.8 the comparison between the different analytical method. Note that Eq. (5.32) will be actually very useful in what follows.

5.4.2 Asymmetric production

If the DM particle is not its own antiparticle, another interesting possibility arises. As in the case of the generation of a baryon asymmetry via the leptogenesis scenario, one could wonder if a DM asymmetry could not be at the origin of the DM relic abundance (see e.g. the reviews of Refs. [207, 304, 305, 306, 307]). Indeed, as Eq. (5.2) shows, the present value of the DM relic abundance is only a factor ∼5 bigger than the baryon relic abundance : $\Omega_{DM} \approx 5\Omega_B$. But why are they so close ? This may be a coincidence, but this may also be a hint that the generation of the

baryon and the DM densities were actually related. In particular, since the present baryon density is expected to come originally from a baryon asymmetry, one could wonder if it is not the case of the DM density too.

For example, if the DM particle is a complex field, it could in principle develop an asymmetry. But how could an asymmetry be generated ? There are several ways an asymmetry can develop. A possibility is that the DM asymmetry is generated by the CP-violating decay of some heavier field, as in the leptogenesis scenario, see for example Ref. [308, 309, 310]. Another possibility is that the DM asymmetry is generated by thermal interaction between the DM and SM particles that carry an asymmetry, in which case the baryon and the DM asymmetries are related through chemical equilibrium conditions, see for example Ref. [311]. This case involves chemical potential equations, not without similarities with the ones we considered in the previous sections. In these two cases, the baryon and the DM relic density are related through

$$\frac{\Omega_{DM}}{\Omega_B} = \frac{m_{DM}}{m_B}\frac{\Delta Y_{DM}}{\Delta Y_B}\bigg|_{\text{today}} . \tag{5.35}$$

We see that if the amount of DM asymmetry is exactly the same as the baryon asymmetry, the DM candidate should have a mass of the order of $m_{DM} \sim 5$ GeV. However, one deviates in general from this idealistic situation because the DM candidate would be so light that one should have already discover it. The factor 5 between the Ω_{DM} and Ω_B is in this case the consequence of an interplay between m_{DM} and ΔY_{DM} through the combination $(m_{DM} \cdot \Delta Y_{DM})$.

Let's note that the symmetric component DM should also undergo a standard freeze-out, so that one could have in general both symmetric and asymmetric DM. In this case, the Boltzmann equation for the DM evolution should be modified in order to account for the DM asymmetry.

5.5 Inert Scalar Doublet Asymmetry as the origin of dark matter

The Inert Doublet Model (IDM) for dark matter has been introduced in section 5.2.2. It is well known that the IDM can account for the observed DM relic abundance via the usual freeze-out mechanism (symmetric production as introduced in section 5.4.1), and be in agreement with direct detection constraints, for DM masses in the ranges $\sim$ [50, 80] GeV and above $\sim$ 540 GeV, up to the $\sim$ 40-50 TeV unitarity bound [290, 291, 312, 292, 313].

However, in the scalar potential in Eq. (5.7), it is interesting to note the presence of the unique term which doesn't conserve the number of inert doublets minus the number of anti-inert doublets :

$$\mathscr{L}^{\text{IDM}} \ni -\frac{\lambda_5}{2}\left[\left(H_1^\dagger H_2\right)^2 + \text{H.c.}\right] , \tag{5.36}$$

to which corresponds the scattering processes $H_2 H_2 \leftrightarrow H_1 H_1$, $H_2 \bar{H}_1 \leftrightarrow H_1 \bar{H}_2$ and their inverse. This interaction reaches thermal equilibrium at $T \sim m_{H_2}$ if at this temperature the corresponding Γ_{λ_5} scattering rate, given in Eq. (E.5) of the Appendix E.1, is larger than the Hubble rate, which

gives the condition

$$|\lambda_5| \gtrsim 10^{-6} \cdot \left(\frac{m_{H_2}}{\text{TeV}}\right)^{1/2} . \tag{5.37}$$

If this equation is satisfied, from chemical potential considerations one has $\mu_{H_1} = \mu_{H_2}$, and both H_1 and H_2 scalar doublets asymmetries are equilibrated, leading potentially to an asymmetric production of the DM relic abundance (at least if a scalar asymmetry ΔH_1 was present), see section 5.4.2. [5] Together with the direct detection constraint in Eq. (5.11) with a 100 keV (180 keV) mass splitting, this means that the λ_5 interaction reaches thermal equilibrium as soon as $m_{H_2} \gtrsim$ 100 GeV (30 GeV), in which case an asymmetry is always created from a H_1 asymmetry.

This is interesting because one generally expects the existence of a $B-L$ asymmetry at high temperature in order to generate the BAU, as for example in the leptogenesis scenarios. This means that a scalar doublet asymmetry ΔH_1 should have been created automatically too at high temperature from thermal equilibrium SM interactions [215]. Therefore, if the λ_5 interaction above has reached thermal equilibrium, a ΔH_2 will be generated automatically too. In other words, even if no H_2 asymmetry is created at high energies, such an asymmetry will be created anyway as soon as the $B-L$ asymmetry is created. [6] Note that it could work also the other way around, i.e. a primordial DM asymmetry could be at the origin of baryogenesis via the same λ_5 equilibration interaction, a possibility we will not consider here (for a scenario of this kind see Ref. [316]).

Therefore a question arises : could the H_2 asymmetry be responsible for most of the present DM relic density ? Or more generally, *what is the fate of the H_2 asymmetry which will anyway be created for $m_{H_2} \gtrsim 100$ GeV ?* This study was made in collaboration with Thomas Hambye [3].

In this section, one will stick to the minimal IDM framework, as defined in section 5.2.2. Let us make two simple starting assumptions. First, let us assume that the symmetric component of the relic density left after freeze-out is smaller than the observed value. Fast SM gauge scatterings automatically care for that for m_{H^0} within the $\sim 120-540$ GeV range, whereas for other values of m_{H^0} large enough $\lambda_{3,4}$ interactions can take care of that [292]. This implies a symmetric annihilation cross section larger than the usual thermal freeze-out value ~ 1 pb, which means a freeze-out temperature T_{fo} smaller than the usual $T_{\text{fo}} \sim m_{H^0}/25$ value. Second, let us assume that a $B-L$ asymmetry has been generated at a temperature T_{B-L} above m_{H_2} and above the ElectroWeak Phase Transition (EWPT) temperature T_{EW} (which we take as the temperature where the vacuum expectation value of the SM scalar field becomes sizable, that is $T_{EW} \approx 165$ GeV, see section 3.3.1). Note that in this way too, the link between the baryon and the DM asymmetry is interestingly totally independent of the way the $B-L$ asymmetry has been created (from any type

[5] Actually, in the few-TeV asymmetric inert DM scenario considered in Ref. [309], it is assumed instead that the λ_5 interaction could have never been in thermal equilibrium. In this case, the DM asymmetry would have been created explicitly at high energies, basically independently of the $B-L$ asymmetry. If the inert scalar is the DM particle, it turns out that the lower bound of Eq. (5.11) implies that Eq. (5.37) must anyway hold for TeV masses.

[6] The inert DM model contains therefore an interaction which basically implies that "Higgsogenesis" [311] production of a DM asymmetry is at work. In Ref. [311], a X_1 fermion singlet DM framework is considered with an extra X_2 fermion doublet and an X-symmetry. An X_2 asymmetry is created from a X-symmetry violating $X_2^2 H_1^2$ non-renormalizable interaction, which is afterwards reprocessed into a X_1 symmetry through X_2 decays. Asymmetric frameworks based on the equilibration of the SM scalar asymmetry with a dark sector asymmetry, based on several new dark sector particles, or based on various possibilities of a $SU(2)_L$ multiplet, can also be found in Refs. [314] and [315] respectively.

of Seesaw or whatever). Thus, we do not care about the way this $B-L$ asymmetry could have been generated. [7]

5.5.1 Asymmetric production and depletion of the H_2 density

In what follows, we will consider in detail and chronologically what happens when the temperature of the Universe cools down from $T \gg m_{H_2}$ to today $T \ll T_{EW}$, crossing $m_{H_2} > T_{\lambda_5} > T_{\rm fo} > T_{EW}$, with T_{λ_5} the temperature where the scattering induced by the λ_5 interaction decouples and $T_{\rm fo}$ the freeze-out temperature at which the total annihilation cross section decouples. This is, we first discuss how an inert doublet asymmetry can be generated and depleted thanks to this λ_5 interaction. Then, we show that there is another depletion mechanism associated to DM oscillations which is at work as soon as the temperature of the Universe goes below the EWPT. A sketch of the scenario is displayed in Fig. 5.11. In this section, we don't consider the Direct Detection constraints, whose consequence will be address in the next section.

A. $\mathbf{T \geq T_{\lambda_5}}$: Inert scalar doublet asymmetry from the SM scalar doublet asymmetry

At temperature above $T_{EW} \approx 165$ GeV, all 2 inert doublet components (η^+ and η^0) have a common mass $m_{H_2} = m_2$, see Eq. (5.7). If Eq. (5.37) is satisfied, the chemical potential of both scalar doublets are equal, $\mu_{H_2} = \mu_{H_1}$. Together with the usual SM chemical equilibrium relations (from thermal equilibrium SM processes [215]), the $\mu_{\eta^+} = \mu_{\eta^0}$ relation (from e.g. $\eta^+\eta^{0*} \leftrightarrow SM$ processes), and the hypercharge relation

$$\sum_i \left(\Delta Y_{Q_i} + 4\Delta Y_{u_i} - 2\Delta Y_{d_i} - \Delta Y_{\ell_i} - 2\Delta Y_{e_i}\right) + \Delta Y_{H_1} + \Delta Y_{H_2} = 0\,, \tag{5.38}$$

it simply gives : [8]

$$\Delta Y_{H_2}(z) = \frac{k(z)}{2}\Delta Y_{H_1} = -\frac{16k(z)}{158+13k(z)}\Delta Y_{B-L}\,, \tag{5.39}$$

where we used the general relation between the chemical potential and the asymmetry (given in Eq. (C.54) in the relativistic limit), i.e. :

$$\Delta Y_{H_2} = \frac{T^2}{6s}\, g_{H_2}\, \mu_{H_2}\, k(z)\,, \tag{5.40}$$

with the k-factor suppression for bosons given by

$$k(z) = \frac{6}{4\pi^2}\int_0^\infty x^2 \sinh^{-2}\left(\frac{1}{2}\sqrt{x^2+z^2}\right) dx \simeq \begin{cases} 2\,, & \text{if} \quad z \ll 1\,, \\ 12\left(\frac{z}{2\pi}\right)^{3/2} e^{-z}\,, & \text{if} \quad z \gg 1\,. \end{cases} \tag{5.41}$$

[7] Let's here mention the "scotogenic model", which is an extension of the IDM with right-handed neutrinos odd under the Z_2 symmetry (already mentioned in section 1.3.1). Indeed, in this model light neutrino mass can be generated at the loop-level [44] and the baryon asymmetry of the Universe can be generated too through the decay of the heavy right-handed neutrinos via the leptogenesis mechanism [292].

[8] We here consider the temperature regime $T \lesssim 10^5$ GeV, where all the SM Yukawa interactions are in thermal equilibrium. This is justified because, in the IDM alone, the inert doublet mass must anyway be smaller than ~ 30 TeV otherwise the symmetric production mechanism generates unavoidably too much DM relic abundance [292].

Eq. (5.39) applies until the λ_5 interaction decouples at z_{λ_5}, where it is given by

$$\Delta Y_{H_2}(z_{\lambda_5}) = -\frac{16k(z_{\lambda_5})}{158+13k(z_{\lambda_5})}\Delta Y_{B-L}\,. \tag{5.42}$$

For practical reasons, let's define the H_2 asymmetry when the λ_5 interaction decouples as

$$\Delta_{H_2}^{\lambda_5} \equiv \left|\Delta Y_{H_2}\left(z_{\lambda_5}\right)\right|\,. \tag{5.43}$$

Let's consider two limiting cases.

No suppression of the asymmetry. Suppose that $z_{\lambda_5} \ll 1$, from the first line of Eq. (5.41) the k-factor just reduce to $k(z_{\lambda_5}) \simeq 2$ so that the H_2 asymmetry would be given by

$$\Delta Y_{H_2} = \Delta Y_{H_1} = -\frac{4}{23}\Delta Y_{B-L}\,. \tag{5.44}$$

As said above, for similar $B-L$ and DM asymmetries, the DM relic density constraint requires m_{DM} to have a mass of few GeV (more exactly, from Eq. (5.44) and taking into account the ΔY_{B-L} to $Y_B^{\rm today}$ ratio which holds in this case, $\Delta Y_{B-L}/Y_B^{\rm today} = 37/12$, one would need $m_{H_2} \approx 10$ GeV). As this possibility is excluded by collider constraints – see section 5.2.2 – this implies that a subsequent suppression of the H_2 asymmetry by a factor of $\sim (10\text{ GeV}/m_{DM})$ must necessarily occur. Two different types of suppressions can naturally take place. The first one, that we now discuss, is the Boltzmann k-factor suppression from asymmetry violating scatterings, used in several other DM models, see e.g. Refs. [317, 311]. The second possible suppression, which we consider after, can arise later when $T \lesssim T_{EW}$ from the combined effect of $\eta^0 \leftrightarrow \eta^{0*}$ oscillations and symmetric annihilations.

Suppression from the k-factor. If the λ_5 interaction is such that it decouples at $z_{\lambda_5} > 1$, from Eq. (5.42) the H_2 asymmetry will undergo a Boltzmann suppression from the k-factor, as can be seen from the second line of Eq. (5.41). This suppression can be understood directly from the Boltzmann equation for ΔY_{H_2} [318], valid for $T \geq T_{EW}$,

$$\frac{d\Delta Y_{H_2}}{dz} = -\frac{4}{sHz}\left(\frac{\Delta Y_{H_2}}{Y_{H_2}^{\rm Eq}} - \frac{\Delta Y_{H_1}}{Y_{H_1}^{\rm Eq}}\right)\gamma_{\lambda_5}\,, \tag{5.45}$$

where $z \equiv m_{H_2}/T$, $H(z)$ is the Hubble rate and $\gamma_{\lambda_5}(z)$ is the reaction density of the λ_5 scatterings, given in Eq. (E.1) of the Appendix E.1. It includes both pair annihilation/creation $H_2H_2 \leftrightarrow H_1H_1$ and "t-channel" $H_2\bar{H}_1 \leftrightarrow H_1\bar{H}_2$ processes, whose rates read $\gamma_{\phi\phi}^{\eta\eta}$ and $\gamma_{\phi\eta}^{\phi\eta}$ respectively. These λ_5-induced processes leave intact the sum of the asymmetries of H_1 and H_2 but not each asymmetry individually. Once T drops below m_{H_2}, the first term in the r.h.s. of Eq. (5.45) is enhanced with respect to the second term by the fact that $Y_{H_2}^{\rm Eq}$ is Boltzmann suppressed, unlike $Y_{H_1}^{\rm Eq}$. This Boltzmann suppression of the asymmetry lasts until the λ_5 induced scatterings decouple, at $T = T_{\lambda_5}$, when $\Gamma_{\lambda_5} \simeq H$. The solution of the Boltzmann equation is approximately given by Eq. (5.42), which is nothing but the solution which makes the r.h.s. of Eq. (5.45) to vanish.

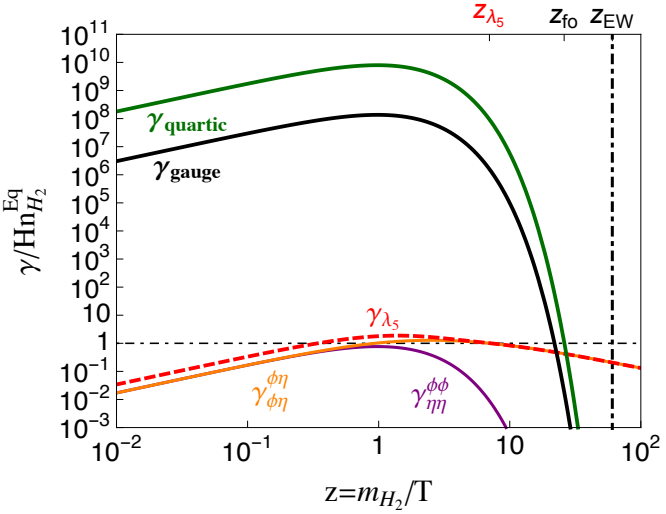

Figure 5.9 – Reaction densities $\gamma/Hn^{\rm Eq}_{H_2}$ as a function of $z = m_{H_2}/T$, for $m_{H_2} = 10$ TeV. The black curve shows the gauge reactions and the green curve shows the annihilation rate from quartic interactions when taking $\lambda_3 = \lambda_4 = 1$. The dashed red curve corresponds to the total λ_5 interaction rate, composed by the sum of the $H_2H_2 \leftrightarrow H_1H_1$ (purple) and $H_2\bar{H}_1 \leftrightarrow H_1\bar{H}$ (orange) channels. We fixed $\lambda_5 = 4\cdot10^{-6}$ for illustration purpose.

Clearly, from Eq (5.42) with $k(z)$ given in (5.41), the λ_5 coupling must not be too large in order to avoid a too strong exponential suppression of the H_2 asymmetry. As emphasized in Ref. [311], for fermion quartic interactions, the last induced channels to decouple are the t-channel ones, simply because they are less Boltzmann suppressed than the other ones. In our context, this means that the $H_2\bar{H}_1 \leftrightarrow H_1\bar{H}_2$ reactions are the last ones to decouple, long after the $H_2H_2 \leftrightarrow H_1H_1$ ones. The value of z_{λ_5} is given by the condition that the Γ_{λ_5} rate is equal to the Hubble rate H, and it is actually very sensitive to the value of λ_5 as can be seen from Fig. 5.9 because of the t-channel scattering. For example, if $m_{H_1} = 10$ TeV one gets $z_{\lambda_5} \approx 2\ldots15$ for $\lambda_5 = 3\cdot10^{-6}\ldots5\cdot10^{-6}$. For somewhat smaller values of λ_5, even if the λ_5 reactions do not enter in thermal equilibrium (as defined by Eq. (5.37)), a numerical integration of the Boltzmann equation shows that still a number of scattering processes occur nevertheless, what can lead to a sizable asymmetry. For these reasons, we will only use the Boltzmann equation in Eq. (5.45) for the numerical results. [9]

B. $T_{\lambda_5} > T > T_{fo}$: Freeze-out in the presence of an asymmetry

During this period, the ΔY_{H_2} asymmetry stays constant unlike the total abundance Σ_{H_2}, whose Boltzmann equation for this period reads

$$\frac{d\Sigma_{H_2}}{dz} = -\frac{\langle\sigma_{H_2}v\rangle s}{zH}\left[\Sigma^2_{H_2} - \Delta^{\lambda_5\,2}_{H_2} - \Sigma^{\rm Eq\,2}_{H_2}\right], \tag{5.46}$$

[9] As an important remark, note that in the example of Fig. 5.9 where $m_{H_2} = 10$ TeV, the value of $\lambda_5 = 4\cdot10^{-6}$ is actually excluded by the Direct Detection bound in Eq. (5.11), which requires $\lambda_5 \lesssim 5\cdot10^{-5}$. Larger values of λ_5 lead in fact to a too strong suppression of the H_2 asymmetry. As we will show in the next section, a dominant asymmetric DM scenario in the IDM alone is actually excluded ! However, one can easily evade the Direct Detection if the inert scalar decays into lighter particles, which therefore constitutes de DM candidate, see section 5.5.4.

where $\langle\sigma_{H_2} v\rangle$ is the effective thermal cross section of the $H_2\bar{H}_2 \leftrightarrow SM\,SM$ annihilations, given in Eq. (E.7) of the Appendix. The total H_2 density is defined by $\Sigma_{H_2} \equiv Y_{H_2} + Y_{\bar{H}_2}$. [10] With a constant $\Delta_{H_2}^{\lambda_5}$, as it is the case during this period, the solution of Eq. (5.46) at freeze-out $z = z_{\rm fo}$ is to a good approximation given by : [11]

$$\Sigma_{H_2}(z_{\rm fo}) \simeq \left[\Delta_{H_2}^{\lambda_5\,2} + \Sigma_{H_2}^{\rm Eq\,2}(z_{\rm fo})\right]^{1/2}, \tag{5.49}$$

where $z_{\rm fo}$ is the usual freeze-out value as defined in Eq. (5.24), given here by the equation

$$z_{\rm fo} \simeq \ln\left[0.0038 \cdot \frac{m_{\rm Planck}\, g_{\Sigma_{H_2}}\, m_{H_2}\langle\sigma_{H_2} v\rangle}{\sqrt{g_* z_{\rm fo}}}\right]. \tag{5.50}$$

If the annihilations are fast enough to leave at $T_{\rm fo}$ a symmetric component smaller than the asymmetric one (which is typically satisfied for $\langle\sigma_{H_2} v\rangle \gtrsim 1$ pb), one has $\Sigma_{H_2}(z_{\rm fo}) \simeq \Delta_{H_2}^{\lambda_5} \gg \Sigma_{H_2}^{\rm Eq}(z_{\rm fo})$. Given the sign of the baryon asymmetry, this means at $T_{\rm fo}$, $\Sigma_{H_2} \sim -\Delta_{H_2} \sim -Y_{\bar{H}_2} \gg Y_{H_2}, \Sigma_{H_2}^{\rm Eq}$.

C. $T_{\rm fo} > T > T_{\rm EW}$: Stagnation of the asymmetry

Nothing is expected to happen during this period. The H_2 total density left at $T_{\rm fo}$ is left intact until T_{EW}, temperature at which the total density and asymmetry are given by :

$$\Sigma_{H_2}(z_{EW}) \simeq \Sigma_{H_2}(z_{\rm fo}) \quad \text{and} \quad \left|\Delta Y_{H_2}(z_{EW})\right| = \Delta_{H_2}^{\lambda_5}. \tag{5.51}$$

For a dominant asymmetric component, one has $\Sigma_{H_2}(z_{EW}) \simeq \left|\Delta Y_{H_2}(z_{EW})\right| = \Delta_{H_2}^{\lambda_5}$.

D. $T < T_{EW}$: Inert scalar doublet asymmetry depletion from $\eta^0 \leftrightarrow \eta^{0*}$ oscillations

Once the temperature drops below T_{EW}, two new effects enter into play : generation of mass splittings between the H^0, A^0 and η^+ components and possibly fast inert particle-antiparticle oscillations $\eta^0 \leftrightarrow \eta^{0*}$, as illustrated in Fig. 5.10. The effect of the mass splittings generated by the SM scalar vev, Eq. (5.9), is of moderate importance as long as $T > \delta m_0 = m_{A^0} - m_{H^0}$ and

[10] We remind that the number of degrees of freedom is given by summing the number of particles (or antiparticles but not both), i.e. $g_{H_2} = 2$ for a $SU(2)_L$ doublet. Therefore, for particles that are not self-conjugated one has $g_{\Sigma_{H_2}} = 2 \cdot g_{H_2}$.

[11] A more precise solution can actually be derived, which reproduce well the shape of the evolution of the Σ_{H_2}. Proceeding in the same way as for Eq. (5.32) in the method 2 of section 5.4.1, one has :

$$\Sigma_{H_2}(z > z'_{\rm fo}) \simeq \left[\Delta_{H_2}^{\lambda_5\,2} + \Sigma'^{\,2}_{H_2}(z)\right]^{1/2} \quad \text{with} \quad \Sigma'_{H_2}(z) = \frac{\Sigma_{H_2}^{\rm Eq}(z'_{\rm fo})}{1 + \frac{\langle\sigma_{H_2} v\rangle s(z)}{H(z)}\left(\frac{z}{z'_{\rm fo}} - 1\right)\Sigma_{H_2}^{\rm Eq}(z'_{\rm fo})}, \tag{5.47}$$

which is the expression we will use in all our numerical results. We recover the solution in Eq. 5.49 by taking the limit where $z \gg z'_{\rm fo}$ in the expression (5.47). As explained above, the value of $z'_{\rm fo}$ corresponds to the temperature at which Σ_{H_2} ceases to follow the equilibrium density $\Sigma_{H_2}^{\rm Eq}$. It is here given by the condition

$$\left.\frac{\Sigma_{H_2}^{\rm Eq\,2} - \Delta_{H_2}^{\lambda_5\,2}}{\Sigma_{H_2}^{\rm Eq}} \frac{s\langle\sigma_{H_2} v\rangle}{zH}\right|_{z'_{\rm fo}} = 1. \tag{5.48}$$

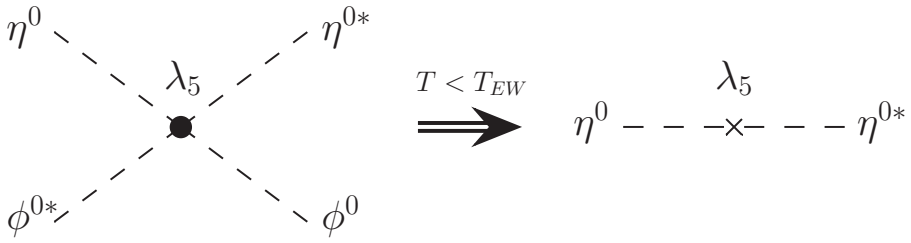

Figure 5.10 – Feynman diagram of the λ_5 interaction involving only neutral scalars. After SSB, the scalar field ϕ^0 acquires a vev leading to $\eta^0 \leftrightarrow \eta^{0*}$ oscillations.

$T > \delta m_\pm = m_{\eta^\pm} - m_{H^0}$. Assuming, as said above, that the H^0 component is the lightest one (i.e. $\lambda_5 < 0$), they imply that the other components will ultimately decay into H^0. But these decays conserve the number of inert scalar particles. They just convert the H_2 asymmetry created before EWSB (with mass m_{H_2}) into a DM relic density of self-conjugated DM particles H^0 (with mass m_{H^0}, different from m_{H_2} unless λ_{H^0} vanishes).

More important is the potential effect of the much faster inert particle-antiparticle oscillations $\eta^0 \leftrightarrow \eta^{0*}$ caused by the λ_5 interaction. The rate of an oscillating particle is simply given by the value of the associated mass splitting [309, 319, 320], i.e. $\Gamma_{\rm osc} = \delta m_0 = m_{A^0} - m_{H^0}$. For $T < T_{EW}$, this rate is very fast compared to the Hubble rate since :

$$\frac{\Gamma_{\rm osc}}{H(T)} \simeq 2 \cdot 10^{15} \cdot |\lambda_5| \cdot \left(\frac{100\,\text{GeV}}{T}\right)^2 \cdot \left(\frac{\text{TeV}}{m_{H^0}}\right) . \tag{5.52}$$

The effect of these oscillations depends obviously on whether they do occur, which Eq. (5.52) doesn't necessarily imply, and on whether symmetric annihilations do occur after EWSB. Actually, even if the freeze-out occurs before EWSB, this does not imply that symmetric annihilations could not restart again after EWSB, due to oscillations [319, 320]. This could easily be the case because, even if one starts with a pure asymmetry, the oscillations will quickly give a number density of each population much larger than their thermal equilibrium values, roughly $n_{\eta^0} \sim n_{\eta^{0*}} \sim |\Delta n_{\eta^0}|/2 \gg n_{\eta^0}^{\rm Eq}$, so that $|\Delta n_{\eta^0}|\langle\sigma v\rangle > H$ can hold even if $n_{\eta^0}^{\rm Eq}\langle\sigma v\rangle < H$. If these annihilations occur, they will anyway reduce the DM abundance, as no inverse processes will occur in this case. Let us consider both possible cases separately.

No symmetric annihilations after EWSB. If no symmetric annihilations arise after EWSB, oscillations have simply no effect. They quickly reconvert a pure η^0 population, or a pure η^{0*} population, into an oscillating mixed η^0-η^{0*} population, but they do not change the number of inert states [319]. In this case, the number of H^0 particles left today will be simply equal to the number of inert scalar particles before EWSB, i.e. $Y_{H^0}^{\rm today} \simeq \Sigma_{H_2}(z_{EW})$.

If the H_2 asymmetry dominates the total density at T_{EW}, the H^0 density is equal to the asymmetry left after λ_5 interaction's decoupling. From Eqs. (5.42) this gives

$$Y_{H^0}^{\rm today} = \frac{16 k\left(z_{\lambda_5}\right)}{158 + 13 k_{H_2}\left(z_{\lambda_5}\right)} \Delta Y_{B-L} , \tag{5.53}$$

with $k(z_{\lambda_5})$ given by Eq. (5.41). Only the relation between the value of Y_B today and ΔY_{B-L} changes after EWSB, as a result of the fact that below T_{EW} the conservation of electric charge holds rather than conservation of Y and T_3. We get

$$Y_B^{\text{today}} \simeq \frac{12}{37}\Delta Y_{B-L}\,. \tag{5.54}$$

As a result, the H^0 density reads

$$Y_{H^0}^{\text{today}} = \frac{148\cdot k\left(z_{\lambda_5}\right)}{474+39\cdot k\left(z_{\lambda_5}\right)}\cdot Y_B^{\text{today}}\,, \tag{5.55}$$

and the present H^0 to baryon density ratio is given by

$$\frac{\Omega_{H^0}}{\Omega_B} = \frac{Y_{H^0}^{\text{today}}}{Y_B^{\text{today}}}\cdot\left(\frac{m_{H^0}}{1\text{ GeV}}\right) = \frac{148\cdot k\left(z_{\lambda_5}\right)}{474+39\cdot k\left(z_{\lambda_5}\right)}\cdot\left(\frac{m_{H^0}}{1\text{ GeV}}\right)\,. \tag{5.56}$$

This is the final result if no symmetric annihilations occur after EWSB and if the asymmetric component ΔY_{H_2} dominates over the total density Σ_{H_2} at T_{EW}. However, it must be stressed that it is not mandatory to avoid symmetric annihilations after EWSB. On the contrary, if the λ_5 interaction above does not provide enough suppression, these scattering processes could easily provide it, without the need of any special tuning. This is what we will now quantify.

Symmetric annihilations after EWSB. Possible effects of dark matter oscillations have been studied in Refs. [319, 320]. As said above, since oscillations reprocess the asymmetry into both particle and antiparticle densities, their main effect is to allow the symmetric annihilations to start again. Even if, as Eq. (5.52) shows, the oscillation rate is much faster than the Hubble rate, this doesn't necessarily mean that oscillations (and thus eventually annihilations) do occur. As shown in these references, if dark matter undergoes fast annihilations or elastic scatterings, these processes can break the coherence of the η^0-η^{0*} states, preventing them from oscillating. The interplay of the oscillations with the other processes is actually more complicated in this inert doublet scenario than in the singlet setups considered in Refs. [319, 320]. This is because on top of η^0-η^{0*} annihilations and η^0 or η^{0*} elastic scatterings, there are charged $\eta^\pm$ states, which at T_{EW} are responsible for half of the asymmetry and do not oscillate. Furthermore, fast inelastic scatterings can change neutral states into these charged states and vice et versa. Moreover, as said above, all states ultimately become real H^0 states, which obviously do not oscillate.

(1) Let us first consider what happens to the neutral states, as if there were no charged states. In this case, one has two important processes. On the one hand, there are $\eta^0\eta^{0*}\to SMSM$ annihilations processes which are dominated by their $\lambda_{3,4}$ interaction contribution. On the other hand there are $\eta^{0(*)}SM\to\eta^{0(*)}SM$ elastic scatterings which are dominated by their t-channel Z exchange contribution, and not by the $\lambda_{3,4}$ elastic scattering contribution. [12] The Z-exchange

[12] For $T\gtrsim m_h$, this stems from the fact that it involves a t-channel mediator whose mass is much smaller than the inert scalar mass, $m_Z\ll m_{H_2}$. As a consequence, it scales as $\Gamma_{\text{scat}}^{\text{gauge}}\simeq G_F^2T^5$ as compared to the quartic coupling elastic contribution which scales as $\Gamma_{\text{scat}}^{\text{quartic}}=n_{H_1}^{\text{Eq}}\langle\sigma v\rangle\simeq\lambda_{3,4}^2T^3/m_{H_2}^2$. For $T<m_h$, the quartic contribution is also sub-leading because it is Boltzmann suppressed, unlike the gauge one.

gauge elastic contribution is the last to decouple, and it is relevant for preventing η^0-η^{0*} states from oscillating because the gauge interaction is odd under η^0-η^{0*} exchange [320], i.e. it basically makes the distinction between η^0 and η^{0*}. Thus the relevant question is, down to which temperature will these processes effectively prevent the oscillations to start ?

At first sight, we could think that oscillations will start only once the scattering rate $\Gamma_{\rm scat}$ goes below the oscillation rate $\Gamma_{\rm osc} = \delta m_0$ (if at this time both rates are still larger than the Hubble rate). This turns out to occur at a rather low temperature, $T_{\rm osc} \sim$ few GeV scale. In this case one would be back to the "no symmetric annihilation" case above, because oscillations have practically no more effect at this temperature, where the annihilation rate is already largely suppressed. However, an integration of the Boltzmann equations shows that oscillations rather start when $(\delta m_0)^2/H = \Gamma_{\rm scat}$, see Ref. [319]. In our scenario, as we have also checked from a numerical integration of the relevant Boltzmann equations, this turns out to happen at a temperature above T_{EW}. Thus we conclude that oscillations start as soon as EWSB occurs.

As a result, annihilations can restart from the EWSB temperature $T_{EW} \approx 165$ GeV. To determine how much of them will annihilate, one can just take the Boltzmann equations with the oscillation and annihilation terms,

$$\frac{d\Sigma_{\eta^0}}{dz} = -\frac{\langle\sigma_0 v\rangle\, s}{2zH}\left[\Sigma_{\eta^0}^2 - \Delta_{\eta^0}^2 - \Xi_{\eta^0}^2 - \Sigma_{\eta^0}^{\rm Eq\ 2}\right], \tag{5.57}$$

$$\frac{d\Delta_{\eta^0}}{dz} = 2i\frac{\delta m_0}{zH}\,\Xi_{\eta^0}, \tag{5.58}$$

$$\frac{d\Xi_{\eta^0}}{dz} = 2i\frac{\delta m_0}{zH}\,\Delta_{\eta^0} - \frac{\langle\sigma_0 v\rangle s}{zH}\,\Xi_{\eta^0}\,\Sigma_0, \tag{5.59}$$

where for any $T \leq T_{EW}$ we define $z \equiv m_{H^0}/T$, with $\langle\sigma_0 v\rangle$ the thermally averaged $\eta^0\eta^{0*} \to SM$ annihilation cross section. Here Δ_{η^0} stems for the usual asymmetry $\Delta_{\eta^0} \equiv \Delta Y_{\eta^0}$, while Ξ_{η^0} is a quantity that accounts for the coherence between the η^0 and η^{0*} components (see [319] for further details). The resolution of these equations leads to a monotonically decreasing $\Sigma_{\eta^0}(z)$ function and to oscillating functions $\Delta_{\eta^0}(z) \propto \cos[f(z)]$ and $\Xi_{\eta^0}(z) \propto \sin[f'(z)]$ whose amplitudes also decrease monotonically. For fast oscillations, and neglecting the $\Sigma_{\eta^0}^{\rm Eq}$ term in Eq. (5.57) (which is indeed suppressed since here $z_{\rm fo} < z_{EW}$), the set of Boltzmann equations can be simplified and solved analytically, at an approximate level, as explained in the Appendix E.2. The solution it gives for Σ_{η^0} is nothing but [13]

$$\Sigma_{\eta^0}(z \geq z_{EW}) = \frac{\Sigma_{\eta^0}(z_{EW})}{1 + \frac{1}{2}\frac{\langle\sigma_0 v\rangle\, s(z)}{H(z)}\left(\frac{z}{z_{EW}} - 1\right)\Sigma_{\eta^0}(z_{EW})}, \tag{5.60}$$

with $z_{EW} = m_{H^0}/T_{EW}$. [14] In the case where the asymmetry dominates the total abundance at T_{EW}, the initial abundance and asymmetry are equal to $\Sigma_{\eta^0}(z_{EW}) = \Delta_{H_2}^{\lambda_5}/2$. The asymmetry Δ_{η^0} and Ξ_{η^0} are, in turn, fast oscillatory functions which are equal to zero on average.

[13] This result is approximately the same than the one obtained in [319] for much smaller δm_0 values – see Eqs (25) and (33) therein – but in which $x_{\rm osc,ann}$ (which depends on δm_0) is now simply replaced by z_{EW}.

[14] If there is no asymmetry and if the freeze-out has occurred prior to EWSB, one recognizes in Eq. (5.60) the usual asymptotic freeze-out behavior, i.e. the freeze-out is not instantaneous, but reaches asymptotically its final value as given in this equation, see Eq. (5.30).

As an important remark, if at $T = T_{EW}$ the equilibrium term $\Sigma_{\eta^0}^{\rm Eq}$ cannot be neglected in the r.h.s. of Eq. (5.57), i.e. if it is large compared to the initial density $\Sigma_{\eta^0}(z_{EW})$, the asymmetry component will be quickly totally destroyed because of the fast $\eta^0\eta^{0*} \leftrightarrow SM\,SM$ scattering processes together with the fast annihilations. This is why one needs to impose $z_{\rm fo} < z_{EW}$ in order to have a possible asymmetric production of the DM relic density. This implies $m_{H_2} \gtrsim 4$ TeV.

The result of Eq. (5.60) looks very similar to what we obtained in Eq. (5.32) of section 5.4.1, and this is not a coincidence. Indeed, this result can also be qualitatively understood in the following way. Once $T \leq T_{EW}$, the fast oscillations reprocess quasi instantaneously the η^0 asymmetry in oscillatory abundances for η^0 and η^{0*}. On average, just after EWSB, we have therefore $n_{\eta^0} \simeq n_{\eta^{0*}} \simeq |\Delta n_{\eta^0}|_{T_{EW}}/2$. Since $T_{\rm fo} > T_{EW}$, when two conjugate particles annihilate to SM particles, the reduction of inert doublet state it implies will not be compensated by any inverse processes. As a result, the Boltzmann equation for Σ_{η^0} one gets along this way is simply given by

$$\frac{d\Sigma_{\eta^0}}{dz} = -\frac{\langle\sigma_0 v\rangle s}{2zH}\,\Sigma_{\eta^0}^2\,, \tag{5.61}$$

to be compared with Eq. (5.29), and whose resolution leads to nothing else than Eq. (5.60). [15]

(2) The next step is to include the contribution of the charged states. Since these states do not oscillate, one could naively expect that the charged asymmetry is essentially left intact until the charged states decay to H^0 states. This doesn't work this way. To see that precisely, one should in principle solve the corresponding set of six coupled Boltzmann equations, for Σ_{η_0}, Δ_{η_0}, Ξ_{η_0}, Π_{η_0}, Σ_{η_+}, Δ_{η_+}, where Π_{η_0} and Ξ_{η_0} are the real and imaginary parts of the quantity that accounts for the coherence effects. Nevertheless in practice we don't need to go that far. It turns out that processes as $\eta^{0(*)}\,SM \leftrightarrow \eta^{\pm}\,SM$ inelastic scatterings are very fast during this period and until T ~few GeV, and these implies that the charged asymmetry follows closely the neutral one as soon as oscillation starts. [16] As a result, in the same way as for the neutral states, one can adopt the simple assumption that as soon as oscillations start, the particle and antiparticle densities for charged states are equilibrated, $Y_{\eta^0} = Y_{\eta^{0*}} = Y_{\eta^+} = Y_{\eta^-}$. At this point, the annihilation processes such as $\eta^+\eta^- \to SMSM$, $\eta^+\eta^{0*} \to SMSM$ and $\eta^-\eta^0 \to SMSM$ can start again, in the same way as the $\eta^0\eta^{0*} \to SMSM$ ones. In parallel with Eq. (5.61), the whole effect can be approximatively

[15] The reason why the two results coincide is in fact more subtle. Since the $\eta^{0(*)}$ oscillatory behavior is given by $Y_{\eta^{0(*)}} = f(z)\left(1 \pm \cos g(z)\right)/2$, the Boltzmann equation in this naive approach should read

$$\frac{d\Sigma_{\eta^0}}{dz} = -2\frac{\langle\sigma_0 v\rangle s}{zH}\,Y_{\eta^0}\,Y_{\eta^{0*}} = -\frac{\langle\sigma_0 v\rangle s}{2zH}\,\Sigma_{\eta^0}^2\,\sin^2 g(z)\,. \tag{5.62}$$

Averaging this expression, we find Eq. (5.61) up to an extra factor 1/2. An extra factor 2 must nevertheless be added to take into account the contribution of the coherence Ξ_{η^0} part, giving back Eq. (5.60).

[16] Indeed, this can be seen from the corresponding term in the Boltzmann equation, which we expect to contain $\Delta\dot{Y}_{\eta^+} \ni -(\Delta Y_{\eta^+} - \Delta Y_{\eta^0})\gamma^{+0}_{\rm scat}$, where $\gamma^{+0}_{\rm scat}$ is the $\eta^+ SM \leftrightarrow \eta^0 SM$ t-channel gauge-mediated scattering rate. Since $\gamma^{+0}_{\rm scat}/n_\eta \gg H$, the asymmetry ΔY_{η^+} follows closely ΔY_{η^0} on average. Note also that the $\eta^0\,SM \leftrightarrow \eta^+\,SM$ (and conjugated) processes not only equilibrate the neutral and charged asymmetries, but also can break the coherence of the η^0-η^{0*} by transforming a coherent neutral state into a charged state which does not oscillate. However, in the same way as for the Z-exchange channel above, its rate goes under $(\delta m_0)^2/H$ before EWSB occurs, so that they do not prevent oscillations to start at $T = T_{EW}$.

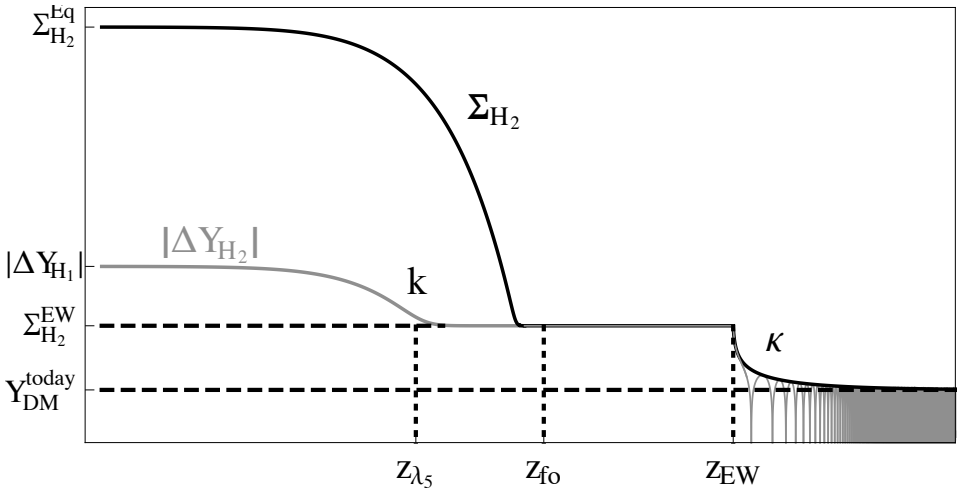

Figure 5.11 – Sketch of the scenario considered in section II and III. We represent, as a function of $z = m_{H^0}/T$, the H_2 asymmetry $|\Delta Y_{H_2}|$ in gray and the total DM density Σ_{H_2} in black. We neglect in this sketch the mass splittings between the different components of H_2. First step : The initial asymmetry ΔY_{H_1} and ΔY_{H_2} are fixed by the $B-L$ asymmetry. Second step : this asymmetry gets suppressed until the λ_5 interactions decouple at z_{λ_5} – the suppression is characterized by the k-factor. Third step : at z_{λ_5} the total annihilation cross section is still in thermal equilibrium and $\Sigma_{H_2}^{\rm Eq}$ follows the equilibrium density $\Sigma_{H_2}^{\rm Eq}$ until it reaches $|\Delta Y_{H_2}|$. Fourth step: at EWSB, oscillations start and reequilibrate the particle-antiparticle populations. At this point, annihilations can start again and if they do they deplete the density – the suppression is characterized by the κ-factor.

accounted by the simple Boltzmann equation

$$\frac{d\Sigma_{H_2}}{dz} = -\frac{\langle\sigma_{H_2} v\rangle s}{zH}\,\Sigma_{H_2}^2\,. \tag{5.63}$$

Similarly to what has been obtained in Eq. (5.60), the resolution of Eq. (5.63), integrated from T_{EW} until now and using the initial condition in (5.51), leads to

$$\Sigma_{H_2}(z \geq z_{EW}) = \frac{\Sigma_{\eta^0}(z_{EW})}{1 + \frac{\langle\sigma_{H_2} v\rangle\, s(z)}{H(z)}\left(\frac{z}{z_{EW}} - 1\right)\Sigma_{\eta^0}(z_{EW})}\,, \tag{5.64}$$

with $\Sigma_{H_2}(z_{EW}) \simeq \Sigma_{H_2}(z_{\rm fo})$ as given in Eq. (5.49). In the case where the asymmetry dominates the total abundance at T_{EW}, the initial abundance and asymmetry are equal to $\Sigma_{\eta^0}(z_{EW}) = \Delta_{H_2}^{\lambda_5}$.

Finally, because of the mass splittings between H^0 and the other components of the inert doublet, this total density in Eq. (5.64) is progressively transferred into a H^0 density through the decays of the heavier components. This occurs typically for a temperature below the mass splittings, i.e. $T < \delta m_0 = m_{A^0} - m_{H^0}$ and $T < \delta m_\pm = m_{\eta^\pm} - m_{H^0}$. Note that, as we will see in the numerical section below, Eq. (5.64) reaches its asymptotic value to a good approximation before T drops below the value of the mass splitting $m_{A^0} - m_{H^0}$. As a result, this splitting can be neglected as it was done to get Eq. (5.64).

5.5.2 Final inert scalar relic density

We summarize in Fig. 5.11 the evolution of the asymmetry $|\Delta Y_{H_2}|$ and total density Σ_{H_2}, if the asymmetry dominates totally the H_2 density before T_{EW}. We remind the main steps :

A. $T \gtrsim T_{\lambda_5}$. The H_2 asymmetry, proportional to the $B-L$ asymmetry, is generated through the λ_5 interactions. The asymmetry undergoes a Boltzmann suppression until the λ_5 interaction decouples (see Eq. (5.42))

$$\Delta_{H_2}^{\lambda_5} \equiv |\Delta Y_{H_2}(z_{\lambda_5})| = \frac{16k\left(z_{\lambda_5}\right)}{158+13k\left(z_{\lambda_5}\right)}\Delta Y_{B-L}\,. \tag{5.65}$$

B. $T_{\lambda_5} > T > T_{EW}$. The symmetric component of Σ_{H_2} follows an exponential suppression, until Σ_{H_2} reaches at $z = z_{fo}$ the value (see Eq. (5.49))

$$\Sigma_{H_2}(z_{\rm fo}) \simeq \left[\Delta_{H_2}^{\lambda_5\,2} + \Sigma_{H_2}^{\rm Eq\,2}(z_{\rm fo})\right]^{1/2}\,. \tag{5.66}$$

From $z_{\rm fo}$ to z_{EW}, the annihilations are momentarily frozen, so that $\Sigma_{H_2}(z_{EW}) \simeq \Sigma_{H_2}(z_{fo})$. During this period, if the contribution from usual freeze-out is negligible (i.e. if the asymmetry dominates the above expression), there are only $\bar{H}_2$ particles in the plasma and $\Sigma_{H_2}(z_{EW}) \simeq \Delta_{H_2}^{\lambda_5}$.

C. $T < T_{EW}$. The fast $\eta^0 \leftrightarrow \eta^{0*}$ oscillations start. They quickly reprocess the $\bar{H}_2$ density in equal abundances (on average) for η^0, η^{0*}, η^+ and η^-. The annihilations can therefore start again and, if they do, they deplete the set of densities, whose sum reads asymptotically

$$\Sigma_{H_2}(z \gg z_{EW}) = \frac{\Sigma_{H_2}(z_{EW})}{1+\frac{\langle\sigma_{H_2} v\rangle\, s(z)}{H(z)}\frac{z}{z_{EW}}\Sigma_{H_2}(z_{EW})}\,. \tag{5.67}$$

At the end of this scenario, for $T \lesssim \delta m_0$ and $T \lesssim \delta m_\pm$, this total density in Eq. (5.67) is progressively transferred into a H^0 density through the decay of the heavier components. The final H^0 abundance is therefore given by

$$Y_{H^0}^{\rm today} = \Sigma_{H_2}(z \gg z_{EW}) = \frac{\Sigma_{H_2}(z_{EW})}{1+\kappa\cdot\Sigma_{H_2}(z_{EW})}\,, \tag{5.68}$$

where we define

$$\kappa \equiv \frac{\langle\sigma_{H_2} v\rangle\, s(z)}{H(z)}\frac{z}{z_{EW}} \simeq 1.3\cdot 10^{13}\cdot\left(\frac{\langle\sigma_{H_2} v\rangle}{1\ {\rm pb}}\right)\,. \tag{5.69}$$

Since ultimately no asymmetry survives, the relation between the baryon and the $B-L$ asymmetry is still given by Eq. (5.54), and the final H^0 to baryon density ratio is given by

$$\boxed{\frac{\Omega_{H^0}}{\Omega_B} = \frac{\Sigma_{H_2}(z_{EW})}{1+\kappa\cdot\Sigma_{H_2}(z_{EW})}\cdot\frac{1}{Y_B^{\rm today}}\cdot\left(\frac{m_{H^0}}{1\ {\rm GeV}}\right)\,.} \tag{5.70}$$

If the asymmetric component dominates, using Eqs. (5.42) and (5.51), one gets simply

$$\frac{\Omega_{H^0}}{\Omega_B} = \frac{148\,k\left(z_{\lambda_5}\right)}{474 + \left(39 + 148\,\kappa\, Y_B^{\text{today}}\right) k\left(z_{\lambda_5}\right)} \cdot \left(\frac{m_{H^0}}{1\text{ GeV}}\right) . \tag{5.71}$$

A number of comments can be done regarding these results. In particular, Eqs. (5.68) and (5.70) show that beside the λ_5 interaction induced "k-factor" suppression in ΔY_{H_2}, see Eq. (5.42), oscillations drive a "κ-factor" suppression. This κ-factor suppression can be sizable as soon as $\kappa \cdot \Sigma_{H_2}(z_{EW}) \gtrsim 1$. This is not surprising since the condition $\kappa \cdot \Sigma_{H_2}(z_{EW}) < 1$ is nothing but the condition $(n_{H_2} + n_{\bar{H}_2})\langle\sigma_{H_2} v\rangle < H$ at $T = T_{EW}$.

As Eq. (5.64) shows, this suppression is neither instantaneous nor exponential. It goes as the inverse of $z/z_{EW} - 1$ until it reaches an asymptotic value. In this sense, imposing that the cross section satisfies the unitarity bound, it is naturally limited but it still can be responsible for the $\sim (10\,\text{GeV}/m_{DM})$ suppression needed, see below. Interestingly, for large values of $\kappa \cdot \Sigma_{H_2}(z_{EW})$, the $Y_{H^0}^{\text{today}}$ relic density obtained doesn't depend anymore on the asymmetry left at T_{EW}, even if this asymmetry is the source of the final H^0 abundance. In this case, we simply get $Y_{DM}^{\text{today}} = 1/\kappa$, and the ratio reads

$$\frac{\Omega_{H^0}}{\Omega_B} \simeq 0.15 \cdot z_{EW} \cdot \left(\frac{1\text{ pb}}{\langle\sigma_{H_2} v\rangle}\right) . \tag{5.72}$$

This means, as we could have anticipated, that for large cross section the asymmetry left is independent of the initial asymmetry, provided this initial asymmetry is large enough. In other terms, if the κ-factor suppression is small, both baryon and H^0 asymmetries are directly connected. If instead it is large, they are not related anymore in a so direct way, since in this case the final relic density depends only on the annihilation cross section. [17] Note interestingly that Eq. (5.72) is nothing but the result of the standard freeze-out scenario, but with the important difference that in the standard case, z_{EW} in Eq. (5.72) must be replaced by z_{fo}, see Eq. (5.34).

5.5.3 Failure of the asymmetric IDM scenario

We now show that the successful generation of the DM relic abundance from a dominant H_2 asymmetry contribution in the IDM alone is actually in conflict with Direct Detection bounds. We proceed step by step : we first compute what is the H_2 asymmetry needed in order to get the correct final DM relic density. We then show what are the corresponding λ_5 values needed.

The final result of Eq. (5.70) depends on three parameters : m_{H^0}, $\Sigma_{H_2}(z_{EW})$ and the total cross section $\langle\sigma_{H_2} v\rangle$ via κ in Eq. (5.69). This means that for given values of the input parameters m_{H^0} and $\langle\sigma_{H_2} v\rangle$, there is only one value of $\Sigma_{H_2}(z_{EW})$ which gives the observed value of Ω_{DM}/Ω_B, as given by the PLANCK best fits, $\Omega_{DM}h^2 \simeq 0.1188$ – see Eq. (5.1) – and $\Omega_B h^2 = 0.022$ – see Eq. (3.5) [206]. Since $\Sigma_{H_2}(z_{EW})$ depends only on these two input parameters (m_{H_2} and $\langle\sigma_{H_2} v\rangle$) and on $\Delta_{H_2}^{\lambda_5}$, this means also that there is only one value of $\Delta_{H_2}^{\lambda_5}$ which gives the correct relic density for fixed values of the two input parameters.

[17] But still, even in this case, they remain similar as the κ factor is bounded from above by unitarity considerations on the total cross section.

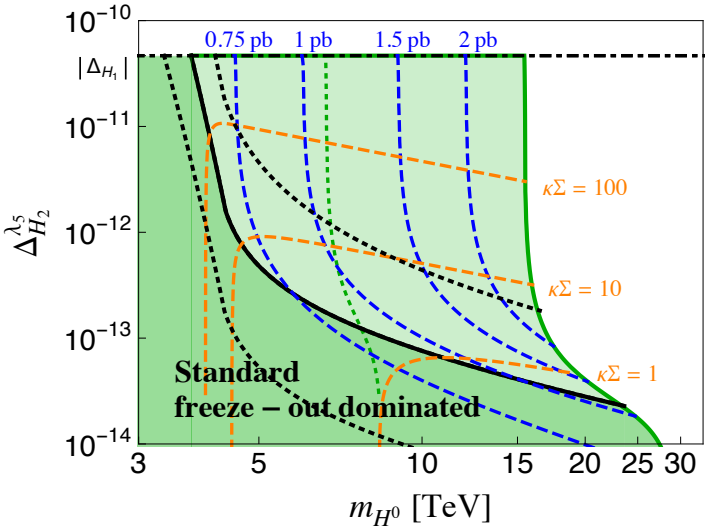

Figure 5.12 – Values of $\Delta^{\lambda_5}_{H_2}$ which give the observed relic density as a function of the input parameters m_{H^0} for various values of $\langle\sigma_{H_2} v\rangle$ (dashed blue lines). The corresponding values of $\kappa\cdot\Sigma_{H_2}(z_{EW})$ are given by the dashed orange lines. The upper horizontal line gives the maximum value of $\Delta^{\lambda_5}_{H_2}$ which is obtained from equilibration with the H_1 and $B-L$ asymmetries. The r.h.s. solid (dashed) green line gives the maximum value of the input parameters imposing that $\lambda_{3,4}$ couplings are smaller than 4π ($\sqrt{4\pi}$). Below $m_{H^0}\sim 4.7$ TeV, the freeze-out occurs after EWSB, which relatively quickly causes a huge suppression. The black lines from top to bottom give the value of the parameters for which 90%, 50%, 10% of the relic density is of asymmetric origin, respectively.

Needed asymmetry as a function of the mass. We show in the left panel of Fig. 5.12 the value of $\Delta^{\lambda_5}_{H_2}$ as a function of m_{H^0} for different values of the cross section. By comparing this value of $\Delta^{\lambda_5}_{H_2}$ to the value this asymmetry would have if there were no "k-factor" suppression – given by the ΔY_{H_1} upper horizontal line – one can read off what is the value of this λ_5 induced "k-factor" suppression, Eq. (5.42) as compared to Eq. (5.44). This figure also shows the corresponding values of the $\kappa\cdot\Sigma_{H_2}(z_{EW})$ factor which lead to the other suppression, i.e. the $1/(1+\kappa\cdot\Sigma_{H_2}(z_{EW}))$ factor in Eq. (5.70).

In Figure 5.12, we also represent for which values of the various parameters the asymmetry produced before the EW transition is responsible for 50% of the final DM relic density (black line). Above (below) this line the relic density is dominantly of asymmetric (symmetric) origin. Similarly, the dotted upper (lower) black line gives the values of the parameters above (below) which the asymmetry is responsible for more (less) than 90% (10%) of the final relic density.

For masses which give a freeze-out below T_{EW}, [18] the $\kappa\cdot\Sigma_{H_2}(z_{EW})$ factor becomes exponentially large because in this case $\Sigma_{H_2}(z_{EW})$ is still exponentially larger than its value at freeze-out.

[18] A comment which must be made at this point concerns the fact that we have considered the electroweak phase transition as if it was an instantaneous process, i.e. as a step function at the temperature $T_{EW}\sim 165$ GeV, see section 3.3.1 and Ref. [210] (see also Ref. [321]) – which as said above is the temperature where the vacuum expectation value of the SM scalar field becomes sizable (i.e. where the oscillations are about to start to reprocess the asymmetry). As the electroweak transition is a crossover, it is clearly an approximation which could be refined. A change of T_{EW} by a given factor would shift all m_{H^0} values in Fig. 5.12 by about the same factor.

Thus, the proportion of $\Sigma_{H_2}(z_{EW})$ which is due to $\Delta_{H_2}^{\lambda_5}$ is exponentially suppressed. This explains why the black lines quickly go up for m_{H^0} below $4-5$ TeV. Note nevertheless that this suppression, even if exponential, is far from instantaneous. As a result we find that, still, the asymmetry can dominate the relic density for a mass equal to 3.7 TeV which is substantially lower than the 4.7 TeV value which gives $T_{\rm fo} = T_{EW}$. [19]

In Fig. 5.12, we recognize several properties expected from the discussion of the previous section. Indeed, for large value of $\kappa \cdot \Sigma_{H_2}(z_{EW})$, the observed relic density doesn't depend anymore on the value of $\Delta_{H_2}^{\lambda_5}$, provided this later quantity is above a certain value. Note that the r.h.s. green curve of Fig. 5.12 is obtained by imposing that all quartic couplings are perturbative, $\lambda_{3,4} < 4\pi$. [20] This line shows that a dominant asymmetric component requires that $m_{H^0} \lesssim 25$ TeV (whereas the same condition gives $m_{H^0} \lesssim 30$ TeV for the standard freeze-out scenario and for a small value of the λ_5 coupling). Such a bound also implies an upper bound on the $\langle \sigma_{H_2} v \rangle$ cross section of about 2.5 pb, that is to say a value about 4 times larger than the ~ 0.7 pb value one needs at these energies along the standard freeze-out scenario. Imposing instead that $\lambda_{3,4} < \sqrt{4\pi}$ one gets $m_{H^0} \lesssim 8$ TeV and $\langle \sigma_{H_2} v \rangle \lesssim 1.1$ pb (dashed green line).

The minimum value of the $\lambda_3^2 + \lambda_4^2$ coupling combination (which enters in $\langle \sigma_{H_2} v \rangle$) that this scenario requires is ~ 2, corresponding to $m_{H^0} \sim 4$ TeV and a cross section of ~ 0.5 pb. This is smaller than the usual ~ 0.7 pb because the associated asymmetry $\Delta_{H_2}^{\lambda_5} \sim |\Delta Y_{H_1}|$ also participates to the depletion of the total density. From Appendix E.3, to these values of $\lambda_{3,4} \sim 1.5$ corresponds a Landau pole at $\sim 10^7$ GeV. This means that new physics is to be expected in this case below this value. The scale of $B-L$ asymmetry production has not to be necessarily below this scale. All what matters for the value of Ω_{DM}/Ω_B is the value of the $B-L$ asymmetry at $T \sim m_{H_2}$.

Needed λ_5 coupling as a function of the mass. In Fig. 5.13, as a function of the same two input parameters m_{H^0} and $\langle \sigma_{H_2} v \rangle$, we show the value of λ_5 which leads to the $\Delta_{H_2}^{\lambda_5}$ value needed in Fig. 5.12. The corresponding value of the $m_{A_0}^2 - m_{H_0}^2$ mass splitting is also given on Fig. 5.13. This figure shows that the scenario leads to the observed relic density for $\lambda_5 \in [5 \cdot 10^{-8}, 8 \cdot 10^{-6}]$, which corresponds to a mass splitting equal to approximately $m_{A_0} - m_{H_0} \in [0.1, 15]$ keV. Larger values of λ_5 quickly lead to a λ_5 decoupling temperature much smaller than m_{H_2}, thus to largely Boltzmann suppressed remaining asymmetries. Smaller values of λ_5 rather quickly lead to no thermalization of the H_2 and H_1 asymmetries, i.e. to no creation of a H_2 asymmetry. In most of the relic density allowed parameter space, both the "k" and "κ" suppressions are active, although it is possible to have only one of the effect to account for all the necessary suppression. As said above, an important constraint that one must satisfy is the direct detection constraint of Eq. (5.11). The value of the mass splitting just quoted are below the ~ 100 keV direct detection lower bound of Eq. (5.11).

[19] To get this 3.7 TeV value we simply applied Eq. (5.64) neglecting the fact that in this case the $\Sigma_{H_2}^{\rm Eq\,2}$ inverse scattering term must be taken into account in the Boltzmann equations (as in Eq. (5.57)). The incorporation of this term would slightly lower further this minimum value of m_{H^0}.

[20] No need to say that with such large values of these quartic couplings, Landau poles are to be typically expected far below the Planck scale. Although the energy scale at which we get a Landau pole depends on the value of other couplings such as λ_2, if there is no cancellations between the contributions of various couplings in the beta functions in Appendix E.3, a value of $\lambda_{3,4} \sim 4\pi$ ($\sqrt{4\pi}$) at $\Lambda = m_{H_2} = 25$ TeV gives a Landau pole at ~ 70 TeV (~ 700 TeV).

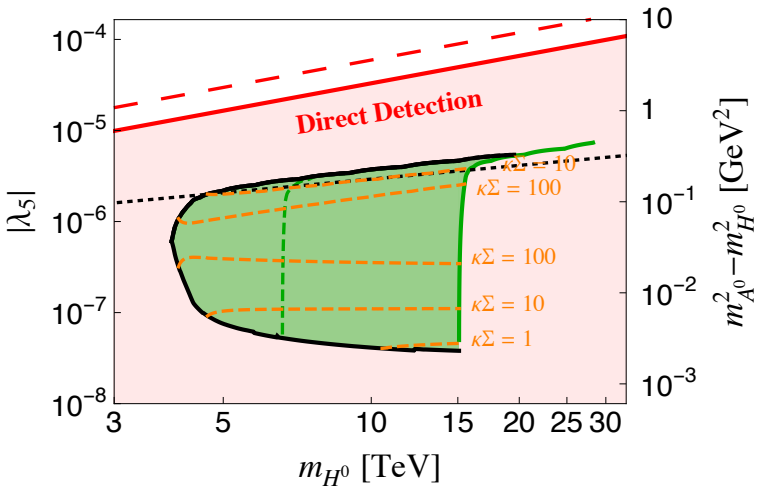

Figure 5.13 – Values of λ_5 which leads to the $\Delta^{\lambda_5}_{H_2}$ values needed in Fig. 5.12, as a function of the input parameters m_{H^0}. The red shaded area is excluded by the direct detection constraint of Eq. (5.11), taking $m_{A^0} - m_{H^0} = 100$ keV. Taking instead $m_{A^0} - m_{H^0} = 180$ keV gives the red dashed line. The dashed black line gives the value of λ_5 below which this interaction never gets in thermal equilibrium, as given by Eq. (5.37). The lowest allowed λ_5 value is obtained for a situation where there is neither a k suppression, nor a κ suppression. In this case one generates directly the observed relic density from having only partial thermalization of the asymmetries.

Thus, unless direct detection would allow a mass splitting as low as the value $m_{A^0} - m_{H^0} \sim 15\,\text{keV}$, which seems very unlikely, this very minimal asymmetric scenario is in fact excluded ! This can also be clearly seen from Fig. (5.13) where the region allowed by direct detection taking in Eq. (5.11) a mass splitting $\delta m_{\text{min}} = 100$ keV has no overlap with the region which gives the observed relic density. Or, in other words, imposing that the mass splitting is above 100 keV, the λ_5 interaction turns out to decouple only at $z_{\lambda_5} \gtrsim 50$ leading to a tiny Ω_{H^0} relic density. Nevertheless, we now show how the inert doublet asymmetry can still be responsible of most of the DM relic abundance by decaying into lighter particles.

So, we conclude that in the very minimal IDM scenario, direct detection constraints implies that there is always creation of an inert doublet asymmetry at $T \sim m_{H_2}$ for $m_{H_2} \gtrsim 100$ GeV, but the fate of this asymmetry is to be too much washed away to account for the observed DM relic density.

5.5.4 Reprocessing the inert doublet asymmetry into a lighter particle DM relic density

Since the very minimal IDM scenario above cannot account for both the relic density and direct detection constraints at the same time, one question one must ask is whether this simple scenario of an IDM asymmetry creation could not be nevertheless at the origin of the DM relic density today in a simple way. This could in fact happen if the DM is made of a lighter species, whose relic density would be due to the reprocessing of the inert doublet asymmetry into this species. Such a reprocessing could for instance take place through decay. For the scalar scenario we consider, this could be the case if there exists a lighter Z_2 odd particle, "S", to which the inert doublet states can

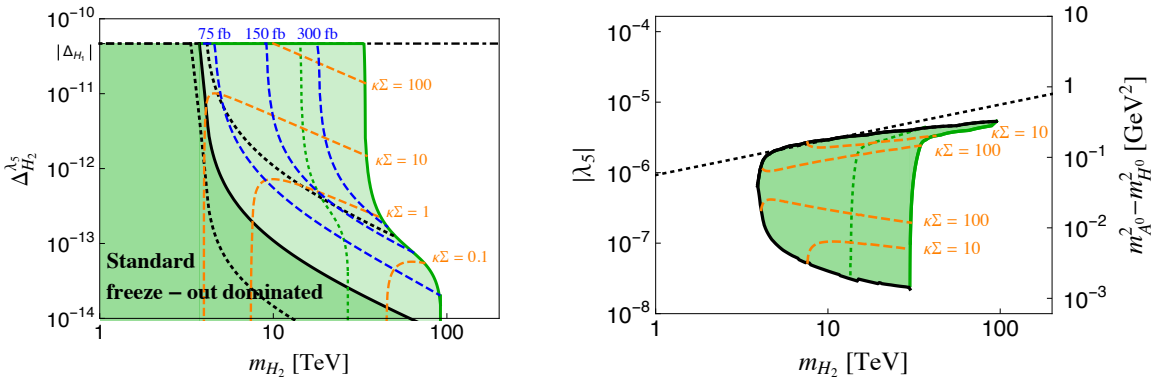

Figure 5.14 – Same as Fig. 5.12 (left) and Fig. 5.13 (right), but allowing the inert scalar to decay into a lighter real scalar singlet S with mass $m_S = m_{H^0}/10$.

decay. In this case, if the asymmetry is fully reprocessed into this lighter particle S, so that each inert scalar component gives one S particle, the results of Figs. 5.12 and 5.13 (without the direct detection constraint) are still fully valid provided the mass of the S particle, m_S, is close to m_{H_2}. If instead it is sizably smaller, this requires to create more inert particles by a factor m_{H_2}/m_S. As an example, Figs. 5.14 show the value of parameters we need to get the observed relic density for a ratio m_{H_2}/m_S equal to 10. Note that such large H_2 asymmetry cases, beside allowing smaller DM masses, also give relaxed lower bounds on the $\lambda_{3,4}$ couplings (in order to suppress sufficiently the symmetric part). Sizably smaller values of these couplings are possible, relaxing accordingly the Landau pole constraints. In order to reprocess the inert doublet asymmetry into such a S specie, various possibilities could be considered. We here consider the case where H_2 decays into a real or a complex scalar singlet – see section 5.2.1.

S as a real scalar singlet. A simple possibility is to consider S as a Z_2-odd scalar singlet, into which the scalar doublet states decay sufficiently slowly to happen after the freeze-out of this singlet DM particle. Such a decay can be accounted for by a $\mathscr{L} \ni \mu_{SH} H_1^\dagger H_2 S$ renormalizable interaction. If so, the main constraint to satisfy along such a scenario is, in order that the S relic density is mainly produced from the IDM asymmetry, that the S particles has a $S^\dagger S \to SM\,SM$ annihilation channel with a large enough cross section to leave a symmetric relic density smaller than the observed one at S freeze-out. These annihilations can be accounted for by a $\mathscr{L} \ni \lambda_{SH} H_1^\dagger H_1 S^\dagger S$ interaction.

As an example, if we take a real scalar singlet, and fix the parameters to be $m_S \sim 2$ TeV (400 GeV) and $m_{H_2} = 10$ TeV, both conditions are fulfilled for $\lambda_{SH} \gtrsim 0.6(0.1)$ and $\mu_{SH} \lesssim 4\cdot 10^{-5}$ GeV ($7\cdot 10^{-6}$ GeV). Also, the λ_{SH} interaction induces elastic scattering on nucleon through SM scalar exchange, $\sigma_N = \lambda_{SH}^2 m_N^4 f_N^2/(\pi m_h^4 m_S^2)$, where m_N is the nucleon mass and the nucleon form factor is approximately given by $f_N \approx 0.3$. The LUX experiment constraint [322], which for $m_{DM} \gtrsim 100$ GeV is $\sigma_N \lesssim 1.2\cdot 10^{-11}(m_S/1\text{ GeV})$ pb (see Eq. (5.16)), is satisfied if $\lambda_{SH} \lesssim 1.6\cdot 10^{-5}(m_S/1\text{ GeV})^{3/2}$. Combining both these lower and upper bounds on λ_{SH} leads to the lower bound $m_S \gtrsim 300$ GeV [270], which is indeed fulfilled in the above example. In the left panel Fig. 5.15 we show the evolution of the asymmetries we get as a function of the temperature for an example of parameter set which leads to the observed relic density.

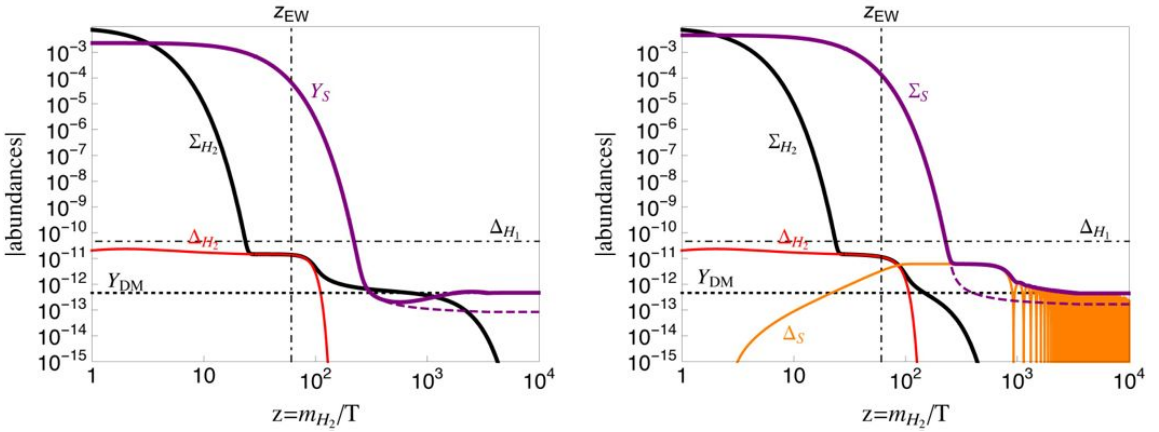

Figure 5.15 – Evolution of the various abundances as a function of $z = m_{H_2}/T$ in the case where the inert doublet decays into a real (left panel) or a complex (right panel) state S after S freeze-out. For the real scalar singlet case (left), we have fixed the H_2-related parameters to $m_{H_2} =$ 10 TeV, $\langle\sigma_{H_2} v\rangle = 0.5$ pb and $\delta m_{H_2} = 3\cdot 10^{-6}$ GeV (corresponding to $\lambda_5 \approx 10^{-6}$), and the S-related parameters to $m_S = 1$ TeV and $\langle\sigma_S v\rangle = 4$ pb, and the connector parameter controlling the decay rate to $\mu_{SH} = 5\cdot 10^{-6}$ GeV. For the complex scalar singlet case (right), we have fixed the H_2-related parameters to $m_{H_2} = 10$ TeV, $\langle\sigma_{H_2} v\rangle = 1$ pb and $\delta m_{H_2} = 3\cdot 10^{-6}$ GeV (corresponding to $\lambda_5 \approx 10^{-6}$), and the S-related parameters to $m_S = 1$ TeV and $\langle\sigma_S v\rangle = 4$ pb, $\delta m_S = 10^{-7}$ eV and the connector parameter controlling the decay rate to $\mu_{SH} = 5\cdot 10^{-5}$ GeV. In both plots, the dashed purple curve shows what would be the evolution of the S density if there were no $H_2 \to H_1 S$ decay.

S as a complex scalar singlet. Similarly to the fermion scenario considered in Ref. [311], another possibility is to consider instead that the decays occur when the freeze-out of the singlet particle S has still not taken place. In this case, the inert doublet asymmetry could also be at the origin of the DM relic density, if the singlet is a complex field and if the inert doublet asymmetry is reprocessed into a S asymmetry. Since inert doublet oscillations start at T_{EW}, this requires the reprocessing to be done prior to EWSB. Imposing in addition for simplicity that the decay occurs after the λ_5 interaction has decoupled at z_{λ_5}, for example for $m_{H_2} = 10$ TeV and $m_S \sim 2$ TeV, one needs $10^{-5}\,\text{GeV} \lesssim \mu_{SH} \lesssim 10^{-3}\,\text{GeV}$. For this scenario to work, one has to make sure that the S asymmetry created in this way is not washed-out by possible S-$S^\dagger$ oscillations. This requires that terms as $\lambda'_{SH} H_1^\dagger H_1 (S^2 + h.c.)$ or $m'^2_S S^2 + h.c.$ are sufficiently suppressed for the oscillations not to occur before S freeze-out. This means the S mass splitting $\delta m_S = (m'^2_S + \theta(T_{EW} - T)\lambda'_S v^2)/2m_S$ must be smaller than

$$\delta m_S \lesssim 10^{-2}\cdot (z^S_{\text{fo}})^{-5/2}\cdot \left(\frac{m_S}{1\,\text{TeV}}\right)^2 \cdot \sqrt{\frac{\langle\sigma_S v\rangle}{1\,\text{pb}}}\,\text{eV}\,, \tag{5.73}$$

with $z^S_{\text{fo}} \gtrsim 20$ the value of m_S/T at which the S freeze-out occurs, and $\langle\sigma_S v\rangle$ the S annihilation cross section. Note that at temperature lower than T^S_{fo}, when the S oscillations starts at z^S_{osc}, they can allow the S annihilations to restart in the same way as for the inert doublet above. Similarly to Eq. (5.68), this causes a suppression of the S asymmetry by a factor equal to $(1 + \kappa_S \Sigma_S(z^S_{\text{fo}}))^{-1}$ with $\kappa_S = \langle\sigma_S v\rangle s z/H(z) z^S_{\text{osc}}$. In the right panel of Fig. 5.15 we show an example of evolution of the H_2 and S asymmetries along such a scenario.

5.6 Summary

In summary, if there exists an inert scalar doublet H_2, unless the λ_5 interaction is tiny, the inert doublet components will automatically develop an asymmetry from thermalization with the ordinary SM scalar doublet and lepton asymmetries. We have studied in detail what is the fate of such an asymmetry at temperature below the value of the inert doublet scalar mass, m_{H_2}. Beside being responsible for the asymmetry creation, the λ_5 interaction also controls the neutral component mass splitting (hence the Z-exchange direct detection rate) and induces a "k-factor" suppression of the inert doublet asymmetry at temperature below m_{H_2}. On top of this suppression one can also have an extra "κ-factor" suppression, from the combined effect of η^0-η^{0*} oscillations (also induced by the λ_5 interaction) and symmetric annihilation. This leads to a scenario which chronologically occurs as represented in Fig. 5.11. We showed that in the few-TeV range, there is a region of parameter space where the H_2 asymmetry survives enough to lead to the observed DM relic density, Fig. 5.12, but this region turns out to lead to a too large Z-exchange direct detection contribution. As a result this scenario is nothing but excluded.

Next we looked at the possibility that the inert scalar asymmetry produced could still be at the origin of the observed DM relic density, which could be the case if it is reprocessed to a lighter specie, S, which satisfies the direct detection constraints. We considered two scenarios where DM is made of a singlet odd under the Z_2 symmetry. a) Slow decay of the asymmetry into the (real or complex) singlet particle, occurring after S freeze-out. b) Reprocessing of the inert scalar doublet asymmetry into a S asymmetry through faster decays occurring before S freeze-out. Both possibilities can lead to the observed DM relic density provided the interaction causing the decay is small enough to induce this decay at the right time.

As most asymmetric DM scenarios, the framework we consider does not explain why the baryon and DM abundances are so similar. Our scenario trades this abundance coincidence for a coincidence between the mass of the proton, the mass of the inert states, the mass of the dark matter particle, and the values of various couplings. Even if both abundances have same origin, these parameters must "cooperate" to lead to a DM abundance so close to the baryon one. Rather than providing a real explanation for the abundance coincidence, this scenario shows instead that the origin of the DM relic density could be of asymmetric origin, due to the generation of an inert scalar asymmetry related to the generation of a $B-L$ asymmetry at high temperature.

General conclusion

In this thesis we focused on three puzzles of modern particle physics : the neutrino masses, the baryon asymmetry of the Universe and the dark matter. Each puzzle resolution requires beyond the Standard Model physics, and each can find an explanation in the context of a plethora of theoretical models. It is essential to consider a maximum of possibilities, as we don't actually know which is the good one yet ! Obviously, the definitive way to distinguish between them is through experiments, which are currently many to work, and many planned. In this context, it is mandatory to probe all the consequences and details of these models.

We discussed in chapter 1 how the smallness of the neutrino masses can find a simple explanation in the framework of the well-motivated Seesaw models. These models are the favorite ones since (i) they generate small neutrino masses through the tree-level exchange of new heavy particles, (ii) they contain all the necessary ingredients to generate enough baryon asymmetry in our Universe through the leptogenesis mechanism, (iii) they can be embedded in Grand Unified Theories, (iv) they generate new processes as for example charged lepton flavor violating processes that could in principle be probed experimentally. However, despite all this pros, there are also cons. Indeed, it is in fact in general difficult to probe the Seesaw models experimentally. For instance, in the type-1 Seesaw model, one generally expects the right-handed neutrinos either to be very heavy or to be light with tiny interactions. In both cases, direct experimental tests are not possible. This is however not always the case. There exists a subclass of models, the Inverse Seesaw models, where sizable rates for charged lepton flavor violation processes can be generated. So it is worth to probe them.

Armed with these considerations, we computed in chapter 2 the rate of the conversion of a muon into an electron in the type-1 Seesaw framework. Since future experiments should reach very high sensibilities on the charged lepton flavor violation processes – up to ~ 6 orders of magnitude better than the present upper bound – it is important to have precise analytical expressions for the rate of these processes in each theoretical model since they could provide very interesting informations about the new physics. In particular, we have shown that the measurement of two or more rates could potentially (i) lead to the determination of the Seesaw scale, and (ii) distinguish between the various Seesaw mechanisms. It is remarkable that low-energy processes could in principle provide such indications on the high-energy parameters. Beside these motivating facts, any non-observation will lead to new bounds on the high-energy parameters of these models.

In chapter 3, we introduced at length the way the matter-antimatter asymmetry of the Universe can be generated in the type-1 Seesaw model along the leptogenesis mechanism. In particular, we highlighted the importance of the flavor effects in this context. From this knowledge, we then analyzed in chapter 4 how leptogenesis can be achieved within the type-2 Seesaw scenario.

Since the scalar triplet can carry an asymmetry, undergoes gauge interactions and has more types of couplings than the type-1 Seesaw, the way the matter-antimatter asymmetry is generated is different from the standard leptogenesis, already before considering flavor issues. This is why, in a first step, the scenario has been analyzed in detail in the one-flavor approximation, where the scalar triplet is assumed to decay into only one lepton flavor. This has allowed us to understand the main features of the scalar triplet leptogenesis. In a second step, we computed the effects of the lepton flavors and the spectator processes. The way flavor manifests itself in type-2 leptogenesis is in many ways different from type-1 leptogenesis. In particular, in contrast with the type-1 Seesaw leptogenesis, we showed that lepton flavors always matter whatever the temperature at which leptogenesis takes place. In this context, we have first determined all the necessary formulas that take into account flavors : decay widths, CP-asymmetries, Boltzmann equations, flavor temperature regimes and associated dynamics. Any reader who would like to calculate the effect of flavors in any type-2 Seesaw model can do it based on these formulas. The procedure to follow is summarized in section 4.4. Subsequently, we have studied various possible new scenarios. In particular, we have highlighted the existence of a totally new regime in which enough matter-antimatter asymmetry can be generated only via pure flavor effects. This is the so-called purely flavored leptogenesis mechanism, which is dominant as soon as the scalar triplet couples more to leptons than to scalars, which is also requested in order to have large rate for the lepton flavor violation processes. We also analyzed how lepton flavor can enhance the leptogenesis efficiency in more general situations.

In chapter 5, we introduce the dark matter puzzle, and showed some beyond the Standard Model extensions which can account for it. Among them, a well-known model is the inert doublet model, in which dark matter (DM) can be accounted for by the neutral component of a second scalar doublet, odd under some discrete symmetry which insures its stability. The usual way the DM is produced in these models is through the usual freeze-out mechanism : the total DM abundances (DM+anti-DM) leaves thermal equilibrium at some freeze-out temperature, function of the interactions of the DM with the plasma, and at this temperature the DM density, being Boltzmann suppressed, is frozen to the present DM relic density. However, there is another way to generate dark matter through the production of a DM asymmetry (DM-anti-DM), not without similarities with the baryon asymmetry case in the previous two chapters. Indeed, the Inert Doublet Model contains an interaction that can be responsible for the generation of a DM asymmetry. Therefore, in the last part of this thesis, we have addressed the following question : is it possible to generate enough dark matter in an asymmetric way in the context of the Inert Doublet Model ? In a pure IDM framework, the answer is actually no. This is because lower bounds from direct detection imply that the interaction responsible for the production of the inert scalar asymmetry is too large to create enough dark matter. Nevertheless, we have shown that the direct detection constraint can be easily evaded if one adds a new particle to which the inert scalars decay. In this context, thanks to the analysis of the fate of the H_2 asymmetry, we have shown in particular that the effect of the inert scalar oscillations can dominate the DM relic density.

Appendix

A Units and conversion factors

A.1 Natural units

We use the natural units, that is we fix $c = \hbar = k_B = 1$. This allows us to express all the standard units in terms of energy unit, expressed in GeV. For example, one has

$$1\text{m} \approx 5.0677 \cdot 10^{15}\ \text{GeV}^{-1} \tag{A.1}$$
$$1\text{s} \approx 1.5193 \cdot 10^{24}\ \text{GeV}^{-1} \tag{A.2}$$
$$1\text{kg} \approx 5.6085 \cdot 10^{26}\ \text{GeV} \tag{A.3}$$
$$1\text{K} \approx 8.6173 \cdot 10^{-14}\ \text{GeV} \tag{A.4}$$
$$1\text{pb} \approx 2.5682 \cdot 10^{-9}\ \text{GeV}^{-2} \tag{A.5}$$

A.2 Parameters and constants

The following parameters and constant values have been used. For the various masses and energy scales :

$$\text{v} = 246\ \text{GeV} \tag{A.6}$$
$$m_{Planck} = 1.22 \cdot 10^{19}\ \text{GeV} \tag{A.7}$$
$$m_h \approx 1.25 \cdot 10^{2}\ \text{GeV} \tag{A.8}$$
$$m_e \approx 5.11 \cdot 10^{-4}\ \text{GeV} \tag{A.9}$$
$$m_\mu \approx 1.06 \cdot 10^{-1}\ \text{GeV} \tag{A.10}$$
$$m_\tau \approx 1.78\ \text{GeV} \tag{A.11}$$
$$m_b \approx 4.18\ \text{GeV} \tag{A.12}$$
$$m_t \approx 1.72 \cdot 10^{2}\ \text{GeV} \tag{A.13}$$
$$m_W \approx 8.04 \cdot 10^{1}\ \text{GeV} \tag{A.14}$$
$$m_Z \approx 9.17 \cdot 10^{1}\ \text{GeV} \tag{A.15}$$

For the couplings :

$$g \approx 6.531 \cdot 10^{1} \quad , \quad \alpha_w \approx 3.394 \cdot 10^{-2} \tag{A.16}$$

$$g_{EM} \approx 3.028 \cdot 10^{1} \quad , \quad \alpha_{EM} \approx 7.297 \cdot 10^{-3} \tag{A.17}$$

$$g_s \approx 1.220 \tag{A.18}$$

$$g_Y \approx 3.581 \cdot 10^{-1} \tag{A.19}$$

$$\theta_w \approx 5.014 \cdot 10^{-1} \quad , \quad s_w \approx 0.481 \quad , \quad c_w \approx 0.877 \tag{A.20}$$

$$G \approx 6.708 \cdot 10^{-39} \tag{A.21}$$

For the cosmological parameters :

$$H_0 = 67.74 \pm 0.46 \text{ (km/s)/Mpc} \tag{A.22}$$

$$\Omega_B h^2 = 0.02205 \pm 0.00028 \tag{A.23}$$

$$\Omega_{DM} h^2 = 0.1199 \pm 0.0027 \tag{A.24}$$

B μ to e conversion in atomic nuclei

B.1 Some useful identities

The mixing unitary matrix U, together with the matrix C defined in Eq. (2.15) obey the following relations :

$$\sum_j^{n_L+n_R} U_{\alpha j} U^*_{\beta j} = \delta_{\alpha\beta} \,, \qquad \sum_j^{n_L+n_R} C_{ij} C^*_{kj} = C_{ik} \,, \qquad \sum_j^{n_L+n_R} U_{\alpha j} C_{ji} = U_{\alpha i} \,, \tag{B.1}$$

$$\sum_j^{n_L+n_R} m_j C_{ij} C_{kj} = 0 \,, \qquad \sum_j^{n_L+n_R} m_j U_{\alpha j} C^*_{jk} = 0 \,, \qquad \sum_j^{n_L+n_R} m_j U_{\alpha j} U_{\beta j} = 0 \,, \tag{B.2}$$

where n_L is the number of left-handed neutrino generations and n_R is the number of right-handed neutrino generations.

B.2 Feynman rules

Because of the Majorana nature of the neutrinos mass eigenstates, one have to pay attention when deriving the Feynman rules, see for example Ref. [323]. In particular, a factor 2 has to be taken into account in the vertices involving Majorana neutrinos and neutral bosons, like the Z or ϕ^0.

External lines

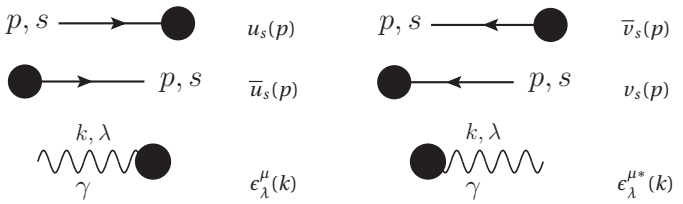

Propagators

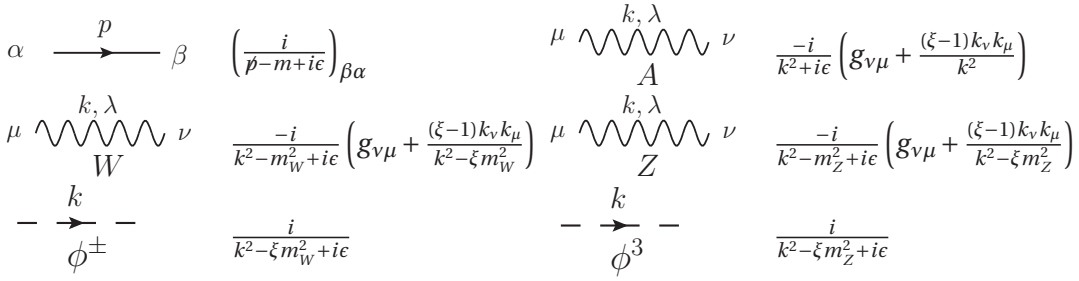

Vertices

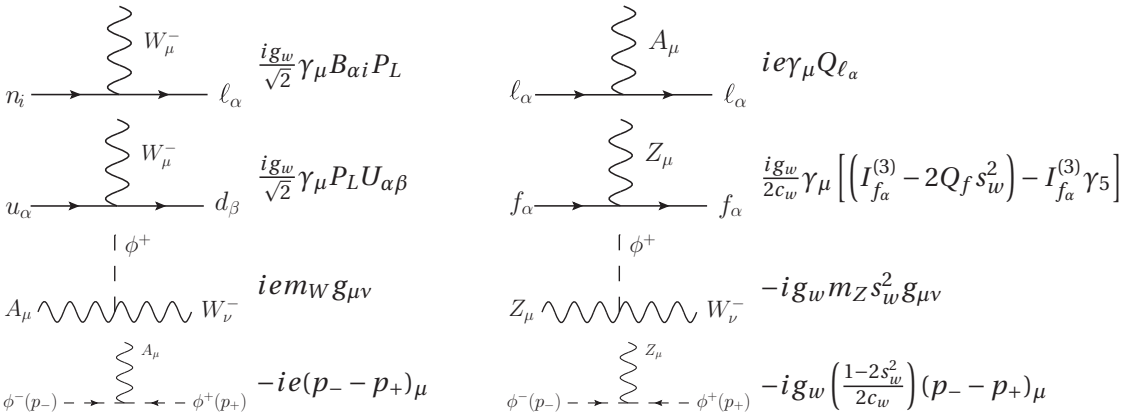

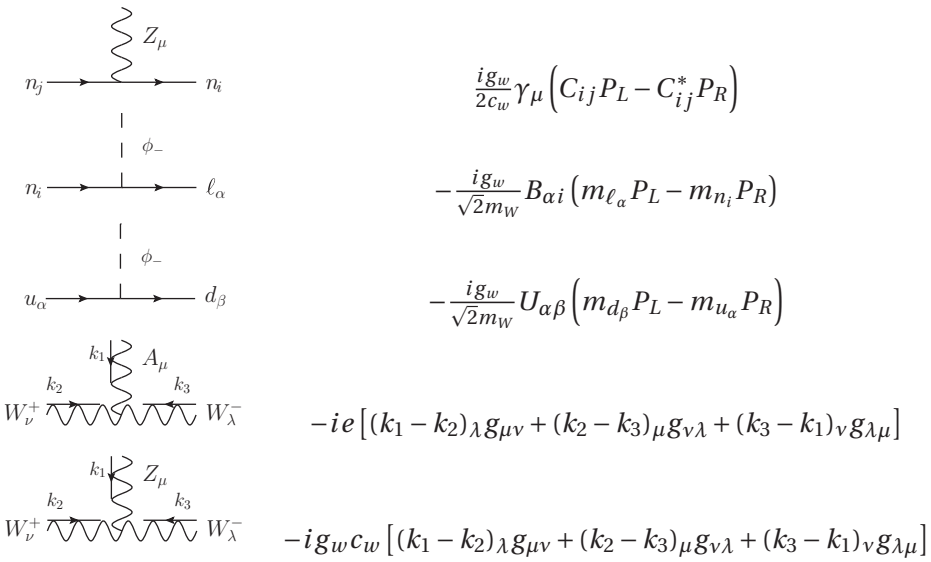

B.3 Feynman diagrams and associated amplitudes

B.3.1 Methodology

As explained in section 2.3.1, in order to compute the effective Lagrangian for comparison with Eq. (2.32), one needs to compute the amplitudes $\mathcal{M}^u$ and $\mathcal{M}^d$ associated to the process involving an up quark, or a down quark. Each amplitude, $\mathcal{M}^u$ and $\mathcal{M}^d$, will receive three contributions, depending on whether the interaction occurs through the exchange of a photon, a Z boson or W's bosons:

$$\mathcal{M}^u = \mathcal{M}^u_\gamma + \mathcal{M}^u_Z + \mathcal{M}^u_W \,, \tag{B.3}$$

$$\mathcal{M}^d = \mathcal{M}^d_\gamma + \mathcal{M}^d_Z + \mathcal{M}^d_W \,. \tag{B.4}$$

Those contributions will be computed separately. The first one, i.e. with the photon exchange, has a common basis with the process $\mu \to e\gamma$ so that we just have to compute the associated amplitude of the latter, without taking a on-shell photon $q^2 \neq 0$, and then to add the line of quarks. This is why we first begin by the calculation of the process $\mu \to e\gamma$. We will check that the divergences cancel, and that the amplitude is gauge invariant. The amplitude is also compared with previous well-known results. Then, we will compute the contribution of the Z boson. The diagrams of this second contribution contains the same topology than the photon one, plus two diagrams that involve two Majorana neutrinos in the loop. The cancellation of the divergences is also verified. Finally, we will compute the contribution of the W's boson. The diagrams involved are box diagrams.

Let's note that the contribution coming from diagrams with scalar boson mediated can be neglect with respect to the one mentioned above. Indeed, these will give correction of order $\sim m_q m_\mu / M_W^2$ to the amplitude, which can be neglected compared to the contributions from the gauge bosons.

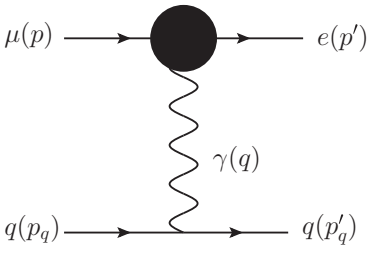

(a) Photon contribution $\mathcal{M}^q_\gamma$

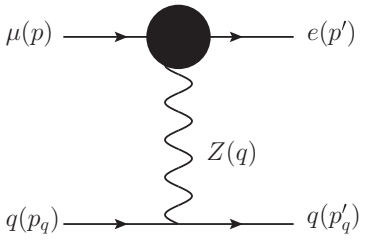

(b) Z contribution $\mathcal{M}^q_Z$

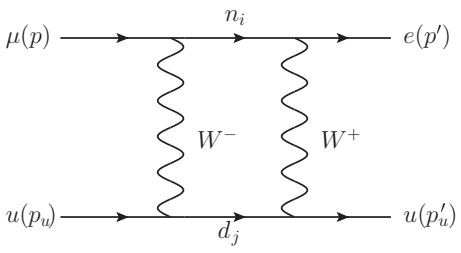

(c) W contribution for u quarks $\mathcal{M}^u_W$

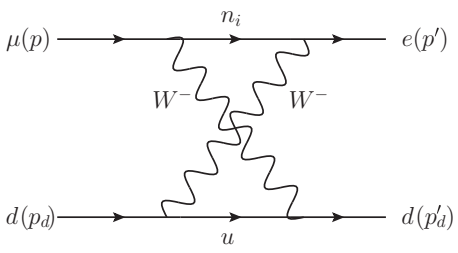

(d) W contribution for d quarks $\mathcal{M}^d_W$

B.3.2 Photon Penguin contribution

We first separate the lepton line from the quark line. This allow to check the amplitude with the well-known $\mu \to e\gamma$ one. The Feynman diagrams, without the quark lines, are given below. Momentum k in the loop are taken clockwise. The associated amplitudes, in the Feynman-t'Hooft gauge $\xi = 1$, are:

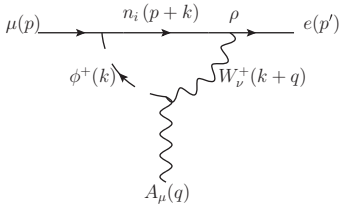

$$i\mathcal{M}_\gamma^A = \sum_i \frac{-eg^2}{2} U_{ei}U_{\mu i}^* \,\overline{u}_e(p')\,\mathscr{I}_\alpha^A\, u_\mu(p)\,\epsilon_\lambda^{\alpha *}(q) \qquad \text{(B.5)}$$

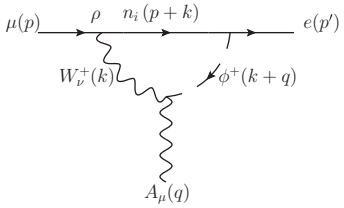

$$i\mathcal{M}_\gamma^B = \sum_i \frac{-eg^2}{2} U_{ei}U_{\mu i}^* \,\overline{u}_e(p')\,\mathscr{I}_\alpha^B\, u_\mu(p)\,\epsilon_\lambda^{\alpha *}(q) \qquad \text{(B.6)}$$

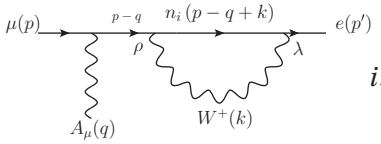

$$i\mathcal{M}_\gamma^C = \sum_i \frac{-eg^2}{2} U_{ei}U_{\mu i}^* \,\overline{u}_e(p')\,\mathscr{I}_\alpha^C\, u_\mu(p)\,\epsilon_\lambda^{\alpha *}(q) \qquad \text{(B.7)}$$

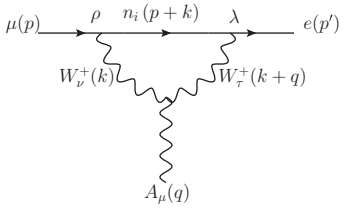

$$i\mathcal{M}_\gamma^D = \sum_i \frac{eg^2}{2} U_{ei}U_{\mu i}^* \,\overline{u}_e(p')\,\mathscr{I}_\alpha^D\, u_\mu(p)\,\epsilon_\lambda^{\alpha *}(q) \qquad \text{(B.8)}$$

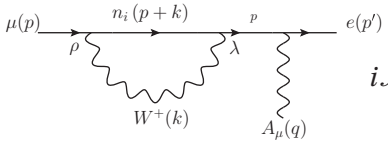

$$i\mathcal{M}_\gamma^E = \sum_i \frac{-eg^2}{2} U_{ei}U_{\mu i}^* \,\overline{u}_e(p')\,\mathscr{I}_\alpha^E\, u_\mu(p)\,\epsilon_\lambda^{\alpha *}(q) \qquad \text{(B.9)}$$

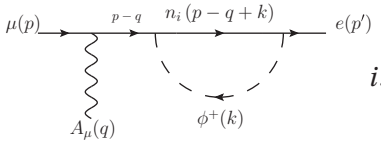

$$i\mathcal{M}_\gamma^F = \sum_i \frac{eg^2}{2m_W^2} U_{ei}U_{\mu i}^* \,\overline{u}_e(p')\,\mathscr{I}_\alpha^F\, u_\mu(p)\,\epsilon_\lambda^{\alpha *}(q) \qquad \text{(B.10)}$$

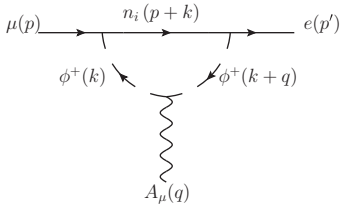

$$i\mathscr{M}_\gamma^G = \sum_i \frac{-eg^2}{2m_W^2} U_{ei}U_{\mu i}^*\,\overline{u}_e(p')\,\mathscr{I}_\alpha^G\,u_\mu(p)\,\epsilon_\lambda^{\alpha *}(q) \qquad \text{(B.11)}$$

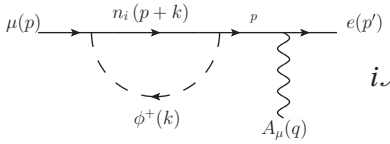

$$i\mathscr{M}_\gamma^H = \sum_i \frac{eg^2}{2m_W^2} U_{ei}U_{\mu i}^*\,\overline{u}_e(p')\,\mathscr{I}_\alpha^H\,u_\mu(p)\,\epsilon_\lambda^{\alpha *}(q) \qquad \text{(B.12)}$$

Neglecting the electron mass, the various integrals $\mathscr{I}_\alpha^j$ are given by

$$\mathscr{I}_\alpha^A = \int \frac{d^4k}{(2\pi)^4} \frac{\gamma_\alpha P_L\left(\not{k}+\not{p}+m_{n_i}\right)\left(m_\mu P_R - m_{n_i}P_L\right)}{\left[k^2-m_W^2\right]\left[(k+q)^2-m_W^2\right]\left[(k+p)^2-m_{n_i}^2\right]} \qquad \text{(B.13)}$$

$$\simeq \left(m_\mu^2 C_u - m_{n_i}^2 C_0\right)\gamma_\alpha P_L + 2m_\mu C_v\, p'_\alpha P_R \qquad \text{(B.14)}$$

$$\mathscr{I}_\alpha^B = \int \frac{d^4k}{(2\pi)^4} \frac{\left(m_e P_L - m_{n_i}P_R\right)\left(\not{k}+\not{p}+m_{n_i}\right)}{\left[k^2-m_W^2\right]\left[(k+q)^2-m_W^2\right]\left[(k+p)^2-m_{n_i}^2\right]}\gamma_\mu P_L \simeq -m_{n_\kappa}^2 C_0\,\gamma_\alpha P_L \qquad \text{(B.15)}$$

$$\mathscr{I}_\alpha^C = \int \frac{d^4k}{(2\pi)^4} \frac{\gamma^\rho\left(\not{k}+\not{p}\,'\right)\gamma_\rho P_L}{\left[k^2-m_W^2\right]\left[(k+p')^2-m_{n_i}^2\right]} \frac{\not{p}\,'+m_\mu}{m_e^2-m_\mu^2}\gamma_\alpha \simeq 0 \qquad \text{(B.16)}$$

$$\mathscr{I}_\alpha^D = \int \frac{d^4k}{(2\pi)^4} \frac{\gamma^\beta(\not{k}+\not{p})\gamma^\nu\left[(-k_\nu-2q_\nu)g_{\alpha\beta}+(2k_\alpha+q_\alpha)g_{\beta\nu}+(-k_\beta+q_\beta)g_{\nu\alpha}\right]}{\left[k^2-m_W^2\right]\left[(k+q)^2-m_W^2\right]\left[(k+p)^2-m_{n_i}^2\right]} P_L \qquad \text{(B.17)}$$

$$\simeq \Big[4(1-D)\tilde{C}_1 + m_\mu^2\,(C_u-2C_{uu}) + 4pp'\,(C_u+C_v-C_{uv})\Big]\gamma_\alpha P_L$$
$$+ m_\mu\left[p_\alpha\,(2C_u-4C_{uu}) - p'_\alpha\,(2C_u+2C_v+4C_{uv})\right]P_R \qquad \text{(B.18)}$$

$$\mathscr{I}_\alpha^E = \gamma_\alpha \frac{\not{p}+m_e}{m_\mu^2-m_e^2}\int \frac{d^4k}{(2\pi)^4} \frac{\gamma^\rho\left(\not{k}+\not{p}\right)\gamma_\rho P_L}{\left[(k+p)^2-m_{n_\kappa}^2\right]\left[k^2-w_W^2\right]} \simeq (2-D)\,\tilde{B}_1\,\gamma_\alpha P_L \qquad \text{(B.19)}$$

$$\mathscr{I}_\alpha^F = \int \frac{d^4k}{(2\pi)^4} \frac{\left(\not{k}+\not{p}\,'\right)\left(m_\mu m_e P_R + m_{n_\kappa}^2 P_L\right) - m_{n_\kappa}^2\left(m_\mu P_R + m_e P_L\right)}{\left[k^2-m_W^2\right]\left[(k+p')^2-m_{n_\kappa}^2\right]} \frac{\not{p}\,'+m_\mu}{m_e^2-m_\mu^2}\gamma_\alpha \qquad \text{(B.20)}$$

$$\simeq m_{n_\kappa}^2 \tilde{B}_0\,\gamma_\alpha P_L \qquad \text{(B.21)}$$

$$\mathscr{I}_\alpha^G = \int \frac{d^4k}{(2\pi)^4} \frac{\left(\not{k}+\not{p}\right)\left(m_\mu m_e P_R + m_{n_i}^2 P_L\right) - m_{n_i}^2\left(m_\mu P_R + m_e P_L\right)}{\left[k^2-m_W^2\right]\left[(k+q)^2-m_W^2\right]\left[(k+p)^2-m_{n_i}^2\right]}\left(2k_\alpha+q_\alpha\right) \qquad \text{(B.22)}$$

$$\simeq 2m_{n_\kappa}^2\tilde{C}_1\,\gamma_\alpha P_L + m_{n_i}^2 m_\mu\left[p_\alpha(C_0-3C_u+2C_{uu}) + p'_\alpha(C_0-2C_v-C_u+2C_{uv})\right]P_R \qquad \text{(B.23)}$$

$$\mathscr{I}_\alpha^H = \gamma_\alpha \frac{\not{p}+m_e}{p^2-m_e^2}\int \frac{d^4k}{(2\pi)^4}\frac{\left(\not{k}+\not{p}\right)\left(m_\mu m_e P_R + m_{n_i}^2 P_L\right) - m_{n_i}^2\left(m_\mu P_R + m_e P_L\right)}{\left[k^2-m_W^2\right]\left[(k+p)^2-m_{n_i}^2\right]} \tag{B.24}$$

$$\simeq m_{n_i}^2\left(\tilde{B}_1-\tilde{B}_0\right)\gamma_\alpha P_L \tag{B.25}$$

In the second equality, we used the equations of motion, we expressed the integrals in terms of Feynman integrals that are given in Appendix B.5, and we neglected the electron mass. The integrals $C_0(x_i)$, $C_v(x_i)$, $C_u(x_i)$, $C_{uu}(x_i)$, $C_{vv}(x_i)$ and $C_{uv}(x_i)$, depending on $x_i = m_{n_i}^2/m_W^2$, are convergent Feynman integrals that are solved using Feynman parametrization. The integrals $\tilde{B}_0(x_i,D)$, $\tilde{B}_1(x_i,D)$ and $\tilde{C}_1(x_i,D)$ are divergent integrals, that we choose to solve by using dimensional regularization method. This means we express these latter in terms of integrals in $D = 4-2\delta$. By doing so, the divergent and convergent parts can be separated. At the end of the computation, we divergent parts must cancel, and a finite result is obtained when taking the limit $\delta \to 0$.

$\mu \to e\gamma$ amplitude and rate

After summation of the amplitudes in Eqs. (B.6)-(B.12), we get

$$i\mathscr{M}(\mu \to e\gamma) = \epsilon_\lambda^{\alpha *}(q)\,\overline{u}_e(p')\Gamma_\alpha u_\mu(p)\,, \tag{B.26}$$

where

$$\Gamma_\alpha = \sum_i \frac{eg^2}{2} U_{ei}U_{\mu i}^*\left[A\gamma_\alpha + B\left(p_\alpha + p'_\alpha\right) + Cq_\alpha\right]\,, \tag{B.27}$$

with

$$A \simeq \Big[\frac{2i}{(4\pi)^2}\ln x_i + 2b_1 - 12c_1 + \left(b_1 - 2c_1 + 2C_0 m_W^2\right)x_i$$
$$-2q^2\left(C_u + C_v - C_{uv}\right) + 2m_\mu^2\left(C_u + C_v - C_{uv} - C_{uu}\right)\Big]P_R\,, \tag{B.28}$$

$$B \simeq -m_\mu\Big[+2C_v + 2C_{uv} + 2C_{uu} + \left(C_0 - 2C_u - C_v + C_{uv} + C_{uu}\right)x_i\Big]P_R\,, \tag{B.29}$$

$$C \simeq -m_\mu\Big[-2C_u - 2C_v - 2C_{uv} + 2C_{uu} - \left(C_u - C_v + C_{uv} - C_{uu}\right)x_i\Big]P_R\,, \tag{B.30}$$

The functions b_1 and c_1 are given in Appendix B.5. By unitarity, all the divergent parts have fallen off. From electromagnetic gauge invariance, we must have that $q_\alpha\Gamma^\alpha = 0$ [134], that is

$$\sum_i U_{ei}U_{\mu i}^*\left(A + Bm_\mu + C\frac{q^2}{m_\mu}\right) = 0\,. \tag{B.31}$$

We have checked that this equality is indeed fulfilled at tree level, and also at first order in q^2/m_W^2 and m_μ^2/m_W^2. Now, using the fact that we can put the amplitude in the form [134] :

$$\Gamma_\alpha = iB\sigma_{\alpha\beta}q^\beta - \frac{C}{m_\mu}\left(q^2\gamma_\alpha - \not{q}q_\alpha\right)\,, \tag{B.32}$$

we finally get the well-known formula [130]-[134]

$$i\mathcal{M}_\gamma = \frac{ieg^2}{2(4\pi)^2 m_W^2}\epsilon_\lambda^\alpha(q)\overline{u}_e(p')\left[F_\gamma^{\mu e}\left(q^2\gamma_\alpha - \not{q}q_\alpha\right)P_L - i\sigma_{\alpha\beta}q^\beta G_\gamma^{\mu e} m_\mu P_R\right]u_\mu(p)\,. \tag{B.33}$$

Keeping only the dominant term, i.e. neglecting the terms proportional to q^2/m_W^2 and m_μ^2/m_W^2 in the integrals, the form factors are given by

$$F_\gamma^{\mu e} = \sum_i U_{ei}U_{\mu i}^* F_\gamma(x_i)\,, \tag{B.34}$$

$$G_\gamma^{\mu e} = \sum_i U_{ei}U_{\mu i}^* G_\gamma(x_i)\,, \tag{B.35}$$

where

$$F_\gamma(x) = \frac{x(7x^2-x-12)}{12(1-x)^3} - \frac{x^2(x^2-10x+12)}{6(1-x)^4}\ln x\,, \tag{B.36}$$

$$G_\gamma(x) = -\frac{x(2x^2+5x-1)}{4(1-x)^3} - \frac{3x^3}{2(1-x)^4}\ln x\,. \tag{B.37}$$

A straightforward computation allows to get the $\mu \to e\gamma$ decay rate, given by [130]-[134]

$$\Gamma = \frac{\alpha_w^3 s_w^2 m_\mu^5}{256\pi^2 m_W^4}|G_\gamma^{\mu e}|^2\,. \tag{B.38}$$

Let's note that the term proportional to $F_\gamma^{\mu e}$ doesn't give any contribution because it vanishes for on-shell photon $q^2 = 0$.

Contribution to μ to e conversion

A explained in section 2.3.1, one needs to separate the local and long-ranged contributions. The long-ranged one is obviously the one involving an on-shell photon. This is the term proportional to $G_\gamma^{\mu e}$ in the amplitude Eq. (B.33), and the amplitude reads

$$i\mathcal{M}_{phot.} = \frac{ieg^2}{2(4\pi)^2 m_W^2}\epsilon_\lambda^\alpha(q)\overline{u}_e(p')\left[-i\sigma_{\alpha\beta}q^\beta G_\gamma^{\mu e} m_\mu P_R\right]u_\mu(p)\,. \tag{B.39}$$

The long-ranged, or non-photonic, contribution of the photon diagrams is the term proportional to $F_\gamma^{\mu e}$ in the amplitude Eq. (B.33). In order to find the associated μ to e conversion amplitude, we just have to replace the $\epsilon_\lambda^\alpha(q)$ by the photon propagator $\Delta_\gamma = -i/q^2$, multiplied by the quark line current. We find

$$i\mathcal{M}_\gamma^q = \frac{ie^2g^2}{2(4\pi)^2 m_W^2}\overline{u}_q(p'_q)\left[Q_q\gamma^\alpha\right]u_q(p_q)\overline{u}_e(p')\left[F_\gamma^{\mu e}\left(\gamma_\alpha - \frac{\not{q}q_\alpha}{q^2}\right)P_L\right]u_\mu(p)\,, \tag{B.40}$$

where Q_q is the electric charge of the quark q.

B.3.3 Z Penguin contribution

As for the photon contributions, we first separate the lepton line from the quark line. The momentum k in the loop is taken clockwise. The Feynman diagrams, without the quark lines, are given below. The associated amplitudes, in the Feynman-t'Hooft gauge $\xi = 1$, are

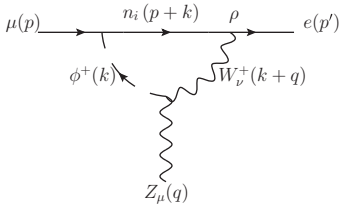

$$i\mathcal{M}_Z^A = \sum_i \frac{g^3 s_w^2}{2c_w} U_{ei} U_{\mu i}^* \, \overline{u}_e(p') \, \mathcal{I}_\alpha^A \, u_\mu(p) \, \epsilon_\lambda^{\alpha *}(q) \qquad \text{(B.41)}$$

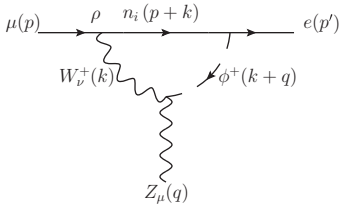

$$i\mathcal{M}_Z^B = \sum_i \frac{g^3 s_w^2}{2c_w} U_{ei} U_{\mu i}^* \, \overline{u}_e(p') \;\; \mathcal{I}_\alpha^B \, u_\mu(p) \, \epsilon_\lambda^{\alpha *}(q) \qquad \text{(B.42)}$$

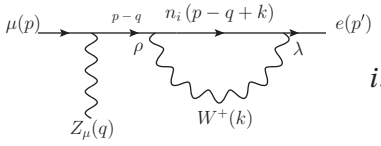

$$i\mathcal{M}_Z^C = \sum_i \frac{-g^3}{4c_w} U_{ei} U_{\mu i}^* \, \overline{u}_e(p') \, \mathcal{I}_\alpha^C \, u_\mu(p) \, \epsilon_\lambda^{\alpha *}(q) \qquad \text{(B.43)}$$

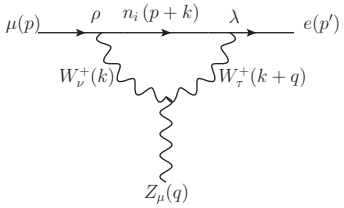

$$i\mathcal{M}_Z^D = \sum_i \frac{g^3 c_w}{2} U_{ei} U_{\mu i}^* \, \overline{u}_e(p') \, \mathcal{I}_\alpha^D \, u_\mu(p) \, \epsilon_\lambda^{\alpha *}(q) \qquad \text{(B.44)}$$

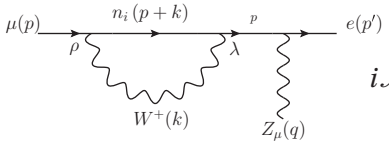

$$i\mathcal{M}_Z^E = \sum_i \frac{-g^3}{4c_w} U_{ei} U_{\mu i}^* \, \overline{u}_e(p-q) \, \mathcal{I}_\alpha^E \, u_\mu(p) \, \epsilon_\lambda^{\alpha *}(q) \qquad \text{(B.45)}$$

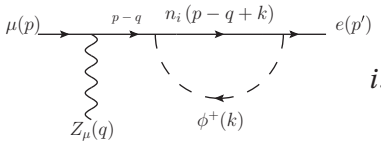

$$i\mathcal{M}_Z^F = \sum_i \frac{g^3}{4m_W^2 c_w} U_{ei} U_{\mu i}^* \, \overline{u}_e(p') \, \mathcal{I}_\alpha^F \, u_\mu(p) \, \epsilon_\lambda^{\alpha *}(q) \qquad \text{(B.46)}$$

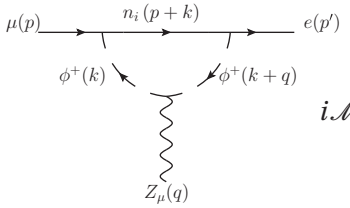

$$i\mathcal{M}_Z^G = \sum_i \frac{-g^3}{2m_w^2}\frac{1-2s_w^2}{2c_w} U_{ei}U_{\mu i}^*\,\overline{u}_e(p')\,\mathscr{I}_\alpha^G\,u_\mu(p)\,\epsilon_\lambda^{\alpha *}(q) \quad \text{(B.47)}$$

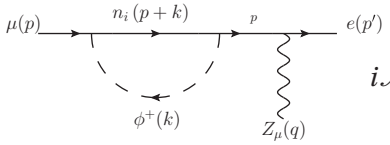

$$i\mathcal{M}_Z^H = \sum_i \frac{g^3}{4m_w^2 c_w} U_{ei}U_{\mu i}^*\,\overline{u}_e(p')\,\mathscr{I}_\alpha^H\,u_\mu(p)\,\epsilon_\lambda^{\alpha *}(q) \quad \text{(B.48)}$$

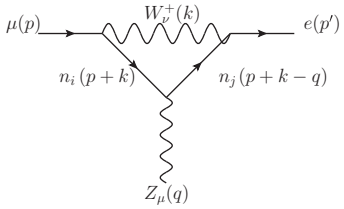

$$i\mathcal{M}_Z^I = \sum_{i,j} \frac{g^3}{4c_w} U_{ej}U_{\mu i}^*\,\overline{u}_e(p')\,\mathscr{I}_\alpha^I\;u_\mu(p)\,\epsilon_\lambda^{\alpha *}(q) \quad \text{(B.49)}$$

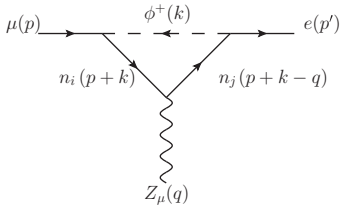

$$i\mathcal{M}_Z^J = \sum_{i,j} \frac{-g^3}{4m_w^2 c_w} U_{ej}U_{\mu i}^*\,\overline{u}_e(p')\,\mathscr{I}_\alpha^J\,u_\mu(p)\,\epsilon_\lambda^{\alpha *}(q) \quad \text{(B.50)}$$

Neglecting the electron mass, the various integrals $\mathscr{I}_\alpha^j$ are given by Eqs. (B.13)-(B.25) and

$$\mathscr{I}_\alpha^I = \int \frac{d^4k}{(2\pi)^4} \frac{\gamma_\beta P_L\left(\not{k}+\not{p}\,'+m_{n_j}\right)\gamma_\alpha\left(C_{ji}P_L - C_{ji}^*P_R\right)\left(\not{k}+\not{p}+m_{n_i}\right)\gamma^\beta P_L}{\left[(k+p)^2-m_{n_i}^2\right]\left[(k+p')^2-m_j^2\right]\left[k^2-m_W^2\right]} \quad \text{(B.51)}$$

$$\begin{aligned}
\simeq C_{ji}\Big\{&\Big[(2-D)^2\tilde{D}_1 + 2m_\mu^2\,(D_{uu}+D_{uv}+D_0-2D_u-D_v) \\
&-2q^2\,(D_{uv}+D_0-D_u-D_v)\Big]\gamma_\alpha P_L \\
&-4m_\mu(D_{uu}-D_u)\,p_\alpha P_R + 4m_\mu\,(D_{uv}+D_0-D_u-D_v)\,p'_\alpha P_R\Big\} \\
&+2C_{ji}^* m_j m_i D_0\,\gamma_\alpha P_L
\end{aligned} \quad \text{(B.52)}$$

$$\mathscr{I}_\alpha^J = \int \frac{d^4k}{(2\pi)^4} \frac{(-m_j P_R)\left(\not{k}+\not{p}\,'+m_{n_j}\right)\gamma_\alpha\left(C_{ji}P_L - C_{ji}^* P_R\right)\left(\not{k}+\not{p}+m_{n_i}\right)\left(m_\mu P_R - m_i P_L\right)}{\left[(k+p)^2-m_i^2\right]\left[(k+p')^2-m_j^2\right]\left[k^2-m_W^2\right]} \tag{B.53}$$

$$\begin{aligned}
\simeq & C_{ji}\left\{\left[m_j^2 m_i^2 D_0 - m_\mu^2 m_j^2 (D_0 - D_u)\right]\gamma_\alpha P_L + 2m_\mu m_j^2 D_v\ p'_\alpha P_R\right\} \\
& + C_{ji}^* m_j m_i \left\{\left[(2-D)\tilde{D}_1 + m_\mu^2(2D_{uu}+2D_{uv}-3D_u) - 2q^2 D_{uv}\right]\gamma_\alpha P_L\right. \\
& \left. + 2m_\mu(3D_u - 2D_{uu}) p_\alpha P_R - 4m_\mu D_{uv}\ p'_\alpha P_R\right\}
\end{aligned} \tag{B.54}$$

In the second equality, we used the equations of motion, and we expressed the integrals in terms of Feynman integrals that are given in Appendix B.5. $D_0(x_i,x_j)$, $D_u(x_i,x_j)$, $D_v(x_i,x_j)$, $D_{uu}(x_i,x_j)$, $D_{vv}(x_i,x_j)$ and $D_{uv}(x_i,x_j)$, where $x_i = m_{n_i}^2/m_W^2$, are convergent Feynman integrals that are solved using Feynman parametrization. $\tilde{D}_1(x_i,x_j,D)$ is a divergent integral that we choose to solve by using dimensional regularization method.

Contribution to μ to e conversion

When summing the various amplitudes Eqs. (B.41)-(B.50), the divergences vanish by unitarity. In order to find the contribution of the Z diagrams to the μ to e conversion amplitude, we just have to replace the $\epsilon_\lambda^\alpha(q)$ by the Z propagator $\Delta_Z = -i/(q^2-m_Z^2)$, multiplied by the quark line current. Because $q^2 \simeq -m_\mu^2$, the propagators is in good approximation $\Delta_Z \simeq i/m_Z^2$. As a consequence, a lot of the terms which have been computed can be neglected, since these will be proportional to $\sim m_\mu^2/m_W^4$ or at this order, compared to the dominant contributions, which gives

$$i\mathscr{M}_Z^q = \frac{ig^4}{2(4\pi)^2 m_W^2}\overline{u}_q(p'_q)\gamma^\alpha\left(I_q^3 P_L - Q_q s_w^2\right)u_q(p_q) \quad \overline{u}_e(p')\ F_Z^{\mu e}\ \gamma_\alpha P_L u_\mu(p)\,, \tag{B.55}$$

where

$$F_Z^{\mu e} = \sum_{i,j=1} U_{ei}U_{\mu j}^*\left(\delta_{ij}F_Z(x_i) + C_{ij}G_Z(x_i,x_j) + C_{ij}^* H_Z(x_i,x_j)\right)\,, \tag{B.56}$$

with

$$F_Z(x) = -\frac{5x}{2(1-x)}\left[1+\frac{x}{1-x}\ln x\right]\,, \tag{B.57}$$

$$G_Z(x,y) = -\frac{1}{2(x-y)}\left[\frac{x^2(1-y)}{1-x}\ln x - \frac{y^2(1-x)}{1-y}\ln y\right]\,, \tag{B.58}$$

$$H_Z(x,y) = \frac{\sqrt{xy}}{4(x-y)}\left[\frac{x^2-4x}{1-x}\ln x - \frac{y^2-4y}{1-y}\ln y\right]\,. \tag{B.59}$$

B.3.4 W boxes contribution

Here, obviously we cannot separate the lepton line from the quark line. The Feynman diagrams are given below. The momentum k in the loop is taken clockwise. The associated amplitudes are given in the Feynman-t'Hooft gauge $\xi = 1$, even if we also made the computation without fixing the gauge.

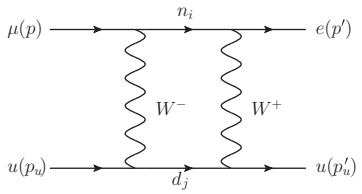

$$i\mathcal{M}_W^A = \sum_i \sum_{d_j} \frac{g^4}{4} U_{ei} U_{\mu i}^* |V_{ud_j}|^2 \, \mathcal{I}_{box}^A \tag{B.60}$$

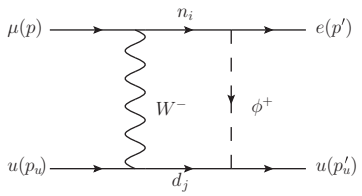

$$i\mathcal{M}_W^B = \sum_i \sum_{d_j} \frac{-g^4}{4m_W^2} U_{ei} U_{\mu i}^* |V_{ud_j}|^2 \, \mathcal{I}_{box}^B \tag{B.61}$$

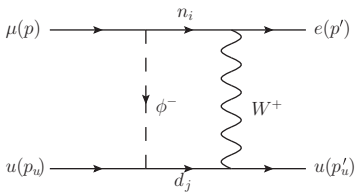

$$i\mathcal{M}_W^C = \sum_i \sum_{d_j} \frac{-g^4}{4m_W^2} U_{ei} U_{\mu i}^* |V_{ud_j}|^2 \, \mathcal{I}_{box}^C \tag{B.62}$$

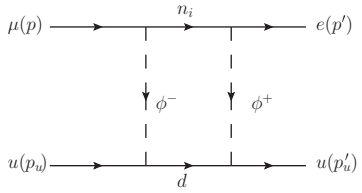

$$i\mathcal{M}_W^D = \sum_i \sum_{d_j} \frac{g^4}{4m_W^4} U_{ei} U_{\mu i}^* |V_{ud_j}|^2 \, \mathcal{I}_{box}^D \tag{B.63}$$

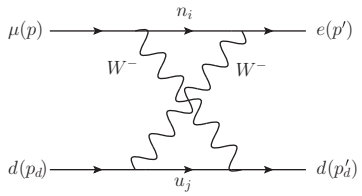

$$i\mathcal{M}_W^E = \sum_i \sum_{u_j} \frac{g^4}{4} U_{ei} U_{\mu i}^* |V_{u_j d}|^2 \, \mathcal{I}_{box}^E \tag{B.64}$$

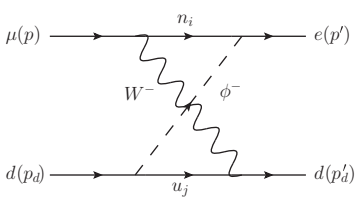

$$i\mathcal{M}_Z^F = \sum_i \sum_{u_j} \frac{-g^4}{4m_W^2} U_{ei} U_{\mu i}^* |V_{u_j d}|^2 \, \mathcal{I}_{box}^F \tag{B.65}$$

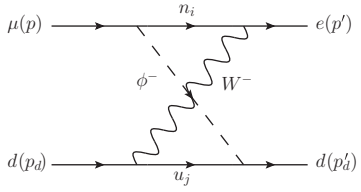

$$i\mathcal{M}_Z^G = \sum_i \sum_{u_j} \frac{-g^4}{4m_W^2} U_{ei} U_{\mu i}^* |V_{u_j d}|^2 \, \mathcal{J}_{box}^G \tag{B.66}$$

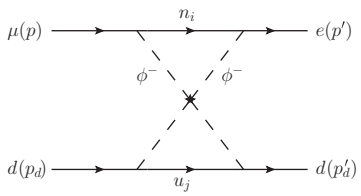

$$i\mathcal{M}_Z^H = \sum_i \sum_{u_j} \frac{g^4}{4m_W^4} U_{ei} U_{\mu i}^* |V_{u_j d}|^2 \, \mathcal{J}_{box}^H \tag{B.67}$$

Here, $V_{u_i d_j}$ stands for the CKM matrix. Neglecting terms in $\sim m_\mu^2/m_W^2$, the various integrals $\mathcal{J}_{box}^j$ are given by,

$$\mathcal{J}_{box}^A \simeq \int \frac{d^4k}{(2\pi)^4} \frac{\overline{u}_e \gamma_\alpha (-\not{k}) \gamma_\beta P_L u_\mu \quad \overline{u}_u \gamma^\alpha (\not{k}) \gamma^\beta P_L u_u}{\left[(p-k)^2 - m_{n_i}^2\right] \left[(q+k)^2 - m_{d_j}^2\right] \left[k^2 - m_W^2\right] \left[(q'-q-k)^2 - m_W^2\right]} \tag{B.68}$$

$$\simeq \overline{u}_e \gamma_\alpha P_L u_\mu \quad \overline{u}_u \gamma^\alpha P_L u_u \quad \left[-16 E_1\left(x_i, x_{d_j}\right)\right] \tag{B.69}$$

$$\mathcal{J}_{box}^B \simeq \int \frac{d^4k}{(2\pi)^4} \frac{\overline{u}_e \left(-m_{n_i}^2\right) \gamma_\mu P_L u_\mu \quad \overline{u}_u \left(m_{d_j}^2\right) \gamma^\mu P_L u_u}{\left[(p-k)^2 - m_{n_i}^2\right] \left[(q+k)^2 - m_{d_j}^2\right] \left[k^2 - m_W^2\right] \left[(q'-q-k)^2 - m_W^2\right]} \tag{B.70}$$

$$\simeq \overline{u}_e \gamma_\alpha P_L u_\mu \quad \overline{u}_u \gamma^\alpha P_L u_u \quad \left[-m_{n_i}^2 m_{d_j}^2 E_0\left(x_i, x_{d_j}\right)\right] \tag{B.71}$$

$$\mathcal{J}_{box}^C \simeq \mathcal{J}_{box}^B \tag{B.72}$$

$$\mathcal{J}_{box}^D \simeq \int \frac{d^4k}{(2\pi)^4} \frac{\overline{u}_e \left(-m_{n_i}^2 \not{k}\right) P_L u_\mu \quad \overline{u}_u \left(m_{d_j}^2 \not{k}\right) P_L u_u}{\left[(p-k)^2 - m_{n_i}^2\right] \left[(q+k)^2 - m_{d_j}^2\right] \left[k^2 - m_W^2\right] \left[(q'-q-k)^2 - m_W^2\right]} \tag{B.73}$$

$$\simeq \overline{u}_e \gamma_\alpha P_L u_\mu \quad \overline{u}_u \gamma^\alpha P_L u_u \quad \left[-m_{n_i}^2 m_{d_j}^2 E_1\left(x_i, x_{d_j}\right)\right] \tag{B.74}$$

$$\mathcal{J}_{box}^E \simeq \int \frac{d^4k}{(2\pi)^4} \frac{\overline{u}_e \gamma_\alpha \not{k} \gamma_\beta P_L u_\mu \quad \overline{u}_d \gamma^\beta \not{k} \gamma^\alpha P_L u_d}{\left[(p-k)^2 - m_{n_i}^2\right] \left[(q'-k)^2 - m_{u_j}^2\right] \left[k^2 - m_W^2\right] \left[(q-q'+k)^2 - m_W^2\right]} \tag{B.75}$$

$$\simeq \overline{u}_e \gamma_\alpha P_L u_\mu \quad \overline{u}_d \gamma^\alpha P_L u_d \quad \left[4 E_1\left(x_i, x_{u_j}\right)\right] \tag{B.76}$$

$$\mathcal{J}_{box}^F \simeq \int \frac{d^4k}{(2\pi)^4} \frac{\overline{u}_e \left(-m_{n_i}^2\right) \gamma_\alpha P_L u_\mu \quad \overline{u}_d \left(-m_{u_j}^2\right) \gamma^\alpha P_L u_d}{\left[(p-k)^2 - m_{n_i}^2\right] \left[(q'-k)^2 - m_{u_j}^2\right] \left[k^2 - m_W^2\right] \left[(q-q'+k)^2 - m_W^2\right]} \tag{B.77}$$

$$\simeq \overline{u}_e \gamma_\mu P_L u_\mu \quad \overline{u}_d \gamma^\mu P_L u_d \quad \left[m_{n_i}^2 m_{u_j}^2 E_0\left(x_i, x_{u_j}\right)\right] \tag{B.78}$$

$$\mathscr{I}^{G}_{box} \simeq \mathscr{I}^{F}_{box} \tag{B.79}$$

$$\mathscr{I}^{H}_{box} \simeq \int \frac{d^4k}{(2\pi)^4} \frac{\overline{u}_e\left(m^2_{n_i}\not{k}\right)P_L u_\mu \quad \overline{u}_d\left(m^2_{u_j}\not{k}\right)P_L u_d}{\left[(p-k)^2-m^2_{n_i}\right]\left[(q'-k)^2-m^2_{u_j}\right]\left[k^2-m^2_W\right]\left[(q-q'+k)^2-m^2_W\right]} \tag{B.80}$$

$$\simeq \overline{u}_e\gamma_\alpha P_L u_\mu \quad \overline{u}_d\gamma^\alpha P_L u_d \quad \left[m^2_{n_i}m^2_{u_j}E_1\left(x_i,x_{u_j}\right)\right] \tag{B.81}$$

In the second equality, we used the equations of motion, and we expressed the integrals in terms of Feynman integrals that are given in Appendix B.5. $E_0(x_i,x_{q_j})$ and $E_1(x_i,x_{q_j})$, where $x_i = m^2_{n_i}/m^2_W$ and $x_{q_j} = m^2_{q_j}/m^2_W$, are convergent Feynman integrals that are solved using Feynman parametrization.

Contribution to μ to e conversion

Summing the various amplitudes Eqs. (B.60)-(B.67), one gets

$$i\mathscr{M}^{q}_{W} = \frac{i\alpha^2_w}{4m^2_W}\overline{u}_q\gamma^\alpha P_L u_q \quad \overline{u}_e\, F^{\mu eqq}_{box}\gamma_\alpha P_L\, u_\mu\,, \tag{B.82}$$

where

$$F^{\mu euu}_{box} = \sum_i \sum_{d_j=d,s,b} U_{ei}U^*_{\mu i}|V_{ud_j}|^2 F_{box}(x_i,x_{d_j})\,, \tag{B.83}$$

$$F^{\mu edd}_{box} = \sum_i \sum_{u_j=u,c,t} U_{ei}U^*_{\mu i}|V_{u_jd}|^2 F_{Xbox}(x_i,x_{u_j})\,, \tag{B.84}$$

with $x_i = m^2_{n_i}/m^2_W$, $x_{q_j} = m^2_{q_j}/m^2_W$ and

$$\begin{aligned} F_{box}(x,y) = \frac{1}{x-y}\Bigg\{&\left(4+\frac{xy}{4}\right)\left[\frac{1}{1-x}+\frac{x^2}{(1-x)^2}\ln x-\frac{1}{1-y}-\frac{y^2}{(1-y)^2}\ln y\right]\\ &-2xy\left[\frac{1}{1-x}+\frac{x}{(1-x)^2}\ln x-\frac{1}{1-y}-\frac{y}{(1-y)^2}\ln y\right]\Bigg\}\,, \end{aligned} \tag{B.85}$$

$$\begin{aligned} F_{Xbox}(x,y) = \frac{1}{x-y}\Bigg\{&\left(1+\frac{xy}{4}\right)\left[\frac{1}{1-x}+\frac{x^2}{(1-x)^2}\ln x-\frac{1}{1-y}-\frac{y^2}{(1-y)^2}\ln y\right]\\ &-2xy\left[\frac{1}{1-x}+\frac{x}{(1-x)^2}\ln x-\frac{1}{1-y}-\frac{y}{(1-y)^2}\ln y\right]\Bigg\}\,. \end{aligned} \tag{B.86}$$

B.4 Summary

The amplitudes associated to the three ingredients, i.e. Eq. (B.39) and Eq. (B.40) for the photon, Eq. (B.55) for the Z, and Eq. (B.82) for the W, can be written as [1]

$$i\mathcal{M}_{\text{phot}} = \frac{i\alpha_w e}{8\pi m_W^2}\epsilon_\lambda^\alpha(q) \quad \overline{u}_e\left[-i\sigma_{\alpha\beta}q^\beta G_\gamma^{\mu e} m_\mu P_R\right] u_\mu\,, \tag{B.87}$$

$$i\mathcal{M}_\gamma^q = \frac{i\alpha_w\alpha}{2m_W^2}\overline{u}_q\gamma^\alpha Q_q u_q \quad \overline{u}_e\left[F_\gamma^{\mu e}\right]\gamma_\alpha P_L u_\mu\,, \tag{B.88}$$

$$i\mathcal{M}_Z^q = \frac{i\alpha_w^2}{2m_W^2}\overline{u}_q\gamma^\alpha\left(I_q^3 P_L - Q_q s_w^2\right)u_q \quad \overline{u}_e\left[F_Z^{\mu e}\right]\gamma_\alpha P_L u_\mu\,, \tag{B.89}$$

$$i\mathcal{M}_{box}^q = \frac{i\alpha_w^2}{4m_W^2}\overline{u}_q\gamma^\alpha P_L u_q \quad \overline{u}_e\left[F_{box}^{\mu eqq}\right]\gamma_\alpha P_L u_\mu\,. \tag{B.90}$$

The sum of the non-photonic contribution, i.e. the last three equations, gives

$$i\mathcal{M}_{\text{non-phot}}^q = \frac{i\alpha_w^2}{2m_W^2}\overline{u}_q\,\gamma^\alpha\left(V_q^{\mu e} + A_q^{\mu e}\gamma_5\right)\,u_q \quad \overline{u}_e\,\gamma_\alpha P_L\,u_\mu\,, \tag{B.91}$$

where

$$V_q^{\mu e} = Q_q s_w^2 F_\gamma^{\mu e} + \left(\frac{I_q^3}{2} - Q_q s_w^2\right)F_Z^{\mu e} + \frac{1}{4}F_{box}^{\mu eqq}\,, \tag{B.92}$$

$$A_q^{\mu e} = -\frac{I_q^3}{2}F_Z^{\mu e} - \frac{1}{4}F_{box}^{\mu eqq}\,, \tag{B.93}$$

where I_q^3 is the weak isospin ($I_u^3 = 1/2\,,\ I_d^3 = -1/2$) and s_w is the sinus of the weak mixing angle. The term proportional to the form factor $A_q^{\mu e}$ doesn't contribute to the coherent conversion as discussed in section 2.3.3. In terms of the above form factors, $V_u^{\mu e}$ and $V_d^{\mu e}$ as defined in Eq. (2.65) are given by

$$V_u^{\mu e} = \frac{2}{3}s_w^2\left(F_\gamma^{\mu e} - F_Z^{\mu e}\right) + \frac{1}{4}\left(F_Z^{\mu e} + F_{box}^{\mu euu}\right)\,, \tag{B.94}$$

$$V_d^{\mu e} = -\frac{1}{3}s_w^2\left(F_\gamma^{\mu e} - F_Z^{\mu e}\right) - \frac{1}{4}\left(F_Z^{\mu e} - F_{box}^{\mu edd}\right)\,. \tag{B.95}$$

In the case of light nuclei, the contribution of the dipolar term can also be casted in a four-fermion interaction amplitude. Replacing the $\epsilon_\lambda^\alpha(q)$ by the photon propagator $\Delta_\gamma = -i/q^2$ and multiplying by the quark line current, it reads

$$i\mathcal{M}_{\gamma-\text{dipole}}^q = \frac{i\alpha_w\alpha}{2m_W^2}\overline{u}_q\gamma^\alpha Q_q u_q\,\overline{u}_e\Big[-i\frac{\sigma_{\alpha\beta}q^\beta}{q^2}\Big]m_\mu G_\gamma^{\mu e} P_L u_\mu\,. \tag{B.96}$$

In this way Eq. (2.67) is obtained

$$\tilde{V}_q^{\mu e} = Q_q s_w^2(F_\gamma^{\mu e} + G_\gamma^{\mu e}) + F_Z^{\mu e}\left(\frac{I_q^3}{2} - Q_q s_w^2\right) + \frac{1}{4}F_{box}^{\mu eqq}\,. \tag{B.97}$$

[1] The term proportional to q_μ in Eqs. (B.33) and (B.40) drops because of quark current conservation.

The loop functions entering the computation of the form factors in Eqs. (B.94-B.96) are : [2]

$$F_\gamma(x) = \frac{x(7x^2-x-12)}{12(1-x)^3} - \frac{x^2(x^2-10x+12)}{6(1-x)^4}\ln x, \tag{B.98}$$

$$G_\gamma(x) = -\frac{x(2x^2+5x-1)}{4(1-x)^3} - \frac{3x^3}{2(1-x)^4}\ln x, \tag{B.99}$$

$$F_Z(x) = -\frac{5x}{2(1-x)} - \frac{5x^2}{2(1-x)^2}\ln x, \tag{B.100}$$

$$G_Z(x,y) = -\frac{1}{2(x-y)}\left[\frac{x^2(1-y)}{1-x}\ln x - \frac{y^2(1-x)}{1-y}\ln y\right], \tag{B.101}$$

$$H_Z(x,y) = \frac{\sqrt{xy}}{4(x-y)}\left[\frac{x^2-4x}{1-x}\ln x - \frac{y^2-4y}{1-y}\ln y\right], \tag{B.102}$$

$$\begin{aligned} F_{box}(x,y) = \frac{1}{x-y}\Bigg\{&\left(4+\frac{xy}{4}\right)\left[\frac{1}{1-x} + \frac{x^2}{(1-x)^2}\ln x - \frac{1}{1-y} - \frac{y^2}{(1-y)^2}\ln y\right] \\ &- 2xy\left[\frac{1}{1-x} + \frac{x}{(1-x)^2}\ln x - \frac{1}{1-y} - \frac{y}{(1-y)^2}\ln y\right]\Bigg\}, \end{aligned} \tag{B.103}$$

$$\begin{aligned} F_{Xbox}(x,y) = \frac{-1}{x-y}\Bigg\{&\left(1+\frac{xy}{4}\right)\left[\frac{1}{1-x} + \frac{x^2}{(1-x)^2}\ln x - \frac{1}{1-y} - \frac{y^2}{(1-y)^2}\ln y\right] \\ &- 2xy\left[\frac{1}{1-x} + \frac{x}{(1-x)^2}\ln x - \frac{1}{1-y} - \frac{y}{(1-y)^2}\ln y\right]\Bigg\}, \end{aligned} \tag{B.104}$$

$$\begin{aligned} G_{box}(x,y) = \frac{-\sqrt{xy}}{x-y}\Bigg\{&\left(4+xy\right)\left[\frac{1}{1-x} + \frac{x}{(1-x)^2}\ln x - \frac{1}{1-y} - \frac{y}{(1-y)^2}\ln y\right] \\ &- 2\left[\frac{1}{1-x} + \frac{x^2}{(1-x)^2}\ln x - \frac{1}{1-y} - \frac{y^2}{(1-y)^2}\ln y\right]\Bigg\}, \end{aligned} \tag{B.105}$$

with the limiting values

$$F_\gamma(0) = 0\,, \tag{B.106}$$

$$G_\gamma(0) = 0\,, \tag{B.107}$$

$$F_Z(0) = 0\,, \tag{B.108}$$

$$G_Z(0,x) = -\frac{x}{2(1-x)}\ln x, \qquad G_Z(0,0) = 0\,, \tag{B.109}$$

$$H_Z(0,x) = 0\,, \qquad H_Z(0,0) = 0\,, \tag{B.110}$$

$$F_{box}(0,x) = \frac{4}{1-x} + \frac{4x}{(1-x)^2}\ln x, \qquad F_{box}(0,0) = 4\,, \tag{B.111}$$

$$F_{Xbox}(0,x) = -\frac{1}{1-x} - \frac{x}{(1-x)^2}\ln x, \qquad F_{Xbox}(0,0) = -1\,, \tag{B.112}$$

$$G_{box}(0,x) = 0\,, \qquad G_{box}(0,0) = 0\,, \tag{B.113}$$

[2] We adopted the notation of Ref. [67] except that here F_{Xbox} is $-F_{box}$ of Ref. [67] whereas our F_{box} is given in Ref. [324] as H_{box}.

and

$$F_\gamma(x) \xrightarrow[x\ll 1]{} -x, \qquad F_\gamma(x) \xrightarrow[x\gg 1]{} -\frac{7}{12} - \frac{1}{6}\ln x, \tag{B.114}$$

$$G_\gamma(x) \xrightarrow[x\ll 1]{} \frac{x}{4}, \qquad G_\gamma(x) \xrightarrow[x\gg 1]{} \frac{1}{2}, \tag{B.115}$$

$$F_Z(x) \xrightarrow[x\ll 1]{} -\frac{5x}{2}, \qquad F_Z(x) \xrightarrow[x\gg 1]{} \frac{5}{2} - \frac{5}{2}\ln x, \tag{B.116}$$

$$G_Z(0,x) \xrightarrow[x\ll 1]{} -\frac{1}{2}x\ln x, \qquad G_Z(0,x) \xrightarrow[x\gg 1]{} \frac{1}{2}\ln x, \tag{B.117}$$

$$F_{box}(0,x) \xrightarrow[x\ll 1]{} 4\left(1 + x\left(1 + \ln x\right)\right), \qquad F_{box}(0,x) \xrightarrow[x\gg 1]{} 0, \tag{B.118}$$

$$F_{Xbox}(0,x) \xrightarrow[x\ll 1]{} -1 - x\left(1 + \ln x\right), \qquad F_{Xbox}(0,x) \xrightarrow[x\gg 1]{} 0. \tag{B.119}$$

In terms of these functions, the form factors read

$$F_\gamma^{\mu e} = \sum_{i=1}^{3+n_N} U_{ei} U_{\mu i}^* F_\gamma(x_i) = \sum_{i=1}^{n_N} U_{eN_i} U_{\mu N_i}^* F_\gamma(x_{N_i}), \tag{B.120}$$

$$G_\gamma^{\mu e} = \sum_{i=1}^{3+n_N} U_{ei} U_{\mu i}^* G_\gamma(x_i) = \sum_{i=1}^{n_N} U_{eN_i} U_{\mu N_i}^* G_\gamma(x_{N_i}), \tag{B.121}$$

$$F_Z^{\mu e} = \sum_{i,j=1}^{3+n_N} U_{ei} U_{\mu j}^* \left(\delta_{ij} F_Z(x_i) + C_{ij} G_Z(x_i, x_j) + C_{ij}^* H_Z(x_i, x_j)\right) \tag{B.122}$$

$$\begin{aligned} &= \sum_{i,j=1}^{n_N} U_{eN_i} U_{\mu N_j}^* \Big[\delta_{N_i N_j}\left(F_Z(x_{N_i}) + 2G_Z(0, x_{N_i})\right) \\ &\quad + C_{N_i N_j}\left(G_Z(x_{N_i}, x_{N_j}) - G_Z(0, x_{N_i}) - G_Z(0, x_{N_j})\right) + C_{N_i N_j}^* H_Z(x_{N_i}, x_{N_j})\Big], \end{aligned} \tag{B.123}$$

$$F_{box}^{\mu euu} = \sum_{i=1}^{3+n_N} \sum_{d_j=d,s,b} U_{ei} U_{\mu i}^* |V_{ud_j}|^2 F_{box}(x_i, x_{d_j}) \simeq \sum_{i=1}^{3+n_N} U_{ei} U_{\mu i}^* F_{box}(x_i, 0) \tag{B.124}$$

$$= \sum_{i=1}^{n_N} U_{eN_i} U_{\mu N_i}^* \left[F_{box}(x_{N_i}, 0) - F_{box}(0,0)\right], \tag{B.125}$$

$$F_{box}^{\mu edd} = \sum_{i=1}^{3+n_N} \sum_{u_j=u,c,t} U_{ei} U_{\mu i}^* |V_{u_j d}|^2 F_{Xbox}(x_i, x_{u_j}) \simeq \sum_{i=1}^{3+n_N} U_{ei} U_{\mu i}^* F_{Xbox}(x_i, 0) \tag{B.126}$$

$$= \sum_{i=1}^{n_N} U_{eN_i} U_{\mu N_i}^* \left[F_{Xbox}(x_{N_i}, 0) - F_{Xbox}(0,0)\right]. \tag{B.127}$$

$$F_{box}^{\mu eee} = \sum_{i,j=1}^{3+n_N} U_{ei} U_{\mu j}^* \left(U_{ei} U_{ej}^* G_{box}(x_i, x_j) - 2\, U_{ei}^* U_{ej} F_{Xbox}(x_i, x_j)\right) \tag{B.128}$$

$$\begin{aligned} &= -2 \sum_{i=1}^{n_N} U_{eN_i} U_{\mu N_i}^* \left[F_{Xbox}(x_{N_i}, 0) - F_{Xbox}(0,0)\right] \\ &\quad + \sum_{i,j=1}^{n_N} U_{eN_i} U_{\mu N_j}^* \Big\{U_{eN_i} U_{eN_j}^* G_{box}(x_{N_i}, x_{N_j}) - 2\, U_{eN_i}^* U_{eN_j} \left[F_{Xbox}(x_{N_i}, x_{N_j})\right. \\ &\quad \left. - F_{Xbox}(0, x_{N_j}) - F_{Xbox}(x_{N_i}, 0) + F_{Xbox}(0,0)\right]\Big\} \end{aligned} \tag{B.129}$$

In the above, $x_{1,2,3} \equiv x_{\nu_{1,2,3}} \equiv m^2_{\nu_{1,2,3}}/m_W^2$, $x_{4,\ldots,3+n_N} \equiv x_{N_{1,\ldots,n_N}} = m^2_{N_{1,\ldots,n_N}}/m_W^2$ and $x_q \equiv m_q^2/m_W^2$. The matrix V is the quark CKM matrix and U is the total $(3+n_N)\times(3+n_N)$ neutrino mixing

matrix defined in Eq. (2.7). The second equality in Eqs. (B.120)-(B.129) is obtained using the unitarity identity $\sum_i U_{ei}U^*_{\mu i}=0$, the diagonalization relation $\sum_i U_{ei}\sqrt{x_i}\,U_{\mu i}=0$, the limiting values of the loop functions in Eqs. (B.130)-(B.135) and the very good approximation for the present analysis in which light neutrino masses are neglected compared to the heavy neutrino masses ($x_{N_{1,\ldots,n_N}} \gg x_{\nu_{1,2,3}}$).

The above form factors in Eqs. (B.120)-(B.129) present the following behavior for low and high masses

$$F_\gamma^{\mu e} \xrightarrow[x\ll 1]{} \sum_{i=1}^{n_N} U_{eN_i}U^*_{\mu N_i}\left[-x_{N_i}\right], \qquad F_\gamma^{\mu e} \xrightarrow[x\gg 1]{} \sum_{i=1}^{n_N} U_{eN_i}U^*_{\mu N_i}\left[\frac{-7}{12}-\frac{1}{6}\ln x_{N_i}\right], \tag{B.130}$$

$$G_\gamma^{\mu e} \xrightarrow[x\ll 1]{} \sum_{i=1}^{n_N} U_{eN_i}U^*_{\mu N_i}\left[\frac{x_{N_i}}{4}\right], \qquad G_\gamma^{\mu e} \xrightarrow[x\gg 1]{} \sum_{i=1}^{n_N} U_{eN_i}U^*_{\mu N_i}\left[\frac{1}{2}\right], \tag{B.131}$$

$$F_Z^{\mu e} \xrightarrow[x\ll 1]{} \sum_{i=1}^{n_N} U_{eN_i}U^*_{\mu N_i}x_{N_i}\left[\frac{-5}{2}-\ln x_{N_i}\right], \qquad F_Z^{\mu e} \xrightarrow[x\gg 1]{} \sum_{i=1}^{n_N} U_{eN_i}U^*_{\mu N_i}\left[\frac{5}{2}-\frac{3}{2}\ln x_{N_i}\right], \tag{B.132}$$

$$F_{box}^{\mu euu} \xrightarrow[x\ll 1]{} \sum_{i=1}^{n_N} U_{eN_i}U^*_{\mu N_i}4\,x_{N_i}\left[1+\ln x_{N_i}\right], \qquad F_{box}^{\mu euu} \xrightarrow[x\gg 1]{} \sum_{i=1}^{n_N} U_{eN_i}U^*_{\mu N_i}\left[-4\right], \tag{B.133}$$

$$F_{box}^{\mu edd} \xrightarrow[x\ll 1]{} \sum_{i=1}^{n_N} U_{eN_i}U^*_{\mu N_i}x_{N_i}\left[-1-\ln x_{N_i}\right], \qquad F_{box}^{\mu edd} \xrightarrow[x\gg 1]{} \sum_{i=1}^{n_N} U_{eN_i}U^*_{\mu N_i}, \tag{B.134}$$

$$F_{box}^{\mu eee} \xrightarrow[x\ll 1]{} \sum_{i=1}^{n_N} U_{eN_i}U^*_{\mu N_i}2\,x_{N_i}\left[1+\ln x_{N_i}\right], \qquad F_{box}^{\mu eee} \xrightarrow[x\gg 1]{} \sum_{i=1}^{n_N} U_{eN_i}U^*_{\mu N_i}\left[-2\right], \tag{B.135}$$

where contributions involving 4 insertions of light-heavy mixing elements have been neglected. This is a good approximation in view of the various experimental bounds which hold on the mixings for the low energy regime, as shown in Fig. 2.8 a, whereas for very high right-handed masses this approximation relies on the perturbativity of the Yukawa couplings (ensured by the bounds in Fig. 2.7 a up to 10 TeV). Dropping these terms with four insertions, the functions V_q and $\tilde{V}_q$ can be written as

$$\begin{aligned} V_u(x) &= \frac{2}{3}s_w^2\Big[F_\gamma(x)-F_Z(x)-2G_Z(0,x)\Big] \\ &\quad +\frac{1}{4}\Big[F_Z(x)+2G_Z(0,x)+F_{box}(x,0)-F_{box}(0,0)\Big], \end{aligned} \tag{B.136}$$

$$\begin{aligned} V_d(x) &= -\frac{1}{3}s_w^2\Big[F_\gamma(x)-F_Z(x)-2G_Z(0,x)\Big] \\ &\quad -\frac{1}{4}\Big[F_Z(x)+2G_Z(0,x)-F_{Xbox}(x,0)+F_{Xbox}(0,0)\Big], \end{aligned} \tag{B.137}$$

$$\tilde{V}_u(x) = V_u(x)+\frac{2}{3}s_w^2G_\gamma(x), \tag{B.138}$$

$$\tilde{V}_d(x) = V_d(x)-\frac{1}{3}s_w^2G_\gamma(x), \tag{B.139}$$

which are the expressions we actually use for all plots.

B.5 Integrals

The divergent integrals are solved using dimensional regularization. These are given by[3]

$$\tilde{B}_0(x,D) \simeq \frac{i}{\mu^{2\delta}(4\pi)^2}\left\{\Delta+1-\ln\frac{m_n^2}{\mu^2}-\frac{1}{x-1}\ln x\right\} \equiv \frac{i\Delta}{\mu^{2\delta}(4\pi)^2}+b_0 \tag{B.140}$$

$$\begin{aligned}\tilde{B}_1(x,D) &\simeq \frac{i}{\mu^{2^\delta}(4\pi)^2}\left\{\frac{\Delta}{2}+\frac{1}{2}-\frac{1}{2}\ln\frac{m_n^2}{\mu^2}+\frac{x+1}{4(x-1)}-\frac{2x-1}{2(x-1)^2}\ln x\right\}\\ &\equiv \frac{i\Delta}{\mu^{2\delta}(4\pi)^2}+b_1\end{aligned} \tag{B.141}$$

$$\begin{aligned}\tilde{C}_1(x,q^2,D) \simeq \frac{i}{\mu^{2\delta}(4\pi)^2}\Bigg\{&\frac{\Delta}{4}+\frac{1}{4}-\frac{1}{4}\ln\frac{m_n^2}{\mu^2}+\frac{x+1}{8(x-1)}-\frac{2x-1}{4(x-1)^2}\ln x\\ &+\frac{q^2}{m_W^2}\left[-\frac{11x^2-7x+2}{72(x-1)^3}+\frac{x^3}{12(x-1)^4}\ln x\right]\Bigg\} \equiv \frac{i\Delta}{\mu^{2\delta}(4\pi)^2}+c_1\end{aligned} \tag{B.142}$$

$$\tilde{D}_1(x,y,D) \simeq \frac{i}{\mu^{2\delta}(4\pi)^2}\left\{\frac{\Delta}{4}+\frac{3}{8}-\frac{1}{4}\ln m_W^2-\frac{1}{4(x-y)}\left[\frac{x^2}{x-1}\ln x+\frac{y^2}{y-1}\ln y\right]\right\} \tag{B.143}$$

The convergent integrals are solved using Feynman parametrization. They read

$$\begin{aligned}C_0(x,q^2) \simeq \frac{-i}{(4\pi)^2 m_W^2}\Bigg\{&-\frac{1}{x-1}+\frac{x}{(x-1)^2}\ln x\\ &+\frac{q^2}{m_W^2}\left[\frac{2x^2+5x-1}{12(x-1)^3}-\frac{x^2}{2(x-1)^4}\ln x\right]\Bigg\}\end{aligned} \tag{B.144}$$

$$\begin{aligned}C_u(x,q^2) \simeq C_v \simeq \frac{-i}{(4\pi)^2 m_W^2}\Bigg\{&-\frac{3x^2-4x+1}{4(x-1)^3}+\frac{x^2}{2(x-1)^3}\ln x\\ &+\frac{q^2}{m_W^2}\left[\frac{3x^3+13x^2-5x+1}{36(x-1)^4}-\frac{x^2}{3(x-1)^5}\ln x\right]\Bigg\}\end{aligned} \tag{B.145}$$

$$\begin{aligned}C_{uu}(x,q^2) \simeq C_{vv} \simeq \frac{-i}{(4\pi)^2 m_w^2}\Bigg\{&-\frac{11x^2-7x+2}{18(x-1)^3}+\frac{x^3}{3(x-1)^4}\ln x\\ &+\frac{q^2}{m_w^2}\left[\frac{12x^4+77x^3-43x^2+17x-3}{240(x-1)^5}-\frac{x^4}{4(x-1)^6}\ln x\right]\Bigg\}\end{aligned} \tag{B.146}$$

[3]The integrals are expanded at zero order in q^2/m_W^2, except the C ones, which are given at first order in q^2/m_W^2. This is because it allows us to check that the relation in Eq. (B.31) is well satisfied. For μ to e conversion, it is enough to keep the zero order.

$$C_{uv}(x,q^2) \simeq \frac{-i}{(4\pi)^2 m_w^2}\left\{-\frac{11x^2-7x+2}{36(x-1)^3}+\frac{x^3}{6(x-1)^4}\ln x \right. \\ \left. +\frac{q^2}{m_w^2}\left[\frac{12x^4+77x^3-43x^2+17x-3}{360(x-1)^5}-\frac{x^4}{6(x-1)^6}\ln x\right]\right\} \tag{B.147}$$

$$D_0(x,y) \simeq \frac{-i}{(4\pi)^2 m_W^2}\left\{\frac{1}{x-y}\left[\frac{x}{x-1}\ln x-\frac{y}{y-1}\ln y\right]\right\} \tag{B.148}$$

$$D_u(x,y) \simeq \frac{-i}{(4\pi)^2 m_W^2}\left\{\frac{1}{x-y}\left[\frac{x}{2(x-1)}-\frac{x^2+xy(x-2)}{2(x-1)^2(x-y)}\ln x+\frac{y^2}{2(y-1)(x-y)}\ln y\right]\right\} \tag{B.149}$$

$$D_v(x,y) \simeq \frac{-i}{(4\pi)^2 m_W^2}\left\{\frac{1}{x-y}\left[\frac{y}{2(y-1)}-\frac{y^2+xy(y-2)}{2(y-1)^2(x-y)}\ln y+\frac{x^2}{2(x-1)(x-y)}\ln x\right]\right\} \tag{B.150}$$

$$D_{uu}(x,y) \simeq \frac{-i}{(4\pi)^2 m_W^2}\left\{\frac{1}{(x-y)^2}\left[\frac{x\left(x^2-3xy-3x+5y\right)}{6(x-1)^2}-\frac{y^3}{3(y-1)(x-y)}\ln y \right.\right. \\ \left.\left. -\frac{x\left(x^2y^2+x^2y+x^2-3xy^2-3xy+3y^2\right)}{3(x-1)^3(x-y)}\ln x\right]\right\} \tag{B.151}$$

$$D_{vv}(x,y) \simeq \frac{-i}{(4\pi)^2 m_W^2}\left\{\frac{1}{(x-y)^2}\left[\frac{y\left(y^2-3xy-3y+5x\right)}{6(y-1)^2}-\frac{x^3}{3(x-1)(x-y)}\ln x \right.\right. \\ \left.\left. -\frac{y\left(x^2y^2+y^2x+y^2-3yx^2-3xy+3x^2\right)}{3(y-1)^3(x-y)}\ln y\right]\right\} \tag{B.152}$$

$$D_{uv}(x,y) \simeq \frac{-i}{(4\pi)^2 m_W^2}\left\{\frac{1}{(x-y)^2}\left[\frac{x^2y-x^2+xy^2-y^2}{6(x-1)(y-1)}-\frac{x^2(2xy+x-3y)}{6(x-1)^2(x-y)}\ln x \right.\right. \\ \left.\left. +\frac{y^2(2xy+y-3x)}{6(y-1)^2(x-y)}\ln y\right]\right\} \tag{B.153}$$

$$E_0(x,y) \simeq \frac{-i}{(4\pi)^2 m_W^4}\left\{\frac{1}{x-y}\left[\frac{1}{1-x}-\frac{1}{1-y}+\frac{x}{(1-x)^2}\ln x-\frac{y}{(1-y)^2}\ln y\right]\right\} \tag{B.154}$$

$$E_1(x,y) \simeq \frac{-i}{4(4\pi)^2 m_W^2}\left\{\frac{1}{x-y}\left[\frac{1}{1-x}-\frac{1}{1-y}+\frac{x^2}{(1-x)^2}\ln x-\frac{y^2}{(1-y)^2}\ln y\right]\right\} \tag{B.155}$$

C Tools for leptogenesis and dark matter genesis

C.1 Thermodynamics of the early Universe : definitions and conventions

C.1.1 Bosons

A boson B obeys the Bose-Einstein statistic. Taking into account its chemical potential μ_B, the associated equilibrium distribution of occupation number of modes of energy $E = \sqrt{\vec{p}^2 + m_B^2}$ at some temperature T is given by

$$f_B^{\rm Eq}(E) = \frac{1}{e^{(E-\mu_B)/T} - 1} \,. \tag{C.1}$$

Accordingly, the number density of a boson B at some temperature T is

$$n_B^{\rm Eq}(E) = g_B \int \frac{d^3\vec{p}}{(2\pi)^3}\, f_B^{\rm Eq}(\vec{p}) \,, \tag{C.2}$$

where g_B is the number of degrees of freedom of B, and the energy density is given by

$$\rho_B^{\rm Eq}(E) = g_B \int \frac{d^3\vec{p}}{(2\pi)^3}\, E\, f_B^{\rm Eq}(\vec{p}) \,. \tag{C.3}$$

The above relations has simple analytical form in some limit.

- If $T \ll m_B$, the boson is non-relativistic and the number density of B in the gas is given, at zero order in μ_B/T, by the Boltzmann's law

$$n_B^{\rm Eq}(E) \approx g_B \left(\frac{m_B T}{2\pi}\right)^{3/2} e^{-m_B/T} \,, \tag{C.4}$$

and

$$\rho_B^{\rm Eq}(E) \approx m_B\, n_B^{\rm Eq}(E) \,. \tag{C.5}$$

The equation of state, that relates the energy E and the pressure p, in the non-relativistic limit is simply $p \approx n_B\ T \approx 0$.

- If $T \gg m_B$, the boson is relativistic and the equilibrium number density of B in the gas is, at first order in μ_B/T,

$$n_B^{\rm Eq}(E) \approx \frac{g_B}{\pi^2}\ T^3 \left(\zeta(3) + \frac{\mu_B}{T}\zeta(2)\right) , \tag{C.6}$$

with the Riemann Zeta function values $\zeta(2) \approx 1.645$ and $\zeta(3) \approx 1.202$. The energy density is, at zero order in μ_B/T,

$$\rho_B^{\rm Eq}(E) \approx g_B \frac{\pi^2}{30}\ T^4 . \tag{C.7}$$

The equation of state, that relates the energy E and the pressure p, in the relativistic limit is simply $p \approx \rho_B/3$. Let's note that the thermodynamical quantities associated to the photons γ, with $g_\gamma = 2$ for the two polarizations, are

$$n_\gamma = \frac{2\zeta(3)}{\pi^2} T^3 , \quad \rho_\gamma = \frac{\pi^2}{15} T^4 , \quad p_\gamma = \frac{1}{3}\rho_\gamma . \tag{C.8}$$

C.1.2 Fermions

A fermion F obeys the Fermi-Dirac statistic. Taking into account its chemical potential μ_F, the associated equilibrium distribution of occupation number of modes of energy $E = \sqrt{\vec{p}^2 + m_F^2}$ at some temperature T is given by

$$f_F^{\rm Eq}(E) = \frac{1}{e^{(E-\mu_F)/T} + 1} . \tag{C.9}$$

Accordingly, the number density of a fermion F at some temperature T is

$$n_F^{\rm Eq}(E) = g_F \int \frac{d^3\vec{p}}{(2\pi)^3}\ f_F^{\rm Eq}(\vec{p}) , \tag{C.10}$$

where g_F is the number of degrees of freedom of F, and the energy density is given by

$$\rho_F^{\rm Eq}(E) = g_F \int \frac{d^3\vec{p}}{(2\pi)^3}\ E\ f_F^{\rm Eq}(\vec{p}) . \tag{C.11}$$

The above relations has simple analytical form in some limit.

- If $T \ll m_F$ and at zero order in μ_B/T, one recover the same results as for the boson case. This is because for $T \ll m_F$ as for $T \ll m_B$, the factor ± 1 in the denominator of the distribution expression can be neglected.

- If $T \gg m_F$, the fermion is relativistic, and one gets at first order in μ_F/T,

$$n_F^{\rm Eq}(E) \approx \frac{g_F}{\pi^2}\ T^3 \left(\frac{3}{4}\zeta(3) + + \frac{\mu_F}{2T}\zeta(2)\right) , \tag{C.12}$$

and, at zero order in μ_F/T,

$$\rho_F^{\rm Eq}(E) \approx \frac{7}{8}\, g_F \frac{\pi^2}{30}\, T^4 \,. \tag{C.13}$$

The equation of state, that relates the energy E and the pressure p, in the relativistic limit is also $p \approx \rho_F/3$.

C.1.3 Maxwell-Boltzmann

In general, it is a good approximation to consider the Maxwell-Boltzmann distribution for both bosons and fermions. This is, the constant term ± 1 is neglected in the boson and fermion distributions :

$$f_X^{\rm Eq}(E_X) \simeq e^{-(E_X-\mu_X)/T} \,, \tag{C.14}$$

where we also took into account the chemical potential μ_X of the species X. The chemical potential of the associated antiparticle $\bar{X}$ is $\mu_{\bar{X}} = -\mu_X$. With the above approximation, the equilibrium number density has a simple analytical form. In the case where $\mu_X = 0$, one has

$$n_X^{\rm Eq} \simeq \frac{g_X}{2\pi^2}\, T^2\, m_X^2\, K_2(m_X/T) \,. \tag{C.15}$$

This is the equilibrium number density that are in general used in the Boltzmann equations. It allows to not make the distinction between bosons and fermions, leading to less complex equations, at the cost of the above approximation.

C.1.4 Gas properties in the early Universe

Energy density. The total energy density ρ is the sum over all the relativistic particle energy densities

$$\rho = \sum_{A=B,F} \rho_A(T_A) \,, \quad \text{where} \quad \rho_A(T_A) = \frac{\pi^2}{30}\, g_A^{\rm eff}\, T_A^4 \,, \tag{C.16}$$

with T_A the temperature of the species A, being a boson (B) or a fermion (F), and $g_A^{\rm eff}$ the effective number of degrees of freedom which is $g_A^{\rm eff} = g_A$ for bosons and $g_A^{\rm eff} = 7/8 \cdot g_A$ for fermions. The total energy density can also be written as

$$\rho = \frac{\pi^2}{30}\, g_*\, T^4 \,, \tag{C.17}$$

where T is the temperature associated to the photons, and

$$g_* \equiv \sum_{\rm bosons} g_A \left(\frac{T_A}{T}\right)^4 + \frac{7}{8} \sum_{\rm fermions} g_A \left(\frac{T_A}{T}\right)^4 \tag{C.18}$$

is the effective number of degrees of freedom in energy. In the early Universe, all the SM particles were relativistic and the effective number of degrees of freedom is $g_* = 106.75$. [1] Today, $T = T_0 \simeq 2.73$ K and the only relativistic species at this temperature are the photons and the neutrinos. It is straightforward to show that the temperature associated to the neutrinos, after CMB and CνB (Cosmic Neutrino Background) decouplings, is related to the photon's one through

$$T_\nu = \left(\frac{4}{11}\right)^{1/3} T \simeq 1.95 \text{ K} \,. \tag{C.19}$$

The total energy density today is then given by

$$\rho_0 = \frac{\pi^2}{30}\left[2 + \frac{21}{4}\left(\frac{4}{11}\right)^{4/3}\right] T_0^4 \simeq 1.68 \cdot \rho_\gamma(T_0) \,, \tag{C.20}$$

where ρ_γ is the energy density of the photons, given in Eq. (C.8).

Entropy. The total entropy density s is the sum over all the relativistic particle entropy densities

$$s = \sum_{A=B,F} s_A(T_A) \,, \quad \text{where} \quad s_A(T_A) = \frac{\rho_A + p_A}{T_A} \,, \tag{C.21}$$

with T_A the temperature, p_A the pressure and ρ_A the energy density of the species A, being a boson (B) or a fermion (F). For a relativistic particles, the energy density and the pressure are related to the temperature through

$$\rho_A = 3p_A = \frac{\pi^2}{30} g_A^{\text{eff}} T_A^4 \,. \tag{C.22}$$

The total entropy density can be expressed as

$$s = \frac{2\pi^2}{45} g_{*s} T^3 \,, \tag{C.23}$$

where T is the temperature associated to the photons, and

$$g_{*s} \equiv \sum_{\text{bosons}} g_A \left(\frac{T_A}{T}\right)^3 + \frac{7}{8} \sum_{\text{fermions}} g_A \left(\frac{T_A}{T}\right)^3 \tag{C.24}$$

is the effective number of degrees of freedom in entropy. In the early Universe, all the SM particles were relativistic and the effective number of degrees of freedom in entropy is $g_{*s} = g_* = 106.75$. [2] Today, using Eq. (C.19), the total entropy density is given by

$$s_0 = \frac{2\pi^2}{45}\left[2 + \frac{21}{4}\left(\frac{4}{11}\right)\right] T_0^3 \simeq 7.04 \cdot n_\gamma(T_0) \,, \tag{C.25}$$

where n_γ is the number density of the photons, given in Eq. (C.8).

[1] Let's note that if we use the Maxwell-Boltzmann distribution, it may be more consistent to compute the effective number of degrees of freedom without taking into account the factor 7/8 in Eq. (C.18). In this case, one can also use $g_* = 117$ in the early Universe.

[2] Using the Maxwell-Boltzmann distribution, one has $g_{*s} = g_* = 117$ in the early Universe.

C.1.5 Equilibrium

Here, we briefly specify the notion of chemical equilibrium, kinetic equilibrium and thermal equilibrium, for gas of particles.

Kinetic (or mechanical) equilibrium. A system of particles is said to be in kinetic equilibrium if the particles exchange energy and momentum efficiently. In this case, the phase space occupancy is given by the familiar Bose-Einstein or Fermi-Dirac distributions.

Chemical (or diffusive) equilibrium. Chemical equilibrium is reached when the sum of the chemical potentials of the reacting particles is equal to the sum of the chemical potentials of the products. The rates of the forward and reverse reactions are then equal.

Thermal (or abusively thermodynamical) equilibrium. Thermal equilibrium is achieved for species which are both in kinetic and chemical equilibrium. These species then share a common temperature $T_i = T$.

C.2 Sphalerons

The global currents associated to the baryon and lepton numbers are non-conserved at the quantum level because of the triangle anomalies. One can show that the associated current derivatives read

$$\partial_\mu j_L^{\mu 5} = \frac{3}{32\pi^2}\left[g^2 W^{\mu\nu}\tilde{W}_{\mu\nu} + g'^2 B^{\mu\nu}\tilde{B}_{\mu\nu}\right] , \tag{C.26}$$

$$\partial_\mu j_B^{\mu 5} = \partial_\mu j_L^{\mu 5} , \tag{C.27}$$

where $\tilde{X}_{\mu\nu} = \epsilon_{\mu\nu\alpha\beta}X^{\alpha\beta}$. As a consequence, from the two equations above, we see that the $B+L$ global symmetry is violated, but clearly not the $B-L$ one since $\partial_\mu(j_B^{\mu 5} - j_L^{\mu 5}) = 0$.

The SM contains therefore processes that violate the sum $B+L$, while conserving the difference $B-L$. These non-perturbative processes are called EW sphalerons [213] and are very fast for temperature typically above the EWSB. More precisely, from Fig. 3.5, one can see that the EW sphalerons rate is faster than the Hubble rate for $T > T_{\text{sphal}} = 132$ GeV.

Let's note that as these EW sphalerons are related to the $SU(2)_L$ gauge group, there are also sphalerons related to the $SU(3)_c$ gauge group, called QCD sphalerons. Our goal here is not to enter in the details of the sphalerons physics, but for our present let's mention the following sphaleron's properties.

- One can associate effective operators to EW and QCD sphalerons processes. They read

$$\mathcal{O}_{EW}^{\text{sphal}} = \prod_i^{N_f} Q_{Li} Q_{Li}^i Q_{Li}^i \ell_{Li}^i \,, \tag{C.28}$$

$$\mathcal{O}_{QCD}^{\text{sphal}} = \prod_i^{N_f} Q_{Li} Q_{Li} u_{Ri}^c d_{Ri}^c \,, \tag{C.29}$$

  where N_f is the number of families. The EW sphalerons operator relates left-handed quarks and leptons and violate $B+L$, while the QCD one relates left-handed and right-handed quarks.

- For $T \ll T_{\text{sphal}} \simeq 132$ GeV, the EW and QCD sphalerons rates are exponentially suppressed :

$$\Gamma_{EW,QCD} \simeq e^{-8\pi^2/g^2} \approx e^{-173} \,, \tag{C.30}$$

  so that they effectively don't occur at all.

- For $T > T_{\text{sphal}}$, sphalerons are fast and their rate are given by [255, 214, 325, 326]

$$\text{Electroweak sphalerons:} \qquad \Gamma_{EW}(T) \simeq 26\,\alpha_{\text{EW}}\,T \,, \tag{C.31}$$

$$\text{QCD instantons:} \qquad \Gamma_{QCD}(T) \simeq 312\,\alpha_{\text{S}}\,T \,. \tag{C.32}$$

- By comparing Eq. (D.44) with the Hubble rate H, the EW sphalerons are much faster than H for $T_{\text{sphal}} \lesssim T \lesssim 10^{12}$ GeV. In this temperature range, the processes generated by effective operator in Eq. (C.28) implies the following chemical equilibrium condition

$$\sum_i \left(3\mu_{Q_i} + \mu_{\ell_i}\right) = 0 \,. \tag{C.33}$$

- By comparing Eq. (D.43) with the Hubble rate H, the QCD sphalerons are much faster than H for $T_{\text{sphal}} \lesssim T \lesssim 10^{13}$ GeV. In this temperature range, the processes generated by effective operator in Eq. (C.28) implies the following chemical equilibrium condition

$$\sum_i \left(2\mu_{Q_i} - \mu_{u_i} - \mu_{d_i}\right) = 0 \,. \tag{C.34}$$

C.3 Boltzmann equations or chemical equilibrium conditions ?

In general, the evolution equations of particle asymmetries in the early Universe couple all particles species and thus involve a large number of reactions. However, a simplification is possible given that for specific temperature regimes different reactions have different timescales. Any reaction occurring in the heat bath will necessarily fall in one of the following categories :

1. Reactions which at a given temperature T_0 are much slower than the Hubble Universe expansion rate $H(T_0)$: $\Gamma_{\text{SR}} \ll H(T_0)$.
2. Reactions which at a given temperature T_0 are much faster than the Hubble Universe expansion rate $H(T_0)$: $\Gamma_{\text{FR}} \gg H(T_0)$.

3. Reactions which at a given temperature T_0 are comparable to the Hubble Universe expansion rate $H(T)$: $\Gamma_{\rm CR} \sim H(T_0)$.

At T_0, reactions falling in category 1 basically have not taken place, so they are generally of no relevance in the evolution of the particle asymmetry. The parameters responsible for such reactions can then be put to zero at the Lagrangian level, leading to the corresponding early Universe effective Lagrangian which involves new global symmetries implying new conservation laws [327]. In contrast, the reactions in 2 at T_0 have occurred so often that the particles involved attain thermodynamic equilibrium and so are subject to chemical equilibrium constraints, which enforce relations among the different particles chemical potentials (the particle asymmetries), see Appendix C.5 below. These chemical equilibrium conditions, when coupled with the constraints implied by the conservation laws of the early Universe effective Lagrangian, allow to express the particle asymmetries of all the species in the thermal bath in terms of quasi-conserved charge asymmetries, the asymmetries related with charges that are only (slowly) broken by the reactions in 3. Finally, reactions of type 3 are not fast enough to equilibrate the distributions of the intervening particles, and so they have to be accounted for via Boltzmann equations, which dictate the evolution of the quasi-conserved charge asymmetries and therefore of all the asymmetries in the heat bath. Note that for reactions of category 1 one has nevertheless to be cautious before dropping them from the Boltzmann equations. A well-known example, relevant in some cases for the dark matter abundance, is the freeze-in regime, i.e. slow production of dark matter particles from an out-of-equilibrium process [328].

C.4 Boltzmann equations formalism

C.4.1 Generalities

The Boltzmann equations are very useful to describe the out-of-equilibrium evolution of a gas of particles submitted to interactions. The evolution equation of the phase space density of a species X has the simple form

$$\mathrm{L}[f_X] = \mathrm{C}[f_X] \,, \tag{C.35}$$

where the Liouville operator L describes typically the space evolution of X and is given by

$$\mathrm{L} = \frac{\partial}{\partial t} + \frac{\partial \vec{x}}{\partial t}\frac{\partial}{\partial \vec{x}} + \frac{\partial \vec{v}}{\partial t}\frac{\partial}{\partial \vec{v}} \,, \tag{C.36}$$

and C is the collision operator. This operator contains all the physics of elastic and/or inelastic collisions, and it therefore includes the matrix element of the probability transitions. By integrating Eq. (C.35), one can derive the Boltzmann equation for the number density n_X, which reads

$$g_X \int \frac{d^3\vec{p}}{(2\pi)^3} \mathrm{L}[f_X] = g_X \int \frac{d^3\vec{p}}{(2\pi)^3} \mathrm{C}[f_X] \,. \tag{C.37}$$

For example, in the case where the species X can interact with other particles through the process $X \leftrightarrow Y + Z$, the collision term in the r.h.s. of Eq. (C.37) reads

$$g_X \int \frac{d^3\vec{p}}{(2\pi)^3} \mathrm{C}[f_X] = \int d\pi_X d\pi_Y d\pi_Z (2\pi)^4 \delta^4(p_X - p_Y - p_Z) \left[f_Y(p_Y) f_Z(p_Z) - f_X(p_X) \right] |\mathscr{M}|^2 \quad \text{(C.38)}$$

with $d\pi_X = d^3\vec{p}_X/(2\pi)^3 2E_X$ and where we used the tree-level approximation $|\mathscr{M}(X \to Y+Z)|^2 = |\mathscr{M}(Y+Z \to X)|^2 \equiv |\mathscr{M}|^2$, which is enough and dominant for this Boltzmann equation.[3] The Liouville term reads, using the Friedmann-Lemaître-Roberston-Walker (FLRW) metric,

$$g_X \int \frac{d^3\vec{p}}{(2\pi)^3} \mathrm{L}[f_X] = \frac{dn_X}{dt} + 3Hn_X \,, \quad \text{(C.39)}$$

where H is the Hubble rate. Equalizing the Liouville and the collision terms, changing variables $n_X \to Y_X = n_X/s$ and $t \to z = m_X/T$ (with $t = 1/2H(z)$), and using the thermal average $\langle m_X/E \rangle = K_1(z)/K_2(z)$ where $K_1(z)$ and $K_2(z)$ are the Bessel functions, one gets the equation

$$\frac{dY_X}{dz} = -\frac{\Gamma_X}{zH(z)} \frac{K_1(z)}{K_2(z)} \left(Y_X - Y_X^{\mathrm{Eq}} \right) , \quad \text{(C.40)}$$

with Γ_X denoting the total decay rate of X. This equation can also be put in the simple form

$$\dot{Y}_X = -\left(\frac{Y_X}{Y_X^{\mathrm{Eq}}} - 1 \right) \gamma_D \,, \quad \text{(C.41)}$$

where $\dot{Y}_X \equiv s(z)H(z)z dY_X/dz$ and where

$$\gamma_D \equiv n_X^{\mathrm{Eq}} \frac{K_1(z)}{K_2(z)} \Gamma_X \quad \text{(C.42)}$$

is the thermally averaged decay/inverse decay rate. We now develop a generic "method", which is actually more a question of notations, that is very useful in deriving the Boltzmann equations an a simple and straightforward way.

C.4.2 Method

The method is the one introduced in Ref. [225]. The difference between a process and its time reversed, weighted by the densities of the initial state, is defined by

$$[A \leftrightarrow B] \equiv \left(\prod_{i=1}^{n} y_{a_i} \right) \gamma_B^A - \left(\prod_{j=1}^{m} y_{b_j} \right) \gamma_A^B \,, \quad \text{(C.43)}$$

where the state A contains the particles $a_1, a_2, \ldots, a_n$ and the state B contains the particles $b_1, b_2, \ldots, b_m$. In the above equation, $\gamma_B^A \equiv \gamma(A \to B)$ is the thermally averaged rate of the process

[3] This approximation doesn't always hold, since one needs to go at the loop level (the CP-asymmetries) for example when computing the Boltzmann equation for the lepton asymmetries. However, it is enough to consider only the tree-level amplitude for the illustration purpose of this section.

$A \to B$, summed over initial and final spin and gauge degrees of freedom, and y_a is defined as

$$y_a \equiv \frac{Y_a}{Y_a^{\rm Eq}} \quad \text{where as usual,} \quad Y_a \equiv \frac{Y_a}{s} \,. \tag{C.44}$$

The difference between the rates of CP-conjugate processes is written $\Delta\gamma_B^A \equiv \gamma_B^A - \gamma_{\bar{B}}^{\bar{A}}$. Let's note that by CPT invariance, one has $\gamma_B^A = \gamma_{\bar{A}}^{\bar{B}}$. Using these notations, the Boltzmann equation for the species X is simply given by

$$\dot{Y}_X = \sum [A \leftrightarrow B] \tag{C.45}$$

where we sum over all the processes responsible for a change in the number of X, which appears at least one times in the final state $B \ni b_1, \ldots, X, \ldots, b_m$.

C.4.3 Example : the type-1 leptogenesis

In the unflavored type-1 leptogenesis scenario, we need the Boltzmann equation governing the evolution of the lepton asymmetry ΔY_L where $Y_L = Y_\ell$. To this end, one needs to sum over the various processes changing the number of L. We must consider all the processes that are at the same order of the CP-asymmetry, that is processes that are proportional to Y_N^4. At this order, considering only the dominant contribution for a sake of illustration, one has

$$\dot{Y}_L = \left(\dot{Y}_L\right)_{\rm sphal} + \left[N_1 \leftrightarrow L\phi\right] + \left[\bar{L}\phi^* \leftrightarrow L\phi\right]' + \left[\phi^*\phi^* \leftrightarrow LL\right] \tag{C.46}$$

$$\dot{Y}_{\bar{L}} = \left(\dot{Y}_{\bar{L}}\right)_{\rm sphal} + \left[N_1 \leftrightarrow \bar{L}\phi^*\right] + \left[L\phi \leftrightarrow \bar{L}\phi^*\right]' + \left[\phi\phi \leftrightarrow \bar{L}\bar{L}\right] \,. \tag{C.47}$$

In the above equation, $(\dot{Y}_L)_{\rm sphal}$ denotes the contribution from the sphalerons in the evolution of L. We will see how to get rid of this term. Also, the primed notation $\left[\bar{L}\phi^* \leftrightarrow L\phi\right]'$ refers to a process with the resonant intermediate state subtracted. This is needed in order to avoid double counting, since the on-shell process $\bar{L}\phi^* \leftrightarrow L\phi$ can be obtained by $\bar{L}\phi^* \to N_1$ followed by $N_1 \to L\phi$. In other terms, the associated rate is given by $\gamma'^A_{BC} = \gamma^A_{BC} - \gamma^A_{N_1} B^{N_1}_{BC}$ with $B^{N_1}_{BC}$ the branching ratio of the decay $N_1 \to B + C$. Using the following practical identities :

$$ab - cd = \frac{1}{2}\left[(a-c)(b+d) + (a+c)(b-d)\right] \,, \tag{C.48}$$

$$ab + cd = \frac{1}{2}\left[(a-c)(b-d) + (a+c)(b+d)\right] \,, \tag{C.49}$$

it is straightforward to show that subtracting Eq. (C.46) and (C.47), one gets, at leading order in Y_N^2 for the washouts term,

$$\Delta\dot{Y}_L \simeq \left(\Delta\dot{Y}_L\right)_{\rm sphal} + \left(y_{N_1} - 1\right)\Delta\gamma^{N_1}_{L\phi} - \left(\Delta y_L + \Delta y_\phi\right)\gamma^{N_1}_{L\phi} \,. \tag{C.50}$$

One can get rid of the first term of this equation by considering, instead of the evolution of L, the evolution of $B - L$. Indeed, the sphalerons conserve $B - L$, i.e. $(\Delta\dot{Y}_L)_{\rm sphal} = (\Delta\dot{Y}_B)_{\rm sphal}$, and the evolution of B is only driven by the sphalerons $\Delta\dot{Y}_B = (\Delta\dot{Y}_B)_{\rm sphal}$, so that the evolution of the difference ΔY_{B-L} doesn't actually depend on the sphaleron at all. In the second term, from the CP-asymmetry definition one has $\Delta\gamma^{N_1}_{L\phi} = \epsilon_{N_1}\gamma_D$, where $\gamma_D \simeq 2\gamma^{N_1}_{L\phi}$ is the thermally average rate of

the total decay of N_1. One has therefore finally, at leading order,

$$\Delta\dot{Y}_{B-L} \simeq -\left(y_{N_1}-1\right)\epsilon_{N_1}\gamma_D + \frac{1}{2}\left(\Delta y_L + \Delta y_\phi\right)\gamma_D \,. \tag{C.51}$$

We cannot solve this equation alone, since there are still unknown quantities. The quantities ΔY_L and ΔY_ϕ are in fact related to Y_{B-L} through chemical equilibrium condition, see section C.5 below. One has, in the unflavored case and neglecting the spectator processes, simply that $\Delta Y_L = -\Delta Y_{B-L}$ and $\Delta Y_\phi = 0$. However, in all the cases the evolution of Y_{N_1} has to be determined. This quantity is a priori not related to the $B-L$ asymmetry and one needs in fact to write down its Boltzmann equation. Using the same approach, it is simply given by

$$\dot{Y}_{N_1} = \left[L\phi \leftrightarrow N_1\right] + \left[\bar{L}\phi^* \leftrightarrow N_1\right], \tag{C.52}$$

which gives, at leading order,

$$\dot{Y}_{N_1} = -\left(y_{N_1}-1\right)\gamma_D \,. \tag{C.53}$$

The two Boltzmann equations in Eqs. (C.51) and (C.53) are the one given in Eqs. (3.36) and (3.35) respectively.

C.5 Chemical equilibrium conditions

C.5.1 Generalities and usual chemical equilibrium conditions

At very high temperatures ($T \gtrsim 10^{15}$ GeV), all SM reactions are frozen in the sense they are much slower than the Hubble rate. As the temperature decreases, certain reactions (those driven by the largest couplings first) attain thermal equilibrium which demands kinetic as well as chemical equilibrium of the corresponding reactions, the latter in turn enforce constraints among the different chemical potentials of the intervening particles.

Indeed, for a relativistic species X, the particle number density-to-entropy ratio is, at leading order in μ_X/T, related with the chemical potential according to Eqs. (C.6) and (C.12). Therefore, the difference $\Delta Y_X = Y_X - Y_{\bar{X}}$ is in fact directly proportional to the chemical potential through :

$$\Delta Y_X = g_X \frac{T^2}{6s}\mu_X \begin{cases} 1\,, & \text{for fermions} \\ 2\,, & \text{for bosons}\,, \end{cases} \tag{C.54}$$

with g_X the number of degrees of freedom of X. In our notation, a singlet fermion has $g_X = 1$, and doublet Dirac fermions has $g_X = 2$, a triplet Dirac fermions has $g_X = 3$, etc. Let's note that there cannot be an asymmetry in the right-handed neutrinos since these are Majorana particles. In the same way, below the EWSB, the light neutrinos are also Majorana particles and they cannot develop an asymmetry. Concerning the boson, only the scalar doublet and the W's can develop an asymmetry, and they have $g_\phi = 2$, $g_W = 3$.

The chemical potentials are important quantities because if a reaction occurs much faster

than the Hubble rate (and is then in thermal equilibrium), $A \leftrightarrow B$ where $A = a_1 + a_2 + \ldots$ and $B = b_1 + b_2 + \ldots$, then the various chemical potentials are related through the chemical equilibrium condition $\sum_i \mu_{a_i} = \sum_i \mu_{b_i}$, where μ_{a_i} and μ_{b_i} are the chemical potentials of species a_i and b_i. From Eq. (C.54), the chemical equilibrium constraints thus relate the different particle asymmetries of those species participating in fast reactions.

In principle, there is a chemical potential (an asymmetry) for each particle in the thermal bath, which implies that *a priori* there are as many chemical potentials as particles in the plasma: 61 (36 quarks+9 leptons+4 scalars+2 W's+1 Z+1 γ+8 gluons). This number, however, is largely reduced due to the constraints imposed by the set of chemical equilibrium conditions and the conservation laws of the early Universe effective Lagrangian. Depending on the temperature regime where the $B-L$ asymmetry is generated, the possible constraints on the chemical potentials are :

1. For $T > T_{EW}$, chemical potentials for all the gauge bosons vanish $\mu_{W^i} = \mu_{\mathscr{B}} = \mu_g = 0$, and so the components of the electroweak and color multiplets have the same chemical potentials [215]. This motivates the above definition of the number of degrees of freedom that we use all along this thesis. This already reduces to 17 the number of independent asymmetries.

   For $T < T_{EW}$, the chemical potential of the charged W's is not zero and the W's can develop an asymmetry. As a consequence, the components of a same multiplets have in general different chemical potential.

2. For $T > T_{EW}$, cosmological hypercharge neutrality must be obeyed. This leads to a relation between the asymmetries and therefore the chemical potentials. For example, in the SM and so in the type-1 leptogenesis (N_1 has zero hypercharge) one has

$$\mathscr{Y} = \sum_\alpha \left(\mu_{Q_\alpha} + 2\mu_{u_\alpha} - \mu_{d_\alpha} - \mu_{\ell_\alpha} - \mu_{e_\alpha}\right) + 2\mu_\phi = 0 \,. \tag{C.55}$$

   For $T < T_{EW}$, the hypercharge is broken and it is instead the cosmological electric charge neutrality that has to be imposed. In the SM and in the type-1 leptogenesis, this means

$$\mathscr{Q} = \sum_\alpha \left[2\left(\mu_{u_{L_\alpha}} + \mu_{u_{R_\alpha}}\right) - 2\left(\mu_{d_{L_\alpha}} + \mu_{d_{R_\alpha}}\right) - 2\left(\mu_{e_{L_\alpha}} + \mu_{e_{R_\alpha}}\right)\right] + 2\mu_{\phi^+} + 4\mu_{W^+} = 0 \,. \tag{C.56}$$

   This expression can be simplified using the result in item 1 and 4.

3. Non-perturbative QCD instanton and electroweak sphaleron reactions – if in thermal equilibrium – enforce the following constraints :

$$\sum_\alpha \left(2\mu_{Q_\alpha} - \mu_{u_\alpha} - \mu_{d_\alpha}\right) = 0 \,, \qquad \sum_\alpha \left(3\mu_{Q_\alpha} + \mu_{\ell_\alpha}\right) = 0 \,. \tag{C.57}$$

   The temperature range at which the QCD instanton reactions attain equilibrium has been estimated to be $T^{QCD}_{\text{sphal}} \in [132, 10^{13}]$ GeV [255, 214] while for electroweak sphaleron processes, being controlled by α_{EW} rather than α_S, it has been found to be about a factor 20 smaller for the upper value [214] so that $T^{EW}_{\text{sphal}} \in [132, 10^{12}]$ GeV, see section C.2.

4. Finally, for $T > T_{EW}$, Yukawa reactions when being in thermal equilibrium lead to the chemical equilibrium constraints:

$$\text{Up-type quarks:} \qquad \mu_{u_\alpha} - \mu_{Q_\alpha} - \mu_\phi = 0\,, \tag{C.58}$$

$$\text{Down-type quarks:} \qquad \mu_{d_\alpha} - \mu_{Q_\alpha} + \mu_\phi = 0\,, \tag{C.59}$$

$$\text{Charged leptons:} \qquad \mu_{e_\alpha} - \mu_{\ell_\alpha} + \mu_\phi = 0\,. \tag{C.60}$$

Top Yukawa-induced reactions are faster than the Hubble rate for $T \lesssim 10^{15}$ GeV. Bottom, charm and tau Yukawa-induced processes are faster than the Hubble rate for $T \lesssim 10^{12}$ GeV, strange and muon for $T \lesssim 10^{9}$ GeV, and the first generation Yukawa-induced processes for $T \lesssim 10^{5}$ GeV [230, 233, 231].

Let's note that below T_{EW}, the scalar boson h acquires a vev and so the neutral component of the scalar doublet cannot develop any asymmetry ($\mu_{\phi^0} = 0$). Using also item 1, one has therefore the relations $\mu_{u_{L_\alpha}} = \mu_{u_{R_\alpha}}$, $\mu_{d_{L_\alpha}} = \mu_{d_{R_\alpha}} = \mu_{u_{L_\alpha}} + \mu_{W^+}$ and $\mu_{e_{L_\alpha}} = \mu_{e_{R_\alpha}} = \mu_{\nu_{L_\alpha}} + \mu_{W^+}$.

The exact number of non-vanishing chemical potentials as well as the number of chemical equilibrium conditions are fixed only when a specific temperature window is settled. Once this is done, the resulting system of equations is solved in terms of a single set of variables. This set of variables is $\mu_{B/3-L_\alpha}$ in the SM and the type-1 leptogenesis. The solution thus provides the relations between the asymmetries of all the particles in the heat bath with the independent asymmetries $\Delta Y_{B/3-L_\alpha}$. In particular, for $T > T_{EW}$, one has the following relations, relating ΔY_{ℓ_α} and ΔY_ϕ to $\Delta Y_{B/3-L_\alpha}$:

$$\Delta Y_{\ell_\alpha} = -\sum_\beta C^\ell_{\alpha\beta}\, \Delta Y_{B/3-L_\beta} \qquad \text{and} \qquad \Delta Y_\phi = -\sum_\alpha C^\phi_\alpha\, \Delta Y_{B/3-L_\alpha}\,, \tag{C.61}$$

where C^ℓ and C^ϕ are matrices of numbers. These matrices have different expressions following the temperature regime at which leptogenesis takes place. The expression of these matrices, derived for example in Ref. [233], is computed in next section.

C.5.2 Temperature regimes and chemical equilibrium conditions for type-1 Seesaw leptogenesis

In what follows we briefly discuss the symmetries of the corresponding early Universe effective Lagrangian and the relevant chemical equilibrium conditions in items 1-4 above, which enable us to calculate the matrices relating the lepton and scalar doublet asymmetries with $Y_{B/3-L_\alpha}$, as given by Eqs. (C.61). We start by discussing the high temperature regime $T > 10^{15}$ GeV, proceeding subsequently to the temperature ranges $T \subset [10^{12}, 10^{15}]$ GeV, $[10^9, 10^{12}]$ GeV, $[10^5, 10^9]$ GeV and $T < 10^5$ GeV. Theses ranges are based on the assumption that all SM interactions that approximately enter in thermal equilibrium at a similar temperature do it effectively at the same temperature. As discussed in section 3.5, this may not be the case since the charged Yukawas, even if faster than the Hubble rate, must also be faster than the inverse decay rate in order that the coherent lepton state looses its coherence. However, we will here consider only the full-flavor regimes corresponding to the cases 1., 2.(b), 3.(c) and 4.(d), plus a "0." one, in which only the top Yukawa-related reactions are in thermal equilibrium.

We stress that some of these temperature "windows" differ from those used in Ref. [233], in particular in what regards the charged lepton Yukawa reaction equilibrium temperatures. They however match with those pointed out in Ref. [230]. [4]

0. *None SM reactions in thermal equilibrium, $T \gtrsim 10^{15}$ GeV*
   In this regime all SM reactions are slower than the Hubble rate. A proper treatment of the problem therefore should be done with the unflavored kinetic equations in Eqs. (3.35) and (3.36). With all SM reactions frozen, only the lepton ℓ_1 and scalar doublets ϕ develop chemical potentials μ_{ℓ_1} and μ_ϕ. These chemical potentials are subject only to the hypercharge neutrality constraint in 2. The associated asymmetries can related to the $B-L$ through the following C^ℓ and C^ϕ values :

   $$C^\ell = 1\,, \qquad C^\phi = 1\,. \tag{C.62}$$

   Taking into account the spectator, from Eq. (C.51), one gets Eq. (3.36) up to a factor 2 in front of ΔY_{B-L}, so that the washout is accordingly stronger. Note that above 10^{15} GeV there is relatively little time for the reheating to occur before the temperature goes below the right-handed neutrino mass (assuming the reheating occurs below the Planck scale).

1. *Only top Yukawa-related reactions in thermal equilibrium, $T \subset [10^{12}, 10^{15}]$ GeV*
   Within this temperature regime, the top Yukawa-related interactions becomes faster than the Hubble rate. Accordingly, we are still in the unflavored regime and the Boltzmann equation that must be used is still the one given in Eq. (C.51).

   The global symmetries of the effective Lagrangian are those of the SM kinetic terms broken only by the top Yukawa coupling, and so the group of global transformations is :

   $$G_{\rm eff} = U(1)_Y \times U(1)_B \times U(1)_e \times U(1)_{\rm PQ} \times SU(3)_d \times SU(3)_e \times SU(2)_Q \times SU(2)_u\,. \tag{C.63}$$

   The $SU(3)$ factors combined with the exact $U(1)_B$, $U(1)_{\rm PQ}$ and the absence of Yukawa couplings for all SM particles, except the top quark, imply : $\mu_{d_\alpha} = \mu_{e_\alpha} = \mu_{u_{1,2}} = \mu_{Q_{1,2}} = \mu_B = 0$ (B being associated to the baryon asymmetry). Taking this constraints into account and the relevant chemical equilibrium conditions in Eqs. (C.55) and (C.58), the latter written only for the top quark, we obtain

   $$C^\ell = 1\,, \qquad C^\phi = 2/3\,. \tag{C.64}$$

2. *QCD instantons, electroweak sphalerons, bottom and charm and tau Yukawa-related reactions in thermal equilibrium, $T \subset [10^9, 10^{12}]$ GeV*
   In this temperature window the lepton doublets lose their quantum coherence due to the tau Yukawa-related interactions being in thermal equilibrium [233, 231]. On the other hand,

[4] Let's note that there is an overall factor 2 difference between the matrices we show here and the matrices given in some papers. This just comes from different notations. Indeed, as an example, ℓ_α accounts in this thesis for the lepton doublet of flavor α with $g = 2$, while for example in Ref. [233], ℓ_α accounts for one of the two components of the lepton doublet with then $g = 1$. This can be quite confusing since the notation can change from one paper to another even if written by the same author (see for example Refs. [233] and [329]). However, the different approaches are consistent with each other since the factor 2 is compensated in the Boltzmann equations, which are in this thesis written in terms of multiplets and not in terms of multiplet's components.

since electroweak sphaleron reactions are in thermal equilibrium, baryon number is no longer conserved, while they conserve the individual $B/3-L_\alpha$ charges. An appropriate study of the evolution of the $B-L$ asymmetry should then be done by tracking the evolution of the flavored charge asymmetries $B/3-L_\alpha$ ($\alpha=a,\tau$, the state a being a coherent superposition of e and μ lepton flavors) with the network of Eqs. (3.62)-(3.63).

The QCD instantons reactions break the global $U(1)_{\rm PQ}$, the bottom and tau Yukawa couplings break the right-handed down-type quark and charged lepton $SU(3)$ flavor multiplet and in addition the tau Yukawa coupling also breaks the global $U(1)_e$. The Lagrangian is as expected "less symmetric", with the group of global transformations given by

$$G_{\rm eff}=U(1)_Y\times SU(2)_d\times SU(2)_e\times U(1)_Q\times U(1)_u\,. \tag{C.65}$$

These global symmetries imply : $\mu_{u_1}=\mu_{Q_1}=0$ and $\mu_{d_\alpha}=\mu_{e_\alpha}=0$ with $\alpha=1,2$, while the complete set of chemical equilibrium conditions correspond to Eqs. (C.55) for hypercharge neutrality (written so to include the now non-vanishing bottom, charm and tau chemical potentials), (C.57) for QCD instantons, (C.57) for electroweak sphalerons, and (C.58), (C.59) and (C.60) written for top, bottom, charm and tau Yukawa interactions. Due to sphaleron reactions, lepton flavor is no longer conserved so that chemical potentials develop in three independent lepton doublets : ℓ_τ, ℓ_a and ℓ_b. Conservation of the $B/3-L_\alpha$ charges however provide the constraint $\mu_{B/3-L_b}=0$, which when coupled with the corresponding chemical equilibrium conditions yields the following flavored $C^{\ell,\phi}$ matrices :

$$C^\ell=\begin{pmatrix}307/359 & -36/359\\ -21/359 & 234/359\end{pmatrix}\,,\quad C^\phi=\begin{pmatrix}82/359 & 112/359\end{pmatrix}\,. \tag{C.66}$$

3. *Strange and muon Yukawa interactions in thermal equilibrium, $T\subset[10^5,10^9]$ GeV :*
As pointed out in Ref. [233, 231], in this temperature regime the lepton doublets completely lose their quantum coherence, implying that chemical potentials develop in each orthogonal lepton flavor doublet : ℓ_τ, ℓ_μ and ℓ_e. Since the second generation Yukawa reactions are faster than the Hubble rate, the symmetries of the effective Lagrangian are reduced to $U(1)$ factors:

$$G_{\rm eff}=U(1)_Y\times U(1)_d\times U(1)_e\times U(1)_Q\times U(1)_u\,. \tag{C.67}$$

These constraints imply $\mu_d=\mu_e=\mu_{Q_1}=\mu_u=0$, and when combined with the corresponding chemical equilibrium conditions (the ones from previous item complemented with Eqs. (C.58), (C.59) and (C.60) for the charm, strange and muon Yukawa interactions) yield :

$$C^\ell=\begin{pmatrix}151/179 & -20/179 & -20/179\\ -25/358 & 344/537 & -14/537\\ -25/358 & -14/537 & 344/537\end{pmatrix}\,, \tag{C.68}$$

$$C^\phi=\begin{pmatrix}37/179 & 52/179 & 52/179\end{pmatrix}\,. \tag{C.69}$$

4. *All SM reactions in thermal equilibrium, $T\lesssim 10^5$ GeV :*
In this case and until electroweak symmetry breaking, the only surviving symmetry is

$U(1)_Y$. Due to all SM reactions being fast, all SM particles develop non-vanishing chemical potentials, with the chemical equilibrium conditions given by the full list in items 1-4. The flavored $C^{\ell,\phi}$ matrices in this regime therefore read :

$$C^{\ell} = \begin{pmatrix} 442/711 & -32/711 & -32/711 \\ -32/711 & 442/711 & -32/711 \\ -32/711 & -32/711 & 442/711 \end{pmatrix}, \tag{C.70}$$

$$C^{\phi} = \begin{pmatrix} 16/79 & 16/79 & 16/79 \end{pmatrix}. \tag{C.71}$$

C.5.3 Relation between the baryon, lepton and $B-L$ asymmetries

In the previous section C.5.2, we gave the relations between the lepton flavor asymmetries ΔY_{ℓ_α} and $\Delta Y_{B/3-L_\alpha}$, as well as the relations between the scalar asymmetry ΔY_ϕ and $\Delta Y_{B/3-L_\alpha}$, for different temperature regimes and for $T > T_{EW}$.

Using the same chemical equilibrium condition, one can also easily derive the relation between the baryon asymmetry ΔY_B and the $B-L$ asymmetry ΔY_{B-L}, which is needed in order to evaluate how much baryon are left today. But it is not necessary to compute this relation for all the temperature regimes considered above. Indeed, once a $B-L$ asymmetry is produced at the end of leptogenesis, it stays intact since it is preserve by sphalerons. [5] Therefore the relation between the asymmetry in B and in $B-L$ changes as the temperature decreases, passing through all the temperature regimes. Just before the EWSB at $T \approx 165$ GeV, we are in the temperature regime of item 4 in page 248 above, and we can easily show that the relation reads

$$\Delta Y_B = \frac{28}{79}\,\Delta Y_{B-L}\,. \tag{C.72}$$

However, when the temperature decreases and crosses the EWPT, the sphalerons are still active until $T \approx 132$ GeV, see Fig. 3.5 in page 86, so that just before the sphalerons decouple and leave the baryon asymmetry intact until today, one has instead

$$\Delta Y_B^{today} = \frac{12}{37}\,\Delta Y_{B-L}\,. \tag{C.73}$$

[5] We suppose of course that no other $B-L$ violation mechanism takes place after the leptogenesis era.

D Type-2 Seesaw leptogenesis

D.1 Tree-level decay rates

We here compute the tree-level decay rates of the Δ^{0*}, Δ^- and Δ^{--} components of the triplets into leptons and scalars. We then explicitly check that the total decay widths of each component are the same for $T > T_{EW}$, respecting gauge invariance.

D.1.1 Leptonic channel

$\underline{\Delta^- \to e_\alpha \nu_\beta}$

We have, neglecting the lepton masses and using $\gamma_0 C u_s^*(p) = v_s(p)$:

$$i\mathscr{M}^0 = i\sqrt{2} Y_\Delta^{\alpha\beta *} \overline{u}_{\nu_\beta} P_R \gamma_0 C u_{e_\alpha}^* = i\sqrt{2} Y_\Delta^{\beta\alpha *} \overline{u}_{\nu_\beta} P_R v_{e_\alpha} , \tag{D.1}$$

so that squaring and summing over the final spins one gets

$$\sum_{spin} \left| i\mathscr{M}^0 \right|^2 = 2 \left| Y_\Delta^{\alpha\beta} \right|^2 \mathrm{Tr}[\not{p} \not{p}' P_L] = 2 \left| Y_\Delta^{\alpha\beta} \right|^2 m_\Delta^2 . \tag{D.2}$$

The partial decay width of the process $\Delta^- \to e_\alpha \nu_\beta$ therefore reads

$$\Gamma\left(\Delta^- \to e_\alpha \nu_\beta\right) = \frac{1}{16\pi m_\Delta} \left| i\mathscr{M}^0 \right|^2 = \frac{m_\Delta}{8\pi} \left| Y_\Delta^{\alpha\beta} \right|^2 , \tag{D.3}$$

and the total decay width to leptons reads

$$\Gamma\left(\Delta^- \to e\nu\right) = \sum_{\alpha,\beta} \Gamma\left(\Delta^- \to e_\alpha \nu_\beta\right) = \frac{m_\Delta}{8\pi} Tr[Y Y^\dagger] . \tag{D.4}$$

$\underline{\Delta^{0*} \to \nu_\alpha \nu_\beta}$

For Δ^{0*}, we just have to pay attention to doublecounting. Indeed, here partial decay width of the process $\Delta^- \to \nu_\alpha \nu_\beta$ must be separated according to whether or not there are two identical particles in the final state. One has

$$\Gamma\left(\Delta^{0*} \to \nu_\alpha \nu_\alpha\right) = \frac{m_\Delta}{8\pi}\left|Y_\Delta^{\alpha\alpha}\right|^2 , \tag{D.5}$$

$$\Gamma\left(\Delta^{0*} \to \nu_\alpha \nu_{\beta\neq\alpha}\right) = \frac{m_\Delta}{4\pi}\left|Y_\Delta^{\alpha\beta}\right|^2 . \tag{D.6}$$

The total decay width therefore reads

$$\Gamma(\Delta^{0*} \to \nu\nu) = \sum_\alpha \Gamma\left(\Delta^{0*} \to \nu_\alpha \nu_\alpha\right) + \sum_{\alpha,\beta>\alpha} \Gamma\left(\Delta^{0*} \to \nu_\alpha \nu_\beta\right) = \frac{m_\Delta}{8\pi}\mathrm{Tr}\left[Y\,Y^\dagger\right] . \tag{D.7}$$

In D.5 we have used the fact that we have 2 identical outgoing particles so we have a factor 1/2 more. In D.7 the sum is such to avoid double counting since $\Gamma(\Delta^{0*} \to \nu_\alpha \nu_\beta) = \Gamma(\Delta^{0*} \to \nu_\alpha \nu_\beta)$

$\underline{\Delta^{--} \to e_\alpha e_\beta}$

Proceeding in the same way as for Δ^{0*}, we get that the decay width are exactly the same and

$$\Gamma(\Delta^{--} \to ee) = \sum_\alpha \Gamma(\Delta^{--} \to e_\alpha e_\alpha) + \sum_{\alpha,\beta>\alpha} \Gamma(\Delta^{--} \to e_\alpha e_\beta) = \frac{m_\Delta}{8\pi}\mathrm{Tr}\left[Y\,Y^\dagger\right] . \tag{D.8}$$

Summary

We see that we get exactly the same decay rate to leptons for each triplet component. It reads :

$$\Gamma\left(\Delta_k^Q \to \bar{\ell}\bar{\ell}\right) \equiv \frac{m_{\Delta_k}}{8\pi}\mathrm{Tr}\left[Y_{\Delta_k} Y_{\Delta_k}^\dagger\right] . \tag{D.9}$$

The partial leptonic decay width can be recast in a single equation which is :

$$\Gamma\left(\Delta_k^Q \to \bar{\ell}_\alpha \bar{\ell}_\beta\right) = \frac{m_{\Delta_k}}{8\pi}\left|Y_{\Delta_k}^{\alpha\beta}\right|^2 \left[1 + |Q-1|\left(1-\delta_{\alpha\beta}\right)\right] , \tag{D.10}$$

D.1.2 Scalar channel

Here there is no subtlety. We quickly find that the total scalar decay width of each triplet component is given by

$$\Gamma\left(\Delta_k^Q \to \phi\phi\right) = \frac{\left|\mu_{\Delta_k}\right|^2}{8\pi m_{\Delta_k}} . \tag{D.11}$$

D.1.3 Total decay width

The total decay rate of a component of the triplet is simply expressed as :

$$\Gamma_{\Delta_k} \equiv (B_\phi^k + B_\ell^k)\Gamma_{\Delta_k} = \frac{1}{8\pi m_{\Delta_k}} \left(m_{\Delta_k}^2 \mathrm{Tr}\left[Y_{\Delta_k} Y_{\Delta_k}^\dagger \right] + \left| \mu_{\Delta_k} \right|^2 \right) \tag{D.12}$$

$$= \frac{1}{8\pi} \frac{m_{\Delta_k}^2 \tilde{m}_{\Delta_k}}{v^2} \frac{B_\phi^k + B_\ell^k}{\sqrt{B_\phi^k B_\ell^k}} , \tag{D.13}$$

where

$$\tilde{m}_{\Delta_k}^2 = \mathrm{Tr}\left[m_\nu^{k\dagger} m_\nu^k \right] = \mathrm{Tr}\left[Y_{\Delta_k}^\dagger Y_{\Delta_k} \right] \left| \mu_{\Delta_k} \right|^2 \frac{\mathrm{v}^4}{m_{\Delta_k}^4} . \tag{D.14}$$

Let's note $\tilde{m}_\Delta^2 = \sum_i m_i^2$ if there is only one scalar triplet.

D.2 CP-asymmetries

The CP-asymmetry in the decay of the scalar triplet Δ_k reads for each components :

$$\epsilon_{\Delta_k^0}^{\ell_\alpha} = 2 \frac{\Gamma(\Delta_k^{0*} \to \nu_\alpha \nu_\alpha) - \Gamma(\Delta_k^0 \to \overline{\nu}_\alpha \overline{\nu}_\alpha)}{\Gamma_{\Delta_k^{0*}} + \Gamma_{\Delta_k^0}} + \sum_{\beta \neq \alpha} \frac{\Gamma(\Delta_k^{0*} \to \nu_\alpha \nu_\beta) - \Gamma(\Delta_k^0 \to \overline{\nu}_\alpha \overline{\nu}_\beta)}{\Gamma_{\Delta_k^{0*}} + \Gamma_{\Delta_k^0}} , \tag{D.15}$$

$$\epsilon_{\Delta_k^+}^{\ell_\alpha} = 2 \frac{\Gamma(\Delta_k^- \to \nu_\alpha e_\alpha) - \Gamma(\Delta_k^+ \to \overline{\nu}_\alpha \overline{e}_\alpha)}{\Gamma_{\Delta_k^-} + \Gamma_{\Delta_k^+}} + 2 \sum_{\beta \neq \alpha} \frac{\Gamma(\Delta_k^- \to \nu_\alpha e_\beta) - \Gamma(\Delta_k^+ \to \overline{\nu}_\alpha \overline{e}_\beta)}{\Gamma_{\Delta_k^-} + \Gamma_{\Delta_k^+}} , \tag{D.16}$$

$$\epsilon_{\Delta_k^{++}}^{\ell_\alpha} = 2 \frac{\Gamma(\Delta_k^{--} \to e_\alpha e_\alpha) - \Gamma(\Delta_k^{++} \to \overline{e}_\alpha \overline{e}_\alpha)}{\Gamma_{\Delta_k^{--}} + \Gamma_{\Delta_k^{++}}} + \sum_{\beta \neq \alpha} \frac{\Gamma(\Delta_k^{--} \to e_\alpha e_\beta) - \Gamma(\Delta_k^{++} \to \overline{e}_\alpha \overline{e}_\beta)}{\Gamma_{\Delta_k^{--}} + \Gamma_{\Delta_k^{++}}} , \tag{D.17}$$

where one has $\Gamma_{\Delta_k^{0*}} + \Gamma_{\Delta_k^0} = \Gamma_{\Delta_k^-} + \Gamma_{\Delta_k^+} = \Gamma_{\Delta_k^{--}} + \Gamma_{\Delta_k^{++}} = 2\Gamma_{\Delta_k}$. The factor 2 in front of the first terms in the r.h.s. of the above equations comes from the fact that the associated scalar triplet decay produces 2 lepton flavors. The factor 2 in front of the second term in the r.h.s. of the second equation comes from the fact that one has $\Delta_k^- \to \nu_\alpha e_\beta$ but also $\Delta_k^- \to \nu_\beta e_\alpha$ contributing to the CP-asymmetry. The one-loop corrections to the tree-level decay depend on the details of the corresponding model.

D.2.1 Pure scalar triplet case

The one-loop Feynman diagrams responsible for a CP-asymmetry in the leptonic decay of Δ_k are depicted in Fig. 4.12. We here compute briefly the CP-asymmetry by considering, for simplicity and in order to avoid double-counting trick, the decay $\Delta_k^- \to e_\alpha \nu_\beta$. The asymmetry produced by the other component has to be the same, by gauge invariance. The tree-level amplitude $i\mathscr{M}^0$ is given in Eq. (D.1). On one hand, the one-loop amplitude of the self-energy lepton conserving

diagram with two leptons in the loop is given by

$$
\begin{aligned}
i\mathscr{M}_\ell^1 =& \sum_{\gamma,\delta} i\sqrt{2}Y_{\Delta_j}^{\alpha\beta *}(\overline{u}_{\nu_\beta}\, P_R\, v_{e_\alpha})\frac{i}{q^2-m_{\Delta_j}^2+im_{\Delta_k}\Gamma_{\Delta_j}}(-1)\\
&\int \frac{d^4k}{(2\pi)^4}\,(i\sqrt{2}Y_{\Delta_j}^{\gamma\delta})\,(i\sqrt{2}Y_{\Delta_k}^{\gamma\beta *})\mathrm{Tr}\left[\frac{-i\not{k}}{k^2+i\epsilon}\frac{-i(\not{q}+\not{k})}{(q+k)^2+i\epsilon}P_L\right]\\
=&\frac{2\sqrt{2}}{m_{\Delta_k}^2-m_{\Delta_j}^2+im_{\Delta_k}\Gamma_{\Delta_j}}Y_{\Delta_j}^{\alpha\beta *}\,\mathrm{Tr}\left[Y_{\Delta_j}Y_{\Delta_k}^\dagger\right]\,(\overline{u}_{\nu_\beta}\,P_R\,v_{e_\alpha})\,\mathscr{I}_\ell\,,
\end{aligned}
\tag{D.18}
$$

where $\mathscr{I}_\ell$ is an integral, containing divergent and convergent parts, given by

$$
\mathscr{I}_\ell \equiv \frac{-im_{\Delta_k}^2}{\mu^{2\delta}(4\pi)^2}\,\mathscr{A} = \frac{-im_{\Delta_k}^2}{\mu^{2\delta}(4\pi)^2}\left[\Delta+\frac{7}{3}-\ln\frac{|q^2|}{\mu^2}-i\pi\theta(q^2)\right]\,,
\tag{D.19}
$$

with $\theta(q^2)$ the Heaviside function (more precisely distribution) of the transferred momentum $q^2=m_{\Delta_k}^2$. On the other hand, the one-loop amplitude of the self-energy lepton violating diagram with two scalars in the loop is given by

$$
\begin{aligned}
i\mathscr{M}_\phi^1 =& i\sqrt{2}Y_{\Delta_j}^{\alpha\beta *}(\overline{u}_{\nu_\beta}\,P_R\,v_{e_\alpha})\frac{i}{q^2-m_{\Delta_j}^2+im_{\Delta_k}\Gamma_{\Delta_j}}\\
&\int\frac{d^4k}{(2\pi)^4}\,(i\sqrt{2}\mu_{\Delta_j}^*)\,(i\sqrt{2}\mu_{\Delta_k})\frac{i}{k^2+i\epsilon}\frac{i}{(q+k)^2+i\epsilon}\\
=&\frac{-2\sqrt{2}}{m_{\Delta_k}^2-m_{\Delta_j}^2+im_{\Delta_k}\Gamma_{\Delta_j}}Y_{\Delta_j}^{\alpha\beta *}\,\mu_{\Delta_j}^*\mu_{\Delta_k}\,(\overline{u}_{\nu_\beta}\,P_R\,v_{e_\alpha})\,\mathscr{I}_\phi\,,
\end{aligned}
\tag{D.20}
$$

where $\mathscr{I}_\phi$ is an integral, containing divergent and convergent parts, given by

$$
\mathscr{I}_\phi \equiv \frac{i}{\mu^{2\delta}(4\pi)^2}\left[\Delta+2-\ln\frac{|q^2|}{\mu^2}-i\pi\theta(q^2)\right]\,.
\tag{D.21}
$$

The decay rate to leptons contains an interference term given by

$$
\begin{aligned}
&\Gamma(\Delta_k^-\to e_\alpha\nu_\beta)\ni\frac{1}{16\pi m_{\Delta_k}}\left[\sum_{spin}\left(i\mathscr{M}_\ell^1+i\mathscr{M}_\phi^1\right)\left(i\mathscr{M}^0\right)^\dagger+h.c.\right]\\
&=\frac{-1}{\mu^{2\delta}(4\pi)^3}\frac{m_{\Delta_k}}{m_{\Delta_k}^2-m_{\Delta_j}^2+im_{\Delta_k}\Gamma_{\Delta_j}}\left[Y_{\Delta_j}^{\alpha\beta *}Y_{\Delta_k}^{\alpha\beta}\left(m_{\Delta_k}^2\mathrm{Tr}\left[Y_{\Delta_j}Y_{\Delta_k}^\dagger\right]\mathscr{A}+\mu_{\Delta_j}^*\mu_{\Delta_k}\mathscr{B}\right)\right]+h.c.
\end{aligned}
\tag{D.22}
$$

For the CP conjugate rate we have :

$$
\Gamma(\Delta_k^+\to\bar{e}_\alpha\bar{\nu}_\beta)\ni\frac{-1}{\mu^{2\delta}(4\pi)^3}\frac{m_{\Delta_k}}{m_{\Delta_k}^2-m_{\Delta_j}^2+im_{\Delta_k}\Gamma_{\Delta_j}}\left[Y_{\Delta_k}^{\alpha\beta *}Y_{\Delta_j}^{\alpha\beta}\left(m_{\Delta_k}^2\mathrm{Tr}\left[Y_{\Delta_k}Y_{\Delta_j}^\dagger\right]\mathscr{A}+\mu_{\Delta_k}^*\mu_{\Delta_j}\mathscr{B}\right)+h.c.\right]
$$

So the CP-asymmetry is given by

$$\begin{aligned}\epsilon^{\ell_\alpha}_{\Delta_k^-} =& 2\sum_\beta \frac{\Gamma(\Delta_k^- \to \nu_\alpha e_\beta) - \Gamma(\Delta_k^+ \to \overline{\nu}_\alpha \overline{e}_\beta)}{2\Gamma_{\Delta_k}} \qquad \text{(D.23)}\\ =& \frac{1}{\Gamma_{\Delta_k}} \frac{-1}{\mu^{2\delta}(4\pi)^3} \frac{m_{\Delta_k}}{m^2_{\Delta_k} - m^2_{\Delta_j} + i m_{\Delta_k}\Gamma_{\Delta_j}} \\ & \left[\left(Y^\dagger_{\Delta_j} Y_{\Delta_k}\right)_{\alpha\alpha} \left(m^2_{\Delta_k} Tr[Y_{\Delta_j} Y^\dagger_{\Delta_k}] \left(\frac{\mathscr{A}}{1+i\alpha} - \frac{\mathscr{A}^*}{1-i\alpha} \right) + \mu^*_{\Delta_j}\mu_{\Delta_k} \left(\frac{\mathscr{B}}{1+i\alpha} - \frac{\mathscr{B}^*}{1-i\alpha} \right) \right) \right. \\ & \left. - \left(Y^\dagger_{\Delta_k} Y_{\Delta_j}\right)_{\alpha\alpha} \left(m^2_{\Delta_k} Tr[Y_{\Delta_k} Y^\dagger_{\Delta_j}] \left(\frac{\mathscr{A}}{1-i\alpha} - \frac{\mathscr{A}^*}{1+i\alpha} \right) + \mu^*_{\Delta_k}\mu_{\Delta_j} \left(\frac{\mathscr{B}}{1-i\alpha} - \frac{\mathscr{B}^*}{1+i\alpha} \right) \right) \right] \qquad \text{(D.24)}\end{aligned}$$

where $\alpha = m_{\Delta_k}\Gamma\Delta_j/(m^2_{\Delta_k} - m^2_{\Delta_j})$. The various quantities entering in the brackets read

$$\frac{\mathscr{A}}{1+i\alpha} - \frac{\mathscr{A}^*}{1-i\alpha} = \frac{1}{1+\alpha^2}\left[2i\,\Im m\left[\mathscr{A}\right] - 2i\alpha\,\Re e\left[\mathscr{A}\right]\right], \qquad \text{(D.25)}$$

$$\frac{\mathscr{A}}{1-i\alpha} - \frac{\mathscr{A}^*}{1+i\alpha} = \frac{1}{1+\alpha^2}\left[2i\,\Im m\left[\mathscr{A}\right] + 2i\alpha\,\Re e\left[\mathscr{A}\right]\right], \qquad \text{(D.26)}$$

$$\frac{\mathscr{B}}{1+i\alpha} - \frac{\mathscr{B}^*}{1-i\alpha} = \frac{1}{1+\alpha^2}\left[2i\,\Im m\left[\mathscr{B}\right] - 2i\alpha\,\Re e\left[\mathscr{B}\right]\right], \qquad \text{(D.27)}$$

$$\frac{\mathscr{B}}{1-i\alpha} - \frac{\mathscr{B}^*}{1+i\alpha} = \frac{1}{1+\alpha^2}\left[2i\,\Im m\left[\mathscr{B}\right] + 2i\alpha\,\Re e\left[\mathscr{B}\right]\right]. \qquad \text{(D.28)}$$

From Eqs. (D.21) and (D.21), we have that $\Im m\left[\mathscr{A}\right] = \Im m\left[\mathscr{B}\right] = -\pi$, so that the CP-asymmetry reads

$$\epsilon^{\ell_\alpha}_{\Delta_k^-} = \frac{1}{\Gamma_{\Delta_k}} \frac{1}{\mu^{2\delta}(4\pi)^2} \frac{m_{\Delta_k}(m^2_{\Delta_k} - m^2_{\Delta_j})}{(m^2_{\Delta_k} - m^2_{\Delta_j})^2 + m^2_{\Delta_k}\Gamma_{\Delta_j}} \Im m\left[\left(Y^\dagger_{\Delta_k} Y_{\Delta_j}\right)_{\alpha\alpha} \left(\mathrm{Tr}\left[Y_{\Delta_k} Y^\dagger_{\Delta_j} \right] m^2_{\Delta_k} + \mu^*_{\Delta_k}\mu_{\Delta_j} \right) \right]. \qquad \text{(D.29)}$$

Finally, dropping δ and replacing Γ_{Δ_k} by its value, one gets

$$\epsilon^{\ell_\alpha}_{\Delta_k^-} = \frac{1}{2\pi} \frac{m^2_{\Delta_k}(m^2_{\Delta_k} - m^2_{\Delta_j})}{(m^2_{\Delta_k} - m^2_{\Delta_j})^2 + m^2_{\Delta_k}\Gamma_{\Delta_j}} \frac{\Im m\left[\left(Y^\dagger_{\Delta_k} Y_{\Delta_j}\right)_{\alpha\alpha} \left(m^2_{\Delta_k} \mathrm{Tr}\left[Y_{\Delta_k} Y^\dagger_{\Delta_j} \right] + \mu^*_{\Delta_k}\mu_{\Delta_j} \right) \right]}{\left(m^2_{\Delta_k} \mathrm{Tr}\left[Y_{\Delta_k} Y^\dagger_{\Delta_k} \right] + |\mu_{\Delta_k}|^2 \right)}. \qquad \text{(D.30)}$$

If $m^2_{\Delta_j} \gg m^2_{\Delta_k}$, it simplifies to

$$\epsilon^{\ell_\alpha}_{\Delta_k^-} = -\frac{1}{2\pi} \frac{m^2_{\Delta_k}}{m^2_{\Delta_j}} \frac{\Im m\left[\left(Y^\dagger_{\Delta_k} Y_{\Delta_j}\right)_{\alpha\alpha} \left(m^2_{\Delta_k} \mathrm{Tr}\left[Y_{\Delta_k} Y^\dagger_{\Delta_j} \right] + \mu^*_{\Delta_k}\mu_{\Delta_j} \right) \right]}{\left(m^2_{\Delta_k} Tr[Y_{\Delta_k} Y^\dagger_{\Delta_k}] + |\mu_{\Delta_k}|^2 \right)}. \qquad \text{(D.31)}$$

D.2.2 Mixed type-1+2 scheme

The one-loop Feynman diagrams responsible for a CP-asymmetry in the leptonic decay of Δ_k are depicted in Fig. 4.12. We here compute briefly the CP-asymmetry by considering, for simplicity and in order to avoid double-counting trick, the decay $\Delta^- \to e_\alpha \nu_\beta$ (we consider only one scalar

triplet in this case). The asymmetry produced by the other component has to be the same, by gauge invariance. The tree-level amplitude $i\mathscr{M}^0$ is still given by Eq. (D.1). The one-loop amplitude is now given by

$$\begin{aligned} i\mathscr{M}^1 = &\sum_i \left(i\sqrt{2}\mu_\Delta\right) \overline{u}_{e_\alpha} \int \frac{d^4k}{(2\pi)^4} \left(\frac{-ig}{\sqrt{2}m_W}\right) U_{\alpha N_i} \left(m_{e_\alpha} P_L - m_{N_i} P_R\right) \frac{i(\not{k} + \not{p} + m_{N_i})}{(k+p)^2 - m_{N_i}^2 + i\epsilon} \\ &\left(\frac{-ig}{\sqrt{2}m_W}\right) \left[C_{N_i\beta}(m_{N_i} P_L + m_{\nu_\beta} P_R) + C^*_{N_i\beta}(m_{N_i} P_R + m_{\nu_\beta} P_L)\right] \frac{i}{k^2 + i\epsilon} \frac{i}{(k+q)^2 + i\epsilon} \, v_{\nu_\beta} \\ \approx &-\sum_i \frac{i\mu_\Delta g^2}{\sqrt{2}(4\pi)^2 m_W^2} U_{\alpha N_i} C^*_{N_i\beta} m_{N_i} \, \overline{u}_{e_\alpha} \, P_R \, v_{\nu_\beta} \, \mathscr{A} \end{aligned} \tag{D.32}$$

where $\mathscr{A} \equiv \left(-\frac{i\pi}{x} \ln x + \Re\right)$, with $\Re$ denoting some real function. Following the same procedure as in pure type-2 case, we find :

$$\epsilon^{\ell_\alpha}_{\Delta^-} = -\sum_{i,\beta} \frac{1}{\Gamma_{N_i}} \frac{g^2\pi}{(4\pi)^3 m_W^2} \frac{m_{N_i}^3}{m_\Delta} \Im m\left[\mu_\Delta Y_\Delta^{\alpha\beta} U_{\alpha N_i} C^*_{N_i\beta}\right] \ln\left(1 + \frac{m_\Delta^2}{m_{N_i}^2}\right) . \tag{D.33}$$

Using $U_{\alpha N_i} = \frac{\mathrm{v}}{\sqrt{2}} Y_{N_i\alpha *}/m_{N_i}$ and $C^*_{N_i\beta} \approx \frac{\mathrm{v}}{\sqrt{2}} Y_{N_i\beta *}/m_{N_i}$, we finally find :

$$\epsilon^{\ell_\alpha}_{\Delta^-} = -\sum_{i,\beta} \frac{1}{4\pi} m_{N_i} \frac{\Im m\left[\mu_\Delta Y_\Delta^{\alpha\beta} Y_{N_i\alpha *} Y_{N_i\beta *}\right]}{m_\Delta^2 \mathrm{Tr}\left[Y_\Delta Y_\Delta^\dagger\right] + \left|\mu_\Delta\right|^2} \ln\left(1 + \frac{m_\Delta^2}{m_{N_i}^2}\right) . \tag{D.34}$$

D.3 Scattering rates

Decay and scattering $1 \leftrightarrow 2$ and $2 \leftrightarrow 2$ reaction densities are given by :

$$\gamma_D = \frac{K_1(z)}{K_2(z)} n_\Sigma^{\mathrm{Eq}} \Gamma_\Delta^{\mathrm{Tot}} , \tag{D.35}$$

$$\gamma_S = \frac{m_\Delta^4}{64\pi^4} \int_{x_{\min}}^\infty dx \sqrt{x} \frac{K_1(z\sqrt{x})\, \widehat{\sigma}_S}{z} . \tag{D.36}$$

Here n_Σ^{Eq} is the $\Sigma = \Delta + \Delta^*$ number density (number density for a non-relativistic species), $x = s/m_\Delta^2$ (s being the center-of-mass energy), Γ_Δ denotes the triplet total decay width, given in Eq. (4.65), whereas $\widehat{\sigma}_S$ the reduced cross section. The integration upper and lower limits are determined by the kinematics of the corresponding scattering process : for gauge boson mediated processes $x_{\min} = 4$, for Yukawa (or scalar) induced reactions $x_{\min} = 0$.

Denoting $\delta = \Gamma_\Delta/m_\Delta$, we have found that the reduced cross sections for the s and t channel $\Delta L = 2$ processes can be written as :

$$\widehat{\sigma}^{\phi\phi}_{\ell_\alpha\ell_\beta} = 3 \cdot 64\pi \, B_\phi \, B_{\ell_{\alpha\beta}} \, \delta^2 \frac{x}{(x-1)^2 + \delta^2} , \tag{D.37}$$

$$\widehat{\sigma}^{\phi\ell_\beta}_{\phi\ell_\alpha} = 3 \cdot 64\pi \, B_\phi \, B_{\ell_{\alpha\beta}} \, \delta^2 \frac{1}{x}\left[\ln(1+x) - \frac{x}{1+x}\right] . \tag{D.38}$$

The reduced cross sections for the s and t channel flavor violating reactions, instead, can be

written according to :

$$\widehat{\sigma}^{\ell_\gamma \ell_\delta}_{\ell_\alpha \ell_\beta} = 3 \cdot 64\pi \, B_{\ell_{\gamma\delta}} \, B_{\ell_{\alpha\beta}} \, \delta^2 \, \frac{x^2}{(1-x)^2+\delta^2} \,, \tag{D.39}$$

$$\widehat{\sigma}^{\ell_\beta \ell_\gamma}_{\ell_\alpha \ell_\delta} = 3 \cdot 64\pi \, B_{\ell_{\gamma\delta}} \, B_{\ell_{\alpha\beta}} \, \delta^2 \left[\frac{x+2}{x+1} - \ln(1+x) \right] . \tag{D.40}$$

Finally, the reduced cross section for gauge induced processes reads [229, 241, 330]

$$\begin{aligned} \widehat{\sigma}_A =& 3 \cdot \frac{2}{72\pi} \left\{ (15C_1 - 3C_2)\, r + (5C_2 - 11C_1)\, r^3 \right. \\ & \left. + 3\left(r^2-1\right)\left[2C_1 + C_2\left(r^2-1\right)\right] \ln\left(\frac{1+r}{1-r}\right) \right\} + \left(\frac{50g^4 + 41g'^4}{48\pi} \right) r^{3/2} \,, \end{aligned} \tag{D.41}$$

where the following notation has been adopted: $r = \sqrt{1-4/x}$ and $C_1 = 12g^4 + 3g_Y^4 + 12g^2 g_Y^2$ and $C_2 = 6g^4 + 3g_Y^4 + 12g^2 g_Y^2$ (with g and g_Y the $SU(2)$ and $U(1)$ SM gauge coupling constants).

In Eqs. (D.37)-(D.41), the numerical pre-factor 3 accounts for the three scalar triplet components. The reaction densities with a resonant intermediate state subtracted can be calculated from Eqs. (D.35), (D.36), (D.37) and (D.39) as follows :

$$\begin{aligned} \gamma'^{\phi\phi}_{\ell_\alpha \ell_\beta} &= \gamma^{\phi\phi}_{\ell_\alpha \ell_\beta} - B_{\ell_{\alpha\beta}} \, B_\phi \, \gamma_D \,, \\ \gamma'^{\ell_\gamma \ell_\delta}_{\ell_\alpha \ell_\beta} &= \gamma^{\ell_\gamma \ell_\delta}_{\ell_\alpha \ell_\beta} - B_{\ell_{\alpha\beta}} B_{\ell_{\gamma\delta}} \gamma_D \,. \end{aligned} \tag{D.42}$$

Rates for the different SM reactions are approximately given by [255, 214, 325, 326] :

$$\text{QCD instantons :} \qquad \gamma_{\rm QCD}(T) \simeq 312 \, \alpha_{\rm S} \, T^4 \,, \tag{D.43}$$

$$\text{Electroweak sphalerons :} \qquad \gamma_{\rm EW}(T) \simeq 26 \, \alpha_{\rm EW} \, T^4 \,, \tag{D.44}$$

$$\text{Yukawa reactions :} \qquad \gamma_{f_\alpha}(T) \simeq 5 \times 10^{-3} \, Y^2_{f_\alpha} \, T \, n^{\rm Eq}_{f_\alpha} = 5 \times 10^{-4} \, Y^2_{f_\alpha} \, T^4 \,, \tag{D.45}$$

where Y_{f_α} denotes the Yukawa coupling of fermion f_α.

D.4 Boltzmann equations

Following the method introduced in Appendix C.4, we here write the main steps in the derivation of the flavored Boltzmann equations for the type-2 leptogenesis.

Scalar triplet density and asymmetry. Thanks to gauge invariance, it is enough to compute the equations associated to only one component of the triplet, that we choose to be $\Delta^\pm$ for simplicity. One gets :

$$\dot{Y}_{\Delta^+} = \left[\phi^+\phi^0 \leftrightarrow \Delta^+\right] + \sum_{\alpha\beta} \left[\bar{e}_\alpha \bar{\nu}_\beta \leftrightarrow \Delta^+\right] + \sum \left[XY \leftrightarrow \Delta^+\Delta^-\right]_{\rm gauge} \,, \tag{D.46}$$

$$\dot{Y}_{\Delta^-} = \left[\phi^-\phi^{0*} \leftrightarrow \Delta^-\right] + \sum_{\alpha\beta} \left[e_\alpha \nu_\beta \leftrightarrow \Delta^-\right] + \sum \left[XY \leftrightarrow \Delta^+\Delta^-\right]_{\rm gauge} \,. \tag{D.47}$$

The gauge interactions was first computed in Ref. [241] and then improved in Ref. [330]. Summing the above equations, one gets easily

$$\dot{Y}_{\Sigma^\pm} \equiv \dot{Y}_{\Delta^+} + \dot{Y}_{\Delta^-} = -\gamma_D^\pm \left(y_{\Sigma^\pm} - 1\right) - 2\gamma_A^\pm \left[y_{\Sigma^\pm}^2 - 1\right] , \tag{D.48}$$

where

$$\gamma_D^\pm = \gamma_{\phi^+\phi^0}^{\Delta^+} + \gamma_{\phi^-\phi^{0*}}^{\Delta^-} + \sum_{\alpha,\beta} \gamma_{\bar{e}_\alpha \nu_\beta}^{\Delta^+} + \gamma_{e_\alpha \bar{\nu}_\beta}^{\Delta^-} , \tag{D.49}$$

and $\gamma_A^\pm$ denote the total decay rate and the total scattering rate of the $\Delta^\pm$ component. Summing over the triplet components, one gets finally the evolution of the total triplet density

$$\dot{Y}_\Sigma = -\gamma_D \left(\frac{Y_\Sigma}{Y_\Sigma^{\rm Eq}} - 1\right) - 2\gamma_A \left[\left(\frac{Y_\Sigma}{Y_\Sigma^{\rm Eq}}\right)^2 - 1\right] , \tag{D.50}$$

where γ_D is the total decay rate as defined in Eq. (4.24). By subtracting the above equations, Eqs. (D.46) and (D.47), one gets instead

$$\Delta\dot{Y}_{\Delta^\pm} \equiv \dot{Y}_{\Delta^+} - \dot{Y}_{\Delta^-} = -\left[\Delta y_\Delta - 2B_\phi \Delta y_\phi + \sum_{\alpha,\beta} B_{\ell_{\alpha\beta}} \left(\Delta y_{\ell_\alpha} + \Delta y_{\ell_\beta}\right)\right] \frac{\gamma_D^\pm}{2} . \tag{D.51}$$

Summing over the triplet component, one gets the evolution of the total triplet asymmetry

$$\Delta\dot{Y}_\Delta = -\left[\frac{\Delta Y_\Delta}{Y_\Sigma^{\rm Eq}} - B_\phi \frac{\Delta Y_\phi}{Y_\phi^{\rm Eq}} + \sum_{\alpha,\beta} B_{\ell_{\alpha\beta}} \left(\frac{\Delta Y_{\ell_\alpha}}{Y_\ell^{\rm Eq}} + \frac{\Delta Y_{\ell_\beta}}{Y_\ell^{\rm Eq}}\right)\right] \gamma_D . \tag{D.52}$$

Lepton asymmetry. Here too, we will focus on the lepton asymmetry generated by only one component of the scalar triplet. One gets for e_α

$$\begin{aligned}
\dot{Y}_{e_\alpha} =& \sum_\beta \left[\Delta^- \leftrightarrow e_\alpha \nu_\beta\right] \\
&+ \sum_\beta \left[\phi^-\phi^{0*} \leftrightarrow e_\alpha \nu_\beta\right]' + \left[\bar{\nu}_\beta \phi^0 \leftrightarrow e_\alpha \phi^+\right] \\
&+ \sum_{\beta,\gamma,\delta} \left[e_\gamma \nu_\delta \leftrightarrow e_\alpha \nu_\beta\right]' + \left[e_\gamma \bar{\nu}_\delta \leftrightarrow e_\alpha \bar{\nu}_\beta\right]
\end{aligned} \tag{D.53}$$

and for $\bar{e}_\alpha$, one just needs to replace all the particle by the associated anti-particle in the above equation. Subtracting the two equations and summing over the lepton components, one gets

$$\begin{aligned}
\Delta\dot{Y}_{\ell_\alpha} =& \left(y_\Sigma + 1\right) \Delta\gamma_{\ell_\alpha \ell_\beta}^{\bar{\Delta}} - \sum_\beta \left(\Delta y_\Delta + \Delta y_{\ell_\alpha} + \Delta y_{\ell_\beta}\right) B_{\ell_{\alpha\beta}} \gamma_D \\
&- \sum_\beta \left(2\Delta y_\phi + \Delta y_{\ell_\alpha} + \Delta y_{\ell_\beta}\right) \left(\gamma_{\ell_\alpha \ell_\beta}^{\prime\phi\phi} + \gamma_{\ell_\alpha \phi}^{\ell_\beta \phi}\right) + 2\sum_\beta \left(B_{\ell_{\alpha\beta}} \Delta\gamma_{\bar{\phi}\bar{\phi}}^{\bar{\Delta}} - B_\phi \Delta\gamma_{\ell_\alpha \ell_\beta}^{\bar{\Delta}}\right) \\
&+ \sum_{\beta,\gamma,\delta} \left(\Delta y_{\ell_\gamma} + \Delta y_{\ell_\delta} - \Delta y_{\ell_\alpha} - \Delta y_{\ell_\beta}\right) \left(\gamma_{\ell_\alpha \ell_\beta}^{\prime\ell_\gamma \ell_\delta} + \gamma_{\ell_\alpha \ell_\delta}^{\ell_\gamma \ell_\beta}\right) + 2\sum_\beta \left(B_{\ell_{\alpha\beta}} \Delta\gamma_{\ell\ell}^{\bar{\Delta}} - B_\ell \Delta\gamma_{\ell_\alpha \ell_\beta}^{\bar{\Delta}}\right)
\end{aligned} \tag{D.54}$$

Here, one has defined the reaction densities with a resonant intermediate state subtracted $\gamma'^{\ell_\gamma \ell_\delta}_{\ell_\alpha \ell_\beta} = \gamma^{\ell_\gamma \ell_\delta}_{\ell_\alpha \ell_\beta} - B_{\ell_{\gamma\delta}} B_{\ell_{\alpha\beta}} \gamma_D$ and $\gamma'^{\phi\phi}_{\ell_\alpha \ell_\beta} = \gamma^{\phi\phi}_{\ell_\alpha \ell_\beta} - B_\phi B_{\ell_{\alpha\beta}} \gamma_D$. Using $\Delta\gamma^{\bar{\Delta}}_{\ell\ell} = -\Delta\gamma^{\bar{\Delta}}_{\phi\phi}$ and $\sum_\beta \Delta\gamma^{\bar{\Delta}}_{\ell_\alpha \ell_\beta} = \epsilon^{\ell_\alpha}_{\Delta} \gamma_D$, one gets finally

$$\begin{aligned}
\Delta \dot{Y}_{\ell_\alpha} = {} & \left(y_\Sigma - 1\right) \epsilon^{\ell_\alpha}_{\Delta} \gamma_D - \sum_\beta \left(\Delta y_\Delta + \Delta y_{\ell_\alpha} + \Delta y_{\ell_\beta}\right) B_{\ell_{\alpha\beta}} \gamma_D \\
& - \sum_\beta \left(2\Delta y_\phi + \Delta y_{\ell_\alpha} + \Delta y_{\ell_\beta}\right) \left(\gamma'^{\phi\phi}_{\ell_\alpha \ell_\beta} + \gamma^{\ell_\beta \phi}_{\ell_\alpha \phi}\right) \\
& + \sum_{\beta,\gamma,\delta} \left(\Delta y_{\ell_\gamma} + \Delta y_{\ell_\delta} - \Delta y_{\ell_\alpha} - \Delta y_{\ell_\beta}\right) \left(\gamma'^{\ell_\gamma \ell_\delta}_{\ell_\alpha \ell_\beta} + \gamma^{\ell_\gamma \ell_\beta}_{\ell_\alpha \ell_\delta}\right)
\end{aligned} \tag{D.55}$$

As usually, the l.h.s. of this equations must be replaced by $(-1)\Delta \dot{Y}_{B/3-L_\alpha}$ in order to express things in terms of sphaleron-conserving quantities. Still, one is left with too many unknown asymmetries in this equations. These must finally be related to the triplet and $B/3 - L_\alpha$ asymmetries trough chemical equilibrium conditions.

D.5 Chemical equilibrium conditions

The way to proceed is the same as in the type-1 Seesaw case in Appendix C.5. The only difference comes from the Hypercharge neutrality condition which reads now

$$\mathcal{Y} = \sum_\alpha \left(\mu_{Q_\alpha} + 2\mu_{u_\alpha} - \mu_{d_\alpha} - \mu_{\ell_\alpha} - \mu_{e_\alpha}\right) + 2\mu_\phi + 6\mu_\Delta = 0 \,. \tag{D.56}$$

Here, we will also write the chemical equilibrium conditions that apply in the situations where the charged lepton Yukawa couplings are not in thermal equilibrium, even if their rate are larger than the Hubble rate. Indeed, as explained in details in section 4.2, in each temperature regime one has different possible flavor regimes, following that the inverse decays are faster or slower than the charged Yukawa reactions. There are therefore parameter space configurations for which lepton flavor coherence is not lost when the SM tau Yukawa reaction (or any other SM lepton Yukawa interaction) becomes fast. In those cases, the C^ℓ and C^ϕ matrices certainly differ from those derived in the case when lepton flavor decoherence takes place at the same temperature at which the corresponding SM Yukawa coupling becomes fast. Although this lepton flavor decoherence "delay" is not inherent to scalar triplet flavored leptogenesis, and it is rather a consequence of parameter choices, here we summarize all possible C^ℓ and C^ϕ matrices including as well those cases. The list presented here thus encompasses all the scenarios one can consider when tracking the $B - L$ asymmetry in triplet scalar flavored leptogenesis scenarios.

Table D.1 displays the different possible temperature regimes, the corresponding reactions which are faster than the Hubble expansion rate, the lepton flavor regimes (full-diagonal, semi-diagonal or general flavor regimes) and the corresponding global symmetries of the effective Lagrangian in the early Universe. In Table D.2, instead, we specify for the different temperature regimes the asymmetry charges for which kinetic evolution equations have to be written and the corresponding C^ℓ and C^ϕ matrices valid in each case. We remind that $T^{f_\alpha}_{\rm decoh}$, as defined in section 4.2.2, refers to the temperature at which the lepton-related triplet inverse decay becomes smaller than the SM lepton f_α Yukawa interaction.

As an example, let's consider the situation where the mass over the scalar triplet is $m_\Delta = 10^9$ GeV, so that leptogenesis takes place in the temperature regime $T \in [10^5, 10^9]$ GeV. Furthermore, suppose that the inverse decays $\ell\ell \to \bar{\Delta}$ are such that only the tau charged lepton Yukawa is active. In this semi-diagonal regime, one has that the strong and EW sphalerons are in equilibrium, as well as the top, bottom, charm, strange and tau Yukawa interactions

$$\sum_\alpha \left(2\mu_{Q_\alpha} - \mu_{u_\alpha} - \mu_{d_\alpha}\right) = 0 \text{ (QCD)} , \qquad \sum_\alpha \left(3\mu_{Q_\alpha} + \mu_{\ell_\alpha}\right) = 0 \text{ (EW)} , \tag{D.57}$$

$$\mu_{u_t} - \mu_{Q_3} - \mu_\phi = 0 \text{ (top)} , \qquad \mu_{u_b} - \mu_{Q_3} + \mu_\phi = 0 \text{ (bottom)} , \tag{D.58}$$

$$\mu_{u_c} - \mu_{Q_2} - \mu_\phi = 0 \text{ (charm)} , \qquad \mu_{u_s} - \mu_{Q_2} + \mu_\phi = 0 \text{ (strange)} , \tag{D.59}$$

$$\mu_{u_\tau} - \mu_{\ell_3} + \mu_\phi = 0 \text{ (tau)} , \tag{D.60}$$

together with the hypercharge relation

$$\mathscr{Y} = \sum_\alpha \left(\mu_{Q_\alpha} + 2\mu_{u_\alpha} - \mu_{d_\alpha} - \mu_{\ell_\alpha} - \mu_{e_\alpha}\right) + 2\mu_\phi + 6\mu_\Delta = 0 . \tag{D.61}$$

In this case, the effective Lagrangian at that time possess the following global symmetries :

$$G_{\text{eff}} = U(1)_Y \times U(1)_Q \times U(1)_u \times U(1)_d \times SU(2)_e , \tag{D.62}$$

so that, assuming that initially the Universe was perfectly symmetric, one has in fact $\mu_{Q_1} = \mu_{u_1} = \mu_{d_1} = \mu_{e_\mu} = \mu_{e_e} = 0$. Now, let's proceed step by step.

The quantities that are conserved by the sphalerons are in this regime the $\Delta Y_{B/3-L_a}$, $\Delta Y_{B/3-L_b}$ and $\Delta Y_{B/3-L_\tau}$ asymmetries. From the relation between the asymmetries and the chemical potential in Eq. (C.54), one has that these are proportional to

$$\Delta Y_{B/3-L_a} \propto \frac{1}{3}\sum_\alpha \left(2\mu_{Q_\alpha} + \mu_{u_\alpha} + \mu_{d_\alpha}\right) - 2\mu_{\ell_a} , \tag{D.63}$$

$$\Delta Y_{B/3-L_b} \propto \frac{1}{3}\sum_\alpha \left(2\mu_{Q_\alpha} + \mu_{u_\alpha} + \mu_{d_\alpha}\right) - 2\mu_{\ell_b} , \tag{D.64}$$

$$\Delta Y_{B/3-L_\tau} \propto \frac{1}{3}\sum_\alpha \left(2\mu_{Q_\alpha} + \mu_{u_\alpha} + \mu_{d_\alpha}\right) - 2\mu_{\ell_\tau} - \mu_{e_\tau} . \tag{D.65}$$

From QCD sphalerons, one has

$$\sum_\alpha \left(\mu_{u_\alpha} + \mu_{d_\alpha}\right) = 2\sum_\alpha \mu_{Q_\alpha} , \tag{D.66}$$

and from EW sphalerons, one has

$$\sum_\alpha \mu_{Q_\alpha} = -\frac{1}{3}\sum_\alpha \mu_{\ell_\alpha} , \tag{D.67}$$

so the asymmetries become, using the tau Yukawa chemical equilibrium condition,

$$\Delta Y_{B/3-L_a} = -\frac{4}{9}\sum_\alpha \Delta Y_{\ell_\alpha} - 2\Delta Y_{\ell_a}\,, \tag{D.68}$$

$$\Delta Y_{B/3-L_b} = -\frac{4}{9}\sum_\alpha \Delta Y_{\ell_\alpha} - 2\Delta Y_{\ell_b}\,, \tag{D.69}$$

$$\Delta Y_{B/3-L_\tau} = -\frac{4}{9}\sum_\alpha \Delta Y_{\ell_\alpha} - 3\Delta Y_{\ell_\tau} + \frac{1}{2}\Delta Y_\phi\,. \tag{D.70}$$

One has to pay attention to the number of degrees of freedom, as well as to the fermion or scalar nature of the asymmetry. Following our conventions, $g_{\ell_\alpha} = g_\phi = 2$ and $g_\Delta = 3$. In order to determine ΔY_ϕ, we use the hypercharge relation, in which we inject the various sphalerons and Yukawa conditions. One has

$$\begin{aligned} & \mu_{Q_2} + \mu_{Q_3} + 2\mu_t + 2\mu_c - \mu_b - \mu_s - \mu_{\ell_a} - \mu_{\ell_b} - \mu_{\ell_\tau} - \mu_{e_\tau} + 2\mu_\phi + 6\mu_\Delta = 0 \\ \Leftrightarrow \quad & 2\mu_{Q_2} + 2\mu_{Q_3} - \mu_{\ell_a} - \mu_{\ell_b} - 2\mu_{\ell_\tau} + 9\mu_\phi + 6\mu_\Delta = 0 \\ \Leftrightarrow \quad & -\frac{5}{3}\mu_{\ell_a} - \frac{5}{3}\mu_{\ell_b} - \frac{8}{3}\mu_{\ell_\tau} + 9\mu_\phi + 6\mu_\Delta = 0 \end{aligned} \tag{D.71}$$

so that the scalar doublet asymmetry reads

$$\Delta Y_\phi = -\frac{4}{9}\Delta Y_\Delta + \frac{10}{27}\Delta Y_{\ell_a} + \frac{10}{27}\Delta Y_{\ell_b} + \frac{16}{27}\Delta Y_{\ell_\tau}\,. \tag{D.72}$$

Injecting this asymmetry in the expression of the $B_3 - L_\alpha$ asymmetries, and inverting the relations, one finally gets the C^ℓ matrix

$$C^\ell = \begin{pmatrix} -\frac{4}{359} & \frac{307}{359} & -\frac{52}{359} & -\frac{36}{359} \\ -\frac{4}{359} & \frac{-52}{359} & \frac{307}{359} & -\frac{36}{359} \\ \frac{26}{359} & -\frac{21}{359} & \frac{-21}{359} & \frac{234}{359} \end{pmatrix}, \tag{D.73}$$

and the C^ϕ one

$$C^\phi = \begin{pmatrix} \frac{172}{359} & \frac{82}{359} & \frac{82}{359} & \frac{112}{359} \end{pmatrix}. \tag{D.74}$$

T (GeV)	In equilibrium	Regime	Global symmetries of the effective $\mathscr{L}$
$\gtrsim 10^{15}$	Hyp.	Full	$U(1)_Y \times U(1)_B \times U(1)_{E_R} \times U(1)_{PQ} \times SU(3)_Q \times SU(3)_u \times SU(3)_d \times SU(3)_e$
$[10^{12}, 10^{15}]$	Hyp., t	Full	$U(1)_Y \times U(1)_B \times U(1)_{E_R} \times SU(2)_Q \times SU(2)_u \times SU(3)_d \times SU(3)_e$
$[10^9, 10^{12}]$:			
$[T^\tau_{\rm decoh}, 10^{12}]$	Hyp., Sphal., t,b,c	Full-diagonal	$U(1)_Y \times U(1)_Q \times U(1)_u \times SU(2)_d \times SU(3)_e$
$[10^9, T^\tau_{\rm decoh}]$	Hyp., Sphal., t,b,c,τ	Semi-diagonal	$U(1)_Y \times U(1)_Q \times U(1)_u \times SU(2)_d \times SU(2)_e$
$[10^5, 10^9]$:			
$[T^\tau_{\rm decoh}, 10^9]$	Hyp., Sphal., t,b,c,s	Full-diagonal	$U(1)_Y \times U(1)_Q \times U(1)_u \times U(1)_d \times SU(3)_e$
$[T^\mu_{\rm decoh}, T^\tau_{\rm decoh}]$	Hyp., Sphal., t,b,c,s,τ	Semi-diagonal	$U(1)_Y \times U(1)_Q \times U(1)_u \times U(1)_d \times SU(2)_e$
$[10^5, T^\mu_{\rm decoh}]$	Hyp., Sphal., t,b,c,s,τ,μ	General	$U(1)_Y \times U(1)_Q \times U(1)_u \times U(1)_d \times U(1)_e$
$\lesssim 10^5$:			
$[T^\tau_{\rm decoh}, 10^5]$	Hyp., Sphal., t,b,c,s,u,d	Full-diagonal	$U(1)_Y \times SU(3)_e$
$[T^\mu_{\rm decoh}, T^\tau_{\rm decoh}]$	Hyp., Sphal., t,b,c,s,u,d,τ	Semi-diagonal	$U(1)_Y \times SU(2)_e$
$[T^e_{\rm decoh}, T^\mu_{\rm decoh}]$	Hyp., Sphal., t,b,c,s,u,d,τ,μ	General	$U(1)_Y \times U(1)_e$
$\lesssim T^e_{\rm decoh}$	Hyp., Sphal., t,b,c,s,u,d,τ,μ,e	General	$U(1)_Y$

Table D.1 – Temperature ranges and the corresponding reactions which are in thermal equilibrium. In the third column we show the corresponding flavor regime that has to be considered and in the fourth column we show the global symmetries of the early Universe effective Lagrangian.

T (GeV)	Flavor(s)	C^ℓ	C^ϕ
$\gtrsim 10^{15}$	$B-L_{1,2,3}$	$\begin{pmatrix}0&1&0&0\\0&0&1&0\\0&0&0&1\end{pmatrix}$	$\begin{pmatrix}2&1&1&1\end{pmatrix}$
$[10^{12},10^{15}]$	$B-L_{1,2,3}$	$\begin{pmatrix}0&1&0&0\\0&0&1&0\\0&0&0&1\end{pmatrix}$	$\begin{pmatrix}\frac{4}{3}&\frac{2}{3}&\frac{2}{3}&\frac{2}{3}\end{pmatrix}$
$[10^9,10^{12}]$:			
$[T^\tau_{\rm decoh},10^{12}]$	$B-L_{1,2,3}$	$\begin{pmatrix}0&\frac{13}{15}&-\frac{2}{15}&-\frac{2}{15}\\0&-\frac{2}{15}&\frac{13}{15}&-\frac{2}{15}\\0&-\frac{2}{15}&-\frac{2}{15}&\frac{13}{15}\end{pmatrix}$	$\begin{pmatrix}\frac{1}{2}&\frac{1}{4}&\frac{1}{4}&\frac{1}{4}\end{pmatrix}$
$[10^9,T^\tau_{\rm decoh}]$	$B/3-L_{a,b,\tau}$	$\begin{pmatrix}-\frac{4}{359}&\frac{307}{359}&-\frac{52}{359}&-\frac{36}{359}\\-\frac{4}{359}&\frac{-52}{359}&\frac{307}{359}&-\frac{36}{359}\\\frac{26}{359}&-\frac{21}{359}&\frac{-21}{359}&\frac{234}{359}\end{pmatrix}$	$\begin{pmatrix}\frac{172}{359}&\frac{82}{359}&\frac{82}{359}&\frac{112}{359}\end{pmatrix}$
$[10^5,10^9]$:			
$[T^\tau_{\rm decoh},10^9]$	$B/3-L_{1,2,3}$	$\begin{pmatrix}0&\frac{13}{15}&-\frac{2}{15}&-\frac{2}{15}\\0&-\frac{2}{15}&\frac{13}{15}&-\frac{2}{15}\\0&-\frac{2}{15}&-\frac{2}{15}&\frac{13}{15}\end{pmatrix}$	$\begin{pmatrix}\frac{1}{2}&\frac{1}{4}&\frac{1}{4}&\frac{1}{4}\end{pmatrix}$
$[T^\mu_{\rm decoh},T^\tau_{\rm decoh}]$	$B/3-L_{a,b,\tau}$	$\begin{pmatrix}-\frac{4}{359}&\frac{307}{359}&-\frac{52}{359}&-\frac{36}{359}\\-\frac{4}{359}&\frac{-52}{359}&\frac{307}{359}&-\frac{36}{359}\\\frac{26}{359}&-\frac{21}{359}&\frac{-21}{359}&\frac{234}{359}\end{pmatrix}$	$\begin{pmatrix}\frac{172}{359}&\frac{82}{359}&\frac{82}{359}&\frac{112}{359}\end{pmatrix}$
$[10^5,T^\mu_{\rm decoh}]$	$B/3-L_{e,\mu,\tau}$	$\begin{pmatrix}-\frac{4}{179}&\frac{151}{179}&-\frac{20}{179}&-\frac{20}{179}\\\frac{11}{179}&-\frac{25}{358}&\frac{344}{537}&-\frac{14}{537}\\\frac{11}{358}&-\frac{25}{358}&-\frac{14}{537}&\frac{344}{537}\end{pmatrix}$	$\begin{pmatrix}\frac{82}{179}&\frac{37}{179}&\frac{52}{179}&\frac{52}{179}\end{pmatrix}$

…see next page for the other regimes…

T (GeV)	Flavor(s)	C^ℓ	C^ϕ
$\lesssim 10^5$:			
$[T^\tau_{\rm decoh}, 10^5]$	$B/3-L_{1,2,3}$	$\begin{pmatrix} 0 & \frac{13}{15} & -\frac{2}{15} & -\frac{2}{15} \\ 0 & -\frac{2}{15} & \frac{13}{15} & -\frac{2}{15} \\ 0 & -\frac{2}{15} & -\frac{2}{15} & \frac{13}{15} \end{pmatrix}$	$\left(\frac{4}{11} \quad \frac{2}{11} \quad \frac{2}{11} \quad \frac{2}{11}\right)$
$[T^\mu_{\rm decoh}, T^\tau_{\rm decoh}]$	$B/3-L_{a,b,\tau}$	$\begin{pmatrix} -\frac{2}{244} & \frac{209}{244} & -\frac{35}{244} & -\frac{24}{244} \\ -\frac{2}{244} & -\frac{35}{244} & -\frac{209}{244} & -\frac{24}{244} \\ \frac{13}{244} & -\frac{33}{488} & -\frac{33}{488} & \frac{156}{244} \end{pmatrix}$	$\left(\frac{86}{244} \quad \frac{41}{244} \quad \frac{41}{244} \quad \frac{56}{244}\right)$
$[T^e_{\rm decoh}, T^\mu_{\rm decoh}]$	$B/3-L_{e,\mu,\tau}$	$\begin{pmatrix} -\frac{8}{481} & \frac{407}{481} & -\frac{52}{481} & -\frac{52}{481} \\ \frac{22}{481} & -\frac{1}{13} & \frac{70}{111} & -\frac{4}{111} \\ \frac{22}{481} & -\frac{1}{13} & -\frac{4}{111} & \frac{70}{111} \end{pmatrix}$	$\left(\frac{164}{481} \quad \frac{2}{13} \quad \frac{8}{37} \quad \frac{8}{37}\right)$
$\lesssim T^e_{\rm decoh}$	$B/3-L_{e,\mu,\tau}$	$\begin{pmatrix} \frac{3}{79} & \frac{442}{711} & -\frac{32}{711} & -\frac{32}{711} \\ \frac{3}{79} & -\frac{32}{711} & \frac{442}{711} & -\frac{32}{711} \\ \frac{3}{79} & -\frac{32}{711} & -\frac{32}{711} & \frac{442}{711} \end{pmatrix}$	$\left(\frac{26}{79} \quad \frac{16}{79} \quad \frac{16}{79} \quad \frac{16}{79}\right)$

Table D.2 – Temperature ranges, as in Table D.1. In the second column, we show the asymmetries for which kinetic equations have to be written. In the third and fourth columns the different C^ℓ and C^ϕ matrices holding in each regime. Note that some of these matrices reduce to those found in the type-1 Seesaw case when removing their first column.

E Asymmetric Dark matter in IDM

E.1 Scattering rates

In Eq. (5.45), the reaction density of the λ_5 scatterings for the η^+ (and similarly for η^0) is given by

$$\gamma_{\lambda_5} = \gamma_{\eta\eta}^{\phi\phi} + \gamma_{\phi\eta}^{\phi\eta}\,, \tag{E.1}$$

where

$$\gamma_{cd}^{ab} = \frac{m_{H_2}^4}{64\pi\, z}\int_4^\infty dx\,\sqrt{x}\,K_1(z\sqrt{x})\,\hat{\sigma}\,(ab\to cd)\ . \tag{E.2}$$

with $\hat{\sigma}(ab\to cd)$ the reduced cross section. These are given by

$$\hat{\sigma}_{\lambda_5}^{s}(\phi\phi\to\eta\eta) = \frac{3\lambda_5^2}{2\pi}\sqrt{1-\frac{4}{x}}\,, \tag{E.3}$$

$$\hat{\sigma}_{\lambda_5}^{t}(\phi\eta\to\phi\eta) = \frac{3\lambda_5^2}{2\pi}\left(1-\frac{1}{x}\right)^2\,. \tag{E.4}$$

In the non-relativistic limit, the corresponding rate is given by

$$\Gamma_{\lambda_5} \equiv \frac{\gamma_{\lambda_5}}{n_{\eta^+}^{\rm Eq}} \equiv n_{\eta^+}^{\rm Eq}\langle\sigma_{\lambda_5}^{s}\,v\rangle + n_{\phi^+}^{\rm Eq}\langle\sigma_{\lambda_5}^{t}\,v\rangle\,, \tag{E.5}$$

where [318]

$$\langle\sigma_{\lambda_5}^{s}\,v\rangle = \frac{3\lambda_5^2}{32\pi\, m_{H_2}^2}\,,\text{and}\quad \langle\sigma_{\lambda_5}^{t}\,v\rangle = \frac{3\lambda_5^2}{16\pi\, m_{H_2}^2}\,. \tag{E.6}$$

In Eq. (5.46) and (5.63), the effective cross section of the $H_2\bar{H}_2\to SM\ SM$ coannihilations is given by [292]

$$\langle\sigma_{H_2}\,v\rangle = \sum_{i,j}\langle\sigma_{ij}\,v\rangle\frac{Y_i^{\rm Eq}}{\Sigma_{H_2}^{\rm Eq}}\frac{Y_j^{\rm Eq}}{\Sigma_{H_2}^{\rm Eq}} \simeq \frac{1}{64\,\pi\, m_{H_2}^2}\left(\frac{3}{8}g^4+\lambda_3^2+\lambda_4^2\right)\,. \tag{E.7}$$

where g is the weak coupling constant. We neglected the λ_5 contribution, and the corrections due to the contributions proportional to $\langle v^2 \rangle$.

E.2 Analytical resolution of the Boltzmann equations

The Boltzmann equations given in Eqs. (5.57)-(5.59) do not in general have a simple analytical solution. However, in the case of very fast oscillations, like it is the case here, a good approximation consists in symmetrizing the equations for Δ_{η^0} and Ξ_{η^0}, i.e. replacing Eqs. (5.58)-(5.59) by

$$\frac{d\Delta_{\eta^0}}{dz} = 2i\frac{\delta m}{zH}\,\Xi_{\eta^0} - \frac{1}{2}\frac{\langle\sigma_0 v\rangle s}{zH}\,\Delta_{\eta^0}\,\Sigma_{\eta^0}\,, \tag{E.8}$$

$$\frac{d\Xi_{\eta^0}}{dz} = 2i\frac{\delta m}{zH}\,\Delta_{\eta^0} - \frac{1}{2}\frac{\langle\sigma_0 v\rangle s}{zH}\,\Xi_{\eta^0}\,\Sigma_{\eta^0}\,. \tag{E.9}$$

In this approximation, the solutions for Δ_{η^0} and Ξ_{η^0} are of the form

$$\Delta_{\eta^0}(z) = f(z)\,\cos[g(z)]\;,\;\Xi_{\eta^0}(z) = i\,f(z)\,\sin[g(z)]\,. \tag{E.10}$$

Furthermore, since we are interested in oscillations happening after the freeze-out, we can neglect $\Sigma_{\eta^0}^{\rm Eq}$ in Eq. (5.57). With these approximations, integrating from z_{EW} to z with the initial conditions $\Delta_{\eta_0}(z_{EW}) = \Sigma_{\eta_0}(z_{EW})$ and $\Xi(z_{EW}) = 0$, the analytical solutions of the Boltzmann equations Eqs. (5.57)-(E.9) are given by Eq. (E.10) and

$$\Sigma_{\eta^0}(z) = \sqrt{\Delta^2_{\eta^0}(z) - \Xi^2_{\eta^0}(z)} = f(z)\,, \tag{E.11}$$

with

$$f(z) = \frac{\Sigma_{\eta_0}(z_{EW})}{1 + \frac{1}{2}\frac{\langle\sigma_0 v\rangle\, s(z)}{H(z)}\left(\frac{z}{z_{EW}} - 1\right)\Sigma_{\eta_0}(z_{EW})}\,, \tag{E.12}$$

$$g(z) = \frac{\delta m}{H(z)}\left(\frac{z^2}{z_{EW}^2} - 1\right). \tag{E.13}$$

The abundance Σ_{η^0} decreases therefore monotonically until it reaches an asymptotical value given by

$$\Sigma_{\eta^0}(z \gg z_{EW}) = \frac{\Sigma_{\eta_0}(z_{EW})}{1 + \frac{1}{2}\frac{\langle\sigma_0 v\rangle\, s(z)}{H(z)}\frac{z}{z_{EW}}\Sigma_{\eta_0}(z_{EW})}\,. \tag{E.14}$$

Note that despite appearance, the denominator doesn't depend on z, since one has $sz/(Hz_{EW}) = 12\sqrt{g_*}M_{Pl}T_{EW}/5\pi^2$.

E.3 Landau Pole

The renormalization group equations for the inert doublet model have been computed in Ref. [290] :

$$16\pi^2 \frac{d\lambda_i}{d\log\Lambda} = \beta_i(\lambda) \,, \tag{E.15}$$

where the beta functions are given by

$$\begin{aligned}
\beta_1 &= 24\lambda_1^2 + 2\lambda_3^2 + 2\lambda_3\lambda_4 + \lambda_4^2 + \lambda_5^2 \,, \\
\beta_2 &= 24\lambda_2^2 + 2\lambda_3^2 + 2\lambda_3\lambda_4 + \lambda_4^2 + \lambda_5^2 \,, \\
\beta_3 &= (12\lambda_3 + 4\lambda_4)(\lambda_1 + \lambda_2) + 4\lambda_3^2 + 2\lambda_4^2 + 2\lambda_5^2 \,, \\
\beta_4 &= 4\lambda_4(\lambda_1 + \lambda_2) + 4\lambda_4^2 + 8\lambda_3\lambda_4 + 8\lambda_5^2 \,, \\
\beta_5 &= 4\lambda_5(\lambda_1 + \lambda_2) + 8\lambda_3\lambda_5 + 12\lambda_4\lambda_5 \,.
\end{aligned} \tag{E.16}$$

Bibliography

[1] R. Alonso, M. Dhen, M. B. Gavela and T. Hambye, JHEP **1301** (2013) 118 [arXiv:1209.2679 [hep-ph]].

[2] D. Aristizabal Sierra, M. Dhen and T. Hambye, JCAP **1408** (2014) 003 [arXiv:1401.4347 [hep-ph]].

[3] M. Dhen and T. Hambye, arXiv:1503.03444 [hep-ph].

[4] E. Fermi, "Trends to a Theory of beta Radiation. (In Italian)," Nuovo Cim. **11** (1934) 1.

[5] C. L. Cowan, F. Reines, F. B. Harrison, H. W. Kruse and A. D. McGuire, Camb. Monogr. Part. Phys. Nucl. Phys. Cosmol. **1** (1991) 41.

[6] G. Danby, J. M. Gaillard, K. A. Goulianos, L. M. Lederman, N. B. Mistry, M. Schwartz and J. Steinberger, Phys. Rev. Lett. **9** (1962) 36.

[7] K. Kodama *et al.* [DONUT Collaboration], Phys. Lett. B **504** (2001) 218 [hep-ex/0012035].

[8] K. A. Olive *et al.* [Particle Data Group Collaboration], Chin. Phys. C **38** (2014) 090001.

[9] Y. Fukuda *et al.* [Super-Kamiokande Collaboration], Phys. Rev. Lett. **81** (1998) 1562 [hep-ex/9807003].

[10] Q. R. Ahmad *et al.* [SNO Collaboration], Phys. Rev. Lett. **87** (2001) 071301 [nucl-ex/0106015].

[11] K. Eguchi *et al.* [KamLAND Collaboration], Phys. Rev. Lett. **90** (2003) 021802 [hep-ex/0212021].

[12] M. H. Ahn *et al.* [K2K Collaboration], Phys. Rev. Lett. **90** (2003) 041801 [hep-ex/0212007].

[13] E. K. Akhmedov and A. Y. Smirnov, Phys. Atom. Nucl. **72** (2009) 1363 [arXiv:0905.1903 [hep-ph]].

[14] R. Davis, Jr., D. S. Harmer and K. C. Hoffman, Phys. Rev. Lett. **20** (1968) 1205.

[15] F. P. An *et al.* [Daya Bay Collaboration], Chin. Phys. C **37** (2013) 011001 [arXiv:1210.6327 [hep-ex]].

[16] F. P. An *et al.* [DAYA-BAY Collaboration], Phys. Rev. Lett. **108** (2012) 171803 [arXiv:1203.1669 [hep-ex]].

[17] Y. Abe *et al.* [Double Chooz Collaboration], Phys. Rev. D **86** (2012) 052008 [arXiv:1207.6632 [hep-ex]].

[18] K. Abe *et al.* [T2K Collaboration], Phys. Rev. Lett. **112** (2014) 061802 [arXiv:1311.4750 [hep-ex]].

[19] M. C. Gonzalez-Garcia, M. Maltoni and T. Schwetz, JHEP **1411** (2014) 052 [arXiv:1409.5439 [hep-ph]].

[20] Y. F. Li, J. Cao, Y. Wang and L. Zhan, Phys. Rev. D **88** (2013) 013008 [arXiv:1303.6733 [hep-ex]].

[21] A. Ghosh, T. Thakore and S. Choubey, JHEP **1304** (2013) 009 [arXiv:1212.1305].

[22] S. B. Kim, arXiv:1412.2199 [hep-ex].

[23] J. Arafune, M. Koike and J. Sato, Phys. Rev. D **56** (1997) 3093 [Phys. Rev. D **60** (1999) 119905] [hep-ph/9703351].

[24] S. K. Agarwalla *et al.* [LAGUNA-LBNO Collaboration], JHEP **1405** (2014) 094 [arXiv:1312.6520 [hep-ph]].

[25] C. Adams *et al.* [LBNE Collaboration], arXiv:1307.7335 [hep-ex].

[26] K. Abe, T. Abe, H. Aihara, Y. Fukuda, Y. Hayato, K. Huang, A. K. Ichikawa and M. Ikeda *et al.*, arXiv:1109.3262 [hep-ex].

[27] C. Weinheimer, B. Degen, A. Bleile, J. Bonn, L. Bornschein, O. Kazachenko, A. Kovalik and E. W. Otten, Phys. Lett. B **460** (1999) 219.

[28] V. N. Aseev *et al.* [Troitsk Collaboration], Phys. Rev. D **84** (2011) 112003 [arXiv:1108.5034 [hep-ex]].

[29] G. Drexlin [KATRIN Collaboration], Nucl. Phys. Proc. Suppl. **145** (2005) 263.

[30] M. Agostini *et al.* [GERDA Collaboration], Phys. Rev. Lett. **111** (2013) 12, 122503 [arXiv:1307.4720 [nucl-ex]].

[31] C. E. Aalseth *et al.* [IGEX Collaboration], Phys. Rev. D **65** (2002) 092007 [hep-ex/0202026].

[32] M. Auger *et al.* [EXO Collaboration], Phys. Rev. Lett. **109** (2012) 032505 [arXiv:1205.5608 [hep-ex]].

[33] A. S. Barabash *et al.* [NEMO Collaboration], Phys. Atom. Nucl. **74** (2011) 312 [arXiv:1002.2862 [nucl-ex]].

[34] A. Gando *et al.* [KamLAND-Zen Collaboration], Phys. Rev. Lett. **110** (2013) 6, 062502 [arXiv:1211.3863 [hep-ex]].

[35] E. Andreotti, C. Arnaboldi, F. T. Avignone, M. Balata, I. Bandac, M. Barucci, J. W. Beeman and F. Bellini *et al.*, Astropart. Phys. **34** (2011) 822 [arXiv:1012.3266 [nucl-ex]].

[36] R. Arnold *et al.* [SuperNEMO Collaboration], Eur. Phys. J. C **70** (2010) 927 [arXiv:1005.1241 [hep-ex]].

[37] R. Gaitskell *et al.* [Majorana Collaboration], nucl-ex/0311013.

[38] F. Granena *et al.* [NEXT Collaboration], arXiv:0907.4054 [hep-ex].

[39] M. C. Chen [SNO+ Collaboration], arXiv:0810.3694 [hep-ex].

[40] P. A. R. Ade *et al.* [Planck Collaboration], Astron. Astrophys. **571** (2014) A16 [arXiv:1303.5076 [astro-ph.CO]].

[41] S. Weinberg, Phys. Rev. Lett. **43** (1979) 1566.

[42] E. Ma, Phys. Rev. Lett. **81** (1998) 1171 [hep-ph/9805219].

[43] P. Minkowski, *Phys. Lett.* B **67** 421 (1977); T. Yanagida, in *Proc. of Workshop on Unified Theory and Baryon number in the Universe*, eds. O. Sawada and A. Sugamoto, KEK, Tsukuba, (1979) p.95; M. Gell-Mann, P. Ramond and R. Slansky, in *Supergravity*, eds P. van Niewenhuizen and D. Z. Freedman (North Holland, Amsterdam 1980) p.315; P. Ramond, *Sanibel talk*, retroprinted as hep-ph/9809459; S. L. Glashow, in*Quarks and Leptons*, Cargèse lectures, eds M. Lévy, (Plenum, 1980, New York) p. 707; R. N. Mohapatra and G. Senjanović, *Phys. Rev. Lett.* **44**, 912 (1980); J. Schechter and J. W. F. Valle, Phys. Rev. D **22** (1980) 2227; Phys. Rev. D **25** (1982) 774.

[44] E. Ma, Phys. Rev. D **73** (2006) 077301 [hep-ph/0601225].

[45] A. Strumia and F. Vissani, hep-ph/0606054.

[46] A. Zee, Phys. Lett. B **93** (1980) 389 [Phys. Lett. B **95** (1980) 461].

[47] A. Zee, Phys. Lett. B **161** (1985) 141.

[48] A. Zee, Nucl. Phys. B **264** (1986) 99.

[49] K. S. Babu, Phys. Lett. B **203** (1988) 132.

[50] A. Broncano, M. B. Gavela and E. E. Jenkins, Nucl. Phys. B **672** (2003) 163 [hep-ph/0307058].

[51] H. Ishida and F. Takahashi, Phys. Lett. B **734** (2014) 183 [arXiv:1403.6460 [hep-ph]].

[52] K. Bhattacharya, J. Chakrabortty, S. Das and T. Mondal, JCAP **1412** (2014) 12, 001 [arXiv:1408.3966 [hep-ph]].

[53] R. Franceschini, T. Hambye and A. Strumia, Phys. Rev. D **78** (2008) 033002 [arXiv:0805.1613 [hep-ph]].

[54] F. del Aguila and J. A. Aguilar-Saavedra, Nucl. Phys. B **813**, 22 (2009) [arXiv:0808.2468 [hep-ph]].

[55] Y. Chikashige, R. N. Mohapatra and R. D. Peccei, Phys. Lett. B **98** (1981) 265.

[56] A. Abada, C. Biggio, F. Bonnet, M. B. Gavela and T. Hambye, JHEP **0712** (2007) 061 [arXiv:0707.4058 [hep-ph]].

[57] R. N. Mohapatra and J. W. F. Valle, Phys. Rev. D **34**, 1642 (1986).

[58] R. N. Mohapatra, Phys. Rev. Lett. **56** (1986) 561.

[59] D. Wyler and L. Wolfenstein, Nucl. Phys. B **218**, 205 (1983).

[60] G. C. Branco, W. Grimus and L. Lavoura, Nucl. Phys. B **312**, 492 (1989).

[61] M.C. Gonzalez-Garcia and J.W.F. Valle, Phys. Lett. **B216** (1989) 316.

[62] R. Barbieri, T. Hambye and A. Romanino, JHEP **0303** (2003) 017 [hep-ph/0302118].

[63] M. Raidal, A. Strumia and K. Turzynski, Phys. Lett. B **609** (2005) 351 [Erratum-ibid. B **632** (2006) 752] [hep-ph/0408015].

[64] J. Kersten and A. Y. Smirnov, Phys. Rev. D **76**, 073005 (2007) [arXiv:0705.3221 [hep-ph]].

[65] M. Shaposhnikov, Nucl. Phys. B **763**, 49 (2007) [arXiv:hep-ph/0605047].

[66] T. Asaka and S. Blanchet, Phys. Rev. D **78**, 123527 (2008) [arXiv:0810.3015 [hep-ph]].

[67] A. Ilakovac and A. Pilaftsis, Nucl. Phys. B **437** (1995) 491 [hep-ph/9403398].

[68] M. B. Gavela, T. Hambye, D. Hernandez and P. Hernandez, JHEP **0909** (2009) 038 [arXiv:0906.1461 [hep-ph]].

[69] S. Blanchet, T. Hambye and F. -X. Josse-Michaux, JHEP **1004** (2010) 023 [arXiv:0912.3153 [hep-ph]].

[70] S. K. Kang and C. S. Kim, Phys. Lett. B **646** (2007) 248 [hep-ph/0607072].

[71] J. Lopez-Pavon, S. Pascoli and C. f. Wong, Phys. Rev. D **87** (2013) 9, 093007 [arXiv:1209.5342 [hep-ph]].

[72] J. Lopez-Pavon, E. Molinaro and S. T. Petcov, arXiv:1506.05296 [hep-ph].

[73] H. Fritzsch and P. Minkowski, Annals Phys. **93** (1975) 193.

[74] H. Georgi and S. L. Glashow, Phys. Rev. Lett. **32** (1974) 438.

[75] J. C. Pati and A. Salam, Phys. Rev. D **10** (1974) 275 [Erratum-ibid. D **11** (1975) 703].

[76] R. N. Mohapatra and J. C. Pati, Phys. Rev. D **11** (1975) 566.

[77] B. Bajc, A. Melfo, G. Senjanovic and F. Vissani, Phys. Rev. D **73** (2006) 055001 [hep-ph/0510139].

[78] G. Lazarides, Q. Shafi and C. Wetterich, Nucl. Phys. B **181** (1981) 287.

[79] B. Bajc, G. Senjanovic and F. Vissani, Phys. Rev. D **70** (2004) 093002 [hep-ph/0402140].

[80] R. N. Mohapatra and J. C. Pati, Phys. Rev. D **11** (1975) 2558.

[81] R. N. Mohapatra and D. P. Sidhu, Phys. Rev. Lett. **38** (1977) 667.

[82] R. N. Mohapatra, F. E. Paige and D. P. Sidhu, Phys. Rev. D **17** (1978) 2462.

[83] R. E. Marshak and R. N. Mohapatra, Phys. Lett. B **91** (1980) 222.

[84] R. N. Mohapatra and R. E. Marshak, Phys. Rev. Lett. **44** (1980) 1316 [Erratum-ibid. **44** (1980) 1643].

[85] R. N. Mohapatra and G. Senjanovic, Phys. Rev. Lett. **44** (1980) 912.

[86] R. N. Mohapatra and G. Senjanovic, Phys. Rev. D **23** (1981) 165.

[87] K. Nakamura *et al.* [Particle Data Group Collaboration], J. Phys. G G **37** (2010) 075021.

[88] A. Broncano, M. B. Gavela and E. E. Jenkins, Phys. Lett. B **552** (2003) 177 [Phys. Lett. B **636** (2006) 332] [hep-ph/0210271].

[89] S. Antusch, C. Biggio, E. Fernandez-Martinez, M. B. Gavela and J. Lopez-Pavon, JHEP **0610** (2006) 084 [hep-ph/0607020].

[90] S. M. Bilenky, S. T. Petcov and B. Pontecorvo, Phys. Lett. B **67** (1977) 309.

[91] J. Adam *et al.* [MEG Collaboration], Phys. Rev. Lett. **110** (2013) 201801 [arXiv:1303.0754 [hep-ex]].

[92] B. Aubert *et al.* [BaBar Collaboration], Phys. Rev. Lett. **104** (2010) 021802 [arXiv:0908.2381 [hep-ex]].

[93] F. Renga [The MEG Collaboration], arXiv:1410.4705 [hep-ex].

[94] T. Aushev, W. Bartel, A. Bondar, J. Brodzicka, T. E. Browder, P. Chang, Y. Chao and K. F. Chen *et al.*, arXiv:1002.5012 [hep-ex].

[95] B. O'Leary *et al.* [SuperB Collaboration], arXiv:1008.1541 [hep-ex].

[96] B. Meadows, M. Blanke, A. Stocchi, A. Drutskoy, A. Cervelli, M. Giorgi, A. Lusiani and A. Perez *et al.*, arXiv:1109.5028 [hep-ex].

[97] U. Bellgardt *et al.* [SINDRUM Collaboration], Nucl. Phys. B **299** (1988) 1.

[98] B. Aubert *et al.* [BaBar Collaboration], Phys. Rev. Lett. **99** (2007) 251803 [arXiv:0708.3650 [hep-ex]].

[99] Y. Miyazaki *et al.* [Belle Collaboration], Phys. Lett. B **660** (2008) 154 [arXiv:0711.2189 [hep-ex]].

[100] A. Blondel, A. Bravar, M. Pohl, S. Bachmann, N. Berger, M. Kiehn, A. Schoning and D. Wiedner *et al.*, arXiv:1301.6113 [physics.ins-det].

[101] T. S. Kosmas, Nucl. Instrum. Meth. A **503** (2001) 247 [nucl-th/0108045].

[102] C. Dohmen *et al.* [SINDRUM II. Collaboration], Phys. Lett. B **317** (1993) 631.

[103] W. Honecker *et al.* [SINDRUM II Collaboration], Phys. Rev. Lett. **76** (1996) 200.

[104] W. H. Bertl *et al.* [SINDRUM II Collaboration], Eur. Phys. J. C **47** (2006) 337.

[105] E. V. Hungerford [COMET Collaboration], AIP Conf. Proc. **1182** (2009) 694.

[106] Y. G. Cui *et al.* [COMET Collaboration], KEK-2009-10.

[107] A. Kurup [COMET Collaboration], Nucl. Phys. Proc. Suppl. **218** (2011) 38.

[108] R. M. Carey *et al.* [Mu2e Collaboration], FERMILAB-PROPOSAL-0973.

[109] R. K. Kutschke, arXiv:1112.0242 [hep-ex].

[110] A. Czarnecki, X. Garcia i Tormo and W. J. Marciano, Phys. Rev. D **84** (2011) 013006 [arXiv:1106.4756 [hep-ph]].

[111] J. Tran Thanh Van, Gif-sur-Yvette, France: Ed. Frontieres (1991) 565 p

[112] R. Akers *et al.* [OPAL Collaboration], Z. Phys. C **67** (1995) 555.

[113] P. Abreu *et al.* [DELPHI Collaboration], Z. Phys. C **73** (1997) 243.

[114] G. Aad *et al.* [ATLAS Collaboration], Phys. Rev. D **90** (2014) 7, 072010 [arXiv:1408.5774 [hep-ex]].

[115] S. Davidson, S. Lacroix and P. Verdier, JHEP **1209** (2012) 092 [arXiv:1207.4894 [hep-ph]].

[116] CMS Collaboration [CMS Collaboration], and studies of the compatibility of its couplings with the standard model," CMS-PAS-HIG-14-009.

[117] K. Hayasaka [Belle Collaboration], PoS ICHEP **2010** (2010) 241 [arXiv:1011.6474 [hep-ex]].

[118] B. Aubert *et al.* [BaBar Collaboration], Phys. Rev. D **77** (2008) 091104 [arXiv:0801.0697 [hep-ex]].

[119] T. Aaltonen *et al.* [CDF Collaboration], Phys. Rev. Lett. **102** (2009) 201801 [arXiv:0901.3803 [hep-ex]].

[120] W. Bonivento and N. Serra, CERN-LHCB-2007-028.

[121] D. Ambrose *et al.* [BNL Collaboration], Phys. Rev. Lett. **81** (1998) 5734 [hep-ex/9811038].

[122] E. Abouzaid *et al.* [KTeV Collaboration], Phys. Rev. Lett. **100** (2008) 131803 [arXiv:0711.3472 [hep-ex]].

[123] M. C. Gonzalez-Garcia and J. W. F. Valle, Mod. Phys. Lett. A **7** (1992) 477.

[124] V. D. Barger, H. Baer, W. Y. Keung and R. J. N. Phillips, Phys. Rev. D **26** (1982) 218.

[125] P. B. Pal, Nucl. Phys. B **227** (1983) 237.

[126] A. Pich, A. Santamaria and J. Bernabeu, Phys. Lett. B **148** (1984) 229.

[127] S. M. Bilenky and S. T. Petcov, Rev. Mod. Phys. **59** (1987) 671 [Erratum-ibid. **61** (1989) 169] [Erratum-ibid. **60** (1988) 575].

[128] R. N. Mohapatra, Phys. Rev. D **46** (1992) 2990.

[129] A. Abada, C. Biggio, F. Bonnet, M. B. Gavela and T. Hambye, Phys. Rev. D **78** (2008) 033007 [arXiv:0803.0481 [hep-ph]].

[130] P. Minkowski, Phys. Lett. B **67** (1977) 421.

[131] C. S. Lim and T. Inami, Prog. Theor. Phys. **67** (1982) 1569.

[132] P. Langacker and D. London, Phys. Rev. D **38** (1988) 907.

[133] W. J. Marciano and A. I. Sanda, Phys. Lett. B **67** (1977) 303.

[134] T. P. Cheng and L. -F. Li, Phys. Rev. Lett. **45** (1980) 1908.

[135] T. P. Cheng and L. F. Li, Oxford, Uk: Clarendon (1984) 536 P. (Oxford Science Publications)

[136] Riazuddin, R. E. Marshak and R. N. Mohapatra, Phys. Rev. D **24** (1981) 1310.

[137] L. N. Chang, D. Ng and J. N. Ng, Phys. Rev. D **50** (1994) 4589 [hep-ph/9402259].

[138] A. Ioannisian and A. Pilaftsis, Phys. Rev. D **62** (2000) 066001 [hep-ph/9907522].

[139] A. Pilaftsis and T. E. J. Underwood, Phys. Rev. D **72** (2005) 113001 [hep-ph/0506107].

[140] F. Deppisch, T. S. Kosmas and J. W. F. Valle, Nucl. Phys. B **752** (2006) 80 [hep-ph/0512360].

[141] A. Ilakovac and A. Pilaftsis, Phys. Rev. D **80** (2009) 091902 [arXiv:0904.2381 [hep-ph]].

[142] F. F. Deppisch and A. Pilaftsis, Phys. Rev. D **83** (2011) 076007 [arXiv:1012.1834 [hep-ph]].

[143] M. Raidal and A. Santamaria, Phys. Lett. B **421** (1998) 250 [hep-ph/9710389].

[144] E. Ma, M. Raidal and U. Sarkar, Nucl. Phys. B **615** (2001) 313 [hep-ph/0012101].

[145] D. N. Dinh, A. Ibarra, E. Molinaro and S. T. Petcov, arXiv:1205.4671 [hep-ph].

[146] D. Aristizabal Sierra, A. Degee and J. F. Kamenik, arXiv:1205.5547 [hep-ph].

[147] S. Weinberg and G. Feinberg, Phys. Rev. Lett. **3** (1959) 111.

[148] J. Bernabeu, E. Nardi and D. Tommasini, Nucl. Phys. B **409** (1993) 69 [hep-ph/9306251].

[149] T. S. Kosmas, G. K. Leontaris and J. D. Vergados, Prog. Part. Nucl. Phys. **33** (1994) 397 [hep-ph/@].

[150] A. Czarnecki, W. J. Marciano and K. Melnikov, AIP Conf. Proc. **435** (1998) 409 [hep-ph/9801218].

[151] Y. Kuno and Y. Okada, Rev. Mod. Phys. **73** (2001) 151 [hep-ph/9909265].

[152] T. S. Kosmas, S. Kovalenko and I. Schmidt, Phys. Lett. B **511** (2001) 203 [hep-ph/0102101].

[153] R. Kitano, M. Koike and Y. Okada, Phys. Rev. D **66** (2002) 096002 [Erratum-ibid. D **76** (2007) 059902] [hep-ph/0203110].

[154] J. D. Vergados, Phys. Rept. **133** (1986) 1.

[155] H. C. Chiang, E. Oset, T. S. Kosmas, A. Faessler and J. D. Vergados, Nucl. Phys. A **559** (1993) 526.

[156] T. S. Kosmas, S. Kovalenko and I. Schmidt, Phys. Lett. B **519** (2001) 78 [hep-ph/0107292].

[157] A. Faessler, T. Gutsche, S. Kovalenko, V. E. Lyubovitskij and I. Schmidt, Phys. Rev. D **72** (2005) 075006 [hep-ph/0507033].

[158] V. Cirigliano, R. Kitano, Y. Okada and P. Tuzon, Phys. Rev. D **80** (2009) 013002 [arXiv:0904.0957 [hep-ph]].

[159] H. De Vries, C. W. De Jager and C. De Vries, Atom. Data Nucl. Data Tabl. **36** (1987) 495.

[160] G. Fricke, C. Bernhardt, K. Heilig, L. A. Schaller, L. Schellenberg, E. B. Shera and C. W. de Jager, Atom. Data Nucl. Data Tabl. **60** (1995) 177.

[161] C. Garcia-Recio, J. Nieves and E. Oset, Nucl. Phys. A **547** (1992) 473.

[162] L. Ray, G. W. Hoffmann, G. S. Blanpied, W. R. Coker and R. P. Liljestrand, Phys. Rev. C **18** (1978) 1756.

[163] G. Pauletta, G. Adams, M. M. Gazzaly, G. Igo, A. T. M. Wang, A. Rahbar, A. Wriekat and G. W. Hoffmann *et al.*, Phys. Lett. B **106** (1981) 470.

[164] T. Suzuki, D. F. Measday and J. P. Roalsvig, Phys. Rev. C **35** (1987) 2212.

[165] R. P. Litchfield, arXiv:1501.04880 [physics.ins-det].

[166] T. Inami and C. S. Lim, Prog. Theor. Phys. **65** (1981) 297 [Erratum-ibid. **65** (1981) 1772].

[167] W. -S. Hou, R. S. Willey and A. Soni, Phys. Rev. Lett. **58** (1987) 1608 [Erratum-ibid. **60** (1988) 2337].

[168] G. Buchalla, A. J. Buras and M. E. Lautenbacher, Rev. Mod. Phys. **68** (1996) 1125 [hep-ph/9512380].

[169] W. Grimus and L. Lavoura, Phys. Rev. D **66** (2002) 014016 [hep-ph/0204070].

[170] A. J. Buras, B. Duling, T. Feldmann, T. Heidsieck and C. Promberger, JHEP **1009** (2010) 104 [arXiv:1006.5356 [hep-ph]].

[171] X. Chu, M. Dhen and T. Hambye, JHEP **1111** (2011) 106 [arXiv:1107.1589 [hep-ph]].

[172] N. Berger [$\mu 3e$ collaboration], arXiv:1110.1504 [hep-ex].

[173] S. Antusch, J. P. Baumann and E. Fernandez-Martinez, Nucl. Phys. B **810** (2009) 369 [arXiv:0807.1003 [hep-ph]].

[174] K. Eitel [KARMEN Collaboration], Nucl. Phys. Proc. Suppl. **91** (2001) 191 [hep-ex/0008002].

[175] P. Astier *et al.* [NOMAD Collaboration], Nucl. Phys. B **611** (2001) 3 [hep-ex/0106102].

[176] D. I. Britton, S. Ahmad, D. A. Bryman, R. A. Burnham, E. T. H. Clifford, P. Kitching, Y. Kuno and J. A. Macdonald *et al.*, Phys. Rev. D **46** (1992) 885.

[177] T. Yamazaki, T. Ishikawa, Y. Akiba, M. Iwasaki, K. H. Tanaka, S. Ohtake, H. Tamura and M. Nakajima *et al.*, Conf. Proc. C **840719** (1984) 262.

[178] R. S. Hayano, T. Taniguchi, T. Yamanaka, T. Tanimori, R. Enomoto, A. Ishibashi, T. Ishikawa and S. Sato *et al.*, Phys. Rev. Lett. **49** (1982) 1305.

[179] G. Bernardi, G. Carugno, J. Chauveau, F. Dicarlo, M. Dris, J. Dumarchez, M. Ferro-Luzzi and J. M. Levy *et al.*, Phys. Lett. B **166** (1986) 479.

[180] G. Bernardi, G. Carugno, J. Chauveau, F. Dicarlo, M. Dris, J. Dumarchez, M. Ferro-Luzzi and J. -M. Levy *et al.*, Phys. Lett. B **203** (1988) 332, and references therein.

[181] F. Bergsma *et al.* [CHARM Collaboration], Phys. Lett. B **166** (1986) 473.

[182] A. Vaitaitis *et al.* [NuTeV and E815 Collaborations], Phys. Rev. Lett. **83** (1999) 4943 [hep-ex/9908011].

[183] P. Abreu *et al.* [DELPHI Collaboration], Z. Phys. C **74** (1997) 57 [Erratum-ibid. C **75** (1997) 580].

[184] A. Atre, T. Han, S. Pascoli and B. Zhang, JHEP **0905** (2009) 030 [arXiv:0901.3589 [hep-ph]].

[185] O. Ruchayskiy and A. Ivashko, JHEP **1206** (2012) 100 [arXiv:1112.3319 [hep-ph]].

[186] E. Kuflik, S. D. McDermott and K. M. Zurek, arXiv:1205.1791 [hep-ph].

[187] K. Kainulainen, J. Maalampi and J. T. Peltoniemi, Nucl. Phys. B **358** (1991) 435.

[188] A. Kusenko, S. Pascoli and D. Semikoz, JHEP **0511** (2005) 028 [hep-ph/0405198].

[189] G. Mangano and P. D. Serpico, Phys. Lett. B **701** (2011) 296 [arXiv:1103.1261 [astro-ph.CO]].

[190] O. Ruchayskiy and A. Ivashko, arXiv:1202.2841 [hep-ph].

[191] A. Pilaftsis, Z. Phys. C **55**, 275 (1992) [hep-ph/9901206].

[192] J. -H. Chen, X. -G. He, J. Tandean and L. -H. Tsai, Phys. Rev. D **81** (2010) 113004 [arXiv:1001.5215 [hep-ph]].

[193] P. S. B. Dev, R. Franceschini and R. N. Mohapatra, arXiv:1207.2756 [hep-ph].

[194] C. G. Cely, A. Ibarra, E. Molinaro and S. T. Petcov, arXiv:1208.3654 [hep-ph].

[195] S. Chatrchyan *et al.* [CMS Collaboration], Eur. Phys. J. C **74** (2014) 2980 [arXiv:1404.1344 [hep-ex]].

[196] A. de Gouvea, arXiv:0706.1732 [hep-ph].

[197] S. Alekhin, W. Altmannshofer, T. Asaka, B. Batell, F. Bezrukov, K. Bondarenko, A. Boyarsky and N. Craig *et al.*, arXiv:1504.04855 [hep-ph].

[198] [MEG-II collaboration], see e.g. R. Sawada, talk at the Neutrino 2012 conference, Tokyo: http://meg.icepp.s.u-tokyo.ac.jp/docs/talks/JPS/2012s/sawada_jps2012s.pdf.

[199] R. Alonso, S. Antusch, M. Blennow, P. Coloma, A. de Gouvea, E. Fernandez-Martinez, B. Gavela and C. Gonzalez-Garcia *et al.*, arXiv:1009.0476 [hep-ph].

[200] R. Alonso., "MINSIS & Minimal Flavour Violation," http://www.lnf.infn.it/sis/frascatiseries/Volume51/Volume51.pdf

[201] J. A. Casas and A. Ibarra, Nucl. Phys. B **618** (2001) 171 [hep-ph/0103065].

[202] A. Ibarra and G. G. Ross, Phys. Lett. B **591** (2004) 285 [hep-ph/0312138].

[203] R. N. Cahn and H. Harari, Nucl. Phys. B **176** (1980) 135.

[204] G. Aad *et al.* [ATLAS Collaboration], Eur. Phys. J. C **72** (2012) 2244 [arXiv:1210.5070 [hep-ex]].

[205] S. Chatrchyan *et al.* [CMS Collaboration], Eur. Phys. J. C **72** (2012) 2189 [arXiv:1207.2666 [hep-ex]].

[206] P. A. R. Ade *et al.* [Planck Collaboration], arXiv:1502.01589 [astro-ph.CO].

[207] A. Strumia, hep-ph/0608347.

[208] N. Suzuki, D. Rubin, C. Lidman, G. Aldering, R. Amanullah, K. Barbary, L. F. Barrientos and J. Botyanszki *et al.*, Astrophys. J. **746**, 85 (2012) [arXiv:1105.3470 [astro-ph.CO]].

[209] A. D. Sakharov, Pisma Zh. Eksp. Teor. Fiz. **5** (1967) 32 [JETP Lett. **5** (1967) 24] [Sov. Phys. Usp. **34** (1991) 392] [Usp. Fiz. Nauk **161** (1991) 61].

[210] M. D'Onofrio, K. Rummukainen and A. Tranberg, Phys. Rev. Lett. **113** (2014) 14, 141602 [arXiv:1404.3565 [hep-ph]].

[211] J. M. Cline, hep-ph/0609145.

[212] D. E. Morrissey and M. J. Ramsey-Musolf, New J. Phys. **14** (2012) 125003 [arXiv:1206.2942 [hep-ph]].

[213] V. A. Kuzmin, V. A. Rubakov and M. E. Shaposhnikov, Phys. Lett. B **155** (1985) 36.

[214] L. Bento, JCAP **0311**, 002 (2003) [hep-ph/0304263].

[215] J. A. Harvey and M. S. Turner, Phys. Rev. D **42**, 3344 (1990).

[216] M. Fukugita and T. Yanagida, Phys. Lett. B **174** (1986) 45.

[217] L. Covi, E. Roulet and F. Vissani, Phys. Lett. B **384** (1996) 169 [hep-ph/9605319].

[218] W. Buchmuller and M. Plumacher, Phys. Lett. B **431** (1998) 354 [hep-ph/9710460].

[219] S. Davidson and A. Ibarra, Phys. Lett. B **535** (2002) 25 [hep-ph/0202239].

[220] M. Flanz, E. A. Paschos and U. Sarkar, Phys. Lett. B **345** (1995) 248 [Phys. Lett. B **382** (1996) 447] [hep-ph/9411366].

[221] A. Pilaftsis, Phys. Rev. D **56** (1997) 5431 [hep-ph/9707235].

[222] A. Pilaftsis and T. E. J. Underwood, Nucl. Phys. B **692** (2004) 303 [hep-ph/0309342].

[223] D. J. H. Chung, E. W. Kolb and A. Riotto, Phys. Rev. D **60** (1999) 063504 [hep-ph/9809453].

[224] J. Martin and C. Ringeval, Phys. Rev. D **82** (2010) 023511 [arXiv:1004.5525 [astro-ph.CO]].

[225] E. Nardi, J. Racker and E. Roulet, JHEP **0709** (2007) 090 [arXiv:0707.0378 [hep-ph]].

[226] W. Buchmuller, P. Di Bari and M. Plumacher, Annals Phys. **315** (2005) 305 [hep-ph/0401240].

[227] G. F. Giudice, A. Notari, M. Raidal, A. Riotto and A. Strumia, Nucl. Phys. B **685** (2004) 89 [hep-ph/0310123].

[228] W. Buchmuller, P. Di Bari and M. Plumacher, Phys. Lett. B **547** (2002) 128 [hep-ph/0209301].

[229] T. Hambye, New J. Phys. **14**, 125014 (2012) [arXiv:1212.2888 [hep-ph]].

[230] R. Barbieri, P. Creminelli, A. Strumia and N. Tetradis, Nucl. Phys. B **575**, 61 (2000) [hep-ph/9911315].

[231] A. Abada, S. Davidson, F. -X. Josse-Michaux, M. Losada and A. Riotto, JCAP **0604**, 004 (2006) [hep-ph/0601083].

[232] S. Blanchet, P. Di Bari, D. A. Jones and L. Marzola, JCAP **1301** (2013) 041 [arXiv:1112.4528 [hep-ph]].

[233] E. Nardi, Y. Nir, E. Roulet and J. Racker, JHEP **0601**, 164 (2006) [hep-ph/0601084].

[234] F. X. Josse-Michaux and A. Abada, JCAP **0710** (2007) 009 [hep-ph/0703084 [HEP-PH]].

[235] S. Blanchet and P. Di Bari, JCAP **0703** (2007) 018 [hep-ph/0607330].

[236] A. De Simone and A. Riotto, JCAP **0702** (2007) 005 [hep-ph/0611357].

[237] T. Hambye, Y. Lin, A. Notari, M. Papucci and A. Strumia, Nucl. Phys. B **695** (2004) 169 [hep-ph/0312203].

[238] E. Ma and U. Sarkar, Phys. Rev. Lett. **80** (1998) 5716 [hep-ph/9802445].

[239] T. Hambye, E. Ma and U. Sarkar, Nucl. Phys. B **602** (2001) 23 [hep-ph/0011192].

[240] T. Hambye and G. Senjanovic, Phys. Lett. B **582**, 73 (2004) [hep-ph/0307237].

[241] T. Hambye, M. Raidal and A. Strumia, Phys. Lett. B **632**, 667 (2006) [hep-ph/0510008].

[242] D. Aristizabal Sierra, J. F. Kamenik and M. Nemevsek, JHEP **1010**, 036 (2010) [arXiv:1007.1907 [hep-ph]].

[243] D. Aristizabal Sierra, F. Bazzocchi and I. de Medeiros Varzielas, Nucl. Phys. B **858**, 196 (2012) [arXiv:1112.1843 [hep-ph]].

[244] W. Buchmuller and M. Plumacher, Phys. Lett. B **511**, 74 (2001) [hep-ph/0104189].

[245] E. Nardi, Y. Nir, J. Racker and E. Roulet, JHEP **0601**, 068 (2006) [hep-ph/0512052].

[246] A. Strumia, Nucl. Phys. B **809**, 308 (2009) [arXiv:0806.1630 [hep-ph]].

[247] S. Lavignac and B. Schmauch, arXiv:1503.00629 [hep-ph].

[248] S. Blanchet, P. Di Bari and G. G. Raffelt, JCAP **0703** (2007) 012 [hep-ph/0611337].

[249] E. W. Kolb and S. Wolfram, Nucl. Phys. B **172**, 224 (1980) [Erratum-ibid. B **195**, 542 (1982)].

[250] R. G. Felipe, F. R. Joaquim and H. Serodio, arXiv:1301.0288 [hep-ph].

[251] G. C. Branco, R. G. Felipe and F. R. Joaquim, Rev. Mod. Phys. **84** (2012) 515 [arXiv:1111.5332 [hep-ph]].

[252] S. Antusch and S. F. King, Phys. Lett. B **597**, 199 (2004) [hep-ph/0405093].

[253] A. Abada, P. Hosteins, F. -X. Josse-Michaux and S. Lavignac, Nucl. Phys. B **809**, 183 (2009) [arXiv:0808.2058 [hep-ph]].

[254] T. Hambye, hep-ph/0412053.

[255] G. D. Moore, Phys. Lett. B **412**, 359 (1997) [hep-ph/9705248].

[256] S. Antusch, P. Di Bari, D. A. Jones and S. F. King, Nucl. Phys. B **856**, 180 (2012) [arXiv:1003.5132 [hep-ph]].

[257] D. Aristizabal Sierra, M. Losada and E. Nardi, Phys. Lett. B **659**, 328 (2008) [arXiv:0705.1489 [hep-ph]].

[258] D. Aristizabal Sierra, L. A. Munoz and E. Nardi, Phys. Rev. D **80**, 016007 (2009) [arXiv:0904.3043 [hep-ph]].

[259] D. Aristizabal Sierra, M. Losada and E. Nardi, JCAP **0912**, 015 (2009) [arXiv:0905.0662 [hep-ph]].

[260] M. C. Gonzalez-Garcia, J. Racker and N. Rius, JHEP **0911**, 079 (2009) [arXiv:0909.3518 [hep-ph]].

[261] W. Chao and H. Zhang, Phys. Rev. D **75** (2007) 033003 [hep-ph/0611323].

[262] D. V. Forero, M. Tortola and J. W. F. Valle, Phys. Rev. D **86**, 073012 (2012) [arXiv:1205.4018 [hep-ph]].

[263] G. L. Fogli, E. Lisi, A. Marrone, D. Montanino, A. Palazzo and A. M. Rotunno, Phys. Rev. D **86**, 013012 (2012) [arXiv:1205.5254 [hep-ph]].

[264] M. C. Gonzalez-Garcia, M. Maltoni, J. Salvado and T. Schwetz, JHEP **1212**, 123 (2012) [arXiv:1209.3023 [hep-ph]].

[265] Y. Sofue and V. Rubin, Ann. Rev. Astron. Astrophys. **39** (2001) 137 [astro-ph/0010594].

[266] S. W. Randall, M. Markevitch, D. Clowe, A. H. Gonzalez and M. Bradac, Astrophys. J. **679** (2008) 1173 [arXiv:0704.0261 [astro-ph]].

[267] C. E. Aisati, M. Gustafsson and T. Hambye, arXiv:1506.02657 [hep-ph].

[268] V. Silveira and A. Zee, Phys. Lett. B **161** (1985) 136.

[269] C. P. Burgess, M. Pospelov and T. ter Veldhuis, Nucl. Phys. B **619** (2001) 709 [hep-ph/0011335].

[270] J. M. Cline, K. Kainulainen, P. Scott and C. Weniger, Phys. Rev. D **88** (2013) 055025 [arXiv:1306.4710 [hep-ph]].

[271] V. Barger, P. Langacker, M. McCaskey, M. Ramsey-Musolf and G. Shaughnessy, Phys. Rev. D **79** (2009) 015018 [arXiv:0811.0393 [hep-ph]].

[272] V. Barger, M. McCaskey and G. Shaughnessy, Phys. Rev. D **82** (2010) 035019 [arXiv:1005.3328 [hep-ph]].

[273] L. M. Krauss and F. Wilczek, Phys. Rev. Lett. **62**, 1221 (1989).

[274] B. Petersen, M. Ratz and R. Schieren, JHEP **0908**, 111 (2009) [arXiv:0907.4049 [hep-ph]].

[275] F. Wilczek and A. Zee, Phys. Rev. Lett. **42**, 421 (1979).

[276] A. Anselm and Z. Berezhiani, Nucl. Phys. B **484**, 97 (1997) [hep-ph/9605400].

[277] Z. Berezhiani and A. Rossi, Nucl. Phys. Proc. Suppl. **101**, 410 (2001) [hep-ph/0107054].

[278] T. Feldmann, M. Jung and T. Mannel, Phys. Rev. D **80**, 033003 (2009) [arXiv:0906.1523 [hep-ph]].

[279] M. E. Albrecht, T. Feldmann and T. Mannel, JHEP **1010**, 089 (2010) [arXiv:1002.4798 [hep-ph]].

[280] B. Grinstein, M. Redi and G. Villadoro, JHEP **1011**, 067 (2010) [arXiv:1009.2049 [hep-ph]].

[281] R. Alonso, M. B. Gavela, L. Merlo and S. Rigolin, JHEP **1107**, 012 (2011) [arXiv:1103.2915 [hep-ph]].

[282] E. Nardi, Phys. Rev. D **84**, 036008 (2011) [arXiv:1105.1770 [hep-ph]].

[283] R. N. Mohapatra, AIP Conf. Proc. **1467**, 7 (2012) [arXiv:1205.6190 [hep-ph]].

[284] J. R. Espinosa, C. S. Fong and E. Nardi, JHEP **1302**, 137 (2013) [arXiv:1211.6428 [hep-ph]].

[285] C. S. Fong and E. Nardi, Phys. Rev. D **89**, no. 3, 036008 (2014) [arXiv:1307.4412 [hep-ph]].

[286] R. Alonso, M. B. Gavela, D. Hernandez and L. Merlo, Phys. Lett. B **715**, 194 (2012) [arXiv:1206.3167 [hep-ph]].

[287] R. Alonso, M. B. Gavela, D. Hernández, L. Merlo and S. Rigolin, JHEP **1308**, 069 (2013) [arXiv:1306.5922, arXiv:1306.5922 [hep-ph]].

[288] R. Alonso, M. B. Gavela, G. Isidori and L. Maiani, JHEP **1311**, 187 (2013) [arXiv:1306.5927 [hep-ph]].

[289] S. D. Aristizabal, M. Dhen, C. S. Fong and A. Vicente, Phys. Rev. D **91** (2015) 9, 096004 [arXiv:1412.5600 [hep-ph]].

[290] R. Barbieri, L. J. Hall and V. S. Rychkov, Phys. Rev. D **74** (2006) 015007 [hep-ph/0603188].

[291] L. Lopez Honorez, E. Nezri, J. F. Oliver and M. H. G. Tytgat, JCAP **0702** (2007) 028 [hep-ph/0612275].

[292] T. Hambye, F.-S. Ling, L. Lopez Honorez and J. Rocher, JHEP **0907** (2009) 090 [Erratum-ibid. **1005** (2010) 066] [arXiv:0903.4010 [hep-ph]].

[293] N. Nagata and S. Shirai, arXiv:1411.0752 [hep-ph].

[294] D. Tucker-Smith and N. Weiner, Phys. Rev. D **64** (2001) 043502 [hep-ph/0101138].

[295] J. Billard, L. Strigari and E. Figueroa-Feliciano, Phys. Rev. D **89** (2014) 2, 023524 [arXiv:1307.5458 [hep-ph]].

[296] P. Cushman, C. Galbiati, D. N. McKinsey, H. Robertson, T. M. P. Tait, D. Bauer, A. Borgland and B. Cabrera *et al.*, arXiv:1310.8327 [hep-ex].

[297] J. H. Davis, Phys. Rev. Lett. **113** (2014) 081302 [arXiv:1407.1052 [hep-ph]].

[298] S. Coutu, APS Physics **6** (2013) 40.

[299] M. Cirelli and G. Giesen, JCAP **1304** (2013) 015 [arXiv:1301.7079 [hep-ph]].

[300] V. Khachatryan *et al.* [CMS Collaboration], Eur. Phys. J. C **75** (2015) 5, 235 [arXiv:1408.3583 [hep-ex]].

[301] E. Lundstrom, M. Gustafsson and J. Edsjo, Phys. Rev. D **79** (2009) 035013 [arXiv:0810.3924 [hep-ph]].

[302] G. Belanger, B. Dumont, U. Ellwanger, J. F. Gunion and S. Kraml, Phys. Rev. D **88** (2013) 075008 [arXiv:1306.2941 [hep-ph]].

[303] E. W. Kolb and M. S. Turner, Front. Phys. **69** (1990) 1.

[304] H. Davoudiasl and R. N. Mohapatra, New J. Phys. **14** (2012) 095011 [arXiv:1203.1247 [hep-ph]].

[305] K. Petraki and R. R. Volkas, Int. J. Mod. Phys. A **28** (2013) 1330028 [arXiv:1305.4939 [hep-ph]].

[306] K. M. Zurek, Phys. Rept. **537** (2014) 91 [arXiv:1308.0338 [hep-ph]].

[307] S. M. Boucenna and S. Morisi, Front. Phys. **1** (2014) 33 [arXiv:1310.1904 [hep-ph]].

[308] N. Cosme, L. Lopez Honorez and M. H. G. Tytgat, Phys. Rev. D **72** (2005) 043505 [hep-ph/0506320].

[309] C. Arina and N. Sahu, Nucl. Phys. B **854** (2012) 666 [arXiv:1108.3967 [hep-ph]].

[310] A. Falkowski, J. T. Ruderman and T. Volansky, JHEP **1105** (2011) 106 [arXiv:1101.4936 [hep-ph]].

[311] G. Servant and S. Tulin, Phys. Rev. Lett. **111** (2013) 15, 151601 [arXiv:1304.3464 [hep-ph]].

[312] M. Cirelli, N. Fornengo and A. Strumia, Nucl. Phys. B **753** (2006) 178 [hep-ph/0512090].

[313] N. Fonseca, R. Z. Funchal, A. Lessa and L. Lopez-Honorez, arXiv:1501.05957 [hep-ph].

[314] Timothy R. Dulaney, Pavel Fileviez Perez, Mark B. Wise, Phys. Rev. **D83** (2011) 023520, arXiv:1005.0617 [hep-ph].

[315] S. M. Boucenna, M. B. Krauss and E. Nardi, arXiv:1503.01119 [hep-ph].

[316] S. Davidson, R. Gonzalez Felipe, H. Serodio and J. P. Silva, JHEP **1311** (2013) 100 [arXiv:1307.6218 [hep-ph]].

[317] E. Nardi, F. Sannino and A. Strumia, JCAP **0901** (2009) 043 [arXiv:0811.4153 [hep-ph]].

[318] C. Arina, F. S. Ling and M. H. G. Tytgat, JCAP **0910** (2009) 018 [arXiv:0907.0430 [hep-ph]].

[319] M. Cirelli, P. Panci, G. Servant and G. Zaharijas, JCAP **1203** (2012) 015 [arXiv:1110.3809 [hep-ph]].

[320] S. Tulin, H. B. Yu and K. M. Zurek, JCAP **1205** (2012) 013 [arXiv:1202.0283 [hep-ph]].

[321] Y. Burnier, M. Laine and M. Shaposhnikov, JCAP **0602** (2006) 007 [hep-ph/0511246].

[322] D. S. Akerib *et al.* [LUX Collaboration], Phys. Rev. Lett. **112** (2014) 9, 091303 [arXiv:1310.8214 [astro-ph.CO]].

[323] J. Gluza and M. Zralek, Phys. Rev. D **45** (1992) 1693.

[324] A. Ilakovac, B. A. Kniehl and A. Pilaftsis, Phys. Rev. D **52** (1995) 3993 [hep-ph/9503456].

[325] B. A. Campbell, S. Davidson, J. R. Ellis and K. A. Olive, Phys. Lett. B **297**, 118 (1992) [hep-ph/9302221].

[326] J. M. Cline, K. Kainulainen and K. A. Olive, Phys. Rev. D **49**, 6394 (1994) [hep-ph/9401208].

[327] C. S. Fong, M. C. Gonzalez-Garcia and E. Nardi, JCAP **1102**, 032 (2011) [arXiv:1012.1597 [hep-ph]].

[328] J. McDonald, Phys. Rev. Lett. **88**, 091304 (2002) [hep-ph/0106249]; L. J. Hall, K. Jedamzik, J. March-Russell and S. M. West, JHEP **1003**, 080 (2010) [arXiv:0911.1120 [hep-ph]]; C. Cheung, G. Elor, L. J. Hall and P. Kumar, JHEP **1103**, 042 (2011) [arXiv:1010.0022 [hep-ph]]; C. E. Yaguna, JHEP **1108**, 060 (2011) [arXiv:1105.1654 [hep-ph]]; M. Frigerio, T. Hambye and E. Masso, Phys. Rev. X **1**, 021026 (2011) [arXiv:1107.4564 [hep-ph]]; X. Chu, T. Hambye and M. H. G. Tytgat, JCAP **1205**, 034 (2012) [arXiv:1112.0493 [hep-ph]].

[329] S. Davidson, E. Nardi and Y. Nir, Phys. Rept. **466**, 105 (2008) [arXiv:0802.2962 [hep-ph]].

[330] M. Cirelli, A. Strumia and M. Tamburini, Nucl. Phys. B **787**, 152 (2007) [arXiv:0706.4071 [hep-ph]].

[331] M. Blennow, E. Fernandez-Martinez, J. Lopez-Pavon and J. Menendez, JHEP **1007** (2010) 096 [arXiv:1005.3240 [hep-ph]].

[332] A. Ibarra, E. Molinaro and S. T. Petcov, JHEP **1009** (2010) 108 [arXiv:1007.2378 [hep-ph]].

[333] A. Ibarra, E. Molinaro and S. T. Petcov, Phys. Rev. D **84** (2011) 013005 [arXiv:1103.6217 [hep-ph]].

[334] J. R. Espinosa, C. Grojean, M. Mühlleitner and M. Trott, arXiv:1207.1717 [hep-ph].

[335] M. C. Gonzalez-Garcia, M. Maltoni and J. Salvado, JHEP **1004** (2010) 056 [arXiv:1001.4524 [hep-ph]].

[336] W. Hu and S. Dodelson, Ann. Rev. Astron. Astrophys. **40** (2002) 171 [astro-ph/0110414].

[337] H. Davoudiasl, R. Kitano, T. Li and H. Murayama, Phys. Lett. B **609** (2005) 117 [hep-ph/0405097].

[338] M. Klasen, C. E. Yaguna and J. D. Ruiz-Alvarez, Phys. Rev. D **87** (2013) 075025 [arXiv:1302.1657 [hep-ph]].

[339] S. D. McDermott, H. B. Yu and K. M. Zurek, Phys. Rev. D **85** (2012) 023519 [arXiv:1103.5472 [hep-ph]].

[340] C. Kouvaris and P. Tinyakov, Phys. Rev. Lett. **107** (2011) 091301 [arXiv:1104.0382 [astro-ph.CO]].

[341] G. Hinshaw *et al.* [WMAP Collaboration], arXiv:1212.5226 [astro-ph.CO].

[342] J. Schechter and J. W. F. Valle, Phys. Rev. D **22**, 2227 (1980); G. Lazarides, Q. Shafi and C. Wetterich, Nucl. Phys. B **181**, 287 (1981); R. N. Mohapatra and G. Senjanovic, Phys. Rev. D **23**, 165 (1981); C. Wetterich, Nucl. Phys. B **187**, 343 (1981);

[343] R. Foot, H. Lew, X. G. He and G. C. Joshi, Z. Phys. C **44**, 441 (1989).

[344] C. S. Fong, E. Nardi and A. Riotto, Adv. High Energy Phys. **2012**, 158303 (2012) [arXiv:1301.3062 [hep-ph]].

[345] G. L. Fogli, E. Lisi, A. Marrone, D. Montanino, A. Palazzo and A. M. Rotunno, Phys. Rev. D **86**, 013012 (2012) [arXiv:1205.5254 [hep-ph]].